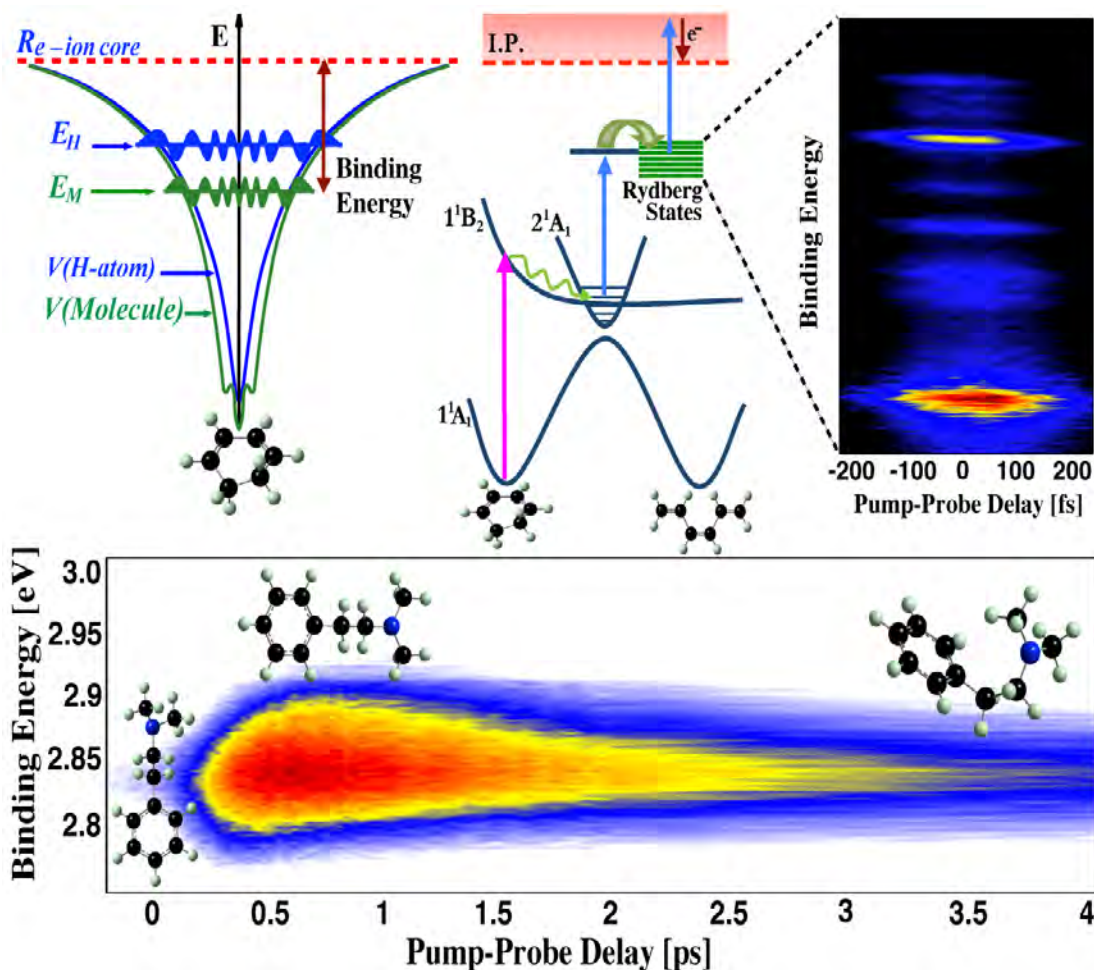


31st Annual Combustion Research Meeting

Airlie Conference Center
Warrenton, Virginia
June 1 – June 4, 2010



U.S. DEPARTMENT OF
ENERGY

Office of
Science

Office of Basic Energy Sciences
Chemical Sciences, Geosciences &
Biosciences Division

31st Annual Combustion Research Meeting

DOE Contractors' Meeting Program and Abstracts

Airlie Conference Center
Warrenton, Virginia
June 1 – June 4, 2010

Chemical Sciences, Geosciences, and Biosciences Division
Office of Basic Energy Sciences
Office of Science
U.S. Department of Energy

Cover Graphics:

The binding energy of a Rydberg electron to a molecular ion core (top left) is a sensitive probe of the molecular structure. Implemented in a time-resolved pump-probe experiment, the structure sensitivity enables ultrafast structural dynamics measurements. Examples include the dynamics of 1,3-cyclohexadiene during the ring-opening process (top right), and the formation of an intramolecular cation-pi bond in phenylethyl-N,N-dimethylamine (bottom). Artwork credit: Sanghamitra Deb, Joseph Bush, Christine Bühler, Michael Minitti (Weber group).

This document was produced under contract number DE-AC05-06OR23100 between the U.S. Department of Energy and Oak Ridge Associated Universities.

The research grants and contracts described in this document are supported by the U.S. DOE Office of Science, Office of Basic Energy Sciences, Chemical Sciences, Geosciences and Biosciences Division.

Foreword

This abstract booklet provides a record of the thirty-first U.S. Department of Energy contractors' meeting focused on gas-phase chemical physics. The reports appearing in this volume present work in progress in basic research contributing to the development of a predictive capability for combustion processes. The work reported herein is supported by the Department of Energy's Office of Basic Energy Sciences (BES) and, in large measure, by the chemical physics program. The long-term objective of this effort is the provision of theories, data, and procedures to enable the development of reliable computational models of combustion processes, systems, and devices.

The objective of this meeting is to provide a fruitful environment in which researchers with common interests will present and exchange information about their activities, will build collaborations among research groups with mutually reinforcing strengths, will identify needs of the research community, and will uncover opportunities for future research directions. The agenda consists of an invited keynote talk, oral presentations by program PIs, and for the first time, invited poster presentations from junior level researchers in an effort to increase the awareness of the Gas Phase Chemical Physics program. Approximately one-third of the PIs in the program speak each year in rotation. With ample time for discussion and interactions, we emphasize that this is an informal meeting for exchange of information and building of collaborations; it is not a review of researchers' achievements or a forum to define the future direction of the program.

During the past year, and a number of preceding years, this program benefited greatly from the leadership and insights of Dr. Larry Rahn. We appreciate the privilege of serving in the management of this research program. In carrying out these tasks, we learn from the achievements and share the excitement of the research of the many sponsored scientists and students whose work is summarized in the abstracts published on the following pages.

We thank all of the researchers whose dedication and innovation have advanced DOE BES research and made this meeting possible and productive. We hope that this conference will help you will build on your successes, and we look forward to our assembly next year for our 32nd annual meeting.

We thank Diane Marceau of the Chemical Sciences, Geosciences and Biosciences Division, and Connie Lansdon and Loretta Friend of the Oak Ridge Institute for Science and Education for their important contributions to the technical and logistical features of this meeting.

Michael Casassa
Mark Pederson
Wade Sisk

Agenda

31st Annual Combustion Research Meeting
U.S. Department of Energy
Office of Basic Energy Sciences

Agenda

Tuesday, June 1, 2010

3:00 pm	<i>Registration</i>
5:00 pm	<i>No-Host Reception at The Whistling Swan Pub</i>
7:00 pm	<i>Dinner</i>

Wednesday, June 2, 2010

7:00 am	<i>Breakfast</i>
----------------	------------------

Session I

Hanna Reisler, Chair & Meeting Co-chair

8:00 am	Welcome and Introduction - Eric Rohlfing, Michael Casassa, Wade Sisk Introduction of Invited Poster Presenters - Stephen Pratt, Meeting Co-chair
8:30 am	Keynote Speaker "Ultrafast Dynamics and Quantum Control of Non-adiabatic Processes," Albert Stolow, National Research Council 1
9:30 am	"Dynamics and Energetics of Elementary Combustion Reactions and Transient Species," Robert Continetti 61
10:00 am	"Bimolecular Dynamics of Combustion Reactions," Floyd Davis 73
10:30 am	<i>Break</i>

Session II

Hua Guo, Chair

11:00 am	"Theoretical Studies of Reaction Dynamics on High-Dimensional Potential Energy Surfaces," Joel Bowman 41
11:30 am	"High-Resolution, Crossed-Molecular-Beam Studies of Collisional Energy Transfer," David Chandler 53
12:00 pm	"Electronically Non-adiabatic Dynamics via Semiclassical Initial Value Methods," William Miller 217

12:30 pm

Lunch

Session III

Nancy Brown, Chair

4:00 pm

“Petascale Direct Numerical Simulation and Modeling of Turbulent Combustion,” Jacqueline Chen 57

4:30 pm

“Turbulence-Chemistry Interactions in Reacting Flows,” Robert Barlow 33

5:00 pm

Poster Session / Reception (Garden Room)
“Quantum Origin of Anomalous Isotope Effect in Ozone Formation,” Dmitri Babikov..... 3
“Combustion Characteristics of Practical Fuels at Elevated Pressures,” Gaurav Mittal..... 7
“Investigation of Molecular Level Composition and Atmospheric Aging of Organic Aerosols,” Sergey Nizkorodov 11
“Structure and Reactivity of Radicals and Elusive Intermediates,” Andrei Sanov..... 13
“Photochemical Combustion Dynamics from the Molecular Level to High Pressure Systems,” Wilton L. Virgo 17
“Catalytic Hydrocarbons Oxidation with Metal Oxide Nanowires,” Xiaolin Zheng..... 19

6:00 pm

Dinner

Session IV

Kent Ervin, Chair

7:00 pm

“Active Thermochemical Tables – Progress Report,” Branko Ruscic..... 277

7:30 pm

“Studies of the Chemistry of Oxygenated Fuels with Photoionization Mass Spectrometry,” Terrill Cool..... 65

Thursday, June 3, 2010

7:00 am

Breakfast

Session V

Phil Westmoreland, Chair

8:00 am

“Variational Transition State Theory,” Donald Truhlar..... 313

8:30 am

“Laser Studies of Combustion Chemistry,” John Hershberger 133

9:00 am

“Flash Photolysis-Shock Tube Studies,” Joe Michael 201

9:30 am

Break

Session VI

William Pitz, Chair

10:00 am “Kinetics and Dynamics of Combustion Chemistry,” David Osborn 245

10:30 am “Exploration and Validation of Chemical-Kinetic Mechanisms,”
Michael Davis 77

11:00 am “Computer-Aided Construction of Chemical Kinetic Models,”
William Green 105

11:30 am “Chemical Kinetics and Combustion Modeling,” James Miller 209

12:00 pm

Lunch

Session VII

Piotr Piecuch, Chair

4:00 pm “Generalized Van Vleck Variant of Multireference Perturbation Theory,”
Mark Hoffman 141

4:30 pm “Theoretical Studies of Potential Energy Surfaces,” Lawrence Harding 125

5:00 pm “A Multireference Study of the Singlet Electronic States of p-Benzyne,”
Carol Parish 249

5:30 pm

Break

Session VIII

Ralf Kaiser, Chair

6:00 pm “Spectroscopy, Kinetics and Dynamics of Combustion Radicals,”
David Nesbitt 229

6:30 pm “Synchrotron Studies of Combustion Radical Reactions and Aerosol
Chemistry,” Stephen Leone 177

7:00 pm

Dinner at the Pavilion

Friday, June 4, 2010

7:00 am *Breakfast*

Session IX

Peter Weber, Chair

8:00 am “Gas-Phase Molecular Dynamics: High Resolution Spectroscopy and Collision Dynamics of Transient Species,” Trevor Sears 281

8:30 am “Quantum Chemistry of Radicals and Reactive Intermediates,” John Stanton 297

9:00 am “Spectroscopic and Dynamical Studies of Highly Energized Small Polyatomic Molecules,” Robert Field 89

9:30 am *Break*

Session X

Wing Tsang, Chair

10:00 am “Particle Diagnostics Development,” Hope Michelsen 205

10:30 am “Scanning Tunneling Microscopy Studies of Chemical Reactions on Surfaces,” George Flynn 93

11:00 am “Elementary Reactions of PAH Formation,” Robert Tranter..... 309

11:30 am Closing Remarks

12:00 pm *Lunch*

Table of Contents

Table of Contents

Foreword	iii
Agenda	v
Table of Contents	ix
Abstracts	1
<u>Invited Presentations</u>	
Albert Stolow – Ultrafast Dynamics and Quantum Control of Non-adiabatic Processes	1
Dmitri Babikov – Quantum Origin of Anomalous Isotope Effect in Ozone Formation	3
Gaurav Mittal – Combustion Characteristics of Practical Fuels at Elevated Pressures	7
Sergey Nizkorodov – Investigation of Molecular Level Composition and Atmospheric Aging of Organic Aerosols.....	11
Andrei Sanov – Structure and Reactivity of Radicals and Elusive Intermediates.....	13
Wilton L. Virgo – Photochemical Combustion Dynamics from the Molecular Level to High Pressure Systems	17
Xiaolin Zheng – Catalytic Hydrocarbons Oxidation with Metal Oxide Nanowires	19
<u>Principal Investigator Presentations</u>	
Millard H. Alexander – Investigation of Non-adiabatic Effects in Reactive and Inelastic Collisions of Molecular Combustion Intermediates.....	21
Wesley D. Allen and Henry F. Schaefer III – Theoretical Studies of Elementary Hydrocarbon Species and Their Reactions.....	25
Tomas Baer – Threshold Photoelectron Photoion Coincidence (TPEPICO) Studies: The Road to ± 0.1 kJ/mol Thermochemistry	29
Robert S. Barlow – Turbulence-Chemistry Interactions in Reacting Flows	33
Josette Bellan – Modeling Reactions in High-Pressure Turbulence in the Cold Ignition Regime.....	37
Joel M. Bowman – Theoretical Studies of Combustion Dynamics.....	41
Nancy J. Brown – Combustion Chemistry	45
Laurie J. Butler – Dynamics of Product Branching in Elementary Combustion Reactions.....	49
David W. Chandler – High-Resolution, Crossed-Molecular-Beam Studies of Collisional Energy Transfer	53
Jacqueline H. Chen – Petascale Direct Numerical Simulation and Modeling of Turbulent Combustion.....	57
Robert E. Continetti – Dynamics and Energetics of Elementary Combustion Reactions and Transient Species.....	61
Terrill A. Cool – Studies of the Chemistry of Oxygenated Fuels with Photoionization Mass Spectrometry.....	65
F. F. Crim – Dissociation Pathways and Vibrational Dynamics in Excited Molecules and Complexes	69

H. Floyd Davis – Bimolecular Dynamics of Combustion Reactions.....	73
Michael J. Davis – Exploration and Validation of Chemical-Kinetic Mechanisms	77
Theodore S. Dibble – Dynamics of Radical Reactions in Biodiesel Combustion	81
Kent M. Ervin – Hydrocarbon Radical Thermochemistry: Gas-Phase Ion Chemistry Techniques.....	85
Robert W. Field – Spectroscopic and Dynamical Studies of Highly Energized Small Polyatomic Molecules	89
George Flynn – Scanning Tunneling Microscopy Studies of Chemical Reactions on Surfaces	93
Jonathan H. Frank – Quantitative Imaging Diagnostics for Reacting Flows.....	97
Michael Frenklach – Mechanism and Detailed Modeling of Soot Formation.....	101
William H. Green – Computer-Aided Construction of Chemical Kinetic Models.....	105
Hua Guo – Quantum Dynamics of Elementary Combustion Reactions	109
Gregory E. Hall – Gas-Phase Molecular Dynamics: High Resolution Spectroscopy and Collision Dynamics of Transient Species	113
Nils Hansen – Flame Chemistry and Diagnostics.....	117
Ronald K. Hanson and Craig T. Bowman – Spectroscopy and Kinetics of Combustion Gases at High Temperatures.....	121
Lawrence B. Harding – Theoretical Studies of Potential Energy Surfaces.....	125
Martin Head-Gordon – Chemical Accuracy from Ab Initio Molecular Orbital Calculations.....	129
John F. Hershberger – Laser Studies of Combustion Chemistry	133
So Hirata – Breakthrough Design and Implementation of Electronic and Vibrational Many-Body Theories.....	137
Mark R. Hoffmann – Generalized Van Vleck Variant of Multireference Perturbation Theory	141
Ahren W. Jasper – Theoretical Kinetics and Non-Born–Oppenheimer Molecular Dynamics.....	145
Ralf I. Kaiser – Probing the Reaction Dynamics of Hydrogen-Deficient Hydrocarbon Molecules and Radical Intermediates via Crossed Molecular Beams	149
Michael E. Kellman – Dynamical Analysis of Highly Excited Molecular Spectra.....	153
Alan R. Kerstein – Theory and Modeling of Small Scale Processes in Turbulent Flow	157
Alexei Khokhlov – First-Principles Petascale Simulations for Predicting Deflagration-to- Detonation Transition in Hydrogen-Oxygen Mixtures	161
Stephen J. Klippenstein – Theoretical Chemical Kinetics	165
Stephen J. Klippenstein and Craig A. Taatjes – Argonne-Sandia Consortium on High-Pressure Combustion Chemistry.....	169
Anna I. Krylov – Theoretical Modeling of Spin-Forbidden Channels in Combustion Reactions.....	173
Stephen R. Leone – Synchrotron Studies of Combustion Radical Reactions and Aerosol Chemistry	177
Marsha I. Lester – Intermolecular Interactions of Hydroxyl Radicals on Reactive Potential Energy Surfaces	181
William A. Lester, Jr. – Theoretical Studies of Molecular Systems.....	185
Robert P. Lucht – Advanced Nonlinear Optical Methods for Quantitative Measurements in Flames	189
R. G. Macdonald – Time-Resolved Infrared Absorption Studies of Radical Reactions.....	193

Alexander M. Mebel – Theoretical Studies of Chemical Reactions Related to the Formation and Growth of Polycyclic Aromatic Hydrocarbons and Molecular Properties of Their Key Intermediates	197
Joe V. Michael – Flash Photolysis-Shock Tube Studies	201
H. A. Michelsen – Particle Diagnostics Development	205
James A. Miller – Chemical Kinetics and Combustion Modeling	209
Terry A. Miller – Detection and Characterization of Free Radicals Relevant to Combustion Processes	213
William H. Miller – Reaction Dynamics in Polyatomic Molecular Systems.....	217
Amy S. Mullin – Dynamics of Activated Molecules	221
Habib N. Najm – Reacting Flow Modeling with Detailed Chemical Kinetics	225
David J. Nesbitt – Spectroscopy, Kinetics and Dynamics of Combustion Radicals.....	229
Daniel M. Neumark – Radical Photochemistry and Photophysics.....	233
C. Y. Ng – Determination of Accurate Energetic Database for Combustion Chemistry by High-Resolution Photoionization and Photoelectron Methods	237
Joseph C. Oefelein – Large Eddy Simulation of Turbulence-Chemistry Interactions in Reacting Multiphase Flows	241
David L. Osborn – Kinetics and Dynamics of Combustion Chemistry	245
Carol A. Parish – Theoretical Studies of the Combustion Reactions of Asphaltene Model Compounds	249
David S. Perry – The Dynamics of Large-Amplitude Motion in Energized Molecules	253
Piotr Piecuch – New Single- and Multi-Reference Coupled-Cluster Methods for High Accuracy Calculations of Ground and Excited States.....	257
William J. Pitz and Charles K. Westbrook – Chemical Kinetic Modeling of Combustion Chemistry	261
Stephen B. Pope – Investigation of Non-premixed Turbulent Combustion.....	265
S. T. Pratt – Optical Probes of Atomic and Molecular Decay Processes	269
Hanna Reisler – Photoinitiated Reactions of Radicals and Diradicals in Molecular Beams ...	273
Branko Ruscic – Active Thermochemical Tables – Progress Report	277
Trevor Sears – Gas-Phase Molecular Dynamics: High Resolution Spectroscopy and Collision Dynamics of Transient Species.....	281
Thomas B. Settersten and Roger L. Farrow – Picosecond Nonlinear Optical Diagnostics	285
Ron Shepard – Theoretical Studies of Potential Energy Surfaces and Computational Methods	289
M. D. Smooke and M. B. Long – Computational and Experimental Study of Laminar Flames.....	293
John F. Stanton – Quantum Chemistry of Radicals and Reactive Intermediates	297
Arthur G. Suits – Universal and State-Resolved Imaging Studies of Chemical Dynamics	301
Craig A. Taatjes – Elementary Reaction Kinetics of Combustion Species.....	305
Robert S. Tranter – Elementary Reactions of PAH Formation	309
Donald G. Truhlar – Variational Transition State Theory.....	313
Wing Tsang – Chemical Kinetic Data Base for Combustion Modeling	317
Angela Violi – Developing a Predictive Model for the Chemical Composition of Soot Nanoparticles: Integrating Model and Experiment	321
Peter M. Weber – Ultrafast Structural Dynamics in Combustion Relevant Model Systems ...	325
Phillip R. Westmoreland – Probing Flame Chemistry with MBMS, Theory, and Modeling ..	329

Margaret S. Wooldridge – The Effects of Oxygenated Fuel Compound Structure on Combustion and Pollutant Reaction Chemistry	333
David R. Yarkony – Theoretical Studies of the Reactions and Spectroscopy of Radical Species Relevant to Combustion Reactions and Diagnostics	337
Hua-Gen Yu – Gas-Phase Molecular Dynamics: Theoretical Studies in Spectroscopy and Chemical Dynamics	341
Timothy S. Zwier – Isomer-Specific Spectroscopy and Isomerization in Aromatic Fuels.....	345
Participant List	349

*Abstracts
of
Invited Presentations*

Ultrafast Dynamics and Quantum Control of Non-adiabatic Processes

Albert Stolow

Steacie Institute for Molecular Sciences, National Research Council Canada
Ottawa, Canada

Femtosecond laser technology has several implications for chemical dynamics. Most obvious is the ability to measure fast chemical processes. Chemical reaction dynamics generally involves the coupled flow of both electronic charge and vibrational energy in a reacting molecule. Time-Resolved Photoelectron Spectroscopy (TRPES) is one probe of these ultrafast 'non-adiabatic' dynamics in polyatomic molecules [1-2] and has been applied to problems ranging from photodissociation dynamics, to excited state proton transfer, to the photostability of DNA. A more kinematically complete TRPES method, called Time-Resolved Coincidence Imaging Spectroscopy (TRCIS), makes use of pairs of 3D particle timing-imaging detectors. This 6D information allows for the detailed study of the time evolution of both scalar and vector correlations in molecular photodissociation. One vector correlation is particularly interesting as it permits angle-energy resolved time-resolved studies from the recoil frame rather than the lab frame - in other words, dynamics from the "molecule's point of view" [3].

Electric forces underlie all of chemistry. Therefore controlling molecular processes with electric fields seems like a natural approach. However, Quantum Control to date has been based upon the multiphoton absorption of light from a coherent laser pulse. We discuss here Quantum Control without the absorption of light, using the non-resonant Dynamic Stark Effect as a tool. Dynamic Stark Control (DSC) applies to both molecular rotation and vibration. We show how DSC, which uses the electric field intensity envelope of a laser pulse rather than its frequency content, can be used to control electronic branching ratios in non-adiabatic photodissociation, without any absorption of light [4].

Some recent proposals for the study of gas phase dynamics are based upon time-resolved scattering, such as electron or X-ray diffraction. By analogy with the differences between powder vs. crystal x-ray diffraction, these experiments will require that the molecules under study be aligned (i.e. 'crystal') in the lab frame, rather than their usual random lab frame alignment (i.e. 'powder'). Here we use DSC to create field-free "fixed in space" molecules, with the alignment persisting long enough to make a femtosecond dynamics measurement. We apply this method to the study of excited state non-adiabatic photodissociation dynamics, once again allowing for studies in the Molecular Frame rather than the Lab Frame [5].

[1] Nature 401, 52, (1999)

[2] Chem.Rev. 104, 1719 (2004); Adv.Chem.Phys. 139, 495 (2008)

[3] Science 311, 219 (2006)

[4] Science 314, 278 (2006)

[5] Science 323, 1464 (2009)

Quantum Origin of Anomalous Isotope Effect in Ozone Formation

Dmitri Babikov, e-mail: dmitri.babikov@mu.edu

Chemistry Department, Marquette University, Milwaukee, Wisconsin 53201

The origin of anomalously large enrichments of stratospheric ozone in heavy isotopes has been a mystery for more than 25 years. The isotope ^{16}O is dominant in the atmosphere, so that most oxygen molecules (O_2) consist of two ^{16}O atoms. However, stratospheric ozone (O_3) is surprisingly observed to be heavily enriched in the isotopes ^{17}O and ^{18}O relative to the atmospheric oxygen from which it's formed. Careful experimental studies have shown that the recombination reaction that forms ozone,



is responsible for the effect. The recombination rates for various isotopic combinations differ by more than 50%, which is a remarkably large isotope effect taking into account small mass difference. It was also demonstrated experimentally that the isotope effect is essentially independent of the identity of the buffer gas M and occurs with M being as simple as Ar or He. For these, the reaction (1) at low pressure is expected to be dominated by the *energy*

transfer mechanism:



where O_3^* is a metastable state (quantum scattering resonance) which lives long enough to be stabilized by the collision M.

We carried out full dimensional quantum scattering calculations of three-body resonances for different isotopologues of non-rotating ozone ($J = 0$) using accurate *ab initio* potential energy surface (PES). We determined energies and lifetimes of the metastable ($^x\text{O}^y\text{O}^z\text{O}$) * states in reaction (2) and found

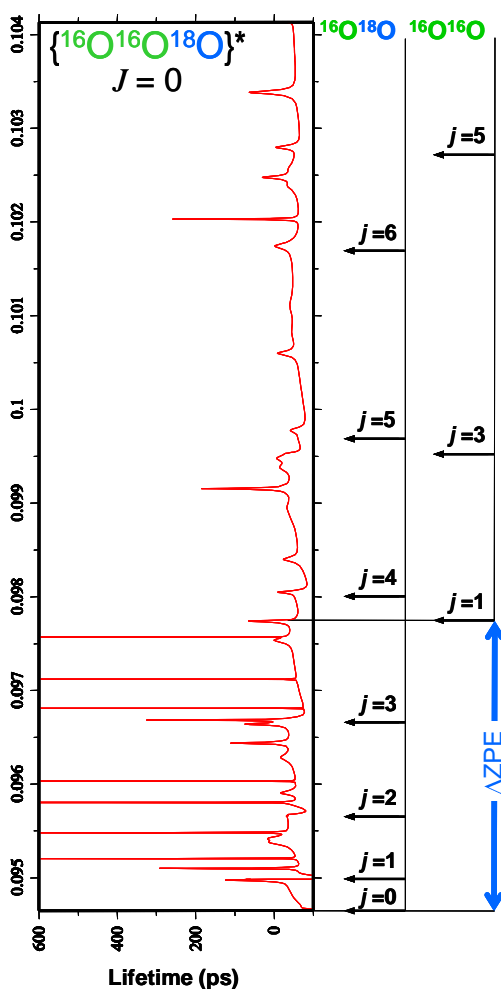
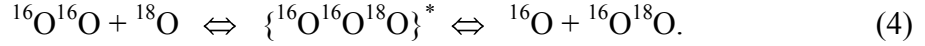


Figure 1: Calculated lifetime spectrum for the metastable $^{16}\text{O}^{16}\text{O}^{18}\text{O}$ ($J = 0$). Vertical axis gives energy of $\text{O}_2 + \text{O}$ collision complex in units of eV. Sharp spikes to the left correspond to long-lived metastable O_3^* states (scattering resonances). Rotational states (j) of the asymptotic $\text{O}_2(v=0)$ products/reactants are indicated for the two exit channels, as well as the ΔZPE energy range.

that the lower part of the spectrum (within the quantum ΔZPE range, see Fig. 1) contains *many metastable states* with lifetimes in the optimum picosecond range to contribute to the recombination, while the upper part of spectrum (above the ΔZPE) is *very sparse* and contains only a few such resonances. Note that this narrow part of spectrum, ΔZPE , has a special property. For example, in the case of $^{16}\text{O}^{16}\text{O}^{18}\text{O}$ shown in Fig. 1 there are two physically distinct entrance/exit channels corresponding to two sides of the barrier-less process:



The quantum ZPE of lighter diatomic, $^{16}\text{O}^{16}\text{O}$, is slightly higher than the ZPE of heavier diatomic, $^{16}\text{O}^{18}\text{O}$, which makes one channel effectively deeper by $\Delta ZPE \sim 25 \text{ cm}^{-1}$. At energies above the ΔZPE both channels are open, but within the ΔZPE energy range one channel is still closed and we found that the long-lived resonances occur only at such conditions (see Fig. 1).

Based on these $J=0$ results we propose a semi-quantitative picture of the remarkable effect of the ΔZPE on recombination rates. Figure 2 gives schematic for formation of ozone isotopologue $^{16}\text{O}^{16}\text{O}^{18}\text{O}$. The experimental formation rates¹ for two entrance channels ($^{16}\text{O}^{16}\text{O} + ^{18}\text{O}$ on the left and $^{16}\text{O} + ^{16}\text{O}^{18}\text{O}$ on the right) are shown at the top of the figure indicating large isotope effect ($\sim 40\%$). Energies below the scattering threshold (yellow part of the figure) correspond to stable O_3 molecules, while the metastable O_3^* can be formed above the threshold. The stabilization of O_3^* to O_3 , reaction (3), is shown schematically by red arrows. This scheme illustrates that the metastable O_3^* states at energies *above* the ΔZPE (striped part) can be formed from both entrance channels; when stabilized they should contribute to recombination rates of both channels about equally. However, the metastable states at energies *within* the ΔZPE (blue part) can be formed only from one, lower entrance channel

$^{16}\text{O} + ^{16}\text{O}^{18}\text{O}$. When such O_3^* states are stabilized they contribute exclusively to the rate of this channel and can be responsible for the anomalous difference in rates for the two channels. Note that it is exactly this ΔZPE region that accommodates

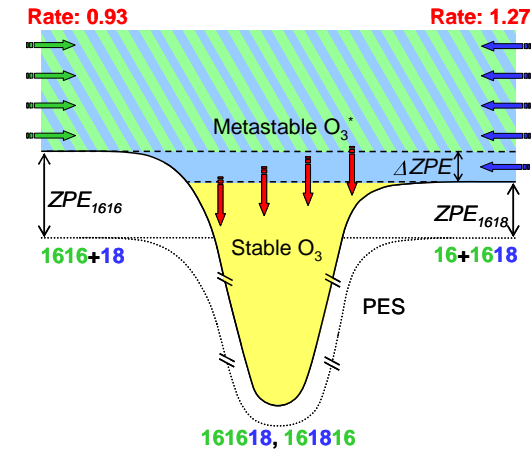


Figure 2: Schematic for recombination process forming the $^{16}\text{O}^{16}\text{O}^{18}\text{O}$ isotopologue. The PES (dotted line), quantum ZPE for each entrance channels and the ΔZPE are shown (not to scale). Note one extra blue arrow on the right side, against the ΔZPE energy range.

¹ Relative to the rate of $^{16}\text{O} + ^{16}\text{O}^{16}\text{O} \rightarrow ^{16}\text{O}^{16}\text{O}^{16}\text{O}$ taken as a reference for other isotopic combinations

many long-lived metastable states (Fig. 1). Also, these states lie closest to the energy of stable O₃ (Fig. 2) and should be stabilized most efficiently by collisions with M.

This preliminary model totally neglects the state-to-state stabilization dynamics and does not permit to separate contributions to the two isotopomers (*e.g.*, ¹⁶O¹⁶O¹⁸O and ¹⁶O¹⁸O¹⁶O) of the same ozone isotopologue, but it is still quite encouraging that the direction of the isotope effect and its order of magnitude predicted for various combinations of ¹⁶O and ¹⁸O in the reactants are consistent with experimental observations. It is now clear that this isotope effect is a *quantum* effect and one can see why classical trajectories could not reproduce it: they have no *ZPE* and follow along the PES (lowest dotted curve in Fig. 2) which has the same energy on both sides of reaction. One also sees that this is a *general* effect which should occur in any ABA type molecule where there is no barrier to dissociation and ΔZPE between the ^xAB and ^yAB is not negligible (*e.g.*, S₃, SO₂, NO₂, CS₂, and many atmospheric ion-molecule collision complexes).

References

1. E. Vetoshkin and D. Babikov, *J. Chem. Phys.* 127, 154312 (2007).
2. E. Vetoshkin and D. Babikov, *Phys. Rev. Lett.* 99, 138301 (2007).
3. E. Vetoshkin and D. Babikov, *J. Chem. Phys.* 127, 154312 (2007).
4. D. Babikov et al, *J. Chem. Phys.* 119, 2577 (2003).
5. D. Babikov et al, *Chem. Phys. Lett.* 372, 686 (2003).
6. D. Babikov et al, *J. Chem. Phys.* 118, 6298 (2003).

Combustion Characteristics of Practical Fuels at Elevated Pressures

Gaurav Mittal

ASEC 101, University of Akron, Akron, OH, 44325

gaurav@uakron.edu

Overview

The focus of the research in High Pressure Combustion Lab is on studying fundamental combustion characteristics of conventional and alternative fuels at elevated pressures and temperatures relevant to engines. It is noted that the experimental data for combustion of practical fuels at conditions of elevated pressures is scarce, and chemical kinetic models remain largely non-validated. Recognizing this need, our objective is to design well-characterized experimental facilities and use them for contributing to the development of comprehensively validated chemical kinetic mechanisms with emphasis on better predictability at elevated pressures.

To this effect, a suite of experimental facilities are in operational and design stage. A CCPRCM (Contained Crevice Piston Rapid Compression Machine) is being used for studying high pressure chemical kinetics of fuels at low-to-intermediate temperatures and elevated pressures. A high pressure JSR (Jet Stirred Reactor) has been built for chemical kinetics investigations at pressures up to 50 atm. Another facility for investigating flame propagation of liquid fuels at elevated pressure is in the fabrication stage. It is expected that the variety of experimental facilities at one location will be extremely valuable for comprehensive investigation of combustion processes. Ultimate objective of this research effort is to provide validated comprehensive and reduced chemical kinetic mechanisms for practical fuels.

Development of Experimental Facilities

Contained Crevice Piston Rapid Compression Machine (CCPRCM) Facility

CCPRCM is a novel facility, recently designed for investigation of homogeneous gas phase chemical kinetics at conditions of elevated pressures (up to 100 atm) and low-to-intermediate temperatures (600-1200 K). The basic operation of the machine is similar to the one designed and used extensively previously [1-3], and the conceptual difference lies in the configuration of the combustion chamber. The novel concept of ‘crevice containment’ gives this facility uniqueness in terms of providing benchmark experimental data. In this approach, crevice zone of RCM is separated from the main reaction zone by means of a seal which engages only when the piston reaches the top dead center (TDC). The design of CCPRCM is validated through extensive CFD simulations. Specifically, it is established that the multi-dimensional effects due to the influence of piston-motion-induced roll-up vortex and non-uniform heat release are minimized by using the approach of ‘crevice containment’. Consequently, this approach allows the simulation of the experimental data by using a zero-dimensional formulation with detailed chemical kinetics for development and validation of chemical kinetic mechanisms. Fig. 1 presents typical experimental pressure histories from CCPRCM for compression of N₂, showing attainment of experimental conditions up to 100 atm by rapid compression process of ~ 25 ms duration. Fig. 2 presents a comparison of the CFD and zero-dimensional simulated ignition delays for CCPRCM for a reactive n-heptane mixture, which suggests that the experiment can be accurately modeled by using the zero-dimensional approach.

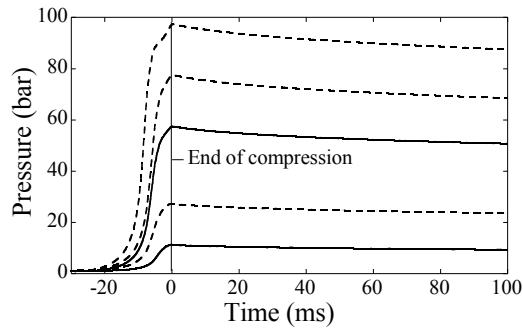


Fig. 1 – Experimental pressure traces from CCPRCM demonstrating the attainable range of compressed pressures up to 100 bar: Gas used: N_2 .

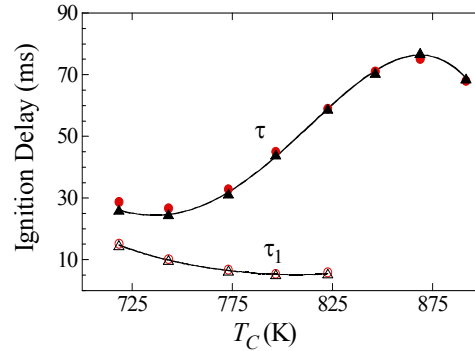


Fig. 2 – Comparison of CFD (triangles) vs zero-dimensional (circles) simulated first-stage (τ_1) and total (τ) ignition delays for CCPRCM. Molar composition: n-heptane/ $O_2/N_2/Ar = 0.3/3.3/33.6/16.16$. $P_C \sim 11$ bar. Kinetic mechanism from Liu et al. [4].

Annular Jet Stirred Reactor

Jet stirred reactors (JSR) are frequently employed for studying homogeneous gas phase chemical kinetics of fuels. Such reactors allow ease of modeling and experimentation with heavy liquid fuels. The most challenging aspect of JSR is the achievement of sufficiently rapid mixing by turbulent jets so that the temperature and concentration fields inside the reactor could be considered homogeneous. JSRs used in combustion community have almost never been validated to ensure that the rapid mixing is indeed achieved. The objective of our research was to explore the mixing inside the popular JSR geometries with the aid of CFD and come up with alternate geometries that could significantly improve mixing characteristics.

Some of the geometries considered are shown in Fig. 3. The geometry #1 consists of a sphere of 4 cm diameter with 4 nozzles, 1 mm diameter each. The geometry #2 is same as #1 except that the diameter of nozzles is 0.25 mm. It is noted that these geometries have been extensively used by various research groups [5-7]. Apart from these, one of the alternative geometries is shown as #3. In geometry #3, the reaction chamber consists of annular region contained between the outside sphere of diameter 4 cm and an inside cylinder of diameter 1.5 cm. It has 4 nozzles, each with 0.25 mm diameter. The arrows in Fig. 3 indicate the directions of jets from the nozzles.

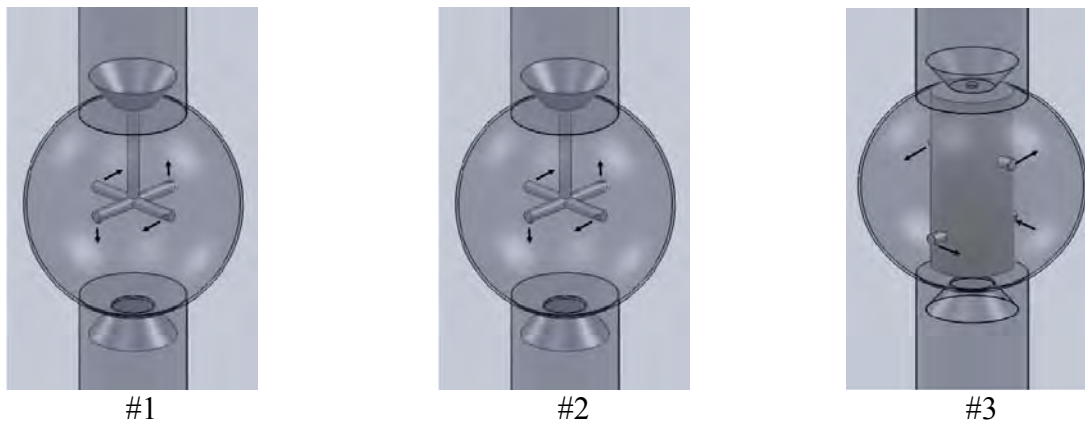


Fig. 3 – Various JSR geometries considered for CFD analysis

In CFD simulations, the steady-state solution for the flow of air is first obtained for the given geometry and boundary conditions. Simulations are conducted using RNG based $k-\epsilon$ turbulence model. The governing equations for flow, turbulence and energy are discretized using the second-order upwind scheme. The steady-state solution is subsequently used for the transient calculations of jet mixing inside the reactor. A tracer pulse is injected in the flow field through nozzles and the evolution of the tracer is then monitored by solving the transient scalar transport equation with the known flow-field.

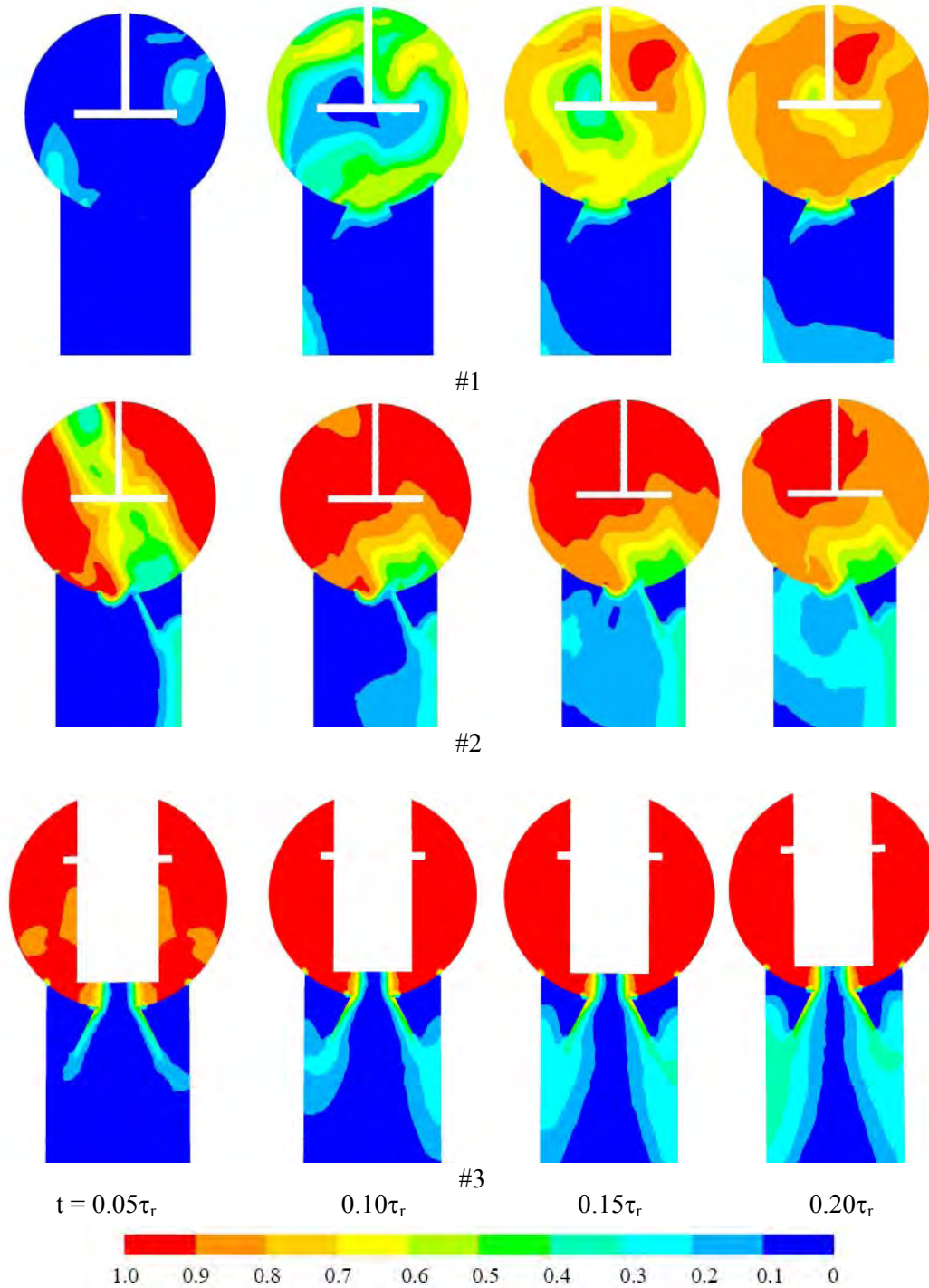


Fig. 4 – Normalized mass fractions of tracer for various geometries. Residence time, $\tau_r \sim 1s$

Figure 4 presents results for a representative case for JSR operation at a pressure of 10 bar and temperature of 800 K. A mass flow rate of 0.0001455 kg/s is specified for all geometries which yield a residence time of ~1 s (0.8 to 1.15 s for different geometries). The Fig. shows the normalized tracer mass fraction distribution at various times after the injection of the tracer pulse. It is noted that the popular geometries are considerably influenced by non-homogeneities and the alternative geometry considered here results in significant improvement. A JSR has been fabricated with the alternative geometry and is being assembled for experiments.

Experimental Data From CCPRCM

The experimental facilities described above are being used for studying homogeneous gas phase chemical kinetics of biofuels and jet fuels. An example of ignition delay measurement from CCPRCM for a Methyl Butanoate mixture at a pressure of 84 bar is shown in Fig. 5. Fig. 6 shows ignition delay data vs inverse of temperature for pressure ~ 20 bar, showing exponential dependence.

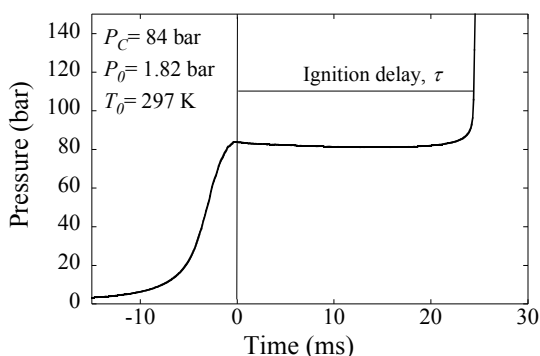


Fig. 5 – Experimental pressure trace from CCPRCM. Molar composition: MB/O₂/N₂/Ar = 1/6.5/46.25/46.25

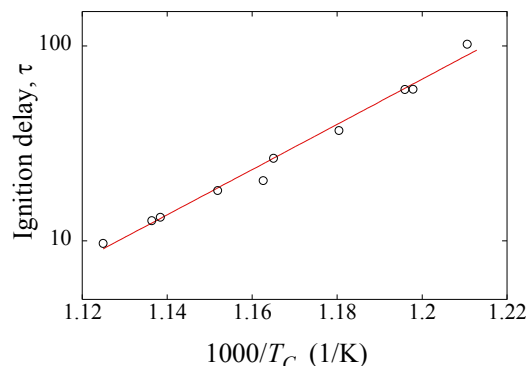


Fig. 6 – Ignition delay vs temperature for $P_c \sim 20$ bar. Molar composition: MB/O₂/Ar = 3.13/20.34/76.53

Future Work

Future work will focus on investigating the chemical kinetics of biodiesel and jet fuel relevant components using JSR and CCPRCM. A GC-MS equipment has been set up for obtaining detailed speciation data from both facilities for rigorous validation of chemical kinetic mechanisms.

References

- [1] G. Mittal, C. J. Sung, *Combust. Sci. Tech.* 179 (2007), 497-530.
- [2] G. Mittal, C. J. Sung, *Combust. Flame* 145 (2006), 160-180.
- [3] G. Mittal, C. J. Sung, R. A. Yetter, *Int. J. Chem. Kin.* 38 (2006) 516-529.
- [4] S. Liu, J.C. Hewson, J. H. Chen, H. Pitsch, *Combust. Flame* 137 (2004) 320-339.
- [5] P. Dagaut, M. Cathonnet, J. P. Rouan, R. Foulatier, A. Quilgars, J. C. Boettner, F. Gaillard, H. James, *J. Phys. E: Sci. Instrum.* 19 (1986) 207-209.
- [6] O. Herbinet, P. M. Marquaire, F. Battin-Leclerc, R. Fournet, *J. Anal. Appl. Pyrolysis* 78 (2007) 419-429.
- [7] R. Rota, F. Bonini, A. Servida, M. Morbidelli, S. Carra, *Ind. Eng. Chem. Res.* 33 (1994) 2540-2553.

Investigation of Molecular Level Composition and Atmospheric Aging of Organic Aerosols

Prof. Sergey Nizkorodov, Department of Chemistry, University of California at Irvine, nizkorod@uci.edu

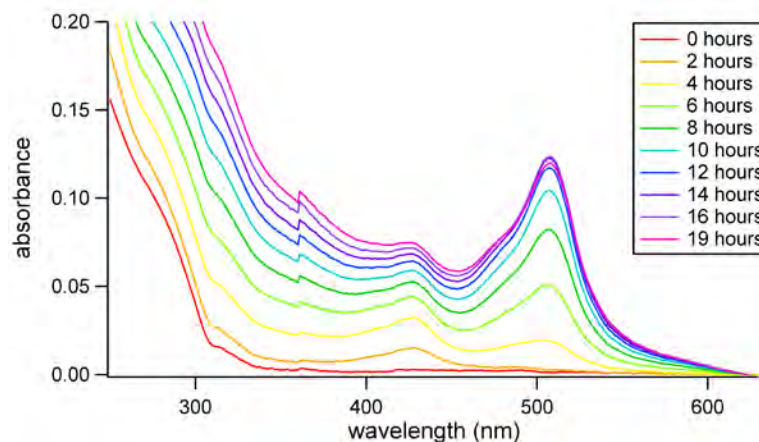
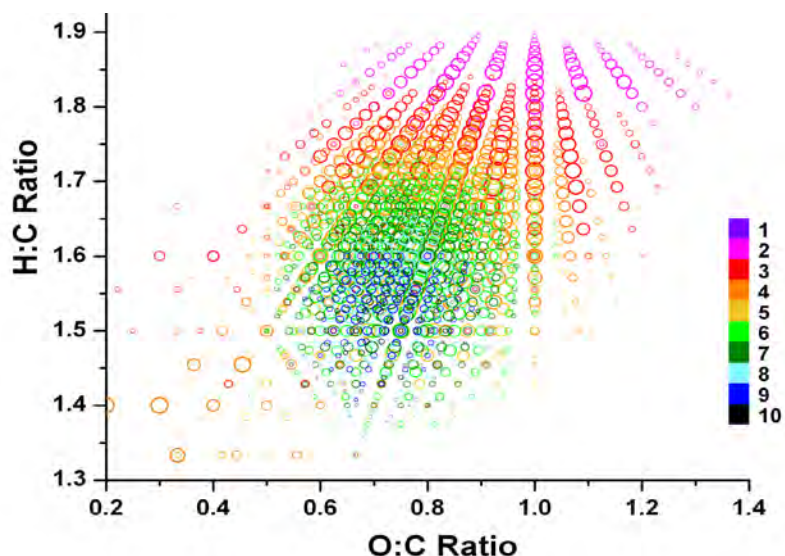
DOE collaborators: Dr. Alexander Laskin and Dr. Julia Laskin, Pacific Northwest National Laboratory, Richland, Washington

Poster Abstract

Atmospheric aerosols play an important role in controlling climate, driving atmospheric chemistry, and contributing to air pollution problems worldwide. This poster presents an overview of our recent research progress in the following areas: 1) detailed characterization of molecular-level composition of organic aerosols; 2) investigation of mechanisms of chemical and photochemical “aging” processes in organic aerosols. In collaboration with Dr. Alexander Laskin and Dr. Julia Laskin from the DOE Pacific Northwest National Laboratory, we have been developing and applying methods of high resolution mass spectrometry to molecular characterization of secondary organic aerosols (SOA). This approach provides unprecedented amount of details about the composition of organic aerosols by supplying molecular formulas for thousands of aerosol species in a single measurement. A detailed analysis of the distribution of chemical formulas reveals useful mechanistic information about chemistry leading to the initial formation and subsequent aging of biogenic and anthropogenic organic aerosols. This collaboration between UC

Irvine and PNNL has resulted in the identification of multifunctional monomeric and oligomeric aerosol compounds in limonene SOA¹ and isoprene SOA,² discovery of chemical pathways leading to colored compounds in “brown” SOA,³ observation of time-dependence of the SOA composition,⁴ and detailed study of the solvent interference in the ESI analysis of SOA.⁵ In addition, Dr. A. Laskin and Dr. J. Laskin have used the same approach for the detailed characterization of N-containing species in biomass burning aerosol.^{6,7} The first graph is just one example illustrating the richness of information provided by this method. It is a Van Krevelen representation of isoprene SOA constituents observed in the negative and positive ion mode mass spectra and color coded by their degree of unsaturation (the number of unsaturated C=C and C=O bonds, as well as rings in the molecules). We are currently working on applications of this powerful method to aerosols generated by fuel combustion and biomass burning.

The term “aging” refers to a combination of processes leading to the change in the chemical composition and physical properties of aerosols on time scales ranging



from minutes to days. We investigate mechanisms of chemical and photochemical aging in secondary organic aerosols using a combination of spectroscopic and mass spectrometric techniques. We recently demonstrated the significance of direct photolysis of carbonyl^{8,9} and peroxide¹⁰ functional groups for photochemical aging of monoterpene SOA. Our more recent work^{3,11} showed that biogenic SOA can also undergo aging catalyzed by reduced nitrogen species (ammonia, amine, and amino acids), which leads to the appearance of light-absorbing “brown” carbon in the SOA on atmospherically relevant time scales. For example, the second graph shows the evolution of absorption spectrum of limonene SOA exposed to low concentrations of ammonia vapor.³ This work has significant implications for the understanding of effects of organic aerosols on climate. Our current efforts focus on unraveling the molecular details of processes responsible for “browning” of SOA.

Relevant Recent Publications

1. Walser, M. L.; Desyaterik, Y.; Laskin, J.; Laskin, A.; Nizkorodov, S. A., High-resolution mass spectrometric analysis of secondary organic aerosol produced by ozonation of limonene. *Phys. Chem. Chem. Phys.* **2008**, *10* (7), 1009-1022.
2. Nguyen, T. B.; Bateman, A. P.; Bones, D. L.; Nizkorodov, S. A.; Laskin, J.; Laskin, A., High-resolution mass spectrometry analysis of secondary organic aerosol generated by ozonolysis of isoprene. *Atm. Environ.* **2010**, *44* (8), 1032-1042.
3. Laskin, J.; Laskin, A.; Roach, P. J.; Slysz, G. W.; Anderson, G. A.; Nizkorodov, S. A.; Bones, D. L.; Nguyen, L. Q., High-resolution desorption electrospray ionization mass spectrometry for chemical characterization of organic aerosols. *Analyt. Chem.* **2010**, *82* (5), 2048-2058.
4. Bateman, A. P.; Nizkorodov, S. A.; Laskin, J.; Laskin, A., Time-resolved molecular characterization of limonene/ozone aerosol using high-resolution electrospray ionization mass spectrometry. *Phys. Chem. Chem. Phys.* **2009**, *11* (36), 7931-7942.
5. Bateman, A. P.; Walser, M. L.; Desyaterik, Y.; Laskin, J.; Laskin, A.; Nizkorodov, S. A., The effect of solvent on the analysis of secondary organic aerosol using electrospray ionization mass spectrometry. *Environ. Sci. Technol.* **2008**, *42* (19), 7341-7346.
6. Smith, J. S.; Laskin, A.; Laskin, J., Molecular characterization of biomass burning aerosols using high-resolution mass spectrometry. *Analyt. Chem.* **2009**, *81* (4), 1512-1521.
7. Laskin, A.; Smith, J. S.; Laskin, J., Molecular characterization of nitrogen-containing organic compounds in biomass burning aerosols using high-resolution mass spectrometry. *Environ. Sci. Technol.* **2009**, *43* (10), 3764-3771.
8. Mang, S. A.; Henriksen, D. K.; Bateman, A. P.; Andersen, M. P. S.; Blake, D. R.; Nizkorodov, S. A., Contribution of carbonyl photochemistry to aging of atmospheric secondary organic aerosol. *J. Phys. Chem. A* **2008**, *112*, 8337-8344.
9. Pan, X.; Underwood, J. S.; Xing, J.-H.; Mang, S. A.; Nizkorodov, S. A., Photodegradation of secondary organic aerosol generated from limonene oxidation by ozone studied with chemical ionization mass spectrometry. *Atm. Chem. Phys.* **2009**, *9*, 3851-3865.
10. Walser, M. L.; Park, J.; Gomez, A. L.; Russell, A. R.; Nizkorodov, S. A., Photochemical Aging of Secondary Organic Aerosol Particles Generated from the Oxidation of d-Limonene. *J. Phys. Chem. A* **2007**, *111* (10), 1907-1913.
11. Bones, D. L.; Henriksen, D. K.; Mang, S. A.; Gonsior, M.; Bateman, A. P.; Nguyen, T. B.; Cooper, W. J.; Nizkorodov, S. A., Appearance of strong absorbers and fluorophores in limonene-O₃ secondary organic aerosol due to NH₄⁺-mediated chemical aging over long time scale. *J. Geophys. Res.* **2010**, *115*, doi:10.1029/2009JD012864.

Structure and reactivity of radicals and elusive intermediates

Andrei Sanov

Department of Chemistry and Biochemistry, University of Arizona, Tucson, AZ 85721-0041
sanov@u.arizona.edu

PROGRAM SCOPE

Chemical bonding is controlled by electrons and it is their behavior that determines bonding structures and the outcomes of chemical reactions. This realization motivates the broadly defined objective of our research: to attain a molecular-level view of electronic structure transformations that are manifest in reactions and intermolecular interactions.

We focus on the structure and dynamics of negative ions and the corresponding neutral molecules using photoelectron imaging and tandem time-of-flight mass-spectroscopy in combination with theoretical modeling techniques. Negative ions are important in many natural and technological processes and their properties are vital to understanding chemistry of solutions, as well as bio- and environmental chemistry. The anions targeted in our studies are selected for their fundamental properties, as well as the potential roles they (or their neutral counterparts) play in relevant reactions. Among others, we are particularly interested in carbon-rich and CN-containing species.

In our experiments, we characterize the bonding motifs of selected molecular systems by observing photoinduced emission of electrons from isolated anions. A pictorial example of the utility of photoelectron imaging in obtaining experimental “signatures” of electronic states is shown in Fig. 1, which illustrates our imaging results for NO_2^- . Analysis of the quantitative details (spectra and angular distributions, which are omitted here) allows us to assign the bands seen in the photoelectron image to specific electronic states of neutral NO_2 formed upon anion photodetachment.

Special emphasis in our work is given to coherence of delocalized charge distributions. A cornerstone of charge transport phenomena, coherence controls unabated charge flow across a molecule or a device. Its limits (*decoherence*) underline the localization of charges and excitations in molecules and nanostructures, imposing restrictions on electro-conductivity of materials. Our work targets coherence at the molecular level, by characterizing interference effects in the photodetachment of symmetric anions with delocalized charge distributions. For example, the work on NO_2^- (Fig. 1) provides a starting (reference) point for our ongoing study of *through-bond* coherence of two equivalent $\text{NO}_2^{\delta-}$ centers in the dinitrobenzene anion.

We are also interested in interactions of negative ions and emitted photoelectrons with neighboring neutral molecules in microscopic solvation environments – clusters.

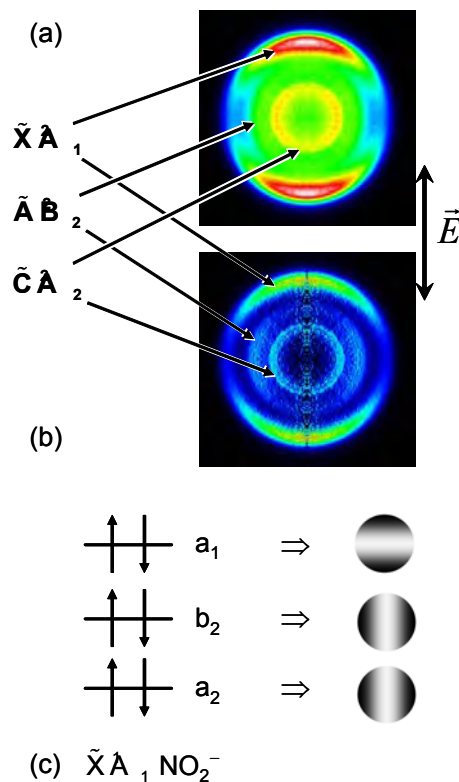


Figure 1. Raw (a) and Abel-inverted (b) photoelectron images of NO_2^- at 266 nm with the bands assigned to electronic states of the neutral. (c) A molecular-orbital diagram for the ground state of the anion with model predictions for the photoelectron angular distributions.

We focus on the mechanisms of molecular-level interactions that control the outcomes of chemical reactions, including those described as solvent-enabled or solvent-controlled chemistry.

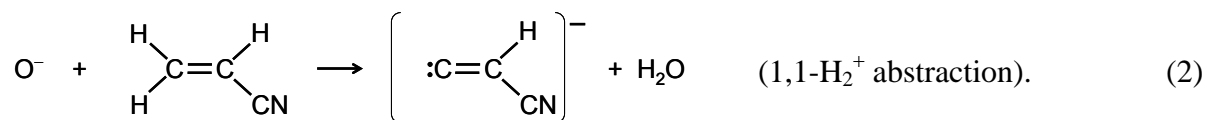
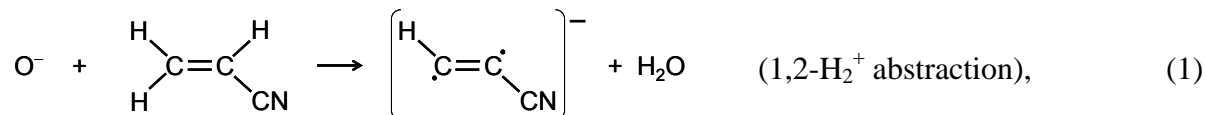
RECENT RESULTS

From its inception, our group has worked on developing the utility of photoelectron imaging in the studies of the electronic structure, photodetachment, and time-resolved dynamics of molecular and cluster anions. We interpret photoelectron images as experimental “signatures” of bound electronic wavefunctions. One example is shown in Fig. 1; another concerns the ground and excited electronic states of *neutral* nitromethane at the equilibrium geometry of the *anion*.¹

The results of some of our experiments are interpreted by considering interference of two effective electron emission centers in the parent anion. In this view, molecular anions are treated as double-slit interferometers, an approach traced back to Cohen and Fano.²

O⁻ CHEMISTRY

In several recent projects, we utilized O⁻ chemistry to generate anions that upon photodetachment provide access to important, yet often elusive neutral species. For example, we used this approach to generate the anions of cyanoacetylene and cyanovinylidene.^{3,4} In this work, the O⁻ radical anions obtained by electron bombardment of N₂O in a supersonic expansion reacted with acrylonitrile, H₂C=CHCN. The desired HCCCN⁻ (scheme 1) and CCHCN⁻ (scheme 2) species were formed via the competing 1,2-H₂⁺ and 1,1-H₂⁺ abstraction reactions:



In the future, we plan to use similar approaches to the generation of other interesting species. For example, the formation of NCCCCN⁻ can be accomplished by replacing acrylonitrile in schemes (1) and (2) with either fumaronitrile or 2-butanedinitrile.

ELUSIVE ANIONS AND REACTIVE INTERMEDIATES

A snapshot of the results for the cyanovinylidene and cyanoacetylene anions, synthesized using schemes (1) and (2) above, is shown in Fig. 2.³ The simultaneous generation of CCHCN⁻ and HCCCN⁻ is exciting for two reasons. First, the photodetachment of these anions provides access to both the *reactant* and *product* sides of the neutral potential energy surface for the cyanovinylidene → cyanoacetylene rearrangement. Similar to vinylidene, cyanovinylidene is a reactive intermediate with a very small rearrangement barrier. Second, our experiment yielded the first laboratory observation of HCCCN⁻.

Cyanoacetylene, HCCCN, is one of the most abundant organic molecules in extraterrestrial environments. Its anionic resonances have been hypothesized to serve as a gateway for formation of carbon-rich and CN-containing anions in space by way of dissociative attachment. Stabilized by geometry relaxation, the adiabatically weakly bound⁵ HCCCN⁻ ions are counterparts of the

dissociative-attachment resonances. These ions had, until recently,³ eluded definitive detection – not only in space, but also in the laboratory. We have concluded that the key to the formation of HCCCN^- is a bent CCC skeleton of the starting reactant (acrylonitrile).

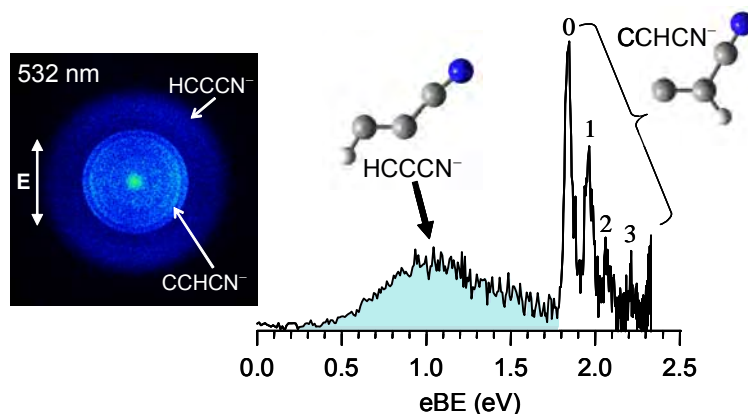


Figure 2. 532 nm photoelectron image and spectrum of the cyano-vinylidene and cyanoacetylene anions. The electron affinity of cyanovinylidene is 1.84 ± 0.01 eV. The vertical detachment energy of HCCCN^- is 1.04 ± 0.05 eV.

RESONANCE-STABILIZED RADICALS

We emphasize selected thermochemical properties, such as C–H bond dissociation energies and electron affinities. These quantities are routinely used for calculating reaction energies and heats of formation of a variety of molecules within the self-consistent framework of thermodynamics.⁶

For example, we determined the C–H bond dissociation energy of malononitrile, $\text{CH}_2(\text{CN})_2$, using the measured electron affinity of the dicyanomethyl radical, $^{\bullet}\text{CH}(\text{CN})_2$.⁷ The results of this work are illustrated in Fig. 3. The C–H bond dissociation energy (BDE) of malononitrile, $\text{BDE}[\text{H}-\text{CH}(\text{CN})_2] = 87.2 \pm 2.1$ kcal/mol, was found to be smaller than that of acetonitrile, $\text{BDE}[\text{H}-\text{CH}_2\text{CN}] = 93.1 \pm 2.1$ kcal/mol.^{7,8} Both are smaller than the BDEs(H-R) of most closed-shell organic molecules [e.g., for methane, $\text{BDE}(\text{H}-\text{CH}_3) = 104.9 \pm 0.4$ kcal/mol].⁶ The relatively weak C–H bonds in CH_3CN and $\text{CH}_2(\text{CN})_2$ reflect the formation of resonance-stabilized radicals, $^{\bullet}\text{CH}_2\text{CN}$ and $^{\bullet}\text{CH}(\text{CN})_2$.

CARBENES

No other class of compounds highlights the power and versatility of photoelectron imaging in unraveling the electronic-structural properties of anions and neutrals as clearly as carbenes. The singlet and triplet states of these important reactive intermediates are accessed by removing electrons from distinct orbitals of the anion, in general resulting in qualitatively different photoelectron angular distributions. Recently, we applied this approach to $\text{CH}_3\text{S}(\text{O})\text{CH}$ and dicyanocarbene. In the first case, we synthesized and characterized carbene anions $\text{CH}_3\text{S}(\text{O})\text{CH}^-$ and $\text{CH}_3\text{S}(\text{O})\text{CH}^- \cdot \text{H}_2\text{O}$.⁹ In the second, we examined the singlet-triplet splitting in the neutral carbene via photoelectron imaging of NCCCN^- .¹⁰

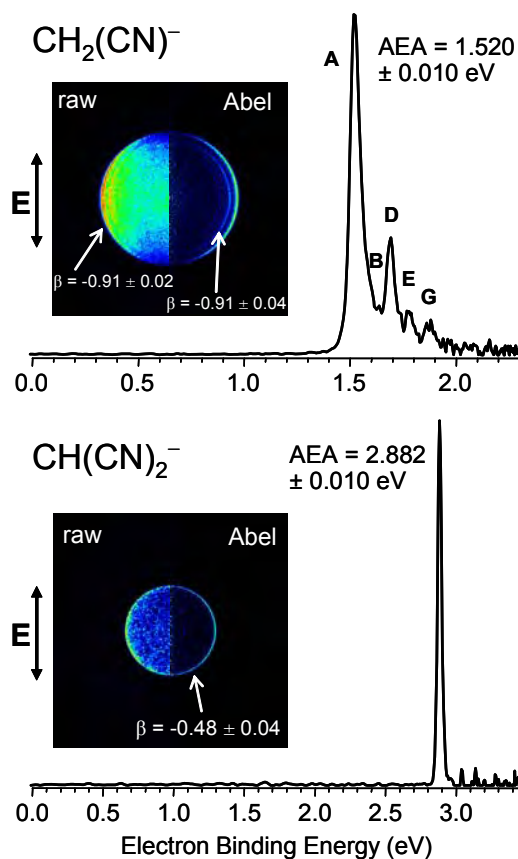


Figure 3. Photoelectron images and spectra of CH_2CN^- and $\text{CH}(\text{CN})_2^-$ at 532 and 355 nm, respectively.

FUTURE PLANS

Our future work in the area of elusive anions and neutral intermediates will focus on structures, electron affinities, bond energies, as well as dynamics and solvent-controlled reactivity.

We plan characterize several chain anions (C_n^- , C_nN^- , and C_nO^-) and examine the effects of different substituents (e.g., $-CN$, $-F$, etc.) on their properties. In selected cases, we will also target high-strain isomers. For example, by reaction of O^- with 2-Cyclopropen-1-one (C_3H_2O) it should be possible to generate the cyclic C_3O^- anion, $\left[\begin{array}{c} \text{C} \\ \parallel \\ \text{C} \end{array} \text{C}=\text{O} \right]^-$. The neutral formed upon its photodetachment, is expected to undergo rapid rearrangement to linear tricarbon monoxide, CCO. Larger cyclic C_nO^- anions are also targets for studies of the corresponding intermediates.

The bond dissociation energies corresponding to the formation of selected organic radicals will be determined by means of photoelectron imaging of their anions. Continuing the recent study of malononitrile,⁷ we will undertake a study of the tricyanomethyl anion, $C(CN)_3^-$. This is a challenging project, because the synthesis of the precursor, tricyanomethane $HC(CN)_3$ (cyanoforn), is not trivial. From the measured electron affinity of the radical, $\cdot C(CN)_3$, combined with the acidity data, the C–H bond dissociation energy of cyanoforn will be determined. This result, reflecting the stability of the corresponding radical, will be compared to the already available bond-dissociation data for the formation of $\cdot CH_3$, $\cdot CH_2(CN)$, and $\cdot CH(CN)_2$, completing the series of these important resonance-stabilized radicals.⁶⁻⁸

Following our recent work on $CH_3S(O)CH$ ^[9] and dicyanocarbene,¹⁰ we will investigate other classes of these intermediates.

- 1) Goebbert, D. J.; Pichugin, K.; Sanov, A., "Low-lying electronic states of CH_3NO_2 via photoelectron imaging of the nitromethane anion", *J. Chem. Phys.* 131, 164308 (2009).
- 2) Cohen, H. D.; Fano, U., "Interference in Photoionization of Molecules", *Phys. Rev.* 150, 30 (1966).
- 3) Goebbert, D. J.; Khuseynov, D.; Sanov, A., "Laboratory observation of the valence anion of cyanoacetylene, a possible precursor for negative ions in space", *J. Chem. Phys.* 131, 161102 (2009).
- 4) Goebbert, D. J.; Khuseynov, D.; Sanov, A., "Photoelectron Imaging of Cyanovinylidene and Cyanoacetylene Anions", *J. Phys. Chem. A* 114, 2259-2265 (2010).
- 5) Sommerfeld, T.; Knecht, S., "Electronic interaction between valence and dipole-bound states of the cyanoacetylene anion", *Eur. Phys. J. D* 35, 207-216 (2005).
- 6) Blanksby, S. J.; Ellison, G. B., "Bond Dissociation Energies of Organic Molecules", *Accounts Chem. Res.* 36, 255 (2003).
- 7) Goebbert, D. J.; Velarde, L.; Khuseynov, D.; Sanov, A., "The C-H Bond Dissociation Energies of Acetonitrile and Malononitrile", *J. Phys. Chem. Lett.* 1, 792-795 (2010).
- 8) Moran, S.; Ellis Jr., H. E.; DeFrees, D. J.; McLean, A. D.; Ellison, G. B., "Carbanion Spectroscopy: CH_2CN^- ", *J. Am. Chem. Soc.* 109, 5996 (1987).
- 9) Velarde, L.; Habteyes, T.; Glass, R. S.; Sanov, A., "Observation and Characterization of the $CH_3S(O)CH^-$ and $CH_3S(O)CH \cdot H_2O$ Carbene Anions by Photoelectron Imaging and Photofragment Spectroscopy", *J. Phys. Chem. A* 113, 3528-3534 (2009).
- 10) Goebbert, D. J.; Pichugin, K.; Khuseynov, D.; Wenthold, P. G.; Sanov, A., "Photoelectron Imaging of $NCCCN^-$: the singlet-triplet splitting of Dicyanocarbene" (in preparation).

**Photochemical Combustion Dynamics From
The Molecular Level to High Pressure Systems**

Wilton L. Virgo

Department of Chemistry, Wellesley College

Wellesley, MA 02481

wvirgo@wellesley.edu

The main problem to be addressed in combustion research is how one can bridge scientific knowledge of combustion at the molecular level to combustion chemistry under high-pressure conditions (tens of atmospheres).

We are currently developing an experimental research program which will elucidate chemically relevant combustion dynamics both at the microscopic quantum level and under high-pressure, fuel-lean conditions.

Velocity map imaging (VMI) will be employed to determine how photochemical energy is partitioned and transformed within hydrogen-rich fuels. Since combustion at the molecular level is governed by the mechanism of bond rupture, experiments involving photodissociation and low-pressure VMI of fuel molecules can be performed to map the pathways for internal energy flow and yield deep insight into fundamental chemistry of hydrocarbons, alcohols and other combustion-relevant fuels.

An original experiment designed to perform high-pressure combustion imaging is a work in progress. The goal is to fully comprehend the fundamental physical chemistry relevant to internal combustion engines that operate under high pressures. An experimental apparatus is being constructed for fuel injection through a small-diameter nozzle into a high-pressure chamber containing a mixture of oxygen and inert gas in order to achieve fuel-lean conditions. Laser-based ignition techniques will be used to precisely control the input energy to drive combustion while maintaining control of the chemical conditions. The propagation of the high-pressure flame will be observed and analyzed using high-speed video technology, particle image velocimetry (PIV) and laser induced fluorescence (LIF). The molecular focus will be on hydrogen or hydrogen-rich fuels (such as propane and natural gas) with high efficiency and low nitrogen oxide (NO_x) emissions. Characterization of the high-pressure flame instability as a function of ignition energy will lead to upgraded models for fuel efficiency.

Catalytic Hydrocarbons Oxidation with Metal Oxide Nanowires

Xiaolin Zheng
Mechanical Engineering, Stanford University
xlzheng@stanford.edu

Catalytic oxidation and partial oxidation of hydrocarbons are essential for many practical applications, including energy generation, petroleum refinement, alternative fuels production, and emission control. Developing cost-effective catalysts for hydrocarbon oxidation will significantly increase the efficiency of these processes and minimize their environmental impact. Nanoparticles of noble metals and metal oxides have been intensively studied and are widely used for the catalytic oxidation of hydrocarbons. However, catalytic nanoparticles are typically anchored to a solid support so that interactions between the support and nanoparticles limit the loading of nanoparticles, restrain the operational temperature, and impede the fundamental understanding of the catalytic properties of individual nanoparticles. There is a great need to develop a new form of catalysts which have surface areas comparable to nanoparticles but require minimum supporting structures.

Our objective is to use catalytic metal oxides in the form of one-dimensional nanowires (NWs) for hydrocarbon oxidation reactions. NWs are attractive alternatives for nanoparticles in the catalytic study because 1) they have large surface area to volume ratios; 2) they can have little interaction with the support since only one end of NWs is in contact with the support; and most importantly 3) their orientations can be controlled to expose a particular crystallographic orientation with more active surface sites. The research focus is two-folded. The first is to synthesize metal oxide NWs in flames and to understand the effects of flame chemistry on the physical and chemical properties of these NWs. The other is to characterize their activities, selectivities and stabilities of these NWs in catalyzing the oxidation of hydrocarbons and to understand the coupling between gaseous and surface reactions. The obtained results are hoped to broaden the applications of cost-effective metal oxide catalysts in many energy conversion systems.

*Abstracts
of
Principal Investigator
Presentations*

Investigation of Non-adiabatic Effects in Reactive and Inelastic Collisions of Molecular Combustion Intermediates

Millard H. Alexander

Department of Chemistry and Biochemistry, University of Maryland
College Park, MD 20742-2021
mha@umd.edu

I. Program Scope

We study inelastic and reactive collisions of small molecules, focusing on radicals important in combustion environments. Most radical encounters involve multiple potential energy surfaces (PESs). Consequently, non-adiabatic effects may be important, even for reactions involving ground-state species. Our work involves first the accurate determination of potential energy surfaces, using multi-reference, configuration-interaction and coupled-cluster techniques. In the subsequent treatment of the collision dynamics it is easiest to work in an electronically diabatic framework, in which there appear electronically off-diagonal PESs. To extract these from a typical *ab initio* calculation, in which electronically adiabatic roots are determined, requires an additional level of computational effort. Our work benefits from a long-standing collaboration with Hans-Joachim Werner, ^{1,2} the developer of the MOLPRO program suite.

After fitting the *ab initio* points to obtain global PESs, we treat the dynamics using time-independent (close-coupling) methods. For inelastic scattering we use our Hibridon code, ³ and, for reactive scattering, the ABC code of Manolopoulos, ⁴ extended to include reactions on multiple PESs. ²

II. Recent Progress

Since inception of our DOE-funded program (fall, 2009) we have focused on the study of the methylene radical (CH_2) in the $c^1\tilde{a}$ state. Inelastic collisions of methylene are currently under experimental study at Brookhaven. ^{5,6} In the fall of 2009 we determined a highly-accurate PES for the interaction of $\text{CH}_2(\tilde{a})$ with He, using CCSD(T) calculations with correlation-consistent basis sets, extrapolated to the complete basis set limit. The calculations were carried out on a grid of 19 values of the CH_2 -He separation and 190 values of the orientation, for a total of 3610 points. These were then fitted, as in our recent paper on collisions of He with H_2O . ⁷ We used, for compactness, an expansion in spherical harmonics in the appropriate inertial frame of CH_2 , in which the z axis lies perpendicular to the C_2 axis, but in the plane of the triatomic.

In Figures 1 and 3 we compare the $\text{CH}_2(\tilde{a})$ -He PES, in which only one lone-pair orbital is occupied, to the $\text{H}_2\text{O}(\tilde{X})$ -He PES, in which both lone-pairs are occupied, determined by Szalewicz and

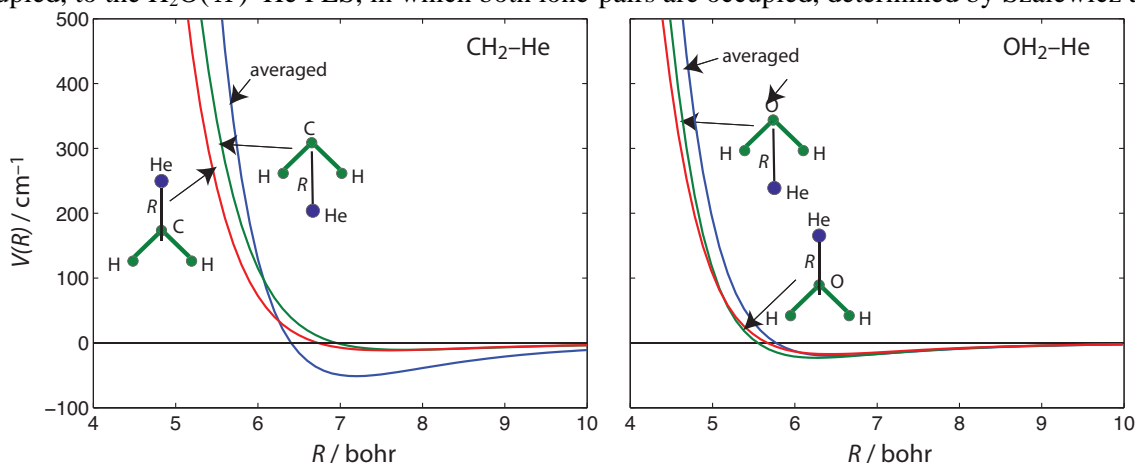


Fig. 1 Comparison on the He-MH₂ distance of the potential energy surface, averaged over all orientations of the H₂, as well a comparison for approach of the He atom along the C₂ axis, both from the C(O) side and from the H₂ side.

co-workers. ⁸ Figure 2 displays a schematic of the geometry of the C(O)H₂-He system, with the z axis aligned along the C₂ axis. Figure 1 shows the dependence on the C(O)H₂-He distance of the PES

averaged over all orientations of the H₂ moiety. This is the isotropic potential, equivalent to the interaction of He with a pseudo-diatomic.

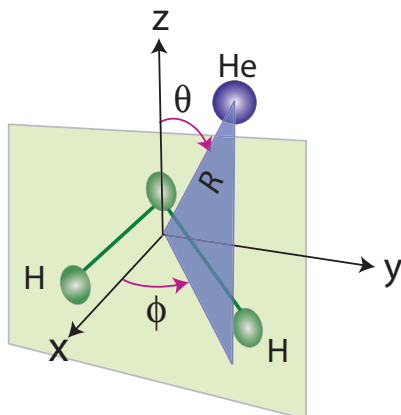


Fig. 2. Geometry of the C(O)H₂-He system, with the z axis aligned along the C₂ axis

Figure 3 compares the dependence on the two angles (illustrated in Fig. 2) of the CH₂(\bar{a})-He and H₂O(\tilde{X})-He potential energy surfaces, for a He-MH₂ distance fixed at the minimum of the isotropic potential shown in Fig. 2, $R = 5.8$ bohr for CH₂(\bar{a})-He and $R = 4.8$ bohr for H₂O(\tilde{X})-He. We see that

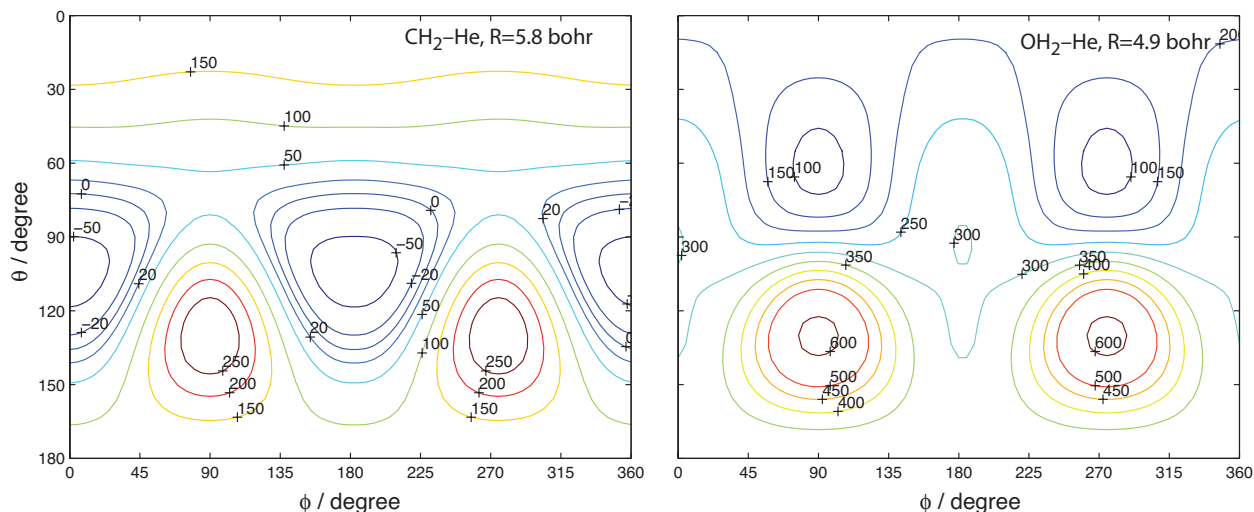


Fig. 3. Contour plots of the C(O)H₂-He potential energy surfaces (in cm⁻¹), with the He distance fixed at the minima in the isotropic potential (see Fig. 1).

the topology of the two PESs is very dissimilar. The PES for CH₂(\bar{a})-He has a considerably deeper minimum and is more strongly anisotropic, when the He approaches at the H₂ end of the molecule. By contrast, the H₂O(\tilde{X})-He PES is more anisotropic, for approach at the O end. This is likely the consequence of the additional, out of plane, lone-pair orbital, which is doubly occupied in the O atom but unoccupied in the C atom in the \bar{a} state of CH₂.

We are now carrying out preliminary scattering calculations, to study inelastic transitions out of, and into, particular JK levels of CH₂(\bar{a}). We utilize our recent extension of the Hibridon program suite to inelastic collisions of asymmetric top molecules.⁷ Figure 4 (next page) shows the rich structure of the lower rotational levels of CH₂(\bar{a}). The rotational levels are labeled *ortho* and *para*, corresponding to the two possible permutation symmetries of the two H nuclei. Collisions with He will not lead to transitions between these two permutation isotopomers. Of particular interest will be the relative propensities for *para* → *para* as compared to *ortho* → *ortho* transitions for $K > 0$. In a symmetric top, these should be

very similar. However, as seen in Fig. 4, for an asymmetric top, even for a given J and K , the energy gaps can be quite different, especially for $K=1$.

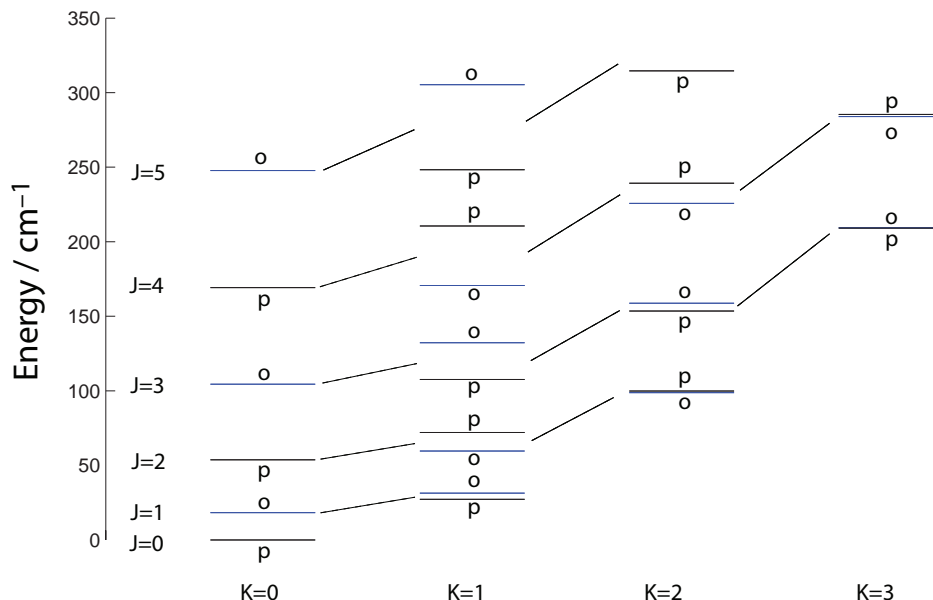


Fig. 4. Positions of the lowest JK rotational levels of the CH_2 molecule in the \tilde{a} state.

Contributing to this project are Lifang Ma (Ph. D. student), Jacek Klos (Research Assistant Professor), and Paul J. Dagdigian (Professor, The Johns Hopkins University).

III. Future Work

During the next year we will complete the $\text{CH}_2(\tilde{a})\text{-He}$ scattering calculations. We (Alexander, Ma, and Dagdigian) will be visiting Brookhaven early in April 2010, to coordinate these calculations with the ongoing experimental work. We will concentrate on modeling inelastic depletion of the lower rotational levels of $\text{CH}_2(\tilde{a})$. Additionally, we will investigate collisional depolarization of the lower rotational levels. Earlier calculations on collisions of H_2O with He showed a striking dependence on the k quantum number of the elastic collisional depolarization.⁷

We then will investigate collisional energy transfer between the \tilde{a} and \tilde{X} states of CH_2 . Initial investigation will involve the diatomic isoelectronic analogue, NH. Here, the equivalent electronically inelastic transition is between the $X^3\Sigma^-$ and $a^1\Delta$ states of the diatomic, induced by spin-orbit coupling. Experimentally, facile energy transfer has been observed.^{9, 10} Collision-induced $a \rightarrow X$ energy transfer in NH and CH_2 are paradigms for spin-orbit induced intersystem crossing in small molecules. Patel-Misra and Dagdigian have discussed, qualitatively, the mechanism for this process in collisions of NH(a). Our goal will be to provide a quantitative prediction of the efficiency of this process, based on quantum scattering studies on accurate potential energy surfaces.

Our initial work will focus on the determination of the PES's for the interaction of the two states (of NH) with He and of the lower (\tilde{X}) state of CH_2 with He, as well as with the determination of the spin-orbit coupling between these two states. Because the \tilde{a} and \tilde{X} have somewhat different geometries, we will need to explore the dependence of the PESs on (at the minimum) the H_2 bending vibration. Initial work will be limited to a vibrationally-averaged treatment.

IV. References

1. H.-J. Werner, B. Follmeg, M. H. Alexander, and D. Lemoine, "Quantum Studies of Electronically Inelastic Collisions of CN ($X^2\Sigma^+$, $A^2\Pi$) with He," J. Chem. Phys. **91**, 5425-5439 (1989).
2. M. H. Alexander, D. E. Manolopoulos, and H. J. Werner, "An investigation of the F+H₂ reaction based on a full ab initio description of the open-shell character of the F(2P) atom," J. Chem. Phys. **113**, 11084-11100 (2000).
3. HIBRIDON is a package of programs for the time-independent quantum treatment of inelastic collisions and photodissociation written by M. H. Alexander, D. E. Manolopoulos, H.-J. Werner and others. More information and/or a copy of the code can be obtained from the website <http://www2.chem.umd.edu/groups/alexander/hybridon/hib43>.
4. D. Skouteris, J. F. Castillo, and D. E. Manolopoulos, "ABC: A Quantum Reactive Scattering Program," Comput. Phys. Comm. **133**, 128-135 (2000).
5. Y. Kim, A. V. Komissarov, G. E. Hall, and T. J. Sears, "Observation of the c^1A_1 state of methylene by optical-optical double resonance," J. Chem. Phys. **123**, (2005).
6. Z. Wang, Y. Kim, G. E. Hall, and T. J. Sears, "State mixing and predissociation in the $c\leftarrow a$ band system of singlet methylene studied by optical-optical double resonance," J. Phys. Chem. A **112**, 9248-9254 (2008).
7. P. J. Dagdigian and M. H. Alexander, "Depolarisation in H₂O-He collisions," Mol. Phys. **XX**, yyyy (2010).
8. K. Patkowski, T. Korona, R. Moszynski, B. Jeziorski, and K. Szalewicz, "Ab initio potential energy surface and second virial coefficient for He-H₂O complex," J. Molec. Struct. (Theochem) **591**, 231-243 (2002).
9. J. S. Adams and L. Pasternack, "Collision-induced intersystem crossing in NH($a^1\Delta$)-NH($X^3\Sigma^-$)," J. Phys. Chem. **95**, 2975-2982 (1991).
10. D. Patel-Misra and P. J. Dagdigian, "State-resolved electronic quenching of NH($a^1\Delta$) by Xe and CO," J. Chem. Phys. **97**, 4871-4880 (1992).

V. Publications and submitted journal articles supported by this project to date

Theoretical Studies of Elementary Hydrocarbon Species and Their Reactions

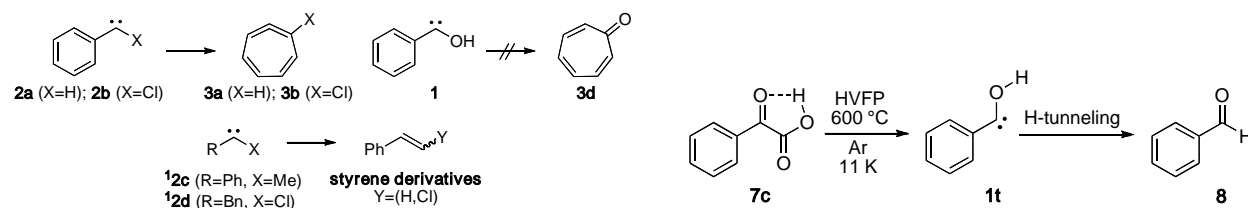
Wesley D. Allen and Henry F. Schaefer III
Center for Computational Chemistry and Department of Chemistry
University of Georgia, Athens, GA 30602-2525
E-mail: wdallen@uga.edu and sch@uga.edu; Phone: (706) 542-7729

Explicitly Correlated R12 Methods for Radicals

The torpid convergence of conventional electron correlation methods to the complete basis set (CBS) limit arises from the inability of one-particle functions to treat the coalescence region between two electrons. The Coulomb singularities in the Hamiltonian require the exact wave function to display a cusp and corresponding depletion of electron density (Coulomb hole) when any interelectronic distance (r_{12}) approaches zero. Two-particle functions that depend explicitly on r_{12} can effectively describe the cusp region without large orbital basis sets. Much progress has been made recently in the development of explicitly correlated methods that incorporate such r_{12} terms into the wave function. We have recently published our research on explicitly correlated ZAPT2 theory for open-shell systems (Ref. 18), which was implemented within the freely available Massively Parallel Quantum Chemistry (MPQC) package. Using a Slater correlation factor represented by Gaussian geminals, together with Peterson's recent F12 and F12-RI basis sets, our ZAPT2-R12 method with a TZ basis consistently outperformed conventional theory applied with an aug-cc-pV6Z basis set, as tested for a set of atomization energies of 20 small molecules. Correlated methods for open-shell states are typically based on semicanonical orbitals, requiring an unrestricted formalism, which for double excitations requires three independent sets of amplitudes. In contrast, *Z*-averaged methods redefine the zeroth-order Hamiltonian with a symmetric exchange operator, thereby allowing a spin-restricted formulation similar in cost to closed-shell computations. Our ZAPT-R12 method thus greatly reduces the cost of explicitly correlated computations on open-shell systems, including the ubiquitous hydrocarbon radicals found in combustion systems.

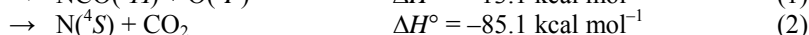
Phenylhydroxycarbene: A Tunneling Phenomenon

In joint work with the experimental group of Peter Schreiner, phenylhydroxycarbene (**1**, Ph-C-OH) was generated for the first time by high vacuum flash pyrolysis (HVFP) of phenylglyoxylic acid (at 600 °C) and spectroscopically (IR, UV/Vis) characterized via immediate matrix isolation in solid Ar at 11 K. The identity of **1** was unequivocally confirmed by precise agreement between observed IR bands and (unscaled) anharmonic vibrational frequencies computed from a CCSD(T)/cc-pVDZ quartic force field. The UV/Vis spectrum of **1** displays a broad band with maximum absorption at 500 ± 25 nm (2.5 ± 0.1 eV) that extends to around 640 nm (1.9 eV), in full accord with combined CCSD(T)/cc-pVQZ and EOM-CCSD/cc-pVTZ computations that yield a gas-phase vertical (adiabatic) excitation energy of 2.7 (1.9) eV. Unlike singlet phenylchlorocarbene **2b**, phenylhydroxycarbene does not undergo photochemical ring expansion. Instead, **1** exhibits quantum mechanical hydrogen tunneling to benzaldehyde underneath a formidable barrier of 28.8 kcal mol⁻¹, even at cryogenic temperatures. The remarkable hydrogen tunneling mechanism is supported by the temperature insensitivity of the observed half-life (2.5 h) and is substantiated by a comparable theoretical half-life (3.3 h) determined from CCSD(T)/aug-cc-pVTZ barrier penetration integrals computed along the intrinsic reaction path. As expected, deuteration turns off the tunneling mechanism, so that *d*-**1** is stable under otherwise identical conditions. The phenylhydroxycarbene system demonstrates the fascinating concept of *tunneling control* of a chemical reaction, whereby the product is not determined by conventional kinetic or thermodynamic factors, but independently by the magnitude of barrier penetration integrals that govern the facility of quantum mechanical tunneling.



OCNO surface

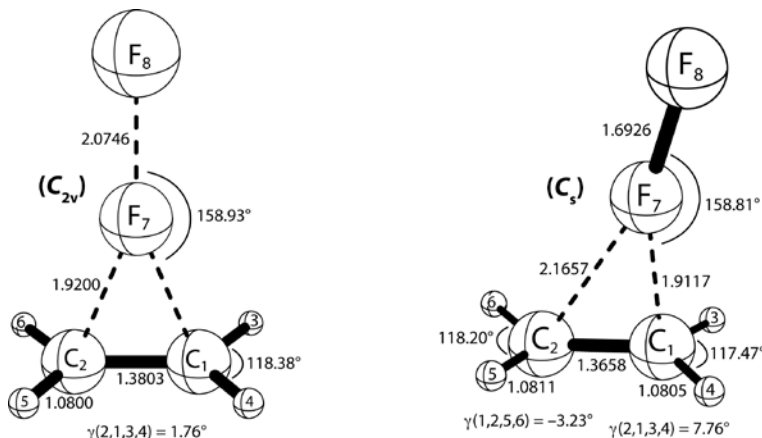
The three dominant pathways for the CN + O₂ reaction are:



Channel (3) proceeds through the OCNO radical, which has been matrix-isolated by two different research groups [(**A**) Y. J. Wu and Y. P. Lee, *J. Chem. Phys.* **123**, 17 (2005); and (**B**) C. S. Jamieson, A. M. Mebel, and R. I. Kaiser, *Phys. Chem. Chem. Phys.* **7**, 4089 (2005)], with characterization by IR spectroscopy. However, discrepancies exist in the vibrational frequencies of Ref. **A** (2045 and 968 cm⁻¹) and Ref. **B** (2113 cm⁻¹). At the ROCCSD(T)/cc-pVQZ level of theory, we find that a cyclic O-C-N-O isomer lies only 2.3 kcal mol⁻¹ higher in energy than the *trans*-bent O-C-N-O form, with an isomerization barrier of just 8.7 kcal mol⁻¹. Therefore, it is possible that both isomers were present in the experiments. We have computed an ROCCSD(T)/cc-pVQZ quartic force field and applied second-order vibrational perturbation theory (VPT2) to determine the fundamentals and isotopic shifts for the *trans*-bent and cyclic isomers of OCNO. Our C-O stretching frequencies for (*trans*-bent, cyclic) OCNO are (2067, 2028) cm⁻¹, which bracket Ref. **A** but are considerably lower than Ref. **B**. The stretching mode observed at 968 cm⁻¹ in Ref. **A** is significantly higher than our computed values of (897, 904) cm⁻¹ for the two isomers. Based on the isotopic shifts, the experimental results are most consistent with formation of the cyclic isomer.

The Problematic C₂H₄ + F₂ Reaction Barrier

Recent crossed molecular beam studies of the ethylene + F₂ reaction show that the fluoroethyl radical and fluorine atom are the exclusive products for collision energies up to at least 11 kcal mol⁻¹ [Y.-J. Lu, T. Xie, J.-W. Fang, H.-C. Shao, and J. J. Lin, *J. Chem. Phys.* **128**, 184302 (2008)]. We have recently published (Ref. 23) a cutting-edge *ab initio* investigation of this archetypical reaction. Laborious geometry optimizations and complete harmonic vibrational analyses were executed at the CCSD(T)/aug-cc-pVQZ level for the reactants, products, and intervening transition states. The reaction energy and barrier height were then subjected to computationally intensive focal point analyses (FPA) in order to converge toward the *ab initio* limits. The largest explicit computations involved the coupled-cluster CCSD(T)/aug-cc-pV5Z and CCSDT(Q)/cc-pVDZ techniques. Auxiliary core correlation, DBOC, and relativistic corrections were also included. As illustrated by the CCSD(T)/aug-cc-pVQZ optimized structures below, there are two competitive stationary points (C_{2v} and C_s) in the transition state region. While lower levels of theory confuse the nature of these points, our pure CCSD(T)/aug-cc-pVQZ computations establish that the C_s structure is the true transition state, the C_{2v} alternative being higher by 2.81 kcal mol⁻¹ (excluding ZPVE) and exhibiting two imaginary frequencies [$\nu_6(a_1) = 319i$ cm⁻¹ and $\nu_{18}(b_2) = 529i$ cm⁻¹]. Our final FPA reaction barrier and reaction enthalpy are 7.97 kcal mol⁻¹ and -7.39 kcal mol⁻¹, respectively. The FPA barrier is 2.5 kcal mol⁻¹ higher than the barrier (5.5 ± 0.5 kcal mol⁻¹) deduced from the crossed molecular beam experiments, which is a considerable disparity considering that benchmarks confirm our reaction energy to be accurate to 0.2-0.3 kcal mol⁻¹.



The perplexing disparity between the state-of-the-art theoretical and experimental barriers for the $C_2H_4 + F_2$ reaction elevates this system as an important testing ground for chemical physics. The issues for theory in predicting these barriers are apparent from our study. There are large oscillations in the electron correlation series for the $C_2H_4 + F_2$ reaction barrier, despite the lack of much multireference character in the transition state. While improving the correlation treatment from CCSD to CCSD(T) lowers the barrier by $12.0 \text{ kcal mol}^{-1}$, further extension to the CCSDT(Q) level produces a change of only $0.2 \text{ kcal mol}^{-1}$. The latter observation indicates good convergence of the final result. Full CCSDTQ and CCSDTQ(P) computations would be beneficial to solidify the convergence; however, these are currently not feasible for this system. The oscillatory pattern of the correlation series suggests that a full CCSDTQ computation would actually increase the reaction barrier above $8.0 \text{ kcal mol}^{-1}$. In brief, if the actual barrier for the $C_2H_4 + F_2$ reaction is indeed near the experimental threshold, surprising aspects of the coupled cluster series remain to be discovered. The interplay between theory and experiment witnessed in the classic $F + H_2$ problem could well be repeated in a next generation of chemical complexity.

C_3H_5 surface

The C_3H_5 potential energy surface hosts a number of species important in combustion and governs some key interconversion reactions. The global minimum allyl radical has been considered as a key species in aromatic ring formation processes that lead to soot. Computational exploration of the C_3H_5 potential energy surface is complicated by orbital symmetry-breaking issues, which preclude a restricted open-shell treatment of the allyl radical. By monitoring both symmetry breaking and spin contamination, we have demonstrated that unrestricted coupled cluster methods can be applied successfully to this problem. Benchmark energetics have been obtained for over 20 stationary points on the C_3H_5 potential energy surface within the focal point analysis (FPA) approach. In the FPA computations, the electron correlation treatments were extended to CCSDT(Q) and extrapolations were performed to the complete basis set (CBS) limit. These results will help determine the accuracy of the various approximations employed in statistical treatments of reactions involving C_3H_5 species.

C_7H_7 isomers

As a resonantly stabilized free radical (RSFR), the benzyl radical is able to accumulate in relatively high concentrations in combustion environments. Benzyl can be generated by abstraction of a hydrogen atom from the methyl group of toluene; abstraction of a ring hydrogen from toluene produces a methylphenyl radical instead. Given their lack of resonance stabilization, the three methylphenyl isomers have been mostly overlooked in flame models, and are usually assumed to be equivalent when they are considered. To address the lack of thermochemical data for these species, we have computed relative energies at the CBS limit of CCSD(T) theory using ZAPT2/cc-pVTZ reference geometries. The (*ortho*, *meta*, *para*) methylphenyl radicals are essentially isoenergetic, lying (23.1 , 23.1 , 23.6) kcal mol^{-1} above benzyl radical. Interconversion requires crossing barriers of over 60 kcal mol^{-1} . By rotating the CH_2 group of benzyl by 90° , therefore preventing delocalization of the unpaired electron into the ring system, we quantified the resonance stabilization energy of the benzyl radical to be $16.1 \text{ kcal mol}^{-1}$ at the CCSD(T) CBS limit.

Publications Supported by DOE: 2007-2010

1. V. Kasalová, W. D. Allen, H. F. Schaefer, E. D. Pillai, and M. A. Duncan, "Model Systems for Probing Metal Cation Hydration," *J. Phys. Chem. A* **111**, 7599-7610 (2007).
2. X. Zhang, A. T. Maccaroni, M. R. Nimlos, S. Kato, V. M. Bierbaum, G. B. Ellison, B. Ruscic, A. C. Simmonett, W. D. Allen, and H. F. Schaefer, "Unimolecular Thermal Fragmentation of *Ortho*-Benzynes," *J. Chem. Phys.* **126**, 044312: 1-20 (2007).
3. S. E. Wheeler, K. A. Robertson, W. D. Allen, H. F. Schaefer, Y. J. Bomble, and J. F. Stanton, "Thermochemistry of Key Soot Formation Intermediates: C_3H_3 Isomers," *J. Phys. Chem. A* **111**, 3819 (2007).
4. P. Bera, Y. Yamaguchi, and H. F. Schaefer, "The Low-Lying Quartet Electronic States of Nitrogen Dioxide," *J. Chem. Phys.* **127**, 174303 (2007).
5. A. C. Simmonett, F. A. Evangelista, W. D. Allen, and H. F. Schaefer, "In Search of Definitive Signatures of the Elusive NCCO Radical," *J. Chem. Phys.* **127**, 014306 (2007).

6. L. Belau, S. E. Wheeler, B. W. Ticknor, M. Ahmed, S. R. Leone, W. D. Allen, H. F. Schaefer, and M. A. Duncan, "Ionization Thresholds of Small Carbon Clusters: Tunable VUV Experiments and Theory," *J. Am. Chem. Soc.* **129**, 10229 (2007).
7. S. E. Wheeler, W. D. Allen, and H. F. Schaefer, "On the Convergence of Z-Averaged Perturbation Theory (ZAPT)," *J. Chem. Phys.* **128**, 074107 (2008).
8. J. J. Wilke, W. D. Allen, and H. F. Schaefer, "Establishment of the $C_2H_5 + O_2$ Reaction Mechanism: A Combustion Archetype," *J. Chem. Phys.* **128**, 074308 (2008).
9. P. P. Bera, Y. Yamaguchi, H. F. Schaefer, and T. D. Crawford, "Born-Oppenheimer Symmetry Breaking in the \tilde{C} State of NO_2 : Importance of Static and Dynamic Correlation Effects," *J. Phys. Chem. A* **112**, 2669 (2008).
10. R. K. Sreeruttun, P. Ramasami, C. S. Wannere, A. C. Simmonett, and H. F. Schaefer, " π - and σ -Phenylethynyl Radicals and their Isomers *o*-, *m*-, and *p*-Ethynylphenyl: Structures, Energetics, and Electron Affinities," *J. Phys. Chem. A* **112**, 2838 (2008).
11. S. Carter, N. C. Handy, Y. Yamaguchi, J. M. Turney, and H. F. Schaefer, "Vibrational Energy Levels for the Electronic Ground State of the Diazocarbene (CNN) Molecule," *Molecular Physics* **106**, 357 (2008).
12. L. D. Speakman, J. M. Turney, and H. F. Schaefer, "Toward the Experimental Observation of Quartet States of the Ozone Radical Cation: Insights from Coupled Cluster Theory," *J. Chem. Phys.* **128**, 214302 (2008).
13. P. R. Schreiner, H. P. Reisenauer, F. C. Pickard, A. C. Simmonett, W. D. Allen, E. Mátyus, and A. G. Császár, "Capture of Hydroxymethylene and Its Fast Disappearance through Tunnelling," *Nature*, **453**, 906-909 (2008). See commentaries and news articles on this work in *Nature* (Vol. 453, p. 862), *Chemistry World* (July 2008, p. 23), and *Angewandte Chemie* (Vol. 47, p. 2).
14. A. U. Sokolov, N. J. Stibrich, and H. F. Schaefer, "BO₃ Molecular Structures: Examples of the Importance of Electron Correlation", *Collect. Czech Chem. Commun.* **73**, 1495 (2008).
15. A. C. Simmonett, H. F. Schaefer, and W. D. Allen, "The Enthalpy of Formation and Anharmonic Force Field of Diacetylene," *J. Chem. Phys.* **130**, 044301 (2009).
16. S. E. Wheeler, K. N. Houk, P. v. R. Schleyer, and W. D. Allen, "A Hierarchy of Homodesmotic Reactions," *J. Am. Chem. Soc.* **131**, 2547 (2009).
17. A. C. Simmonett, N. J. Stibrich, B. N. Pappas, H. F. Schaefer, and W. D. Allen, "Barrier to Linearity and Anharmonic Force Field of the Ketenyl Radical," *J. Phys. Chem. A* **113**, 11643 (2009).
18. J. J. Wilke and H. F. Schaefer, "The Subtleties of Explicitly Correlated Z-Averaged Perturbation Theory: Choosing an R12 Method for High-Spin Open-Shell Molecules," *J. Chem. Phys.* **131**, 244116 (2009).
19. S. E. Wheeler and H. F. Schaefer, "Thermochemistry of the HOSO Radical, a Key Intermediate in Fossil Fuel Combustion," *J. Phys. Chem. A* **113**, 6779 (2009).
20. T. Lu, A. C. Simmonett, F. A. Evangelista, Y. Yamaguchi, and H. F. Schaefer, "Diphosphene and Diphosphenylidene," *J. Phys. Chem. A* **113**, 13227 (2009).
21. E. Prochnow, F. A. Evangelista, H. F. Schaefer, W. D. Allen, and J. Gauss, "Analytic Gradients for the State-Specific Multireference Coupled Cluster Singles and Doubles Model," *J. Chem. Phys.* **131**, 064109 (2009).
22. P. R. Schreiner, H. P. Reisenauer, E. Mátyus, A. G. Császár, A. Siddiqi, A. C. Simmonett, and W. D. Allen, "Infrared Signatures of the NCCO Radical," *Phys. Chem. Chem. Phys.* **11**, 10385 (2009).
23. H. Feng and W. D. Allen, "The Problematic $C_2H_4 + F_2$ Reaction Barrier," *J. Chem. Phys.* **132**, 094304 (2010).
24. J. A. Miller, S. J. Klippenstein, Y. Georgievskii, L. B. Harding, W. D. Allen, and A. C. Simmonett, "Reactions between Resonance-Stabilized Radicals: Propargyl + Allyl," *J. Phys. Chem. A* **114**, 4881 (2010).
25. U. B. Ozkaya, J. M. Turney, Y. Yamaguchi, and H. F. Schaefer, "The Barrier Height, Unimolecular Rate Constant, and Lifetime for the Decomposition of HN_2 ," *J. Chem. Phys.* **132**, 064308 (2010).
26. Q. Wu, Q. Cheng, Y. Yamaguchi, Q. Li, and H. F. Schaefer, "Triplet States of Cyclopropenylidene and Its Isomers," *J. Chem. Phys.* **132**, 044308 (2010).
27. D. Gerbig, H. P. Reisenauer, C.-H. Wu, D. Ley, W. D. Allen, and P. R. Schreiner, "Phenylhydroxycarbene," *J. Am. Chem. Soc.*, submitted (2010).

Annual Progress report April 2010
**Threshold Photoelectron Photoion Coincidence (TPEPICO) Studies:
The Road to ± 0.1 kJ/mol Thermochemistry**

Tomas Baer (baer@unc.edu)
Department of Chemistry
University of North Carolina
Chapel Hill, NC 27599-3290
DOE Grant DE-FG02-97ER14776

Program Scope

The threshold photoelectron photoion coincidence (TPEPICO) technique is utilized to investigate the dissociation dynamics and thermochemistry of energy selected medium to large organic molecular ions. The reactions include parallel and consecutive steps that are modeled with the statistical theory in order to extract dissociation onsets for multiple dissociation paths. These studies are carried out with the aid of molecular orbital calculations of both ions and the transition states connecting the ion structure to their products. The results of these investigations yield accurate heats of formation of ions, free radicals, and stable molecules. In addition, they provide information about the potential energy surface that governs the dissociation process. Isomerization reactions prior to dissociation are readily inferred from the TPEPICO data.

The TPEPICO Experiment

The threshold photoelectron photoion coincidence (TPEPICO) experiment in Chapel Hill is carried out with a laboratory H₂ discharge light source. Threshold electrons are collected by velocity focusing them into a 1.5 mm hole on a mask located at the end of the 12 cm drift tube. Some hot electrons pass through a 2x5 mm opening located next to the central 1.5 mm hole. In this fashion, two TPEPICO spectra are simultaneously collected, one for threshold and one for hot electrons. Hot electron free data are obtained by subtracting a fraction of the hot from the threshold TPEPICO data. The ion TOF is either a linear version or a reflectron for studying H loss processes. The electrons provide the start signal for measuring the ion time of flight distribution. When ions dissociate in the microsecond time scale, their TOF distributions are asymmetric. The dissociation rate constant can be extracted by modeling the asymmetric TOF distribution. A high-resolution version of this experiment with a molecular beam source and an electron imaging detector at the Swiss Light Source (SLS) has been constructed and has been collecting data since August, 2008. Because of the high photon flux, we have implemented the first multi-start multi-stop coincidence scheme using a master clock as the time base. The maximum photon resolution and flux have not yet been achieved due to some alignment issues. However, 2 meV resolution (0.2 kJ/mol) is routinely available, which is yielding very precise heats of formation of some key molecules, radicals and ions.

Recent Results

The Heats of Formation of the Allyl Radical and Ion by TPEPICO Spectroscopy: The 0 K onset of $C_3H_6 \rightarrow C_3H_5^+ + H^\bullet$ was measured in Chapel Hill by Threshold Photoelectron-Photoion Coincidence (TPEPICO) spectroscopy. From the onset (11.898 ± 0.024 eV) the heat of formation of the allyl ion ($CH_2CHCH_2^+$) was determined to be $\Delta_f H_{0K}^0 = 967.2$; $\Delta_f H_{298K}^0 = 955.4 \pm 2.5$ kJ mol⁻¹. This value is significantly more positive than prior determinations, and resolves a discrepancy between measurements of the allyl radical and allyl ion heats of formation and

recent precise measurement of the allyl radical adiabatic ionization energy (8.1309 eV) by the Merkt group. Our derived radical heat of formation is 170.9 ± 2.5 kJ/mol, which compares very well with the accepted value of 171 ± 4 kJ mol⁻¹. The new allyl ion heat of formation leads to a new proton affinity for proadiene (allene) of 765.0 ± 2.5 kJ/mol, which is 10 kJ/mol lower than the previously accepted value. The 0 K onset for H loss from the propene ion was made difficult

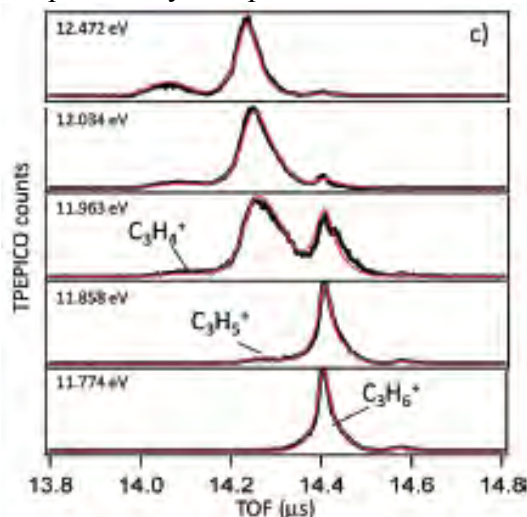


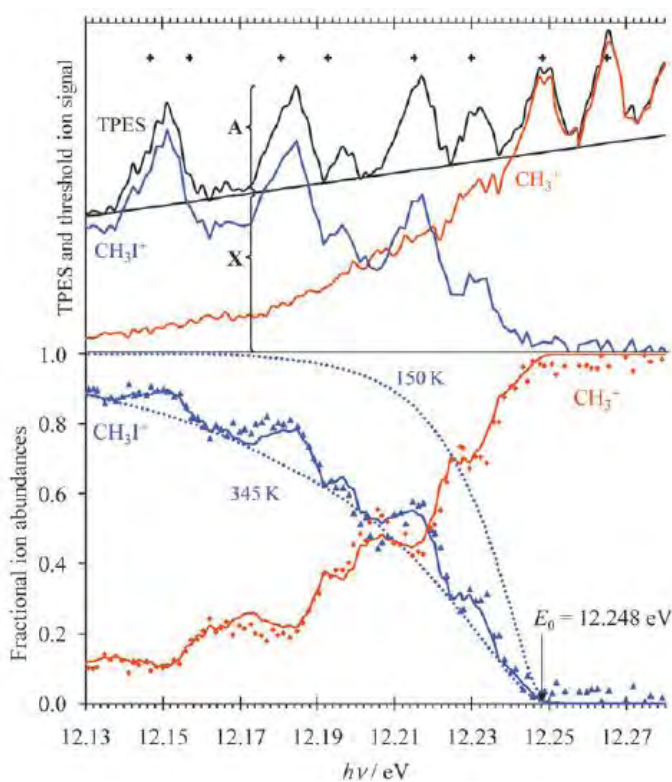
Figure 1. Ion TOF distributions for the photoionization of propene at various photon energies.

by the slow loss of the hydrogen atom, as well as competition at a slightly higher energy by H₂ loss. As shown in the figure, the asymmetry of the H loss peak due to the slow reaction is barely visible because of the small mass loss. However, modeling of the reaction dynamics when using both LinTOF and ReTOF mass spectrometers at various ion temperatures, provided a good fit to all the data, and sufficient information content to extract an accurate onset energy.

An attempt is made to determine the CH₃CCH₂⁺ heat of formation by measuring the 0 K onset of $2\text{-ClC}_3\text{H}_5 \rightarrow \text{C}_3\text{H}_5^+ + \text{Cl}^\bullet$. However, $2\text{-ClC}_3\text{H}_5^+$ dissociates through numerous parallel channels, preventing an accurate determination, and in any case C_3H_5^+ appears at too low an energy to be the higher energy CH₃CCH₂⁺ structure. Rather, $2\text{-ClC}_3\text{H}_5^+$ undergoes a concerted hydrogen transfer and Cl-loss via an intramolecular SN-2 like mechanism to produce the allyl ion. The 0 K onset of $3\text{-ClC}_3\text{H}_5 \rightarrow \text{C}_3\text{H}_5^+ + \text{Cl}^\bullet$ is measured (11.108 ± 0.010 eV) to determine the $3\text{-ClC}_3\text{H}_5^+$ heat of formation ($\Delta H_{f,0\text{K}}^0=14.9$; $\Delta H_{f,298\text{K}}^0=1.1 \pm 2.7$ kJ mol⁻¹). $3\text{-ClC}_3\text{H}_5^+$ is suggested to readily isomerize to trans $1\text{-ClC}_3\text{H}_5^+$ prior to dissociation.

On the ionization and dissociative photoionization of iodomethane: a definitive experimental enthalpy of formation of CH₃I:

The dissociative photoionization onset energy of the $\text{CH}_3\text{I} \rightarrow \text{CH}_3^+ + \text{I}$ reaction was studied at the VUV beamline of the Swiss Light Source (SLS) using a new imaging photoelectron photoion coincidence (iPEPICO) apparatus operating with a photon resolution of 2 meV and a threshold electron kinetic energy resolution of about 1 meV. Three previous attempts at establishing this value accurately, namely a pulsed field ionization (PFI)-PEPICO measurement, *ab initio* calculations and a mass analyzed threshold ionization (MATI) experiment, in which the onset energy was bracketed by state-selected excitation to vibrationally excited ²A₁ A states of the parent ion, have yielded contradictory results. It is shown that dimers and adducts formed in the supersonic molecular beam affected the PFI-PEPICO onset energy. The room temperature iPEPICO experiment yields an accurate 0 K onset of 12.248 ± 0.003 eV, from which we derive a $\Delta_f H_{298\text{K}}^0(\text{CH}_3\text{I}) = 15.4 \pm 0.3$ kJ mol⁻¹. This high precision value can now be utilized as an anchor for calculations involving other alkyl halides, such as C₂H₅I. The room temperature breakdown diagram shows a fine structure that corresponds to the threshold photoelectron spectrum (TPES) of the A state. Low internal energy neutrals seem to be preferentially ionized in the A state when compared with the X state, and A state peaks in the TPES are Stark-shifted as a function of the DC field, whereas the dissociative



photoionization of X state ions is not affected. This suggests that there are different competing mechanisms at play to produce ions in the A state vs. ions in the X state. The competition between field ionization and autoionization in CH₃I is compared with that in Ar, N₂ and in the H-atom loss energy region in CH₄⁺. The binding energies of the neutral and ionic Ar-CH₃I clusters were found to be 26 and 66 meV, respectively.

Figure 2 shows the TPES in region of the CH₃I⁺ A state. The peaks are assigned to A state vibrational levels, while the broad background is a result of the X state continuum. The parent and daughter ion coincidence yield curves show that the A state peaks show up only in the parent ion structure, thereby demonstrating that A state excitation yields ion in lower rotational states than the X state ions. The bottom shows the breakdown diagram modeled with two temperatures.

Experimental Thermochemistry of SiCl₃R (R = Cl, H, CH₃, C₂H₅, C₂H₃, CH₂Cl, SiCl₃), SiCl₃⁺, and SiCl₃[•]: The 0 K onsets (E_0) of a series of trichlorosilane derivatives SiCl₃R → SiCl₃⁺ + R[•] (R = Cl, H, CH₃, C₂H₅, C₂H₃, CH₂Cl, SiCl₃) were measured by Threshold Photoelectron-Photoion Coincidence (TPEPICO) spectroscopy. The well-known heat of formation of SiCl₄ is used as an anchor to determine the heat of formation of SiCl₃⁺, which is in turn used as an anchor to determine the heats of formation of the other alkyltrichlorosilanes investigated. A series of isodesmic reactions at the G3 and CBS-QB3 levels accurately reproduced the experimental heats of formation, and this scheme was used to calculate the heat of formation of Si₂Cl₆, from which the measured E_0 determines the SiCl₃[•] heat of formation. The measured values then determine the IE of SiCl₃[•] along with the Si-R bond dissociation enthalpies of the six neutral species investigated. The experimental heats of formation are also used in a series of isodesmic reaction calculations to determine the heats of formation of SiH₃R (R= H, CH₃, C₂H₅, C₂H₃, CH₂Cl, SiCl₃).

Work in Progress and Future Plans

Some papers in progress include an accurate and reliable measurement of the propyl ion heat of formation. SLS experiments on C₃H₈, C₃H₇X (X = Cl, Br, I) have yielded accurate onsets (± 2 meV), which will result in very accurate heats of formation for C₃H₇⁺ as well as for C₃H₇X (X = Cl, Br, I), all to within ± 0.2 kJ/mol. This will provide a proton affinity for propene, and will greatly aid in establishing heats of formation for a range of alkyl halides. Another project in progress involves the dissociation of C₆H₅X⁺, X = NO, Cl, Br, I. The common ion for these dissociation reactions is the C₆H₅⁺, which is an important species in Ruscic's Active Thermochemical Tables. This joint project with Ruscic will incorporate our accurate onsets for these reactions into the Active Tables. Finally, we are in the final stages of writing up a very

interesting paper with John Stanton on tunneling in the H atom loss from HCOOH^+ to produce the HOCO^+ ion.

Future directions involve the installation of the Ruscic free radical source at the iPEPICO experiment at the Swiss Synchrotron. This will permit the study of a number alkoxy and peroxy radicals. The unique approach will involve dissociative photoionization by iPEPICO rather than just measuring the IE, which is often made difficult by poor FC factors.

Publications from DOE supported work 2008 – 2010

Nicholas S. Shuman, Melony A. Ochieng, Bálint Sztáray, Tomas Baer, TPEPICO Spectroscopy of Vinyl Chloride and Vinyl Iodide: Neutral and Ionic Heats of Formation and Bond Energies, *J. Phys. Chem. A* **112**, 5647-5652 (2008)

Nicholas S. Shuman, James P. Kercher, and Tomas Baer, The Dissociation Dynamics of Energy-Selected Neopentylamine Ions: Heats of Formation of Neopentylamine and Neopentyl Alcohol, *Int. J. Mass Spectrom.* **287** 26-31 (2008)

Nicholas S. Shuman, Linda Ying Zhao, Michael Boles, Bálint Sztáray, and Tomas Baer, The Heats of Formation of HCCl_3 , HCCl_2Br , HCClBr_2 , HCB_3 , and their ions studied photoelectron photoion coincidence. *J. Phys. Chem. A* **112**, 10533-10538 (2008)

William Stevens, Bálint Sztáray, Nicholas S. Shuman, Tomas Baer, and Jürgen Troe, Specific Rate Constants $k(E)$ of the Dissociation of Halobenzene Ions: Analysis by Statistical Unimolecular Rate Theories. *J. Phys. Chem. A* **113** 573-582 (2009)

Andras Bodi, Melanie Johnson, Thomas Gerber, Zsolt Gengeliczki, Bálint Sztáray, and Tomas Baer, Imaging photoelectron photoion coincidence spectroscopy with velocity focusing electron optics, *Rev. Sci. Instrum.* **80** 034101/1-7 (2009)

Balázs Hornung Andras Bodi Csaba I. Pongor, Zsolt Gengeliczki Tomas Baer and Bálint Sztáray, Dissociative photoionization of $\text{X}(\text{CH}_3)_3$ ($\text{X} = \text{N}, \text{P}, \text{As}, \text{Sb}, \text{Bi}$): mechanism, trends and accurate energetics, *J. Phys. Chem. A* **113** 8091-8098 (2009)

Nicholas S. Shuman, Austin Spencer, and Tomas Baer, Experimental thermochemistry of SiCl_3R ($\text{R} = \text{Cl}, \text{H}, \text{CH}_3, \text{C}_2\text{H}_5, \text{C}_2\text{H}_3, \text{CH}_2\text{Cl}, \text{SiCl}_3$), SiCl_3^+ , and SiCl_3^\bullet , *J. Phys. Chem. A* **113** 9458 – 9466 (2009)

Nicholas S. Shuman, William R. Stevens, Katherine E. Lower, and Tomas Baer, The heat of formation of the allyl ion by TPEPICO spectroscopy, *J. Phys. Chem. A* **113** 10710-10717 (2009)

Andras Bodi, Nicholas S. Schuman, and Tomas Baer, On the ionization and dissociative photoionization of iodomethane: a definitive experimental enthalpy of formation of CH_3I , *Phys. Chem. Chem. Phys.* **11** 11013-11021 (2009)

Nicholas S. Shuman, Andras Bodi, and Tomas Baer, Heats of formation of *t*-butyl peroxy radical and *t*-butyl diazyl ion: RRKM vs SSCAM rate theories in systems with kinetic and competitive shifts, *J. Phys. Chem. A* **114** 232-240 (2010)

William R. Stevens, S. Hunter Walker, Nicholas S. Shuman[†], and Tomas Baer, Dissociative Photoionization Study of Neopentane: A path to an accurate heat of formation of the *t*-butyl ion, *t*-butyl iodide, and *t*-butyl hydroperoxide, *J. Phys. Chem. A* **114** 804 – 810 (2010)

Turbulence-Chemistry Interactions in Reacting Flows

Robert S. Barlow
Combustion Research Facility
Sandia National Laboratories, MS 9051
Livermore, California 94550
barlow@sandia.gov

Program Scope

This program is directed toward achieving a more complete understanding of turbulence-chemistry interactions in flames and providing detailed measurements for validation of combustion models. In the Turbulent Combustion Laboratory (TCL), simultaneous line imaging of spontaneous Rayleigh scattering, Rayleigh scattering, and two-photon laser-induced fluorescence (LIF) of CO is applied to obtain spatially and temporally resolved measurements of temperature, the concentrations of all major species, mixture fraction, and reaction progress, as well as gradients in these quantities in hydrocarbon flames. The instantaneous three-dimensional orientation of the turbulent reaction zone is also measured by imaging of OH LIF in two crossed planes, which intersect along the laser axis for the multiscalar measurements. These combined data characterize both the thermo-chemical state and the instantaneous flame structure, such that the influence of turbulent mixing on flame chemistry may be quantified. Our experimental work is closely coupled with international collaborative efforts to develop and validate predictive models for turbulent combustion. This is accomplished through our visitor program and through the TNF Workshop series. Although the past emphasis has been on nonpremixed and partially premixed combustion, the workshop and this program are expanding their scope to address a broad range of combustion modes, including premixed and stratified flames. We are also working to extend our quantitative multiscalar diagnostics to more complex fuels. Entry into these new research areas has prompted developments in both hardware and methods of data analysis to achieve unprecedented spatial resolution and precision of multiscalar measurements. Within the CRF we collaborate with Joe Oefelein to use highly-resolved large-eddy simulations (LES) of our experimental flames in order to gain greater fundamental understanding of the dynamics of multi-scale flow-chemistry interactions. We also collaborate with Tom Settersten and Jonathan Frank to refine our quantitative LIF methods and to apply complementary imaging diagnostics to selected turbulent flames.

Recent Progress

Turbulent Stratified and Premixed Flames

In stratified combustion a turbulent flame propagates through a nonuniform mixture of fuel and oxidizer. This mode of combustion is common on practical systems but is not well understood at a fundamental level, so it represents an important challenge for combustion models. Stratified combustion is also challenging for laser diagnostics because high precision in the measurement of the local equivalence ratio, ϕ , is required and thin reaction zones demand high spatial resolution. We have been collaborating with Cambridge University (S. Hochgreb and M. Sweeney) and the Technical University of Darmstadt (A. Dreizler, F. Seffrin, F. Fuest) to investigate stratified turbulent flames using three burner configurations that cover ranges of turbulence level and flow field complexity. The first burner (Fig. 1a) uses parallel slots and a mesh at the burner exit plane to create a mildly turbulent mixing layer between two streams to

different equivalence ratio. Data from this burner have been analyzed to extract statistics on the instantaneous dissipation of reaction progress variable, which is an important quantity for some modeling approaches and which had not previously been measured in any turbulent stratified flame. Statistics of the flame surface density, curvature, and orientation have also been reported. The burners shown in Fig. 1b and 1c, operate at higher turbulence levels and were both designed as target burners for model calculations. Both have co-annular flows that generate a turbulent mixing layer between them. The TU Darmstadt burner uses a central premixed pilot to anchor the conical turbulent flame. The Cambridge/Sandia burner (Fig. 1c) has a central bluff body rather than a pilot to stabilize the flame, and it includes variable swirl in the outer annular flow. Recirculation and swirl add complexity to the flow field, increasing the modeling challenge. Both burners have long entry lengths to simplify the description of inflow conditions for simulations.

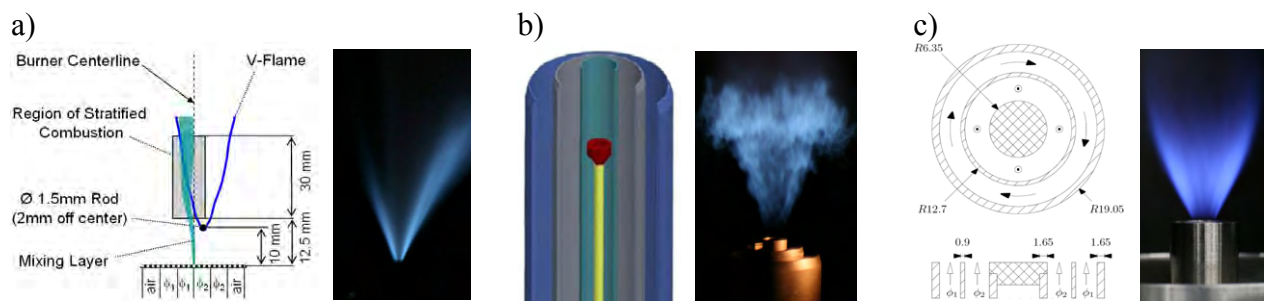


Figure 1. a) Cambridge stratified slot burner diagram and flame image; b) TU Darmstadt stratified annular burner and flame image; and c) Cambridge/Sandia stratified swirl burner and flame image.

During the past year we completed extensive experiments on the Cambridge/Sandia burner, including stratified and premixed methane-air flames with varying stratification ratio and swirl number (12 cases in total). Premixed cases are included, so that the effects of stratification on flame structure may be isolated. Analysis of these data has only started, but this work has already revealed unexpected effects of transport on the structure of turbulent premixed flames. These new measurements show that the C/H atom ratio is not necessarily conserved going through the turbulent flame brush in this burner configuration. Figure 2 illustrates the effect by comparing results from a planar unstrained laminar premixed flame with those from a turbulent premixed flame stabilized on the Cambridge burner. In each case the measurements are plotted vs. temperature to expand the internal structure of the flame, and results are compared to unstrained laminar flame calculations at the appropriate reactant equivalence ratio. Calculations were done using Chemkin with GRI 3.0 and multi-component transport. Measurements from the laminar flame agree well with the calculation. However, the turbulent flame measurements reveal changes in the behavior of the C/H ratio and several other scalars within the flame and in the fully reacted products. The C/H ratio, which varies through the interior of the laminar flame due to differential molecular diffusion, does not return to its starting value of 0.25 in the turbulent flame. This is believed to result from a combination of molecular and turbulent transport, such that H_2 diffuses preferentially through the preheat zone and is further transported away from the local flame brush by turbulent advection. The elevated carbon level translates to higher than expected CO_2 mass fraction and lower O_2 mass fraction (not shown). Thus, the equivalence ratio, calculated from the atom balance of the measured species, is higher in the

products than in the reactants, with the difference being about 10%. These effects were not observed in the premixed slot burner flame (Fig. 1a), which has very low turbulence and no shear. It is possible that shear is a contributing factor, along with high turbulence and the relatively high angle between the flame brush normal and the mean streamlines of the reactant flow. Velocity measurements are in progress at Cambridge University and will help in developing a more complete understanding of the physical mechanisms contributing to this newly observed (as far as we are aware) combustion phenomenon.

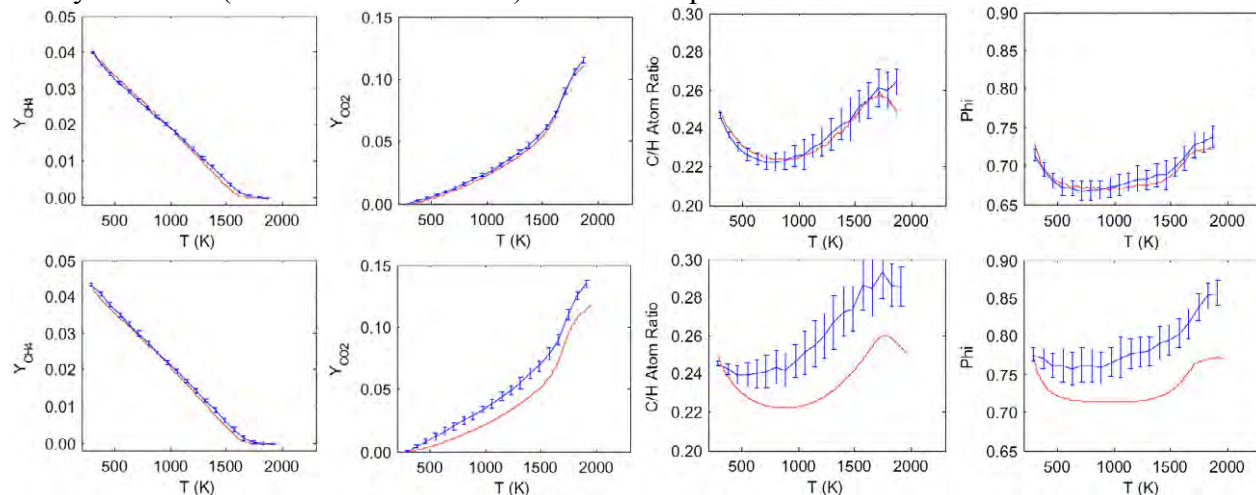


Figure 2. Measured mean and rms ($\pm\sigma$ shown as error bars) CH₄ and CO₂ mass fractions, C/H atom ratio, and local equivalence ratio in a planar unstrained laminar premixed CH₄-air flame at $\phi = 0.73$ (upper row) and in a turbulent premixed flame at $\phi = 0.77$ (lower row). Results of laminar unstrained flame calculations at the appropriate reactant equivalence ratio are also shown in each graph.

Data Evaluation for DME Flames

In collaboration with F. Fuest and A. Dreizler (TU Darmstadt) and J.-Y. Chen (UC Berkeley) we have been developing methods for interpretation of Raman/Rayleigh measurements in laminar and turbulent partially premixed flames of dimethyl ether (DME). This work is a continuation of exploratory studies on laminar and turbulent jet flames of ethane, ethylene, DME, and propane conducted early in 2009. The hydrocarbon intermediates in DME flames, including CH₄, CH₂O, C₂H₂, C₂H₄, and C₂H₆, have lower Rayleigh and Raman cross sections than the parent fuel, and the total mole fraction of these intermediates is high enough to significantly influence results. Therefore, the composition and effective cross sections for the mixture must be modeled as part of the Raman/Rayleigh data analysis. Our initial approach is to describe the mixture cross sections as functions of temperature, based on compositions from laminar opposed-flow flame calculations at representative strain rates. This approach works well for processing Raman/Rayleigh data from laminar flames. However, we expect that a more sophisticated approach will be needed to interpret signals from turbulent partially premixed flames with local extinction, so work will continue in this area.

Future Plans

Our highest priority for the coming year will be to move forward with analysis and interpretation of the very substantial data set from the stratified swirl burner. This work will be conducted in collaboration with Cambridge University. In addition to further investigation of the transport effects described above, we will be extracting conditional statistics on scalar quantities

relevant to both geometrically-based and dissipation-based modeling approaches for turbulent stratified and premixed flames. This work will take advantage of long 30,000-shot records acquired near the intersection of the flame brush and the mixing layer in each stratified case. It is likely that multi-scalar experiments will also be conducted on the TU Darmstadt stratified burner at some point during the next year. However dates have not been established.

We also plan to conduct experiments on a series of turbulent partially premixed DME-air jet flames stabilized on the Sydney piloted burner. These experiments will be conducted at the highest practical Reynolds number and will include multiple steps in the probability of localized extinction. Both of these projects are consistent with research priorities established for the TNF Workshop.

BES Supported Publications (2008 - present)

G.H. Wang, N.T. Clemens, P.L. Varghese, R. S. Barlow, "Turbulent Time Scales in a Nonpremixed Turbulent Jet Flame by Using High-Repetition Rate Thermometry," *Combust. Flame*, **152**, 317-335 (2008).

G.H. Wang, R.S. Barlow, "Spatial resolution effects on the measurement of scalar variance and scalar dissipation in turbulent nonpremixed jet flames", *Exp. Fluids* **44**, 633-645 (2008).

T.G. Drozda, G.H. Wang, V. Sankaran, J.R. Mayo, J.C. Oefelein, R.S. Barlow, "Scalar Filtered Mass Density Functions in Nonpremixed Turbulent Jet Flames," *Combust. Flame*, **155**, 54-96 (2008).

R.S. Barlow, G.H. Wang, P. Anselmo-Filho, M. S. Sweeney, S. Hochgreb, "Application of Raman/Rayleigh/LIF Diagnostics in Turbulent Stratified Flames," *Proc. Combust. Inst.* **32**, 945-953 (2009).

P. Anselmo-Filho, S. Hochgreb, R.S. Barlow, R.S. Cant, "Experimental Measurements of Geometric Properties of Turbulent Stratified Flames," *Proc. Combust. Inst.* **32**, 1763-1770 (2009).

M.J. Dunn, A.R. Masri, R.W. Bilger, R.S. Barlow, G.H. Wang, "The Compositional Structure of Highly Turbulent Piloted Premixed Flames Issuing into Hot Coflow," *Proc. Combust. Inst.* **32**, 1779-1786 (2009).

J. Cai, D.H. Wang, C. Tong, R.S. Barlow, A.N. Karpetis, "Investigation of sub-grid-scale mixing of mixture fraction and temperature in turbulent partially premixed flames," *Proc. Combust. Inst.*, **32**, 1517-1525 (2009).

R.S. Barlow, H.C. Ozarovsky, A.N. Karpetis, R.P. Lindstedt, "Piloted Jet Flames of CH₄/H₂/Air: Experiments on Localized Extinction in the Near Field at High Reynolds Numbers," *Combust. Flame* **156**, 2117-2128 (2009).

M.J. Dunn, A.R. Masri, R.W. Bilger, R.S. Barlow. "Finite Rate Chemistry Effects in Highly Sheared Turbulent Premixed Flames," *Flow. Turb. Combust.* (accepted).

F. Fuest, R.S. Barlow, D. Geyer, F. Seffrin, A. Dreizler, "A Hybrid Method for Evaluation of 1D Raman Spectroscopy," *Proc. Combust. Inst.* (accepted).

TNF Workshop Information: <http://www.sandia.gov/TNF>

Modeling Reactions in High-Pressure Turbulence in the Cold Ignition Regime

Josette Bellan

Mechanical Engineering Department, California Institute of Technology
Pasadena, CA 91125

Josette.Bellan@jpl.nasa.gov

I. Program Scope

This study addresses issues highlighted in the Basic Energy Needs for Clean and Efficient Combustion of 21st Century Transportation Fuels (DOE BES, 2003) under the topic of Combustion under Extreme Pressure. It is there noted that “the most basic concepts of thermal autoignition” are “based on experience and theory at near atmospheric pressures” and that “as pressure increases significantly..., many of these conceptual pictures begin to change or disappear”. It is also stated “A better description of the coupling and interaction of high pressure flow and molecular transport processes with chemistry is also necessary”, particularly because “Ignition and flame propagation of alternative and renewable fuels, as well as of the changing feed stocks of conventional fossil-based fuels, are very likely to be much different at very high pressures than under the more familiar, lower pressure conditions of current engines.” Recognizing that “Under such (*increasing pressure*) conditions distinctions between gas and liquid phases become moot, new equations of state must be used...”, it is immediately apparent that there must be “a re-examination of the basic assumptions that govern the physics and chemistry related to combustion; and the need for this type of re-examination increases as the combustion pressure increases.” This recognition is also stated under the topic of Multiscale Modeling since due to the new equations of state “The combination of unexplored thermodynamic environments and new physical and chemical fuel properties results in complex interactions among multiphase (*according to the above, the multiphase distinction becomes moot with increasing pressure*) fluid dynamics, thermodynamic properties, heat transfer, and chemical kinetics that are not understood even at a fundamental level.” From the theoretical viewpoint for “systems at high pressure, fluid dynamic time scales can be comparable to chemical time scales.” and therefore “completely diffusion-controlled reactions ... can become important”.

Thus, the objective of this study is the investigation of the coupling among thermodynamics, transport properties, intrinsic kinetics and turbulence under the high-pressure and the relatively (with respect to combustion) low-temperature conditions typical of the auto-ignition regime, with particular emphasis on the manifestation of this coupling on the effective kinetic rate. It is also planned to establish collaboration with Dr. Joseph Oefelein of the Combustion Research Facility at Sandia Livermore to work together towards implementing the models developed in this research into the high-pressure Large Eddy Simulation code under development by him at Sandia.

II. Recent Progress

This program was initiated in September 2009 and thus has not yet benefited of a full year of study. Additionally, the Post Doc who will work with the PI and be entirely dedicated to this project will only come on board somewhat later than anticipated due to a delay in finishing her PhD thesis. Therefore, the study has so far been mainly conducted by the PI, and, due to the limited time that contractually the PI can currently devote to this work, the

investigation has primarily concentrated on understanding the implications on this reactive-flow work from recent results obtained in a precursor study on high-pressure mixing, under different sponsorship. These recent results were derived after the present work was proposed and it is very satisfying to find out that they reinforce the proposed direction of the study while adding further considerations which are not necessarily restricted to high-pressure studies but become amplified under high-pressure conditions. In the following, we will discuss what we have learned from these recent results and how they may add to the work already underway.

We had made the case that supercritical-pressure mixing studies have shown that the scalar dissipation dominates viscous and heat dissipation. This conclusion came from Direct Numerical Simulations (DNSs) of temporal mixing layers the results of which showed the formation of high density-gradient magnitude (HDGM) regions where the scalar dissipation had most of its activity. Because these HDGM regions were also experimentally observed in fully turbulent flows [i – iii], the natural, but **indirect**, conclusion was that the scalar dissipation dominates the total dissipation even in fully turbulent flows. Recently, we have had **direct** evidence that for non-reactive flows undergoing species mixing, the scalar dissipation indeed dominates the entire dissipation [iv]. By non-dimensionalizing the source term of the entropy equation, which represents the dissipation, we have shown that both the viscous and heat dissipation scale as $O(Re^{-1})$, whereas the scalar dissipation does not scale with Re , where Re denotes the Reynolds number. Thus, as Re increases (e.g. from DNS to fully turbulent flows) both the viscous and thermal dissipation decrease, whereas the scalar dissipation is independent of the Re value. For the high-pressure flows under consideration, the coefficients resulting from the non-dimensionalization were computed at transitional times of different DNS realizations and their calculated value did not modify the conclusions of the non-dimensionalization. The question is: Would the same conclusion remain valid for high-pressure reactive flows? This is a subject which we should investigate once we have available DNS realizations of such reactive flows. In particular, this means that we should develop the mathematical expression for the source term in the entropy equation in the case of reactive flows and perform the non-dimensionalization of the reaction-based term to compare it to the three flux-originated modes of dissipation studied in [iv]. The implications of the results could be far reaching for conducting Large Eddy Simulation (LES) in that the difficulty in LES is to reproduce the dissipation through models; knowing where most of the effort should be devoted will not only enhance the LES quality but also reduce the time to develop the needed models.

Another set of results [v] added increasing perspective to performing LES of high-pressure flows, and generally to performing LES in any situation in which there are strong non-uniformities in the flow, as for example the present HDGM regions. Such HDGM regions have already been observed in fully turbulent high-pressure reactive flows [vi]. We recall that the LES equations are obtained by filtering the governing equations, yielding two types of terms: (a) terms which can be directly computed from the LES solution, and (b) subgrid (SGS) terms which must be modeled. But the SGS terms are not only the ubiquitous SGS fluxes (for species, momentum and enthalpy) which originate from the convective terms of the original equations, but also terms each expressing a difference between a filtered term and the same term computed as a function of the filtered (i.e. LES) solution resulting from **all** terms in the original equations. These differences, usually neglected, embed SGS information which may be considerable if there are strong flow non-uniformities and/or if the LES grid is much

coarser than that for a well-resolved DNS would be. Modeling performed in [v] showed how one of these important additional SGS terms [vii], based on the pressure gradient, could be modeled using a Taylor series expansion. Another type of modeling was used for the divergence of the heat flux [viii], based on the approximate deconvolution model (ADM), and it was shown how this model led to an irreducible error which is inherent to the coarser LES grid compared to DNS. The implication for reactive flows is that the corresponding SGS terms obtained from filtering the reaction terms could be modeled using similar approaches. The strong non-linearity of the additional SGS terms already modeled bodes well for applying the same techniques to reactive flow modeling.

Finally, there is strong indication that the definition of scalar variance currently used in combustion for the conserved scalar, particularly for modeling flamelets, is no longer valid for high-pressure flows. This issue must be addressed for supercritical-pressure reactive flows because it will impact combustion modeling at the most fundamental level. In particular, this issue is directly related to the questioning by Barlow [ix] of the current concept of progress variable, as used even for atmospheric flows. Discrepancies between currently established concepts for atmospheric-pressure flows and future concepts needed for studies incorporating detailed molecular transport properties become amplified as the pressure increases. The PI is currently exploring the possibility of spending considerably more of her time on this crucial study.

As of now, the PI has initiated collaboration with Dr. Oefelein by transmitting SGS models specifically describing high-pressure mixing, and he will soon start discussing the details of their implementation into the Sandia code. Also, the supercritical-pressure reactive-flow conservation equations have been derived using a 4 steps and 5 species kinetics [x] for heptane/air reactions in the auto-ignition regime. To allow the study of turbulence/reaction coupling at the incipient turbulence Reynolds number values achievable in DNS, the pre-exponential factor of the reactions rates provided in [x] will be proportionally modified to adjust the reactions' characteristic times to those of these incipient turbulence flows.

III. Future Plans

To code the conservation equations, the following will be achieved in the near future:

- Implement a multispecies diffusive model.
- Develop a real-gas equation of state representing the 5 species system.
- Develop boundary conditions for supercritical-pressure reacting flows obeying real-gas equations of state, much as those in [xi] for perfect-gas flows.

We expect to debug the code, obtain the baseline DNS solution and perform analysis of the results before the next year meeting.

IV. References

- i. Chehroudi, B; Talley, D.; Coy, E. AIAA 99-0206, **1999**.
- ii. Oswald, M. and Schik, A. *Exp. Fluids* **1999**, 27, 497.
- iii. Segal, C.; Polikhov, S. *Phys. Fluids* **2008**, 20, 052101-7.
- iv. Okong'o, N; Bellan, J. *Comp. Fluids* **2010**, doi 10.1016/j.compfluid.2010.02.001
- v. Taşkinoğlu, E. S.; Bellan, J. *J. Fluid Mech.* **2010**, 645, 211.
- vi. Singla, G. Etude des flammes cryotechniques oxygène liquide/méthane à haute pression, PhD thesis **2005**, École Centrale de Paris.
- vii. Selle, L. C. ; Okong'o, N. A. ; Bellan, J. ; Harstad, K. G. *J. Fluid Mech.* **2007**, 593, 57.

- viii. Taşkınoğlu, E. S.; Bellan, J. AIAA 2010-0206, **2010**.
- ix. Barlow, R. S., March 22, **2010**, communication
- x. Müller, U. C.; Peters, N.; Linan, A. *Proc. Symp. Inst.* **1992**, 24, 777.
- xi. Sutherland, J. C; Kennedy, C. A. *J. Comp. Phys.* **2003**, 191, 502.

V. Publications and submitted articles supported by this project September 2009-March 2010

None yet.

Theoretical Studies of Combustion Dynamics (DE-FG02-97ER14782)

Joel M. Bowman

Cherry L. Emerson Center for Scientific Computation and Department of Chemistry,
Emory University Atlanta, GA 30322, jmbowma@emory.edu

Program Scope

The research program supported by this Department of Energy grant focuses on the development of rigorous computational methods to model the chemical and physical processes of importance in gas-phase combustion. This includes the development of full-dimensional, global, *ab initio*-based potential energy surfaces (PESs) that describe complex unimolecular and bimolecular reactions. Dynamics on these potentials, which may contain multiple minima and saddle points, can be done for long times and can reveal new pathways and mechanisms of chemical reactions. Large amplitude motion, including isomerization, "roaming", energy transfer in collisions with atoms and molecules can be studied with these potentials. The choice of reaction system to study is always motivated by experiments that challenge and ultimately advance basic understanding of combustion reaction dynamics.

Recent Progress

CH₃CHO Photodissociation

We have developed a new global PES for CH₃CHO that includes thousands of MRCI/aVTZ energies in the regions of multireference character. This potential, like the first version,^{P3} has been used in quasiclassical trajectory calculations of the photodissociation of CH₃CHO, over a large wavelength range to determine the extent of "roaming" in the dissociation dynamics.^{1, P3, P4} Preliminary results indicate that this unusual pathway to molecular products is a major one, in agreement with results published in 2008.^{P4} The final state distributions of the radical products CH₃ and HCO have also been calculated and compare well with recent experiments of Kable and co-workers.²

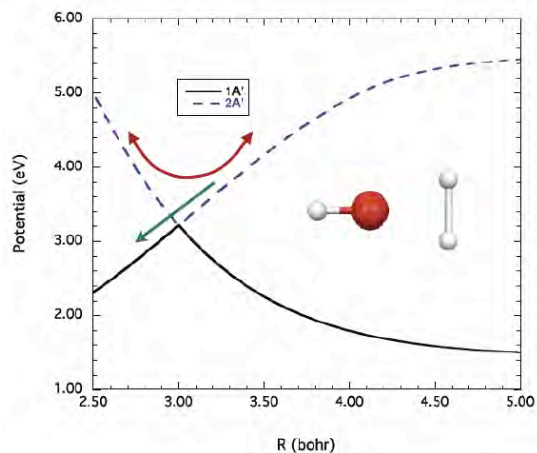
F+CH₄ reaction

We developed a full-dimensional, *ab initio*-based PES for the F+CH₄ reaction,^{P9} based on fitting roughly 20 000 highly accurate electronic energies. This PES is the most accurate one currently available and has been used by us in dynamics calculations of HF final state distributions, which agree well with experimental results of Nesbitt and co-workers.³ More recently we reported a study of interesting and surprising mode-specific effects in the F+CD₃H(*v*_{CH} = 0,1) reaction.^{P13} This was motivated by crossed molecular beam experiments, reporting these effects, by Lui and co-workers.⁴

Electronic Quenching of OH* by H₂

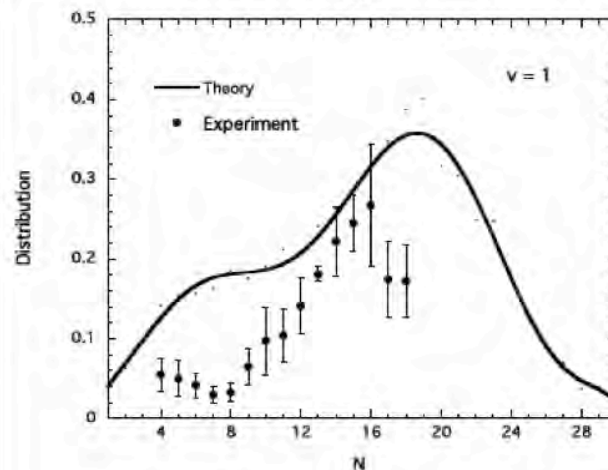
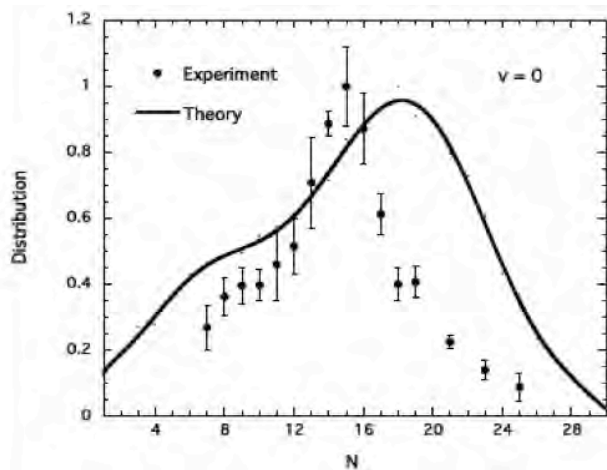
Motivated by experiments of the Lester group^{5,6} and the Davis group⁷ we developed a global potential energy surface for the ground electronic state and electronically excited states in the vicinity of thirteen conical intersections identified previously by Hoffman and Yarkony.⁸ These surfaces were used to study the reactive and non-reactive quenching channels OH* + H₂ → H₂O+H, OH+H₂. The first set of calculations were done by initiating tens of thousands of classical trajectories at each of these conical intersections, using two microcanonical distributions of initial momenta for

each atom. These are indicated in the figure below, which serves to define the "adiabatic" and "diabatic" microcanonical models for the dynamics. Each of these models bypasses the need to obtain the non-adiabatic dynamics and gives what we terms "post quenching" dynamical predictions of the reactive to non-reactive branching and final state distributions of the products. In the adiabatic model, indicated by the red two-headed arrow, momenta at conical intersections are



selected fully microcanonically, consistent with a long-lived collision complex on the upper adiabatic potential (indicated as 2A'). In the diabatic model, indicated by the green single-headed arrow, the negative sign of the initial relative speed of the distance between the centers of mass of the OH* and H₂, denoted R, is assumed to be preserved at the conical intersections. This is consistent with immediate passage to the ground electronic state through the conical intersections.

These two models results in widely different predictions of the reactive to non-reactive branching fraction (as expected) with the diabatic one being in much closer agreement with experiment. Both, however, predict, virtually identical final state distributions, and example of which is shown below for the OH ro-vibrational distributions. Comparisons with the Lester group experiments are also given and we



we are quite encouraged with the level of agreement with experiment, especially given the simplicity of the model. We close this section by also noting that the new ground state global PES is being used in quantum scattering calculations of the state-to-state cross sections.⁹

Future Plans

(1) We plan to extend the study of multi-electronic state dynamics calculations of the H₂CO photodissociation that will explicitly consider the non-adiabatic coupling. (2) We plan reduced dimensionality quantum calculations of the F+CD₃H reaction in order to make direct comparisons with the experiments of Kopin Liu, who has presented some evidence of a possible resonance in this reaction. Liu's experiments detect the correlated products CD₃(v=0)+HF(v') and CD₂H(v=0)+DF(v'). (3) We will complete potential energy surfaces and non-adiabatic coupling for excited states of the OH*+H₂ reaction and begin coupled non-adiabatic dynamics calculations of this quenching. Finally, (4) we will begin studies of energy transfer in complex systems such as vibrationally excited CH₃CHO, formed from the association reaction CH₃+HCO.

References

1. P. L. Houston and S. H. Kable, Proc. Natl. Acad. Sci. USA, **103**, 16079 (2006).
2. B. R. Heazlewood, S. J. Rowling, A. T. Maccarone, M. J. T. Jordan, and S. H. Kable, J. Chem. Phys. **130**, 054310 (2009).
3. W. W. Harper, S. G. Nizkorodov, and D. J. Nesbitt, J. Chem. Phys. **113**, 3670 (2000).
4. (a) W. Shiu, J. Lin, and K. Liu, Phys. Rev. Lett. **92**, 3201 (2004); (b) J. Zhou, J. J. Lin, and K. Liu J. Chem. Phys. **119**, 8289 (2003); (c) Science
5. M. W. Todd, D. T. Anderson, and M. I. Lester, J. Phys. Chem. A **105**, 10031 (2001).
6. P. A. Cleary, L. P. Dempsey, C. Murray, M. I. Lester, J. Klos, and M. H. Alexander, J. Chem. Phys. **126**, 204316 (2007).
7. M. Ortiz-Suarez, M. F. Witinski, and H. F. Davis, J. Chem. Phys. **124**, 201106 (2006).
8. B. C. Hoffman and D. R. Yarkony, J. Chem. Phys. **113**, 10091 (2000).
9. S. Althorpe, private communication.

PUBLICATIONS SUPPORTED BY THE DOE (2008-present)

1. Photodissociation dynamics of formaldehyde initiated at the T₁/S₀ minimum energy crossing configurations (Letter), B. Shepler, E. Epifanovsky, P. Zhang, J. M. Bowman, A. I. Krylov, and K. Morokuma, J. Phys. Chem. A **112**, 13267 (2008).
2. Further aspects of the roaming mechanism in formaldehyde dissociation, S. A. Lahankar, V. Goncharov, F. Suits, J. D. Farnum, J. M. Bowman, and A. G. Suits, Chem. Phys. **347**, 288 (2008).
3. "Roaming" dynamics in CH₃CHO photodissociation revealed on a global potential energy surface, B. C. Shepler, B. J. Braams, and J. M. Bowman, J. Phys. Chem. A **112**, 9344 (2008).
4. Roaming is the dominant mechanism for molecular products in acetaldehyde photodissociation, B. R. Heazlewood, M. J. T. Jordan, S. H. Kable, T. M. Selby, D. L. Osborn, B. C. Shepler, B. J. Braams, and J. M. Bowman, Proc. Natl. Acad. Sci. USA **105**, 12719 (2008).
5. The theoretical prediction of infrared spectra of *trans*- and *cis*-hydroxycarbene calculated using full dimensional ab initio potential energy and dipole moment

- surfaces, L. Koziol, Y. M. Wang, B. J. Braams, J. M. Bowman, and A. I. Krylov, *J. Chem. Phys.* **128**, 204310 (2008).
6. Accurate ab initio structure, dissociation energy, and vibrational spectroscopy of the F⁻-CH₄ anion complex, G. Czako, B. J. Braams, and J. M. Bowman, *J. Phys. Chem. A* **112**, 7466 (2008).
 7. Probing the structure of CH₅⁺ by dissociative charge exchange, J. E. Mann, Z. Xie, J. D. Savee, B. J. Braams, J. M. Bowman, and R. E. Continetti, *J. Am. Chem. Soc.* **130**, 3730 (2008).
 8. Three Reaction Pathways in the H+HCO → H₂+CO reaction, K. M. Christoffel and J. M. Bowman, Three reaction pathways in the H + HCO → H₂ + CO reaction, K. Christoffel and J. M. Bowman, *Phys. Chem. A*, **113**, 4138 (2009).
 9. Accurate ab initio potential energy surface, dynamics, and thermochemistry of the F + CH₄ → HF + CH₃ reaction, G. Czako, B. C. Shepler, B. J. Braams, and J. M. Bowman, *J. Chem. Phys.* **130** 084301 (2009).
 10. Quasiclassical Trajectory Calculations of the HO₂+NO Reaction on a Global Potential Surface, C. Chen, B. C. Shepler, B. J. Braams and J. M. Bowman, *Phys. Chem. Chem. Phys.* **11**, 4722 (2009).
 11. Production of vibrationally excited H₂O from charge exchange of H₃O⁺ with cesium, J. E. Mann, Z. Xie, J. D. Savee, J. M. Bowman, and R. Continetti, *J. Chem. Phys.* **130**, 041102 (2009).
 12. Full-dimensional *ab initio* potential energy surface and vibrational configuration interaction calculations for vinyl. A. R. Sharma, B. J. Braams, S. Carter, B. C. Shepler, and J. M. Bowman, *J. Chem. Phys.* **130**, 174301 (2009).
 13. CH stretching excitation steers the F atom to the CD bond in the F + CHD₃ reaction, G. Czako and J. M. Bowman, *J. Am. Chem. Soc.* **131**, 17534 (2009).
 14. Roaming dynamics in formaldehyde-d₂ dissociation, V. Goncharov, S. A. Lahankar, J. D. Farnum, J. M. Bowman, and A. G. Suits, *J. Phys. Chem. A* **113** (52), 15315 (2009).
 15. Permutationally invariant potential energy surfaces in high dimensionality, B. J. Braams and J. M. Bowman, *Int. Rev. Phys. Chem.* **28**, 577 (2009).
 16. Permutationally invariant polynomial basis for molecular energy surface fitting via monomial symmetrization, Z. Xie and J. M. Bowman, *J. Chem. Theo Comp.* **6** (1), 26 (2010).
 17. Seven-degree-of-freedom, quantum scattering dynamics study of the H₂D⁺+H₂ reaction, D. Y. Wang, Z. Xie, and J. M. Bowman, *J. Chem. Phys.* **132** (8) (2010).
 18. Communications: Classical trajectory study of the postquenching dynamics of OH A²Σ⁺ by H₂ initiated at conical intersections, E. Kamarchik, B. N. Fu, and J. M. Bowman, *J. Chem. Phys.* **132** (9) (2010).

COMBUSTION CHEMISTRY
Principal Investigator: Nancy J. Brown
Environmental Energy Technologies Division
Lawrence Berkeley National Laboratory
Berkeley, California, 94720
510-486-4241
NJBrown@lbl.gov

PROJECT SCOPE

Combustion processes are governed by chemical kinetics, energy transfer, transport, fluid mechanics, and their complex interactions. Understanding the fundamental chemical processes offers the possibility of optimizing combustion processes. The objective of our research is to address fundamental issues of chemical reactivity and molecular transport in combustion systems. Our long-term research objective is to contribute to the development of reliable combustion models that can be used to understand and characterize the formation and destruction of combustion-generated pollutants. We emphasize studying chemistry at both the microscopic and macroscopic levels. Our current work is concerned with improving the calculation of transport properties for combustion modeling.

RECENT PROGRESS

Diffusion, viscosity, thermal conductivity, and thermal diffusion are critically important in combustion processes. They affect profile shapes, flame velocities, and pollutant production. Sensitivity analysis [Brown and Revzan, 2005] revealed that influential transport properties can be as important in flame modeling as influential reaction rates, and both should be taken into account when building chemical mechanisms.

A review of transport property formalisms and their underlying parameterizations has been completed. This review examines current approximations and approaches that underlie the evaluation of transport properties for combustion modeling applications. Viscosity data (post 1970) were used to benchmark the various approaches and approximations because it is the most accurately measured (errors less than 0.5%) of the properties, and there is significant data for experimentally determined viscosity coefficients for pure substances and binary mixtures.

Discussed in the review are: the intermolecular potential and its descriptive molecular parameters; various approaches to evaluating collision integrals; supporting data required for the evaluation of transport properties; the quality of experimental measurements and their importance for validating or rejecting approximations to property estimation; the interpretation of corresponding states; combination rules that yield pair molecular potential parameters for unlike species from like species parameters; and mixture approximations. The insensitivity of transport properties to intermolecular forces is noted, especially the non-uniqueness of the supporting potential parameters. When suitable potential parameters are used, the accuracy of transport property evaluation for pure substances and binary mixtures is acceptable when they are calculated using the approaches of Kee et al.(TRANLIB), Mason, Kestin, and Uribe(MKC), Paul and Warnatz (DRFM), Ern and Giovangigli(EGLIB). Although the approach to treating

polar molecules appears to be different in TRANLIB and DRFM, they yield quite similar results when the supporting data required by each is accurate. Recommendations from the review include a strong plea for revisiting the supporting data required by the various approaches, and updating the data sets with accurate potential parameters, dipole moments, and polarizabilities. Potential parameters and the slope of the trough line [see Bastien et al., 2010] characterizing the relationship between the energy and length-scaling Lennard-Jones potential parameters should also be part of the supporting data sets for each molecule. Combining rules were found to under predict the viscosity in most of the cases, and we recommend that improved rules be developed. There are very few measurements of transport properties for radical species, and we strongly recommend additional measurements. Thermal conductivity, which is important for the fuel and oxidizer in the early stages of flame development, must have accurate values of the molecular heat capacity for its evaluation.

There are many combining rules and several of these appear to be quite ad hoc without much physical basis. We used our optimum potential parameters obtained by fitting binary mixture viscosities for twelve types of binary mixtures to generate a new approach to combining rules. Plotting the σ_{ij} 's versus the pure species collision diameters σ_{ii} 's and σ_{jj} 's resulted in a rather smooth and nearly planar surface as shown in Bastien et al. [2010]. The equation of the plane yielding the best fit is:

$$\sigma_{ij} = 0.43 \cdot (\sigma_{ii} + \sigma_{jj}) + 0.46 \quad (I)$$

This yields good results, with deviations frequently less than 2% from the best fit values, but there are outliers with deviations exceeding 3%.

T* greater than 10: MKC observed a slight failure in the Law of Corresponding States when the LJ 12-6 potential was used for values of T* greater than 10 and suggest that it be replaced a Born-Mayer exponential repulsive potential [$V_0 \exp(-r/\rho)$] thereby introducing two additional potential parameters. There are very few viscosity data for T* > 10.0. We investigated rare gases, H₂, and N₂ and calculated the viscosity using the Lennard Jones and Born-Mayer potentials as seen in the Figure 1 for H₂.

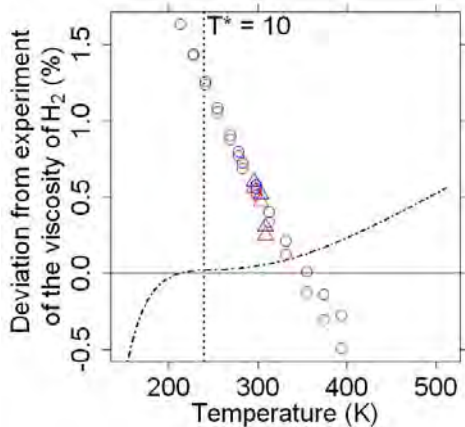


Figure1: Deviation of calculated viscosities from experimental values for H₂.

The red symbols correspond to viscosities computed with the 2-parameter correlation. The blue symbols correspond to viscosities computed the 4-parameter correlation. The dots and dashes lines correspond to deviation between the two correlations (the 2-parameter correlation is the reference value). The T*=10.0 line is the vertical line in the figure.

The viscosities calculated with the two potentials track each other very well, and have small and acceptable deviations. We recommend using the L-J potential in this temperature range since it appears to work well, and requires only two molecular parameters.

Thermal conductivity: In contrast with viscosity and diffusion, internal degrees of freedom of polyatomic molecules contribute to the thermal conductivity, and the effects of inelastic collision where energy is transferred among the various degrees of freedom must be considered. Measurements of thermal conductivity via the hot wire technique, the preferred experimental approach, have larger errors associated with them (5 %) than viscosities. The TRANLIB, MKC, and DRFM approaches to computing thermal conductivity are different and each has its own approach for accounting for the internal degrees of freedom, but all use the heat capacity. Each separates the contributions of the different degrees of freedom and evaluates them with approaches that are quite empirical. We computed thermal conductivities for a number of molecules using the three approaches and computed their deviations from experimental values for: Ar, N₂, O₂, CO₂, and CH₄. Each approach gave satisfactory results with deviations less than 5 % when compared with experiment. The TRANLIB code must be corrected for an algebraic error as indicated in the review.

Transport codes: Two codes that are used most widely in the combustion community are TRANLIB and the EGLIB codes of Ern and Giovangigli [2004]. EGLIB is a general purpose Fortran library for multicomponent mixture transport property evaluation of order (NS)², where NS is the number of species. EGLIB uses the formalism developed for transport linear systems, contains the TRANLIB data base, and uses the TRANLIB evaluation of collision integrals. EGLIB also provides a new approach to transport properties in mixtures involving the treatment of vanishing mass fractions that is of order NS. We recommend using the EGLIB code and modifying the supporting data base by including better values for the potential parameters, dipole moments, and polarizabilities. Thermal conductivity coefficient calculations could be improved if more accurate values of the heat capacity were used.

Current Research

Our research has shown that a simple Lennard-Jones 12-6 (LJ) potential is adequate for the calculation of viscosity of simple molecules taken as pure species and binary mixtures. Viscosity measurements of a single chemical species allow direct estimation of the parameters that describe the interaction between two molecules of the same species, ϵ_{ii} and σ_{ii} , the conventional energy and length scaling parameters associated with the L-J potential. We found that many different (ϵ_{ii} , σ_{ii}) pairs can yield predicted viscosities that agree with experimental values with less than 1% error over a wide range of temperatures. In order to explore the consequences of this finding, which suggests a significant insensitivity of transport to the intermolecular surface, we are conducting sensitivity studies of the deflection function, cross section and collision integrals to the intermolecular potential. We are also assembling a set of supporting data for flame studies of H₂/air and CH₄/air flames using a variety of techniques: ab initio calculations, correlations, and literature searches, and are examining the reliability of thermal diffusion calculations. We will use the new transport data in flame modeling studies with Bell and Chang.

Publication supported by DOE for last two years:

Lunden, M.M., Kirchstetter, T.W., Thatcher, T.L., Hering, S.V., and Brown, N.J. (2008) “Factors affecting the indoor concentration of carbonaceous aerosols of outdoor origin.” Atmospheric Environment doi:10.1016/j.atmosenv.2008.03.017. LBNL Report No. 60877.

Jin, L., Tonse, S.R., Cohan, D.S., Mao, X., Harley, R.A., Brown, N.J., Sensitivity analysis of ozone formation and transport for a Central California air pollution episode, Environmental Science & Technology 42, 3683-3689, (2008).

Tonse, S.; Brown, N.J.; **Jin, L.**; Harley, R.A. A Process-Analysis Based Study of the Ozone Weekend Effect. Atmospheric Environment 42, pp7728-7736 (2008).

Ling Jin, Nancy Brown, Robert A. Harley, Jian-Wen Bao, Sarah Michelson, James M. Wilzak, Seasonal versus Episodic Performance Evaluation for an Eulerian Photochemical Model, in press Journal Geophysical Research Atmospheres (2009)

Bastien, L.A.J., Price, P.N. and Brown, N.J. “Intermolecular Potential Parameters and Combining Rules Determined from Viscosity Data,” submitted to International Journal of Chemical Kinetics (2010).

Brown, N.J., Bastien, L., and Price, P. N., “Transport Properties for Combustion Modeling”, Submitted to Progress in Energy and Combustion Science, (2010).

References

Brown, N.J.,K.L. Revzan, Int. J. Chemical Kinetics, 37 (2005) 538-553.

Bzowski, J., J. Kestin, E. Mason, F.J. Uribe, J. Phys. Chem. Ref. Data, 19 (1990) 1179-1232.

Ern, A. and Giovangigli, V. “EGLIB: A General Purpose FORTRAN Library for Multicomponent Transport Property Evaluation, EGLIB Version 3.4 July 12, 2004.

Kee, R.J., G. Dixon-Lewis, J. Warnatz, M.E. Coltrin, J.A. Miller, *A FORTRAN Computer Package for the Evaluation of Gas-Phase Multicomponent Transport Properties*, SANDIA, 1986.

Mason, E.A., F.J. Uribe, in: Transport Properties of Fluids (Their Prediction, Estimation, and Correlations), Cambridge University Press, 250-283, 1996.

Paul P.H., *DRFM: A New Package for the Evaluation of Gas-Phase Transport Properties*, Sandia, 1997.

Paul, P.H., J. Warnatz, Boulder, Colorado, 1998, pp. 495-504.

Dynamics of Product Branching in Elementary Combustion Reactions

Laurie J. Butler

The University of Chicago, The James Franck Institute
5640 South Ellis Avenue, Chicago, IL 60637
L-Butler@uchicago.edu

I. Program Scope

The elementary reactions that determine the performance of a combustion system range from direct H-atom abstraction reactions to complex reactions involving competing addition/elimination mechanisms. While the total rate constant for many elementary reactions is well-characterized, understanding the product branching in complex reactions presents a formidable challenge. To study such reactions, our experiments directly probe the dynamics of the product channels that arise from long-lived radical intermediates along the bimolecular reaction coordinates. The work uses the methodology developed in my group in the last eight years, using both imaging and scattering apparatuses. The experiments generate a particular isomeric form of an unstable radical intermediate along a bimolecular reaction coordinate and investigate the branching between the ensuing product channels of the energized radical as a function of its internal energy under collision-less conditions.

The experiments use a combination of: 1) measurement of product velocity and angular distributions in a crossed laser-molecular beam apparatus, with electron bombardment detection in my lab and with tunable vacuum ultraviolet photoionization detection at Taiwan's National Synchrotron Radiation Research Center (NSRRC), and 2) velocity map imaging using state-selective REMPI ionization and single photon VUV ionization of radical intermediates and reaction products. Our publications this year include the final experimental paper on our comprehensive study of product branching in the O + allyl reaction and our first study of a radical intermediate of the OH + ethene reaction, the 2-hydroxyethyl radical. Our results develop insight on product channel branching in reactions that proceed via an addition/elimination mechanism and provide a key benchmark for theoretical predictions of polyatomic reactions that proceed through unstable radical intermediates.

II. Recent Progress and Ongoing Work

A. O + Allyl

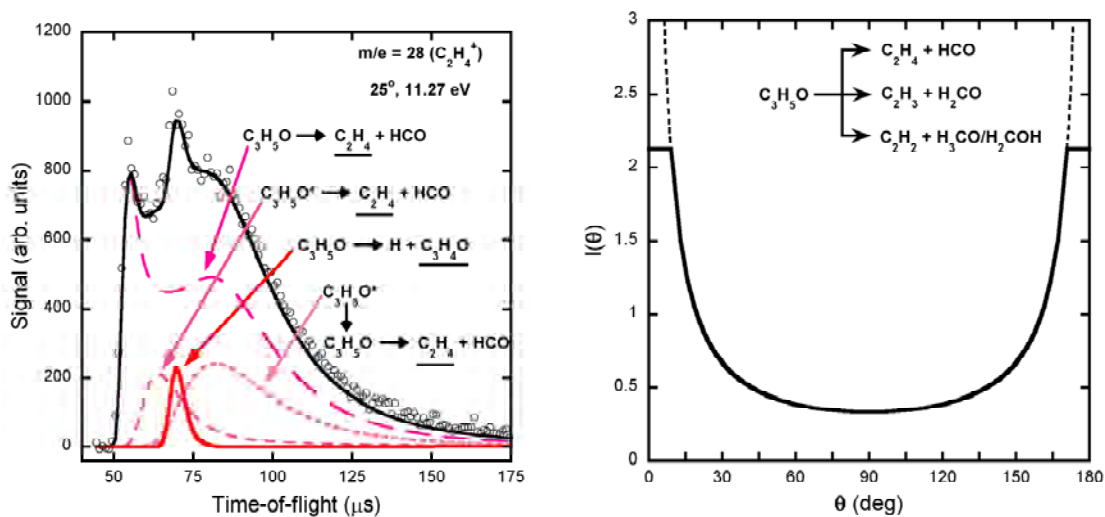
Our work this year completed our studies on the complex dynamics of the O + allyl reaction. The work included imaging and scattering experiments in our lab at Chicago, CCSD(T) calculations on the relevant radical intermediates and transition states on the path to the energetically allowed product channels, and extensive scattering experiments at the NSRRC in Taiwan in collaboration with J. J. Lin on the product channels accessed from the radical intermediate formed when the O atom adds to a terminal C atom. To measure the branching between product channels accessed from this intermediate, our experiments corrected the relative signal levels by calibrating, in separate experiments, the photoionization cross sections of some of the radical and molecular products with respect to Cl atoms, ethene and vinyl. The work also allowed us to measure the photoionization cross section of HCO radicals, as they are produced in a one-to-one ratio with ethene in this system.

Before our work, a few key studies on the O + allyl reaction had attempted to probe the product branching and dynamics of this reaction. The early bulk kinetics work of Gutman et al. (J. Phys. Chem. 94, 3652 (1990)) identified only the acrolein + H product channel as a primary one, putting a <20% upper limit on the H₂CO + C₂H₃ product channel. Later crossed molecular beam experiments by Choi et al (J. Chem. Phys. 116, 2675 (2002); 117, 2017 (2002); 120, 7976

(2004)) focused on detecting only OH and H atom products; they also computationally characterized (J. Chem. Phys. **119**, 8966 (2003)) the multiple reaction pathways that can result from the addition of O atoms to an end vs. the central C atom. More recently, Casavecchia et al (Phys. Chem. Chem. Phys. **9**, 1307 (2007)) used soft-electron impact ionization in a crossed-molecular beams experiment to try to identify all the product channels. The data evidenced that acrolein + H is a major product channel, but they were unable to definitively assign the product channels resulting in their signal at $m/e=29$ and 27 , so concluded that “one or more C-C fission product channels” contribute to the product branching. Most recently, Hoyermann et al. (Proc. Combust. Inst. **32**, 157 (2009)) used laser flash photolysis to generate the O and allyl reactants and quantitative FTIR spectroscopy to determine the room temperature product branching.

Our prior experiments on this system (J. Chem. Phys. **129**, 084301 (2008)) photolytically generated the $\text{OCH}_2\text{CHCH}_2$ radical intermediate, definitively identified three major product channels, H + acrolein, $\text{H}_2\text{CO} + \text{C}_2\text{H}_3$ and $\text{HCO} + \text{C}_2\text{H}_4$, and determined the product branching to the H + acrolein product channel. Our work this year focused on determining the branching fractions to all the other product channels from this radical intermediate. Initiating the dynamics from the radical intermediate instead of from the O + allyl reactants allows us to study the dynamics at energies where the product branching is critically sensitive to the energetics of the intermediate transition states, and to quantum tunneling. Our photolytic precursor produced highly rotationally excited radicals, so we used the measured onset of the H + acrolein product channel to estimate the rotational energy partitioning to the radicals.

The $\text{O}(^3\text{P})$ + allyl radical intermediate dissociated to three competing C-C bond fission channels. Analysis of the velocity distribution of the momentum-matched signals from the $\text{HCO} + \text{C}_2\text{H}_4$ products and the $\text{H}_2\text{CO} + \text{C}_2\text{H}_3$ products shows that the dissociation of the radical intermediate imparts a high relative kinetic energy, peaking near 20 kcal/mol, between the products. The strongly forward-backward peaked angular distributions (see figure below) and the high kinetic energies result from tangential recoil during the dissociation of highly rotationally excited nascent radicals formed photolytically in this experiment.



The data identifies four dominant product channels: acrolein + H, ethene + HCO, $\text{H}_2\text{CO} + \text{C}_2\text{H}_3$, and $\text{HCCH} + \text{CH}_3\text{O}/\text{CH}_2\text{OH}$. The most exothermic product channel, $\text{C}_2\text{H}_5 + \text{CO}$, does not contribute significantly to the product branching. Our integrated signals at C_2H_4 vs. C_2H_3 at 11.27 eV photoionization, corrected for kinematic effects and their photoionization cross section, gave the $\text{HCO} + \text{C}_2\text{H}_4 : \text{H}_2\text{CO} + \text{C}_2\text{H}_3$ branching ratio of 4.5 ± 0.5 . Here we have used the photoionization cross section for C_2H_4 put on an absolute scale by Cool et al., Int. J. Mass Spectrom. **247**, 18 (2005)) and the photoionization spectrum of vinyl radicals measured by C.

Taatjes in conjunction with our low-resolution photoionization efficiency curve. This data also allowed us to determine the absolute photoionization cross section of HCO radicals as 8.8-11.6 Mb at 11.27 eV (averaged over the NSRRC bandwidth), and to put the entire photoionization spectrum of HCO from 10 to 11.5 eV on an absolute scale. Likewise, we used our integrated signals at C₂H₄ vs. HCCH to determine the HCO + C₂H₄ : HCCH + CH₃O/CH₂OH branching ratio; it is 3.1 ± 0.5. Using the branching fraction to the H + acrolein product channel of 18% measured previously, we obtained branching fractions for all the significant product channels. They are: 53 % for the HCO + C₂H₄ product channel; 12 % to the C₂H₃ + formaldehyde product channel; and 17% to the HCCH + H₃CO/H₂COH product channels. The statistical predictions for the product branching are in reasonable agreement with the experiment, with the exception of the branching to the acetylene product channel. The experimentally determined branching to that channel is significantly larger than that predicted by the statistical calculations; we are presently re-examining the data related to that channel.

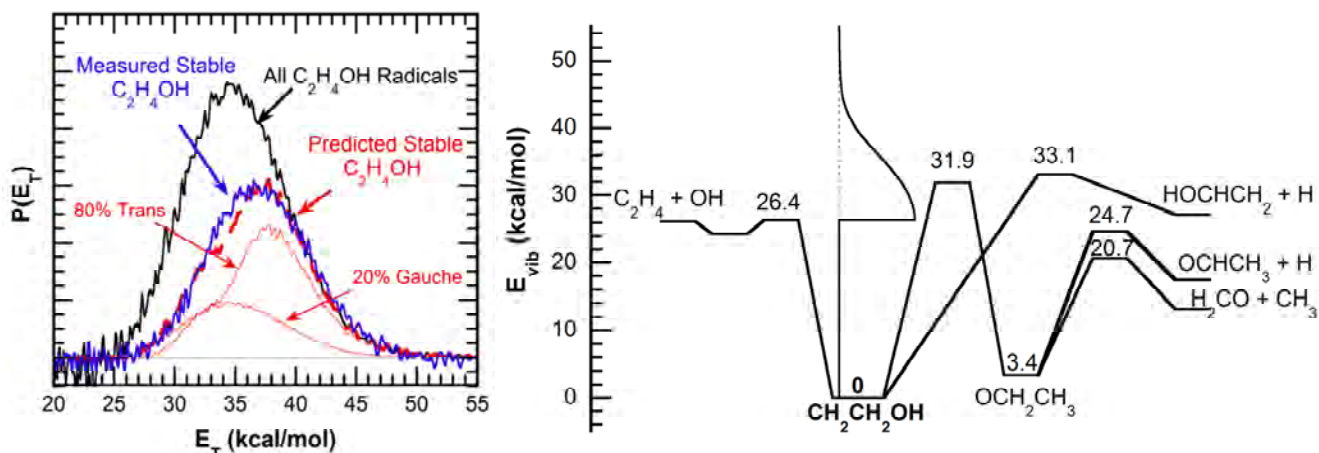
This system serves as a key benchmark to theoretical studies designed to predict product branching in combustion systems. The O + allyl elementary reaction includes two key dynamical features that control the product branching in reactions of radicals with unsaturated hydrocarbon species. First, the initial radical adduct in the addition/elimination channel has direct bond fission channels that compete with isomerization of the radical intermediate via an H atom transfer. This makes the product branching sensitive to quantum tunneling. Second, the intermediate isomerization pathway may not be dynamically separated from the simple bond fission dynamics to H + acrolein; this renders some of the assumptions made in predicting product branching with statistical theories invalid.

B. OH + Ethene

Our other major effort this year centered on the radical intermediate formed when an OH radical adds to ethene. There has been extensive experimental and theoretical work on the OH + ethene reaction: thirteen prior theoretical studies and a shocking thirty-eight prior experimental studies, many focusing on the temperature and pressure dependence of the total rate constant. Our work investigates the products from the addition of OH to the C=C bond of ethene, forming the HOCH₂CH₂ radical intermediate. Upon forming this adduct, one can expect a competition between collisional stabilization of the adduct in the bulk and, if the adduct is formed with high enough internal energy, its direct dissociation to ethenol + H, and its isomerization, via H-atom transfer, to a second radical intermediate, OCH₂CH₃. This second radical intermediate leads to the formaldehyde + CH₃ and acetaldehyde + H product channels. Interestingly, there have been two recent reports (Taatjes et al, *Science* **308**, 1887 (2005) and *J. Phys. Chem. A* **110**, 3254 (2006) and Cool et al, *J. Chem. Phys.* **119**, 8356 (2003)) of ethenol production in ethene flames; this observation is attributed to the ethenol + H product channel in the OH + ethene reaction.

Our work, Pub. 2 below, photolytically generates, from 2-bromoethanol photodissociation, the 2-hydroxyethyl radical intermediate of the OH + ethene reaction and measures the velocity distribution of the stable radicals. This precursor is known to produce radicals with substantial rotational energy, so to render it useful for product branching studies our work developed a model for predicting the partitioning between rotational and vibrational energy in the radicals prepared photolytically, one that explicitly includes the change in impact parameter due to the vibrational modes of the photolytic precursor. The experiments used velocity map imaging to separately resolve the C₂H₄OH + Br(²P_{3/2}) and C₂H₄OH + Br(²P_{1/2}) photodissociation channels, allowing us to account for the 10.54 kcal/mol partitioned to the Br(²P_{1/2}) co-fragment. Energy and momentum conservation give the distribution of total internal energy, rotational and vibrational, in the C₂H₄OH radicals. Then, using 10.5 eV photoionization, we measured the velocity distribution of the radicals that are stable to subsequent dissociation. The onset of

dissociation reflects the significant amount of rotational energy imparted to the C_2H_4OH photofragment. Instead of estimating the mean rotational energy with an impulsive model from the equilibrium geometry of 2-bromoethanol, our model explicitly includes weighting over geometries across the quantum wavefunction with zero, one, and two quanta in the harmonic mode that most strongly alters the exit impact parameter. The model gives a nearly perfect prediction of the measured velocity distribution of stable radicals near the dissociation onset using a G4 prediction of the C-Br bond energy and the dissociation barrier for the OH + ethene channel. The vibrational energy distribution of our radicals is shown below superimposed on the theoretical transition states of Senosiain et al., *J. Phys. Chem. A*, **110**, 6960 (2006).



Having fully characterized the vibrational energy distribution of this OH + ethene radical intermediate, we turned to measuring the product branching. The data directly test the ratios between microcanonical rates predicted from theory. We just concluded taking data at the NSRRC on the ethenol + H, vinyl + H_2O , acetaldehyde + H, and formaldehyde + CH_3 product channels. They should allow us to directly determine the relative energies of the OH + ethene entrance channel, the isomerization barrier to the OCH_2CH_3 radical, which leads to the formaldehyde + CH_3 and acetaldehyde + H product channels, and the barrier for direct dissociation of the $HOCH_2CH_2$ radical intermediate to ethenol + H. Senosiain et al. predict that the barrier to ethenol + H is higher by 1.2 kcal/mol than the isomerization barrier. In contrast other recent theoretical work by M. C. Lin et al (*Chem. Phys. Lett.* **408**, 25 (2005)) predicts the barrier to isomerize to OCH_2CH_3 is higher, not lower, than the barrier for the CH_2CH_2OH radical intermediate to dissociate to ethenol + H. They conclude that the ethenol + H product channel would be the only significant product channel to compete with the direct abstraction reaction that forms $H_2O + C_2H_3$. Our ongoing experiments offer a direct measurement of the product channel branching for this reaction.

IV. Publications Acknowledging DE-FG02-92ER14305 (2008 or later)

1. Investigation of the O + allyl addition/elimination reaction pathways from the OCH_2CHCH_2 radical intermediate, B. L. FitzPatrick, K. -C. Lau, L. J. Butler, S. -H. Lee, and J. J. Lin, *J. Chem. Phys.* **129**, 084301 (2008).
2. Modeling the Rovibrationally Excited C_2H_4OH Radicals from the Photodissociation of 2-Bromoethanol at 193 nm, B. J. Ratliff, C. C. Womack, X. N. Tang, W. M. Landau, L. J. Butler, and D. E. Szpunar, *J. Phys. Chem. A*, Article ASAP, 10.1021/jp911739a (2010).
3. Primary Photodissociation Pathways of Epichlorohydrin and Analysis of the C-C Bond Fission Channels from an $O(^3P)$ + Allyl Radical Intermediate, B. L. FitzPatrick, B. W. Alligood, L. J. Butler, S. -H. Lee, and J. J. Lin, submitted to *J. Chem. Phys.* (2010).

High-Resolution, Crossed-Molecular-Beam Studies of Collisional Energy Transfer.

David W. Chandler
Combustion Research Facility
Sandia National Laboratory
Livermore, CA 94551-0969
Email:chand@sandia.gov

Program Scope:

My research focuses on the chemical dynamics of gas phase molecular species. Chemical dynamics is the detailed study of the motion of molecules and atoms on potential energy surfaces in order to learn about the details of the surface as well as the dynamics of their interactions. We have recently developed two molecular beam techniques for studying in greater detail the velocity and quantum state dependence of elastic and inelastic energy transfer un greater detail. The first utilizes velocity chirped molecular beam pulses in conjunction with time- and-space resolved detection of the scattering products thereby improving the velocity resolution of the scattering experiments. We are also developing a technique for the study of collisions of electronically excited state molecules. We excite a molecule at the crossing of the molecular beams (or atomic beams) in order to create an electronically excited state molecule in a particular ro-vibrational state. Within the radiative lifetime (200 ns for NO(A)) the molecule undergoes elastic, rotationally or vibrationally inelastic, or electronically nonadiabatic collisions producing new quantum states of the molecule. Quantum-state-selective ionization of the product molecules and projection of those ions onto an imaging detector allow us to observe, for the first time, differential cross sections and alignment moments for electronically excited state species.

Progress Report:

Velocity chirped molecular beams:

In our laboratory, the techniques of velocity-chirped, crossed-molecular-beam scattering and transient-electronic-state scattering were derivative from the crossed molecular beam scattering experiments studies we have been carrying out on maximizing and detecting molecules that are collisionally cooled in the laboratory reference frame. Although we have recently produced measurable amounts of cold atoms and molecules, having tens of milli-Kelvin temperatures, using a unique crossed molecular beam scattering technique we call Kinematic Cooling, we were unable to isolate the cold samples for further studies due to secondary collisions. We believe that these secondary collisions originate from collisions from a secondary effusive beam that is produced as the molecular beam sources are closing. In order to eliminate these effusive “after beams” and to isolate our kinematically cooled atoms, Kr, and molecules, ND₃ and NO, we installed choppers between the nozzle source and the scattering center. This has worked to lengthen the observation time of the cold molecules and afforded us a method for chirping the molecular beam pulses. The choppers are at a distance from the collision interaction volume, therefore the chopped molecular beams spread in time as they travel to the scattering center due to the velocity spread in the beam. Although the chopper was able to turn off the molecular beam in about 5 microseconds at the position of the scattering volume they have of 30 to 40 microseconds long tails. These tails are velocity chirped. The velocity dispersion necessarily leads to a narrowing of the instantaneous velocity distribution in the tail of the pulse: molecules

in the tail of the pulse enter the collision volume with a much smaller range of velocities than the molecules in the leading portion of the pulse. By observing scattering that only occurred during a few μs time duration at the crossing of these “tails” the spread in the velocity distribution associated with the observed scattering was cut by about a factor of 7 for each molecular beam. A 40 m/s velocity spread was reduced to an approximately 7 m/s velocity spread. The impact of this is seen in Fig. 1 on the NO + Ar scattering.

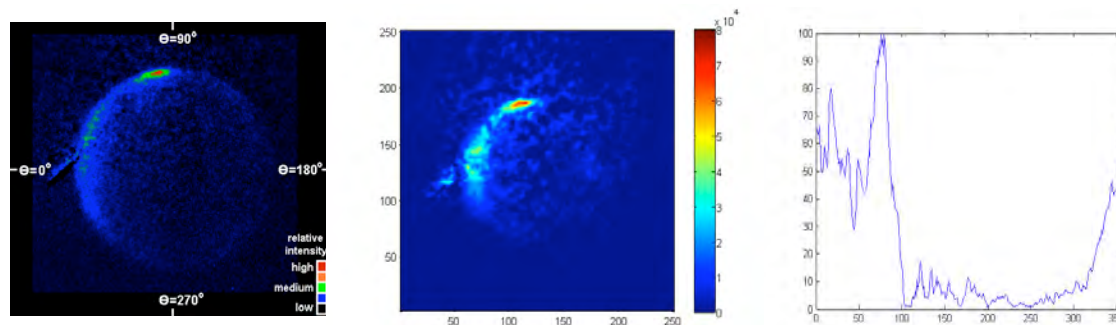


Figure 1: Scattering of $\text{NO}(j=0.5) + \text{Ar} \rightarrow \text{NO}(j=7.5) + \text{Ar}$. Left panel is scattering observed with an unchirped molecular beam (~ 40 m/s spreads), middle panel is scattering observed with chirped molecular beams (~ 7 m/s spreads) revealing structure in the forward scattering direction, right panel is intensity profile around the middle image showing structure around 20 degrees associated with forward scattering.

In the left panel of Fig. 1 is the scattering image taken with the full velocity distribution of the molecular beams present at the scattering center. In this image a smooth forward scattered differential cross section is observed in the forward, 0° , scattering direction. An intense spot is observed at 90° due to the production of cold molecules that build up during the scattering of the beams. In the middle panel of Fig. 1 is the image taken when to “chopped” tails of the molecular beams overlap in the scattering volume. The beams are significantly weaker but structure is evident in the forward scattering region of the differential cross section. This Fraunhofer interference, first observed by Faubell, in the scattering is always predicted but rarely seen for molecular systems. The right hand panel of Fig. 1 is an intensity profile around the middle image quantifying the structure at low angle scattering. Fraunhofer scattering assumes that plane matter waves are diffracting from a sharp-edged, hard, object. Recently theory by Lemeshko and Friedrich has provided direct comparison to the scattering and alignment measurements we have previously published with lower velocity resolution. Their calculated alignment moments show oscillating behavior at low scattering angle. We were not able to determine alignment moments at low angle due to interference with the parent molecular beams and the velocity spreads inherent in our atomic and molecular beams. Our new experimental geometry will allow us to measure more accurately the Fraunhofer scattering inherent in rotationally inelastic collisions.

Scattering experiments with electronically excited molecules:

When faced with the desire to scatter Kr atoms from Kr atoms to generate a millikelvin samples of Kr atoms the problem become trying to detect the approximately 10^8 atoms/cc cold Kr atoms in the scattering center that are interdispersed with approximately 10^{13} atoms/cc hot supersonic Kr atoms in the parent molecular beam. The solution shown in Figure 2 is to “tag” the Kr atoms by exciting, via two-photon transition at 214.7 nm, the atoms into the $4s^2 4p^5 ({}^2P_{3/2}) 5p[3/2]_2$ state¹ which fluoresces primarily at 760 nm into the $4s^2 4p^5 ({}^2P_{3/2}) 5s[3/2]_2^0$ metastable (45 second

lifetime) excited state. Then by waiting a few microseconds before ionizing the excited state atoms with a second 266-nm laser pulse one allows the faster supersonic atoms to leave the scattering / ionization volume leaving only cold Kr atoms (and Kr atoms moving along the laser beam axis) to be detected. Figure 2 shows a series of images of Kr with various time delays between the 214-nm and the 266-nm laser beam pulses.

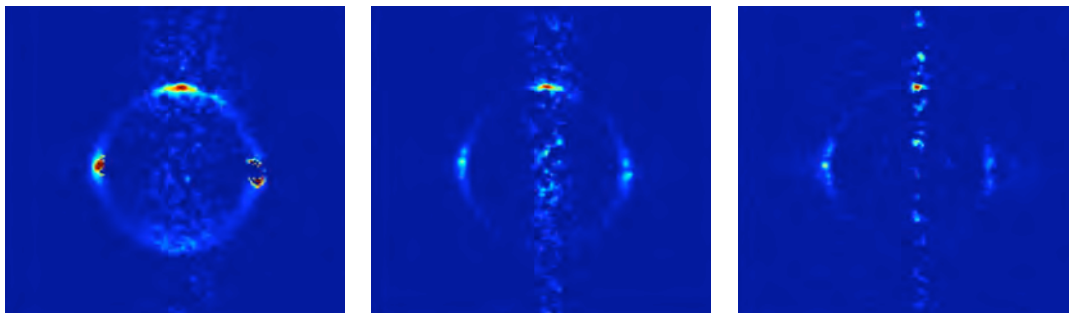


Figure 2: Images of Kr atoms following Kr / Kr scattering. The Kr is tagged and put into a long-lived metastable state (see text). This metastable state is subsequently ionized a short time later. The left most image has a time delay of 400 nsec between lasers. Middle image has time delay of 1 microsecond between laser pulses and the right most image has a 3 microsecond time delay between images.

Inspection of Fig. 2 shows three main features. At early times, left panel of Fig. 2, the parent molecular beams are still within the laser volume and are observed at 0° and 180° (left and right side of image). At this 400 ns delay and the 1 μ s delay (middle panel) an entire elastic scattering sphere is observed as there is elastic scattering of the ground, pre tagging, and the electronically excited metastable atoms, post tagging emanating from both atomic beams. Finally at the top of the images is the sample of milli-Kelvin cold Kr atoms (red color coded spot at 270°). As the time delay is increased the faster moving molecular beam and forward scattered atoms leave the ionization volume of the 266nm beam but the cold molecules remain. This tagging technique can be used for LIF tagging and measuring of flow velocities containing Kr if the quenching of the metastable state is not too severe as there is a “two level” cycling transition associated with this metastable state.

Inspired by the strength of these results, we undertook an investigation into excited-state scattering in molecules. The observation of elastic scattering of Kr atoms in the above experiments 400 ns after excitation implies that molecules in short-lived electronically excited states can undergo sufficient collisions to generate angle-resolved scattering images from which differential cross sections and alignment moments can be easily recovered. The NO(A) state lifetime is about 200 ns, therefore if we excite NO(X) to the NO(A, $j=0$) state within scattering volume and wait 400 ns then $\sim 10\%$ of the NO(A) will survive and some fraction of those molecules will have a collision and change rotational states. After a 400 ns delay the NO(A, $j=5$) molecules are selectively ionizing the by (1 + 1) REMPI through the NO(E) state at ~ 620 nm and those ions are velocity-mapped Ion Imaged. In Fig 3 are images of NO(A, $J=7$) from such an experiment where one beam containing 5%NO in Ar intersects a beam containing Ne. The two images on the left side of the figure were taken with different polarizations of the 620-nm light. The images are different because the NO(A, $j=7$) molecules are aligned by the collision. (Note that our scheme allows us to align the NO(A) molecule before the collision as well!) Because there is absolutely no NO(A, $j=7$) in the parent molecular beam there is no beam spot to subtract out as there was in the earlier NO(X) state scattering. Because of this we can measure the entire

forward scattering differential cross section with no interference and are able to see structure, as predicted, in the Fraunhofer scattering. This work is being done in collaboration with the group of Ken McKendric and Matt Costen (Harriott-Watt Univeristy).

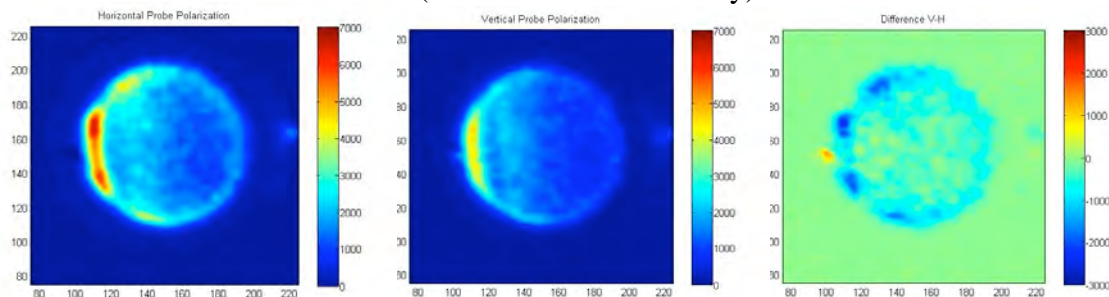


Figure 3: Differential cross section measurements of $\text{NO } A(j=0) + \text{Ar} \rightarrow \text{NO } A(j=7) + \text{Ar}$ where detection is via $1 + 1$ REMPI Through the E state of NO.

Proposed Work:

Over the next funding period we plan on continuing our study of inelastic energy transfer in electronically excited state molecules. The success of the present set of experiments opens the door for several new avenues of investigation. Excitation of a molecule just below its dissociation energy followed by collision induced dissociation and velocity map imaging of the product fragments. Both NO_2 and C_2H_2 are candidate molecules for this kind of study. This study will provide both a direct measure of the entire $P(E, E')$ excitation curve of a dissociating molecule and provide information on a process that is the microscopic reverse of a three body recombination process. Very short ($\sim 10 \mu\text{s}$) molecular beam pulses will be utilized in these new experiments in order for the beams to be highly chirped when scattering. This will significantly improve in velocity resolution for crossed molecular beam experiments.

Publications 2008-2010:

- 1) Cold and Ultracold molecules: Spotlight on Orbiting Resonances, Chandler DW, J Chem. Phys. Vol.132 110901 (2010).
- 2) Differential Cross Sections for Rotational Excitation of ND_3 by Ne, Kay JJ, van de Meerakker SYT, Wade EA, Chandler DW et al., J. Phys. Chem. A Vol. 113 (52) 14800-14806 (2009).
- 3) A compact molecular beam machine, Jansen P, Chandler DW, Strecker KE, Rev. Sci. Instru. Vol. 80 (8) Article Number: 083105 (2009).
- 4) Production of cold ND_3 by kinematic cooling, Kay JJ, van de Meerakker SYT, Strecker KE, Chandler DW et al., Faraday Disc. Vol. 142, 143-153 (2009).
- 5) The kinematic cooling of molecules with laser-cooled atoms, Takase K, Rahn LA, Chandler DW, et al., New J. of Phys. Vol.11 Article Number: 055033(2009).
- 6) Imaging the rotationally state-selected $\text{NO}(A,n)$ product from the predissociation of the A state of the NO-Ar van der Waals cluster Roeterdink WG, Strecker KE, Hayden CC, Chandler DW, et al., J. Chem. Phys. Vol.130 (13) Article Number: 134305 (2009).
- 7) The Quest for Cold and Ultracold Molecules, Chandler DW, Strecker KE, ChemPhysChem Vol 10(5) 751-754 (2009)
- 8) Inelastic Energy Transfer: The NO-rare gas system, David W. Chandler and Steven Stolte, in Gas Phase Molecular Reaction and Photodissociation Dynamics, Editors K. C. Lin and P. D. Kleibert, Transworld Research Network, India. 2008.
- 9) Kinematic Cooling of Molecules, David W. Chandler and Kevin Strecker, in Low Temperature and Cold Molecules by World Scientific, editor IWM Smith. (2008)
- 10) Kinematic production of isolated millikelvin molecules, Strecker KE, Chandler DW, Phys. Rev. A Vol 78(6) Article Number: 063406 (2008).

Petascale Direct Numerical Simulation and Modeling of Turbulent Combustion

Jacqueline H. Chen (PI) and Ed Richardson

Sandia National Laboratories, Livermore, California 94551-0969

Email: jhchen@sandia.gov

Program Scope

In this research program we have developed and applied massively parallel three-dimensional direct numerical simulation (DNS) of building-block, laboratory scale flows that reveal fundamental turbulence-chemistry interactions in combustion. The simulation benchmarks are designed to expose and emphasize the role of particular physical subprocesses in turbulent combustion. The simulations address fundamental science issues associated with chemistry-turbulence interactions that underly all practical combustion devices: extinction and reignition, flame propagation and structure, stratified combustion, flame stabilization in autoignitive flows, flame-wall interactions, and reactive scalar mixing in turbulent jet flames. In addition to the new understanding provided by these simulations, the data have been used to develop and validate predictive models required in engineering simulations.

Recent Progress

With petascale computing the following turbulence-chemistry interactions were amenable to study by DNS and form the basis of the target simulations performed in the past year – an autoignitive lifted ethylene/air turbulent jet flame [19], a reactive turbulent hydrogen jet in crossflow [18], and stratified combustion in turbulent methane/air slot jet flames. The DNS data were used to glean fundamental insight into specific ‘turbulence-chemistry’ interactions and to develop and test RANS and LES models for turbulent combustion [4,6,8,15,20,22,24,26]. The data were also used to aid in the interpretation of measurements by relating scalar statistics obtained from lower-dimensional measurements to those of the true three-dimensional quantity [5,23]. Highlights of our accomplishments in the past year are summarized below, followed by a summary of future research directions.

Stabilization of lifted turbulent ethylene/air jet flames in heated coflow

Direct numerical simulation (DNS) of the near field of three-dimensional spatially-developing turbulent ethylene [19] jet flames in highly-heated coflow was performed with a reduced mechanism to investigate the stabilization mechanism. The DNS was performed at a jet Reynolds number of 10,000 with over 1.29 billion grid points. The results showed that auto-ignition in a fuel-lean mixture at the flame base is the main source of stabilization of the lifted jet flame. This is verified by employing chemical explosive mode (CEM) analysis [12,25] as a diagnostic to unambiguously identify the spatial and temporal boundaries ignition, flame regions and the lifted stabilization point in the DNS of the jet flame. A chemical explosive mode (CEM) is the eigenmode associated with a positive eigenvalue of the Jacobian of the chemical source term. A reactive mixture in the presence of a CEM is intrinsically explosive and otherwise non-explosive, and can be correspondingly classified as unburned and burned, respectively. In spatially non-homogeneous systems, the competition between CEM and loss can be approximately quantified with a Damköhler number, Da , the ratio of the chemical time scale to a diffusive loss time scale, where the scalar dissipation rate is taken as a reciprocal time scale of diffusive loss. A mixture with $Da \gg 1$ indicates a dominant CEM that will likely result in actual ignition; otherwise ignition may be suppressed as the CEM is strongly strained.

Figure 1a shows the time scales of CEM in a spanwise slice of the DNS data, with unburned highly explosive mixtures shown in red and burned mixtures in blue. The transition layer between the burned (red) and unburned (blue) mixtures in Fig. 1a is therefore a (partially) premixed flame front, as discussed in [12,25]. Highly explosive mixtures precede the premixed flames. Consequently, this suggests that auto-ignition may be a dominant flame stabilization mechanism in this flame. To further verify this point, Fig. 1b shows the spatial distribution of the Damköhler number where a large positive Da , shown in red hues, indicates that the CEM dominates transport such that the mixture is autoigniting. A large negative Da , shown in blue hues, indicates a fast reacting burned mixture, whose overall progression can be limited by the slower transport. As such, the dark blue zones in Fig. 1b contain the diffusion flame kernels, and ignition in portions of the high speed fuel rich central fuel jet is suppressed. Two strips of

auto-igniting mixtures upstream of the lifted flame can be clearly seen in Fig. 1b resulting in islands of ignited mixtures disconnected from the lifted flame. Therefore, this result confirms that auto-ignition is a dominant factor, leading to the burned regions downstream of the stabilization points.

Figure 1c shows the controlling variables, temperature and species concentrations, in different regions of the lifted jet flame as identified by the explosion index **EI** [12,25]. The figure is colored with the average of selected variables, namely temperature (red), HO₂(green), O (blue), CH₃ (yellow), OH (magenta), CO (cyan), and CH₃CHO (gray), weighted by the local Damköhler number on a logarithmic scale. It is seen that while O and OH control the auto-igniting layers close to the heated coflow, temperature and HO₂ control various ignition zones near the jet center. Furthermore, CO and CH₃CHO are the controlling species in the post flame zones of premixed flames and the diffusion flame kernels downstream.

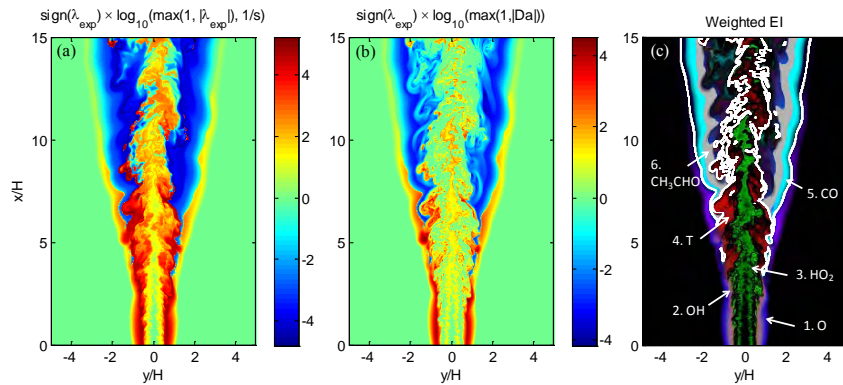


Figure 1. Structure of the lifted ethylene jet flame in a heated air coflow, obtained by CEMA (a) time scales of CEM or the decaying mode evolved from a CEM. Red hues indicate unburned mixture ($\lambda_{exp} > 0$) and blue indicates burned mixture ($\lambda_{exp} < 0$); (b) isocontour of Da , with red indicating auto-igniting zones and blue indicating the diffusion flame zone; (c) controlling variables, temperature and species, identified by explosion index [12,25], weighted locally by normalized Da . The white isocontour shows the partially premixed flame fronts, where $\lambda_{exp} = 0$, identified in (a).

In addition to auto-ignition, Lagrangian tracking of the flame base [19] revealed the passage of large-scale flow structures and their correlation with the fluctuations of the flame base similar to lifted hydrogen/air jet flames in [11]. It is observed that the present ethylene lifted flame base exhibits a cyclic ‘saw-tooth’ shaped movement marked by rapid movement upstream followed by a slower movement downstream. This is a consequence of the lifted flame being stabilized by a balance between consecutive auto-ignition events in hot fuel-lean mixtures and convection induced by the high speed jet and coflow velocities.

Reactive Transverse Fuel Jets-In-Crossflow (JICF)

A reactive transverse fuel jet in cross-flow (JICF) configuration is studied using three-dimensional direct numerical simulation (DNS) with detailed chemical kinetics in order to investigate the mechanism of flame stabilization in the near field of a fuel jet nozzle [18]. JICF configurations are used in practical applications where high mixing rates are desirable between the jet and the crossflow fluids. Classical applications of JICF configurations are fuel injection nozzles and dilution holes in gas turbine combustors. This study examines the case of a nitrogen-diluted hydrogen transverse jet exiting a nozzle perpendicularly into a cross-flow of heated air. Improved understanding of the flame stabilization mechanism acting downstream of the transverse fuel jet will enable the formulation of more reliable guidelines for design of fuel injection nozzles characterized by minimal flame holding behavior and intrinsic flashback safety. Results show that the flame is stabilized on the downstream side of the fuel jet at the location of the vortex shedding generated by the jet shear layer. The core of the heat release is located near the trailing edge of the fuel jet, at approximately 4 nozzle diameters away from the wall, and is characterized by the simultaneous occurrence of locally stoichiometric reactants and low flow

velocities in the mean. Instantaneously, upstream flame movement is observed through propagation into the outer layers of jet vortices. Downstream of the stabilization region there is significant penetration of small vortices into the flame, and hence combustion occurs in the thin and broken reaction zones regimes.

DNS of turbulent stratified methane-air slot jet flame

DNS of a turbulent stratified methane-air slot jet flame was performed with a reduced methane-air mechanism to provide understanding of the stratified combustion regime. The benchmark simulation data resulting from this study provides a unique test-bed for predictive engineering models in the challenging partially-premixed regime. As the initial fuel-air stratification dissipates due to turbulent mixing, the flames are subjected to steep, time varying equivalence ratio gradients. Locations where the equivalence ratio gradients align normal to the flame exhibit greatly modified burning rates and flame propagation speeds, S_d compared to the perfectly premixed case. Variation of the propagation speed with the flame normal equivalence ratio gradient, indicates enhanced flame speeds when the products are richer than the reactants, with the reverse also true. Studying this effect using computations of strained one-dimensional counterflow flames in the presence of equivalence ratio gradients [17] revealed the thermo-chemical basis for this observation. Specifically, equivalence ratio gradients resulting in flames with richer, higher temperature products lead to enhanced equilibrium concentrations of species such as the hydroxyl radical in the flame's carbon monoxide-hydrogen recombination layer. Diffusion of these highly reactive intermediate species towards the reactant side of the flame, as opposed to thermal diffusion, is the main source of the increased reaction rate.

Future Plans

DNS Parameter Studies: Effects of Momentum Ratio, Injection Angle, Nozzle Shape, and Fuel on Flame Stabilization in a Reactive Fuel Jet in Crossflow (JICF)

Extending our JICF research we plan to perform parametric studies to investigate the effects of varying the momentum ratio between the transverse jet and the cross flow, the shape of the nozzle (i.e. circular, square, or elliptical cross-sections), the angle of injection, and the thickness of the approaching cross-flow boundary layer on the flow and reactive scalar mixing fields. We are especially interested in these effects on flame anchoring mechanisms relevant to stationary gas turbines for power generation. A further parameter we plan to vary is the fuel itself, e.g., ethylene, syngas (CO+H₂ blend), or di-methyl ether, could provide insight into how switching the fuel to the off-gas from a solid oxide fuel cell or operating on biofuels could influence the combustion process, and especially flame anchoring and flashback.

Effect of Turbulent Velocity in Scalar Transport in Reactive Fuel Jets in Crossflow

To obtain a better understanding of the large-scale properties of the velocity, scalar mixing, and reaction rates in the crossflowing fuel jet flame and their coupling, we propose to analyze scalar-velocity statistics in the natural coordinate system of the JICF, i.e. we will determine the jet centerline trajectory, the jet width in terms of the jet centerline coordinate, and the velocity and scalar concentration decay in this jet trajectory coordinate system. Averages and co-variances of various turbulence quantities including the velocity, mixture fraction and progress variable terms will be extracted along the trajectory-normal coordinate as a function of downstream position. Specifically, the scalar flux components that represent the unresolved terms in the Reynolds-averaged scalar transport equation will be obtained. Regions in the JICF exhibiting gradient diffusion will be distinguished from those exhibiting counter-gradient scalar diffusion. Modeling implications of gradient and counter-gradient scalar transport in reactive scalar mixing in JICF will also be explored. Another quantity of direct relevance to models for stratified combustion is the filtered density function for the mixture fraction and partially premixed progress variable c . We propose to extract these quantities from the DNS at several different LES filter scales, compare to traditional functional forms used for approximation, and explore modeling implications.

BES Publications (2008-2010)

1. D. Lignell, J. H. Chen, and P. J. Smith, "Three-dimensional DNS of Soot Formation and Transport in a Temporally-Evolving Non-premixed Ethylene Jet Flame," *Combust. Flame* 155:316-333 (2008).

2. C. S. Yoo, J. H. Chen, J. H. Frank, "A Numerical Study of Transient Ignition and Flame Characteristics of Diluted Hydrogen Versus Heated Air in Counterflow," *Combust. Flame* **156**(1) 140-151 (2009).
3. N. Chakraborty, E. R. Hawkes, J. H. Chen, and S. Cant, "The Effects of Strain Rate and Curvature on Surface Density Function Transport in Turbulent Premixed Methane-Air and Hydrogen-Air Flames: A Comparative Study," *Combust. Flame* **126**(3):1617-1629 (2008).
4. F. Bisetti, J. Y. Chen, E. R. Hawkes, and J. H. Chen, "Probability Density Function Treatment of Turbulence-Chemistry Interactions during the Ignition of a Temperature-Stratified Mixture for Application to HCCI Engine Modeling," *Combust. Flame* **155**(4):571-584 (2008).
5. E. R. Hawkes, R. Sankaran, J. H. Chen, S. Kaiser, and J. H. Frank, "An Analysis of Lower-Dimensional Approximations to the Scalar Dissipation Rate using DNS of Flame Jet Flames," *Proc. Combust. Inst.*, **32**(1):1455-1463 (2009).
6. E. S. Richardson, C. S. Yoo, and J. H. Chen, "Analysis of Second-Order Conditional Moment Closure Applied to an Autoignitive Lifted Hydrogen Jet Flame," *Proc. Combust. Inst.*, **32**(2):1695-1703 (2009).
7. U. D. Lee, C. S. Yoo, J. H. Chen, and J. H. Frank, "Effects of H₂O and NO on Extinction and Reignition of Vortex-Perturbed Hydrogen Counterflow Flames," *Proc. Combust. Inst.*, **32**(1): 1059-1066 (2009).
8. D. Lignell, J. C. Hewson, and J. H. Chen, "A priori Analysis of Conditional Moment Closure Modeling of a Temporal Ethylene Jet Flame with Soot Formation using DNS," *Proc. Combust. Inst.*, **32**(1):1491-1498 (2009).
9. F. Bisetti, J. Y. Chen, E. Hawkes, and J. H. Chen, "Differential Diffusion Effects During Ignition of a Thermally Stratified H₂/Air Mixture Subject to Turbulence," *Proc. Combust. Inst.*, **32**(1): 1465-1472 (2009).
10. T. Lu, C. K. Law, C. S. Yoo, and J. H. Chen "Dynamic Stiffness Removal for Direct Numerical Simulation," *Combust. Flame*, **156**(8):1542-1551 (2009).
11. C. S. Yoo, R. Sankaran, and J. H. Chen "3D Direct Numerical Simulation of a Turbulent Lifted Hydrogen/Air Jet Flame in Heated Coflow: Stabilization and Structure," *J. Fluid Mech.* **460**:453-481 (2010).
12. T. Lu, C. S. Yoo, J. H. Chen, and C. K. Law, "3D Direct Numerical Simulation of a Turbulent Lifted Hydrogen/Air Jet Flame in Heated Coflow: Explosive Mode Analysis," in press, *J. Fluid Mech.* (2009).
13. A. Gruber, R. Sankaran, E. R. Hawkes and J. H. Chen, "A Flame-Wall Interaction: A DNS Study," in press, *J. Fluid Mech.* (2010).
14. U. Lee, C. S. Yoo, J. H. Chen, J. H. Frank, "Effect of NO on Extinction and Reignition of Vortex-Perturbed Hydrogen Flames," *Combust. Flame* **157**(2): 217-229 (2010).
15. E. S. Richardson, R. Sankaran, R. W. Grout, and J. H. Chen, "Numerical Analysis of Reaction-Diffusion Effects in Turbulent Premixed Methane-Air Combustion," *Combust. Flame* **157**:506-515 (2010).
16. J. H. Chen, A. Choudhary, B. de Supinski, M. DeVries, E. R. Hawkes, S. Klasky, W. K. Liao, K. L. Ma, J. Mellor-Crummey, N. Podhorszki, R. Sankaran, S. Shende, C. S. Yoo, *Comput. Sci. Disc.* **2** (2009) 015001.
17. E. S. Richardson, V. E. Granet, A. Eyssartier, and J. H. Chen, "Effects of Equivalence Ratio Variation on Lean, Stratified Methane-Air Laminar Counterflow Flames," in press *Combust. Theory and Modelling* (2009).
18. R. W. Grout, A. Gruber, J. H. Chen and C. S. Yoo, "Direct Numerical Simulation of Flame Stabilization Downstream of a Transverse Fuel Jet in Cross-Flow," submitted to *Proc. Combust. Inst.*
19. C. S. Yoo, E. S. Richardson, R. Sankaran, and J. H. Chen, "A DNS Study of the Stabilization Mechanism of a Turbulent Lifted Ethylene Jet Flame in Highly-Heated Coflow," submitted to *Proc. Combust. Inst.* (2009).
20. E. R. Hawkes, O. Chatakonda, R. Sankaran, O. Colin and J. H. Chen, "An Algebraic Flame Surface Density Model for LES in the Thin Reaction Zones Regime," submitted to *Proc. Combust. Inst.* (2009).
21. L. Wang, E. R. Hawkes, and J. H. Chen, "Flame Edge Statistics in Turbulent Combustion," submitted to *Proc. Combust. Inst.* (2009).
22. R. S. Cant, O. Chatakonda, R. Sankaran, R. W. Grout, J. H. Chen, and E. R. Hawkes, "DNS of Flame Surface Density Transport in Turbulent Bunsen Flames," submitted to *Proceedings Proc. Combust. Inst.* (2009).
23. E. R. Hawkes, R. Sankaran, and J. H. Chen, "Estimates of the 3D Flame Surface Density and All Terms in its Transport Equation from 2D Measurements," submitted to *Proc. Combust. Inst.* (2009).
24. N. P. unati, J. C. Sutherland, A. R. Kerstein, E. R. Hawkes, and J. H. Chen, "An Evaluation of the One-Dimensional Turbulence Model: Comparison with Direct Numerical Simulations of CO/H₂ Jets with Extinction and Reignition," submitted to *Proc. Combust. Inst.* (2009).
25. T. Lu, C. S. Yoo, E. S. Richardson and J. H. Chen, "Chemical Explosive Mode Analysis for a Turbulent Lifted Ethylene Jet Flame in Heated Coflow," submitted to *Proc. Combust. Inst.* (2009).
26. E. S. Richardson and J. H. Chen, "Application of the Euclidian Minimum Spanning Tree Mixing Model to Premixed Flames with Differential Diffusion," submitted to *Combust. Flame* (2010).

Dynamics and Energetics of Elementary Combustion Reactions and Transient Species

Grant DE-FG03-98ER14879

Robert E. Continetti
Department of Chemistry and Biochemistry
University of California San Diego
9500 Gilman Drive
La Jolla, CA 92093-0340
rcontinetti@ucsd.edu

I. Program Scope

This research program examines the energetics and dynamics of transient neutral species and collision complexes relevant to combustion phenomena. The experimental approach used in these studies involves measurement of the photodetachment and dissociative photodetachment (DPD) of negative ion precursors of important neutral combustion intermediates. This year we have achieved an important technological advance in the experiments, with the successful commissioning of a cryogenically cooled linear electrostatic ion trap that allows the preparation of the precursor negative ions with well-characterized internal temperatures and also allows us to use for the first time high-intensity low-duty-cycle ion sources in these high-repetition-rate coincidence experiments. This development has allowed us to reexamine the DPD of cooled HOCO^- at 388 nm, probing the stability of the HOCO free radical and the potential energy surface that governs the $\text{OH} + \text{CO} \rightarrow \text{H} + \text{CO}_2$ reaction without uncertainties resulting from vibrationally excited HOCO^- in the beam.^{1,2,3,4}

Integration of the trap with the photoelectron-photofragment coincidence (PPC) spectrometer is a major advance. Both the sensitivity and resolution of the new trap are *higher* than the old single-pass configuration of the spectrometer. While we would have preferred to have more published results to date, this important experimental advance has been worth the effort in our view, and will allow us to now more accurately extend these studies to larger oxygenated radicals and other systems, including the larger carboxyl radicals that were initiated in the first year of the current grant. Our goal remains the determination of the energetics and reaction dynamics of these important combustion intermediates, allowing more quantitative evaluation of their roles in combustion and validation of theoretical approaches to predicting the dynamics of combustion reactions. In the following sections, the experimental advances will be reviewed, followed by the new results on the HOCO system and future plans.

II. Recent Progress

A. Cryogenically cooled linear electrostatic ion beam trap

The cryogenically cooled electrostatic ion beam trap (EIBT) is now fully functional, allowing measurements, *in coincidence*, of atomic and molecular neutral products along with photodetached electrons from trapped, cooled ions bunched and synchronized with a Ti:Sapphire regenerative amplifier. The trap consists of two electrostatic mirrors that reflect bunches of ions along a central axis, analogous to an optical resonator.⁵ Ions oscillating in the trap have well-defined momenta, which makes it ideal for the PPC experiments. By storing ions from an inherently colder low-repetition rate source in a cold, ultrahigh vacuum environment where they can continue to cool radiatively, this method provides cooled ions but maintains the high duty cycle required for coincidence experiments. Since the center of this type of trap is essentially field free, a velocity map imaging electron detector is placed intracavity allowing detached electrons to be collected in coincidence with the resultant neutral particles which continue along the center-of-mass trajectory out of the trap. All products are collected on an event-by-event

basis as before using time- and position-sensitive detectors for a full kinematic reconstruction of the DPD event.⁶ In fact, a range of masses can be trapped, and recording photoelectron spectra in coincidence with the neutral products under these conditions allows for the simultaneous acquisition and separation of photoelectron spectra for many different anions.

Currently 7 keV ion beams are trapped at a pressure of 7×10^{-11} torr, giving trapping I/e lifetimes well in excess of one second, although there is a trade-off between beam divergence and trapping lifetime. With a ~ 1 V pk-pk RF waveform phase-locked to the master oscillator of the laser system, the ions can be bunched to 50 – 200 ns width and synchronized to the laser with an RMS jitter of ~ 10 . This is essential, as the coincidence experiment requires photodetachment of the ions when they are heading towards the multiparticle neutral detector. A small DC repulsion and correction field in the center of the trap allows orthogonal extraction of electrons to the intracavity electron detector. Calibration by O_2^- photodetachment has shown an electron kinetic energy (eKE) resolution of $\Delta(\text{eKE})/\text{eKE} \leq 4\%$. Photoelectron images reveal a strong Doppler shift for poor bunching and synchronization, allowing quick tuning of the system.

B. Probing the $\text{OH} + \text{CO} \rightarrow \text{HOCO} \rightarrow \text{H} + \text{CO}_2$ reaction by photodetachment of HOCO^-

In earlier studies we have used the photodetachment and DPD of HOCO^- to probe the potential energy surface that governs the $\text{OH} + \text{CO} \rightarrow \text{HOCO} \rightarrow \text{H} + \text{CO}_2$ reaction, low lying excited states of HOCO, novel resonance-mediated two-photon photodetachment processes and recoil-frame photoelectron angular distributions for the DPD of HOCO^- . As discussed above, however, the energy partitioning in the DPD of HOCO^- to $\text{OH} + \text{CO}$ in particular was either inconsistent with the relatively well known thermochemistry of OH, CO, H and CO_2 or a result of vibrationally excited anions. The $\text{H} + \text{CO}_2$ channel, in addition was seen in this earlier work to be operative below the calculated barriers for dissociation,⁷ consistent with a tunneling process or vibrational excitation in the parent anions. It is in this context that we have revisited this question with the cryogenic EIBT.

The new results show significant quantitative differences from earlier work primarily due to the removal of hot bands from the photoelectron spectra for the product channels: $\text{HOCO} + e^-$, $\text{H} + \text{CO}_2 + e^-$ and $\text{OH} + \text{CO} + e^-$. Additionally, as a result of the higher spectral resolution, these new results further constrain the mechanism for the poorly understood $\text{H} + \text{CO}_2$ exit channel,

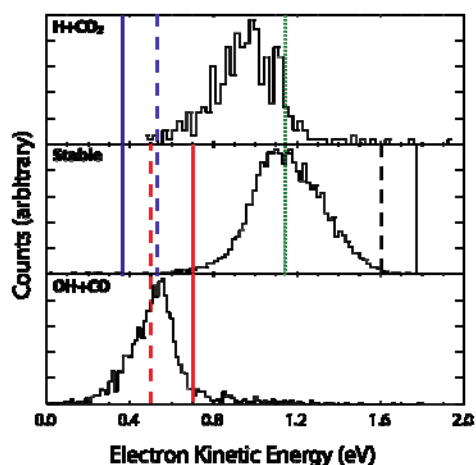


Figure 1. Channel-resolved photoelectron spectra. (a) $\text{H} + \text{CO}_2 + e^-$, (b) $\text{HOCO} + e^-$, (c) $\text{OH} + \text{CO} + e^-$. Dashed (solid) lines represent maximum predicted eKE for *cis*- (*trans*-) isomers. The dotted line is maximum eKE for dissociation through C-HCO₂.

suggesting a new possible explanation for dissociation of HOCO to $\text{H} + \text{CO}_2$ well below the calculated barrier to dissociation from the *cis*-HOCO well. Figure 1 summarizes the observed photoelectron spectra for each product channel. As opposed to the earlier data, three distinct regions of the photoelectron spectrum now become apparent, each corresponding to a specific process on the HOCO potential energy surface. The photoelectron spectrum obtained from events leading to stable HOCO neutrals is shown in Figure 1(b), with maximum predicted electron kinetic energies (eKEs) shown for detachment of HOCO^- . Clearly all photoelectrons in this spectrum fall below the predicted maxima, while the earlier results revealed photoelectrons more than 0.2 eV beyond these limits, providing strong evidence for ion precursors with significantly lower internal energy in this experiment. For dissociation to $\text{H} + \text{CO}_2$, shown in Figure 1(a), nearly all photoelectrons occur above the maximum expected eKE, consistent with earlier observations that all

dissociation to $\text{H}+\text{CO}_2$ limit occurs *below* the calculated barrier for $\text{cis-HOCO} \rightarrow \text{H} + \text{CO}_2$. This spectrum too shows an overall shift towards lower eKE of more than 0.2 eV due to the cooled precursor anions. Finally, the photoelectron spectrum for dissociation to $\text{OH}+\text{CO}$ in Figure 1(c) exhibits significant narrowing and a shift of more than 0.5 eV from previous data.

One major outstanding question is the relative contribution of *cis*- and *trans*-isomers to the overall dynamics on the HOCO surface. In the $\text{OH} + \text{CO}$ channel the majority of the photoelectrons detected lie above the calculated barrier from the *cis*-HOCO well but below that for *trans*-HOCO, providing strong evidence that this process is dominated by dissociation from *trans*-HOCO. In the case of detachment to stable HOCO, all photoelectrons occur below the limits for either isomer. While the observed maximum eKE agrees well with the predicted maximum eKE for detachment from *cis*-HOCO, Franck-Condon calculations and measurements closer to the photodetachment threshold should help resolve this discrepancy.

More detailed dynamical information can be extracted from the coincidence spectra for the $\text{H}+\text{CO}_2$ and $\text{OH}+\text{CO}$ channels. Figure 2(a) shows the spectrum for dissociation to $\text{OH}+\text{CO}$ fragments, with a pair of diagonal lines representing the predicted total energy release ($E_{\text{TOT}} = \text{eKE} + \text{KER}$) for *cis*- and *trans*-HOCO⁻ isomers. These results also lie below the predicted maximum E_{TOT} as expected in the case of cold ions. This spectrum is dominated by a narrow diagonal feature with FWHM of less than 0.1 eV. No vibrational excitation in either the OH or CO products is observed, and the width of this peak approaches experimental resolution implying low rotational excitation. Since the primary geometric difference between the anion and neutral species in either isomer is elongation of the central O-C bond, this channel is likely driven primarily by the O-C stretching mode.

Figure 2(b) shows the spectrum for dissociation to $\text{H}+\text{CO}_2$, truncated at $\text{KER} < 0.2$ eV to reduce the number of false coincidences caused by the large disparity in product masses. The diagonal lines in this spectrum again represent the predicted maximum E_{TOT} for each anion isomer, and again nearly all data falls below these limits. In this channel the diagonal band is quite broad, > 0.5 eV, indicating a high level of internal excitation in the CO_2 product. All dissociation is seen to occur above the limits for both isomers, however there appears to be a kink in the diagonal band in the range of 1.1 – 1.2 eV which results in a horizontal feature towards low KER. This feature correlates energetically with the energy of the C_{2v} HCO_2 isomer on the neutral surface, suggesting the detachment of HOCO^- to HOCO is followed by isomerization to HCO_2 prior to dissociation to $\text{H}+\text{CO}_2$, an alternative to direct tunneling through the dissociation barrier from the *cis*-HOCO isomer. Once again, however, the calculated barrier to this isomerization is much higher and would also require a tunneling mechanism given the calculated energetics.

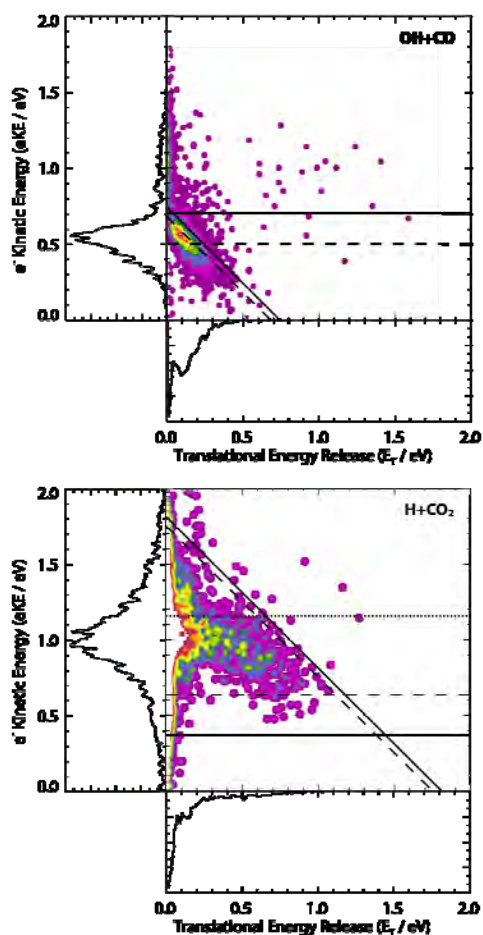


Figure 2. PPC spectra. (a) $\text{OH} + \text{CO} + \text{e}^-$ (b) $\text{H} + \text{CO}_2 + \text{e}^-$. Horizontal lines represent barrier heights, while diagonal lines represent maximum E_{TOT} values.

The three mechanisms inferred here involve three distinct regions in the HOCO potential energy surface, the lowest of which leads exclusively to stable HOCO. However it is interesting to note that while the next

highest region leads almost exclusively to H+CO₂, the highest region leads almost exclusively to OH+CO even though both channels are energetically allowed. Once the OH + CO channel opens, it dominates the decomposition dynamics, inconsistent with the RRKM calculations reported in conjunction with the six-dimensional quantum dynamics simulations of the DPD of HOCO⁻ by Gray, Goldfield and co-workers.⁸ Also, these simulations did not predict the observed production of H + CO₂ at lower energies in the HOCO well. These new results resolve experimental uncertainties and point anew to the need for a more refined global potential energy surface for this fundamental combustion reaction.

III. Future plans

We are now prepared to study the photodetachment and the two-photon DPD of HOCO⁻ at 775 nm to better determine the electron affinity and examine the population of HOCO⁻ isomers in the ion beam. Two-photon photodetachment opens up the possibility of examining interference phenomena and controlling the product branching ratio. We are now in a position to pursue completion of our studies of the carboxyl radicals and reaction complexes involving the hydroxyl radical with polyatomic molecules starting with ionic complexes such as OH⁻(CH₃) ↔ O⁻(CH₄). We are also collaborating with the Sandia CRF on the examination of energy transfer in complexes like CH₃O₂ – Ar, where a detailed understanding is essential to explain pressure-dependent phenomena in combustion. A project to develop a new multiparticle detector is also well underway. Finally, the integration of the new trap with the PPC spectrometer opens up new vistas. Low-duty cycle ion sources, coupled with accumulator traps will now be usable, including laser-desorption ionization, electrospray, and even aerosol sources. In addition, with trapped ions, experiments involving vibrational excitation and photoisomerization of the anion precursors will now be feasible with new light sources in the laboratory. This is a time of exciting opportunities for the use of negative ion precursors to study combustion phenomena.

IV. DOE Publications: 2007 – 2010

1. Z. Lu, Q. Hu, J.E. Oakman and R.E. Continetti, “Dynamics on the HOCO potential energy surface studied by dissociative photodetachment of HOCO⁻ and DOCO⁻.”, *J. Chem. Phys.* **126**, 194305-1 – 194305-11 (2007).
2. Z. Lu and R.E. Continetti, “Alignment of a molecular anion via a shape resonance in near-threshold photodetachment.”, *Phys. Rev. Lett.* **99**, 113005-1 – 113005-4 (2007).
3. Z. Lu, J.E. Oakman, Q. Hu and R.E. Continetti, “Photoelectron-photofragment angular correlations in the dissociative photodetachment of HOCO⁻.”, *Molec. Phys.* **106**, 595-606 (2008).
4. C.J. Johnson and R.E. Continetti, “Dissociative Photodetachment of Cold HOCO⁻ and below-barrier dissociation to H+CO₂.”, submitted to *J. Phys. Chem. Lett.* (2010).

References Cited

-
1. T.G. Clements, R.E. Continetti and J.S. Francisco, *J. Chem. Phys.* **117**, 6478 (2002).
 2. Z. Lu, Q. Hu, J. E. Oakman, and R. E. Continetti, *J. Chem. Phys.* **126**, 19305 (2007).
 3. Z. Lu and R.E. Continetti, *Phys. Rev. Lett.* **99**, 113005 (2007).
 4. Z. Lu, J.E. Oakman, Q. Hu and R.E. Continetti, *Molec. Phys.* **106**, 595 (2008).
 5. M. Dahan, R. Fishman, O. Heber, M. Rappaport, N. Altstein, D. Zajfman, and W. J. van der Zande, *Rev. Sci. Instrum.* **69**, 76 (1998).
 6. K.A. Hanold, A.K. Luong, T.G. Clements, and R.E. Continetti, *Rev. Sci. Instr.* **70**, 2268 (1999).
 7. H.-G. Yu, J.T. Muckerman and T. Sears, *Chem. Phys. Lett.* **349**, 547 (2001).
 8. S. Zhang, D. M. Medvedev, E. M. Goldfield, and S. K. Gray, *J. Chem. Phys.* **125**, 164312 (2006).

Studies of the Chemistry of Oxygenated Fuels with Photoionization Mass Spectrometry

Terrill A. Cool
School of Applied and Engineering Physics
Cornell University, Ithaca, New York 14853
tac13@cornell.edu

I. Project Scope

Clean-burning renewable oxygenated bio-derived fuels are potentially important replacements for conventional gasoline and diesel fuels, which may reduce dependence on imported petroleum and lower net greenhouse-gas emissions. Our current research focuses on the chemistry of 13 simple methyl and ethyl esters chosen as surrogates for the long-chain esters that are primary constituents of biodiesel fuels. Principal goals of these studies are: (1) show how fuel-specific structural differences including degree of unsaturation, linear vs branched chain structures, and methoxy vs ethoxy functions affect fuel-destruction pathways, (2) understand the chemistry leading to potential increases in the emissions of hazardous air pollutants including aldehydes and ketones inherent in the use of biodiesel fuels, and (3) define the key chemical reaction mechanisms responsible for observed reductions in polycyclic aromatic hydrocarbons and particulate matter when oxygenated fuels are used as replacements for conventional fuels. Experimental measurements of the composition of reaction intermediates for each of the 13 selected model compounds, performed with flame-sampling molecular-beam synchrotron photoionization mass spectrometry, combined with comprehensive kinetic modeling, are key steps toward predictive descriptions of the combustion of practical biodiesel fuels.

II. Recent Progress

A. Fuel-Specific Influences on the Composition of Reaction Intermediates in Premixed Flames of Three $C_5H_{10}O_2$ Ester Isomers. Bin Yang, Terrill A. Cool, Charles K. Westbrook, Nils Hansen, Katharina Kohse-Höinghaus.

Measurements of the composition of reaction intermediates in low-pressure premixed flames of three simple esters, the methyl butanoate (MB), methyl isobutanoate (MIB), and ethyl propanoate (EP) isomers of $C_5H_{10}O_2$, enable further refinement and validation of a detailed chemical reaction mechanism originally developed with modeling studies of similar flames of methyl formate, methyl acetate, ethyl formate, and ethyl acetate [1]. Photoionization mass spectrometry (PIMS), using monochromated synchrotron radiation, reveals significant differences in the compositions of key reaction intermediates between flames of the MB, MIB, and EP isomers studied under identical flame conditions. Detailed kinetic modeling describes how these differences are related to molecular structures leading to unique fuel destruction pathways for each of these isomers. Despite the simple structures of these small esters, they contain structural functional groups expected to account for fuel-specific effects observed in the combustion of practical biodiesel fuels. The good agreement between experimental measurements and detailed reaction mechanisms applicable to these simple esters demonstrates that major features of each flame can be predicted with reasonable accuracy by building a hierarchical reaction mechanism based on three factors: 1) unimolecular decomposition of the

fuel, especially by complex bond fissions; 2) H-atom abstraction reactions followed by β -scission of the resulting radicals leads to nearly all of the observed intermediate species detected experimentally in each flame; 3) the rates of these H-atom abstraction reactions are effectively the same for each distinct type of terminal alkyl radical group (i.e., methoxy, ethoxy, methyl, ethyl, propyl) for ester fuels with comparable structural groups.

B. Absolute Cross-Sections for Dissociative Photoionization of Some Small Esters. Juan Wang, Bin Yang, Terrill A. Cool, Nils Hansen

Absolute cross-sections for molecular and dissociative photoionization are needed for quantitative flame-sampling molecular beam PIMS studies of the flame chemistry of ester fuels. Dissociative ionization of several small esters has been extensively studied by several groups, using a full range of experimental techniques. These studies have focused on the measurement of appearance energies for photofragment ions, the structural identities of these fragments and the dynamic mechanisms responsible for their formation. Dissociative ionization channels often arise from complex isomerization processes in competition with direct bond scission of the parent molecular ion.

Despite considerable interest in these intrinsic features of dissociative photoionization of esters, absolute photoionization cross-sections have been reported for only methyl and ethyl acetate [2]. We have now completed measurements of absolute cross-sections for near-threshold molecular and dissociative photoionization for 11 additional small esters (methyl formate, ethyl formate, vinyl acetate, methyl propanoate, ethyl propanoate, methyl butanoate, methyl isobutanoate, methyl propenoate, ethyl propenoate, methyl crotonate, methyl methacrylate) [3]. The cross-sections for these esters exhibit qualitative features similar to those found for simple alkanes. Their total photoionization cross-sections rise gradually from threshold in a quasi-linear fashion, with major contributions from numerous dissociative ionization channels. The parent ion cross-sections rise to plateaus at photon energies coincident with the onset of dissociative photoionization (typically ≈ 0.5 - 0.8 eV above threshold), which extend to the 11.75 eV limit of the present studies.

An extensive literature exploring isomerization/dissociation mechanisms is available for six of these molecules. However, dissociative ionization of ethyl propanoate has received scant attention and no previous observations of dissociative ionization are available for four simple monounsaturated esters: methyl propanoate, ethyl propanoate, methyl crotonate, and methyl methacrylate. We have measured appearance energies and have made tentative identifications of dissociative photoionization products for these five molecules, although definitive studies of dissociation mechanisms with a variety of experimental techniques are clearly needed. Indeed, the appearance of numerous pathways for dissociative photoionization at photon energies just above the adiabatic ionization energies for these molecules makes them interesting candidates for detailed studies of isomerization/dissociation mechanisms.

III. Future Plans

To date, we have completed experimental measurements and data analysis for 13 simple ester fuels. Kinetic modeling is complete for 7 of these. During the next few months modeling will be completed for the remaining 6 fuels (methyl crotonate, ethyl propanoate, methyl methacrylate, methyl propenoate, vinyl acetate, and methyl propanoate).

We propose to use flame-sampling synchrotron PIMS to validate and refine current kinetic models for the combustion of dimethoxymethane, $\text{C}_3\text{H}_8\text{O}_2$, and dimethyl carbonate, $\text{C}_3\text{H}_6\text{O}_3$. Measurements of the composition of reaction intermediates reveal the influences of fuel destruction mechanisms. Detailed kinetic modeling, accounting for these influences, identifies these fuel-specific decomposition processes and yields rate constant estimates for key reaction steps.

A primary goal of the proposed research is the study of flames of DMM, DMC and blended DMM/ethane and DMC/ethane oxygenate/hydrocarbon flames. Our approach may permit the first measurements of the concentrations of several key radicals in the pool of reaction intermediates. Two radicals, methoxy, CH_3O , and methoxy formyl, $(\text{C}=\text{O})\text{OCH}_3$, are prime targets of the proposed studies. The unimolecular decompositions



are important components of the fuel-destruction pathways for DMM and DMC and all methyl esters. *Ab initio* studies of these reactions by Good and Francisco [4], Butler and coworkers [5], and recent experimental measurements of Glaude et al. [6] for DMC show that reaction (1) is strongly favored over reaction (2). The proposed experimental and modeling studies should provide quantitative determinations of the influences of these reactions in the destruction of DMM and DMC.

The principal investigator also plans to work with Nils Hansen of the Sandia CRF to improve the resolution of the mass spectrometer and resolve present uncertainties in the identification of reaction intermediates of key importance in determinations of detailed reaction pathways.

References

1. C. K. Westbrook, W. J. Pitz, P. R. Westmoreland, F. L. Dryer, M. Chaos, P. Obwald, K. Kohse-Höinghaus, T. A. Cool, J. Wang, B. Yang, N. Hansen, T. Kasper, "A Detailed Chemical Kinetic Mechanism for Oxidation of Four Small Alkyl Esters in Laminar Premixed Flames", *Proc. Combust. Inst.*, **2009**, 32, 221-228.
2. J. Wang, B. Yang, T. A. Cool, N. Hansen and T. Kasper, "Near-threshold Absolute Photoionization Cross Sections of some Reaction Intermediates in Combustion", *Int. J. Mass Spectrom.*, **2008**, 269(3), 210-220.
3. J. Wang, B. Yang, T. A. Cool, N. Hansen, "Absolute Cross-Sections for Dissociative Photoionization of Some Small Esters", *Int. J. Mass Spectrom.*, **2010**, xxx, xxx-xxx (in press); available online 20 February 2010.
4. D. A. Good, J. S. Francisco, "Tropospheric oxidation mechanism of dimethyl ether and methyl formate", *J. Phys. Chem. A* **2000**, 104, 1171-1185.
5. L. R. McCunn, K.-C. Lau, M. J. Krisch, L. J. Butler, J.-W. Tsung, J. J. Lin, "Unimolecular dissociation of the CH_3OCO radical: an intermediate in the $\text{CH}_3\text{O} + \text{CO}$ reaction", *J. Phys. Chem. A* **2006**, 110, 1625-1634.
6. P. A. Glaude, W. J. Pitz, M. J. Thomson, "Chemical kinetic modeling of dimethyl carbonate in an opposed-flow diffusion flame", *Proc. Combust. Inst.*, **2005**, 30, 1111-1118.

IV. DOE Publications, 2008-present

B. Yang, T. A. Cool, C. K. Westbrook, N. Hansen, K. Kohse-Höinghaus, "Fuel-specific influences on the composition of reaction intermediates in premixed flames of three $\text{C}_3\text{H}_{10}\text{O}_2$ ester isomers", *Proc. Combustion Institute*, 33 (submitted).

W. Li, M. E. Law, P. R. Westmoreland, T. Kasper, N. Hansen, J. Wang, T. A. Cool, K. Kohse-Höinghaus “Competing Paths for Aromatic Species Formation in Cyclohexane Premixed Flat Flames,” *Proc. Combustion Institute*, 33 (submitted).

N. Hansen, T. Kasper, B. Yang, T. A. Cool, W. Li, P. R. Westmoreland, P. Oßwald, K. Kohse-Höinghaus “Fuel-Structure Dependence of Benzene Formation Processes in Premixed Flames Fueled by C₆H₁₂ Isomers”, *Proc. Combustion Institute*, 33 (submitted).

J. Wang, B. Yang, T. A. Cool, N. Hansen, “Absolute Cross-Sections for Dissociative Photoionization of Some Small Esters”, *Int. J. Mass Spectrom.*, **2010**, xxx, xxx-xxx (in press); available online 20 February 2010.

K. Kohse-Höinghaus, P. Oßwald, T. A. Cool, T. Kasper, N. Hansen, F. Qi, C. K. Westbrook, P. R. Westmoreland, “Biofuel combustion chemistry: from ethanol to biodiesel”, *Angew. Chem. Int. Ed.*, accepted 12/2009 (invited review article).

N. Hansen, J. A. Miller, P. R. Westmoreland, T. Kasper, K. Kohse-Höinghaus, J. Wang, T. A. Cool, “Isomer-Specific Combustion Chemistry in Allene and Propyne Flames”, *Combust. Flame*, **2009**, 156 (11), 2153-2164.

T. Kasper, P. Oßwald, U. Struckmeier, K. Kohse-Höinghaus, C. A. Taatjes, J. Wang, T. A. Cool, M. E. Law, A. Morel, P. R. Westmoreland, “Combustion chemistry of the propanol isomers—investigated by electron ionization and VUV-photoionization molecular-beam mass spectrometry”, *Combust. Flame*, **2009**, 156 (6), 1181-1201.

J. Wang, M. Chaos, B. Yang, T. A. Cool, F. L. Dryer, T. Kasper, N. Hansen, P. Oßwald, K. Kohse-Höinghaus, P. R. Westmoreland, “Composition of reaction intermediates for stoichiometric and fuel-rich dimethyl ether flames: Flame-sampling mass spectrometry and modeling studies”, *Phys. Chem. Chem. Phys.*, **2009**, 11 (9), 1328-1339.

N. Hansen, T. A. Cool, P. R. Westmoreland, K. Kohse-Höinghaus, “Recent Contributions of Flame-Sampling Molecular-Beam Mass Spectrometry to a Fundamental Understanding of Combustion Chemistry”, *Progress in Energy and Combustion Science*, **2009**, 35, 168-191.

J. Wang, U. Struckmeier, B. Yang, T. A. Cool, P. Oßwald, K. Kohse-Höinghaus, T. Kasper, N. Hansen, P. R. Westmoreland, “Isomer-specific influences on the composition of reaction intermediates in dimethyl ether/propene and ethanol/propene flames”, *J. Phys. Chem. A*, **2008**, 112, 9255-9265.

C. K. Westbrook, W. J. Pitz, P. R. Westmoreland, F. L. Dryer, M. Chaos, P. Oßwald, K. Kohse-Höinghaus, T. A. Cool, J. Wang, B. Yang, N. Hansen, T. Kasper, “A Detailed Chemical Kinetic Mechanism for Oxidation of Four Small Alkyl Esters in Laminar Premixed Flames”, *Proc. Combust. Inst.*, **2009**, 32, 221-228.

A. Lucassen, P. Oßwald, U. Struckmeier, K. Kohse-Höinghaus, T. Kasper, N. Hansen, T. A. Cool, P. R. Westmoreland, “Species identification in a laminar premixed low-pressure flame of morpholine as a model substance for oxygenated nitrogen-containing fuels”, *Proc. Combust. Inst.*, **2009**, 32, 1269-1276.

N. Hansen, J. A. Miller, T. Kasper, K. Kohse-Höinghaus, P. R. Westmoreland, J. Wang, T. A. Cool, “Benzene Formation in Premixed Fuel-Rich 1,3-Butadiene Flames”, *Proc. Combust. Inst.*, **2009**, 32, 623-630.

C. A. Taatjes, N. Hansen, D. L. Osborn, K. Kohse-Höinghaus, T. A. Cool, P. R. Westmoreland, “Imaging Combustion Chemistry via Multiplexed Synchrotron-Photoionization Mass Spectrometry”, *Phys. Chem. Chem. Phys.*, **2008**, 10(1), 20-34.

J. Wang, B. Yang, T. A. Cool, N. Hansen and T. Kasper, “Near-threshold Absolute Photoionization Cross Sections of some Reaction Intermediates in Combustion”, *Int. J. Mass Spectrom.*, **2008**, 269(3), 210-220.

N. Hansen, S. J. Klippenstein, P. R. Westmoreland, T. Kasper, K. Kohse-Höinghaus, J. Wang and T. A. Cool, “A Combined ab initio and Photoionization Mass Spectrometric Study of Polyynes in Fuel-Rich Flames”, *Phys. Chem. Chem. Phys.*, **2008**, 10(3), 366-374.

Dissociation Pathways and Vibrational Dynamics in Excited Molecules and Complexes

F.F. Crim
Department of Chemistry
University of Wisconsin–Madison
Madison, Wisconsin 53706
ffrim@chem.wisc.edu

Our research investigates the chemistry of vibrationally excited molecules. The properties and reactivity of vibrationally energized molecules are central to processes occurring in environments as diverse as combustion, atmospheric reactions, and plasmas and are at the heart of many chemical reactions. The goal of our work is to unravel the behavior of vibrationally excited molecules and to exploit the resulting understanding to determine molecular properties and to control chemical processes. A unifying theme is the preparation of a molecule in a specific vibrational state using one of several excitation techniques and the subsequent photodissociation of that prepared molecule. Because the initial vibrational excitation often alters the photodissociation process, we refer to our double-resonance photodissociation scheme as *vibrationally mediated photodissociation*. In the first step, fundamental or overtone excitation prepares a vibrationally excited molecule, and then a second photon, the photolysis photon, excites the molecule to an electronically excited state from which it dissociates. Vibrationally mediated photodissociation provides new vibrational spectroscopy, measures bond strengths with high accuracy, alters dissociation dynamics, and reveals the properties of and couplings among electronically excited states.

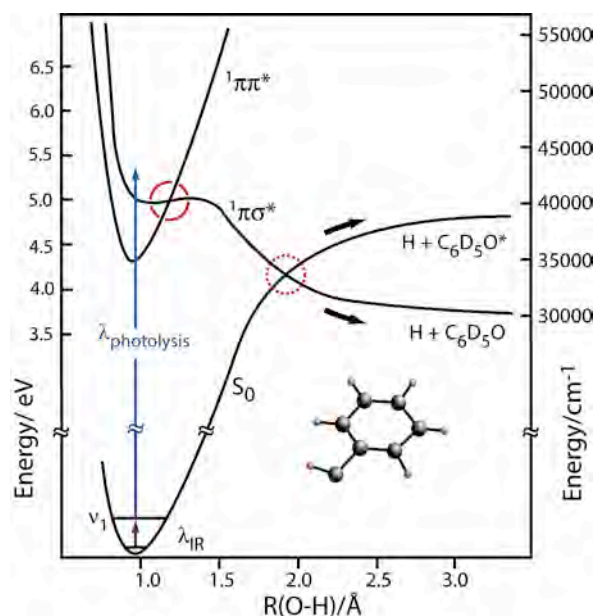
We have used ion imaging to follow the adiabatic and nonadiabatic dissociation pathways in ammonia, to make new measurements on the vibrationally mediated photodissociation of the hydrogen bonded dimer of formic acid, and to study the influence of vibrational excitation on the dynamics at conical intersections in phenol. Phenol is particularly interesting because of well-characterized one-photon photodissociation dynamics and clear theoretical predictions about changes arising from vibrational excitation prior to dissociation. We have begun measurements on the complex of phenol with CO to understand the influence of complexation on the competition between adiabatic and nonadiabatic dissociation and, in particular, its influence on the vibrationally mediated photodissociation. We are also obtaining our first results on ammonia dimers with an eye toward understanding the vibrationally mediated photodissociation dynamics of complexes.

The goals of these studies are to understand and prepare vibrations in the ground electronic state, to study the vibrational structure of the electronically excited molecule, and to probe and control the dissociation dynamics of the excited state.

Phenol

Phenol is one of several heteroaromatic molecules that have multiple conical intersections that are accessible at different excitation energies. Our goal in studying phenol is to discover the influence that vibrational excitation has on the passage through or around these crossings. We have performed both one-photon and vibrationally mediated photodissociation ion-imaging experiments to extract the recoil energy

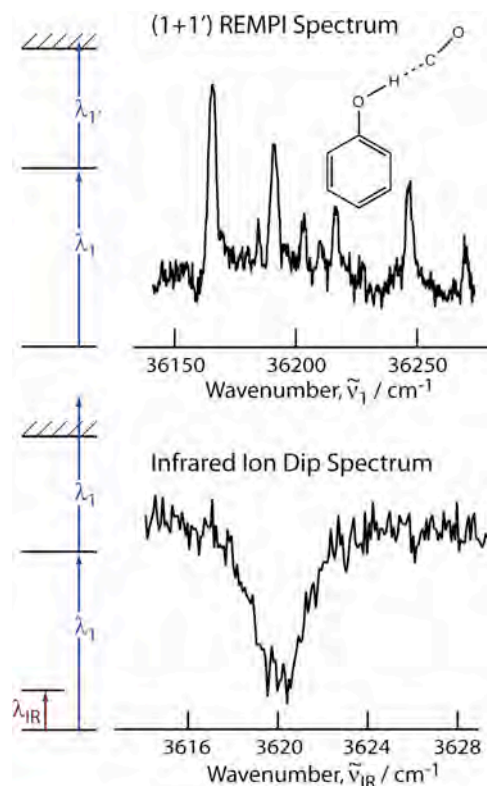
distributions. The figure shows schematic diabatic potential curves for the ground (S_0) and first two excited states ($^1\pi\pi^*$ and $^1\pi\sigma^*$). The development of the wave function of the system as it passes through both intersections, $^1\pi\pi^* \rightarrow ^1\pi\sigma^*$ (solid circle) and $^1\pi\sigma^* \rightarrow S_0$ (dotted circle), determines the branching at the second intersection to form either ground state phenoxyl by nonadiabatic dissociation or excited state phenoxyl by adiabatic dissociation. Comparing the recoil energy distributions of the fragments from one-photon dissociation of phenol- d_5 with those from vibrationally mediated photodissociation shows that initial vibrational excitation strongly influences the disposal of energy into relative translation. Dissociation of phenol- d_5 molecules initially excited in the O-H stretching region produces significantly more fragments with low recoil energies than does one-photon dissociation at the same total energy. This difference appears to come from the increased probability of adiabatic dissociation in which the initially vibrationally excited molecule passes around the conical intersection between the dissociative state and the ground state to produce electronically excited phenoxyl- d_5 radicals.



phenoxyl by adiabatic dissociation. Comparing the recoil energy distributions of the fragments from one-photon dissociation of phenol- d_5 with those from vibrationally mediated photodissociation shows that initial vibrational excitation strongly influences the disposal of energy into relative translation. Dissociation of phenol- d_5 molecules initially excited in the O-H stretching region produces significantly more fragments with low recoil energies than does one-photon dissociation at the same total energy. This difference appears to come from the increased probability of adiabatic dissociation in which the initially vibrationally excited molecule passes around the conical intersection between the dissociative state and the ground state to produce electronically excited phenoxyl- d_5 radicals.

Phenol-CO Complexes

Our experience with phenol, ammonia, and formic acid dimers prepares the way for our studies of the influence of an adduct on dissociation pathways and dynamics in vibrationally excited molecules. Because complexation can influence the course of a bimolecular reaction, our vibrationally mediated photodissociation studies potentially provide insights that have consequences beyond excited-state dissociation. We have begun studying one-photon dissociation in complexes of phenol with CO because we know that conical intersections are important in the dissociation of phenol and that vibrational excitation influences the course of that dissociation. We are in the position of studying both vibrational predissociation of the ground-state complex and vibrationally mediated photodissociation of the excited state complex. The figure shows types of spectra that we have observed in the phenol-CO complex. The top part of the figure is the (1+1') REMPI spectrum obtained by observing the parent ion in an expansion of phenol with CO in a mixture of He and Ar. The features in the spectrum agree with a previous observation of the transitions (J. Chem. Phys. **111**, 1947 (1999)), and using this spectrum we have optimized the conditions for the production of the complex of phenol with only one CO molecule. Production of higher clusters, such as phenol-(CO) $_2$, is a competing channel that we have learned to diagnose and

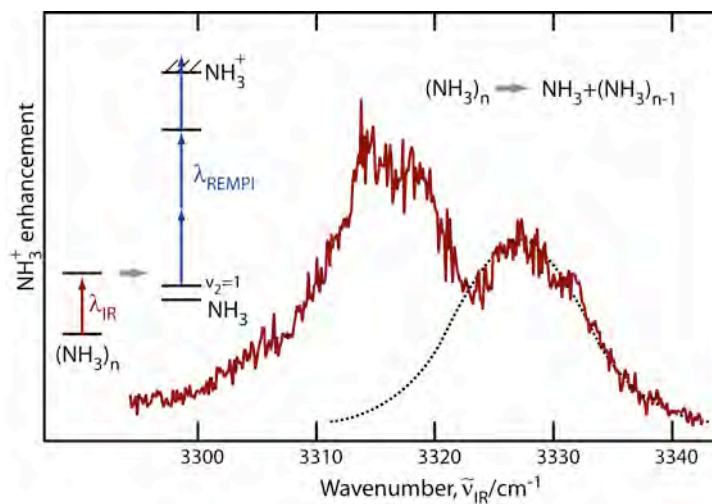


avoid. The lower part of the figure shows the infrared ion dip spectrum obtained by observing the depletion of the (1+1') REMPI signal upon excitation of the O-H stretching vibration of the complex. We observe ion dip spectra of both the bare phenol and the phenol-CO complex shifted from each other by about 30 cm^{-1} , in agreement with previous measurements (J. Phys. Chem. A **106**, 10124 (2002)). These two measurements set the stage for our next experiments. We intend to monitor the CO product of the vibrational predissociation and of the vibrationally mediated photodissociation to explore the effects of complexation on the dissociation dynamics.

Ammonia Dimers and Complexes

The detailed insights that have come from our studies of the influence of vibrational excitation on the excited state dynamics of ammonia suggest that the vibrationally mediated photodissociation of ammonia dimers and complexes of ammonia with other small molecules could reveal novel behavior. Our two central concerns are the influence of complexation on the dynamics at the conical intersection and the changes that complexation produces in the vibrationally mediated photodissociation of ammonia. There are detailed studies of the photodissociation of bare ammonia molecules, which provide a starting point for our work. New studies of the vibrational predissociation of ammonia complexes with C_2H_2 , and with H_2O by Reisler and coworkers (J. Phys. Chem. A **111**, 7589 (2007) and J. Phys. Chem. A **113**, 10174 (2009)) provide a similar starting point for understanding the ground-electronic state behavior in some of the complexes we intend to investigate.

We have begun studying the ammonia dimer in order to master its characterization and to understand ground-electronic state vibrational dynamics. Expansion of ammonia in He produces a collection of oligomers. Exciting the N-H stretching vibration in an oligomer produces vibrationally and rotationally excited ammonia fragments that we detect by (2+1) REMPI through the B state. The figure shows the infrared excitation spectrum obtained by observing the enhanced production of NH_3 fragments with one quantum of excitation in the umbrella vibration (ν_2). These features are consistent with the transitions observed in He droplets (J. Phys. Chem. A **111**, 7460 (2007)). The dotted line in the figure shows the region corresponding to the symmetric stretching vibrations of the dimer. The absorption at lower energies likely comes from larger clusters.



Future Directions

The variety of complexes available, including ones with different bonding motifs, offers a rich array of possibilities in which to study the influence of an adduct and initial vibrational excitation. Our immediate goal is to study complexes with ammonia as well as other bare and complexed molecules where we can use vibrational excitation to influence the passage through conical intersections.

PUBLICATIONS SINCE 2008 ACKNOWLEDGING DOE SUPPORT

Vibrational Action Spectroscopy of the C-H and C-D Stretches in Partially Deuterated Formic Acid Dimer, Y. Heidi Yoon, Michael L. Hause, Amanda S. Case, and F. Fleming Crim, *J. Chem. Phys.* **128**, 084305 (2008).

Dynamics at Conical Intersections: The Influence of O-H Stretching Vibrations on the Photodissociation of Phenol, Michael L. Hause, Y. Heidi Yoon, Amanda S. Case, and F. Fleming Crim, *J. Chem. Phys.* **128**, 104307 (2008).

Vibrationally Mediated Photodissociation of Ammonia: Product Angular Distributions from Adiabatic and Nonadiabatic Dissociation. Michael L. Hause, Y. Heidi Yoon, and F. Fleming Crim, *Mol. Phys.* **106**, 1127 (2008).

Reactive Scattering: Quantum-State-Resolved Chemistry, F. Fleming Crim, in *Tutorials in Molecular Reaction Dynamics*, Eds. Mark Brouard and Claire Vallance (Royal Society of Chemistry, London, 2010) (*in press*).

Bimolecular Dynamics of Combustion Reactions

H. Floyd Davis

Department of Chemistry and Chemical Biology
Baker Laboratory, Cornell University, Ithaca NY 14853-1301
hfd1@Cornell.edu

I. Program Scope:

The aim of this research program is to better understand the mechanisms and product energy disposal in elementary bimolecular reactions fundamental to combustion chemistry. Using the crossed molecular beams method, a molecular beam containing highly reactive free radicals is crossed with a molecular beam. The angular and velocity distributions of the neutral products from single reactive collisions are measured using “universal” mass spectrometry with single photon pulsed vacuum ultraviolet (VUV) photoionization, or for reactions leading to H, D, or O products, by Rydberg tagging time-of-flight (TOF) methods.

II. Recent Progress:

Over the past few years, it has become clear that in order to successfully study the dynamics of elementary radical reactions beyond simple atom + molecule systems using universal mass spectrometric detection of products, it is desirable to *greatly* improve detection sensitivity over that possible using conventional electron impact ionization methods. Casavecchia has employed “soft” low energy electron impact ionization methods to study a range of interesting bimolecular reactions.¹ Using continuous molecular beams and a continuous electron impact ionization source, it is possible to substantially reduce fragmentation of desired product molecules while minimizing contributions from interfering species. However, many of the polyatomic radicals important in combustion (e.g., H, OH, C₂H₃, C₆H₅ etc.) are best produced using pulsed photolytic sources. The inherent mismatch in duty cycle between the continuous nature of electron impact ionizer detectors and pulsed radical beams imposes severe limitations on the use of soft electron impact ionization methods. Several groups have employed synchrotron radiation sources for single photon VUV ionization of products from bimolecular reactions in crossed beam studies. At the National Synchrotron Radiation Research Center in Taiwan, an apparatus employing tunable VUV (10^{16} photons/s) is currently used, demonstrating good signal to noise ratios in a number of crossed beam studies.² However, the quasicontinuous nature of the synchrotron light source is again not well-matched to the use of pulsed photolytic radical beams. Also, synchrotron light sources are not widely available.

Hydrogen Rydberg tagging TOF spectroscopy (HRTOF) has been used with great success in studies of the dynamics of elementary 3-atom³ and 4-atom⁴ systems. Several years ago, we introduced a similar technique for detection of O atoms (ORTOF) produced from bimolecular reactions.⁵ However, for studies of the polyatomic radical reactions relevant to combustion, which frequently have small cross sections, we found that small signals and high background levels made studies extremely difficult or even impossible. The primary source of interfering signal was from photodissociation of radicals or parent molecules by the residual UV light from VUV generation.

In order to substantially improve the sensitivity in Rydberg tagging experiments, and to greatly expand the range of systems that can be studied using universal pulsed photoionization detection⁶ (previously limited to 7.9 eV using an F₂ excimer), during the current funding period we have

devoted great effort to implementing new VUV light sources (8-11 eV) on two different crossed beams machines in our laboratory. The highest possible efficiency for VUV generation using pulsed nanosecond lasers involves a method first proposed by Smith and Alford⁷ and then demonstrated experimentally by Muller and coworkers.⁸ It employs 4-wave mixing of collimated (*i.e.*, *unfocussed*) nanosecond pulses in a 1m long cell containing mercury (Hg) vapor. This approach is most general and efficient if *three* independent input laser beams are each tuned near Hg resonances at the precise wavelengths where index matching may be achieved.⁸ Pulsed beams in the VUV at the millijoule level⁸ and continuous wave (CW) Lyman- α (121 nm)⁹ have been produced using variants of this approach.

For production of 130 nm light necessary for ORTOF, three unfocussed input nanosecond pulses are simultaneously tuned near a one photon, two photon, and Rydberg resonance (*i.e.*, 255 nm + 404 nm + 777 nm) in a 1 meter long Hg heat pipe, producing very intense 130 nm light (Fig. 1). The VUV is spatially separated by off-axis transmission through a movable MgF₂ lens and reflected into the interaction region using a remotely-adjustable VUV mirror (Fig. 2). We have found that this method leads to unprecedented signal levels with dramatic reduction of background levels. Assuming 1 mJ/pulse at 30Hz in the 130nm range, we produce VUV photon fluxes that are nearly identical to that using a synchrotron source, *i.e.*, 2×10^{16} photons/s. In our experiments, products are ionized in universal TOF experiments by scanning the ionization laser over the range of arrival times for products at the detector, maintained below 1×10^{-10} Torr. Thus essentially all of the VUV photons are usable for

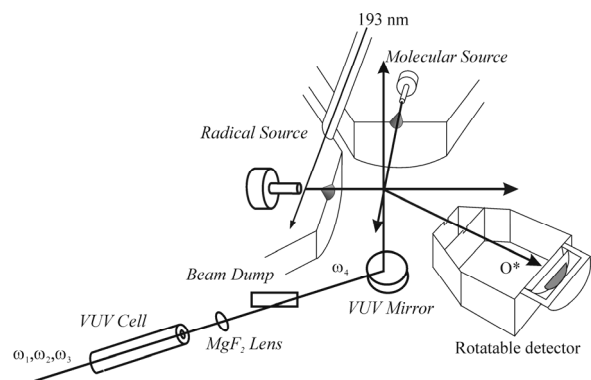


Fig. 2: Schematic of newly-configured Rydberg Tagging Apparatus (not to scale). VUV (ω_4) produced in 1m long Hg cell passes beam dump whereas fundamental beams (ω_1 , ω_2 , and ω_3) are dumped.

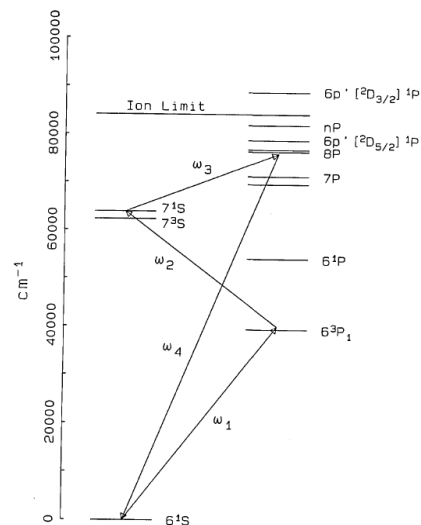


Fig. 1: Four-wave mixing scheme of Smith and Alford (Ref. 7). Three tunable pulsed lasers are simultaneously tuned near one, two, and three photon resonances in Hg. Phase matching at any ω_4 is achieved by precisely tuning ω_1 .

ionization, whereas using pulsed radical sources with continuous synchrotron ionization methods, the duty cycle is at best only 1%. This results in a dramatic increase in sensitivity over that possible using pulsed beams with synchrotron light sources.

In the following, we illustrate some recent results on two different machines using high-brightness VUV pulsed light sources employing collimated beams. For “universal” mass spectrometric detection, we have studied several reactions involving phenyl radicals. To optimize and characterize the method for ORTOF, we photolyzed N₂O at 130 nm, producing O(³P) + N₂ (A,B) which may be probed by ORTOF

i) Crossed Beams Study of Phenyl Oxidation:

Phenyl radicals (C_6H_5) react with oxygen molecules (O_2) to form phenylperoxy radicals (C_6H_5OO). These intermediates have been calculated to decompose either through O-O bond fission forming $C_6H_5O + O$, or through a series of isomerization steps producing $C_5H_5 + CO_2$, $C_5H_5O + CO$ or $C_6H_4O_2 + H$ ¹⁰ (Fig. 3).

In this study, the reaction of phenyl radicals with molecular oxygen is investigated at a mean collision energy of 64 kJ/mol using the crossed molecular beams technique, employing detection via pulsed single photon ionization at 9.9 eV. Here we monitor the formation of phenoxy radicals (C_6H_5O) from the $C_6H_5O + O$ channel, providing insight into the lifetimes of the C_6H_5OO intermediates. The measured distributions imply that the C_6H_5OO lifetimes (τ) are at least comparable to their rotational timescales, i.e. $\tau \geq 1$ ps (Fig. 4). Our lower limit for τ is at least 100 times longer than an upper limit inferred from a previous crossed beams experiment carried out at a higher collision energy employing a pyrolytic phenyl radical source.¹¹

ii) A Study of the Electronically Metastable Products from 130.2 nm N_2O Photodissociation Using Unfocussed Lasers for VUV Generation:

To optimize the production of 130.2 nm light using collimated lasers, and to further characterize the ORTOF method, we have reexamined the photodissociation of N_2O in the VUV. The photodissociation of N_2O in the vacuum ultraviolet (VUV) leads primarily to production of $N_2(X^1\Sigma_g^+) + O(^1S_0)$, together with minor contributions from the $N_2(A^3\Sigma_u^+) + O(^3P_J)$ and $N_2(B^3\Pi_g) + O(^3P_J)$ channels. Because radiative transitions from $O(^1S_0)$ to the lower $O(^3P_J)$ and $O(^1D_2)$ states are dipole forbidden, the radiative lifetime of $O(^1S_0)$ is quite long ($\tau \approx 0.84$ s). Consequently, the chemistry and quenching of $O(^1S_0)$ is important in a number of environments. In the present study, we found that the nascent metastable $O(^1S_0)$ from the dominant $N_2(X^1\Sigma_g^+) + O(^1S_0)$ channel can be detected without further excitation by impact on a microchannel plate. An inverted $N_2(X^1\Sigma_g^+)$ vibrational distribution with very little rotational excitation is consistent with dissociation from near-linear N_2O geometries. The $N_2(A^3\Sigma_u^+) + O(^3P_J)$ and $N_2(B^3\Pi_g) + O(^3P_J)$ channels are detected by two methods, oxygen Rydberg tagging time-of-flight (ORTOF) spectroscopy and metastable $N_2(A^3\Sigma_u^+)$ TOF spectroscopy.

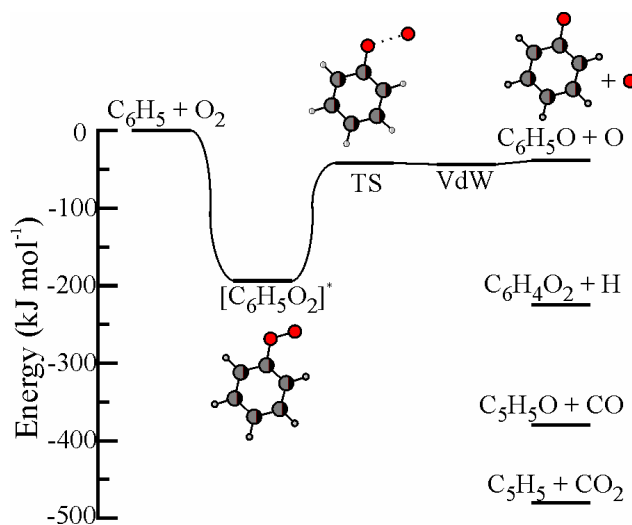


Fig. 3 Energetics of phenyl + O_2 reaction (Ref. 10).

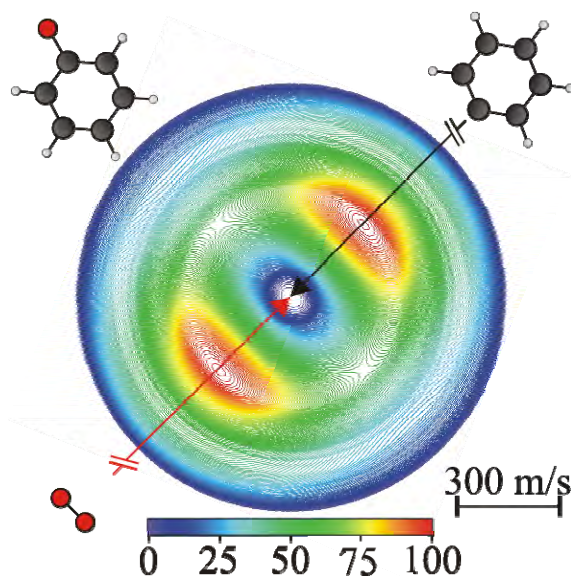


Fig. 4: Product flux contour map for C_6H_5O from $C_6H_5 + O_2$ reaction at $E_{coll} = 64$ kJ/mol.

III. Future Studies:

The dramatic increase in VUV intensities combined with decreased background levels will facilitate high resolution measurements of the $\text{H} + \text{O}_2 \rightarrow \text{OH} + \text{O}({}^3\text{P}_j)$ reaction using ORTOF. By measuring the angular and velocity distributions of individual $\text{O}({}^3\text{P}_j)$ levels, the correlated OH rovibrational energy distributions will be measured as a function of scattering angle. The results will be compared to recent high-level calculations by Guo's group.¹² Other key combustion systems producing atomic products of interest include $\text{C}_2\text{H}_3 + \text{O}_2 \rightarrow \text{C}_2\text{H}_3\text{O} + \text{O}$, $\text{OH}(\text{X}, \text{A}) + \text{H}_2 \rightarrow \text{H}_2\text{O} + \text{H}$ (and isotopologues), as well as $\text{OH} + \text{CO} \rightarrow \text{CO}_2 + \text{H}$.

To understand the dynamics of competing reaction pathways in polyatomic radical reactions, the tunable high brightness pulsed VUV source (8-11eV) will be used to study a range of important reactions including simple hydrocarbon free radicals (C_2H_3 , C_2H_5 , C_3H_7 , C_4H_9 , *etc.*) with O_2 using our rotatable source apparatus. To better understand the competing reaction channels producing enols in combustion, bimolecular reactions of OH (X) with ethene and propene will be studied.

IV. Publications citing DOE Support for 2008-Present:

1. Daniel R. Albert and H. Floyd Davis, "Collision Complex Lifetimes in the Reaction $\text{C}_6\text{H}_5 + \text{O}_2 \rightarrow \text{C}_6\text{H}_5\text{O} + \text{O}$ ", *J. Phys. Chem. Lett.* **1**, 1107 (2010).
2. David L. Proctor, Daniel R. Albert and H. Floyd Davis, "Improved piezoelectric actuators for use in high-speed pulsed valves", *Rev. Sci. Instrum.* **81**, 023106 (2010).
3. Martha Beckwith, David L. Proctor, Daniel R. Albert and H. Floyd Davis, "A Study of the Electronically Metastable Products from 130 nm N_2O Photodissociation Using Unfocussed Lasers for VUV Generation", *J. Chem. Phys.*, submitted for publication.

V. References:

-
1. P. Casavecchia, F. Leonori, N. Balucani, R. Petrucci, G. Capozza, and E. Segoloni, *Phys. Chem. Chem. Phys.* **11**, 46 (2009).
 2. S.-H. Lee, W.-K. Chen, and W.-J. Huang, *J. Chem. Phys.* **130**, 054301 (2009)
 3. W. Dong, C. Xiao, T. Wang, D. Dai, X. Yang, and D.H. Zhang, *Science* **327**, 1501 (2010).
 4. B. Strazisar, C. Lin and H.F. Davis, *Science* **290**, 958 (2000).
 5. C. Lin, M. F. Witinski, and H. F. Davis, *J. Chem. Phys.* **119**, 251 (2003)
 6. D. Proctor and HF Davis, *Proc. Nat. Acad. Sci. Am.* **105**, 12673 (2008).
 7. A.V. Smith and W.J. Alford, *J. Opt. Soc. Am. B.* **4**, 1765 (1987).
 8. H. Muller, D.D. Lowenthal, M.A. DeFaccio, and A. V. Smith, *Opt. Lett.* **13**, 651 (1988).
 9. K.S.E. Eikema, J. Walz, and T.W. Hansch, *Phys. Rev. Lett.* **83**, 3828 (1999).
 10. Tokmakov, I.V.; Kim, G.S.; Kislov, V.V.; Mebel, A.M.; Lin, M.C. *J. Phys. Chem. A*, **109**, 6114 (2005).
 11. Gu, X.; Zhang, F.; Kaiser, R.I. *Chem. Phys. Lett.* **448**, 7 (2007).
 12. Z. Sun, D.H. Zhang, C. Xu, S. Zhou, D. Xie, G. Lendvay, S-Y. Lee, Y. Shi, H. Guo *J. Am. Chem. Soc.* **130**, 14962 (2008).

Exploration and validation of chemical-kinetic mechanisms

Michael J. Davis

Chemistry Division
Argonne National Laboratory
Argonne, IL 60439
Email: davis@tcg.anl.gov

The main focus of the work is on the exploration and theoretical validation of chemical-kinetic mechanisms, which combines global sensitivity analysis with the exploration of the characteristics of the sensitivity analysis over the physical and chemical parameters. The exploration is expedited by using the tools of DACE,¹ coupled with methods for updating and exploring the response surface generated from sampling. The tools used for generating these sensitivity maps can be applied to other types of fitting and optimization problems. We are in the process of implementing several of these procedures for fitting potential energy surfaces.

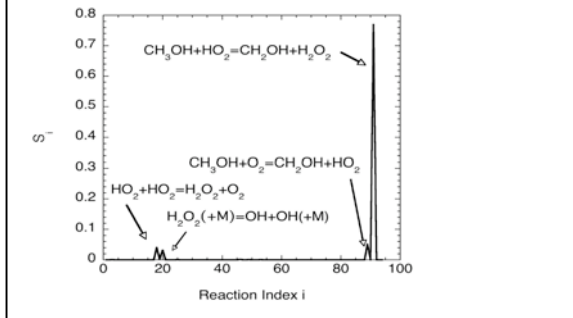
Recent Progress

Theoretical Validation of the methanol mechanism

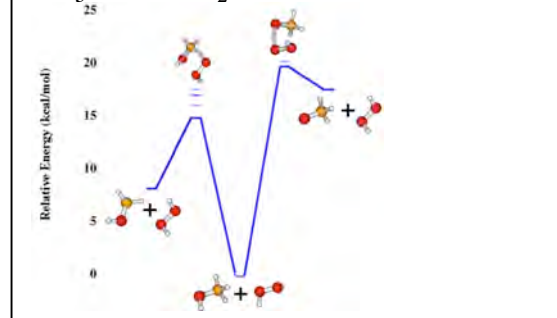
This project is a collaboration with Stephen Klippenstein and Larry Harding at Argonne, Rex Skodje (Colorado), and Alison Tomlin (Leeds). The validation procedure is described in the figure. Global sensitivity analysis² was used to study the ignition properties of methanol/air mixtures under constant volume conditions, using the mechanism of Li *et al.*³ The rate constants of all the reactions in the mechanism were varied over their uncertainty ranges with Monte Carlo sampling. This leads to a distribution of ignition delay times. This distribution is analyzed by decomposing its variance in terms of individual reactions leading to a set of first-order sensitivity coefficients (the fraction of the total variance attributable to each reaction), and is plotted in the upper left of the figure. Over 70% of the variance is attributable to $\text{CH}_3\text{OH} + \text{HO}_2 = \text{CH}_2\text{OH} + \text{H}_2\text{O}_2$. The rate constant for this reaction was calculated (the next two panels). The new rate constant is about an order of magnitude lower than that used in the mechanism of Ref. 3. The use of this rate constant leads to two important results. The overall uncertainty of the ignition delay times is decreased and the nominal ignition delay time is increased significantly as demonstrated in the last panel of the figure.

When the updated uncertainty of the rate constant for the reaction $\text{CH}_3\text{OH} + \text{HO}_2 = \text{CH}_2\text{OH} + \text{H}_2\text{O}_2$ is used for a new set of set of calculations, the reaction $\text{CH}_3\text{OH} + \text{O}_2 = \text{CH}_2\text{OH} + \text{HO}_2$, which has a small but noticeable variance fraction in the first panel of the figure, becomes the reaction with the highest fractional variance. The rate constant for this reaction was calculated and its value was once again approximately a factor of ten lower than in the original mechanism, once again increasing the ignition delay time.

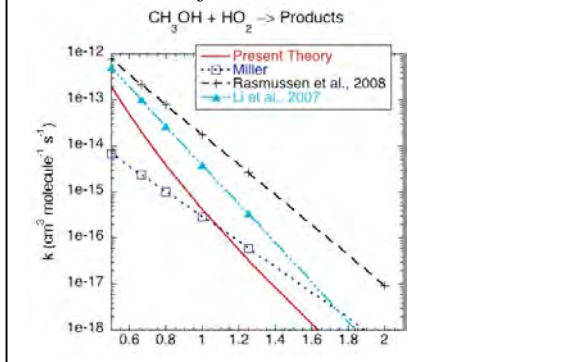
Identification of the key reactions using global sensitivity analysis



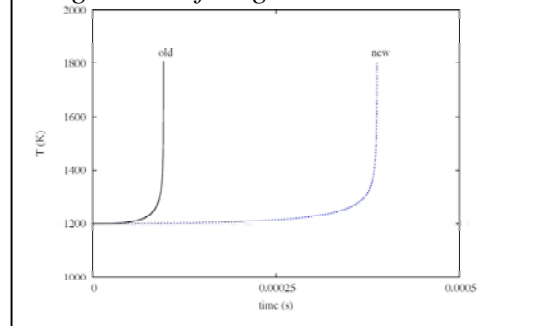
Calculation of the energetics of CH₃OH + HO₂



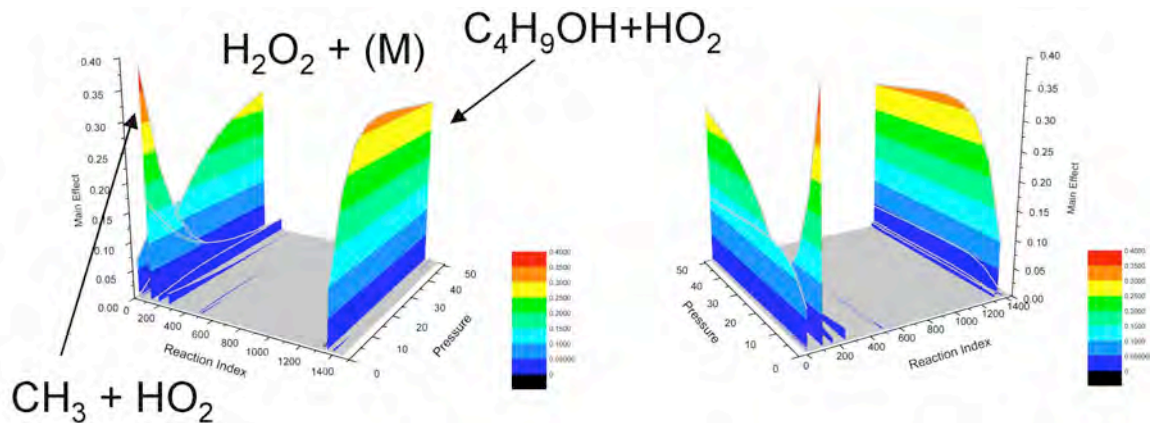
Calculation of the rate constant



The new rate constant leads to much longer times for ignition.



Global Sensitivity analysis of n-Butanol



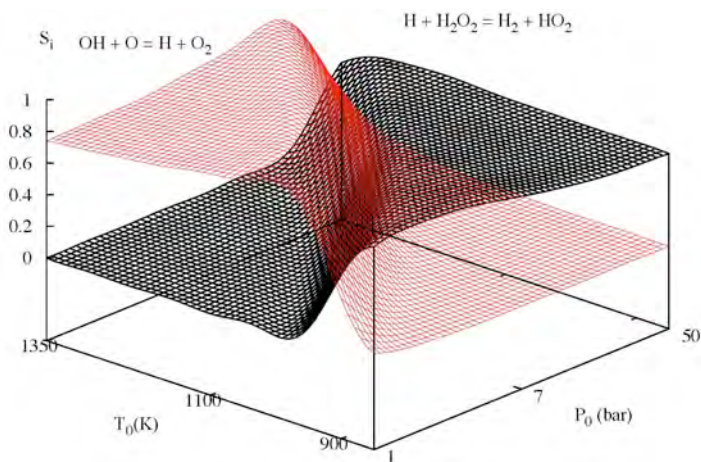
The study of methanol ignition has led us in two directions. The first is the study of larger mechanisms. This project is a collaboration with Dingyu Zhou and Rex Skodje, (Colorado). The mechanism of Ref. 4 was used to study ignition properties of n-butanol,

in pure oxygen. The sensitivity indices are studied as a function of pressure, temperature and stoichiometry. The figure shows results for stoichiometric mixtures of n-butanol and oxygen with an initial temperature of 1200 K. Once again reactions with HO_2 have the highest fractional variance, with $\text{CH}_3 + \text{HO}_2$ being dominant near $P = 1$ bar and $n\text{-C}_4\text{H}_9\text{OH} + \text{HO}_2$ at elevated pressure. The decomposition of H_2O_2 also has significant fractional variance at elevated pressure.

Global sensitivity surfaces for chemical-kinetic mechanisms. Generation and exploration

The second research direction involves two tasks. The first task extends the theoretical validation procedure, by studying the ways in which the sensitivity indices change with initial conditions. It involves the implementation/development of the tools necessary to explore the physical and chemical space with global sensitivity analysis using the DACE methodology.^{1,5-6} The second task is a more detailed investigation of the procedures used in the methanol study, including improvements in the algorithms used to generate the sensitivity indices.

The H_2/O_2 mechanism was used to implement these two tasks because it is small enough to investigate in great detail, and as the above plot of the n-butanol results demonstrates, these reactions carry significant fractions of the variance for the ignition properties of n-butanol. The x-axes in the plots of the previous figure are labeled “Reaction Index”, which indicates the sequence of the reactions in the mechanism and are in approximate order of the numbers of carbon atoms in each reaction. These plots demonstrate that most of the variance in the ignition delay times is due to the primary fuel, n-butanol, and the hydrogen and C_1 species.



The H_2/O_2 project is a collaboration with Skodje (Colorado) and Tomlin (Leeds) and involves two publications, one in the publication list, and the other in preparation.⁵ There are two reactions which have the highest fractional variance over a large range of pressures, temperatures, and stoichiometry, as noted in the figure above. The surfaces shown in the figure were generated for stoichiometric mixtures of H_2 and O_2 , and were created using the Gaussian process model.¹ The initial sample was a maximin Latin

hypercube sample.⁶ Points were added to the original sample based on domain decomposition⁵ and the error function estimate inherent in the Gaussian process interpolator.⁶ The surfaces in this figure show a rather sharp transition from OH + O to H + H₂O₂, and at the present time we are investigating the correlation between this transition and the well-studied explosion limits for this system.⁵

Future Plans

This research will be extended in three ways. We intend on using large numbers of parallel processors to extend the ignition work to larger mechanisms, including n-heptane. We plan on extending the validation work to different combustion situations, with the first being one-dimensional, steady, premixed flames. The third important way this work will be extended is the fitting of potential energy surfaces using the Gaussian process model. Preliminary work, reported in last year's abstract, will be extended to the formaldehyde potential surface. The potential fitting work will include comparisons to moving least-squares, in collaboration with Al Wagner. It will also include a toolkit of techniques that have been developed elsewhere, such as multi-fidelity fitting.⁶

References

- ¹ T. J. Santner, B. J. Williams, I. W. Notz, *The Design and Analysis of Computer Experiments*, Springer, New York (2003).
- ² A. Saltelli *et al*, *Global sensitivity analysis: The primer*, Wiley (2008).
- ³ J. Li, Z. Zhao, A. Kazakov, M. Chaos, and F. I. Dryer, *Int. J. Chem. Kin.* **39**, 109 (2007).
- ⁴ G. Black, H.J. Curran, S. Pichon, J.M. Simmie, and V. Zhukov, *Combustion and Flame* **157**, 363 (2010).
- ⁵ M. J. Davis and R. T. Skodje, "Global sensitivity surfaces for chemical-kinetic mechanisms. Generation and exploration."
- ⁶ A. I. J. Forrester, A. Sobester, and A. Keane, *Engineering design via surrogate modeling. A practical guide*, Wiley (2008).

Publications

- M. J. Davis and A. S. Tomlin, "Spatial dynamics of steady flames 1. Phase space structure and the dynamics of individual trajectories", *J. Phys, Chem. A.* **112**, 7768 -7783 (2008).
- M. J. Davis and A. S. Tomlin, "Spatial dynamics of steady flames 2. Low-dimensional manifolds and the role of transport processes", *J. Phys, Chem. A.* **112**, 7784-7805 (2008).
- S. J. Klippenstein, L. B. Harding, M. J. Davis, A. S. Tomlin, and R. T. Skodje, "Uncertainty driven theoretical kinetics studies for CH₃OH ignition: HO₂ + CH₃OH and O₂ + CH₃OH", submitted to the 2010 Combustion Symposium.
- R. T. Skodje, A. S. Tomlin, S. J. Klippenstein, L. B. Harding, and M. J. Davis, "Theoretical validation of chemical-kinetic mechanisms: The combustion of methanol", to be submitted.
- M. J. Davis, R. T. Skodje, and A. S. Tomlin, "Global sensitivity analysis of chemical-kinetic reaction mechanisms", to be submitted.

PROJECT NARRATIVE

Dynamics of Radical Reactions in Biodiesel Combustion

Theodore S. Dibble
Chemistry Department
SUNY-Environmental Science and Forestry
Syracuse, NY 13210
tsdibble@syr.edu

PROJECT SCOPE

The ignition of diesel fuel depends on isomerization of peroxy radicals ($\text{ROO}\bullet$) via a hydrogen shift reaction:



Production of multiple OH radicals (chain branching) in the chemistry following reaction (1) leads to autoignition. Processes such as reaction (2):



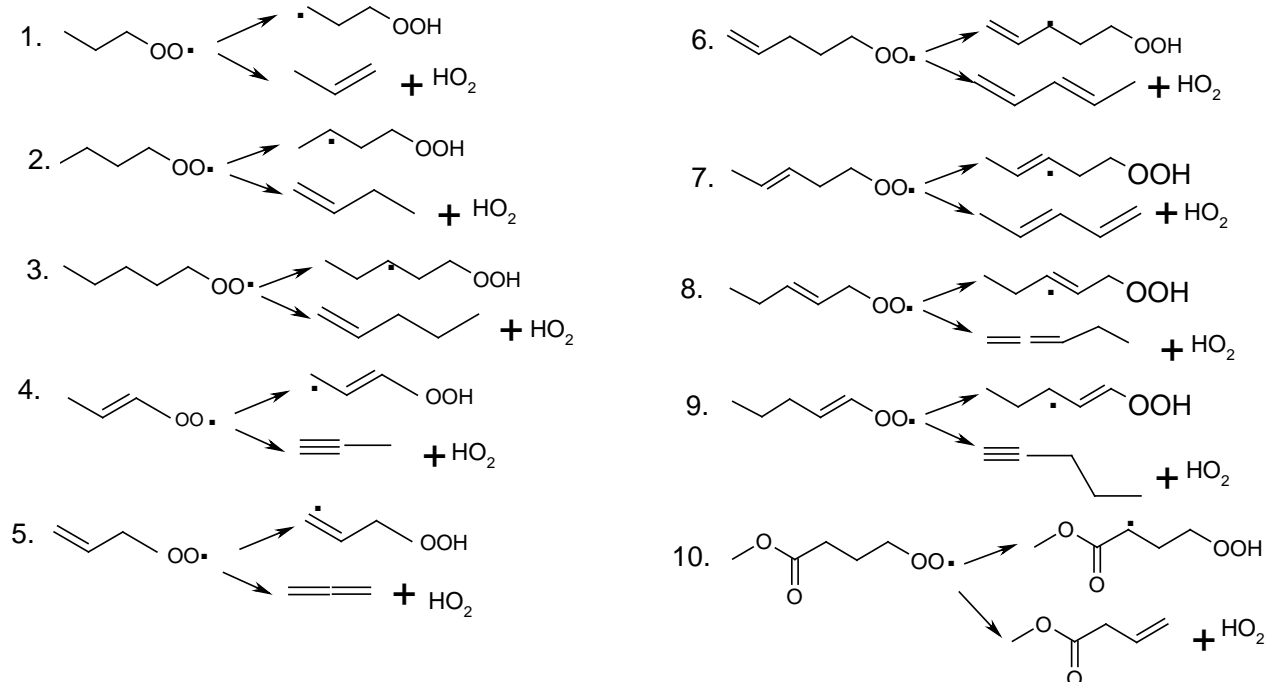
compete with chain branching. Experimentalists face several difficulties in gaining an understanding of this chemistry, and no QOOH species has ever been detected by experiment! This has inspired many computational studies of these processes. Another limitation is that the peroxy radicals studied to date have been almost exclusively those derived from alkanes.

Biodiesel fuel is increasingly being used worldwide. Although we have a fair understanding of the molecular details of the chemistry of peroxy radicals derived from alkanes, biodiesel fuels contain ester and olefin groups which significantly impact the thermodynamics and kinetics of biodiesel ignition.¹ The broader goal of this research is to carry out systematic computational studies of the elementary kinetics of this chemistry for compounds that are models for biodiesel ignition. This includes not only reactions (1) and (2), but also reactions leading to chain branching. In addition, the research will:

- include rigorous treatments of tunneling effects
- quantify the effect of chemically activated processes
- synthesize the results into structure-activity relations (SARs)

RECENT PROGRESS

To date, we have investigated reactions (1) and (2) in a variety of peroxy radicals containing olefin and ester functional groups (see scheme 1). The size and asymmetry and number of the species to be investigated will require using an efficient computational approach for determining the potential energy surface, i.e., density functional theory. We started with the recently developed M05-2X functional,² which has been optimized for kinetics and thermodynamics.^{3, 4} The 6-31+G(d,p) basis set was employed, and calculations were carried out with the spin-unrestricted formalism. The GAUSSIAN09 system of programs has been used to determine structures, energies, and vibrational frequencies of reactants, products, and saddle points. The nature of the saddle points has been determined by close inspection of saddle point structures and animation of the imaginary vibrational frequency.



Scheme 1. 1,5 H-shift and HO₂ elimination in peroxy radicals, including model compounds for studying combustion of fatty-acid methyl esters.

To investigate basis set effects, calculations were repeated on these three model systems using M05-2X/6-311G(2df,2p). Basis set effects were no more than 1.0 Kcal/mole on reaction energies, and less than that on activation barriers. Relative energies were compared to benchmark calculations published previously on ethyl, 1-propyl and 1-butyl peroxy radicals.^{5, 6, 77} The relative energies at M05-2X were in good agreement with the benchmark calculations for the H-shift reactions, with no obvious bias. The M05-2X relative energies tend to be 1-3 kcal/mole higher than the benchmark values for HO₂ elimination reactions.

Figure 1 depicts the potential energy profiles for unimolecular reactions of 1-pentylperoxy with a C=C bond at either carbons 1, 2, 3, or 4. It can readily be seen that activation barriers for HO₂ elimination are very highly correlated with thermodynamics, but those for 1,5 H-shift show more variability. For the pent-3-ene-1-peroxy and pent-2-ene-1-peroxy radicals, the hydrogen atom being transferred is located on a sp² hybridized carbon atom. These C-H bonds are strong, leading to very similar and significantly positive (+26 kcal/mole) reaction energies for their 1,5 H-shift reactions. By contrast, 1,5 H-shift reactions of pent-1-ene-1-peroxy and pent-4-ene-1-peroxy radicals are both nearly thermoneutral. The range of activation barriers for these four reactions span a range of only 10 kcal/mole, and the activation barriers for these reactions in pent-1-ene-1-peroxy and pent-4-ene-1-peroxy differ by 5 kcal/mole when their reaction energies only vary by 1 kcal/mole. Clearly, the barriers to 1,5 H-shift reactions are strongly influenced by factors other than thermochemistry.

To investigate the effects of different functional groups on the mechanism of reaction (1) and (2), three species consisting of alkane, alkene and ester respectively were chosen as model molecules (see molecule 3, 6 and 10 in Scheme 1). Figure 2 depicts the effect of these three functional groups on the series of 1,5 H-shift reactions. Comparing with the saturated pentyl-

peroxy radical, alkane group decreases the barrier and reaction energy much more than ester group.

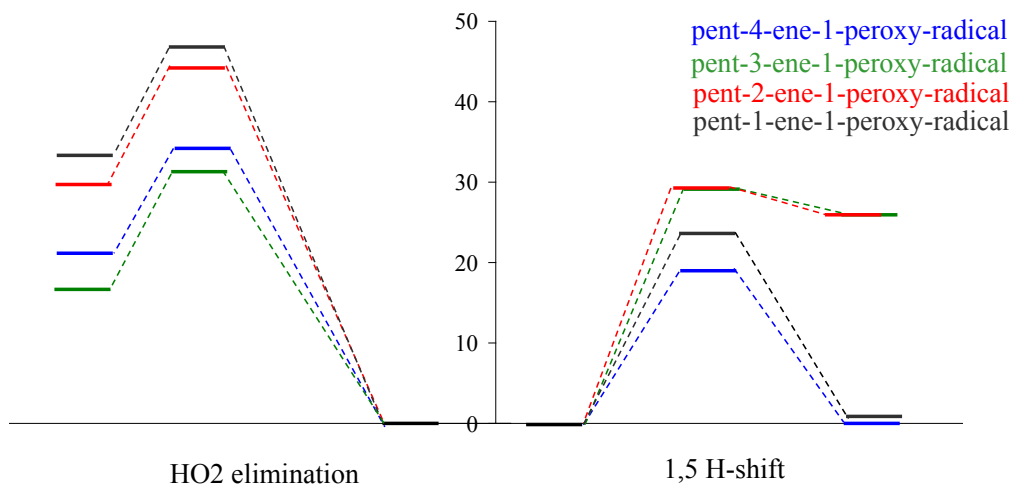


Figure 1. Potential energy profiles (kcal/mole) for unimolecular reactions of 1-pentylperoxy with a C=C bond at either carbons 1, 2, 3, or 4.

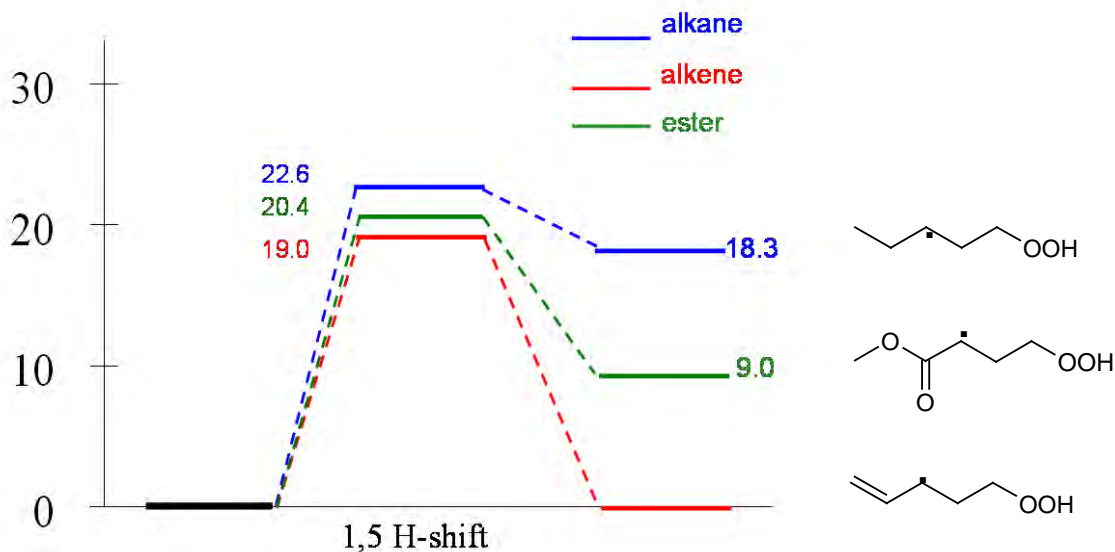


Figure 2. Potential energy profiles (kcal/mole) for 1,5 H-shift reactions of 1-alkylperoxy (internal H-atom transfer from carbon 3) with alkyl, alkene and ester groups at carbon 4. The structures of the three reaction products are shown to the right.

FUTURE PLANS

High level *ab initio* computations such as the CBS-QB3 method will be performed to correct the activation and reaction energies. Rate constants for the reactions of interest will be investigated as a function of temperature and pressure using RRKM/Master Equation calculations. For the H-shift processes, tunneling effect could play significant roles. Multi-dimensional tunneling corrections to thermal rate constants will be computed and compared to the Wigner and Eckart models. Calculations will be extended to the kinetics of QOOH and •OOQOOH radicals. RRKM/Master Equation calculations will be carried out to determine the stable products of this chemistry.

PUBLICATIONS ACKNOWLEDGING BES SUPPORT 2009-PRESENT

F. Zhang and T. S. Dibble, Effects of ester and olefin functional groups on kinetics of unimolecular reactions of peroxy radicals, *in preparation*.

REFERENCES

- [1] R. Sumathi and W. H. Green, Oxygenate. Oxyalkyl and alkoxy carbonyl thermochemistry and rates for hydrogen abstraction from oxygenates. *Phys. Chem. Chem. Phys.*, **2003**, *5*, 3402-17.
- [2] Y. Zhao and D. G. Truhlar. How Well Can New-Generation Density Functionals Describe the Energetics of Bond-Dissociation Reactions Producing Radicals? *J. Phys. Chem. A*, **2008**, *112*, 1095-99.
- [3] Y. Zhao and D. G. Truhlar. Design of Density Functionals That Are Broadly Accurate for Thermochemistry, Thermochemical Kinetics, and Nonbonded Interactions. *J. Phys. Chem., A*, **2005**, *109*, 5656-67.
- [4] Y. Zhao and D. G. Truhlar. Density Functionals with Broad Applicability in Chemistry. *Accts. Chem. Res.*, **2008**, *41*, 157-67.
- [5] J. J. Wilke, W. D. Allen, and H. F. Schaefer III, Establishment of the C₂H₅+O₂ reaction mechanism: A combustion archetype. *J. Chem. Phys.*, **2008**, *128*, 074308.
- [6] J. K. Merle, C. J. Hayes, S. J. Zalyubovsky, B. G. Glover, T. A. Miller, and C. M. Hadad, Theoretical Determinations of the Ambient Conformational Distribution and Unimolecular Decomposition of n-Propylperoxy Radical. *J. Phys. Chem. A*, **2005**, *109*, 3637-3446.
- [7] J. D. DeSain, C. A. Taatjes, J. A. Miller, S. J. Klippenstein and D. K. Hahn, Infrared frequency-modulation probing of product formation in alkyl + O₂ reactions Part IV. Reactions of propyl and butyl radicals with O₂. *Faraday Discuss.* **2001**, *119*, 101-120.

Hydrocarbon Radical Thermochemistry: Gas-Phase Ion Chemistry Techniques

Kent M. Ervin
Department of Chemistry and Chemical Physics Program
University of Nevada, Reno
Reno, NV 89557-0216
ervin@unr.edu

I. Program Scope

Gas-phase ion chemistry and mass spectrometry techniques are employed to determine energetics of hydrocarbon radicals that are important in combustion processes and to investigate the dynamics of ion–molecule reactions. Tandem mass spectrometry is used to measure the activation of endoergic ion-molecule reactions as a function of kinetic energy. Modeling the measured reaction cross sections using statistical rate theory [1] or empirical reaction models allows extraction of reaction threshold energies. These threshold energies yield relative gas-phase acidities, proton affinities or hydrogen atom affinities, which may then be used to derive neutral R–H bond dissociation enthalpies using thermochemical cycles involving established electron affinities or ionization energies [2]. The reactive systems employed in these studies include endoergic bimolecular proton transfer reactions, hydrogen-atom transfer reactions, and collision-induced dissociation of heterodimer complex anions and cations. Electronic structure calculations are used to evaluate the possibility of potential energy barriers or dynamical constrictions along the reaction path, and as input for RRKM and phase space theory calculations. Existing guided ion beam tandem mass spectrometry experiments in the Ervin group are being complemented by development of a Quadrupole Ion Trap/Time-of-Flight tandem mass spectrometer.

II. Recent Progress

A. Energy-Resolved Collision-Induced Dissociation

We continue work to measure gas-phase acidities and other energetics of oxygen-containing hydrocarbons and of highly unsaturated hydrocarbons that are of interest in combustion kinetic systems.

Energy-resolved collision induced dissociation is used to measure energetics of ionic systems that can be related to neutral hydrocarbon molecules and radicals via thermochemical cycles.

In recent work [3], we have carried out experiments on the threshold collision-induced dissociation of peroxyformate anion, HCOOO^- . Figure 1 shows preliminary cross section data

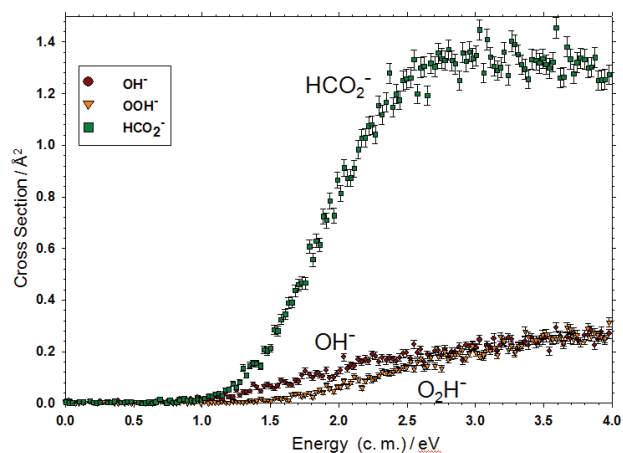


Figure 1. Energy-resolved collision-induced dissociation of peroxyformate anion.

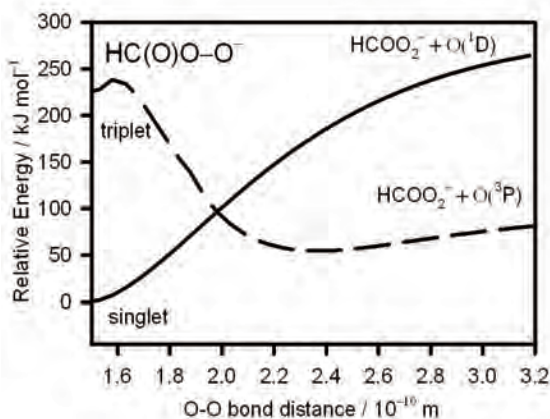


Figure 2. Singlet and triplet potential energy surfaces for dissociation of peroxyformate.

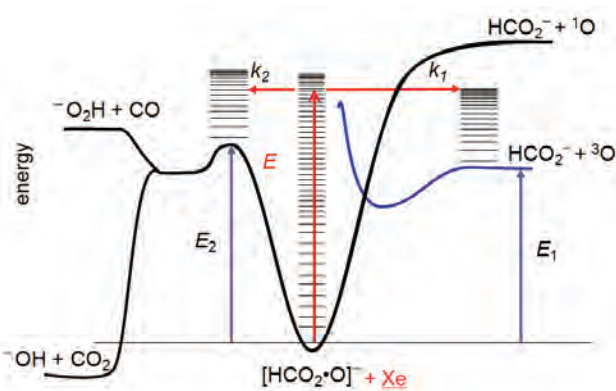


Figure 3. Scheme for dissociation of peroxyformate.

for collision-induced dissociation with xenon as the target gas. The primary product with the lowest threshold energy is formate anion, HCO_2^- , with loss of O atom. The observed threshold energy is much too low for the products to be on the spin-conserved singlet electronic surface. Therefore, efficient conversion to the ground triplet state products must be occurring along the dissociation path. Figure 2 shows calculated energies of the singlet and triplet surfaces. We identify a singlet-triplet intersection that is below the asymptotic energy of the products. That allows formation of the ground state products with no excess barrier, so the measured threshold energy is an upper limit for the anion dissociation energy, $D(\text{HCOO}^- - \text{O})$. The minor products at higher energy in Figure 1 are OH^- and O_2H^- . The formation of $\text{OH}^- + \text{CO}_2$ is exothermic overall, but using density functional theory calculations we find that the OH^- and O_2H^- product channels share a common transition state with an energy above that for the formate anion channel. The overall potential energy surface and scheme for the modeling the kinetic and competitive shifts using RRKM theory is shown in Figure 3.

Using our measured threshold energy, recent measurements of the gas-phase acidity of HCO_3H and electron affinity of HCO_3^- [4], and the known acidities and enthalpy of formation of formic acid, HCO_2H , we can obtain the first experimental value for the enthalpy of formation of the neutral peroxyformic acid, HCO_3H . These results also provide the enthalpy of formation for $\text{HC}(\text{O})\text{OO}\cdot$, the neutral formyloxyl radical. Preliminary values agree well with energies from computational chemistry.

B. Instrumental Development

We are also continuing development of a Quadrupole Ion Trap/Time-of-Flight tandem mass spectrometer [5, 6] for future ion-molecule reaction kinetics and product velocity distribution measurements. In recent work [7], we have developed a novel pulsed extraction method. In conventional operation of a QIT/TOF instrument, the Quadrupole Ion Trap itself is used as the first acceleration stage for Wiley-McLaren spatial focusing of the ions (either at the detector for linear time-of-flight or at an earlier point with energy refocusing for reflectron time-of-flight). However, the differential acceleration of ions at different initial axial positions in the trap causes a very wide energy spread in the extracted ion packet. The differential acceleration is essential for Wiley-McLaren spatial re-focusing, but the energy spread is very undesirable for using the ion packet for energy-resolved reactive collisions. We have characterized a short-pulse extraction method that creates a narrow energy spread of ions in the packet. The extraction pulse ends before any ions reach the exit aperture, giving them all the same total acceleration. That

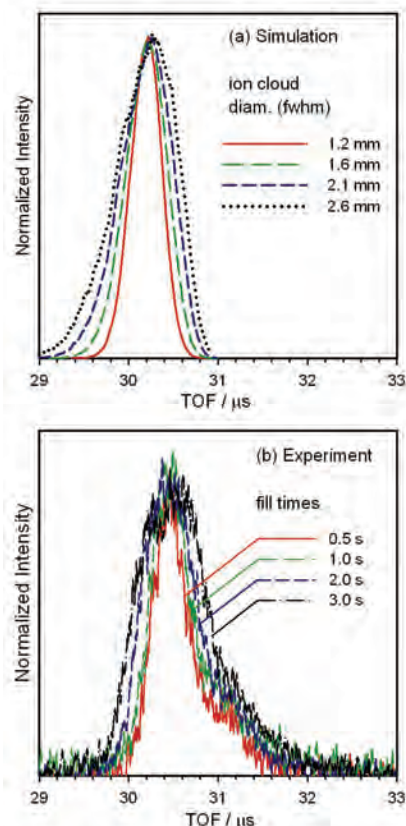


Figure 4. Time-of-flight peak profiles for short-pulse extraction used for diagnostics of the ion cloud size in the quadrupole ion trap.

precludes Wiley-McLaren spatial focusing, but instead provides a well-defined energy with a narrow distribution. Using ion trajectory simulations compared with experiment, we have demonstrated that the short-pulse mode can also be used to diagnose the size of the ion cloud in the ion trap prior to extraction. Results comparing experimental and simulations peak profiles for different ion cloud sizes (varied by changing the ion fill times and number of ions in the trap) are shown in Figure 4.

During this project year, we have also upgraded the power supply and control system for the magnet on our magnetic sector mass spectrometer on the guided ion beam tandem mass spectrometer. This replaces obsolete 1970s era electronics that came with a MAT double focusing mass spectrometer that we cannibalized for the instrument nearly 20 years ago. With field control using a Hall effect sensor and a stable power supply, we can now reliably tune to a known mass (m/z) and stay there, which greatly simplifies experimental protocols.

C. Franck-Condon Analysis Software

Continuing previous collaborations [8-10], we have further developed the PESCAL program for Franck-Condon simulations of photoelectron spectra and photodetachment threshold spectra. The PESCAL code has been used by several other groups, for example references [4, 11-16] since 2009.

III. Future Work

Experimental work will continue on the ion thermochemistry experiments detailed above and related work involving proton affinities in cationic systems. In the near term, we plan to extend the work on peroxyformate anion to the similar peroxyacetate system. We are also further developing our quadrupole ion trap/time-of-flight mass spectrometer apparatus with future applications related to combustion systems.

IV. References

- (1) Armentrout, P. B.; Ervin, K. M.; Rodgers, M. T. *J. Phys. Chem. A* **2008**, *112*, 10071.
- (2) Ervin, K. M. *Chem. Rev.* **2001**, *101*, 391. Erratum, *ibid.* **2002**, *102*, 855.
- (3) Nickel, A. A.; Lanorio, J. G.; Ervin, K. M. **2010** (work in progress).
- (4) Villano, S. M.; Eyet, N.; Wren, S. W.; Ellison, G. B.; Bierbaum, V. M.; Lineberger, W. *C. J. Phys. Chem. A* **2010**, *114*, 191.
- (5) Sassin, N. A.; Everhart, S. C.; Cline, J. I.; Ervin, K. M. *J. Chem. Phys* **2008**, *128*, 234305.
- (6) Sassin, N. A.; Everhart, S. C.; Dangi, B. B.; Ervin, K. M.; Cline, J. I. *J. Am. Soc. Mass Spectrom.* **2009**, *20*, 96.
- (7) Dangi, B. B.; Sassin, N. A.; Ervin, K. M. *Rev. Sci. Instrum.* **2010** (submitted).

- (8) Wren, S. W.; Vogelhuber, K. M.; Ervin, K. M.; Lineberger, W. C. *Phys. Chem. Chem. Phys.* **2009**, *11*, 4745.
- (9) Adams, C. L.; Schneider, H.; Ervin, K. M.; Weber, J. M. *J. Chem. Phys.* **2009**, *130*, 073407.
- (10) Vogelhuber, K.; Wren, S. W.; McCoy, A.; Ervin, K. M.; Lineberger, W. C. **2010**, (*work in progress*).
- (11) Yen, T. A.; Garane, E.; Shreve, A. T.; Neumark, D. M. *J. Phys. Chem. A* **2010**, *114*, 3215.
- (12) Soorkia, S.; Trevitt, A. J.; Selby, T. M.; Osborn, D. L.; Taatjes, C. A.; Wilson, K. R.; Leone, S. R. *J. Phys. Chem. A* **2010**, *114*, 3340.
- (13) Trevitt, A. J.; Goulay, F.; Meloni, G.; Osborn, D. L.; Taatjes, C. A.; Leone, S. R. *Int. J. Mass Spectrom.* **2009**, *280*, 113.
- (14) Goulay, F.; Trevitt, A. J.; Meloni, G.; Selby, T. M.; Osborn, D. L.; Taatjes, C. A.; Vereecken, L.; Leone, S. R. *J. Am. Chem. Soc.* **2009**, *131*, 993.
- (15) Miller, S. R.; Schultz, N. E.; Truhlar, D. G.; Leopold, D. G. *J. Chem. Phys.* **2009**, *130*, 024304.
- (16) Villalta, P. W.; Leopold, D. G. *J. Chem. Phys.* **2009**, *130*, 024303.

V. Publications and submitted journal articles supported by this project 2008-2010

- Jia, B.; Ervin, K. M. "Threshold collision-induced dissociation of hydrogen-bonded dimers of carboxylic acids", *J. Phys. Chem. A* **2008**, *112*, 1773-1782.
- Shi, Y.; Ervin, K. M. "Hydrogen atom transfer reactions of C_2^- , C_4^- , and C_6^- . Bond dissociation energies of $H-C_{2n}^-$ and $H-C_{2n}$ ($n = 1, 2, 3$)", *J. Phys. Chem. A* **2008**, *112*, 1261-1267.
- Armentrout, P. B.; Ervin, K. M.; Rodgers, M. T. "Statistical rate theory and kinetic energy-resolved ion chemistry: Theory and applications", *J. Phys. Chem. A* **2008**, *112*, 10071-10085.
- K. M. Ervin, PESCAL, Fortran program for Franck-Condon simulation of photoelectron spectra, <http://wolfweb.unr.edu/~ervin/pes/> (major revision 2008; minor revisions 2009, 2010).
- Adams, C. L.; Schneider, H.; Ervin, K. M.; Weber, J. M. "Low-energy photoelectron imaging spectroscopy of nitromethane anions: Electron affinity, vibrational features, anisotropies and the dipole-bound state." *J. Chem. Phys.* **2009**, *130*, 074307:1-10.
- S. W. Wren, K. M. Vogelhuber, K. M. Ervin, and W. C. Lineberger, "The photoelectron spectrum of CCl_2^- : The convergence of theory and experiment after a decade of debate", *Phys. Chem. Chem. Phys.* **2009**, *11*, 4745-4753.

Spectroscopic and Dynamical Studies of Highly Energized Small Polyatomic Molecules

Robert W. Field
Massachusetts Institute of Technology
Cambridge, MA 02139
rwfield@mit.edu

I. Program Scope

The fundamental goal of this program is to develop the experimental techniques, diagnostics, interpretive concepts, and pattern-recognition schemes needed to reveal and understand how large-amplitude motions are encoded in the vibration-rotation energy level structure of small, gas-phase, combustion-relevant polyatomic molecules. We are focusing our efforts on unimolecular isomerization in several prototypical systems, including the $\text{HNC} \leftrightarrow \text{HCN}$ and $\text{HCCH} \leftrightarrow \text{CCH}_2$ isomerization systems. We are developing chirped-pulse millimeter wave (CPmmW) spectroscopy as a technique that can be used in conjunction with Stimulated Emission Pumping (SEP) and the Stark effect to populate and identify molecular states with high excitation in *local* vibrational modes, which are of key importance in understanding isomerization processes.

II. Recent Progress

A. CPmmW Spectroscopy

1. Chirped Pulse/Slit jet spectrometer

Chirped-Pulse Millimeter-Wave (CPmmW) spectroscopy is the first truly broadband and high resolution technique for spectroscopy in the millimeter wave region. We designed the technique in collaboration with the Brooks Pate research group at the University of Virginia, based on their pioneering Chirped-Pulse Fourier-Transform Microwave (CP-FTMW) spectrometer, which operates at frequencies up to 20 GHz. We have built and tested a CPmmW spectrometer that operates in the 70–102 GHz frequency range. The spectrometer can acquire up to 12 GHz of spectral bandwidth at better than 100 kHz resolution in a single shot, and initial tests indicate significant advantage over existing millimeter-wave spectrometers in sensitivity times spectral bandwidth. The slit jet apparatus that we are in the process of constructing will increase the sensitivity of our CPmmW experiments by at least a factor of 100. The gas load of the slit jet will be 10 times of that of the regular axial jet that we currently use. Another factor of 10 or more in signal-to-noise improvement will come from reduced Doppler profile in the slit configuration. In order to facilitate supersonic expansion and minimize collisional broadening in the molecular beam, the slit jet needs to operate at 2 mTorr or less background pressure. After modeling pumping of the expected 1 mbar•L/pulse gas load, we designed a custom vacuum chamber pumped by a 2100 L/ turbo-molecular pump, which should satisfy the pumping requirements. This equipment has been ordered and is being assembled in our lab. The sensitivity and accurate relative intensities of the CPmmW technique will translate into new classes of spectral diagnostics that will enable us to attack new regimes of spectral congestion and dynamical complexity.

2. C_2H

An ongoing CPmmW project is the study of the C_2H radical. C_2H is a small but complicated molecule due to a ferocious vibronic coupling between the $\tilde{X}^2\Sigma$ and the $\tilde{A}^2\Pi$ states, which are separated by only $\sim 3000 \text{ cm}^{-1}$. C_2H also presents the possibility of exhibiting bond-breaking isomerization along the same $\angle\text{CCH}$ coordinate as acetylene. Recent preliminary experiments in our group exploit the increased sensitivity and bandwidth of the CPmmW technique to enable measurement of several molecular properties in C_2H that are sensitive reporters of geometry and electronic wavefunction mixing. These include the dipole moment via the Stark effect, as well as the spin-spin splitting and the Fermi contact hyperfine interaction. We have successfully generated C_2H using discharge methods and have detected it via its ground-state rotational spectrum. Excited vibrational states can be produced by a variety of methods, including photolysis and IR excitation, and will then be probed by CPmmW spectroscopy.

In conjunction with our experimental investigation of C_2H , we are working on a theoretical treatment. As part of a collaboration with Prof. J. F. Stanton, we have used the Köppel, Domcke, and Cederbaum

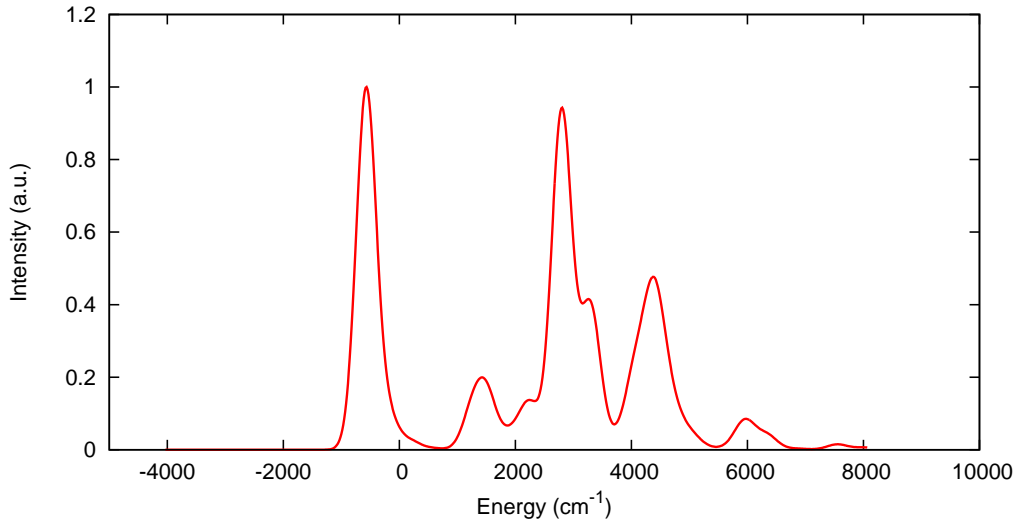


Figure 1: Simulated photodetachment spectrum of C_2H^- . The calculation is performed using the KDC quasideiabatic model, with parameters obtained at the EOMIP-CCSDT/ANO1 level of theory. The horizontal axis is offset by the ~ 3 eV anion photodetachment energy.

(KDC) quasideiabatic model to calculate the vibronic levels of C_2H . The agreement with experiment at the EOMIP-CCSDT/ANO1 level is excellent, and we plan to use this model Hamiltonian to calculate vibronically averaged properties of the bending levels of the $\tilde{X}^2\Sigma$ state for comparison with CPmmW measurements. The calculated photodetachment spectrum of C_2H^- is shown in Fig. 1.

B. High- and low-barrier unimolecular isomerization in S_0 and S_1 HCCH

The goal of our studies on the acetylene \leftrightarrow vinylidene system is to observe barrier-proximal vibrational states. Many studies have demonstrated that the vibrational eigenstates of acetylene and similar molecules undergo a normal-to-local transition in which the normal modes appropriate to describe small displacements from the equilibrium geometry evolve into local modes in which the excitation is isolated in a single C-H bond stretch or $\angle CCH$ bend. The evolution of vibrational character is of particular interest in the acetylene bending system, because the local-bending vibration bears a strong resemblance to the reaction coordinate for isomerization from acetylene to vinylidene, with one hydrogen moving a large distance off of the C-C bond axis while the other hydrogen remains nearly stationary.

1. PUMP-DUMP-PROBE experiments on local-bender eigenstates

While the existence of local-bender eigenstates in S_0 acetylene has been predicted by a variety of theoretical models, including effective Hamiltonian fits to the available experimental data, experimental verification of the large-amplitude character of these vibrational eigenstates has been difficult to achieve. We have observed the first direct evidence of the S_0 local-bender states. Using local-bender-pluck states on the S_1 surface as SEP intermediates, we recorded spectra that show a degenerate pair of levels with g/u symmetries in the energy region where the local-benders are predicted to emerge. The observed degeneracy corresponds with expectations for the local-bender states. The large geometric distortions associated with these states should lead to large vibrationally-averaged dipole moments, which will distinguish them from the vast majority of strongly mixed, small-amplitude, ergodic states.

Recently we undertook PUMP-DUMP-PROBE laser experiments with the goal of observing Stark mixing of the g/u paired local-bender eigenstates as evidence of their local mode character. The spectra recorded contained previously unobserved $K' = 3$ levels of the S_1 state, as well as new information about Franck-Condon access to and from interesting vibrational states on both electronic surfaces. While no Stark mixing has yet been observed in these laser experiments, the PUMP-DUMP-PROBE spectra have emerged as a promising new way to detect and characterize large amplitude motion states. Using members of a class of special vibrational eigenstates as launch states for the PROBE spectrum allows definitive and

immediate identification of which upper states would be ideal PUMP states for extending access to ever larger-amplitude-motion states.

2. Observation and theoretical treatment of vibrational levels of S_1 *cis* acetylene

Aside from its utility as an intermediate for studying highly excited vibrational states of the S_0 surface, the S_1 state also presents the possibility of characterizing low-barrier isomerization from its *trans*-geometry minimum to a local minimum at the *cis*-bent geometry. This isomerization has been the focus of many theoretical studies, but it has been difficult to study experimentally because, though the *trans* minimum has been exhaustively characterized, the transition from the ground electronic state to the S_1 *cis* geometry is electronically forbidden and no transitions to this conformer have previously been observed. In the course of characterizing the S_1 surface, several vibrational levels were observed which could not be ascribed to S_1 -*trans* or other electronic states. S_1 -*cis* seems a likely candidate for explaining these interloper levels, which were, surprisingly, observed below the energy of the calculated barrier to *trans-cis* isomerization, and must therefore owe their observed intensity to mixing via tunneling with *trans*-geometry-localized states.

Evidence continues to mount in favor of the S_1 *cis* assignment of these interloper levels. A three dimensional discrete variable representation (DVR) calculation has been performed that reproduces the S_1 vibrational level structure to within 2% for the fundamental vibrational levels, and can generate at least qualitatively correct spectral intensities, although the comparison of intensities is complicated by many factors. The calculation predicts *cis-trans* mixing as well as the unexpected spectral features, in agreement with the proposed explanation of low barrier *cis-trans* isomerization. Furthermore, $^{13}\text{C}_2\text{H}_2$ LIF spectra for one of the interloper bands shows isotope shifts that agree extremely well with the predicted isotope shifts for its *cis* assignment, but which cannot be reconciled with any possible *trans* well assignment.

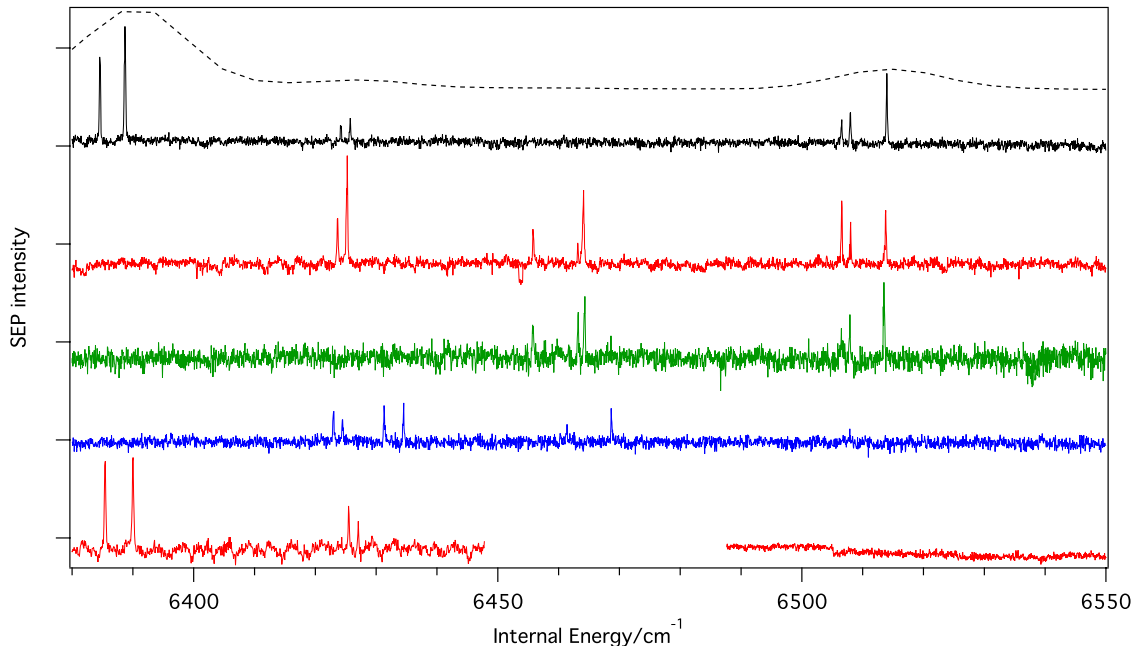


Figure 2: SEP spectra of the $N = 10$ pure bending polyad of S_0 C_2H_2 . From top to bottom, the S_1 PUMP states are $2^1 3^2$, the 3 members of $3^2 B^2$ from high to low energy, and 4^3 . (The $2^1 3^2$ DF spectrum is shown as a dashed trace.) SEP spectra from 4^3 and $2^1 3^2$ are expected to have the same relative intensity distribution within a polyad, yet the features near 6510 cm^{-1} are missing from the 4^3 spectrum. Since these features are present in spectra from PUMP states that are expected to light up $v_4'' = N$ and $v_4'' = N - 2$, e. g. $2^1 3^2$ and $3^2 B^2$, it seems plausible that a mixing of 4^3 with the analogous $2^1 3^1 6^2$ might interfere destructively with the transition amplitude to those S_0 states. Accordingly, the spectral features near 6390 cm^{-1} that appear only from $2^1 3^2$ and not from $3^2 B^2$ are unaffected in the 4^3 spectrum.

3. Upper state mixing revealed in SEP spectra

Reduced dimension DVR calculations predict a three-state interaction involving one of the S_1 interloper bands. According to the calculation, this *cis* interloper state engenders an indirect coupling between

the *trans* $2^13^16^2$ and 4^3 zero-order states, causing the eigenstates to lie substantially farther apart than one might expect, and lending intensity to the *cis* 3^16^1 interloper band that appears between them. These predictions agree quite well with experimental observations. The intrapolyad intensity patterns observed in SEP spectra from the *cis* interloper were expected to reveal the character of the intensity-lending *trans* state or states. Preliminary SEP spectra from the 4^3 state contain evidence of an unexpected interference effect resulting from this proposed three-state coupling. S_0 intrapolyad intensity distributions are, as a rule, governed solely by the fractionation of the (single) bright state. However, as shown in Fig. 2, the intensity distribution in the SEP spectrum observed from the 4^3 state deviates from the expected pattern, and seems to contain an interfering combination of the bright state patterns seen in the 2^13^2 and the 3^2B^2 spectra. This type of indirect effect can yield much information about state mixing, and is particularly interesting in this case since its effects on the level structure cannot reasonably be accounted for by effective Hamiltonian models that rely solely on polyads.

III. Future Work

We plan to continue to improve the sensitivity of our CPmmW spectrometer by taking advantage of new millimeter-wave technology and by incorporating a slit-jet molecular beam chamber. These enhancements will enable us to measure the populations of vibrationally-excited photolysis and pyrolysis products and locate the acetylene local-bender states. Combining our S_1 DVR results with the survey capability of CPmmW/DF spectra will guide us towards conclusive SEP experiments. We will record Stark effect spectra of the S_0 highly vibrationally excited levels, in order to measure the large predicted vibrationally-averaged dipole moments of the local-bender barrier-proximal states.

Publications supported by this project 2008–2010

- [1] H. A. Bechtel, A. H. Steeves, B. M. Wong, and R. W. Field. Evolution of chemical bonding during HCN/HNC isomerization as revealed through nuclear quadrupole hyperfine structure. *Angewandte Chemie International Edition*, 47(16):2969–2972, 2008.
- [2] A. J. Merer, N. Yamakita, S. Tsuchiya, A. H. Steeves, H. A. Bechtel, and R. W. Field. Darling–Dennison resonance and Coriolis coupling in the bending overtones of the \tilde{A}^1A_u state of acetylene, C_2H_2 . *The Journal of Chemical Physics*, 129(5):054304, 2008.
- [3] A. H. Steeves, A. J. Merer, H. A. Bechtel, A. R. Beck, and R. W. Field. Direct observation of the symmetric stretching modes of \tilde{A}^1A_u acetylene by pulsed supersonic jet laser induced fluorescence. *Mol. Phys.*, 106(15):1867–1877, 2008.
- [4] A. J. Merer, Z. Duan, R. W. Field, and J. K. G. Watson. Perturbations in the $4\nu_3$ level of \tilde{A}^1A_u state of acetylene, C_2H_2 . *Canadian Journal of Physics*, 87(5):437–441, 2009.
- [5] A. H. Steeves, H. A. Bechtel, A. J. Merer, N. Yamakita, S. Tsuchiya, and R. W. Field. Stretch-bend combination polyads in the \tilde{A}^1A_u state of acetylene, C_2H_2 . *Journal of Molecular Spectroscopy*, 256(2):256–278, 2009.
- [6] G. B. Park, A. H. Steeves, and R. W. Field. A Chirped-Pulse Millimeter-Wave Spectrometer in the 70–100 GHz Range. *Journal of Molecular Spectroscopy*, in preparation, 2010.

Scanning Tunneling Microscopy Studies of Chemical Reactions on Surfaces

George Flynn, Department of Chemistry, Columbia University

Mail Stop 3109, 3000 Broadway, New York, New York 10027

gwf1@columbia.edu

Introduction:

Our work is focused on fundamental chemical events taking place on carbon surfaces^{1,2} with the intent of shedding light on their role in mediating the formation of polycyclic aromatic hydrocarbons (PAHs) from small molecular precursors and the growth of soot particles.³⁻⁷ One of the exciting developments in this area of research has been the discovery of techniques for preparing and studying single graphite sheets or graphene⁸, a two-dimensional material whose chemical reactivity is substantially greater than that of multi-sheet graphite.^{1,2,4}

We use scanning tunneling microscopy (STM) to study the interfacial structure and chemistry of graphene mainly because of its ability to investigate surface structure and dynamics with molecular or even atomic resolution. In addition we employ micro-Raman scattering to identify and distinguish among single, double and triple layered graphene samples and to assess the amount of electron or hole “doping” caused by surface adsorbates. Atomic force microscopy (AFM) is also employed to determine the large scale “flatness” of graphene on different substrates.

The electronic and structural properties of graphene are quite unusual and depend on both the size and shape of the graphene flakes, which are themselves essentially giant PAHs. Furthermore, evidence is mounting (see below) that the relative smoothness and hence chemistry of graphene samples is dependent on the nature of the underlying substrate on which they are mounted. Graphene is an interesting model system in which to study the kind of carbon chemistry that is likely to shed light on the properties of soot-like materials.

In terms of chemical reactivity, the edges of large PAHs and the surfaces of soot particles in the third stage of growth are analogous to the edges of pits, defect sites and step edges on graphite and graphene. Exposure of well characterized, defected graphite and graphene surfaces to oxygen or hydrocarbon fuels (e.g. C₂H₂) in a controlled manner under ultra-high vacuum (UHV) conditions, thus, provides an opportunity to investigate the fundamental chemical steps involved in carbon chemistry and soot formation. Interest in soot is ultimately driven by the environmental and health implications arising from its formation in combustion reactions (particularly those involving heavier, diesel fuels containing catalytic metal atoms⁹⁻¹¹), which are nearly ubiquitous throughout our society.³⁻⁷

Results: “Ultra-flat” Graphene on Mica

The fabrication and characterization of high-quality ultraflat graphene monolayers has been realized by making use of a mica support that provides atomically flat terraces over large areas. The key to the success of these experiments was the preparation of an atomically flat substrate for deposition of single-layer graphene crystals. For this purpose mica, a material composed of negatively charged aluminosilicate layers that are linked by single layers of potassium ions, was chosen. Since cleavage takes place readily along the

potassium layer, atomically smooth surfaces with lateral dimensions as large as 100 μm can be routinely produced.

Graphene monolayers were prepared by the standard method⁸ of mechanical exfoliation of kish graphite on both mica and bulk SiO_2 substrates for comparative studies. (Both the cleavage of mica and the transfer of graphene sheets to the resulting mica surface were carried out in a dry glove box to minimize the effects of atmospheric water vapour on the samples.) AFM topographic images for regions surrounding the edges of graphene samples on both SiO_2 and mica substrates were readily obtained. Histograms of the corresponding height distribution over $200 \times 200 \text{ nm}^2$ regions of the surfaces show significant variations among the different substrates. For the bare SiO_2 surface, the parameters describing the height variation (σ) and correlation length (l) are, respectively, $\sigma = 168 \text{ pm}$ and $l = 16 \text{ nm}$. For the graphene monolayer on SiO_2 , we find a comparable (or slightly diminished) degree of roughness, with $\sigma = 154 \text{ pm}$ and $l = 22 \text{ nm}$, indicating that graphene monolayers largely follow the underlying substrate morphology.

In sharp contrast to these results, our AFM images on the mica substrate exhibit a much smoother landscape. For the bare mica surface, we obtain $\sigma = 34.3 \text{ pm}$ and $l = 2 \text{ nm}$. (The low value of l can be attributed to residual AFM noise, rather than to physically meaningful features.) Taking the measured value of σ as a guide, the surface of mica is seen to be at least 5 times smoother than that of the SiO_2 substrate. When placed on such a flat mica terrace, graphene monolayers display an exceedingly flat structure, one quite different from that observed for graphene/ SiO_2 . This difference can be seen qualitatively by simply comparing the 3D, stereographic presentations of the AFM topographic images. More quantitatively, for graphene on mica, we obtain $\sigma = 24.1 \text{ pm}$ and $l = 2 \text{ nm}$. This topography is at least 5 times smoother than that of graphene on SiO_2 . Since the interlayer distance in bulk graphite is 340 pm, with an observed height variation of only 24.1 pm, we can consider graphene on mica as having reached the limit of atomic flatness with respect to ripples, *i.e.*, a height variation substantially less than the diameter of an atom when probed with our lateral resolution of 7nm.

Present and Future Experimental Program

It should be possible to probe oxidation of both ultra-flat graphene on mica and “bumpy” graphene on SiO_2 in an ultra-high vacuum chamber at temperatures ranging from 300-800 K. From our studies of the oxidation of graphene on SiO_2 carried out at atmospheric pressure, we know that single sheet graphene shows evidence of oxidation at a lower temperature than double and triple sheet samples². We suspect that this is due to the locally bumpy nature of single sheet graphene on SiO_2 . This idea can be tested by studying the oxidation of single sheet graphene on mica. When the oxidation is carried out in an ultra-high vacuum chamber, STM can be used to follow the atomic scale surface features that are most reactive. The importance of defect structures can also be assessed by punching nanoscopic holes in graphene with the STM tip, followed by exposure to O_2 gas. Our expectation is that anything, which breaks the aromatic symmetry and hence interrupts the delocalization of electrons over the graphene sheet, will also affect the chemical reactivity of this material. Similar experiments can be

carried out using acetylene as the fuel. Earlier work on graphite surfaces from our laboratory suggests that graphene or defected graphene will also be reactive toward hydrocarbons such as acetylene¹.

References

1. Li Liu, Kwang Taeg Rim, Daejin Eom, Tony Heinz, and George W. Flynn “Direct Observation of Atomic Scale Graphitic Layer Growth,” *Nanoletters*, **8**, 1872-1878 (2008)
2. Li Liu, Sunmin Ryu, Michelle R. Tomasik, Elena Stolyarova, Naeyoung Jung, Mark S. Hybertsen, Michael L. Steigerwald, Louis E. Brus, George W. Flynn, “Graphene Oxidation: Thickness-Dependent Etching and Strong Chemical Doping”, *Nanoletters*, **8**, 1965-1970 (2008)
3. J. A. Miller and G. A. Fisk, “Combustion Chemistry”, *Chem. & Eng. News*, **65** (35), 22-46, August 31, 1987
4. Russell Whitesides, Dominik Domin, Romelia Salomon-Ferrer, William A. Lester, Jr., Michael Frenklach, “Graphene Layer Growth Chemistry: Five- and Six-Member Ring Flip Reaction”, *Journal of Physical Chemistry A*, **112**, 2125-2130 (2008)
5. Laszlo Nemes, Anna M. Keszler, Christian G. Parigger, James O. Hornkohl, Hope A. Michelsen, Vadim Stakhursky, “Spontaneous emission from the C₃ radical in carbon plasma”, *Applied Optics*, **46**, 4032-4040 (2007)
6. H. A. Michelsen, M. A. Linne, B. F. Kock, M. Hofmann, B. Tribalet, C. Schulz, “Modeling laser-induced incandescence of soot: enthalpy changes during sublimation, conduction, and oxidation”, *Applied Physics B: Lasers and Optics*, **93**, 645-656 (2008)
7. H. A. Michelsen, “Derivation of a temperature-dependent accommodation coefficient for use in modeling laser-induced incandescence of soot”, *Applied Physics B: Lasers and Optics*, **94**, 103-117 (2009)
8. K. S. Novoselov, D. Jiang, F. Schedin, T. J. Booth, V. V. Khotkevich, S. V. Morozov, A. K. Geim”, “Two-dimensional atomic crystals”, *Proc. Nat’l Acad. of Sci. of the U.S.* **102**, 10451-10453 (2005)
9. Kwang Taeg Rim, Mohamed Siaj, Shengxiong Xiao, Matthew Myers, Vincent D. Carpentier, Li Liu, Chaochin Su, Michael L. Steigerwald, Mark S. Hybertsen, Peter H. McBreen, George W. Flynn, and Colin Nuckolls, Forming Aromatic Hemispheres on Transition Metal Surfaces, *Angew. Chem. Int. Ed.* **46**, 7891-7895 (2007)
10. Daejin Eom, Deborah Prezzi, Kwang T. Rim, Hui Zhou, Michael Lefenfeld, Colin Nuckolls, Mark S. Hybertsen, Tony F. Heinz, and George W. Flynn, “Structure and Electronic Properties of Epitaxial Graphene on Co(0001)”, *Nanoletters*, **9**, 2844-2848 (2009)
11. R. Rosei, M. De Crescenzi, F. Sette, C. Quaresima, A. Savoia, and P. Perfetti, “Structure of graphitic carbon on Ni(111): A surface extended-energy-loss fine-structure study” *Phys. Rev. B* **28**, 1161-1164 (1983).

DOE Publications: (2008-2010)

1. Boaz Ilan, Gina M. Florio, Mark S. Hybertsen, Bruce J. Berne and George W. Flynn, "Scanning Tunneling Microscopy Images of Alkane Derivatives on Graphite: Role of Electronic Effects", *Nanoletters*, 8, 3160-3165 (2008)
2. Elena Stolyarova, Daniil Stolyarov, Li Liu, Kwang T. Rim, Yuanbo Zhang, Melinda Han, Mark Hybertsen, Philip Kim and George Flynn, "STM Studies of Ultrathin Graphitic (Graphene) Films on an Insulating Substrate under Ambient Conditions", *J. Phys. Chem. C*, 112, 6681-6688 (2008)
3. Li Liu, Kwang Taeg Rim, Daejin Eom, Tony Heinz, and George W. Flynn "Direct Observation of Atomic Scale Graphitic Layer Growth," *Nanoletters*, 8, 1872-1878 (2008)
4. Li Liu, Sunmin Ryu, Michelle R. Tomasik, Elena Stolyarova, Naeyoung Jung, Mark S. Hybertsen, Michael L. Steigerwald, Louis E. Brus, George W. Flynn, "Graphene Oxidation: Thickness-Dependent Etching and Strong Chemical Doping", *Nanoletters*, 8, 1965-1970 (2008)
5. E. Stolyarova, D. Stolyarov, K. Bolotin, S. Ryu, L. Liu, M. Klima, M. Hybertsen, I. Pogorelsky, I. Pavlishin, K. Kusche, J. Hone, P. Kim, L. Brus, H. L. Stormer, V. Yakimenko, G. Flynn, "Observation of Graphene Bubbles and Effective Mass Transport Under Graphene Films", *Nanoletters*, 9, 332-337 (2009)
6. Daejin Eom, Deborah Prezzi, Kwang T. Rim, Hui Zhou, Michael Lefenfeld, Colin Nuckolls, Mark S. Hybertsen, Tony F. Heinz, and George W. Flynn, "Structure and Electronic Properties of Epitaxial Graphene on Co(0001)", *Nanoletters*, 9, 2844-2848 (2009)
7. Kwang Taeg Rim, Daejin Eom, Li Liu, Elena Stolyarova, Joan Marie Raitano, Siu-Wei Chan, Maria Flytzani-Stephanopoulos, and George W. Flynn, "Charging and Chemical Reactivity of Gold Nanoparticles and Adatoms on the (111) Surface of Single Crystal Magnetite: A Scanning Tunneling Microscopy/Spectroscopy Study", *J. Phys. Chem. C*, 113, 10198-10205 (2009)
8. Chun Hung Lui, Li Liu, Kin Fai Mak, George W. Flynn, and Tony F. Heinz, "Ultraflat Graphene", *Nature*, 462, 339-342 (2009)
9. E. Stolyarova, K. Rim, K. Douglass, D. Eom, R. Opila, T. Heinz, A. V. Tepyakov, G. W. Flynn, "STM and XPS Studies of Graphene Films Prepared by Sonication-Assisted Dispersion", in preparation

Quantitative Imaging Diagnostics for Reacting Flows

Jonathan H. Frank
Combustion Research Facility
Sandia National Laboratories
Livermore, CA 94551-0969
jhfrank@sandia.gov

Program Scope

The primary objective of this project is the development and application of laser-based imaging diagnostics for studying the interactions of fluid dynamics and chemical reactions in reacting flows. Imaging diagnostics provide temporally and spatially resolved measurements of species, temperature, and velocity distributions over a wide range of length scales. Multi-dimensional measurements are necessary to determine spatial correlations, scalar and velocity gradients, flame orientation, curvature, and connectivity. Current efforts in the Advanced Imaging Laboratory focus on planar laser-induced fluorescence and Rayleigh scattering techniques for probing the detailed structure of both isolated flow-flame interactions and turbulent flames. The investigation of flow-flame interactions is of fundamental importance in understanding the coupling between transport and chemistry in turbulent flames. These studies require the development of new imaging diagnostic techniques to measure key species in the hydrocarbon-chemistry mechanism as well as to image rates of reaction and dissipation. Recent advances in diagnostic capabilities enable us to probe the temporal evolution of turbulent flames as well.

Recent Progress

Effects of heat release on dissipation structures in turbulent jet flames

Ongoing comparisons of non-reacting turbulent flows and flames reveal the effects of heat release on the morphology of fine-scale turbulence structures in flames. High-resolution imaging of laser Rayleigh scattering in turbulent $\text{CH}_4/\text{H}_2/\text{N}_2$ jet flames and non-reacting propane jets enabled us to isolate the effects of flow shear and heat release on the dissipation field. Recent analysis quantified the effects of flame heat release on distributions of the local curvature and angular orientation of dissipation structures. The morphology of fine-scale turbulence structures within the reaction zone is indicative of significant reductions in local turbulence levels. The damping of turbulence in the reaction zone also alters the fine-scale turbulence structure in the outer regions of the jet flame. The reaction zone forms a viscous buffer that shields the outer mixing layer from the highly turbulent flow near the jet centerline. Insights from these experiments are being used in the development of turbulent combustion models, as described in the following section.

Coupling imaging diagnostics and large eddy simulations

Experimental studies of turbulent jet flames and non-reacting jets are coupled with high-fidelity LES calculations of J. Oefelein (Sandia) to evaluate how LES represents small-scale mixing and what the effect of resolution is on the time evolving dissipation fields. Recently, we have focused on understanding resolved-scale dynamics in simulations of turbulent non-reacting jets. The aim of these passive scalar mixing studies is to establish a foundation for simulating turbulent mixing processes before tackling the additional complexities of chemical reactions and heat release in turbulent flames. We have assessed the effects of LES grid size on the evolution of the mixture fraction and dissipation fields in turbulent axisymmetric jet flows. Figure 1 shows an example of comparisons between measured and simulated radial profiles of mean dissipation using three different LES grids. The experimental data were spatially filtered to match the resolution of the corresponding LES grids. The resolved-scale scalar mixing contains significant errors on the coarser grids and systematically approaches the actual mean distribution of dissipation as the grid is refined. This result highlights the compounding effect that errors

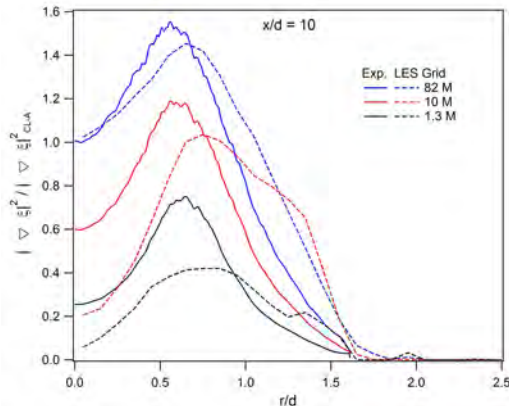


Fig. 1. Measured (Exp.) and computed (LES) radial profiles of mean scalar dissipation in a non-reacting propane jet with $Re=14,500$. Comparisons are shown at $x/d = 10$ for three LES grids, ranging from 1.3 to 82 million cells. Dissipation values are normalized by the corresponding centerline values for the 82 M cell grid. The measurements are spatially filtered to match the resolution of the corresponding LES grids.

in the mixture fraction field have on the overall mixing characteristics of the LES. The primary errors are most likely due to temporal damping and dispersion of the spatially evolving structures, which is an artifact of transporting the filtered quantities in LES with different levels of resolution. Further analysis of the temporal and spatial evolution of these errors is underway. We are also evaluating the effect of Reynolds number on these errors using a wide range of jet flow conditions.

High-repetition rate imaging for studying temporal evolution of turbulent flames

Efforts to develop a high-repetition rate imaging facility in the CRF's Advanced Imaging Laboratory are ongoing. This new capability will significantly enhance our research program by enabling us to probe the complex time history of interactions between turbulent flows and flames. Measurements of time history effects are particularly important for understanding intermittent phenomena, such as localized extinction and re-ignition. Our efforts to build up this capability at Sandia have been enhanced through collaborations with other laboratories that have invested in high-repetition rate imaging equipment. In a collaboration with W. Meier (DLR Stuttgart, Germany), we used simultaneous particle imaging velocimetry (PIV) and crossed-plane OH-LIF measurements to probe the temporal evolution of turbulent non-premixed jet flames with localized extinction. The crossed-plane configuration provided insight into the 3-D structure of the flame and reduced biases from out-of-plane motion that are inherent in 2-D planar high-speed measurements. Results demonstrated the importance of edge-flame propagation as a re-ignition mechanism and revealed a wide range of local edge-flame propagation speeds.

Impact of turbulence on reaction rates in premixed flames

We initiated a study on the local perturbation of reaction rates by turbulence in premixed counterflow flames in collaboration with A. Gomez (Yale Univ.). Work focused on the effects of turbulence on CO to CO_2 conversion rates in stoichiometric and lean premixed $CH_4/O_2/N_2$ flames with a turbulent Karlovitz number of approximately 5. The oxygen content of the different reactant mixtures was adjusted to maintain similar laminar flame speeds and adiabatic flame temperatures. Simultaneous OH-LIF and two-photon CO-LIF imaging measurements probed the CO oxidation via the $CO + OH = CO_2 + H$ reaction. Although the stoichiometric and lean flames ($\phi=0.7, 0.58$) occupied the same position on the extended Borghi diagram, they exhibited very different behavior with regard to CO oxidation. The stoichiometric flame was the least robust with the $CO + OH$ reaction almost entirely quenched. Results provide new evidence of turbulence affecting CO oxidation in premixed flames and highlight inadequacies of current frameworks for representing regimes of turbulent premixed combustion.

Future Plans

Recent comparisons of experiments and LES in non-reacting jets indicate the need for a thorough examination of widely used modeling assumptions in LES and a more complete understanding of the effects of grid resolution. A comparison of measurements and simulations near the jet exit will be used to examine the evolution of filtered quantities from the nascent jet flow to the downstream positions already investigated. High-repetition rate LIF imaging will be used to expand comparisons of experiments and LES to the time domain. This new capability will enable us to assess the effects of temporal filtering on the evolution of turbulence structures.

The continued development of a high-repetition rate imaging facility with simultaneous scalar and velocity measurements remains an essential goal of our research plan. As new capabilities are added, we will use them to study the dynamics of flow-flame interactions in turbulent premixed, non-premixed, and stratified modes of combustion.

In collaboration with J. Chen (Sandia), we established a joint experimental and computational capability for investigating the coupling of transport and chemistry in isolated flow-flame interactions using vortex-perturbed counterflow flames. In the next phase of this work, we plan to study extinction and re-ignition of oxygenated fuels, such as dimethyl ether. We will test the ability of different chemical mechanisms and transport models to capture the wide range of thermochemical states involved in extinction and re-ignition.

We plan to conduct detailed studies of turbulent stratified combustion in which premixed flames propagate into inhomogeneous mixtures of fuel and oxidizer. Despite its practical significance, stratified combustion has been studied in much less detail than perfectly premixed or non-premixed combustion. These studies will be performed in collaboration with experimental and computational groups from Technical University of Darmstadt, Cambridge University, and Sandia. Initial experiments are focused on methane-air flames in the Darmstadt coannular stratified burner (Fig. 2) and are conducted in collaboration with A. Dreizler (TU Darmstadt, Germany). The equivalence ratios and velocities of the outer annular slots can be varied independently to change the stratification and flow shear, respectively. We plan to study the effects of stratification and shear on the local flame structure. We will also explore approaches for conditioning measurements on the degree of local stratification.

We plan to develop a new mixing diagnostic technique that could be used for measuring either the local mixture stratification in the reactants and products of stratified premixed flames or the mixture fraction in non-premixed flames. This approach uses a noble gas as a chemically inert tracer that can be seeded into one of the flow streams. The tracer is detected using two-photon LIF imaging. We recently demonstrated the feasibility of two-photon LIF imaging of krypton seeded into turbulent jet flames in collaboration with N. Clemens (UT Austin). The combination of two-photon Kr LIF and laser Rayleigh scattering could be used to determine mixture fraction and temperature. Most previous mixture fraction imaging techniques have used combined measurements of chemically reactive species and temperature to construct a conserved scalar. The advantage of this new approach is that the tracer gas remains chemically inert in a wide range of conditions. Quantitative mixing measurements will require knowledge of the temperature-dependent collisional quenching rates of krypton by major flame species. Quenching measurements will be performed in collaboration with R. Farrow and T. Settersten (Sandia).

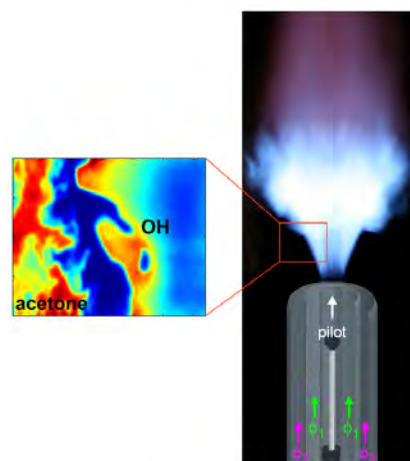


Fig. 2. Stratified premixed flame stabilized on the piloted coannular Darmstadt burner. Composite image of simultaneous single-shot LIF measurements of OH and acetone used to mark the flame front and the flow issuing from the outer slot, respectively.

BES-Supported Publications (2008-present)

- J.H. Frank and S.A. Kaiser, "High-resolution imaging of dissipative structures in a turbulent jet flame with Rayleigh scattering," *Exp. Fluids* **44**, 221-233 (2008).
- W.D. Kulatilaka, B.D. Patterson, J.H. Frank, and T.B. Settersten, "Comparison of nanosecond and picosecond excitation for interference-free two-photon laser-induced fluorescence detection of atomic hydrogen in flames," *Appl. Opt.* **47**, 4672-4683 (2008).
- S. Schlachter, A.D. Elder, J.H. Frank, A. Grudinin, and C.F. Kaminski, "Spectrally resolved confocal fluorescence microscopy with a supercontinuum laser," *Microscopy and Analysis* **22**, 11-13 (2008)
- C.F. Kaminski, R.S. Watt, A.D. Elder, J.H. Frank, and J. Hult, "Supercontinuum radiation for applications in chemical sensing and microscopy," *Appl. Phys. B* **92**, 367-378 (2008).
- C.S. Yoo, J.H. Chen, and J.H. Frank, "A numerical study of transient ignition and flame characteristics of diluted hydrogen versus heated air in counterflow," *Combust. Flame* **156**, 140-151 (2009).
- S. Schlachter, A.D. Elder, A. Esposito, G.S. Kaminski, J.H. Frank, L.K. van Geest, and C.F. Kaminski, "mhFLIM: Resolution of heterogeneous fluorescence decays in widefield lifetime microscopy," *Opt. Express* **17**:1557-1570 (2009)
- U.D. Lee, C.S. Yoo, J.H. Chen, J.H. Frank, "Effects of H₂O and NO on extinction and re-ignition of vortex-perturbed hydrogen counterflow flames," *Proc. Combust. Inst.* **32**, 1059-1066 (2009).
- E.R. Hawkes, R. Sankaran, J.H. Chen, S.A. Kaiser, J.H. Frank, "An analysis of lower-dimensional approximations to the scalar dissipation rate using direct numerical simulations of plane jet flames," *Proc. Combust. Inst.* **32**, 1455-1463 (2009).
- W.D. Kulatilaka, J.H. Frank, T.B. Settersten, "Interference-free two-photon LIF imaging of atomic hydrogen in flames using picosecond excitation," *Proc. Combust. Inst.* **32**, 955-962 (2009).
- S.A. Kaiser and J.H. Frank, "Spatial scales of extinction and dissipation in the near field of non-premixed turbulent jet flames," *Proc. Combust. Inst.* **32**, 1639-1646 (2009).
- W. D. Kulatilaka, J. H. Frank, B. D. Patterson, and T. B. Settersten, "Analysis of 205-nm photolytic production of atomic hydrogen in methane flames," *Appl. Phys. B* **97**, 227-242 (2009).
- J.H. Frank and R. S. Barlow, "Nonpremixed turbulent combustion," in *Combustion Phenomena: Selected Mechanisms of Flame Formation, Propagation, and Extinction*, J. Jarosinski and B. Veyssiere, Eds., CRC Press, 2009, pp. 153-162.
- A.D. Elder, C.F. Kaminski, and J.H. Frank, " ϕ^2 FLIM: a technique for alias-free frequency domain fluorescence lifetime imaging," *Opt. Express* **17**, 23181-23203 (2009).
- U.D. Lee, C.S. Yoo, J.H. Chen, J.H. Frank, "Effect of NO on extinction and re-ignition of vortex-perturbed hydrogen flames," *Combust. Flame* **157**, 217-229 (2010).
- J.H. Frank, S.A. Kaiser, J.C. Oefelein, "Analysis of scalar mixing dynamics in LES using high-resolution imaging of laser Rayleigh scattering in turbulent non-reacting jets and non-premixed jet Flames," Submitted to *Proc. Combust. Inst.*, 2010.
- A.G. Hsu, V. Narayanaswamy, N.T. Clemens, J.H. Frank, "Mixture fraction imaging in turbulent non-premixed flames with two-photon LIF of krypton," Submitted to *Proc. Combust. Inst.*, 2010.
- B. Böhm, J.H. Frank, A. Dreizler, "Temperature and mixing field measurements in stratified lean premixed turbulent flames," Submitted to *Proc. Combust. Inst.*, 2010.
- A.M. Steinberg, I. Boxx, C.M. Arndt, J.H. Frank, W. Meier, "Experimental study of flame-hole re-ignition mechanism in a turbulent non-premixed jet flame using sustained multi-kHz PIV and crossed-plane OH PLIF," Submitted to *Proc. Combust. Inst.*, 2010.
- B. Coriton, J.H. Frank, A.G. Hsu, M.D. Smooke, A. Gomez, "Effect of quenching of the oxidation layer in highly turbulent counterflow premixed flames," Submitted to *Proc. Combust. Inst.*, 2010.
- J.H. Frank and S.A. Kaiser, "High-resolution imaging of turbulence structures in jet flames and non-reacting jets with laser Rayleigh scattering," Submitted to *Exp. Fluids*, 2010.

MECHANISM AND DETAILED MODELING OF SOOT FORMATION

Principal Investigator: Michael Frenklach

Department of Mechanical Engineering

The University of California

Berkeley, CA 94720-1740

Phone: (510) 643-1676; E-mail: myf@me.berkeley.edu

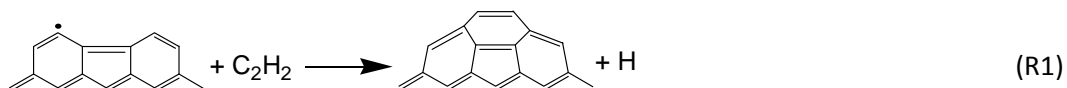
Project Scope: Soot formation is one of the key environmental problems associated with operation of practical combustion devices. Mechanistic understanding of the phenomenon has advanced significantly in recent years, shifting the focus of discussion from conceptual possibilities to specifics of reaction kinetics. However, along with the success of initial models comes the realization of their shortcomings. This project focuses on fundamental aspects of physical and chemical phenomena critical to the development of predictive models of soot formation in the combustion of hydrocarbon fuels, as well as on computational techniques for the development of predictive reaction models and their economical application to CFD simulations. The work includes theoretical and numerical studies of gas-phase chemistry of gaseous soot particle precursors, soot particle surface processes, particle aggregation into fractal objects, and development of economical numerical approaches to reaction kinetics.

Recent Progress:

Graphene-Edge Surface Kinetics Model: Bay Capping Reactions (with X. You, R. Whitesides, D. Zubarev, and W. A. Lester, Jr.)

Controlling formation of soot in modern combustion systems requires a good mechanistic understanding of soot particle growth. One of the biggest unknowns, particle inception, received substantial attention in recent years and its mechanistic picture steadily advances toward a unified theory. Another part of the mechanism, surface growth, has transformed from an empirical rate law to a simple elementary-reaction model to a complex, multi-step process. The complexity of the surface growth mechanism stems from numerous possibilities of chemical transformations taking place at graphene edges, presumed to be the building units of soot particles. Among them are game-changing processes: migrations of lone and embedded five-member rings, which give rise to rapid lateral translation of five-member rings along zigzag edges.

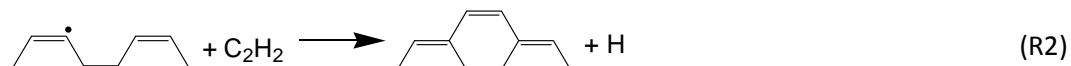
Last year, we reported a new detailed kinetic Monte-Carlo (KMC) model of graphene-edge growth with a total of 42 surface transformations ([7] in the publication list). Evolving edge morphology and growth rate were found to be affected by the rates of key reactions. One of the most interesting among them is capping, addition of acetylene to an embedded five-member ring,



The significance of this reaction step is several-fold. First, it pins down the five-member ring and prevents it from migrating. As ring migration generally leads to smoother surfaces, this aspect of capping works against it. Second, capping forms armchair-like sites that initiate zipper-type growth of new layers. Finally, capping permanently embeds five-member rings into the growing graphene structure and hence causes it to curve.

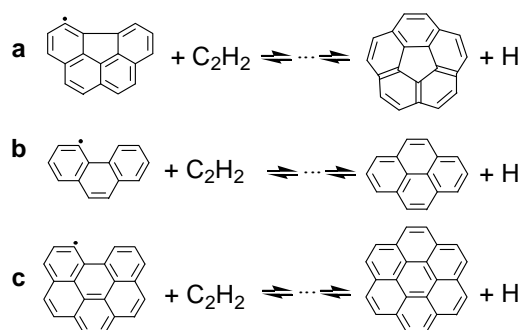
In [7], reaction R1 was assumed to have the rate coefficient of its zigzag-edge analog because no rate data were available. The importance of reaction R1 called for a thorough examination of its kinetics.

Capping an embedded five-member ring looks very similar to the acetylene-addition step of the primary HACA sequence, the one that takes place on an armchair bay,



We hence set out to compare the rate coefficients of the two reactions and their influence on graphene-edge growth. A graphene sheet becomes curved during ring-closure in capping an embedded five-member ring on a zigzag edge, while it remains planar when capping a boat site on an armchair edge.

Re-evaluation of reaction R2 turned out to be important in its own right. The two prior theoretical studies of this reaction were performed at semi-empirical levels of quantum theory, PM3 and AM1. In the present study, we reexamine the kinetics of the complete system of reaction R2, performing calculations at a higher level of theory, density functional theory (DFT) at the B3LYP/6-311G(d,p) level,

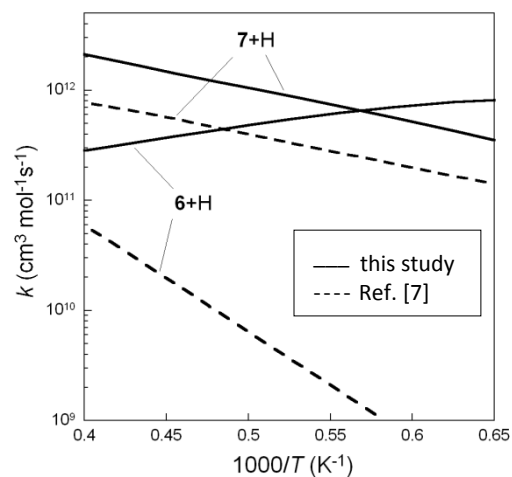


the same employed in recent studies of similar-size systems.

To examine the effect of substrate size, we performed the calculations for reaction R2 using two substrates, 3- and 6-ring molecular structures, as shown in the figure on the left.

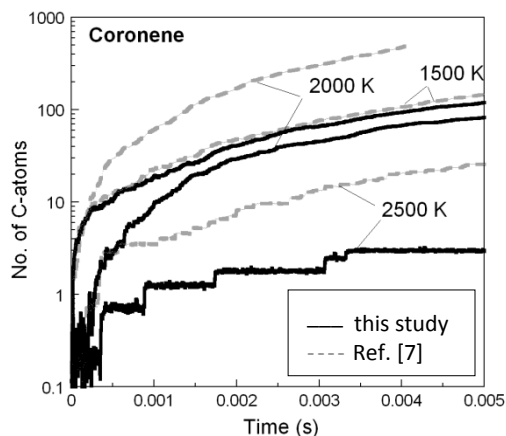
The kinetics were examined using the MultiWell suite of codes, covering temperatures from 1500 to 2500 K and pressures from 0.1 to 10 atm, thus spanning conditions from typical laboratory studies to practical combustion devices. No pressure dependence was found for the rate coefficients of all three reaction systems.

The rate coefficients computed for the main reaction channels, $1+\text{C}_2\text{H}_2 \rightarrow 6+\text{H}$ and $1+\text{C}_2\text{H}_2 \rightarrow 7+\text{H}$ (systems **a** and **c**, respectively) are displayed in the figure on the right. These results show that the rate coefficient of the step generating 7+H of **a** is about twice that of **c**. The new rate coefficient value for capping the five-member-ring bay is of the same order of magnitude as its prior estimate, yet with a substantially different activation energy. The calculated rate coefficient for capping the six-member-ring bay is one order magnitude lower than that used in prior KMC studies and is close to an older evaluation.

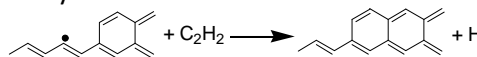


To examine the influence of the new kinetic data, we performed detailed kinetic Monte Carlo simulations changing the rate coefficients of the bay-capping reactions of the initial model [7]. The simulations track the evolution of a graphene structure in gaseous environments typical of combustion. At each time step, a reaction event is selected stochastically from a total of 42 surface transformations. Particular emphasis is given to incorporation of five-member rings and resulting curvature and edge defects. To properly account for the evolving curvature, after application of the KMC step, the molecular structure was optimized using the MM3 potential with the TINKER molecular mechanics package.

The simulations were run on five different substrates: pyrene, coronene, pentacene, decacene, and icosacene, at three constant temperatures 1500, 2000, 2500 K, and a constant gas-phase composition with mole fractions of C₂H₂, H₂, and H set to 0.1, 0.1, and 0.01, respectively. The replacement of the three reactions rates produced, generally, similar effects on the growth rates for the five substrates studied. Compared with the previous results [7], C-atom addition remained nearly the same at 1500 K, but slowed down at 2000 and 2500 K, and especially at 2000 K, as can be seen in the figure below.



Performing KMC simulations with changing rates individually revealed that the difference in the growth-rate pattern is mainly due to the change in the rate of KMC reaction $1+C_2H_2 \rightarrow 7+H$, namely



Among other computed measures, f_{R5} , the fraction of five-member rings, increased from 0.24 to 1.01 % at 0.004 s for coronene growth at 2000 K because the number of six-member rings was significantly decreased after lowering the rate of R3.

Previous KMC studies [7] showed that the difference in the growth rate and morphology of the evolving graphene edge was due to competition among corner, interior, and embedded-ring nucleation events initiating zipper-type growth. The mechanism of graphene-edge growth changes with temperature. At 1500 K, graphene-edge growth is promoted by the stable five-member rings incorporated in the growing layer that create interior nucleation sites. Embedded-ring nucleation via capping the embedded five-member ring is also possible at this temperature. Since the new rates of the five-member-ring capping do not change significantly, the growth rate and f_{R5} at 1500 K are not appreciably affected by these changes. With the increase in temperature, the thermodynamic and kinetic stability of five-member rings decreases. The increasingly frequent desorption of five-member rings leaves the structure composed of predominantly six-member rings, which promotes the relative importance of boat-site cyclization, reaction R3. Decreasing its rate tenfold has the most dramatic effect at 2000 K to reduce the growth rate and to increase the value of f_{R5} . At 2500 K, growth becomes much less frequent and five-member rings are rarely incorporated into the structure. The reaction mechanism at this temperature is dominated by corner nucleation via formation of six-member rings; and hence lowering the rate of R3, which propagates edge growth, causes a smaller reduction in the overall growth rate.

At the same time, the change in the rate coefficients did not affect the phenomenon of curving obtained for graphene-edge evolution in the previous study [7]. The molecular structure formed at 1500 K is significantly curved because of the high fraction of five-member rings in the structure. As temperature rises, the embedded five-member rings are more likely to escape from the surface; therefore, the resulting structure is less curved at 2000 K, and stays planar at 2500 K without much growth.

Most recently ([9] in the publication list), with an improved code, we performed KMC simulations for the conditions of Homann's flames and compared our numerical predictions with the experimentally determined H/C ratios of aromatic molecules as well as with recent numerical results of Kraft and co-workers (Raj et al., *Combust. Flame* 156:896, 2009). The results show that our model tends to predict species with lower hydrogen content than the experiments. Five-member ring incorporation, included in our model but not in the Raj et al. model, leads to curved structures that have smaller edges relative to un-curved species with the same number of carbon atoms and thus have fewer hydrogen atoms per molecule. In contrast, the model of Raj et al. tends to produce species with higher hydrogen content than those measured. Inclusion of surface "rounding" reactions in a more recent work by Raj, et al. (*Carbon* 48:319, 2010) has improved this to some degree but does not achieve full agreement. The disagreement between the experiment and the models for C/H ratios may be a result of overprediction of curvature in our model and underprediction in the Raj et al. model. As suggested in [7], interlayer effects may hinder curvature and thereby reduce the rate of curvature inducing reactions. Further analysis is in progress.

Local Electronic Structure and Stability of Polyaromatic Oxyradicals (with D. Yu. Zubarev, X. You, J. McClean, and W. A. Lester, Jr.)

During the past two years, we turned our attention to soot oxidation. As the first step in this direction we have examined thermodynamic stability of critical oxygenated intermediates. The initial analysis of local electronic structure of a series of pentacene oxyradicals showed that the relative stability of linear PAHs can be explained by fragmentation of the delocalized π -electron system of the precursor molecule and formation of locally aromatic fragments ([8] in the publication list). During the past year, we investigated relative stability of oxyradicals of two-dimensional PAH substrates to establish the role of the adjacent edges and the interior regions and identify the structural fragments responsible for the structural relaxation and stabilization upon oxidation. The analysis is in progress.

Future Plans

Graphene Layer Growth and Oxidation Chemistry: We will continue exploration of reactions on graphene edges. This work will be performed in collaboration with William Lester's group, performing DFT analysis of the reaction systems and then QMC analysis on most critical reaction steps identified in the prior DFT studies. For every reaction system, a complete set of rate coefficients will be established in master-equation solutions.

Graphene Layer Evolution: We will continue exploration of the evolution of graphene sheets through our newly-developed detailed KMC approach, by inclusion of additional reaction steps as they become available and by extending the simulation conditions and constraints.

DOE-BES Supported Publications (2008-2010)

1. "Isomer Energy Differences for the C_4H_3 and C_4H_5 Isomers Using Diffusion Monte Carlo," D. Domin, W. A. Lester Jr., R. Whitesides, and M. Frenklach, *J. Phys. Chem.* **112**, 2065 (2008).
2. "Graphene Layer Growth Chemistry: Five- and Six-Member Ring Flip Reaction," R. Whitesides, D. Domin, R. Salomón-Ferrer, W. A. Lester Jr., and M. Frenklach, *J. Phys. Chem.* **112**, 2125 (2008).
3. "Embedded-Ring Migration on Graphene Zigzag Edge," R. Whitesides, D. Domin, W. A. Lester Jr., and M. Frenklach, *Proc. Combust. Inst.* **32**, 577 (2009).
4. "Molecular Dynamics Simulations of PAH Dimerization," D. Wong, R. Whitesides, C. A. Schuetz and M. Frenklach, in *Combustion Generated Fine Carbon Particles* (H. Bockhorn, A. D'Anna, A. F. Sarofim, H. Wang, Eds.), Karlsruhe University Press, Karlsruhe, Germany, 2009, p. 245.
5. "A New Graphene Edge Surface Kinetics Model," R. Whitesides and M. Frenklach, *Proceedings of the 6th U.S. National Combustion Meeting*, Ann Arbor, MI, May 17-19, 2009.
6. "Time Integration of Chemical Kinetics with Computational Singular Perturbation and Tabulation," B. Debusschere, B. Rhoads, H. Najm, Y. Marzouk, M. Valorani, D. Goussis, and M. Frenklach, Fall Meeting of the Western States Section of the Combustion Institute, Irvine, CA, October 26-27, 2009.
7. "Detailed Kinetic Monte-Carlo Simulations of Graphene-Edge Growth," R. Whitesides and M. Frenklach, *J. Phys. Chem. A* **114**, 689-703 (2010), Feature Article.
8. "Local Electronic Structure and Stability of Pentacene Oxyradicals," D. Y. Zubarev, N. Robertson, D. Domin, J. McClean, J. Wang, W.A. Lester, Jr., R. Whitesides, X. You, and M. Frenklach, *J. Phys. Chem. C* **114**, 5429 (2010).
9. "Extended Simulations of Graphene Growth with Updated Rate Coefficients," R. Whitesides, X. You, and M. Frenklach, Spring Technical Meeting, Western States Section of the Combustion Institute, Boulder, CO, March 22-23, Paper No. 10S-22.
10. "Modeling Particle Dynamics with MOMIC," M. Frenklach, in *Modeling and Computation of Nanoparticles in Fluid Flows*, Lecture Series of van Karman Institute for Fluid Mechanics, in press.
11. "Modeling Particle Aggregation," M. Frenklach, in *Modeling and Computation of Nanoparticles in Fluid Flows*, Lecture Series of van Karman Institute for Fluid Mechanics, in press.
12. "Modeling Nanoparticle Formation," M. Frenklach and R. Whitesides, in *Modeling and Computation of Nanoparticles in Fluid Flows*, Lecture Series of van Karman Institute for Fluid Mechanics, in press.

Computer-Aided Construction of Chemical Kinetic Models

William H. Green
Department of Chemical Engineering, M.I.T.
Cambridge, MA 02139
whgreen@mit.edu

I. Program Scope

The combustion chemistry of even simple fuels can be extremely complex, involving hundreds or thousands of kinetically significant species. The most reasonable way to deal with this complexity is to use a computer not only to numerically solve the kinetic model, but also to construct the kinetic model in the first place. Our research spans a wide range from quantum chemical calculations on individual molecules and elementary-step reactions, through the development of improved rate/thermo estimation procedures, the creation of algorithms and software for constructing and solving the simulations, the invention of methods for model-reduction while maintaining error control, through comparisons with experiment. We are developing methods needed to make computer-construction of accurate combustion models practical, as well as tools to make it feasible to handle and solve the resulting large kinetic models, even in multidimensional reacting flows. Many of the parameters in the models are derived from quantum chemistry, and the models are compared with experimental data measured in our lab or in collaboration with others.

II. Recent Progress

A. Methodology for Computer-Aided Kinetic Modeling

The main focus of our research continues to be the development of methodology for constructing, reducing, and solving combustion simulations. With funding from NSF, we are integrating our extensible open-source reaction-mechanism-generation software RMG (<http://rmg.sourceforge.net>) with the PrIME database (<http://primekinetics.org>). In August 2009 we released RMG v.3.1, which builds kinetic models valid over the user-specified range of pressure and temperature. This automatically identifies and computes the rates of chemically-activated and other formally-direct reactions. We have incorporated an improved version of the approximate solution technique for the master equation suggested by NJB Green [i] into RMG v 3.1, this allows more accurate computations of $k(T,P)$ at reasonable computational cost. Our prior work used the Modified-Strong-Collision approximation, which is very efficient and robust, but which introduces errors up to about a factor of 3 in $k(T,P)$ in unfavorable cases; the user can choose which method to use. This new version of the RMG software package has already been downloaded by dozens of users.

Motivated by practical fuel problems in diesel engines, we are extending RMG so that it can construct kinetic models for reactions in liquid phase, not just gas phase. With separate funding we have recently reviewed methods for computing solvent effects [ii], and are currently implementing an automatic method in RMG for automatically estimating the solvation energies of all the species on-the-fly as the kinetic model is being constructed.

We continue to make progress in automated mechanism reduction, to facilitate the use of detailed fuel chemistry models in reacting flow simulations. We recently published a new model-reduction method, adaptively using principal orthogonal decomposition to reduce the chemical dimensionality.[9] Our current work is focused on clarifying the mathematical relationships between competing model-reduction methods, providing an equal basis for comparisons between different methods, and (with separate funding) implementation of error-controlled adaptive chemistry model-reduction into practical engine CFD simulators such as KIVA.

We have also developed a fast numerical solution method [15] for simulations of McEnally and Pfeifferle's doped methane 2-d diffusion flame experiments [iii], making it practical to model that extensive series of experiments in chemical detail as discussed below.

B. Quantum Calculations and Measurements of Individual Reaction Rates

We have directly measured the rate coefficients of several reactions of the vinyl radical using laser flash photolysis.[8,10,14] Unexpectedly, our measured rate coefficients for addition of vinyl radical to different alkenes do not follow the trend expected from Evans-Polanyi relations or the Hammond postulate. Similar findings have been previously reported based on quantum chemistry calculations for other addition reactions by Radom and by Marin. However, most existing large combustion chemistry models assume Evans-Polanyi or similar relations to estimate the rates of addition reactions and their reverse beta-scission reactions. We have performed high-level quantum calculations to understand this in detail, and recently published our explanation of this phenomena in *J. Phys. Chem. A*. [14] Reactions through the adduct compete with direct H-abstraction reactions that yield resonantly-stabilized radicals; next we plan to measure the branching ratio to allyl radical resulting from vinyl + propene.

We have computed the rates of many intramolecular reactions of ROO and HOOQOO species.[16] From these calculations have developed more accurate rate-estimation rules, and a better method for handling the coupling between internal rotors which occurs in long-chain species with stable ring conformers; this will allow us to build more accurate models for ignition and cool flame chemistry.

C. Applications: Large Kinetic Models and Engine Simulations

We have modeled McEnally & Pfefferle's measurements [iii] on aromatic formation in methane diffusion flames doped by several isomers of hexadiene in detail.[15] The chemistry is fairly complicated, for example the hexadienes form cyclic C5 species, and several of the important reactions required high-level quantum chemistry and variational transition state theory. We have also published manuscripts on the reaction $C_5H_5 + CH_3$, [13] which ultimately leads to benzene, and on the rates for C_5H_5 or C_5H_6 plus several C3 species (leading to styrene).[12]

Researchers at Shell and John Heywood at MIT have discovered that the R+M/2 octane test procedure used in the USA does not correctly rank the engine behavior of gasolines (i.e. some gasolines with low R+M/2 ratings are very resistant to knock in modern engines, and vice-versa.) We collaborated with Heywood to clarify the chemical-kinetic origin of the problem [iv], and are exploring how to appropriately bring this information to the awareness of groups in charge of setting fuel quality standards.

With separate funding, we have used RMG to construct detailed models for combustion of 3 of the 4 isomers of butanol, a biofuel which is scheduled to go into commercial production by 2012. We have validated these models with a wide variety of experimental data. Manuscripts describing these models have recently been submitted to *Combustion & Flame* and *I&ECR*.

III. Future Work

A. Methodology

We are completing a manuscript comparing different methods for computing $k(T,P)$, comparing accuracy, computer time (important for very large kinetic models), and robustness of the numerical methods.

As we become capable of accurately modeling more complicated fuels, we have begun to run into computer memory problems during mechanism construction (even if the final model at the end of the construction process is small enough to handle easily). We are developing improved mechanism construction algorithms to reduce peak memory requirements and to take advantage of the capabilities of modern multicore computers.

We are also writing a manuscript showing that several different model-reduction methods have the same mathematical structure, and so these methods can be compared in a general way.

We are working with Bozzelli, Marin, and the group from Nancy to reconcile discrepancies in procedures for automatically estimating thermochemistry, and plan to publish a unified group-contribution database, highlighting any unresolved issues. As part of this work, we have recently completed high level quantum calculations of the thermochemistry for 170 species important in propane combustion. We are also developing new ways to compute the thermochemistry for intermediates formed

from fused-ring fuel species. So far, most researchers have focused on C,H,O species, but we plan to add methods for estimating species containing N and S heteroatoms, as these species are important in some fuels. We have begun to construct group values for C,H,N,O species [6].

B. Individual Reactions: Quantum Chemistry & Experiments

We have recently predicted product distributions from several reactions of vinyl radicals with unsaturated species.[8,14] We plan to test these predictions by directly measuring the yield of allylic radical products using flash photolysis with long-pulse laser absorption spectroscopy, and to use mass spectrometry to measure the branching ratios to other product channels. After completing these measurements, we plan to measure reactions of carbonyl radicals formed when alcohols are oxidized. We are collaborating with Bob Field to develop new spectroscopic methods to more precisely quantify radical yields.

We have recently collaborated with Stephen Klippenstein to compute the reaction allyl + HO₂ and the decomposition reactions of the resulting allyloxy radical, and submitted that work for presentation at the Combustion Symposium.

C. Large Kinetic Models and Applications

We have initiated a collaboration with Charlie Westbrook and Rolf Reitz to develop a model for a new type of two-fuel two-injector engine invented at Wisconsin, which has been demonstrated to achieve a very impressive 53% thermal efficiency.[v] The amount of each fuel is varied to maintain the engine near its optimal efficiency over a broad range of operating conditions. In one practical manifestation of this new type of engine, it appears it would be helpful to add cetane improvers such as di-tertiary butyl peroxide to gasoline, and we are developing a kinetic model for that unusual mixture.

With additional funding from other sources, we are using the computer-aided modeling tools developed by this project to construct many other fuel chemistry models. We are collaborating with Hai Wang to develop a kinetic model for the combustion of isobutanol, the last butanol isomer. We are also independently constructing a kinetic model for the combustion of 1-hydroxy-2-butene, another possible biofuel, which is expected to be easier than butanol to make in high yield from genetically engineered bacteria. We are also creating a detailed chemical kinetic model for JP-10, a specialized fused-ring fuel used in military and NASA applications.

IV. References

- i. Green, NJB; Bhatti, ZA. Steady-state master equation methods. *Phys. Chem. Chem. Phys.* 9 (31): 4275-4290 (2007).
- ii. Jalan, A.; Ashcraft, RW; West, RH; Green,WH; "Predicting Solvation Energies for Kinetic Modeling", *Annu. Rep. Prog. Chem., Sect. C*, **106**, 1-49 (2010).
- iii. See for example: McEnally, C, Pfefferle L. "Decomposition and Hydrocarbon Growth Processes for Hexenes in Nonpremixed Flames" *Combustion and Flame*, 143, 246-263 (2005).
- iv. Mittal, V; Heywood, J; Green, W H; "The Underlying Physics and Chemistry Behind Fuel Sensitivity" *SAE 10PFL-0468* (2010).
- v. "Blending Fuels to Boost Efficiency", *Mechanical Engineering* (November 2009) p. 18.

V. Publications and submitted journal articles supported by this project 2008-2010

1. William H. Green, "Building and Solving Accurate Combustion Chemistry Simulations", *Journal of the Combustion Society of Japan* **50**, 19-28 (2008).
2. John P. Angelos, Marcel Pignou, Morgan M. Andrae, Wai K. Cheng, William H. Green & Michael A. Singer, "Detailed Chemical Kinetic Simulations of HCCI Engine Transients", *International Journal of Engine Research*, **9**, 149-164 (2008).
3. John Z. Wen, Henning Richter, William H. Green, Jack B. Howard, Meri Treska, Paula M. Jardim and John B. Vander Sande, "Experimental study of catalyst nanoparticle and single walled carbon

- nanotube formation in a controlled premixed combustion”, *J. Materials Chem.*, **18**, 1561-1569 (2008)
4. Jason Ploeger, William H. Green, and Jefferson W. Tester, “Co-oxidation of ammonia and ethanol in supercritical water, part 2: Modeling demonstrates the importance of H_2NNO_x ”, *Int. J. Chem. Kinet.* **40**, 653-662 (2008).
 5. Alexander Mitsos, Geoffrey M. Oxberry, Paul I. Barton, and William H. Green, “Optimal Automatic Reaction and Species Elimination in Kinetic Mechanisms”, *Combustion & Flame* **155**, 118-132 (2008).
 6. Robert W. Ashcraft and William H. Green, “Thermochemical Properties and Group Values for Nitrogen-Containing Molecules”, *J. Phys. Chem. A* **112**, 9144 (2008).
 7. Sandeep Sharma, C. Franklin Goldsmith, Teppei Ogura, Michael R. Harper, Gregory R. Magoon, Huzeifa Ismail, John P. Angelos, and William H. Green, “Pulling it all Together: Fuel chemistry modeling across the scales from individual molecules to engine simulations”, *Prepr. ACS Div. of Fuel Chemistry* (2008).
 8. C. Franklin Goldsmith, Huzeifa Ismail, Paul R. Abel, and William H. Green, “Pressure and Temperature Dependence of the Reaction of Vinyl Radical with Alkenes II: Measured Rates and Predicted Product Distributions for Vinyl + Propene”, *Proc. Combust. Inst.* **32**, 139-148 (2009).
 9. M.A. Singer and W.H. Green, “Using adaptive proper orthogonal decomposition to solve the reaction-diffusion equation”, *Appl. Num. Math.* **59**, 272 (2009).
 10. H. Ismail, P.R. Abel, W.H. Green, A. Fahr, L. Jusinski, A. Knepp, J. Zador, G. Meloni, T. Selby, D. Osborn, and C.A. Taatjes, “Temperature-Dependent Kinetics of the Vinyl Radical (C_2H_3) Self-Reaction”, *J. Phys. Chem. A* **113**, 1278-1286 (2009).
 11. Richard H. West, Michael R. Harper, William H. Green, “21st-Century Kinetics: Quantitative Predictions from First Principles”, *Proceedings of the 8th World Congress of Chemical Engineering*, Montreal, 0242 (2009).
 12. Sandeep Sharma and William H. Green, “Formation of Styrene from propargyl and cyclopentadienyl”, *Proceedings of the 6th US National Combustion meeting*, Ann Arbor, 22E3 (2009).
 13. Sandeep Sharma and William H. Green, “Computed rate coefficients and product yields for $C_5H_5 + CH_3 =$ products”, *Journal of Physical Chemistry A* **113**, 8871-8882 (2009).
 14. C. Franklin Goldsmith, Huzeifa Ismail, and William H. Green, “Pressure and Temperature Dependence of the Reaction of Vinyl Radical with Alkenes III: Measured Rates and Predicted Product Distributions for Vinyl + Butene”, *J. Phys. Chem. A* **113**, 13357-13371 (2009).
 15. Sandeep Sharma, Michael R. Harper, and William H. Green, “Modeling of 1,3-hexadiene, 2,4-hexadiene and 1,4-hexadiene doped methane flames: Flame modeling, Benzene and Styrene formation”, *Combustion & Flame* (2010, accepted)
 16. Sandeep Sharma, Sumathy Raman, and William H. Green, “Intramolecular Hydrogen Migration in Alkylperoxy and Hydroperoxyalkylperoxy Radicals: Accurate Treatment of Hindered Rotors”, *J. Phys. Chem. A* (2010, accepted)

Quantum Dynamics of Elementary Combustion Reactions

Hua Guo (hguo@unm.edu)

Department of Chemistry and Chemical Biology, University of New Mexico

Many combustion reactions are of complex-forming nature, in which the reaction path is dominated by a deep potential well. One such example is the $\text{H} + \text{O}_2 \rightarrow \text{HO} + \text{O}$ reaction, which forms the bottleneck in combustion of hydrogen and hydrocarbon fuels.¹ We have recently focused on the elucidation of the reaction dynamics of this important combustion reaction and other complex-forming reactions using quantum mechanical approaches. The codes developed in our group are based on the highly accurate and efficient Chebyshev propagator,² and are capable of calculating both initial state-resolved and state-to-state scattering attributes including differential cross sections.³

Quantum mechanical characterization of such seemingly simple reactions is very challenging. First, accurate potential energy surfaces (PESs) are needed. For dynamic calculations, a large basis is often needed because of the deep well and the long-range interactions in the product channel. In the wave packet approach, long propagation is also expected because of the long-lived intermediate complex. The difficulties are compounded by the floppy nature of the reaction intermediate, which renders many commonly used dynamical approximations (e.g., the centrifugal sudden approximation) inadequate. In addition, the barrierless reaction pathway requires a large number of partial waves.

We have continued our exploration of the most important combustion reaction ($\text{H} + \text{O}_2 \rightarrow \text{HO} + \text{O}$), extending our earlier work by including rotational excitation of the O_2 reactant.⁴ It was found that the excited O_2 plays an important role in this reaction and it yields a better agreement with experiment (Fig. 1). In another study, we have collaborated with M. Alexander at Maryland to obtain accurate rate constants for the reverse $\text{HO} + \text{O} \rightarrow \text{H} + \text{O}_2$ reaction.⁵ This paper has attracted much attention as one of 20 most downloaded paper at J. Chem. Phys. in January 2010.

In the mean time, we have extended the capability of our scattering codes to include non-adiabatic couplings. Using this code, we have recently reported a thorough theoretical study of the $\text{O}(^1\text{D}) + \text{H}_2 \rightarrow \text{OH} + \text{H}$ reaction, which has three possible reaction pathways, among which one is a non-adiabatic one. The results, which include both differential and integral cross sections, are in excellent agreement with experimental results of K. Liu⁶

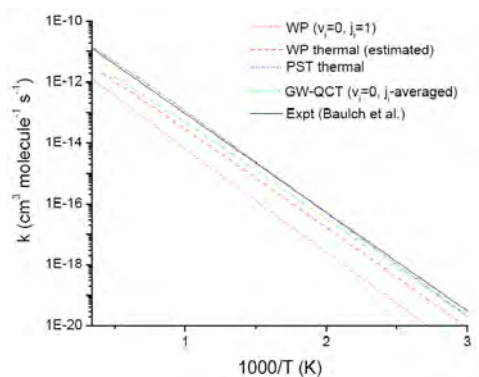


Fig. 1 Temperature dependence of various calculated rate constants, including the initial state ($v_i=1, j_i=1$) specified rate constant obtained using the quantum wave packet method, the estimated quantum mechanical thermal rate constant, the PST thermal rate constant, and the GW-QCT rate constant averaged over all j_i levels of the ground state vibrational manifold. The experimental rate constant is also included for comparison.

and represent a significant improvement over previous theoretical studies. A similar non-adiabatic code has been developed for tetratomic systems and applied to the photodissociation of NH_3 .⁷ It sheds light on the dramatic mode selectivity observed by the Crim group.⁸

We plan to utilize this code to investigate several other non-adiabatic scattering systems, including the $\text{N}(^2\text{D}) + \text{H}_2 \rightarrow \text{NH} + \text{H}$ and $\text{H} + \text{O}_2 \rightarrow \text{HO} + \text{O}$ reactions. To achieve this, we have been collaborating with D. Xie at Nanking University to generate the PESs for both the ground and excited states of NH_2 and HO_2 . The PESs for NH_2 has recently been published,⁹ and those for HO_2 are near completion. Preliminary spectroscopic studies have indicated high quality of the excited state PES. We have used the ground state NH_2 PES to investigate the $\text{NH} + \text{H}$ exchange reaction.¹⁰

To make our computer codes more efficient, we have recently published an extensive study of the propagators commonly used in scattering calculations.¹¹ Our results indicate that the Chebyshev propagator is significantly more accurate than and equally efficient as the commonly used second-order differencing propagator, particularly when resonances are important in scattering. This piece of work attracted much attention and was one of the 10 most downloaded J. Chem. Phys. papers in May 2009. Such accuracy and efficiency in propagation allowed us to tackle challenging problems in quantum scattering, such as the $\text{O} + \text{O}_2$ exchange reaction.¹² Our recent results indicated that this reaction is highly non-statistical as evidenced by the forward dominated differential cross section (Fig. 2), raising questions about the RRKM treatment of the related ozone recombination process.¹³ Our theoretical analysis of the reaction also provided an in-depth understanding of a recent molecular beam experiment on this reaction.¹⁴

Finally, we note that we continued our investigations of highly excited vibrational spectroscopy of polyatomic molecules.¹⁵ A review article on energy localization has recently been published.¹⁶

In the near future, we would like to expand the capacity of our state-to-state quantum scattering codes to larger systems. One such system is the $\text{F} + \text{H}_2\text{O}$ reaction,¹⁷⁻¹⁸ which is affected by strong non-adiabatic coupling.¹⁹ We have started developing codes for such processes.

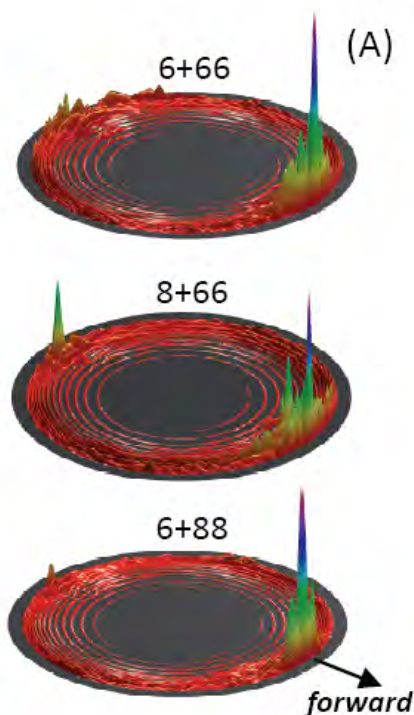


Fig. 2. Calculated DCSs for $^{16}\text{O} + ^{32}\text{O}_2 \rightarrow ^{32}\text{O} + ^{16}\text{O}$ (denoted as 6+66), $^{18}\text{O} + ^{32}\text{O}_2 \rightarrow ^{34}\text{O}_2 + ^{16}\text{O}$ (8+66) and $^{16}\text{O} + ^{36}\text{O}_2 \rightarrow ^{34}\text{O}_2 + ^{18}\text{O}$ (6+88) processes at collision energy of 0.05eV.

References (* indicates DOE funded work in the past year):

1. J. A. Miller, R. J. Kee and C. K. Westbrook, *Annu. Rev. Phys. Chem.* **41**, 345 (1990).
2. H. Guo, *Rev. Comput. Chem.* **25**, 285-347 (2007).
3. S. Y. Lin and H. Guo, *Phys. Rev. A* **74**, 022703 (2006).
- *4. S. Y. Lin, H. Guo, G. Lendvay and D. Xie, *Phys. Chem. Chem. Phys.* **11**, 4715 (2009).
- *5. F. Lique, M. Jorfi, P. Honvault, P. Halvick, S. Y. Lin, H. Guo, D. Q. Xie, P. J. Dagdigian, J. Klos and M. H. Alexander, *J. Chem. Phys.* **131**, 221104 (2009).
6. S.-H. Lee and K. Liu, *J. Chem. Phys.* **111**, 4351 (1999).
- *7. W. Lai, S. Y. Lin, D. Xie and H. Guo, *J. Phys. Chem. A*, **114**, 3121 (2010).
8. M. L. Hause, Y. H. Yoon and F. F. Crim, *J. Chem. Phys.* **125**, 174309 (2006).
- *9. S. Zhou, Z. Li, D. Xie, S. Y. Lin and H. Guo, *J. Chem. Phys.* **130**, 184307 (2009).
- *10. Z. Li, D. Xie, Z. Sun, D. H. Zhang, S. Y. Lin and H. Guo, *J. Chem. Phys.* **131**, 124313 (2009).
- *11. Z. Sun, S.-Y. Lee, H. Guo and D. H. Zhang, *J. Chem. Phys.* **130**, 174102 (2009).
- *12. Z. Sun, L. Liu, S. Y. Lin, R. Schinke, H. Guo and D. H. Zhang, *Proc. Nat. Acad. Sci.* **107**, 555 (2010).
13. Y. Q. Gao and R. A. Marcus, *Science* **293**, 259-263 (2001).
14. A. L. Van Wyngarden, K. A. Mar, K. A. Boering, J. J. Lin, Y. T. Lee, S.-Y. Lin, H. Guo and G. Lendvay, *J. Am. Chem. Soc.* **129**, 2866-2870 (2007).
- *15. S. Lin, D. Xie and H. Guo, *J. Phys. Chem. A* **113**, 7314 (2009).
- *16. S. C. Farantos, R. Schinke, H. Guo and M. Joyeux, *Chem. Rev.* **109**, 4248 (2009).
17. M. Ziemkiewicz, M. Wojcik and D. J. Nesbitt, *J. Chem. Phys.* **123**, 224307 (2005).
18. A. M. Zolot and D. J. Nesbitt, *J. Chem. Phys.* **129**, 184305 (2008).
19. M. P. Deskevich, D. J. Nesbitt and H.-J. Werner, *J. Chem. Phys.* **120**, 7281 (2004).

Gas-Phase Molecular Dynamics: High Resolution Spectroscopy and Collision Dynamics of Transient Species

Gregory E. Hall
Chemistry Department, Brookhaven National Laboratory
Upton, NY 11973-5000
gehall@bnl.gov

Program Scope

This research is carried out as part of the Gas-Phase Molecular Dynamics program in the Chemistry Department at Brookhaven National Laboratory. Chemical intermediates in the elementary gas-phase reactions involved in combustion chemistry are investigated by high resolution spectroscopic tools. Production, reaction, and energy transfer processes are investigated by transient, double resonance, polarization and saturation spectroscopies, with an emphasis on technique development and connection with theory as well as specific molecular properties.

Recent Progress

A. Double-resonance methods for spectroscopy and dynamics

A range of spectroscopic measurements have been performed using frequency-modulated near-infrared probe lasers in combination with tunable ns lasers to acquire new, rotationally state-labeled spectra of CH₂. Using a counterpropagated, chopped or amplitude modulated saturation laser (instead of a tunable ns laser) in combination with the frequency-modulated probe beam allows sub-Doppler saturation spectra to be acquired on transient species. Spectroscopic applications of these methods to CH₂ and CN are described in Trevor Sears' abstract. Once the frequency-domain information is understood, one can exploit the time-dependent signals to learn about energy-transfer collisions, depolarization kinetics, velocity-changing elastic collisions, and thereby pick apart in the time and frequency domain the processes responsible for pressure broadening of molecular transitions and some of the collision processes closely related to transport properties. Several applications of these types of measurements are summarized below.

B. Dynamics of mixed-state collisions in the intersystem crossing of CH₂

When applied to the electronically mixed singlet/triplet gateway states of CH₂, double resonance saturation recovery and saturation transfer measurements confirm the efficient collisional interconversion within an orthogonal pair of mixed states inferred in our previous, less direct experiments.[1] A pulsed optical depletion of the population in one eigenstate of mixed spin character leads rapidly to a collisionally-induced depletion of its partner eigenstate on a timescale faster than normal rotational energy transfer, prior to full rotational thermalization. We envision this process as a long-range dephasing of the coherent two-level superposition states, driven by the differential interaction of the collision partner with singlet and triplet van der Waals potentials. Even without an explicit spin-changing interaction, a sequence of dephasing collisions can have the net result of transferring population between the weakly coupled singlet and triplet surfaces. A systematic experimental study of these collisions provides new insights into the mechanism of spin conversion in the small molecule limit with weak coupling.

C. Saturation recovery double-resonance studies of energy transfer and depolarization

The combination of transient FM absorption spectroscopy and pulsed optical hole-burning offers a precision tool for the study of collision dynamics. Originally implemented in our laboratory in order to

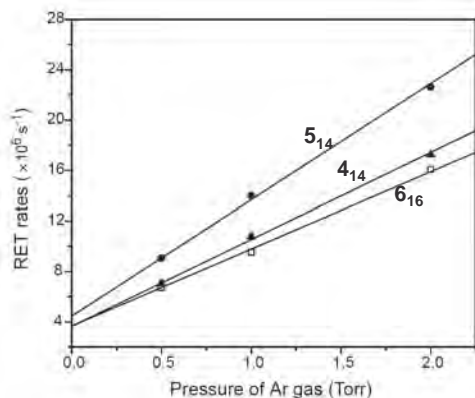


Figure 1. Saturation recovery rates observed for selected rotational states of singlet CH_2 undergoing collisions with ketene and variable amounts of Ar.

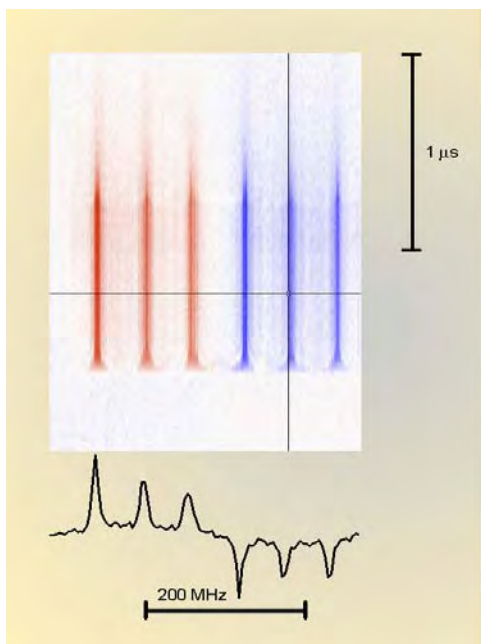


Figure 2. Transient sub-Doppler hole-burning in CN. A cut through the two-dimensional (time and frequency) data set shows a spectrum at fixed time during a square pulse of bleach light. Color depth encodes transient saturation intensity in response to the bleach laser exposure. Red and blue spectra are duplicates of the three strong hyperfine transitions with opposite sign, separated by the 191 MHz FM sideband frequency.

investigate the collisions of perturbed singlet/triplet mixed states in CH_2 , we are finding surprises and useful new information in the study of the simpler process of rotational energy transfer for polyatomic molecules even for scattering on a single electronic surface. The method allows for simultaneous measurement of collision-induced population recovery, following transient bleaching, as well as the collisional loss of polarization. Bleaching and recovery signals for a rotational state of CH_2 depend on the relative polarization of collinear bleach and probe lasers, providing both population and alignment kinetics. The difference between the parallel and perpendicular recovery signals decays faster than the polarization-weighted population recovery signal. These measurements can be related quantitatively to the integral cross sections for rotationally inelastic collisions and elastic depolarization. Surprisingly large and non-monotonic variations in the integral cross sections for inelastic collisions are observed among rotational states of the same nuclear spin symmetry and slowly varying energy. Figure 1 illustrates a few such unexpected observations. The “trend” is qualitatively consistent, perhaps fortuitously, with a simple geometrical angular momentum transfer model of rotational energy transfer proposed by McCaffery and co-workers[2] to treat their NH_2+H inelastic collision data. Quantum scattering calculations are underway, in collaboration with Alexander and Dagdigian, to compare with the experimental energy transfer and depolarization measurements.

D. Collision studies of sub-Doppler transient hole-burning

Extending work described in Sears’ abstract on the hyperfine-resolved saturation spectroscopy of CN radicals, we are investigating the time- and frequency-domain response of the polarized FM probe to rapid switching in the intensity of a counterpropagating bleach laser beam. Figure 2 illustrates the different response to switching on and off the saturation beam at the bottom and top of the sharp colored stripes, respectively. As the narrow-band bleach laser is switched on, coherent transients are observed in the form of damped Rabi oscillations (not visible at the graphical resolution of Figure 2). The frequency of the

oscillations depends on the laser power, detuning, and transition moment, while inhomogeneous geometrical effects and damping due to collisions affects the contrast of the oscillations. After a few

hundred ns, a photo-stationary state is achieved, where the optical pumping and collisional relaxation rates are comparable and the saturation spectrum is power and pressure-broadened, but stationary. When the bleach beam is switched off, approximately exponential recoveries are observed, with rates linear in the partial pressures of the sample constituents. No differential polarization effects have been observed in the sub-Doppler recovery kinetics, consistent with the interpretation that it is unlikely for an elastic depolarization event (M-changing, J conserving) to occur without a concurrent velocity change. Taken alone, the sub-Doppler saturation recovery kinetics measurements are a blend of A-state and X-state relaxation effects, including both elastic and inelastic contributions. The paragraph below discusses ongoing work to isolate these contributions, using a conventional ns dye laser to saturate without velocity selection, and with the use of both two-level and three-level double resonance schemes.

Future Work

A. Double-resonance studies of elastic and inelastic collisions

The simplicity of using the same tunable laser beam for saturation and probe in a counterpropagating geometry for sub-Doppler spectroscopy leads to the kinetic complication in the two-level system that relaxation in both upper and lower states will contribute to the observed kinetics. A three-level (V or Λ) configuration removes this ambiguity, but would seem to require an additional high-resolution laser. The normally annoying ‘crossover resonances’ that complicate spectral assignments in saturation spectroscopy

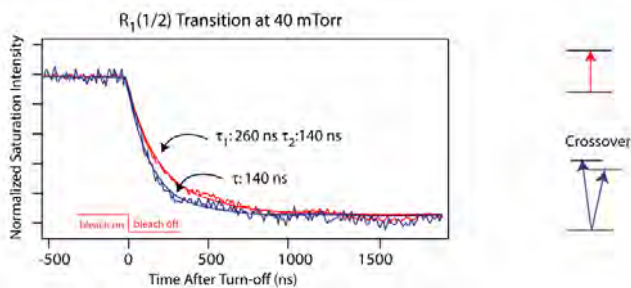


Figure 3. Sub-Doppler saturation recovery kinetics on a two-level (red) and three-level (blue) hyperfine resonances within the $R_1(1/2)$ rotational line of CN A-X (1-0) band near 919 nm.

are indeed three-level sub-Doppler resonances, and thus allow upper or lower state relaxation kinetics to be measured separately, as shown in Figure 3. When pyruvonnitrile (CH_3COCN) is used as the photolytic precursor and collision partner, two distinct saturation recovery times are observed in the two-level sub-Doppler signal, corresponding to a faster refilling of the X state velocity hole and a slower dissipation of the velocity-selected excited state level. A crossover resonance measured only 30 MHz to the red of the two-level resonance has bleach and probe transitions terminating in different velocity components of different A-state hyperfine levels, so the recovery kinetics is exclusively sensitive to the rate of refilling in the X state. A single exponential recovery suffices for the cross-over kinetics. We expect the primary difference is that the rotationally inelastic collisions are substantially less efficient for A-state CN than for X-state CN with the polar collision partner CH_3COCN , since the A-state dipole moment is much smaller than in the X state. When nonpolar NCCN is used as a CN precursor and collision partner, the two-level and three-level saturation recovery kinetics are slower and essentially indistinguishable. A series of measurements with added Ar, He and N_2 buffer gases provide collisional data for velocity-changing and rotationally inelastic collisions in these systems.

Experiments are currently in progress using a ns tunable laser to saturate all velocity components of selected X-state rotational levels, to independently measure the inelastic contributions to the saturation recovery. A measurement of the rates of sub-Doppler saturation recovery, compared to the recovery following broad-band bleaching, permits independent determination of various elastic and inelastic contributions relevant to phenomena such as pressure broadening or transport properties. No trace of velocity preserving, elastic depolarization is observed, and rotationally elastic, velocity changing

collisions make an increasingly minor contribution to the total rate of saturation recovery for collisions with rare gases, and the photolytic CN precursors C₂N₂ and CH₃COCN. With minor variations, it may be possible to resolve the relative inelastic rates for fine structure changing and conserving inelastic collisions in CN (*X*, *v*=0) from saturation transfer measurements.

B. Surface studies using a laser comb-based Fourier transform instrument

We seek to exploit and share new opportunities and applications of frequency comb lasers with our colleagues in condensed phase and interfacial chemistry. In addition to the ultra-high resolution offered by applications of frequency combs to time and frequency standards, there can be applications of frequency combs that offer broadband advantages of high speed and low noise spectral acquisition, for instance in combination with FTIR. One approach to improving the sensitivity of FTIR measurements, already demonstrated,[3] is to replace the conventional global source by a laser-based comb. The comb output passes through the sample, and into the interferometer. The light reaching the detector after the interferometer contains the normal interference signal resulting from the travel of the moving mirror, but the interferogram is now encoded as a radio frequency signal at the comb repetition frequency. Phase-sensitive detection, similar to our frequency modulation laser experiments, yields in-phase and quadrature interferograms, that are Fourier transforms of the absorption and dispersion spectra. The main advantage comes from the fact that the detected signal is encoded at frequencies of 100-500 MHz frequency of the comb spacing, where the 1/*f* and technical noise is substantially lower than at the tens of kHz normally encountered in FT spectrometers. We are initiating a construction project to combine a near-infrared frequency comb source with a commercial interferometer, attempting to improve sensitivity and acquisition speed for near-infrared attenuated internal reflection measurements of aqueous/semiconductor surface species of relevance to catalytic and photocatalytic water splitting.

Publications supported by this project since 2008

- State mixing and predissociation in the $\tilde{c} - \tilde{a}$ band system of singlet methylene studied by optical-optical double resonance, Z. Wang, Y. Kim, G. E. Hall and T. J. Sears, *J. Phys. Chem. A*, **112**, 9248-9254 (2008)
- Sub-Doppler laser absorption spectroscopy of the $A^2\Pi_i - X^2\Sigma^+$ (1,0) band of CN. Measurement of the ¹⁴N hyperfine parameters in $A^2\Pi_i$ CN. M. L. Hause, G. E. Hall, and T. J. Sears, *J. Mol. Spectr.* **253** 122-128 (2008); Corrigendum: *J. Mol. Spectr.* **260** 138 (2010).
- Sub-Doppler Stark spectroscopy in the $A - X$ (1,0) band of CN. M. L. Hause, G. E. Hall, and T. J. Sears, *J. Phys. Chem. A*, **113** 13342-13346 (2009).
- Pseudo-continuous resonance-enhanced multiphoton ionization: application to the determination of the hyperfine constants of ²⁰⁸Pb¹⁹F. P. Sivakumar, C. P. McRaven, P. M. Rupasinghe, T. Zh. Yang, N. E. Shafer-Ray, G. E. Hall and T. J. Sears, *Mol. Phys.* (2010). (in press).
- Frequency modulated circular dichroism spectroscopy: application to ICN photolysis. G. Hancock, G. Richmond, G.A.D. Ritchie, S. Taylor, M. L. Costen and G. E. Hall, *Mol. Phys.* (2010). (in press)

References

-
- ¹ A. V. Komissarov, A. Lin, T. J. Sears, and G.E. Hall, *J. Chem. Phys.* **125**, 084308 (2006)
- ² Z. T. AlWahabi, N. A. Besley, M. A. Osborne, and Z. Rawi, *J. Chem. Phys.* **102**, 7945 (1995).
- ³ J. Mandon, G. Guelachvili and N. Picque, *Nature Photonics*, **3**, 99 (2009).

Flame Chemistry and Diagnostics

Nils Hansen

Combustion Research Facility, Sandia National Laboratories, Livermore, CA 94551-0969

Email: nhansen@sandia.gov

SCOPE OF THE PROGRAM

The goal of this program is to provide a rigorous basis for the elucidation of chemical mechanisms of combustion, combining experimental measurements employing state-of-the-art combustion diagnostics with detailed kinetic modeling. The experimental program concentrates on the development and application of combustion diagnostics for measurements of key chemical species concentrations. These measurements are carried out in low-pressure, one-dimensional laminar flames and are designed to serve as benchmarks for the validation of combustion chemistry models. Comparison of experimental data to models employing detailed chemical kinetics is critical to determining important chemical pathways in combustion and in pollutant formation in combustion systems. As turbulent combustion models become increasingly sophisticated, accurate chemical mechanisms will play a larger role in computations of realistic combustion systems. Verification of detailed chemistry models against a range of precise measurements under thoroughly characterized steady conditions is necessary before such flame models can be applied with confidence in turbulent combustion calculations.

PROGRESS REPORT

Molecular Beam Mass Spectrometry at the Advanced Light Source

In collaboration with T. A. Cool of Cornell University, K. Kohse-Höinghaus of Bielefeld University, and P. R. Westmoreland of the University of Massachusetts, great progress has been made measuring low-pressure flames using molecular-beam mass spectrometry (MBMS) with synchrotron photoionization at the Advanced Light Source (ALS) of the Lawrence Berkeley National Laboratory. In the past year, different flames fueled by larger hydrocarbons and oxygenated species have been characterized over a wide range of stoichiometries. The data is currently being processed for comparison to detailed kinetic flame models.

Combustion Chemistry in Flames fueled by Oxygenates and Hydrocarbon

Fuel-consumption and initial steps of aromatic ring formation were studied in fuel-rich flames of 1,3-butadiene, 1-hexene, cyclohexane, methylcyclopentane, and 3,3-dimethyl-1-butene. These experimental studies provide a broad database for flame modeling.

Fuel-Structure Dependence of Benzene Formation Processes in Premixed Flames Fueled by C₆H₁₂ Isomers: The fuel-structure dependent significance of various benzene formation pathways was

analyzed using data from rich ($\phi=1.7$) flames fueled by four C_6H_{12} isomers: 1-hexene, cyclohexane, methylcyclopentane, and 3,3-dimethyl-1-butene. Isomer-resolving photoionization efficiency curves and quantitative mole fraction profiles revealed the dominant fuel destruction pathways, the influence of different fuel consumption processes on the formation of commonly considered benzene precursors, and the contributions of several routes towards benzene formation. While propargyl and allyl radicals dominate benzene formation in the combustion of 1-hexene (see below), contributions from reactions involving $i-C_4H_5$ and C_5H_5 radicals were revealed in the flames of 3,3-dimethyl-1-butene and methylcyclopentane, respectively. Close to the burner surface, successive dehydrogenation of the fuel was found to be important for the cyclohexane flame and to some smaller extent for the methylcyclopentane flame.

The Importance of Fuel Dissociation and the Propargyl + Allyl Reaction for the Formation of Benzene in a 1-Hexene Flame: Fuel decomposition and benzene formation processes in a premixed laminar low-pressure flame of 1-hexene were investigated by comparing quantitative mole fraction profiles of flame species with kinetic modeling results from the group of P. R. Westmoreland. The premixed flame, which was stabilized on a flat-flame burner under a reduced pressure of 30 Torr was analyzed by flame-sampling molecular-beam time-of-flight mass spectrometry which utilizes photoionization by tunable vacuum-ultraviolet synchrotron radiation. The model calculations included the latest rate coefficients for 1-hexene decomposition (J.H. Kiefer *et al.*, *J. Phys. Chem. A* **2009**, *113*, 13570) and for the propargyl (C_3H_3) + allyl ($\alpha-C_3H_5$) reaction (J.A. Miller *et al.*, *J. Phys. Chem. A* **2010**, doi10.1021/jp910604b]. The predicted mole fractions as a function of distance from the burner were at least in acceptable and often in very good agreement with the experimentally observed profiles, thus allowing an assessment of the importance of various fuel decomposition reactions and benzene formation routes. The results clearly indicated that 1-hexene is dominantly decomposed via unimolecular dissociation forming allyl ($\alpha-C_3H_5$) and n -propyl ($n-C_3H_7$). Minor fuel-decomposition pathways include H-abstraction reactions producing various C_6H_{11} radicals and subsequent β -scission into C_2 , C_3 , and C_4 intermediates. The reaction path analysis also highlighted an outstanding contribution of the propargyl (C_3H_3) + allyl ($\alpha-C_3H_5$) reaction to the formation of benzene. In this flame, benzene is dominantly formed through H-assisted isomerization of fulvene, which itself is almost exclusively produced by the aforementioned $C_3H_3 + \alpha-C_3H_5$ reaction.

Measurement of Aromatic Flame Species by Multi-Photon Ionization: A new experiment has been set up to detect aromatic flame constituents, such as benzene, toluene and smaller polycyclic aromatic hydrocarbons (PAH's) by flame-sampling molecular-beam mass spectrometry (MBMS) employing photoionization with UV light, either in resonant or non-resonant ionization processes. Preliminary data has been taken for flames fueled by acetylene, allene, propyne, propene, and 1,3-

butadiene. The data is currently being analyzed and, if possible, compared to literature data. The species with the largest mass and a distinctive height profile is currently found at $m/z = 202$, but experimental improvements are under way to extend the detectable mass range.

FUTURE DIRECTIONS

One key immediate task is the analysis of the large body of ALS data accumulated in the past years, which may compel further or confirmatory measurements during subsequent beam cycles. We will continue to explore isomer specific pathways of fuel-consumption and aromatic ring formation in flames fueled by C_5 - C_7 species. More work is needed on the determination of the absolute molar composition of flames fueled by the isomeric C_6H_{12} species. The fuels will present the classes of long-chain alkenes, fully saturated and methyl-substituted cycloalkanes, and branched alkenes. The combustion chemistry of these fuels will be investigated in unprecedented detail using otherwise identical flame conditions. Important fuel destruction and aromatic ring formation pathways will be elucidated. In this context, the flame chemistry of the methyl-substituted derivative of cyclohexane, methylcyclohexane, will also be studied. In light of the recent findings regarding the fuel-consumption and benzene formation pathways in a fuel-rich 1-hexene flame, we deem it best to expand our studies to additional fuels with a similar structural feature, i.e. an allylic C-C bond. We therefore plan to study the combustion chemistry of flames fueled by 1-butene and 1-pentene.

Furthermore, we want to replace the existing linear time-of-flight set-up of the ALS flame machine with a reflectron time-of-flight mass spectrometer. This modification will lead to a significant increase in mass resolution which is currently limited to $m/\Delta m \approx 400$. A reflectron time-of-flight spectrometer offers the appeal that a mass resolution of $m/\Delta m \approx 3000$ can be obtained, and thus, unambiguous identifications of flame species of near-equal mass would be achievable.

These studies of fuel-consumption and aromatic ring formation employing synchrotron generated VUV photoionization will be complemented by the multiphoton ionization experiments in the laser laboratory. Resonantly enhanced multiphoton ionization (REMPI) is an ionization technique, where the ionization energy is transferred to the molecule with two or more photons. It can be used for flame studies for the detection of aromatic species like benzene, substituted benzenes, and polycyclic aromatic hydrocarbons (PAH's). It is known that a single wavelength near 269 nm can be used to efficiently ionize polyaromatics up to about C_{20} -PAH's, while for larger species a wavelength of 208 nm will be profitable.

In recent years, tightened regulations for emissions from internal combustion engines have stimulated a pronounced interest in non-conventional oxygenated fuels. The initiated studies of oxygenated fuel chemistry will continue with experimental and modeling investigations of flames fueled by cyclic ethers which, as contents in biomass derived fuels, are of considerable interest. Well suited as

model fuels to learn more about the characteristic combustion chemistry of cyclic ethers are tetrahydrofuran (THF) and tetrahydropyran (THP).

PUBLICATIONS ACKNOWLEDGING BES SUPPORT 2008-PRESENT

1. C. A. Taatjes, N. Hansen, D. L. Osborn, K. Kohse-Höinghaus, T. A. Cool, P. R. Westmoreland, “‘Imaging’ Combustion Chemistry via Multiplexed Synchrotron-Photoionization Mass Spectrometry”, *Phys. Chem. Chem. Phys.*, **10**, 20-34 (2008).
2. N. Hansen, S. J. Klippenstein, P. R. Westmoreland, T. Kasper, K. Kohse-Höinghaus, J. Wang, T. A. Cool, “A Combined *ab-initio* and Photoionization Mass Spectrometric Study of Polyynes in Fuel-Rich Flames”, *Phys. Chem. Chem. Phys.*, **10**, 366-374 (2008).
3. J. Wang, B. Yang, T. A. Cool, N. Hansen, T. Kasper, “Near-threshold Absolute Photoionization Cross Sections of some Reaction Intermediates in Combustion”, *Int. J. Mass Spectrom.*, **269**, 210-220 (2008).
4. J. D. Cardoza, F. M. Rudakov, N. Hansen, P. M. Weber, “Identification of Isomeric Hydrocarbons by Rydberg Photoelectron Spectroscopy”, *J. Electron Spectrosc.*, **165**, 5-10 (2008).
5. J. Wang, U. Struckmeier, B. Yang, T. A. Cool, P. Oßwald, K. Kohse-Höinghaus, T. Kasper, N. Hansen, P. R. Westmoreland, “Isomer-Specific Influences on the Composition of Reaction Intermediates in Dimethyl Ether/Propene and Ethanol/Propene Flames”, *J. Phys. Chem. A*, **112**, 9255-9265 (2008).
6. N. Hansen, J. A. Miller, T. Kasper, K. Kohse-Höinghaus, P. R. Westmoreland, J. Wang, T. A. Cool, “Benzene Formation in Premixed Fuel-Rich 1,3-Butadiene Flames”, *Proc. Combust. Inst.*, **32**, 623-630 (2009).
7. A. Lucassen, P. Oßwald, U. Struckmeier, K. Kohse-Höinghaus, T. Kasper, N. Hansen, T. A. Cool, P. R. Westmoreland, “Species identification in a laminar premixed low-pressure flame of morpholine as a model substance for oxygenated nitrogen-containing fuels”, *Proc. Combust. Inst.*, **32**, 1269-1276 (2009).
8. C. K. Westbrook, W. J. Pitz, P. R. Westmoreland, F. L. Dryer, M. Chaos, P. Oßwald, K. Kohse-Höinghaus, T. A. Cool, J. Wang, B. Yang, N. Hansen, T. Kasper, “A Detailed Chemical Kinetic Mechanism for Oxidation of Four Small Alkyl Esters in Laminar Premixed Flames”, *Proc. Combust. Inst.*, **32**, 221-228 (2009).
9. N. Hansen, T. A. Cool, P. R. Westmoreland, K. Kohse-Höinghaus, “Recent Contributions of Flame-Sampling Molecular-Beam Mass Spectrometry to a Fundamental Understanding of Combustion Chemistry”, *Prog. Energy Combust. Sci.*, **35**, 168-191 (2009).
10. J. Wang, M. Chaos, B. Yang, T. A. Cool, F. L. Dryer, T. Kasper, N. Hansen, P. Oßwald, K. Kohse-Höinghaus, P. R. Westmoreland, “Composition of Reaction Intermediates for Stoichiometric and Fuel-Rich Dimethyl Ether flames: Flame-Sampling Mass Spectrometry and Modeling Studies”, *Phys Chem. Chem. Phys.*, **11**, 1328-1339 (2009).
11. N. Hansen, J. A. Miller, P. R. Westmoreland, T. Kasper, K. Kohse-Höinghaus, J. Wang, T. A. Cool, “Isomer-Specific Combustion Chemistry in Allene and Propyne Flames”, *Combust. Flame*, **156**, 2153-2164 (2009).
12. K. Kohse-Höinghaus, P. Oßwald, T. A. Cool, T. Kasper, N. Hansen, F. Qi, C. K. Westbrook, P. R. Westmoreland, “Biofuel Combustion Chemistry: From Ethanol to Biodiesel”, *Angew. Chem.*, in press.
13. U. Struckmeier, A. Lucassen, N. Hansen, T. Wada, N. Peters, K. Kohse-Höinghaus, “Demonstration of a Burner for the Investigation of Partially Premixed Low-Temperature Flames”, *Combust. Flame*, in press.
14. J. Wang, B. Yang, T. A. Cool, N. Hansen, “Absolute Cross-Sections for Dissociative Photoionization of Some Small Esters”, *Int. J. Mass Spectrom.*, in press.
15. W. Li, M. E. Law, P. R. Westmoreland, T. Kasper, N. Hansen, J. Wang, T. A. Cool, K. Kohse-Höinghaus, “Competing Paths for Aromatic Species Formation in Cyclohexane Premixed Flames”, *Proc. Combust. Inst.*, submitted.
16. N. Hansen, T. Kasper, B. Yang, T. A. Cool, W. Li, P. R. Westmoreland, P. Oßwald, K. Kohse-Höinghaus, “Fuel-Structure Dependence of Benzene Formation Processes in Premixed Flames Fueled by C₆H₁₂ Isomers”, *Proc. Combust. Inst.*, submitted.
17. B. Yang, T. A. Cool, C. K. Westbrook, N. Hansen, “Fuel-Specific Influences on the Composition of Reaction Intermediates in Premixed Flames of Three C₅H₁₀O₂ Ester Isomers”, *Proc. Combust. Inst.*, submitted.

SPECTROSCOPY AND KINETICS OF COMBUSTION GASES AT HIGH TEMPERATURES

Ronald K. Hanson and Craig T. Bowman
Department of Mechanical Engineering
Stanford University, Stanford, CA 94305-3032
rkhanon@stanford.edu, ctbowman@stanford.edu

Program Scope

This program involves two complementary activities: (1) development and application of cw laser absorption methods for the measurement of concentration time-histories and fundamental spectroscopic parameters for species of interest in combustion; and (2) shock tube studies of reaction kinetics relevant to combustion.

Species currently being investigated in the spectroscopic portion of the research include H₂O (at 2.5 μm), CO₂ (at 2.7 μm), OH (at 306 nm) and several species with strong deep UV absorption features including CH₃ (at 216 nm), HO₂ radical (at 225 nm), and H₂O₂ (at 244 nm).

In parallel with these spectroscopic studies, kinetics research has advanced on several fronts. (1) New shock tube methods have been applied to generate near-constant-volume measurements of propane ignition delay times. (2) An OH laser absorption diagnostic has been applied to investigate oxidation processes in dimethyl ether (DME) systems. (3) H₂O and OH diagnostics have been used to provide improved measurements of several hydroperoxyl radical rate coefficients in the H₂/O₂/H₂O₂/HO₂ system, including those for the reactions OH + HO₂ → H₂O + O₂ and OH + H₂O₂ → H₂O + HO₂. (4) The OH diagnostic has been used to measure the rate coefficients for a series of reactions of the larger alkanes +OH and selected alkenes +OH.

Recent Kinetics Progress:

Propane Ignition Delay Times: Shock tube measurements of ignition delay times with high activation energies are strongly sensitive to variations in reflected shock temperatures. At longer shock tube test times, as are needed at low reaction temperatures, small gradual increases in pressure (and simultaneous increases in temperature) that result from incident shock wave attenuation and boundary layer growth can significantly shorten measured ignition delay times. To obviate this pressure increase, we made use of a recently developed driver-insert method of Hong et al. (2009) that allows generation of near-constant-volume test conditions for reflected-shock measurements. Using this method, we measured propane ignition delay times in lean mixtures (0.8% C₃H₈/ 8% O₂/ Ar) at temperatures between 980 and 1400 K and nominal pressures of 6, 24 and 60 atm, under both conventional shock tube operation (with post-shock fractional pressure variation $dP_5/dt \sim 1-7$ %/ms) and near-constant-volume operation (with $dP_5/dt \sim 0$ %/ms). The near-constant-volume ignition delay times provide a database for low-temperature propane model development that is independent of non-ideal fluid flow and heat transfer effects. Comparison of these near-constant-volume measurements with predictions using the JetSurF v1.0 mechanism of Sirjean et al. (2009) (using CHEMKIN) shows good agreement at all pressures; see Figure 1. Ignition delay times measured with finite dP_5/dt were found to be significantly shorter at the lowest temperatures and highest pressures studied. However, these ignition times are successfully simulated using the same detailed mechanism when an appropriate gasdynamic model (CHEMSHOCK) that accounts for changes in pressure and temperature is used.

DME Chemistry: The first high-temperature rate coefficient measurements of two dimethyl ether (DME) reactions, (1) $\text{DME} + \text{Ar} \rightarrow \text{CH}_3\text{O} + \text{CH}_3 + \text{Ar}$ and (2) $\text{DME} + \text{OH} \rightarrow \text{CH}_3\text{OCH}_2 + \text{H}_2\text{O}$, were measured in a shock tube by monitoring OH radicals. OH was measured with narrow-linewidth laser absorption using the well-known $\text{R}_1(5)$ line of the A-X(0,0) transition at 306.7 nm. OH radicals were formed by shock-heating mixtures of DME and O_2 in Ar. These mixtures take advantage of the rapid decomposition of the product CH_3O , forming H-atoms, which quickly react with O_2 to form OH. In carefully chosen mixtures, OH concentration is primarily sensitive to k_1 and the well-known rate coefficient of $\text{H} + \text{O}_2 \rightarrow \text{OH} + \text{O}$. See Figures 2 and 3. The rate coefficient k_1 is in the falloff regime at high temperatures, so it was measured at several pressures from 0.6 – 11.5 atm and temperatures from 1349 – 1790 K. Uncertainty in the k_1 measurements was estimated to be $\pm 35\%$. The rate coefficient measurements were then modeled using RRKM theory, which describes the data quite well. Both the rate coefficient measurements and RRKM model were fit from 1000 to 1800 K using the Troe falloff form: $k_{1,\infty}(T) = 4.38 \cdot 10^{21} \text{ T}^{-1.57} \exp(-42220 \text{ K}/T) \text{ s}^{-1}$, $k_{1,0} = 7.52 \cdot 10^{15} \exp(-21537 \text{ K}/T) \text{ cm}^3 \text{ mol}^{-1} \text{ s}^{-1}$, and $F_{\text{cent}} = 0.454 \exp(-T/2510)$. The rate coefficient k_2 was measured at pressures near 1.6 atm and temperatures of 923 – 1423 K. OH radicals were generated by the thermal decomposition of the OH precursor tert-butyl hydroperoxide (TBHP), and k_2 was inferred from the observed decay of OH with an estimated uncertainty of $\pm 40\%$. The high-temperature measurements were compared to several rate coefficient evaluations and previous low-temperature measurements. The evaluation by Curran et al. of $k_2 = 6.32 \times 10^6 * \text{T}^2 * \exp(328/T \text{ [K]}) \text{ (cm}^3/\text{mol/s)}$ was found to provide an excellent fit to both the previous low-temperature measurements and this work.

Reactions in the $\text{H}_2/\text{O}_2/\text{H}_2\text{O}_2/\text{HO}_2$ System: The rate coefficient of reaction (3) $\text{OH} + \text{HO}_2 \rightarrow \text{H}_2\text{O} + \text{O}_2$ can be inferred at high temperatures from measurements of the rate coefficient of its reverse reaction (-3) $\text{H}_2\text{O} + \text{O}_2 \rightarrow \text{OH} + \text{HO}_2$. We used laser absorption of both H_2O and OH (simultaneously) to study the reverse reaction (-3) in shock-heated $\text{H}_2\text{O}/\text{O}_2/\text{Ar}$ mixtures over the temperature range 1600 to 2200 K. Initial H_2O concentrations were determined using tunable diode laser absorption near 2.5 μm , and OH concentration time-histories were measured using UV ring-dye-laser absorption near 306.7 nm. Detailed kinetic analysis of the OH time-history profiles yielded a value for the rate coefficient k_3 of $(3.3 \pm 0.9) \times 10^{13} \text{ [cm}^3\text{mol}^{-1}\text{s}^{-1}]$ between 1600 and 2200 K; see Figure 4. This value is consistent with the extrapolation of the negative temperature dependence seen in the measurements by Keyser (1988) at lower temperatures and in the model of Gonzalez et al. (1992).

Similarly, the rate coefficients of the reactions (4) $\text{OH} + \text{H}_2\text{O}_2 \rightarrow \text{H}_2\text{O} + \text{HO}_2$ and (5) $\text{H}_2\text{O}_2 + \text{M} \rightarrow 2\text{OH} + \text{M}$ were measured in shock-heated $\text{H}_2\text{O}_2/\text{Ar}$ mixtures using laser absorption diagnostics for H_2O and OH. Initial H_2O_2 concentrations were determined by noting that there is a direct correspondence between the measured change in H_2O concentration (from reaction initiation to completion) and the initial H_2O_2 concentration. Based on simultaneous measurements of the OH and H_2O time-histories, k_4 was found to be $4.6 \times 10^{13} \exp(-2630/T) \text{ [cm}^3\text{mol}^{-1}\text{s}^{-1}]$ over the temperature range 1020 to 1460 K at 1.8 atm. These rate coefficient values differ significantly at high temperature from those of Hippler et al. (1992, 1995). Additional measurements of k_4 near 1 atm indicated no significant pressure dependence. Similarly, k_5 was found to be $9.5 \times 10^{15} \exp(-21250/T) \text{ [cm}^3\text{mol}^{-1}\text{s}^{-1}]$ over the same temperature and pressure range.

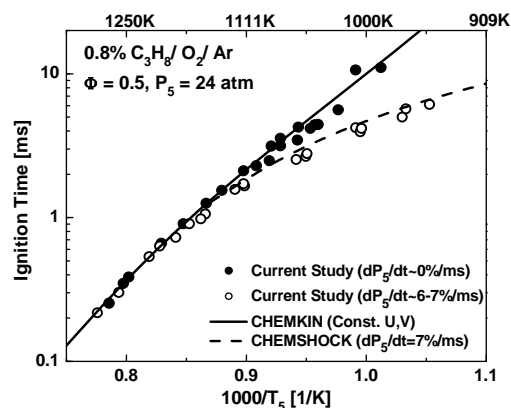


Figure 1. High-pressure propane ignition delay time data ($P_5 = 24$ atm), along with CHEMKIN and CHEMSHOCK modeling using JetSurF v1.0 mechanism.

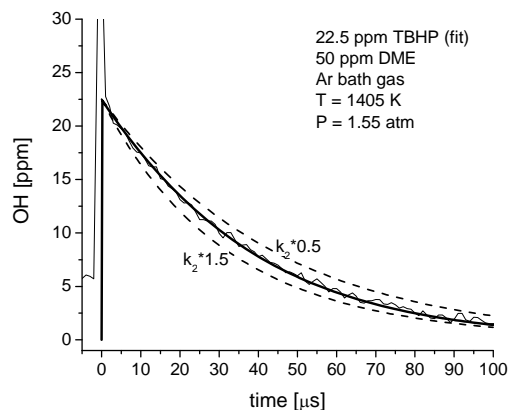


Figure 3. Representative DME + OH rate coefficient measurement. The solid line is fit to the data by adjusting k_2 and initial TBHP, while the dashed lines show the best fit of $k_2 \pm 50\%$.

Reactions of Alkanes and Alkenes with OH: Work has begun on measuring the overall rate coefficients of a series of reactions of alkanes and alkenes with OH. As in previous studies in our laboratory, tert-butyl hydroperoxide is used as a precursor for OH, and laser absorption at 306 nm is used to follow OH concentration time-histories during the pseudo-first-order removal of OH in the presence of excess fuel. Current work for the alkane series is concentrated on measurements of the rate coefficient for n-heptane+OH and, in particular, accurately determining the initial n-heptane concentration using mid-IR laser absorption at 3.39 μm . For the alkene series, initial measurements of the rate coefficients for ethylene+OH, propene+OH, and butadiene+OH have been performed and are currently being analyzed. Analysis will include RRKM modeling of these reaction rate coefficients.

Spectroscopy: A new Coherent™ MIRA Ti-Sapphire laser system is being applied to study deep-UV absorption features of several combustion species. This laser system allows significantly improved operation (higher power and wider tuning range) over previous systems. Using this laser high SNR time-histories of CH_3 during ethane decomposition have been

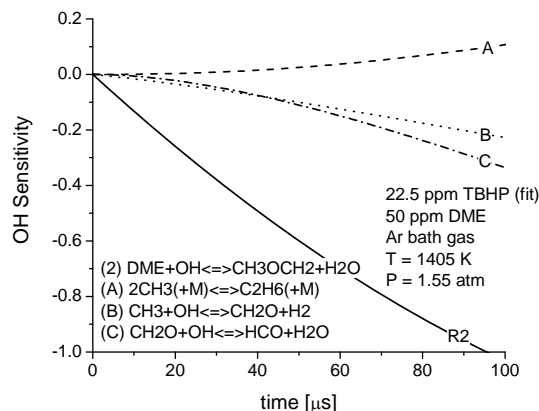


Figure 2. OH sensitivity plot for rate coefficient measurement of $\text{DME} + \text{OH} \leftrightarrow \text{CH}_3\text{OCH}_2 + \text{H}_2\text{O}$.

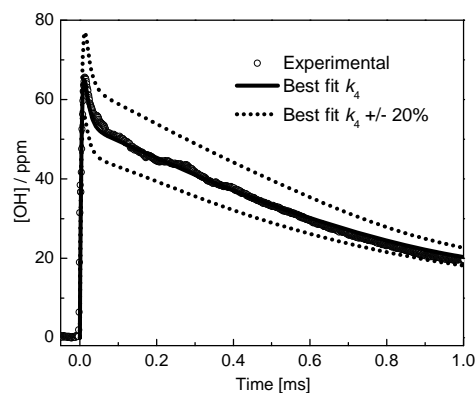


Figure 4. Representative OH time-history data used for the determination of k_4 for $\text{OH} + \text{H}_2\text{O}_2 \rightarrow \text{H}_2\text{O} + \text{HO}_2$. Initial reflected shock conditions: 1192 K, 1.95 atm, 2216 ppm H_2O_2 /1364ppm H_2O /682ppm O_2 /Ar.

acquired; see Figures 5 and 6. These measurements demonstrate the relatively high fidelity of the modified GRI-Mech v3.0 reaction mechanism for modeling ethane decomposition.

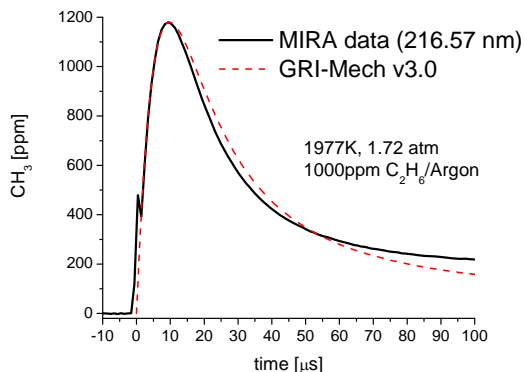


Figure 5. Representative CH_3 time-histories acquired using the MIRA Ti-sapphire laser system.

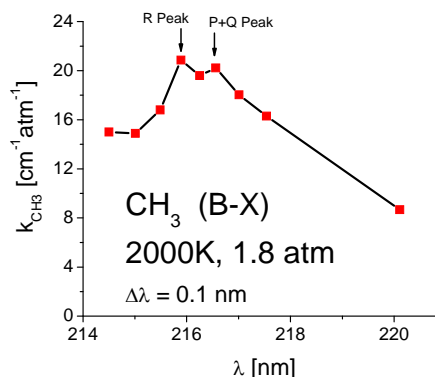


Figure 6. CH_3 absorption coefficient as a function of wavelength measured using the MIRA Ti-Sapphire laser system.

Future Plans

We plan to continue investigations of the high-temperature rate coefficients of alkanes+OH and alkenes+OH. In particular, we will extend study to larger n-alkanes (i.e. n-dodecane) and to cyclo-alkanes (e.g. methycycloalkane). We also plan to investigate decomposition pathways of various methyl esters using a tunable diode laser CO_2 diagnostic, which provides a method to characterize the bond breakage pathways in and adjacent to the ester group. The MIRA Ti-Sapphire laser system will be used to investigate the reaction of CH_3+HO_2 .

List of Recent Publications

- Z. Hong, S. S. Vasu, D. F. Davidson, R. K. Hanson, "Experimental Study of the Rate of $\text{OH}+\text{H}_2\text{O}=\text{H}_2\text{O}+\text{O}$ at High Temperatures Using the Reverse Reaction," under review, *Journal of Physical Chemistry A*.
- Z. Hong, R. D. Cook, D. F. Davidson, R. K. Hanson, "A Shock Tube Study of $\text{OH}+\text{H}_2\text{O}_2=\text{H}_2\text{O}+\text{HO}_2$ and $\text{H}_2\text{O}_2+\text{M}=2\text{OH}+\text{M}$ using Laser Absorption of H_2O and OH ," under review, *Journal of Physical Chemistry A*.
- K.-Y. Lam, Z. Hong, D. F. Davidson, R. K. Hanson, "Shock Tube Ignition Delay Time Measurements in Propane/ O_2 /Argon Mixtures at Near-Constant-Volume Conditions," under review, *Proceedings of the Combustion Institute*.
- D. F. Davidson, S. C. Ranganath, K.-Y. Lam, M. Liaw, Z. Hong, R. K. Hanson, "Ignition Delay Time Measurements of Normal Alkanes and Simple Oxygenates," in press, *Journal of Propulsion and Power*.
- Z. Hong, A. Farooq, E. A. Barbour, D. F. Davidson, R. K. Hanson, "Hydrogen Peroxide Decomposition Rate: A Shock Tube Study Using Tunable Laser Absorption of H_2O near 2.5 μm ," Paper 09F65, Western States Section/Combustion Institute Fall 2009 Meeting, Irvine CA.
- R. D. Cook, D. F. Davidson, R. K. Hanson, "High-Temperature Shock Tube Measurements of Dimethyl Ether Decomposition and the Reaction of Dimethyl Ether with OH ," *Journal of Physical Chemistry A* 113 (2009) 9974-9980.
- D. F. Davidson, R. K. Hanson, "Recent Advances in Shock Tube/Laser Diagnostic Methods for Improved Chemical Kinetics Measurements," *Journal of Shock Waves* 19 (2009) 271-283.
- Z. Hong, G. A. Pang, S. S. Vasu, D. F. Davidson, R. K. Hanson, "The Use of Driver Inserts to Reduce Non-Ideal Pressure Variations behind Shock Waves," *Journal of Shock Waves* 19 (2009) 113-123.
- R. D. Cook, D. F. Davidson, R. K. Hanson, "Rate Measurements of DME Decomposition and $\text{DME}+\text{OH}$ at Elevated Temperatures," to be presented at the U. S. Combustion Meeting, Ann Arbor MI, May 2009.

Theoretical Studies of Potential Energy Surfaces*

Lawrence B. Harding
Chemical Sciences and Engineering Division
Argonne National Laboratory, Argonne, IL 60439
harding@anl.gov

Program Scope

The goal of this program is to calculate accurate potential energy surfaces for both reactive and non-reactive systems. Our approach is to use state-of-the-art electronic structure methods (CASPT2, MR-CI, CCSD(T), etc.) to characterize multi-dimensional potential energy surfaces. Depending on the nature of the problem, the calculations may focus on local regions of a potential surface (for example, the vicinity of a minimum or transition state), or may cover the surface globally. A second aspect of this program is the development of techniques to fit multi-dimensional potential surfaces to convenient, global, analytic functions that can then be used in dynamics calculations.

Recent Progress

Decomposition pathways for Propane: The existence of roaming radical mechanisms for the decomposition of formaldehyde and acetaldehyde is now well established. An important question for combustion modeling is do roaming pathways contribute significantly to the decomposition of fuel molecules? Our calculations predict the existence of a roaming radical path for the decomposition of propane. This pathway leads to the formation of methane and ethylene with a threshold slightly below that for CC bond cleavage. This year Stephen Klippenstein and I have begun a collaborative theoretical/experimental effort (with Raghu Sivaramakrishnan and Joe Michael) to determine the importance of roaming radical pathways in the thermal decomposition of hydrocarbon fuels. Shock-tube measurements indicate that in the thermal decomposition of propane the ratio of hydrogen atoms produced to propane molecules consumed is less than one (approximately 0.9). The CC bond cleavage mechanism is expected to give a ratio of exactly one because each propane molecule makes one ethyl and one methyl and then each ethyl rapidly dissociates to an H atom plus ethylene. That the observed ratio is 0.9 implies the existence of a competing mechanism contributing ~10%. We have completed a thorough theoretical study of possible decomposition pathways for propane. The results are shown schematically in Figure 1. We have characterized five pathways leading to carbenes along with the two CH bond cleavage pathways and the roaming radical path to $\text{CH}_4 + \text{C}_2\text{H}_4$. Transition state theory calculations based on these results predict that, under the conditions of the shock-tube experiments, the carbene pathways contribute less than 0.02% relative to CC bond cleavage and the CH bond cleavages less than 0.1%. Therefore none of these pathways can be the competing mechanism and we tentatively conclude that the roaming mechanism contributes ~10% to the thermal

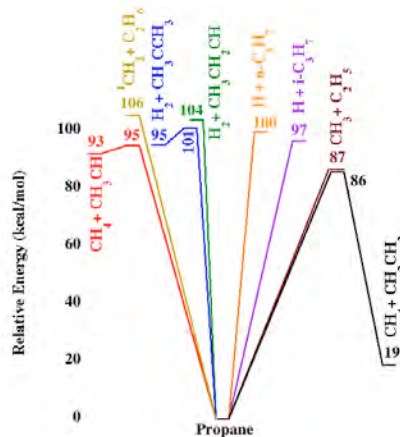


Figure 1

decomposition of propane. Similar calculations are underway for iso-butane and neo-pentane where the shock tube studies indicate roaming channel contributions of 22-25%.

Decomposition pathways for Dimethyl Ether: In another theoretical/experimental collaboration we have examined decomposition pathways for dimethyl ether, again as an aid in the interpretation of shock tube measurements. CASPT2 calculations predict the existence of a roaming methyl radical pathway lying 1.4 kcal/mol below the $\text{CH}_3+\text{CH}_3\text{O}$ asymptote. This roaming methyl pathway leads to $\text{CH}_4+\text{H}_2\text{CO}$ via a very shallow van der Waals minimum. In Figure 2 we show a schematic including this pathway along with the results of CCSD(T)/CBS calculations for possible competing pathways. From these results it is clear that the only pathway that will compete to a significant extent with CO bond cleavage is the roaming radical path. Preliminary shock tube studies indicate that

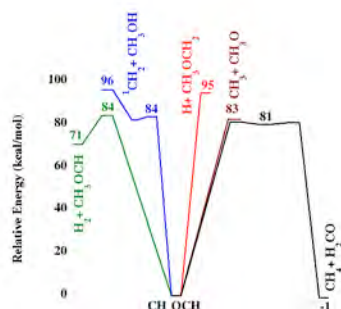
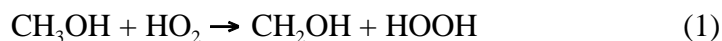


Figure 2.

the roaming methyl path contributes 20% to the total rate of decomposition.

$\text{CH}_3\text{OH} + \text{HO}_2$: Starting with the Li et al¹ mechanism for methane oxidation, global sensitivity analyses by Rex Skodje (Colorado), Alison Tomlin (Leeds), and Mike Davis indicated that the reaction of CH_3OH with HO_2 contributes most strongly to uncertainties in calculated ignition delays under certain conditions. No direct measurements of the rate of this reaction have been reported and previous estimates differ by more than an order of magnitude. For this reason we undertook a detailed theoretical analysis with the goal of reducing the uncertainty in the rate coefficients for reactions (1) and (2).



Rovibrational properties of the saddle points were determined using CASPT2/aug-cc-pvtz calculations and final relative energies with CCSD(T) calculations extrapolated to the complete basis set (CBS) limit at the CASPT2 geometries. The results are shown schematically in Figure 3. A total of five unique saddle points were found for reaction (1) and two for reaction (2). These saddle points are related to each other via internal rotations. The transition state structures shown in Figure 3 correspond to the lowest energy rotamers and horizontal lines depict the energies of the higher rotamers. These results were then used by Stephen Klippenstein to obtain transition state theory estimates of the rate coefficients. The results of these calculations are shown in Figure 4. From this plot it can be seen that reaction (1) is dominant at all temperatures. The rate of reaction (2) comes within a factor of four of reaction (1) only at the highest temperatures. The current predictions are approximately a factor of ten below the rate used in the original model and exhibit a temperature dependence similar to that in the original model. The current results are in best agreement with the earlier estimate of Miller² although the predicted temperature dependence is significantly stronger.

A similar study of the reaction of CH_3OH with O_2 has also been completed. The present predictions for the rate of this reaction are also approximately one order of magnitude below the rate used in the original model.

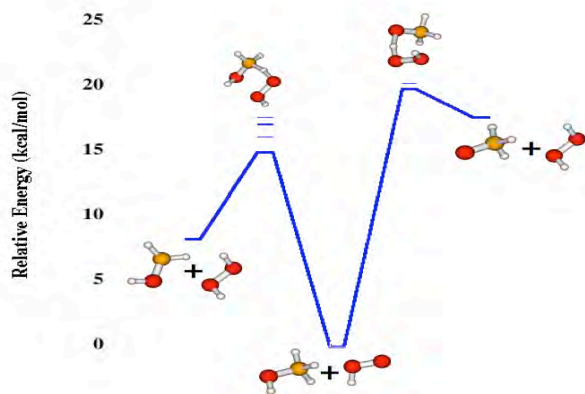


Figure 3.

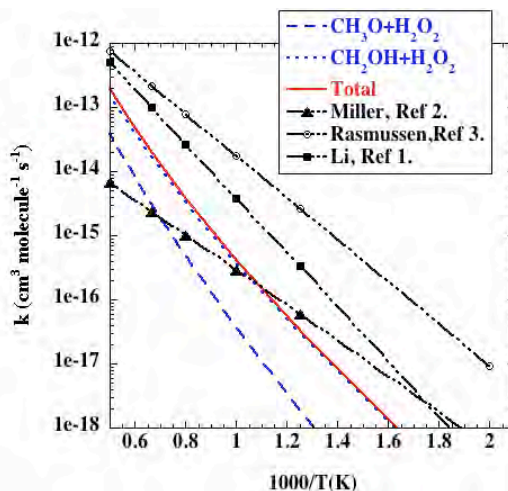


Figure 4.

Future Plans

One of the reactions we plan to focus on in the near future is $\text{OH} + \text{HO}_2 \rightarrow \text{H}_2\text{O} + \text{O}_2$. Combustion mechanisms have shown a high sensitivity to this reaction but there is considerable uncertainty in the rate of this reaction. There is also some evidence for a highly non-Arrhenius temperature dependence.

As noted above we also plan to continue our studies of roaming radical pathways in saturated hydrocarbons, ethers and peroxides. These studies will involve a collaborative effort with Ahren Jasper, Richard Dawes (Sandia) and Al Wagner using reduced dimensional, IMLS, potential energy surfaces to study roaming radical reactions. Our first two target molecules will be propane and dimethyl ether.

Acknowledgement: This work was performed under the auspices of the Office of Basic Energy Sciences, Division of Chemical Sciences, Geosciences and Biosciences, U.S. Department of Energy, under Contract DE-AC02-06CH11357.

References:

- (1) J. Li, Z. Zhao, A. Kazakov, M. Chaos, F. L. Dryer, *Int. J. Chem. Kinet.* **39**, 109 (2007)
- (2) J. A. Miller, private communication
- (3) C. L. Rasmussen, K. H. Wassard, K. Dam-Johansen, P. Glabert, *Int. J. Chem. Kin.* **40**, 423 (2008)

PUBLICATIONS (2008 - Present):

The Thermal Decomposition of CF₃ and the Reaction of CF₂+OH → CF₂O+H

N. K. Srinivasan, M.-C. Su, J. V. Michael, A. W. Jasper, S. J. Klippenstein and L. B. Harding, *J. Phys. Chem. A* **112**, 31-37 (2008)

The Kinetics of CH + N₂ Revisited with Multi-Reference Methods

L. B. Harding, S. J. Klippenstein and J. A. Miller, *J. Phys. Chem. A* **112**, 522-532 (2008)

Quantum States of the Endohedral Fullerene Li@C₆₀

M. Zhang, L. B. Harding, S. K. Gray, S. A. Rice, *J. Phys. Chem. A* **112**, 5478-5485(2008)

Kinetics and Product Branching Ratios of the Reaction of ¹CH₂ with H₂ and D₂

K. L. Gannon, M. A. Blitz, M. J. Pilling, P. W. Seakins, S. J. Klippenstein and L. B. Harding *J. Phys. Chem. A* **112**, 9575-9583 (2008)

Kinetics of the H + NCO Reaction

S. J. Klippenstein and L. B. Harding
32nd Symposium (International) on Combustion **32**, 149-155(2009)

Theoretical Rate Coefficients for the Reaction of Methyl Radical with Hydroperoxyl Radical and for Methylhydroperoxide Decomposition

A. W. Jasper, S. J. Klippenstein and L. B. Harding
32nd Symposium (International) on Combustion **32**, 279-286(2009)

A Crossed-Molecular Beam Study on the Formation of the Exotic Cyanoethynyl Radical in Titan's Atmosphere

X. Gu, R. I. Kaiser, A. M. Mebel, V. V. Kislov, S. J. Klippenstein, L. B. Harding, M. C. Liang, and Y. L. Yung, *Astrophysical Journal* **701**, 1797-1803 (2009)

The Thermal Decomposition of NH₂OH and Subsequent Reactions: Ab Initio Transition State Theory and Reflected Shock Tube Experiments

S. J. Klippenstein, L. B. Harding, B. Ruscic, R. Sivaramakrishnan, N. K. Srinivasan, M.-C. Su, and J. V. Michael, *J. Phys. Chem. A* **113**, 10241-10259 (2009)

Shock Tube and Theory Investigation of Cyclohexane Decomposition

J. H. Kiefer, K. Gupte, L. B. Harding and S. J. Klippenstein
J. Phys. Chem. A **113**, 13570-13583 (2009)

Roaming Radical Kinetics in the Decomposition of Acetaldehyde

L. B. Harding, Y. Georgievskii and S.J. Klippenstein, *J. Phys. Chem. A* **114**, 765-777 (2010)

The Effect of Spin-Orbit Splitting on the Association Kinetics of Barrierless Halogen Atom-Hydrocarbon Radical Reactions

A. W. Jasper, S. J. Klippenstein, L. B. Harding, *J. Phys. Chem. A* (accepted)

CHEMICAL ACCURACY FROM AB INITIO MOLECULAR ORBITAL CALCULATIONS

Martin Head-Gordon

Department of Chemistry, University of California, Berkeley, and,
Chemical Sciences Division, Lawrence Berkeley National Laboratory,
Berkeley, CA 94720.
mhg@cchem.berkeley.edu

1. Scope of Project.

Short-lived reactive radicals and intermediate reaction complexes play central roles in combustion, interstellar and atmospheric chemistry. Due to their transient nature, such molecules are challenging to study experimentally, and our knowledge of their structure, properties and reactivity is consequently quite limited. To expand this knowledge, we develop new theoretical methods for reliable computer-based prediction of the properties of such species [9]. We apply our methods, as well as existing theoretical approaches, to study prototype radical reactions, often in collaboration with experimental efforts. These studies help to deepen understanding of the role of reactive intermediates in diverse areas of chemistry. They also sometimes reveal frontiers where new theoretical developments are needed in order to permit better calculations in the future.

2. Summary of Recent Major Accomplishments.

2.1 *Improved density functionals.*

We have systematically optimized a new density functional called ω B97 that includes 100% exact exchange at long range, thereby eliminating long-range self-interaction error [4]. Tests show that ω B97, and an additional functional, ω B97X [4], which includes a fraction of short-range exact exchange also, statistically out-perform widely used density functionals such as B3LYP [4]. Intermolecular interactions can be further improved by including atom-atom dispersion corrections, yielding ω B97X-D [16]. Even greater reductions in self-interaction may be possible by using different separators [5,27]. Or, at additional computational expense, one can also include 2nd order non-local correlation [8], leading to a double-hybrid functional of the same family, termed ω B97X-2 [32], which is probably our most accurate to date.

2.2 *Excited states of large molecules without self-interaction errors.*

For excited states, we recently developed the quasidegenerate scaled opposite spin (SOS) doubles correction to single excitation CI. SOS-CIS(D0) [10] has a number of desirable properties. The cost scales only 4th order with molecular size, versus 5th order for conventional perturbation methods such as CIS(D). It is self-interaction free, and charge-transfer excited states are correctly described. We have formulated and implemented the analytical gradient [22] to enable the exploration of excited state potential energy surfaces of molecules in the 20-50 atom regime. Numerical tests of accuracy [30] suggest that it generally out-performs TDDFT with B3LYP and is comparable to more computationally expensive methods such as CC2. We have also co-developed a double

spin-flip (SF) approach (with Anna Krylov) that can treat excited states where up to 4 electrons are strongly correlated [19], and extended this approach to define a restricted active space (RAS) SF method [31] that can be applied to quite large molecules.

2.3 *Optimizing orbitals with low-order perturbation theory.*

Second order Moller-Plesset (MP2) theory can perform very poorly for radicals because of spin-contamination. For instance, the conjugated radical, phenalenyl, C₁₃H₉, (\cdot), exhibits $\langle S^2 \rangle > 2.0$ rather than 0.75. This problem can be resolved by optimizing the orbitals in the presence of 2nd order electron correlation, an approach we call O2. Furthermore, O2 potential energy curves that are smoother than standard MP2 [24]. MP2 forces and dipole moments are discontinuous when orbitals change from restricted to unrestricted, while O2 is continuous. Indeed, the MP2 effective density matrices can be non-n-representable (i.e. unphysical) while those for O2 are not [24]. This suggests that orbital optimized double hybrid density functionals should be developed, as existing double hybrids have the same weaknesses as MP2.

2.4 *Pairing methods for strong electron correlations.*

To treat large molecules that have strong electron correlations (e.g. singlet biradicaloids), we have been developing generalized valence bond coupled cluster methods, which systematically approximate CASSCF. Perfect pairing is the starting point: exact for one pair, and extensive. The next well-defined level is the perfect quadruples model [20], which is exact for two pairs and extensive. This is to be followed by a theory which correctly correlates up to three pairs of electrons – perfect hexuples – which is underway. As well as being a virtually exact approximation to CASSCF for computational organic chemistry, PH should also not suffer from symmetry-breaking in aromatics which we have shown arises due to neglect of 3-pairs correlations [1,17].

2.5 *Valence bond methods for strong electron correlations.*

Instead of approximating the CASSCF limit for treating strong correlations, another, relatively unexplored possibility is to approximate the spin-coupled valence bond limit (also exponentially expensive). We have made exciting recent progress on this problem, yielding a new approximate valence bond method that can break any number of chemical bonds with only a quadratic number of spin-coupling variables, maintaining extensivity, and spin-purity [21]. It still remains to treat the remaining essentially dynamical correlations, and we have started to develop a multireference density functional theory framework [28] towards this goal – it requires the reference system to be partially interacting rather than non-interacting as in Kohn-Sham DFT.

2.6 *Fundamental studies of chemical bonding.*

As a result of understanding the changes in chemical bonding with oxidation state in 4-membered CuPCuP heterocycles [7], we have developed a simple and potentially broadly useful method for computational evaluation of metal oxidation states [33]. We have also gained insight into the origin of the generation of small amounts of electricity from the oxidation of CO to CO₂ on a Pt thin-film catalyst – a nonadiabatic effect we show is associated with electron transfer from CO₂(δ^-) to the surface as the nascent product linearizes after crossing the barrier to reaction between CO(ads) + O(ads) [25].

3. Summary of Research Plans.

- Testing, and if necessary, further refining the new density functionals.
- Extensions of the coupled cluster pairing & CC-VB approaches to strong correlation
- Dynamic correlation corrections to coupled cluster pairing
- Density-functional approaches to augmenting the CC-VB method
- New studies of the properties of reactive radicals and radical reactions.

4. Publications from DOE Sponsored Work, 2008-present.

- [1] "Symmetry-breaking in benzene and larger aromatic molecules within generalized valence bond coupled cluster methods", K.V. Lawler, G.J.O. Beran, and M. Head-Gordon, *J. Chem. Phys.* 128, 024107 (2008) (13 pages).
- [2] "The limits of local correlation theory: electronic delocalization and chemically smooth potential energy surfaces", J.E. Subotnik, A. Sodt and M. Head-Gordon, *J. Chem. Phys.* 128, 034103 (2008) (12 pages).
- [3] "Central moments in quantum chemistry", D.W. Small and M. Head-Gordon, *Int. J. Quantum Chem.* 108, 1220-1231 (2008)
- [4] "Systematic optimization of long-range corrected hybrid density functionals", Jeng-Da Chai and M. Head-Gordon, *J. Chem. Phys.* 128, 084106 (2008).
- [5] "A two-parameter Coulomb attenuator with a cutoff radius for two-electron repulsion integrals: the effect of attenuation on correlation energies", A.D. Dutoi and M. Head-Gordon, *J. Phys. Chem A* 112, 2110-2119 (2008).
- [6] "Hartree-Fock exchange computed using the atomic resolution of the identity approximation", A. Sodt and M. Head-Gordon. *J. Chem. Phys.* 128, 104106 (2008).
- [7] "A Delicate Electronic Balance between Metal and Ligand in [Cu-P-Cu-P] Diamondoids: Oxidation State Dependent Plasticity and the Formation of a Singlet Diradical", Y.M. Rhee and M. Head-Gordon, *J. Am. Chem. Soc.* 130, 3878-3887 (2008)
- [8] "Semiempirical double-hybrid density functional with improved description of long-range correlation", T. Benighaus, R.A. Distasio Jr., R.C. Lochan, J.D. Chai and M. Head-Gordon, *J. Phys. Chem. A*, 112, 2702-2712 (2008).
- [9] "Chemistry at the Computer," M.Head-Gordon & E.Artacho, *Physics Today*, 61(4), 58 (2008)
- [10] "Quasidegenerate scaled opposite spin second order perturbation corrections to single excitation configuration interaction", D. Casanova, Y.M. Rhee and M. Head-Gordon, *J. Chem. Phys.* 128, 164106 (2008).
- [11] "Near infrared spectroscopy of nitrogenated polycyclic aromatic hydrocarbon cations from 0.7 to 2.5 micrometers", A.L. Mattioda, L. Rutter, J. Parkhill, M. Head-Gordon, T.J. Lee, and L.J. Allamandola, *Astrophys. J.* 680, 1243-1255 (2008).
- [12] "Exploring the accuracy of relative molecular energies in local correlation theory", J.E. Subotnik and M. Head-Gordon, *J. Phys.: Condens. Matter* 20 (2008) 294211.
- [13] "Effects of ligands and spin-polarization on the preferred conformation of distannynes" W. Kurlancheek, Y. Jung and M. Head-Gordon, *Dalton Trans.* 33, 4428-4435 (2008).
- [14] "The spin-flip extended single excitation configuration interaction method", D. Casanova and M. Head-Gordon, *J. Chem. Phys.* 129, 064104 (2008).
- [15] "Direct observation of photoinduced bent nitrosyl excited state complexes", K.R. Sawyer, R.P. Steele, E.A. Glascoe, J.F. Cahoon, J.P. Schlegel, M. Head-Gordon and C.B. Harris, *J. Phys. Chem. A*, 112, 8505-8514 (2008).
- [16] "Long-range corrected hybrid density functionals with damped atom-atom dispersion corrections", J.-D. Chai and M. Head-Gordon, *Phys. Chem. Chem. Phys.* 44, 6615 (2008).

- [17] “Penalty functions for combining coupled cluster and perturbation amplitudes in local correlation methods with optimized orbitals”, K.V. Lawler, J.A. Parkhill and M. Head-Gordon, *Mol. Phys.* 106, 2309-2324 (2008).
- [18] “Optimal operators for Hartree-Fock exchange from long-range corrected hybrid density functionals”, J.D. Chai and M. Head-Gordon, *Chem. Phys. Lett.* 467, 176-178 (2008).
- [19] “Double spin-flip approach within equation-of-motion coupled cluster and configuration interaction formalisms: Theory, implementation and examples” D. Casanova, L.V. Slipchenko, A.I. Krylov, and M. Head-Gordon, *J. Chem. Phys.* 130, 044103 (2009).
- [20] “The perfect quadruples model for electron correlation in a valence active space”, J.A. Parkhill, K.V. Lawler, and M. Head-Gordon, *J. Chem. Phys.* 130, 084101 (2009)
- [21] “Tractable spin-pure methods for bond-breaking: Local many-electron spin-vector sets and an approximate valence bond model”, D.W. Small and M. Head-Gordon, *J. Chem. Phys.* 130, 084103 (2009).
- [22] “Quartic-scaling analytical gradient of quasidegenerate scaled opposite spin second order perturbation corrections to single excitation configuration interaction”, Y.M. Rhee and M. Head-Gordon, *J. Chem. Theor. Comput.* 5, 1224-1236 (2009).
- [23] “The numerical condition of electron correlation theories when only active pairs of electrons are spin-unrestricted”, K.V. Lawler, J.A. Parkhill, and M. Head-Gordon, *J. Chem. Phys.* 130, 184113 (2009) (7 pages)
- [24] “Violations of N-representability from spin-unrestricted orbitals in Møller-Plesset perturbation theory and related double-hybrid density functional theory”, W. Kurlancheek and M. Head-Gordon, *Mol. Phys.* 107, 1223-1232 (2009).
- [25] “Chemistry of fast electrons”, S.N. Maximoff and M. Head-Gordon, *Proc. Natl. Acad. Sci. USA* 106, 11461-11465 (2009).
- [26] “Improving approximate optimized effective potentials by imposing exact conditions: Theory and application to electronic statics and dynamics”, Y. Kurzweil and M. Head-Gordon, *Phys. Rev. A* 80, 012509 (2009).
- [27] “The exchange energy of a uniform electron gas experiencing a new, flexible range separation”, J.A. Parkhill, J.-D. Chai, A.D. Dutoi and M. Head-Gordon, *Chem. Phys. Lett.* 478, 283-286 (2009).
- [28] “Analysis of multi-configuration density functional theory methods: Theory and model application to bond-breaking”, Y. Kurzweil, K.V. Lawler and M. Head-Gordon, *Mol. Phys.* 107, 2103-2110 (2009).
- [29] “Hartree-Fock solutions as a quasidiabatic basis for non-orthogonal configuration interaction”, A.J.W. Thom and M. Head-Gordon, *J. Chem. Phys.* 131, 124113 (2009).
- [30] “Performance of quasidegenerate scaled opposite spin perturbation corrections to single excitation configuration interaction for excited state structures and excitation energies with application to the Stokes shift of 9-methyl-9,10-dihydro-9-silaphenanthrene”, Y.M. Rhee, D. Casanova, and M. Head-Gordon, *J. Phys. Chem. A* 113, 10564-76 (2009).
- [31] “Restricted active space spin-flip configuration interaction approach: Theory, implementation and examples” D. Casanova and M. Head-Gordon, *Phys. Chem. Chem. Phys.* 11, 9779-9790 (2009).
- [32] “Long-range corrected double hybrid density functionals”, J.-D. Chai and M. Head-Gordon, *J. Chem. Phys.* 131, 174105 (2009) (13 pages).
- [33] “LOBA: A localized orbital bonding analysis to calculate oxidation states, with application to a model water oxidation catalyst”, A.J.W. Thom, E. Sundstrom, and M. Head-Gordon, *Phys. Chem. Chem. Phys.* 11, 11297-11304 (2009)

Laser Studies of Combustion Chemistry

John F. Hershberger

Department of Chemistry and Molecular Biology
North Dakota State University
NDSU Dept. 2735, PO Box 6050
Fargo, ND 58108-6050
john.hershberger@ndsu.edu

Time-resolved infrared diode laser absorption and laser-induced fluorescence spectroscopy are used in our laboratory to study the kinetics and product channel dynamics of chemical reactions of importance in the gas-phase combustion chemistry of nitrogen-containing species. This program is aimed at improving the kinetic database of reactions crucial to the modeling of NO_x control strategies such as Thermal de-NO_x, RAPRENO_x, and NO-reburning. The emphasis in our study is the quantitative measurement of both total rate constants and product branching ratios.

NCCO Kinetics

We have successfully detected the NCCO radical using high-resolution infrared absorption spectroscopy for the first time. NCCO is formed by the photolysis of methyl cyanofornate or ethyl cyanofornate:



A previous report attributed an emission feature at 2093 cm⁻¹ to the ν₁ mode of NCCO.¹ Our initial detection attempts were therefore conducted to search for transient absorption signals in the 2050-2110 cm⁻¹ range. Although several signals were found, all were attributable either to CN or to highly vibrationally excited states of CO. More recently, high level ab initio calculations suggested that the strongest infrared band is the ν₂ mode, located near 1898 cm⁻¹.² Our subsequent searches have found several transitions, including lines at 1887.42, 1887.72, 1888.11, 1888.76, and 1889.46 cm⁻¹. Identical signals were obtained using both different precursors, eliminating the possibility that CH₃OCO (a possible minor photolysis channel from the methyl precursor) is the source of the signals. We are therefore confident in our assignment of NCCO as the spectral carrier of these signals.

We have studied the kinetics of NCCO with molecular oxygen:



We find a slow, pressure-dependent rate constant of

$$k_3 (298 \text{ K}) = (5.2 \pm 0.3) \times 10^{-13} \text{ cm}^3 \text{ molecule}^{-1} \text{ s}^{-1} \text{ at 2 Torr pressure of N}_2.$$

Our result is in good agreement with the one previous kinetic study which used mass spectrometric detection.³ Channel (3a), the NCC(O)OO adduct, which we cannot spectroscopically detect, appears to be the major product channel in this reaction, but we have detected a significant yield into channel (3b) by using isotopically labeled $^{18}\text{O}_2$ and detecting the mixed isotope $^{16}\text{O}^{12}\text{C}^{18}\text{O}$ product. We estimate the branching ratio $\phi_{3\text{b}} = 0.28 \pm 0.06$ at 3.2 Torr total pressure. This is in qualitative agreement with a recent ab initio calculation⁴ which predicted that both (3a) and (3b) may be present. Channel (3c) is unimportant, with $\phi_{3\text{c}} < 0.03$.

We have also studied the kinetics of NCCO with NO:



This reaction also displays pressure-dependent kinetics:

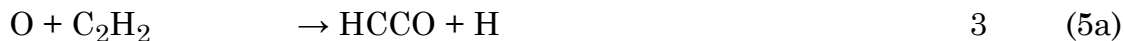
$k_4 (298 \text{ K}) = (3.2\text{-}27.1) \times 10^{-13} \text{ cm}^3 \text{ molecule}^{-1} \text{ s}^{-1}$ over the total pressure range 3.0-25.0 Torr. This result suggests that channel (4d) is important. In fact, we only detect extremely small yields of CO and CO₂ in this reaction, suggesting that $\phi_{4\text{a}}$, $\phi_{4\text{b}}$, and $\phi_{4\text{c}}$ are all less than 0.02.

We have also calculated critical points on both the triplet and singlet potential energy surfaces of this reaction. We find that all pathways to product channels (4a), (4b), and (4c) involve high energy barriers, and are therefore inaccessible at moderate temperatures. In summary, both experiment and theory are in agreement that this reaction is dominated by collisional stabilization of the NCC(NO)O adduct, channel (4d).

Work is in progress on the NCCO + NO₂ reaction. This reaction appears to be substantially faster than NCCO+NO. One complication is that CN produced in the photolysis reacts quickly with NO₂, producing some of the same products. We are investigating the possibility of using a hydrocarbon or other reagent to quickly remove CN radicals without removing NCCO.

HCNO Kinetics

Previous to recent studies in our laboratory, there have been no literature data available on the kinetics of HCNO, the fulminic acid molecule. Recent modeling studies have suggested the importance of this molecule in NO-reburning mechanisms.¹ In combustion, HCNO is primarily formed via acetylene oxidation:



Earlier reports have summarized our results for several reactions involving HCNO, including O+HCNO, OH+HCNO, CN+HCNO, and NCO+HCNO.

More recently, we have been performing experiments on the Cl+HCNO reaction:



Because we cannot directly detect Cl atoms, we are using a relative rate experiment similar to that employed in our earlier study of the O+HCNO reaction. We are using deuterated hydrocarbons as competitive reactants:



We measure the yield of the DCl product as a function of [HCNO]/[C₂D₆]. Knowledge of k₈ then allows determination of k₇. Our preliminary results indicate a slow rate constant for k₇, with an upper limit of <2×10⁻¹³ cm³ molecule⁻¹ s⁻¹. Work in progress includes switching to CD₄ as a slower competitive reactant in order to obtain a more precise estimate.

References

1. W. McNavage, W. Dailey, and J.-L. Dai, *Can. J. Chem.* **82**, 925 (2004).
2. A.C. Simmonett, F.A. Evangelista, W.D. Allen, H.F. Schaefer III, *J. Chem. Phys.* **127**, 14306 (2007).
3. T. Imamura, N. Washida, *Int. J. Chem. Kinet.* **33**, 440 (2001).
4. Y. Tang, R. Wang, B. Wang, *J. Phys. Chem.* **112**, 5295 (2008).

Publications acknowledging DOE support (2006-present)

1. "Ab Initio Study of the HCCO+NO₂ Reaction", J.P. Meyer and J.F. Hershberger, *Chem. Phys.* **325**, 545 (2006).
 2. "Kinetics of the OH+HCNO Reaction", W. Feng, J.P. Meyer, and J.F. Hershberger, *J. Phys. Chem. A* **110**, 4458 (2006).
 3. "Kinetics of the CN+HCNO Reaction", W. Feng and J.F. Hershberger, *J. Phys. Chem. A* **110**, 12184 (2006).
 4. "Kinetics of the NCO+HCNO Reaction", W. Feng and J.F. Hershberger, *J. Phys. Chem. A* **111**, 3831 (2007).
 5. "Kinetics of the O+HCNO Reaction", W. Feng and J.F. Hershberger, *J. Phys. Chem. A* **111**, 10654 (2007).
 6. "Theoretical Study of the Reaction of O(³P) with HCNO", W. Feng and J.F. Hershberger, *Chem. Phys. Lett.* **457**, 307 (2008).
 7. "Kinetics of Reactions of CN with chlorinated Methanes", V. Samant and J.F. Hershberger, *Chem. Phys. Lett.* **460**, 64 (2008).
 8. "A Re-investigation of the Branching Ratio of the CN + O₂ Reaction", W. Feng and J.F. Hershberger, *J. Phys. Chem. A* **113**, 3523 (2009).
 9. "Infrared Diode Laser Study of the Kinetics of the NCCO + O₂ Reaction", W. Feng and J.F. Hershberger, *Chem. Phys. Lett.* **488**, 140 (2010).
- "Experimental and Theoretical Study of the Kinetics of the NCCO + NO Reaction, W. Feng and J.F. Hershberger, manuscript in preparation.

Breakthrough Design and Implementation of Electronic and Vibrational Many-Body Theories

So Hirata (principal investigator: DE-FG02-04ER15621)

Quantum Theory Project and The Center for Macromolecular Science and Engineering,
Departments of Chemistry and Physics, University of Florida, Gainesville, FL 32611

hirata@qtp.ufl.edu

Program Scope

Predictive chemical computing requires hierarchical many-body methods of increasing accuracy for both electrons and vibrations. Such hierarchies are established, at least conceptually, as configuration-interaction (CI), many-body perturbation (MP), and coupled-cluster (CC) methods, which all converge at the exact limit with increasing rank of a hierarchical series. These methods can generate results of which the convergence with respect to various parameters of calculations can be demonstrated and which can thus be predictive in the absence of experimental information.

The wide use of the hierarchical electronic and vibrational many-body methods has, however, been hindered (1) by the immense cost of *executing* the calculations with these methods and, furthermore, the non-physical rapid increase of the cost with increasing molecular size, (2) by the complexity and cost of *developing* some of the high-rank members of these methods, and (3) by the slow convergence of electronic energies and wave functions with respect to one-electron basis set sizes, which further drives up the cost of execution.

The overarching goal of our research is to address all three difficulties for electrons and vibrations in small molecules in the gas phase as well as in solids and molecules in condensed phases. We have eradicated the second difficulty for electrons by developing a computerized symbolic algebra system that completely automates the mathematical derivations of electron-correlation methods and their implementation. For vibrations, an assortment of vibrational many-body methods has been implemented in the general-order algorithm that allows us to include anharmonicity and vibrational mode-mode couplings to any desired extent. We have also addressed the third difficulty by departing from the conventional Gaussian basis sets and introduce a new hierarchy of converging electron-correlation methods with completely flexible but rational (e.g., satisfying asymptotic decay and cusp conditions) basis functions such as numerical basis functions on interlocking multi-center quadrature grids and explicit r_{12} (inter-electronic distance) dependent basis functions.

This year, we have made significant progress that primarily addresses the first difficulty and enables these hierarchical electronic and vibrational many-body calculations of infinitely extended systems.

Recent Progress

Two complementary computational approaches⁶ have been explored to speedup the systematic electron-correlation calculations of solids. One is the delocalized orbital approach or the so-called crystal orbital (CO) theory in which the periodic-symmetry-adapted orbitals are used as one-electron basis. The other is the localized orbital approach in which the total energy of molecular clusters and crystals is approximated as the sum of energies of overlapping dimers in embedding electrostatic fields.

The delocalized approach is inevitable for delocalized wave functions such as in metals and conjugated polymers. Here, the Brillouin-zone (BZ) integration of correlation energy contributions incurs the largest computational cost, which is proportional to cubic or higher power of the number of wave vector (k vector) sampling points in the BZ. We have proposed several schemes to dramatically speedup this computational step by introducing various downsampling approximations in the reciprocal space. These approximations are shown to have a firm physical justification based on our knowledge of the long-range decay rate of chemical interactions.

The localized approach is well suited for molecular clusters and crystals. Our proposed method enables routine applications of MP and CC methods to infinite one-, two-, and three-dimensional crystals. It can obtain energies, lattice structures, and harmonic and anharmonic vibrational frequencies in the Γ approximation (see below) in a linear-scaling, size-extensive fashion. Corrections to basis-set superposition errors can also be made. It has the additional advantages of being easily implemented and naturally parallel.

Formulas of the whole array of vibrational many-body methods have been derived for anharmonic lattice vibrations (phonon) in solids. Size dependence of terms has been carefully analyzed to ensure that the

methods are size-extensive. Some of these methods have been applied to the frequencies of the infrared- and/or Raman-active vibrations of polyethylene and polyacetylene in the Γ approximation (see below). This is first such calculations that are based on *ab initio* electronic and *ab initio* vibrational methods.

Since the 30th Annual Combustion Research Meeting, 7 papers⁴⁻¹⁰ have been published including 2 invited articles.^{5,6} 3 book chapters¹⁻³ are also in press and 4 more papers²³⁻²⁶ are being reviewed. In total, 26 publications¹⁻²⁶ (including 4 submitted) have resulted from this grant in 2008–10. In the same period, the PI has been an invited speaker at 10 conferences (including the 30th Combustion Meeting) and 8 university seminars. In 2009, the PI has been selected to receive the National Science Foundation's CAREER Award and the Camille Dreyfus Teacher-Scholar Award. The PI has also been invited to join the Editorial Advisory Boards of *Phys. Chem. Chem. Phys.* and *Theor. Chem. Acc.* His students working on the DOE project have won an ACS Graduate Student Award in Computational Chemistry and a Best Poster Prize.

Second-order many-body perturbation calculations on solid hydrogen fluoride.²⁶ A linear-scaling, local-basis MP2 method based on a truncated many-body expansion of energies has been applied to crystalline hydrogen fluoride in three dimensions. The energies, equilibrium lattice structures, and molecular dipole moments of two structures (parallel and anti-parallel, **Fig. 1**) have been determined, taking account of one- and two-body Coulomb (electrostatic), exchange, and correlation interactions exactly (within MP2/aug-cc-pVDZ) and three-body and higher-order Coulomb interactions approximately. Counterpoise corrections of the basis-set superposition errors have also been made. Previous three experimental studies (neutron diffraction, NMR, and infrared absorption) advocated three different structures (parallel, anti-parallel, and disordered, respectively), whereas previous three computational studies were split between the parallel and anti-parallel structures. Our calculations have shown that the anti-parallel structure is considerably more stable than the parallel one and that, furthermore, the latter does not have a potential minimum near the observed lattice constants, finally resolving the controversy. Our computed lattice constants of the anti-parallel structure also agree with the observed within 0.3 Å.

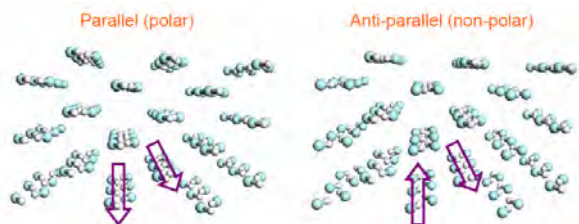


Fig. 1. Parallel and anti-parallel structures of solid hydrogen fluoride

Modulo second-order many-body perturbation method for extended systems.^{8,12} The cost of an MP2 CO calculation on a one-dimensional extended system (e.g., polymer) exhibits the steep cubic dependence on the number of wave vector (k vector) sampling points in the first BZ. Reducing this number (K) as much as possible is the key to making MP2 routinely applicable to solids. The validity and accuracy of various ways of drastically reducing K has been investigated. We have proposed the mod- n scheme in which the k vectors are downsampled by a factor of n only in the MP2 step, holding fixed the number of k vectors in the HF step. In one variant of this approximation, the correlation energies of polyethylene and polyacetylene are recovered within 1% of converged values at less than a tenth of usual computational cost. The quasi-particle energy bands have also been reproduced quantitatively with the same approximation. In the most drastic approximation, in which only one zone-center k point (Γ point) in the BZ is sampled (the Γ approximation), the correlation energies are recovered within 10% of the converged values with a speedup by a factor of 80–100. The (angle-resolved) photoelectron spectra of *trans*- and *cis*-polyacetylenes, polyethylene, and polydiacetylene have been reproduced accurately or predicted by MP2 with this scheme (**Fig. 2**).

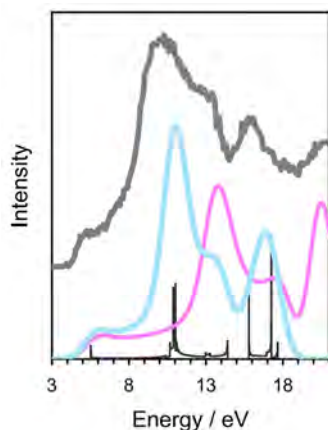


Fig. 2 Photoelectron spectra of *trans*-polyacetylene. The grey curves: experiment; red curves: HF/6-31G*; blue curves: MP2/6-31G*; black histogram: MP2/6-31G* density of states.

Logarithm second-order many-body perturbation method for extended systems.²⁵ We have proposed progressive downsampling of k vectors: higher-lying unoccupied and lower-lying occupied Bloch orbitals are subject to downsampling by an exponentially increasing factor (with base n), making the total number of orbitals grow only logarithmically with respect to the number of basis functions per unit cell. Unlike the mod- n downsampling

scheme proposed by us earlier,^{8,12} this log- n scheme reduces the *scaling* of the cost and thus achieves a greater speedup as the unit cell size and/or the basis set size increases. Correct band indexing is found to be essential for maintaining high accuracy. Also, each lattice sum contribution must be multiplied by an appropriate quadrature weight, which is a function of four bands involved. We have laid out algorithms for the band indexing and quadrature weights. A combined log- n and mod- n scheme has been found to speedup the MP2/6-31G** energy and energy band calculations of polyacetylene easily by a factor of 20–30.

Explicitly correlated second-order many-body perturbation method for extended systems.⁴ A formalism of the explicitly correlated MP2 employing basis functions that depend explicitly on the electron-electron distances (MP2-R12 or F12) has been derived and implemented for extended systems. The excitation amplitudes on these functions have been held fixed at values that satisfy the first-order cusp condition. Necessary many-electron integrals over Gaussian basis functions of a Slater-type geminal have been evaluated by means of the resolution-of-the-identity approximation using a complementary auxiliary basis set. These integrals and the correlation energy are shown to have the correct size dependence. The valence MP2 correlation energy of polyethylene near the complete-basis-set limit has been obtained and shown to be considerably greater in magnitude than the value obtainable from the conventional MP2 without the R12 treatment.

First-principles methods for anharmonic lattice vibrations.^{23,24} Size-extensive generalizations of vibrational self-consistent field (VSCF), vibrational MP (VMP), and vibrational CC (VCC) methods have been made to anharmonic lattice vibrations in solids. Copious terms in the formalisms of VSCF that have nonphysical size dependence are identified algebraically and eliminated, leading to compact and strictly size-extensive equations. They have no contributions from cubic and odd-order force constants and alter only the transition energies from a subset of quartic and even-order force constants. The second-order VMP and VCC are shown

to be size-extensive and account for anharmonic effects due to all odd- and even-order force constants.

We have applied a vibrational truncated CI (VCI) method to the frequencies of the infrared- and/or Raman-active ($k = 0$) vibrations of polyethylene and polyacetylene. The size-extensivity has been restored by the Γ approximation. The one-, two-, and three-dimensional slices of the potential energy surfaces in the normal coordinates have been computed by the

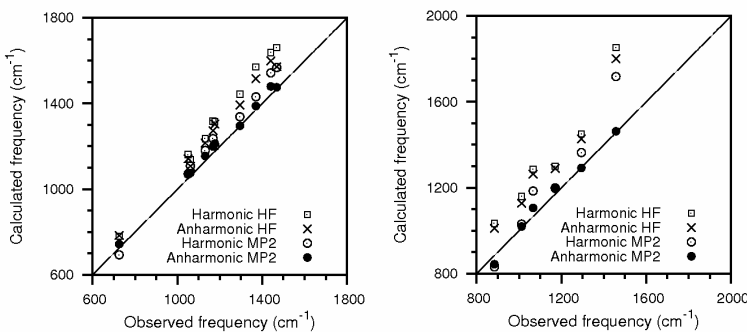


Fig. 3. Vibrational frequencies of polyethylene (left) and polyacetylene (right).

CO theory at the HF and MP2 electronic structure levels. It is shown that accounting for *both* electron correlation *and* anharmonicity is essential in achieving good agreement between the computed and observed frequencies, especially for the in-phase C=C stretching mode in polyacetylene (**Fig. 3**). The VCI calculations have also explained the appearance of the Fermi resonances involving the ν_2 ($k = 0$) fundamental and ν_8 ($k = \pi$) first overtone.

Future Plans

We plan to further explore various novel sampling schemes in the reciprocal space not only to accelerate the extended-system calculations with existing methods but also to design a new method. We have promising preliminary data showing that the mod- n scheme can make CC singles and doubles (CCSD) routinely applicable to polymers. We are also trying to formulate size-extensive CI for metallic extended systems.

The localized approach has proven extremely useful. With this scheme, we are applying MP2 to the phonon dispersion and phonon density of states of proton-ordered phase of ice. We are hopeful that we can resolve the controversy surrounding the two distinct “hydrogen-bond stretching” peaks in the inelastic neutron scattering spectra of ice.

We are implementing the general vibrational many-body methods for solids, which go beyond the Γ approximation and thus can compute anharmonic phonon dispersion curves and phonon density of states that include overtones and combinations. We plan to work out *ab initio* theory for anharmonic effects on lattice structures and hence thermal expansion coefficients.

Publications of DOE Sponsored Research (2008–Present)

1. **Book chapter:** S. Hirata, O. Sode, M. Keçeli, and T. Shimazaki, “Electron correlation in solids: delocalized and localized orbital approaches,” in *Accurate Condensed-Phase Quantum Chemistry* (in press, Taylor & Francis, 2010).
2. **Book chapter:** S. Hirata, T. Shiozaki, E. F. Valeev, and M. Nooijen, “Eclectic electron-correlation methods,” in *Recent Progress in Coupled-Cluster Methods: Theory and Application* (in press, Springer, 2010).
3. **Book chapter:** S. Hirata *et al.*, “Computational interstellar chemistry,” in *Recent Advances in Spectroscopy: Astrophysical, Theoretical and Experimental Perspective* (in press, Springer, 2010).
4. T. Shiozaki and S. Hirata, *J. Chem. Phys. (Communications)* (in press, 2010), “Explicitly correlated second-order Møller–Plesset perturbation method for extended systems.”
5. **Invited article:** T. Shiozaki, E. F. Valeev, and S. Hirata, *Annual Reports of Computational Chemistry* **5**, 131–148 (2009), “Explicitly correlated coupled-cluster methods.”
6. **Invited article:** S. Hirata, *Phys. Chem. Chem. Phys.* [Perspective] **11**, 8397–8412 (2009), “Quantum chemistry of macromolecules and solids.”
7. S. Hirata, E. B. Miller, Y.-Y. Ohnishi, and K. Yagi, *J. Phys. Chem. A* [Pitzer Special Issue] **113**, 12461–12469 (2009), “On the validity of the Born–Oppenheimer separation and the accuracy of diagonal corrections in anharmonic molecular vibrations.”
8. S. Hirata and T. Shimazaki, *Phys. Rev. B* **80**, 085118 (2009) (7 pages), “Fast second-order many-body perturbation method for extended systems.”
9. T. Shiozaki, S. Hirata, and E. F. Valeev, *J. Chem. Phys.* **131**, 044118 (2009) (12 pages), “Explicitly correlated combined coupled-cluster and perturbation methods.”
10. K. Yagi, H. Karasawa, S. Hirata, and K. Hirao, *ChemPhysChem* **10**, 1442–1444 (2009), “First-principles quantum vibrational simulations of the guanine-cytosine base pair.”
11. M. Keçeli, T. Shiozaki, K. Yagi, and S. Hirata, *Mol. Phys.* [Schaefer Special Issue] **107**, 1283–1301 (2009), “Anharmonic vibrational frequencies and vibrationally-averaged structures of key species in hydrocarbon combustion: HCO^+ , HCO , HNO , HOO , HOO^- , CH_3^+ , and CH_3 .”
12. T. Shimazaki and S. Hirata, *Int. J. Quantum Chem.* [Harris Special Issue] **109**, 2953–2959 (2009), “On the Brillouin-zone integrations in second-order many-body perturbation calculations for extended systems of one-dimensional periodicity”
13. O. Sode, M. Keçeli, S. Hirata, and K. Yagi, *Int. J. Quantum Chem.* [Hirao Special Issue] **109**, 1928–1938 (2009), “Coupled-cluster and many-body perturbation study of energies, structures, and phonon dispersions of solid hydrogen fluoride.”
14. T. Shiozaki, M. Kamiya, S. Hirata, and E. F. Valeev, *J. Chem. Phys.* **130**, 054101 (2009) (10 pages), “Higher-order explicitly correlated coupled-cluster methods.”
15. S. Hirata, *J. Chem. Phys.* **129**, 204104 (2008) (11 pages), “Fast electron-correlation methods for molecular crystals: An application to the α , β_1 , and β_2 modifications of solid formic acid.”
16. **Invited article:** S. Hirata and K. Yagi, *Chem. Phys. Lett.* **464**, 123–134 (2008) [a Frontiers article], “Predictive electronic and vibrational many-body methods for molecules and macromolecules.”
17. T. Shiozaki, M. Kamiya, S. Hirata and E. F. Valeev, *J. Chem. Phys. (Communications)* **129**, 071101 (2008) (4 pages), “Explicitly correlated coupled-cluster singles and doubles method based on complete diagrammatic equations.”
18. **Book chapter:** S. Hirata, P.-D. Fan, T. Shiozaki, and Y. Shigeta, “Single-reference methods for excited states in molecules and polymers” in *Radiation Induced Molecular Phenomena in Nucleic Acid: A Comprehensive Theoretical and Experimental Analysis* edited by Jerzy Leszczynski and Manoj Shukla (Springer, 2008).
19. S. Hirata, K. Yagi, S. A. Perera, S. Yamazaki, and K. Hirao, *J. Chem. Phys.* **128**, 214305 (2008) (9 pages), “Anharmonic vibrational frequencies and vibrationally averaged structures and nuclear magnetic resonance parameters of FHF^- .”
20. **Invited article:** T. Shiozaki, M. Kamiya, S. Hirata, and E. F. Valeev, *Phys. Chem. Chem. Phys.* **10**, 3358–3370 (2008) [in the issue on “Explicit-R12 correlation methods and local correlation methods”], “Equations of explicitly-correlated coupled-cluster methods.”
21. K. Yagi, S. Hirata, and K. Hirao, *Phys. Chem. Chem. Phys.* **10**, 1781–1788 (2008), “Vibrational quasi-degenerate perturbation theory: Application to Fermi resonances in CO_2 , H_2CO , and C_6H_6 .”
22. M. Kamiya, S. Hirata, and M. Valiev, *J. Chem. Phys.* **128**, 074103 (2008) (11 pages), “Fast electron correlation methods for molecular clusters without basis set superposition errors.”

Submitted Publications of DOE Sponsored Research (2008–Present)

23. S. Hirata, M. Keçeli, and K. Yagi (submitted, 2010), “First-principles methods for anharmonic lattice vibrations: formalisms.”
24. M. Keçeli, S. Hirata, and K. Yagi (submitted, 2010), “First-principles methods for anharmonic lattice vibrations: applications to polyethylene and polyacetylene in the Γ approximation.”
25. Y.-Y. Ohnishi and S. Hirata (submitted, 2010), “Logarithm second-order many-body perturbation method for extended systems.”
26. O. Sode and S. Hirata (submitted, 2010), “Second-order many-body perturbation study of solid hydrogen fluoride.”

Generalized Van Vleck Variant of Multireference Perturbation Theory

Mark R. Hoffmann
University of North Dakota
Chemistry Department
Grand Forks, ND 58202-9024
Email: mhoffmann@chem.und.edu

I. Project Scope

There is need for cutting edge theoretical and computational electronic structure methods to support the study of complex potential energy surfaces (PESs). While standard methods of computational chemistry are usually adequate for studying the ground electronic states of molecular species near their equilibrium geometries, reaction intermediates, transition states and excited states generally require advanced methods that take into account their multiconfigurational nature. Multireference (MRPT) and quasidegenerate (QDPT) perturbation theories have been demonstrated to be efficient and effective for the description of electron correlation in essentially arbitrarily complex molecules. Recent work demonstrated that the mathematically robust and physically correct structures in our MRPT, called Generalized van Vleck Perturbation Theory (GVVPT), are amenable to highly efficient algorithms. Specifically, second- and third-order approximations of GVVPT (i.e., GVVPT2 and GVVPT3) utilize routines in common with our highly efficient macroconfiguration-based, configuration-driven MRCISD¹. Consequently, theoretical and computational development can proceed by first addressing the structurally simpler equivalent CI problem. Chemical problems that are not addressed readily by other theoretical methods become accessible to MRPT or QDPT: problems such as the descriptions of large regions of excited electronic state PESs of polyatomics, especially when the characters of the excited states are doubly excited relative to the ground state, and the characterizations of multiple PESs of the same symmetry in close proximity. Within the scope of this grant, we intend to apply these theoretical techniques to combustion-relevant Group 15 oxides, and to develop their descriptions of derivative and spin-orbit nonadiabatic couplings.

II. Recent Progress

A. Derivatives. In the present work, we show that, based on the fully variational Lagrangian functional formalism developed by Helgaker and Jørgensen², an alternative method for calculating the MRCISD energy derivatives and nonadiabatic coupling matrix elements can be developed that does not impose any restrictions on the choice of weights within the SA-MCSCF procedure. While the Lagrangian technique is elegant, applicable to all computational methods, and realizes automatically the idea of Handy and Schaefer³ leading to the simplest final expressions, this technique has received little attention in calculating MRCISD derivatives. A previous use of the Helgaker-Jørgensen Lagrangian approach for the MRCISD procedure was restricted to the simplest case of MOs optimized at the single state MCSCF level⁴. We extend the Lagrangian technique to the case of using MOs optimized at the SA-MCSCF level in a way in which restrictions on variations of the MCSCF CI coefficients are accounted for through the Lagrangian multipliers (N.B. Thereby avoiding the necessity to introduce any state rotation operators within the MCSCF space). In addition, we show that the task of determination of sets of redundant orbital rotations, which is highly nontrivial in the general case, is simplified drastically and becomes trivial if the MCSCF and MRCISD configuration spaces are generated using the recently developed macroconfiguration approach⁵. One of the most important results of the present work is that we show how the Lagrangian technique can directly be used for calculating the nonadiabatic coupling terms at the MRCISD level; moreover, this result is also applicable to calculating such coupling terms at other levels of theory.

The desired MRCISD nonadiabatic coupling term can be written as the total partial geometry derivative,

$$g_{AA'}^\alpha = \frac{dg_{AA'}}{dx_\alpha} = \frac{\partial g_{AA'}}{\partial x_\alpha} + \frac{\partial g_{AA'}}{\partial \Delta} \frac{\partial \Delta}{\partial x_\alpha}, \quad (1)$$

of the function

$$g_{AA'}(\mathbf{x}, \Delta(\mathbf{x})) = (\mathbf{A}_T^A)^+ \left[\langle \mathbf{F}_T | e^{\Delta(\mathbf{x})} e^{A_0 \Delta(\mathbf{x})} | \mathbf{F}_T \rangle + \frac{1}{E_{AA'}^{MRCI} - E_A^{MRCI}} \langle \tilde{\mathbf{F}}_T | e^{-\Delta(\mathbf{x})} H(\mathbf{x}) e^{\Delta(\mathbf{x})} | \tilde{\mathbf{F}}_T \rangle \right] \mathbf{A}_T^{A'}, \quad (2)$$

To avoid the problem of calculating $g_{AA'}^{\alpha, \Delta} = \frac{\partial g_{AA'}}{\partial \Delta} \frac{\partial \Delta}{\partial x_\alpha}$, we define the Lagrangian functional associated with function (2),

$$\mathcal{L}_{AA'}(\mathbf{x}, \boldsymbol{\lambda}(\mathbf{x}), \boldsymbol{\eta}_{AA'}^\lambda(\mathbf{x})) = g_{AA'}(\mathbf{x}, \Delta(\mathbf{x})) + \langle \boldsymbol{\eta}_{AA'}^\lambda(\mathbf{x}) | \mathbf{e}(\mathbf{x}, \boldsymbol{\lambda}(\mathbf{x})) \rangle, \quad (3)$$

where the set of the multipliers $\boldsymbol{\eta}_{AA'}^\lambda(\mathbf{x}) = (\boldsymbol{\eta}_{AA'}^{v\Delta}(\mathbf{x}), \boldsymbol{\eta}_{AA'}^{r\Delta}(\mathbf{x}), \boldsymbol{\eta}_{AA'}^C(\mathbf{x}))$ is related to restrictions on the nonredundant, redundant, and MCSCF CI coefficients, respectively. Note that the Lagrangian depends on the MCSCF CI matrix $\mathbf{C}_{MP}(\mathbf{x})$ only through the restriction functions $\mathbf{e}(\mathbf{x}, \boldsymbol{\lambda}(\mathbf{x}))$ [N.B. the geometry dependence of the MRCISD vectors \mathbf{A}_T^A and $\mathbf{A}_T^{A'}$ has already been taken into account in Eq. (2)].

Using the Lagrangian approach formalism, it can be shown that the desired MRCISD nonadiabatic coupling matrix elements subject to restrictions are equal to the explicit geometry partial derivatives of the Lagrangian (3),

$$g_{AA'}^\alpha = \frac{dg_{AA'}}{dx_\alpha} = \frac{\partial \mathcal{L}_{AA'}}{\partial x_\alpha} = g_{AA'}^{\alpha, x} + \left\langle \boldsymbol{\eta}_{AA'}^{v\Delta} \left| \frac{\partial \mathbf{e}^{v\Delta}}{\partial x_\alpha} \right. \right\rangle + \left\langle \boldsymbol{\eta}_{AA'}^{r\Delta} \left| \frac{\partial \mathbf{e}^{r\Delta}}{\partial x_\alpha} \right. \right\rangle + \left\langle \boldsymbol{\eta}_{AA'}^C \left| \frac{\partial \mathbf{e}^C}{\partial x_\alpha} \right. \right\rangle, \quad (4)$$

if the Lagrangian multipliers $\boldsymbol{\eta}_{AA'}^\lambda$ at \mathbf{x}_0 satisfy appropriate equations. These equations involve only the corresponding explicit partial derivatives and force all the parameters $\boldsymbol{\lambda}(\mathbf{x}) = \{v\Delta(\mathbf{x}), r\Delta(\mathbf{x}), \mathbf{C}_{MP}(\mathbf{x})\}$ to be variational for the Lagrangian at the reference geometry.

B. Relativistic effects. Two types of relativistic corrections are considered in this work. One is the scalar part that is taken into account by the Douglas–Kroll–Hess (DKH) transformation of the one-electron Hamiltonian^{6,7}, which modifies the values of non-relativistic one-electron integrals but maintains their structure so that non-relativistic programs can be applied directly. The other type of relativistic correction is spin–orbit coupling (SOC), which can be obtained by the construction and diagonalization of a spin–orbit (SO) Hamiltonian matrix. Obara–Saika recursive forms⁸ for the spin–orbit and pVp-type integrals are used. The SOCI Hamiltonian matrix is constructed based on a configuration-driven GUGA algorithm.

The SOC terms, as matrix elements of a spin-dependent CI Hamiltonian, can be evaluated using the UGA⁹ or GUGA¹⁰ techniques. We are particularly interested in an uncontracted SOCI program, based on a configuration-driven GUGA algorithm, and developed an approach that uses aspects of both. Furthermore, the uncontracted SOCI program will serve as a basis for the implementation of uncontracted SO-GVVPT2. Following the vector-recoupling and UGA techniques and the use of “real spherical” spin functions^{10,11}, the formulas for the SOC terms were derived for a configuration-driven SOCI program.

In SOCI, uncoupled *L-S* electronic states usually have different spin and space symmetries. Prior to this work, the MCSCF program in the in-house electronic structure code (i.e., UNDMOL) was restricted to only one irreducible representation for the optimization of molecular orbitals. It was necessary to extend the MCSCF program so that multiple states of different symmetries could be considered simultaneously with equal or different weights.

The original macroconfiguration program is restricted to one irreducible representation with specified total spin number. It needed to be modified to include all the symmetries defined by the user in an input file. The indexing of CSFs must be treated carefully at the configuration level. In the macroconfiguration program for MCSCF, the number of CSFs has a $(2S+1)$ degeneracy for each spin number S , while for SOCI, the $(2S+1)$ degeneracy must be unfolded and one fictitious electron needs to be added for a system with an odd number of electrons.

The configuration-driven CFGCI algorithm can be directly applied to an SOCI program. Besides the SOC terms, no significant modifications are required until the final evaluation of non-relativistic Hamiltonian matrix elements. Instead of one fixed S , several total spin numbers, as specified in an input file, are considered. The viable configurations generated from a configuration, or modified, Distinct Row Table (mDRT) are also relaxed to all allowed irreducible representations. The indexing and ordering of CSFs are modified accordingly to allow all possible M values. In the case of systems with odd numbers of electrons, the calculated Hamiltonian elements are either duplicated, if they are stored on disk, or used twice in the evaluation of sigma vectors for the bifurcated sets of CSFs.

The SOC terms are evaluated with a new subroutine when there is exactly one orbital difference between the bra and ket configuration pair. This subroutine is adapted from the one used for calculating two-particle-two-hole (i.e. two orbital difference) coupling coefficients. Only the exchange products of segment values are kept. Inside the subroutine, there is a loop over all allowed spins of the bra (S_{bra}) configuration that embeds a minor loop over three possible spins for the ket configuration ($S_{ket} = S_{bra}, S_{bra}\pm 1$), subject to all other restrictions and user specifications on spins. All possible values of M and S dependent pre-factors (i.e., the so-called $A, B, C, D,$ and G functions) are pre-computed and stored in fast memory. In the case of $S_{ket} = S_{bra} - 1$, an additional factor is multiplied with the product of segmented values $(F_{ij})_N$ to avoid explicit use of $C', D',$ and G' functions.

C. NO dimer. The nitric oxide dimer $(NO)_2$ poses both experimental and theoretical challenges and has attracted much attention over the years. In its ground (\tilde{X}^1A_1) state, the dimer has planar C_{2v} symmetry and is formed by the pairing of two π^* orbitals of NO, leading to a weak ($D_0 = 710\pm 10 \text{ cm}^{-1}$) but covalent N-N bond. While the ground state properties of the dimer, including its equilibrium geometry, dipole moment, and fundamental frequencies, are experimentally, but not theoretically, well characterized, there are neither experimental electronic excitation energies nor reliable predictions of excited state properties reported in the literature.

The lowest 8 electronic ($1,2^1A_1, 1^1A_2, 1^3A_2, 1^1B_1, 1^3B_1, 1,2^3B_2$) states of the dimer, correlating with the ground $NO(X^2\Pi) + NO(X^2\Pi)$ asymptote are purely valence. At the ground state equilibrium geometry, they are grouped within 1 eV and separated by a gap of about 5-6 eV from the numerous states that correlate with the higher lying asymptotes and involve the competitive $\pi \rightarrow \pi^*$ and $\pi^* \rightarrow$ Rydberg excitations. Even the lowest energy states have significant multireference character, which can change drastically with geometry. Consequently, accurate theoretical treatments must ensure a balanced description of dynamic and nondynamic correlations at all geometries. Furthermore, quite large atomic basis sets (at least at the aug-cc-pVTZ level) must be used to describe well energetically close valence and Rydberg excitations.

Even in the case of the states correlating with the ground asymptote, there are many unsolved problems (e.g., are the 1^1B_1 and 2^1A_1 states weakly bound and is the 1^3B_2 state quasibound?), and there exist essentially more problems related to states correlating with higher lying asymptotes. E.g., in previous studies, the existence of the lowest excited asymptote $NO(X^2\Pi) + NO(a^4\Pi)$ (with a relative energy of 4.77 eV) has not been taken into account. As a result, the asymptotic energy of the eight triplet states ($1,2^3A_1, 2,3^3A_2, 2,3^3B_1, 3,4^3B_2$) correlating with this asymptote and their qualitative natures (e.g., at large NN distances they must be valence and not Rydberg) have not been evaluated correctly. Some of these states are of special interest, with some expected to be bound (e.g., 2^3A_2 and 2^3B_1) or quasibound (2^3A_1). Our

studies have used GVVPT2 to characterize all singlet and triplet states that correlate with the ground and first excited asymptotes.

III. Future Work

We expect continued progress in all three areas identified above. In regard to nonadiabatic coupling, work will continue optimizing the computer code for MRCISD wavefunctions and to derive and develop the corresponding algorithm for GVVPT2. We expect to make quick progress on the GVVPT2 nonadiabatic coupling, since there are many common elements with MRCISD. Spin-orbit coupling matrix elements have been realized for MCSCF wavefunctions. With use of the in-house configuration-driven UGA code, extension to MRCISD, for both true SOCI and primary space CI, will be pursued next. The initial study of the (NO)₂ potential energy surfaces for all singlet and triplet states that correlate to the lowest two dissociation limits at the GVVPT2 level needs to be continued using more accurate methods of electronic structure theory and specifically GVVPT3 and MRCISD, with Davidson-type corrections for the effects of higher than double excitations. All three areas will allow the eventual study of dynamics on the NO+NO surface, with inclusion of nuclear derivative and spin-orbit nonadiabatic coupling.

IV. References

- ¹ W. Jiang, Y. G. Khait, and M. R. Hoffmann, *J. Phys. Chem. A* **113**, 4374 (2009).
- ² T. Helgaker and P. Jørgensen, *Adv. Quantum Chem.* **19**, 183 (1988); *Theor. Chim. Acta* **75**, 111 (1989).
- ³ N. C. Handy and H. F. Schaefer III, *J. Chem. Phys.* **81**, 5031 (1984).
- ⁴ H. Koch, H. J. A. Jensen, P. Jørgensen, T. Helgaker, G. E. Scuseria, and H. F. Schaefer III, *J. Chem. Phys.* **92**, 4924 (1990).
- ⁵ Y. G. Khait, J. Song, and M. R. Hoffmann, *Int. J. Quantum Chem.* **99**, 210 (2004).
- ⁶ M. Douglas and N. M. Kroll, *Ann. Phys. (NY)* **82**, 89 (1974).
- ⁷ B. A. Hess, *Phys. Rev. A* **33**, 3742 (1980).
- ⁸ S. Obara and A. Saika, *J. Chem. Phys.* **84**, 3963 (1986); **89**, 1540 (1988).
- ⁹ R. D. Kent and M. Schlesinger, *Phys. Rev. A* **42**, 1155 (1990); **50**, 186 (1994).
- ¹⁰ S. Yabushita, Z. Zhang, and R. M. Pitzer, *J. Phys. Chem.* **103**, 5791 (1999).
- ¹¹ R. M. Pitzer and N. W. Winter, *J. Phys. Chem.* **92**, 3061 (1988).

V. Publications and Submitted Journal Articles Supported by this Project 2009-2010

M. R. Hoffmann, D. Datta, S. Das, D. Mukherjee, A. Szabados, Z. Rolik, and P. R. Surjan, Comparative study of multireference perturbation theories for ground and excited states, *J. Chem. Phys.* **131**, 204104 (2009).

D. P. Theis, Y. G. Khait, S. Pal, and M. R. Hoffmann, Molecular dipole moments using the GVVPT2 variant of multireference perturbation theory, *Chem. Phys. Lett.* **487**, 116 (2010).

Y. G. Khait, D. P. Theis, and M. R. Hoffmann, Geometrical derivatives and nonadiabatic coupling terms in MRCISD using the lagrangian technique (*submitted*).

Theoretical Kinetics and Non-Born–Oppenheimer Molecular Dynamics

Ahren W. Jasper
Combustion Research Facility, Sandia National Laboratories
Livermore, CA 94551-0969
ajasper@sandia.gov

I. Program Scope

The goal of this project is the development and validation of theoretical methods for obtaining quantitative rate coefficients for elementary reactions and for elucidating reaction mechanisms. An accurate and complete first principles theoretical description is the goal for small to moderate sized systems, and more approximate methods are required for larger and more complex systems. We are particularly focused on extending the applicability of the theoretical models to a broader range of systems, including non-Born–Oppenheimer processes, which involve multiple, coupled electronic states. This work relies upon a combination of quantum chemistry, transition state theory, master equation, and molecular dynamics calculations. This program benefits considerably from interactions with experimentalists at the CRF and elsewhere who provide data with which to test the theoretical methods. In turn, theoretical insights gained using the validated models are useful for interpreting data obtained under less straightforward experimental conditions.

II. Recent Progress

A. Theoretical Chemical Kinetics

For many chemical kinetics calculations, the dominant source of error is the treatment of collisional energy transfer, which accounts for the activation and stabilization of the intermediate complexes. In collaboration with J. A. Miller, direct molecular dynamics calculations were carried out to compute energy transfer parameters for use in master equation calculations for the $\text{CH}_4 \rightleftharpoons \text{CH}_3 + \text{H}$ reaction in helium. A computationally efficient strategy (requiring only several hundreds of trajectories) was developed and employed, and the resulting values of the exponential-down-model energy transfer parameters ($\alpha = 110 (T/300 \text{ K})^{0.81} \text{ cm}^{-1}$) are in good agreement with previous empirically adjusted values. The results of master equation calculations using the calculated values for α , along with previous ab initio calculations of the properties of the reactants and the barrierless kinetics, are in good agreement with experimental rates.ⁱ This work provides a complete first-principles characterization of the temperature and pressure dependent kinetics for this simple single-well system.

In collaboration with S. J. Klippenstein and L. B. Harding, a theoretical study of the kinetics of the $\text{CH}_3 + \text{HO}_2$ reaction was performed at temperatures and pressures relevant to combustion. The predicted product branching ratio of 4:1 for the $\text{CH}_3\text{O} + \text{OH}$ and $\text{CH}_4 + \text{O}_2$ products was found to be in close agreement with revised values recently obtained in two modeling studies.ⁱⁱ Earlier theoretical and modeling studies predicted significantly more formation of $\text{CH}_3\text{O} + \text{OH}$. This result has important consequences for understanding ignition in hydrocarbon combustion at high pressures. Rate coefficients for the $\text{CH}_3\text{O} + \text{OH}$ reaction and for CH_3OOH decomposition were also presented.

The effect of spin-orbit splitting on the barrierless association rates was quantified for six hydrocarbon radical–halogen atom reactions ($\text{R} + \text{X}$, with R = methyl and allyl, X = F, Cl, and Br). For five of the six reactions, spin-orbit splitting resulted in only a small (5–15%) perturbation to the nonrelativistic rate. For one reaction (allyl + Br), the effect was much larger, lowering the rate by a factor of 2. For this reaction, spin-orbit splitting had a nonperturbative effect on the barrierless kinetics, shifting the transition states to shorter fragment separations.

The decomposition of diacetyl was characterized theoretically in collaboration with shock tube measurements of R. S. Tranter and J. H. Kiefer. The major product channel (diacetyl \rightarrow 2 acetyl) is

barrierless and was treated using Klippenstein's direct variable reaction coordinate transition state theory. Temperature and pressure dependent rates obtained from master equation calculations were in close agreement with the experimental results. In the course of this study (and informed by other work by Tranter, Kiefer, Harding, and Klippenstein), the rate for $C_2H_6 + Kr \rightarrow 2 CH_3 + Kr$ was revised, with the new rate $\sim 30\%$ lower than the previously reported rate for 1200–1500 K and low pressures.

In another combined theoretical/experimental study with Tranter and Kiefer, the decomposition pathways of dioxane were mapped out using single reference and multireference

quantum chemistry, and the results are shown in Fig. 1. Four low-energy ring opening pathways were found (SP1–SP4), and three of these (SP1–SP3) involve a concerted H-atom transfer across the ring as it opens. For each of the concerted pathways, related stepwise pathways were found with weakly-bound diradical intermediates (not shown in Fig. 1). The

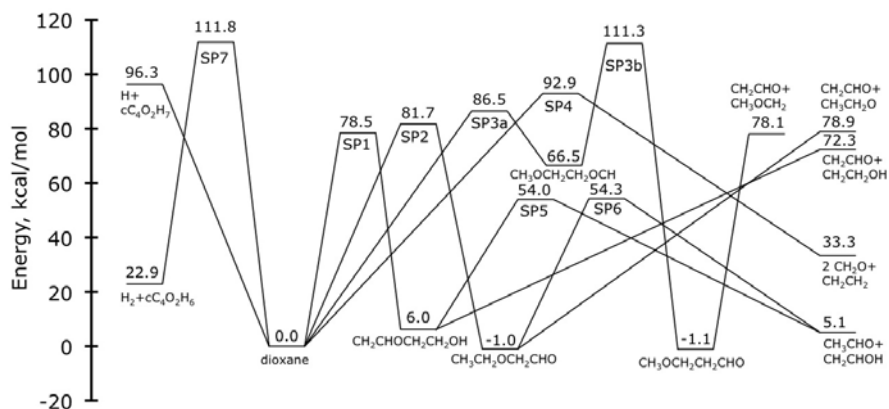


Figure 1: Potential energy diagram for 1,4-dioxane decomposition

The major immediate products of dioxane ring opening are $CH_2CHOCH_2CH_2OH$ and $CH_3CH_2OCH_2CHO$, which subsequently decompose at the central bond to radical and molecular products.

The reaction of propene with OH was studied theoretically in collaboration with C. A. Taatjes, J. Zádor, and J. A. Miller, and good agreement between the theoretical results and available measurements was obtained. At temperatures above ~ 1200 K, H abstraction is the dominant processes, giving allyl and propenyl radicals and water. Vinyl alcohol, formed via decomposition of the adduct, was identified as a minor but measurable product.

B. Non-Born–Oppenheimer Molecular Dynamics Simulations

In collaboration with D. G. Truhlar, the photodissociation of NH_3 was studied using a fitted set of coupled potential energy surfaces and NBO molecular dynamics calculations. This system features a conical intersection (CI) at extended N–H distances and planar geometries. Trends in the production of excited state amino radicals as a function of initial state preparation were computed and compared with the experimental results of Crim and co-workers.ⁱⁱⁱ The experimental results suggest an enhancement in the production of excited state products when the antisymmetric stretch of NH_3 is excited, with the interpretation that excitation of the antisymmetric stretch causes the system to go “around” the CI and thus inhibits electronic state quenching. The NBO MD trajectory results do not support this interpretation. We find that the system is efficiently quenched via the seam of CIs when either the antisymmetric or symmetric stretches are excited. The NBO MD calculations predict that the production of excited state amino radicals depends on the total energy, and no state specificity is observed. Detailed descriptions of the most accurate, well-validated multistate trajectory methods have been given in a recent review.

III. Future Work

A. Theoretical Chemical Kinetics

We will continue to use established theoretical kinetics techniques to make quantitative predictions for important elementary combustion reactions. Several applications are underway,

including a collaboration with S. J. Klippenstein and D. L. Osborn studying the phenyl + propargyl reaction. We will also study the applicability of transition state theory for systems that are currently not well described by statistical theories. For example, barrierless abstraction reactions pose challenges to current theories. For these reactions variable reaction coordinate TST is appropriate for characterizing the kinetics at low temperatures, but the assumptions involved in this approach are not suitable at higher temperatures where the reacting fragments are significantly distorted from their isolated geometries at the important dynamical bottlenecks. A two transition state approach will be applied to study these systems.

We will continue to develop our trajectory-based method for studying energy transfer. We will compute fully ab initio (i.e., parameter-free) rate coefficients for a series of saturated hydrocarbon systems (vinyl, ethane, propane, etc.), as well as unsaturated molecules and radicals (C_2H_3 , ethylene, etc). We will consider both atomic (He, Ar, Kr, etc.) and molecular (H_2O , N_2 , etc.) bath gases. In addition to providing improved theoretical kinetics for pressure dependent reactions involving these species, the proposed systematic studies of energy transfer will be used to guide the development of simple models and predictive rules for parameterizing collisional energy transfer models in master equation calculations.

B. Non-Born–Oppenheimer Molecular Dynamics Simulations

A major component of future work will involve the application of our validated NBO molecular dynamics (MD) methods to polyatomic systems, including: (1) The photodissociation of vinyl halides, which will be useful for interpreting the experimental results of D. L. Osborn and co-workers^{iv} and others. (2) Intersystem crossing in spin-orbit coupled systems formed from the addition of oxygen atoms to hydrocarbons. (3) Direct NBO MD simulations of the photodissociation of HNCO and of the $H + NCO$ reaction. Upon photoexcitation to the S_1 state, HNCO may decay by one of several pathways: adiabatically to form $^1NH + CO$, nonadiabatically to $^3NH + CO$ via a spin-forbidden transition to the T_1 state, or nonadiabatically via a transition to the S_0 state to form either $H + NCO$ or $^1NH + CO$. This system has been well characterized experimentally^v and provides an excellent test case for the validation and development of the NBO MD methods.

To complement our previous study of the energetic effect of spin-orbit coupling discussed above, we will study the dynamical effect of spin-orbit coupling using NBO MD. Transition state theory allows for the efficient computation of accurate rate coefficients as long as the so-called “transmission coefficient” is close to unity or can be calculated. The transmission coefficient may deviate from unity for three reasons: (1) tunneling through potential barriers, (2) single surface recrossing at the dividing surface, and (3) electronically nonadiabatic surface switches. Methods exist for reliably estimating the magnitudes of the first two effects, but only approximate methods exist for treating the third. We will use direct NBO MD simulations to compute electronically nonadiabatic transmission coefficients for the $CH_3 + F$, Cl , and Br reactions.

C. Quantum Chemistry

An important practical bottleneck for performing NBO MD simulations is the need for inexpensive and accurate potential energy surfaces and their couplings. Two strategies will be pursued for obtaining potential energy surfaces in the NBO MD simulations. Direct dynamics methods will be developed based on single reference methods (DFT, MP2, etc) for spin-orbit coupled systems and multireference methods (CASPT2, etc) for valence coupled systems.

Semiautomated surface fitting strategies will also be implemented.^{vi} One project will involve developing general strategies for automatically generating analytic potential energy surfaces describing the six-dimensional interaction of two rigid fragments using IMLS. These potentials will allow for barrierless kinetics calculations carried out using higher-level quantum chemistry methods as well as more extensive explorations of transition state dividing surfaces.

Schemes for modeling the coupling between the electronic surfaces will also be developed.

IV. References

- i. M. Brouard, M. T. Macpherson, and M. J. Pilling, *J. Phys. Chem.* **93**, 4047 (1989).
- ii. J.J. Scire Jr., F.L. Dryer and R.A. Yetter, *Int. J. Chem. Kinet.* **33**, 784 (2001). H.J. Curran, Combustion Chemistry Centre Reaction Mechanism, private communication, 2007.
- iii. A. Bach, J. M. Hutchison, R. J. Holiday, and F. F. Crim, *J. Phys. Chem. A* **107**, 10490 (2003).
- iv. P. Zou, K. E. Strecker, J. Ramirez-Serrano, L. E. Jusinski, C. A. Taatjes, and D. L. Osborn, *Phys. Chem. Chem. Phys.* **10**, 713 (2008).
- v. T. Droz-Georget, M. Zyrianov, H. Reisler, and D. W. Chandler, *Chem. Phys. Lett.* **276**, 316 (1997). H. L. Berghout, S. Hsieh, and F. F. Crim, *J. Chem. Phys.* **114**, 10835 (2001).
- vi. See, e.g., O. Godsi, C. R. Evenhuis, and M. A. Collins, *J. Chem. Phys.* **125**, 104105 (2006). O. Tishchenko and D. G. Truhlar, *J. Chem. Theory Comput.* **3**, 938–948 (2007). R. Dawes, D. L. Thompson, Y. Guo, A. F. Wagner, and M. Minkoff, *J. Chem. Phys.* **126**, 184108 (2007).

V. Publications and submitted journal articles supported by this project 2008-2010

1. A. W. Jasper and D. G. Truhlar, “Non-Born–Oppenheimer molecular dynamics for conical intersections, avoided crossings, and weak interactions,” in *Conical Intersections: Theory, Computation, and Experiment*, edited by W. Domcke, D. R. Yarkony, and H. Koppel (World Scientific, 2010), in press.
2. A. W. Jasper, S. J. Klippenstein, and L. B. Harding, “The effect of spin-orbit splitting on the association kinetics of barrierless halogen atom–hydrocarbon radical reactions,” *J. Phys. Chem. A*, accepted.
3. R. Dawes, A. W. Jasper, C. Tao, C. Richmond, C. Mukarakate, S. H. Kable, and S. A. Reid, “Theoretical and experimental spectroscopy of the S₂ state of CHF and CDF: Dynamically weighted multireference configuration interaction calculations for high-lying electronic states,” *J. Phys. Chem. Lett.* **1**, 641 (2010).
4. J. Zádor, A. W. Jasper, and J. A. Miller, “The reaction between propene and hydroxyl,” *Phys. Chem. Chem. Phys.* **11**, 11040 (2009).
5. X. Yang, A. W. Jasper, J. H. Kiefer, and R. S. Tranter, “The dissociation of diacetyl: A shock tube and theoretical study,” *J. Phys. Chem. A* **113**, 8318 (2009).
6. D. Bomhommeau, R. Valero, D. G. Truhlar, and A. W. Jasper, “Coupled-surface investigation of the photodissociation of NH₃(\tilde{A}): Effect of exciting the symmetric and antisymmetric stretching modes,” *J. Chem. Phys.* **130**, 234303 (2009).
7. A. W. Jasper and J. A. Miller, “Collisional energy transfer in unimolecular reactions: Direct classical trajectories for CH₄ \rightleftharpoons CH₃ + H in Helium,” *J. Phys. Chem. A* **113**, 5612 (2009).
8. A. W. Jasper, S. J. Klippenstein, and L. B. Harding, “Theoretical rate coefficients for the reaction of methyl radical with hydroperoxyl radical and for methylhydroperoxide decomposition,” *Proc. Combust. Inst.* **32**, 279 (2009).
9. R. Valero, D. G. Truhlar, and A. W. Jasper, “Adiabatic states derived from a spin-coupled diabatic transformation: Semiclassical trajectory study of photodissociation of HBr and the construction of potential curves for LiBr⁺,” *J. Phys. Chem. A* **112**, 5756 (2008).
10. N. K. Srinivasan, M.-C. Su, J. V. Michael, A. W. Jasper, S. J. Klippenstein, and L. B. Harding, “Thermal decomposition of CF₃ and the reaction of CF₂ + OH \rightarrow CF₂O + H,” *J. Phys. Chem. A* **112**, 31 (2008).

Probing the Reaction Dynamics of Hydrogen-Deficient Hydrocarbon Molecules and Radical Intermediates via Crossed Molecular Beams

Ralf I. Kaiser

Department of Chemistry, University of Hawai'i at Manoa, Honolulu, HI 96822

ralfk@hawaii.edu

1. Program Scope

The major goals of this project are to explore experimentally in crossed molecular beams experiments the reaction dynamics and potential energy surfaces (PESs) of hydrocarbon molecules and their corresponding radical species which are relevant to combustion processes. The reactions are initiated under single collision conditions by crossing two supersonic reactant beams containing radicals and/or closed shell species under a well-defined collision energy and intersection angle. By recording angular-resolved time of flight (TOF) spectra, we obtain information on the reaction products, intermediates involved, on branching ratios for competing reaction channels, on the energetics of the reaction(s), and on the underlying reaction mechanisms. These data are of crucial importance to understand the formation of carbonaceous nanostructures as well as of polycyclic aromatic hydrocarbons and their hydrogen deficient precursors in combustion flames.

2. Recent Progress

2.1. Dynamics of Phenyl, $C_6H_5(X^2A_1)$, Radical Reactions

We completed the crossed molecular beam studies of phenyl radicals with C_4H_6 isomers: 1,3-butadiene, 1,2-butadiene, 1-butyne, and 2-butyne. Selected experiments were also conducted with (partially) deuterated reactants to pin down the position(s) of the atomic hydrogen versus deuterium loss pathway(s). Electronic structure calculations were conducted in collaboration with Alexander Mebel (FIU).

2.2. Formation of the Phenyl, $C_6H_5(X^2A_1)$, Radical under Single Collision Conditions

Besides the reactions of the phenyl radical - one of the most important transient species to initiate the formation of PAHs - we also investigated the formation of this species under single collision conditions via the reaction of dicarbon molecules plus 1,3-butadiene. This reaction represents a potential, but hitherto unnoticed route to synthesize the first aromatic C_6 ring in hydrocarbon flames, where concentrations of dicarbon transient species are significant. Here, crossed molecular beams experiments of dicarbon molecules in their $X^1\Sigma_g^+$ electronic ground state and in the first electronically excited $a^3\Pi_u$ state have been conducted with 1,3-butadiene and two partially deuterated counterparts (1,1,4,4-D4-1,3-butadiene and 2,3-D2-1,3-butadiene) at two collision energies of 12.7 and 33.7 kJmol^{-1} . Combining these scattering experiments with electronic structure and RRKM calculations on the singlet and triplet C_6H_6 surfaces, our investigation reveals that the aromatic phenyl radical is formed predominantly on the triplet surface via indirect scattering dynamics through a long lived reaction intermediate. Initiated by a barrier-less addition of triplet dicarbon to one of the terminal carbon atoms of 1,3-butadiene, the collision complex undergoes trans-cis isomerization followed by ring closure and hydrogen migration prior to hydrogen atom elimination ultimately forming the phenyl radical. The latter step emits the hydrogen atom almost perpendicularly to the rotational plane of the decomposing intermediate and almost parallel to the total angular momentum vector. On the singlet surface, smaller contributions of phenyl radical could not be excluded; experiments with partially deuterated 1,3-butadiene indicate the formation of the thermodynamically less stable acyclic $H_2CCHCCCCH_2$ isomer. This study presents the very first experimental evidence - complimented by theoretical

studies – that under single collision conditions an aromatic hydrocarbon molecule can be formed in a bimolecular gas phase reaction via reaction of two acyclic molecules involving cyclization processes at collision energies relevant to combustion flames.

2.3. Ionization Potentials of Transient Hydrocarbon Species

We have expanded our collaboration with Musa Ahmed (LBNL) at the Chemical Dynamics Beamline to investigate the ionization energies of resonantly stabilized C_4H_3 radicals utilizing laser ablation of graphite in combination with seeding the ablated species in neat methylacetylene gas, which also acted as a reagent. Photoionization efficiency (PIE) curves were recorded of photoionized isomers at the Advanced Light Source. The PIE curve suggests the formation of four C_4H_3 radicals: two acyclic structures *i*- C_4H_3 and *E/Z*-*n*- C_4H_3 and two cyclic isomers. This study provides a novel interpretation of previous data on C_4H_3 radicals in hydrocarbon flames. Experiments were also conducted on the ionization energies of C_7H_6 and C_7H_5 isomers synthesized in situ via laser ablation of carbon and reaction with seeded benzene molecules. This process also leads most likely to the formation of multiple phenylpolyacetylene molecules [$C_6H_5(C\equiv C)_n-H$], whose ionization energies are currently explored.

2.4. Development of a Supersonic Beam Source of Methylidyne Radicals (CH)

We generated a pulsed supersonic beam of ground state methylidyne radicals via photolysis at 248 nm at 30 Hz of helium-seeded bromoform ($CHBr_3$) at seeding fractions of 0.12 % by bubbling helium gas (99.9999 %; Gaspro) at a pressure of 2.2 atm through a stainless steel bubbler which houses the bromoform at a temperature of 283 K and feeding this gas mixture into a pulsed piezoelectric valve. The latter is operated at a repetition rate of 60 Hz, pulse widths of 80 μs , and a voltage of minus 400 V to 450 V. Here, by focusing 60 mJ per pulse output of excimer laser (Lambda Physik, COMPEX) with a 1 meter focus lens downstream of the nozzle to an area of about 4 mm by 0.7 mm, a few 10^{12} radicals cm^{-3} can be formed in the interaction region of the scattering chamber. Although it is not feasible to eliminate $CHBr_2$, $CHBr$, and CBr in the supersonic beam, these molecules have – due to the heavy bromine atom – distinct center-of-mass angles when reacting with the hydrocarbon molecules. Therefore, the dynamics can be distinguished from those of the methylidyne reactions based on the distinct mass-to-charge ratios and due to different center-of-mass angles and hence scattering ranges of the products. The velocity and speed ratio of the radical beam can be determined on-axis in the TOF mode. Since signal at $m/z = 13$ (CH^+) also originates from dissociative ionization of, for instance, non-photolyzed bromoform, operating the electron impact ionizer in the *soft ionization* mode, here at 34 eV, for the beam characterization is important. This translates into a narrow range of peak velocities of 1680 – 1800 ms^{-1} with speed ratios of 12 - 18. We also utilized laser induced fluorescence to characterize the rotational and vibrational modes of the methylidyne radical, $CH(X^2\Pi)$, in the interaction region of the scattering chamber. Methylidyne radicals are detected using $A^2\Delta - X^2\Pi$ transitions: (0,0) vibrational band for excitation near 431 nm and (0,1) band for detection near 490 nm. The interference filter in front of the photomultiplier tube (PMT; Andover Corp.) is centered at 490 nm with a 10 nm bandwidth; this discriminates against scattered laser light. Figure 1 shows the LIF spectrum of the methylidyne radical beam with a peak velocity of about 1700 ms^{-1} as characterized with the TOF technique. Sixteen detection laser shots were averaged for each point. The spectrum was analyzed utilizing a LIFBASE database and spectral simulation program for diatomic molecules by Jorge Luque. The best fit simulation suggests a rotational temperature of 14 ± 1 K in the vibrational ground state; less than 6 % of the radicals are in the first vibrationally excited state population.

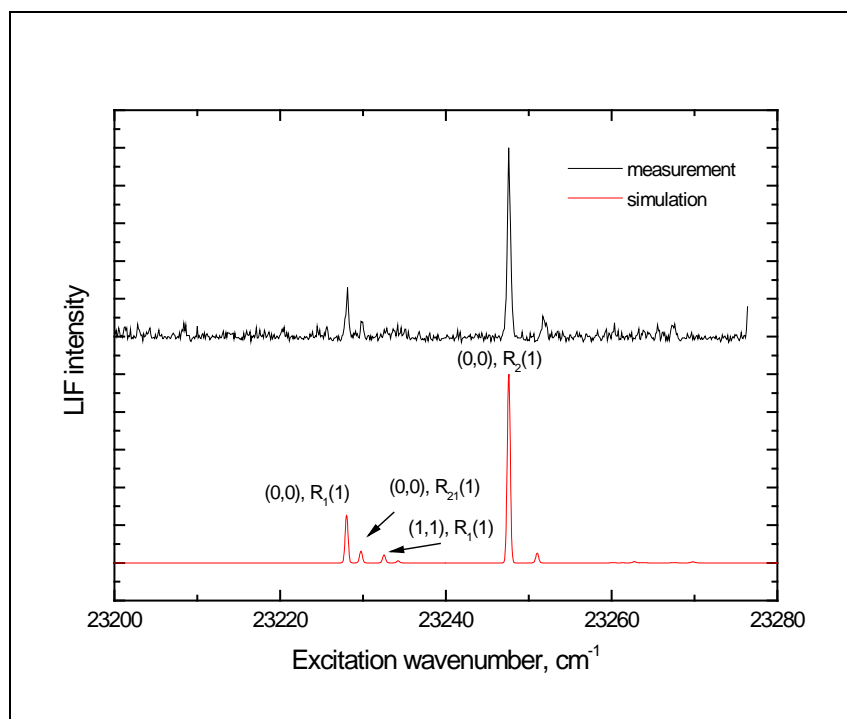


Figure 1: LIF spectrum of helium-seeded methylidyne radicals (top) together with the simulation. Parameters of the best fit simulation suggest a rotational temperature of 14 K and relative populations of $v = 1$ level of less than 6 % based on the $(1,1)$, $R_1(1)$ peak.

2.5. Crossed Beam Reactions of $\text{CH} + \text{C}_2\text{H}_2$, $\text{CD} + \text{C}_2\text{H}_2$, and $\text{CH} + \text{C}_2\text{D}_2$

One of our objectives in this funding period is also to investigate the unimolecular decomposition of chemically activated, resonantly stabilized free C_3H_3 radicals, among them the important propargyl isomer. This leads to the formation of combustion-relevant C_3H_2 [cyclopropenylidene (*c*- C_3H_2), propargylene (HCCCH), vinylidene carbene (H_2CCC)] and C_3H isomers [2-cyclopropyn-1-yl (*c*- C_3H), 2-propynylidene (*l*- C_3H)]. We accessed the C_3H_3 potential energy surface via bimolecular gas phase reactions of the methylidyne radical (CH ; $X^2\Pi$) with acetylene (C_2H_2 ; $X^1\Sigma_g^+$) at a collision energy of about 16 kJ mol^{-1} . A preliminary analysis of the time-of-flight (TOF) and laboratory angular distributions obtained at mass-to-charges of 38, 37, and 36 suggests the existence of three channels: the formation of the *c*- C_3H_2 isomer, the synthesis of HCCCH and/or H_2CCC , and finally, the *l*- C_3H plus molecular hydrogen pathway. The atomic hydrogen loss dominated the dynamics with branching ratios of *c*- C_3H_2 to $\text{HCCCH}/\text{H}_2\text{CCC}$ of about 1:4. The molecular hydrogen channel was a minor component. Due to the presence of ground state carbon atoms in the beam, so far only upper limits of about 25 % could be derived. We also conducted the experiments of $\text{CD} + \text{C}_2\text{H}_2$ and $\text{CH} + \text{C}_2\text{D}_2$ to assign the position of the hydrogen versus deuterium loss and the detection of the D_2 versus H_2 versus HD . The data analysis and fitting of these experiments is currently in progress.

2.6. Tunable VUV Light Generation

In order to utilize ionization techniques complementary to electron impact ionization, we have started to generate tunable vacuum ultraviolet (VUV) light (5 – 15 eV) utilizing resonance enhanced sum ($2\omega_1 + \omega_2$) and difference ($2\omega_1 - \omega_2$) frequency nonlinear mixing. This will assist to ionize molecules according to their ionization potentials. By accessing the different resonance lines of krypton, xenon, and mercury, VUV light may be generated in the wavelength range of 81 – 256 nm at fluxes from $10^{13} - 10^{16}$ photons pulse $^{-1}$.

3. Future Plans

We plan to continue with the studies of the C_3H_3 potential energy surface via the reaction of ground state carbon atoms ($C(^3P_j)$) with vinyl radicals ($C_2H_3; X^2A'$). Secondly, we aim to untangle the reaction dynamics of phenyl radicals at low collision energies utilizing a photolytic phenyl radical source with selected hydrocarbon molecules accessing the C_9H_x ($x = 8, 10$) and $C_{10}H_x$ ($x = 6, 8, 10$) PESs and, hence, the formation of bicyclic aromatic (like) species holding the indene and naphthalene carbon skeletons.

4. Acknowledgements

This work was supported by US Department of Energy (Basic Energy Sciences; DE-FG02-03-ER15411).

5. Publications Acknowledging DE-FG02-03-ER15411 (2008-2010)

X. Gu, R.I. Kaiser, A.M. Mebel, *Chemistry of Energetically Activated Cumulenes - From Allene (H_2CCCH_2) to Hexapentaene ($H_2CCCCCH_2$)*. Invited Review. Chem. Phys. Chem. 9, 350-369 (2008).

F. Zhang, X. Gu, R.I. Kaiser, *Formation of the Diphenyl Molecule in the Crossed Beam Reaction of Phenyl Radicals with Benzene*. JCP 128, 084315/1-5(2008).

F. Zhang, X. Gu, Y. Guo, R. I. Kaiser, *Reaction Dynamics of Phenyl Radicals (C_6H_5) with Propylene (CH_3CHCH_2) and Its Deuterated Isotopologues*. JPCA 112, 3284-3290 (2008).

X. Gu, F. Zhang, R.I. Kaiser, *A Crossed Molecular Beam Study of the Phenyl Radical Reaction with 1,3-Butadiene and its Deuterated Isotopomers*. JPCA 113, 998-1006 (2009).

X. Gu, R.I. Kaiser, *Reaction Dynamics of Phenyl Radicals in Extreme Environments - A Crossed Molecular Beam Study*. Acc. Chem. Res. 42, 290-302 (2009).

X. Gu, F. Zhang, R. I. Kaiser, V. V. Kislov, A.M. Mebel, *Reaction Dynamics of the Phenyl Radical with 1,2-Butadiene*. CPL 474, 51-56 (2009).

R.I. Kaiser, F. Zhang, X. Gu, V.V. Kislov, A.M. Mebel, *Reaction Dynamics of the Phenyl Radical (C_6H_5) with 1-Butyne ($HCCC_2H_5$) and 2-Butyne (CH_3CCCH_3)*. CPL 481, 46-53 (2009).

R.I. Kaiser, A.M. Mebel, O. Kostko, M. Ahmed. *On the Ionization Potentials of C_4H_3 Isomers*. CPL 485, 281-285 (2010).

R.I. Kaiser, *Reaction Dynamics of Carbon-Centered Radicals in Extreme Environments Studied by the Crossed Molecular Beams Technique*. in: Carbon-Centered Radicals: Structure, Dynamics and Reactivity. Malcolm D. E. Forbes, Editor, Wiley, p. 221-248 (2010).

F. Zhang, B. Jones, P. Maksyutenko, R. I. Kaiser, C. Chin, V.V. Kislov, A.M. Mebel, *Formation of the Phenyl Radical [$C_6H_5(X^2A_1)$] under Single Collision Conditions - A Crossed Molecular Beam and Ab Initio Study*. JACS 132, 2672-2683 (2010).

X. Gu, R.I. Kaiser, *Comment on 'Collision Complex Lifetimes in the Reaction $C_6H_5 + O_2 \rightarrow C_6H_5O + O$ by Davis et al.'* JPCA (submitted 2010).

DYNAMICAL ANALYSIS OF HIGHLY EXCITED MOLECULAR SPECTRA

Michael E. Kellman

Department of Chemistry, University of Oregon, Eugene, OR 97403

kellman@uoregon.edu

PROGRAM SCOPE:

The highly excited vibrational dynamics of small molecular species are crucial to understanding fundamental processes important for combustion systems. The goal of our program is to develop theoretical tools to understand spectra and dynamics of highly excited systems. It is clear that anharmonic effects lead to profound changes in the vibrational dynamics of molecules when nonlinearities can no longer be treated as perturbative effects. The standard picture of anharmonic normal modes breaks down. We emphasize particularly the role of bifurcations and the “birth of new modes in bifurcations from the low energy normal modes”. We use bifurcation analysis of semiclassical versions of the effective Hamiltonians used by spectroscopists to fit complex experimental spectra. Observable phenomena associated with bifurcations such as changes in spectral patterns have been predicted and observed. A developing focus is systems approaching and undergoing chemical reactivity, including intramolecular (isomerization) reactions.

RECENT PROGRESS AND FUTURE PLANS: The progress described below is in collaboration with postdoctoral associates Aniruddha Chakraborty (who completed his work June, 2009), and continuing postdoctorals Vivian Tyng and George Barnes. Our current research is pursuing two main directions:

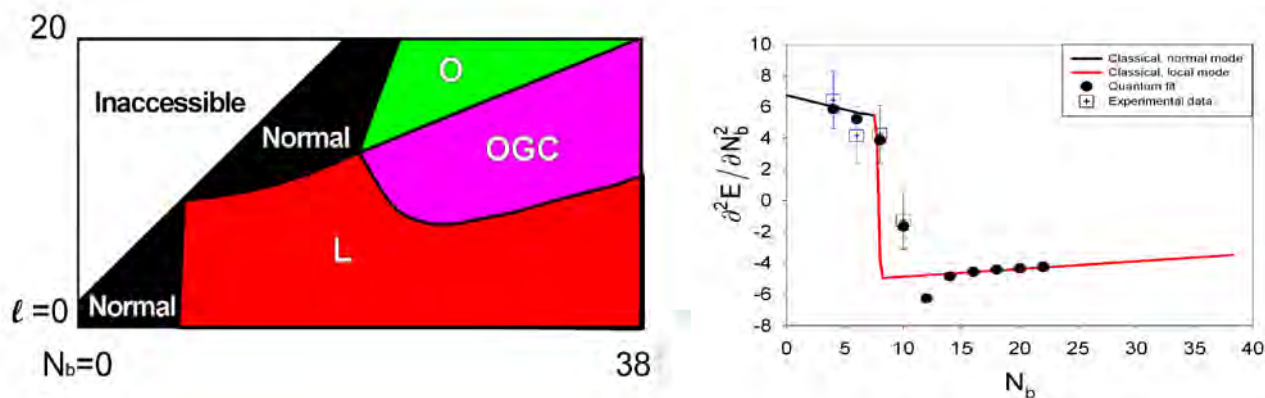
CRITICAL POINTS BIFURCATION ANALYSIS OF EFFECTIVE SPECTROSCOPIC HAMILTONIANS. The goal is to decipher the dynamical information for increasingly complex molecular systems. Current progress has been in three areas:

High- l bending dynamics of acetylene. This is a general analysis of the different types of modes encountered in highly excited bending dynamics of acetylene, resulting in Ref. 3. In this paper, building on our earlier work for the $l = 0$ spectra of Field and coworkers, the bending dynamics of acetylene with pure vibrational angular momentum excitation and high quantum number $l > 0$ are analyzed through the method of critical points bifurcation analysis to find new anharmonic modes born in bifurcations of the low-energy normal modes. It is found that the local L, orthogonal O, precessional P, and counter-rotator CR families persist for all l . In addition, for $l > 8$ there is a fifth family of critical points which, unlike the previous families, has no fixed relative phase (“off great circle” OGC). The concept of the *minimum energy path in the polyad space* is developed. With restriction to $l = 0$ this is the local mode family L. This has an intuitive

relation to the minimum energy path or reaction mode for acetylene-vinylidene isomerization. With $l > 0$ included as a polyad number, the $l = 0$ minimum energy path forms a trough-like channel in the *minimum energy surface in the polyad space*, which consists of a complex mosaic of L, O, and OGC critical points. There is a division of the complete set of critical points into layers, the minimum energy surface forming the lowest.

High- l bending dynamics of acetylene: a phase diagram with tetracritical point, no monodromy, and new spectral patterns.

Critical points and bifurcations are considered for the acetylene effective Hamiltonian in the polyad space of total bend and vibrational angular momentum quantum numbers $[N_b, l]$. A “phase diagram” (below, left) is constructed for the surface of minimum energy critical points. The phases denote vibrational modes of different character, including new types of anharmonic modes born in bifurcations from the ordinary normal modes. A tetracritical point is the outstanding feature of the diagram. Patterns in the energy levels are considered, starting with quantum monodromy. No monodromy is found, in contrast with other types of bifurcating systems. Instead, patterns are predicted in the first and second derivatives of the energy with respect to the quantum numbers, in close analogy with the theory of phase transitions. The tetracritical point finds striking manifestation in these patterns. This may be amenable to experimental test. Moreover, the minimum energy path, analogous to the reaction path, has derivative patterns which can already be compared with experiment. Agreement of theory and experiment is found within experimental error (below right).



Future Plans: Bifurcation analysis of rotation-vibration dynamics through molecular spectroscopic Hamiltonians (with Dr. Vivian Tyng). Our method to connect experiment and theory has been to use the effective spectroscopic fitting Hamiltonian. We analyze the dynamics of the effective Hamiltonian via a semiclassical form of the effective Hamiltonian by subjecting it to bifurcation analysis using the method of critical points. A great deal of progress using the critical points analysis has been made on purely vibrational problems. However, to our knowledge no analysis using

the tools of nonlinear dynamics has ever been performed on the effective Hamiltonian of a real molecular rotation-vibration system, probably because of the greater complexity of the problem. We have successfully tackled that problem in work being prepared for publication. There are now available for analysis some high quality rotation-vibration fitting Hamiltonians of real molecular data at relatively high levels of both vibrational and rotational excitation. We are completing our first paper in this area, on CO₂. Future work is planned on C₂H₂, for which there is adequate experimental data and a good spectroscopic fitting Hamiltonian.

POLYAD BREAKING GENERALIZED EFFECTIVE HAMILTONIANS.

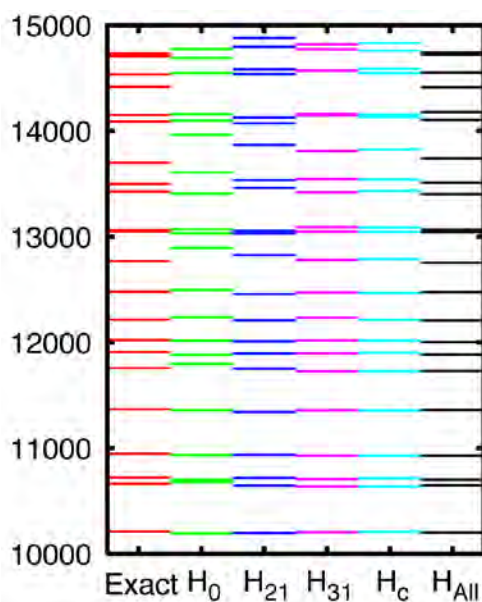
Spectroscopic fitting Hamiltonians are enormously useful as a tool to analyze molecular spectra. The fitting Hamiltonian is an effective quantum matrix Hamiltonian. Virtually all spectroscopic fitting Hamiltonians to date invoke the “polyad approximation” of a conserved total vibrational quantum number. However, at sufficiently high energy, the polyad approximation must fail. Spectra of systems that break the polyad action, time-dependent transport in these systems, and the representation of these phenomena with a generalized effective fitting Hamiltonian are mostly unexplored areas. Recently we have been working to construct effective spectroscopic Hamiltonians to encompass polyad breakdown. We have done this in two steps. The first is for a model system of coupled anharmonic oscillators. The second is for a much more realistic two-mode model of the HO₂ complex important in the combustion reaction $H + O_2 \rightarrow HO_2 \rightarrow O + O$.

Polyad Breaking Effective Hamiltonian for Chaotic Coupled Anharmonic

Oscillators. We have been testing a simple generalized effective Hamiltonian capable of encompassing the major dynamical and spectral effects of the polyad breakdown, using a model system of two coupled anharmonic oscillators as test “data”. Our first results have been published as a Communication to the Journal of Chemical Physics [3]; further publications of the detailed method are in preparation. We demonstrate that a generalized effective Hamiltonian successfully describes the polyad breaking by successively adding a very small number of additional resonance couplings. Each additional resonance coupling induces bifurcations to give new low-order periodic orbits, incompatible with the original polyad number, that reorganize the surrounding phase space structure into large-scale resonance zones. In a quantum system, the spectrum shows clear signatures of these new structures that should be observable in experiments.

It is noteworthy that these fits have been obtained using Hamiltonians constructed with shift operators defined to have the simple action of harmonic raising and lowering operators, even up to dissociation energy $E = 1.0$. This extends the practice of spectroscopic fitting at low energy – it has not been necessary to use operators adapted to the special characteristics of the anharmonic oscillator system, here coupled Morse oscillators. In this sense we have performed a “fair” test of the effective Hamiltonian, even though we knew the nature of the exact model system. The success of ordinary harmonic raising and lowering operators bodes well for fitting real systems without the need for too much prior knowledge.

Polyad Breaking Effective Hamiltonian for Isomerization in HO₂. We have developed a two-dimensional model for the isomerization in the hydroperoxyl radical HO₂. The model takes a slice of the realistic potential surface obtained by H. Guo and coworkers. Energy levels and wave functions are calculated with the help of a large DVR basis. The potential encompasses the isomerization and dissociation channels of the system. Effective spectroscopic fitting Hamiltonians with just a few polyad breaking terms are capable of reproducing large scale vibrational structure above isomerization barriers. (See below, lefthand and righthand columns for comparison of exact and best fit results.) Insight into the dynamical nature of isomerization is also gained through classical trajectories. It is seen that contrary to physical intuition the bend mode is not a “reaction mode,” but rather isomerization requires excitation in both stretch and bending modes. The dynamics reveals two “Farey trees” formed from the 2:1 and 3:1 resonances building off of a prominent 5:2 (2:1+3:1) feature. The 3:1 tree is associated with isomerization while the 2:1 tree leads to trapping and perhaps dissociation at higher energies than those considered in this work.



Recent publications (in print, in press 2008-2010) related to DOE supported research:

1. A. Chakraborty and M.E. Kellman, “Effective Hamiltonian for Chaotic Coupled Oscillators”, J. Chem. Phys. 129, 171104 (2008).
2. V. Tyng and M.E. Kellman, “Catastrophe Map and the Role of Individual Resonances in C₂H₂ Bending Dynamics”, J. Chem. Phys. 130, 144311, 1-14 (2009).
3. V. Tyng and M.E. Kellman “Critical Points Bifurcation Analysis of High- l Bending Dynamics in Acetylene”, J. Chem. Phys. 131, 244111, 1-11 (2009).
4. V. Tyng and M.E. Kellman, “Spectral Intensity Patterns and Vibrational Phase Space Structure”, J. Phys. Chem. A 113, 13246–13250 (2009).
5. V. Tyng and M.E. Kellman, “The Bifurcation Phase Diagram For C₂H₂ Bending Dynamics Has A Tetracritical Point With Spectral Patterns But No Monodromy”, submitted to J. Phys. Chem. A.
6. S. Yang and M.E. Kellman, “Resonance induced spectral tuning”, submitted to Phys. Rev. A.

Theory and Modeling of Small Scale Processes in Turbulent Flow

Alan R. Kerstein
Combustion Research Facility
Sandia National Laboratories
Livermore, CA 94551-0969
Email: arkerst@sandia.gov

PROJECT SCOPE

The goal of this project is to model turbulent reacting flow in a way that makes efficient use of existing knowledge of chemical kinetics and heat, mass, and momentum transfer processes in order to simulate turbulent combustion accurately and affordably. Recognizing that a combusting flow is in essence a collection of flame states, it is natural to turn to flame models for guidance. Indeed, this perspective motivated the development of the flamelet modeling approach [A] and related methods, such as conditional moment closure [B]. In their simplest forms, these models live on a 1D state-space coordinate, usually mixture fraction.

The approach taken in this project is to evolve the flame on a 1D physical-space coordinate, as in counter-flow and related flame computations, but to broaden the scope of this formulation by introducing a representation of all scales of turbulent motion on the 1D coordinate, thus obtaining an economical multi-scale modeling capability. This is accomplished by introducing a map-based representation of fluid motion. The familiar (in other contexts) numerical technique of conservative Lagrangian displacement of an entire flow field, i.e., a map of the entire flow onto itself, has been recast into a map-based method that emulates turbulent motions in 1D (and also has uses in higher-dimensional simulation, as noted below).

During this project, two map-based 1D formulations have been developed, the Linear-Eddy Model (LEM), which predicts mixing under prescribed flow conditions but does not predict the flow *per se*, and One-Dimensional Turbulence (ODT), a predictive simulation of turbulent flow as well as mixing within it. Coupled arrays of LEM or ODT domains are used to perform 3D simulations in which 3D motions are captured at coarse scales (larger than the separation of adjacent domains) and motions at smaller scales are captured in 1D on the individual domains. If LEM is used, flow information must be supplied, e.g. by a conventional 3D coarse-grained simulation or by the 3D ODT method. ODT is a complete enough flow representation so that the coupled array of ODT domains can in principle simulate 3D turbulent flow with no coarse-grained advancement operation. Development and demonstration of a novel flow simulation strategy, Autonomous Microscale Evolution (AME), based on this concept is a major goal of planned future efforts.

RECENT PROGRESS

Both LEM and ODT provide significant demonstrated capabilities to simulate turbulence-chemistry interactions and other relevant flame phenomena. Two developments offer new opportunities to perform direct quantitative comparisons between these models and turbulent combustion data. One is the increasing availability of directly comparable direct-numerical-simulation (DNS) results. The other is the pending completion of a new algorithmic and physical modeling framework for ODT that is directly analogous to turbulent round jet diffusion flames (see Future Work).

The ODT formulation currently used for combustion simulations is limited to planar geometry and temporal advancement. There are no precisely analogous combustion experiments, but 3D DNS results for planar temporal configurations are increasingly available. One such data set, for a syngas (CO, H₂, N₂) diffusion flame in air [C], has been compared to an ODT simulation [8] using the same kinetics (11 species, 21 reactions) as in the DNS. ODT parameters were set to match the lateral spread of momentum and species. DNS and ODT conditional statistics of temperature, species, and scalar dissipation were then compared.

The accuracy of the ODT results was comparable to current state-of-the-art turbulent combustion modeling methods. Notably, ODT reproduced the extinction and re-ignition seen in the DNS. In ODT, there was somewhat more extinction, after which re-ignition brought the ODT mixture-fraction-conditioned mean temperature profile into good agreement with the DNS. Consistent with this, the tails of ODT conditional probability density functions (PDFs) of scalar dissipation are longer than the analogous DNS PDFs at early times, but are shorter at late times. It is unclear at present whether this is related to the ODT representation of intermittency in turbulence or whether it is a consequence of the choice of the subset of the DNS results used to set ODT parameters. This will be investigated further.

ODT includes a representation of buoyant as well as shear forcing and hence is useful for simulating buoyant stratified turbulent flows. One such case, corresponding to ocean mixing conditions, is of particular interest because it develops thin interfaces analogous to flames in turbulence. In the ocean, this occurs because heat and salt have different diffusivities (non-unity Lewis number Le), such that stable salinity jumps form barriers between thermally driven convective layers.

In addition to Le , this flow is described by the Prandtl number Pr , the Richardson number Ri (normalized shear forcing), and Rayleigh number Ra (normalized vertical scale). ODT has been used to explore the rich phenomenology of this four-parameter space, with emphasis on comparison to a promising algebraic-Reynolds-stress closure model of oceanic vertical transport [D, E]. ODT is consistent with this model for cases that both can address, but is more general in that only ODT can address Le and Pr dependences, enabling parameter studies relevant to convective transport in planets and stars.

The independent variables of the closure model are quantities that are not easily measured in the ocean. In order to provide a link between the closure model and ocean mixing measurements, ODT is being used to relate closure-model variables to measurable quantities.

A 3D ODT-based simulation method previously set up and validated for homogeneous turbulence has been extended to channel flow. Initial results indicate that the method performs as expected, with no artifacts arising from its extension to inhomogeneous wall-bounded flow.

FUTURE WORK

As noted in Recent Progress, one development enabling more direct ODT (and LEM, where applicable) comparisons to turbulent combustion data is the availability of 3D DNS data. ODT simulations corresponding to existing and anticipated DNS data sets will be performed. The objectives of these comparisons are first, to validate ODT for various combustion regimes, and second, to perform wider-ranging parameter studies than are affordable using 3D DNS. These parameter studies will check whether inferences based on the DNS cases are valid under more turbulent conditions or with more detailed kinetic mechanisms than can be run affordably in DNS.

One DNS target case is a planar Bunsen methane-air flame in which the co-flow consists of combustion products at an equivalence ratio not necessarily the same as in the reactant flow. Another target case is a planar ethylene jet diffusion flame with soot kinetics and radiative coupling. Also, comparison of DNS and LEM will be performed for an initially chemically uniform but thermally non-uniform constant-volume configuration that idealizes a homogeneous-charge compression-ignition (HCCI) regime. LEM has been compared [2] to 2D DNS of a hydrogen-air HCCI regime [F], and will be compared to a planned 3D DNS study in which the fuel is dimethyl ether.

Key ingredients for ODT simulations directly analogous to round jet diffusion flames (cylindrical symmetry, spatial advancement, multi-step chemical kinetics, and radiation coupling) have been developed individually but not previously combined in any one code. To enable this and allow for other future extensions, an object-oriented ODT code is being written. It uses an adaptive mesh to allow Lagrangian implementation of advection. This is needed for the cylindrical spatial ODT formulation. One goal of this effort is to gain understanding of the apparent universality of scalar dissipation spectra recently measured in turbulent round jet diffusion flames at the Combustion Research Facility.

The new code will also serve as a suitable platform for future development of 3D ODT-based combustion simulations. This approach can be implemented without requiring input from a coarse-grained advancement procedure. Hence it is termed Autonomous Microscale Evolution (AME).

The existing 3D ODT-based method that is discussed in Recent Progress is not autonomous in this sense. It involves a coarse-grained pressure-projection step whose outcome is communicated down-scale to the ODT-resolved flow field. AME is a pseudo-compressible formulation that avoids this down-scale coupling.

Development of AME is ongoing. Near-term target applications include flame stabilization in recirculating flows and internal-wave effects in stably stratified buoyant flows.

ODT will be used to investigate primary breakup of turbulent liquid jets. For this application, immiscible fluid phases with interfacial surface tension will be incorporated into ODT. This application is challenging due to the wide range of droplet sizes that are generated. An experimental study of primary breakup [G] yielded results consistent with the interpretation that breakup ceases when the flow residence time exceeds the time scale for formation of a droplet as large as the jet width. This interpretation seems counterintuitive; ODT will be used to check the validity of this versus other possible interpretations.

One effect of particle inertia in turbulent flow is clustering due the centrifuging effect of turbulent eddies, which tends to expel particles from vortical regions, causing them to accumulate outside those regions. In previous work [H], a simple representation of inertial-particle response to maps (surrogate eddies) was formulated, involving particle slip relative to the map-induced displacement of fluid, with slip magnitude proportional to Stokes number St . It was shown mathematically that this formulation captures key features of the St dependence of particle clustering for low St .

This result applies to suitably defined maps in any number of spatial dimensions. A given degree of clustering implies far more collisions in 1D than in 3D, so for coalescence modeling, the slip-modified map is applied to slabs in 3D space, with randomly chosen slab orientations (to

represent isotropic turbulence), rather than to intervals on a line. Algorithmically, the method evolves a list of particle locations, hence is grid-free and economical in 3D as well as in 1D. It will be used to study the parameter dependences of the particle collision rate, focusing on comparison to collision rates obtained by DNS [I, J]. This will be followed by investigation of droplet coalescence coupled to other relevant processes, such as gravitational sedimentation and condensational growth, under conditions relevant to rain formation in clouds.

REFERENCES

- A. N. Peters, *Turbulent Combustion* (Cambridge Univ. Press, Cambridge 2000).
- B. A. Klimenko, *Combust. Theory Model.* **5**, 275 (2001).
- C. E. R. Hawkes, R. Sankaran, J. C. Sutherland, and J. H. Chen, *Proc. Combust. Inst.* **31**, 1633 (2007).
- D. V. M. Canuto, A. Howard, Y. Cheng, and M. S. Dubovikov, *J. Phys. Oceanogr.* **32**, 240 (2002).
- E. V. M. Canuto, Y. Cheng, and A. Howard, *Geophys. Res. Lett.* **35**, L02613 (2008).
- F. E. R. Hawkes, R. Sankaran, P. P. Pebay, and J. H. Chen, *Combust. Flame* **145**, 145 (2006).
- G. P.-K. Wu and G. M. Faeth, *Phys. Fluids* **7**, 2915 (1995).
- H. A. R. Kerstein and S. K. Krueger, *Phys. Rev. E* **73**, 025302 (2006).
- I. O. Ayala, B. Rosa, L.P. Wang, and W.W. Grabowski, *New J. Phys.* **10**, 075015 (2008).
- J. C. N. Franklin, P. A. Vaillancourt, M. K. Yau, and P. Bartello, *J. Atmos. Sci.* **62**, 2451 (2005).

PUBLICATIONS SINCE 2008

1. J. R. Mayo and A. R. Kerstein, "Fronts in Randomly Advected and Heterogeneous Media and Nonuniversality of Burgers Turbulence: Theory and Numerics," *Phys. Rev. E* **78**, 056307 (2008).
2. M. Oevermann, H. Schmidt, and A. R. Kerstein, "Investigation of Autoignition under Thermal Stratification using Linear-Eddy Modeling," *Combust. Flame* **155**, 370 (2008).
3. A. R. Kerstein, "One-Dimensional Turbulence: Stochastic Simulation of Multi-Scale Dynamics," *Lect. Notes Phys.* **756**, 291 (2009).
4. S. E. Woosley, A. R. Kerstein, V. Sankaran, A. J. Aspden, and F. Roepke, "Type Ia Supernova: Calculations of Turbulent Flames Using the Linear Eddy Model," *Astrophys. J.* **704**, 255 (2009).
5. J. R. Schmidt, J. O. L. Wendt, and A. R. Kerstein, "Non-equilibrium Wall Deposition of Inertial Particles in Turbulent Flow," *J. Stat. Phys.* **137**, 233 (2009).
6. R. C. Schmidt, A. R. Kerstein, and R. J. McDermott, "ODTLES: A Multi-Scale Model for 3D Turbulent Flow Based on One-Dimensional Turbulence Modeling," *Comput. Methods Appl. Mech. Engrg.* **199**, 865 (2010).
7. A. J. Ricks, J. C. Hewson, A. R. Kerstein, J. P. Gore, S. R. Tieszen, and Wm. T. Ashurst, "A Spatially Developing One-Dimensional Turbulence (ODT) Study of Soot and Enthalpy Evolution in Meter-Scale Buoyant Turbulent Flames," *Combust. Sci. Tech.* (in press).
8. N. Punati, J. C. Sutherland, A. R. Kerstein, E. R. Hawkes, and J. H. Chen, "An Evaluation of the One-Dimensional Turbulence Model: Comparison with Direct Numerical Simulations of CO/H₂ Jets with Extinction and Reignition," *Proc. Combust. Inst.* (in press).

First-principles petascale simulations for predicting deflagration-to-detonation transition in hydrogen-oxygen mixtures

Alexei Khokhlov¹, Joanna Austin², Charles Bacon³,
Shashi Aithal⁴ and Katherine Riley³

1. Dept. of Astronomy and the Enrico Fermi Institute, The University of Chicago, AAC 136, 5640 S. Ellis Ave., Chicago, IL 60637; ajk@oddjob.uchicago.edu
2. The University of Illinois at Urbana-Champaign, Dept. of Aerospace Engineering, 306 Talbot Laboratories, 104 S Wright St, Urbana, IL 61821; jmaustin@illinois.edu
3. Argonne Leadership Computing Facility, The Argonne National Laboratory, 9700 South Cass Avenue, Building 360, Argonne, IL 60439; bacon@alcf.anl.gov, riley@alcf.anl.gov
4. Mathematics and Computer Science Division, The Argonne National Laboratory, 9700 South Cass Avenue, Building 360, Argonne, IL 60439; aithal@mcs.anl.gov

I. Program Scope

The goal of this program is to create first-principles petascale simulation tools for predicting high-speed combustion and detonation (HSCD) phenomena, in particular, for predicting the transitory regimes of rapid flame acceleration and deflagration-to-detonation transition (DDT). Our immediate attention is on the problem of DDT arising in applications involving hydrogen-oxygen mixtures. Hydrogen is emerging as an important fuel across a range of industries as a means of achieving energy independence and to reduce emissions. DDT and the resulting detonation waves in gaseous fuels can have catastrophic consequences. Hydrogen fuels are particularly sensitive to detonation, with autoignition times several orders of magnitude less than that of a liquid hydrocarbon such as gasoline. The widespread commercial use of hydrogen requires the development of new safety standards for gas handling, storage, and transport [1].

The run distance to detonation in a turbulent flame accelerating in a long pipe is a critical parameter used in safety assessments. Current theory is not capable of calculating the DDT and run distance a priori. As a result, safety assessments rely on empirical correlations found in DDT experiments carried out for various fuel compositions, ambient pressures, and tube geometries. However, the experiments are challenging and the existing data are sparse. First-principles numerical simulations of DDT are required for an in-depth understanding of the phenomena, and can quantify the relative importance of the various controlling parameters such as stoichiometry, ambient conditions, pipe geometry and surface roughness [2-4]. Such an understanding will enable these simulations to be used as a predictive tool for future design of safe hydrogen systems.

II. Recent Progress

During the first six months of the project we implemented the high-speed combustion and detonation (HSCD) code for predicting flame acceleration and DDT in H₂-O₂ mixtures. HSCD is a distributed memory parallel adaptive mesh refinement (AMR) reactive flow Navier-Stokes code [5,6] augmented with the appropriate eight-species equation of state (EOS), coupled multi-species microscopic transport, and chemical kinetics suitable for hydrogen combustion [7-13].

A distinct feature of the HSCD code is a dynamic cell-by-cell AMR based on a parallel fully threaded tree (FTT) structure. In ordinary trees pointers are directed from parents to children. In FTT, the pointers are inverted and directed from groups of children to parents and parent's siblings. This arrangement eliminates expensive tree searches which are notoriously difficult to parallelize and it allows all operations, including mesh refinement and de-refinement, to be performed in parallel. A space-filling curve approach is used in FTT for domain decomposition. The mesh can be refined around shocks, discontinuities and in regions containing large gradients of physical variables such as density, temperature, pressure, chemical composition, vorticity, and so on. AMR is performed dynamically every fourth timestep after which the cells are rebalanced across the domain decomposition boundaries using a heuristic to minimize the maximum amount of work, the number of ghost cells, and the number of MPI send/receive operations per MPI rank.

As each physical model is incorporated into the HSCD code, the implementation is being verified against results obtained using Cantera[14]. Cantera is open-source suite of software tools for reacting flow problems and has been used for calculation of thermodynamic and transport properties, chemical equilibrium conditions, and chemical production rates. The detailed chemical mechanism of O Conaire et al., containing 8 species and 19 reactions, has been initially selected [8]. This mechanism has been previously validated against shock tube ignition delay data for temperatures up to 2700 K and pressures up to 64 atm (over a temperature range of 1650 to 1930 K)[15]. Reasonable temperature and pressure limits for detonation post-shock conditions in hydrogen-oxygen mixtures are 700 to 2200K and 10 to 40 atm respectively.

We analyzed the computational requirements and upgraded the code for petascale simulations by converting the straight MPI parallel implementation of the code to the hybrid OpenMP/MPI implementation and optimizing the indirect memory access patterns for better utilization of the cache. We successfully performed first test AMR simulations of strong point explosion and shock propagation in $100 \times 1.25 \times 1.25 \text{ cm}^3$ and $100 \times 2.5 \times 2.5 \text{ cm}^3$ tubes filled with stoichiometric $2H_2 - O_2$ mixture at atmospheric pressure and room temperature.

The simulations were carried out with spatial resolution of $\simeq 7$ microns and spatial dynamic range $\simeq 1.4 \times 10^5$ utilizing up to 3×10^9 computational cells on 32K cores of Sun Linux Cluster Ranger at Texas Advanced Computational Center and 131K cores of BG/P Intrepid at Argonne National Laboratory. Two papers describing this work have been submitted to CLADE 2010 and Supercomputing 2010 conferences.

III. Future Work

During the second half of this year we will begin a systematic validation of component processes by carrying reactive flow Navier-Stokes simulations of ignition and laminar flames, flame acceleration and development of a boundary layers, shock ignition and ignition delays, and comparing the results with the existing experimental data. We have begun evaluating suitable test cases from the literature and compiling a validation database. During the second year of the project we plan to carry out simulation of flame acceleration and DDT in smooth tubes.

On the code development side, we plan further optimization of OpenMP/MPI programming model and scaling the code to upcoming generation of manycore and GPU-accelerated clusters. We also plan to implement comprehensive visualization and on-the-fly analysis capabilities for detecting and zooming in on the rapid transient processes such as non-steady shock-flame flame interaction, auto-ignition of hot spots, and DDT taking place on very small temporal and spatial scales.

IV. References

1. W. Breitung, in *Hydrogen Technology*, A. Len (ed.), Berlin Heidelberg: Springer-Verlag, 2008, chapter 9, pp. 335-376.
2. Urtiew, P.A., Oppenheim, A.K., *Experimental observation of the transition to detonation in an explosive gas*, Proc. R. Soc. A 295, 13-53 (1966).
3. M. Kyznetsov, V. Alexeev, I. Matsukov, S. Dorofeev, *DDT in a smooth tube filled with a hydrogen-oxygen mixture*, Shock Waves, 14 (2005) 205-215.
4. G. Ciccarelli and S. Dorofeev, *Flame acceleration and transition to detonation in ducts*, Prog. Energy and Combust. Sciences 34:499-550, 2008.
5. A.M. Khokhlov, *Fully threaded tree algorithms for adaptive refinement fluid dynamics simulations*, J. Comp. Phys., 143 (1998) 519.
6. A.M. Khokhlov, A.Yu. Chtchelkanova, *Fully Threaded Tree Algorithms for Massively Parallel Computations*, in Proceedings of the Ninth SIAM Conference on Parallel Processing for Scientific Computing, San Antonio, Texas, USA, March 22-24, 1999.
7. G. Dixon-Lewis, *Kinetic mechanism, structure and properties of premixed flames in hydrogen-oxygen-nitrogen mixtures*, Philosophical Transactions of the Royal Society of London. Series A, 292 (1979) 45-99.
8. M. O Conaire, H.J. Curran, J.M. Simmie, W.J. Pitz and C.K. Westbrook, *A comprehensive modeling study of hydrogen oxidation*, Int. J. Chem. Kinetics, 36 (2004) 603-622.
9. A.A. Konnov, *Remaining uncertainties in the kinetic mechanism of hydrogen combustion*, Combustion & Flame, 152 (2008) 507-528.
10. A. Burkat and B. Ruscic, *Third Millennium Ideal Gas and Condensed Phase Thermochemical Database for Combustion and Updates from Active Thermochemical Tables*, Technical report ANL-05/20, Argonne national laboratory, 2005.

11. R.A. Svehla, *Estimated viscosities and thermal conductivities at high temperatures*, NASA Technical report R-132, 1962
12. C.F. Curtiss & R.B. Bird, *Multicomponent diffusion*, Ind. Eng. Chem. Res., 38 (1999) 2515-2522.
13. Wilke, *A viscosity equation for gas mixtures*, J. Chem. Phys., 18 (1950) 517-519.
14. D. Goodwin, Caltech
15. E.L. Peterson, D. F. Davidson, M. Rohrig and R.K. Hanson, *High pressure shock tube measurements of ignition times in stoichiometric H₂/O₂/Ar mixtures* 20th Int. Symp. on Shock Waves, (1996) 941-946.

V. Publications and submitted journal articles supported by this project

2. A. Khokhlov, C. Bacon, S. Aithal, K. Riley, J. Austin, *Towards First-Principles Simulations of Deflagration-to-Detonation Transition in Hydrogen-Oxygen Mixtures*, submitted to Challenges of Large Applications in Distributed Environments (CLADE) conference, 2010.
2. A. Khokhlov, C. Bacon, S. Aithal, K. Riley, J. Austin, *First-Principles Simulations of High-Speed Combustion and Detonation in Hydrogen-Oxygen Mixtures*, submitted to Supercomputing 2010.

THEORETICAL CHEMICAL KINETICS

Stephen J. Klippenstein
Chemical Sciences and Engineering Division
Argonne National Laboratory
Argonne, IL, 60439
sjk@anl.gov

Program Scope

The focus of this program is the theoretical estimation of the kinetics of elementary reactions of importance in combustion chemistry. The research involves a combination of *ab initio* quantum chemistry, variational transition state theory (TST), classical trajectories, and master equation simulations. The emphasis of our current applications is on reactions that are of importance in (i) soot formation, (ii) radical oxidation, or (iii) NO_x chemistry. We are also interested in a detailed understanding of the limits of validity of and, where feasible, improvements in the accuracy of specific implementations of transition state theory. Detailed comparisons with experiment and with other theoretical methods are used to explore and improve the predictive properties of the transition state theory models. Dynamics simulations are performed as a means for testing the statistical assumptions, for exploring reaction mechanisms, and for generating theoretical estimates where statistical predictions are clearly inadequate. Master equation simulations are used to study the pressure dependence of the kinetics and to obtain phenomenological rate coefficients for use in kinetic modeling.

Recent Progress

Spin-Orbit Interactions and TST

In collaboration with Ahren Jasper (Sandia) and Larry Harding (Argonne) we have studied the effect of the geometry dependence of the spin-orbit splitting on transition state theory predictions for radical-radical recombination rate coefficients. The reactions of three halogen atoms (F, Cl, and Br) with two hydrocarbon radicals (CH₃ and CH₂CHCH₂) were studied with direct variable reaction coordinate transition state theory including explicit treatment of the geometry dependent spin-orbit splitting. These systems exhibit a range of spin-orbit strengths and a range of attractiveness along the minimum energy path. The simple neglect of the variation in the spin-orbit splitting yields reasonably accurate rate coefficients for all but the CH₂CHCH₂ + Br reaction, where this neglect overestimates the rate coefficient by up to a factor of 2.

Soot Formation

In collaboration with Jim Miller (Sandia), Wes Allen (Georgia), and Larry Harding we have employed *ab initio* transition state theory based master equation calculations to predict the temperature and pressure dependent phenomenological kinetics for the reaction between the two resonantly stabilized radicals, allyl and propargyl. Direct variable reaction coordinate transition state theory is used to predict the microcanonical rate coefficients for the barrierless channels. This study indicates that the formation of cyclic C₆H₇ and C₆H₈ species are suppressed by elevated pressures. Overall, it suggests that the formation of five-membered rings from this reaction is not as important as previously thought.

Hydrocarbon Oxidation

In a joint study with Mike Davis (Argonne), Rex Skodje (Colorado), Alison Tomlin (Leeds), and Larry Harding we have employed a combination of global uncertainty screening and *ab initio* transition state theory to improve the appropriateness at high pressure of the mechanism of Li et al. for the ignition of CH₃OH. The screening analysis suggests the importance of first the CH₃OH + HO₂ reaction and then the CH₃OH + O₂ reaction. The revised mechanism, incorporating the *ab initio* TST predictions for the kinetics of these two reactions, yields ignition delays that are up to a factor of 4 greater than those from the original mechanism.

In collaboration with Hanna Reisler (USC) we have studied the D-atom products arising from the predissociation of rovibrationally excited CD₂CD₂OH. The theoretical component of the analysis, which builds on our earlier study of C₂H₄ + OH with Senosiain et al., indicates that (i) the D-producing channels are minor compared to the OH + C₂D₄ channel, constituting at most a few percent; (ii) the branching ratio is more favorable towards these products when the reactant radicals have low rotational energy; and (iii) the vinyl alcohol channel is strongly favored over the acetaldehyde channel at all but the lowest excess energies.

Nitrogen Chemistry

In collaboration with Ed Law (Princeton) we have performed an *ab initio* TST based master equation analysis of the decomposition kinetics of monomethyl hydrazine (CH₃NHNH₂). The simple CN and NN fissions to produce NH₂ + CH₃NH and CH₃ + NHNH₂ dominate the kinetics, and so were studied with direct variable reaction coordinate transition state theory. The comparison with experiment suggests the need for an improved understanding of some of the secondary chemistry for the pyrolysis of this propellant.

Future Directions

We will continue our studies of aromatic ring formation, hydrocarbon oxidation, and NO_x chemistry. In collaboration with Talitha Selby (Wisconsin-Washington), Dave Osborn (Sandia), and Ahren Jasper we are studying the kinetics of the reaction between phenyl and propargyl radicals, which may be a key step in the formation of the second aromatic ring. This collaboration involves the comparison of *ab initio* transition state theory based master equation calculations with multiplexed photoionization based measurements of the product distributions. Our work with Tranter (Argonne) on the self-reaction of phenyl radicals has suggested the importance of benzyne radicals to the PAH growth process. Thus, we are initiating some studies of the kinetics of these radicals. We have made preliminary theoretical predictions for the self-reaction of *o*-C₆H₄. In collaboration with Wang (USC) we have begun an analysis of the reactions of ortho-benzyne with alkynes and alkenes. The reaction with C₄H₂ may provide a significant pathway to naphthalene.

We continue to collaborate with Jim Miller on various soot related reactions. This year we plan to study the reaction of propargyl with OH, which may provide an important oxidative loss channel for this key resonantly stabilized radical. We also intend to study the reaction of vinyl radical with 1,3 butadiene, which may provide an important ring formation pathway in ethylene flames. Both of these studies will involve complicated multiple well *ab initio* transition state theory based master equation calculations. In collaboration with Jim Miller and Peter Glarborg (Denmark) we plan to study the kinetics of NNH + O₂ and its effect on thermal de-NO_x.

Our work on delineating the contribution from roaming radical pathways under combustion conditions continues on various fronts. In a joint theory/experiment collaboration with Larry Harding and Joe Michael (Argonne) we are now studying the decomposition of various saturated alkanes, and of dimethyl ether. In these studies, a comparison of theoretical predictions for molecular loss via tight transition states with experimental observations of radical branching ratios provide quantitative estimates of the extent of any roaming contribution. A collaboration with Ahren Jasper and Al Wagner (Argonne) will provide accurate *ab initio* surfaces for reduced dimensional trajectory studies of roaming in various reactions, including propane and dimethyl ether. We are also exploring a statistical theory based treatment of the roaming radical contribution.

DOE Supported Publications, 2008-Present

1. **Thermal Decomposition of CF₃ and the Reaction of CF₂ + OH → CF₂O + H**, N. K. Srinivasan, M.-C. Su, J. V. Michael, A. W. Jasper, S. J. Klippenstein, and L. B. Harding, *J. Phys. Chem. A*, **112**, 31-37 (2008).
2. **A Combined Ab Initio and Photoionization Mass Spectrometric Study of Polyynes in Fuel-Rich Flames**, N. Hansen, S. J. Klippenstein, P. R. Westmoreland, T. Kasper, K. Kohse-Hoinghaus, J. Wang, and T. A. Cool, *Phys. Chem. Chem. Phys.*, **10**, 366-374 (2008).
3. **Kinetics of CH + N₂ Revisited with Multireference Methods**, L. B. Harding, S. J. Klippenstein, and J. A. Miller, *J. Phys. Chem. A*, **112**, 522-532 (2008).
4. **Theory of Low Temperature Gas-Phase Reactions**, S. J. Klippenstein and Y. Georgievskii, in "Low Temperatures and Cold Molecules", edited by I. W. M. Smith, (Imperial College, London, 2008), p. 175-231.
5. **Reactions over Multiple, Interconnected Potential Wells: Unimolecular and Bimolecular Reactions on a C₃H₅ Potential**, J. A. Miller, J. P. Senosiain, S. J. Klippenstein, and Y. Georgievskii, *J. Phys. Chem. A*, **112**, 9429-9438 (2008).
6. **Kinetics and Product Branching Ratios of the Reaction of ¹CH₂ with H₂ and D₂**, K. L. Gannon, M. A. Blitz, M. J. Pilling, P. W. Seakins, S. J. Klippenstein, L. B. Harding, *J. Phys. Chem. A*, **112**, 9575-9583 (2008).
7. **An Experimental and Theoretical High Temperature Kinetic Study of the Thermal Unimolecular Dissociation of Fluoroethane**, B. R. Giri, J. H. Kiefer, H. Xu, S. J. Klippenstein, and R. S. Tranter, *Phys. Chem. Chem. Phys.*, **10**, 6266-6273 (2008).
8. **A Shock Tube and Theory Study of the Dissociation of Acetone and Subsequent Recombination of Methyl Radicals**, S. Saxena, J. H. Kiefer, and S. J. Klippenstein, *Proc. Comb. Inst.*, **32**, 123-130 (2009).
9. **Kinetics of the H + NCO Reaction**, S. J. Klippenstein and L. B. Harding, *Proc. Comb. Inst.*, **32**, 149-155 (2009).
10. **Theoretical Rate Coefficients for the Reaction of Methyl Radical with Hydroperoxyl Radical and for Methylhydroperoxide Decomposition**, A. W. Jasper, S. J. Klippenstein, and L. B. Harding, *Proc. Comb. Inst.*, **32**, 279-286 (2009).
11. **Detailed Balance in Multiple-Well Chemical Reactions**, J. A. Miller, S. J. Klippenstein, S. H. Robertson, M. J. Pilling, and N. J. B. Green, *Phys. Chem. Chem. Phys.*, **11**, 1128-1137 (2009). [Perspectives Article]

12. **A Crossed Molecular Beams Study on the Formation of the Exotic Cyanoethynyl Radical in Titan's Atmosphere**, X. Gu, R. I. Kaiser, A. M. Mebel, V. V. Kislov, S. J. Klippenstein, L. B. Harding, M. C. Liang, Y. L. Yung, *Astrophysical J.*, **701**, 1797-1803 (2009).
13. **The Thermal Decomposition of NH₂OH and Subsequent Reactions: Ab Initio Transition State Theory and Reflected Shock Tube Experiments**, S. J. Klippenstein, L. B. Harding, B. Ruscic, R. Sivaramakrishnan, N. K. Srinivasan, M.-C. Su, and J. V. Michael, *J. Phys. Chem. A*, **113**, 10241-10259 (2009).
14. **Shock Tube and Theory Investigation of Cyclohexane and 1-Hexene Decomposition**, J. H. Kiefer, K. S. Gupte, L. B. Harding, and S. J. Klippenstein, *J. Phys. Chem. A*, **113**, 13750-13583 (2009).
15. **On the Temperature Dependence of Two Key Interstellar Reactions of H₃⁺: O(³P) + H₃⁺ and CO + H₃⁺**, S. J. Klippenstein, Y. Georgievskii, and B. J. McCall, *J. Phys. Chem. A*, **114**, 278-290 (2010).
16. **Direct Observation of Roaming Radicals in the Thermal Decomposition of Acetaldehyde**, R. Sivaramakrishnan, J. V. Michael, and S. J. Klippenstein, *J. Phys. Chem. A*, **114**, 755-764 (2010).
17. **Roaming Radical Kinetics in the Decomposition of Acetaldehyde**, L. B. Harding, Y. Georgievskii, and S. J. Klippenstein, *J. Phys. Chem. A*, **114**, 765-777 (2010).
18. **Reactions between Resonance Stabilized Radicals: Propargyl + Allyl**, J. A. Miller, S. J. Klippenstein, Y. Georgievskii, L. B. Harding, W. D. Allen, and A. C. Simmonett, *J. Phys. Chem. A*, ASAP (2010).
19. **The Effect of Spin-Orbit Splitting on the Association Kinetics of Barrierless Halogen-Atom-Hydrocarbon Radical Reactions**, A. W. Jasper, S. J. Klippenstein, and L. B. Harding, *J. Phys. Chem. A*, in press (2010).
20. **D-Atom Products in Predissociation of CD₂CD₂OH from the 202-215 nm Photodissociation of 2-bromoethanol**, L. W. Edwards, M. Ryazanov, H. Reisler, and S. J. Klippenstein, *J. Phys. Chem. A*, in press (2010).
21. **Uncertainty Driven Theoretical Kinetics Studies for CH₃OH Ignition: HO₂ + CH₃OH and O₂ + CH₃OH**, S. J. Klippenstein, L. B. Harding, M. J. Davis, A. S. Tomlin, and R. T. Skodje, *Proc. Comb. Inst.*, submitted (2010).
22. **Ab Initio Kinetics for the Decomposition of Monomethylhydrazine (CH₃NHNH₂)**, P. Zhang, S. J. Klippenstein, H. Sun, and C. K. Law, *Proc. Comb. Inst.*, submitted (2010).
23. **Formation of CH₂NH and NH₃ in Titan's Upper Atmosphere**, R. V. Yelle, V. Vuitton, P. Lavvas, S. J. Klippenstein, M. Smith, S. Horst, and J. Cui, *Faraday Discussions*, submitted (2010).
24. **An Experimental and Theoretical Investigation of the Self-Reaction of Phenyl Radicals**, R. S. Tranter, S. J. Klippenstein, L. B. Harding, B. R. Giri, X. Yang, and J. H. Kiefer, *J. Phys. Chem. A*, submitted (2010).

ARGONNE-SANDIA CONSORTIUM ON HIGH-PRESSURE COMBUSTION CHEMISTRY

Stephen J. Klippenstein (PI), Michael J. Davis, Lawrence B. Harding, Joe V. Michael,
Branko Ruscic, Raghu Sivaramakrishnan, Robert S. Tranter

Chemical Sciences and Engineering Division, Argonne National Laboratory, Argonne, IL, 60439
sjk@anl.gov

Craig A. Taatjes (PI), Ahren W. Jasper, James A. Miller, David L. Osborn, Judit Zádor

Combustion Research Facility, Mail Stop 9055, Sandia National Laboratories
Livermore, CA 94551-0969
cataatj@sandia.gov

Program Scope

The goal of this project is to explore the fundamental effects of high pressure on the chemical kinetics of combustion and to use that knowledge in the development of accurate models for combustion chemistry at the high pressures of current and future engines. Such accurate chemical models will aid in the effective use of novel alternative fuels, in the development of advanced engine designs, and in the reduction of pollutants. We design and implement novel experiments, theory, and modeling to probe high-pressure combustion kinetics from elementary reactions, to submechanisms, to flames. The work focuses on integrating modeling, experiment, and theory (MET) through feedback loops at all levels of chemical complexity. We are developing and testing the methodology for propane, n-heptane, and 1-butanol as key prototype fuels, and will extend this approach to a general fundamental theory of pressure effects. The consortium expands and enhances collaborations between Argonne's Dynamics in the Gas Phase Group and the Combustion Chemistry Group in Sandia's Combustion Research Facility and also interacts closely with the Princeton-led Combustion Energy Frontier Research Center (CEFRC).

Recent Progress

Propane Oxidation. Our initial efforts have focused on implementing the MET paradigm for the combustion of propane. As a first step we have initiated a large-scale collaborative study of the oxidation of propyl radical. This study involves a collaboration between Taatjes, Klippenstein, and Bill Green (MIT). In the Taatjes lab, measurements of OH formation from pulsed-photolytic Cl-initiated propane oxidation have been carried out as a function of temperature (525 K to 763 K) at pressures of 10 bar. The formation of OH shows clear evidence of formally direct OH production at these pressures, as seen in previous studies on cyclohexane oxidation.

Meanwhile, Green and Klippenstein have performed a high level ab initio transition state theory based master equation analysis of the kinetics of the second O₂ reaction in propyl oxidation. The energies for the stationary points in both the CH₂CH₂CH₂OOH + O₂ and CH₃CH(OOH)CH₂ + O₂ reactions have been obtained with an ~RQCISD(T)/CBS//B3LYP/6-311++G(d,p) approach. For the barrierless channels in these two reactions, we have implemented

direct CASPT2/cc-pvdz based variable reaction coordinate transition state theory treatments. Our master equation calculations implement these VRC-TST treatments in combination with more standard rigid-rotor harmonic oscillator based TST treatments for the isomerizations and decompositions with well-defined barriers.

The phenomenological rate coefficients arising from these master equation studies of the $C_3H_6OOH + O_2$ reactions and related studies for the $C_3H_7 + O_2$ reactions provide the core of a mechanism developed by Green and Taatjes for the conditions of Taatjes's high pressure Cl-initiated propyl oxidation experiments. The remainder of the mechanism is obtained with Green's RMG automated mechanism generator. Work in progress is comparing the predicted and observed time-dependent OH concentrations.

Propane Decomposition. At higher temperatures it is generally important to understand the competition between thermal decomposition of the fuel and oxidation of the fuel radicals generated via abstraction reactions of H, OH, and HO_2 with the fuel. As a first step in accurately modeling this competition, Harding and Klippenstein have begun a theoretical study of the decomposition of propane. This work leverages our related core BES work where, in a collaboration with Michael, we are studying the contribution of the roaming radical pathways to this decomposition. Michael's shock tube studies have yielded the decomposition rate constants at relatively low pressures of ~ 1 bar. Our ab initio transition state theory based master equation calculations are providing meaningful extrapolations to high pressures, e.g., 100 bar.

Uncertainty Analysis and HO_2 chemistry. As described in MJD's abstract, Davis, Rex Skodje (Colorado), and Alison Tomlin (Leeds) have implemented a novel uncertainty screening approach that provides a direct indication of where additional theoretical predictions and/or experimental measurements would be most effective in reducing the uncertainty of the global predictions of quantities such as the ignition delay. As part of the current high-pressure combustion chemistry project, Davis and Skodje have been implementing this approach for the ignition of propane at high pressures. Their results suggest the dominant importance of the $C_3H_8 + HO_2$ abstraction reaction at high pressures.

More generally, this uncertainty screening indicates the importance to ignition at high pressure of improved kinetic estimates for reactions of the HO_2 radical. This importance arises from (i) the increasing importance of the HO_2 radical as a chain propagator with increasing pressure and (ii) the current lack of meaningful estimates for its kinetics. The latter shortcoming is due to the great difficulty of making high temperature experimental kinetics measurements for HO_2 due to its instability. Thus, we are currently studying theoretically the kinetics of a number of reactions of the HO_2 radical.

For example, we are extending our earlier work on the kinetics of the $CH_3 + HO_2$ reaction to larger alkyl radicals. Klippenstein and Harding have work now in progress for both ethyl and propyl radicals. Preliminary direct VRC-TST calculations yield a rate of $2 \times 10^{-11} \text{ cm}^3 \text{ molecule}^{-1} \text{ s}^{-1}$ for the ethyl + HO_2 reaction with primary formation of $CH_3CH_2O + OH$. Also, in collaboration with Green, we have predicted the kinetics of the allyl + HO_2 bimolecular reaction, the thermal decomposition of C_3H_5OOH , and the unimolecular reaction of C_3H_5O . Direct variable reaction coordinate transition state theory is used to characterize the barrierless transition states for the allyl + HO_2 and $C_3H_5O + OH$ reactions. The predicted rate coefficients for allyl + $HO_2 \rightarrow C_3H_5OOH \rightarrow$ products are in good agreement with experimental values. The calculations for allyl + $HO_2 \rightarrow C_3H_6 + O_2$ underpredict the observed rate. The new rate

coefficients suggest that the reaction of allyl + HO₂ will promote chain branching significantly more than presumed in prior models.

High-Pressure Multiplexed Photoionization Mass Spectrometry (MPIMS) Reactor. A Laboratory Directed Research and Development (LDRD) project at Sandia constructed a first version of a high-pressure, high-temperature cell that has been interfaced with the existing Sandia MPIMS kinetics machine (see DLO and CAT abstracts). The interrogation of high-pressure reacting mixtures by MPIMS will facilitate unraveling isomer-specific pathways of autoignition and molecular weight growth chemistry; for example, ketohydroperoxides have recently been detected from butane oxidation in an atmospheric-pressure jet-stirred reactor by Qi, Battin-Leclerc, and coworkers (*Angew. Chem. Int. Ed.*, DOI: 10.1002/anie.200906850). The initial testing of the Sandia high-pressure MPIMS cell will also be used to design a new machine that will be optimized for high-pressure experiments.

Thermochemistry. The thermochemistry of gaseous substances is normally expressed and tabulated as if these substances followed ideal gas behavior. However, real gases behave approximately as ideal gases only in the limit of low pressure, with differences between the ideal and real gas thermochemistry tending to grow exponentially as the pressure increases. Ruscic has started exploratory investigations under the assumption that the essential nature of the departure of real gas thermochemistry from its ideal counterpart can be successfully described by combining the ideal-gas thermochemistry of the monomer, dimer, trimer, etc. The inverse of this assumption is currently being explored within Active Thermochemical Tables by applying it to test cases that involve the process of extracting ideal-gas vaporization enthalpies from actual real-gas measurements under the assumption that the latter pertain to equilibrium mixtures of the monomer, dimer, etc., each of which behaves as if it were an ideal gas.

Future Directions

We will continue working on the development of an accurate mechanism for the combustion of propane at high-pressures over a range of temperatures. Miller will generate an improved starting point for the core mechanism via updates to his current C1-C3 mechanism. Another key aspect of this work will involve the implementation of the global uncertainty screening of Davis for the Cl initiated oxidation experiments of Taatjes. This analysis will help direct further experiments in delineating the processes that contribute to the chain branching processes in the negative temperature coefficient regime. The modeling work will also be extended to the consideration of various additional flame properties such as flame speeds and species profiles. Klippenstein and Harding will study the propane + HO₂ abstraction reaction with high level ab initio transition state theory.

Jasper and Miller will implement their first principles treatment of energy transfer for a number of reactions of importance to propane combustion. Initially, they will study HO₂, which, as mentioned in the current progress section, is of key importance at high pressures. This study will provide insight into the relative importance of the chain terminating reaction H + O₂ (+M) → HO₂ (+M) as compared to the chain branching reaction H + O₂ → OH + O. The predicted kinetics will be compared with available experimental results. We will also perform first principles studies of energy transfer in the propane and propyl radical decompositions.

We will continue our work at implementing novel experimental and theoretical tools.

Tranter has begun to develop a miniature high-repetition rate shock tube to provide well defined high-temperature, high pressure conditions to investigate gas phase chemistry and particle formation mechanisms. The shock tubes will act as reactors that can be coupled to multiple analytical devices through a differentially pumped molecular beam sampling system (MBS) and be compatible with the size and duty cycle requirements of experimental stations at the ALS and APS. An orifice in the endwall of the shock tube will act as the first stage of the MBS. A fast-acting piloted valve, based on a design by Combs et al. [*Rev. Sci. Instrum.*, **75**, 270 (2004)], will be employed for the driver section at pressures up to 35 bar. This valve can be operated at repetition rates of 6 Hz and achieves very high gas throughput. It will be coupled to a 6 mm bore driven section equipped at multiple points with valves that permit rapid evacuation of the driven section, a key to reducing cycle time. Consideration has also been given to the data acquisition and control hardware and software that will be required and a new timing device has been constructed that should permit timing information from several hundred experiments to be acquired at the desired repetition rates.

Klippenstein and Harding will develop automated procedures for theoretically predicting the kinetics at high pressure. Our initial focus in this area will involve treatments that consider all torsional motions in simple abstraction reactions and that allow for consideration of all beta-bond fissions from a given radical. Ruscic's work on exploring the effects of high-pressure on combustion thermochemistry will continue. Klippenstein and Harding will develop novel approaches for treating the effects of vibrational anharmonicities on the rate constants. Jasper, Harding, and Klippenstein will explore theoretical methods for treating the radical complex mechanism. Our initial efforts will focus on the $\text{CH}_3 + \text{O}_2$ reaction, where interesting experimental observations have been made.

Osborn has devised a novel experiment to probe the energy transfer process, via a half-collision approach, using negative ion dissociative photodetachment. Utilizing a recently upgraded apparatus in the laboratory of Robert Continetti (UC San Diego), we will form negative ion complexes $[\text{ROOM}]^-$, where R is a hydrocarbon free radical, and M is a bath gas molecule, such as Ar, Xe, CO_2 , or H_2O . By measuring the kinetic energy of the detached electron in coincidence with the breakup of the remaining neutral cluster, we will measure energy deposition into the fragments from an energy-selected parent cluster. This work will provide a direct measure of the energy transfer function $P(E, E')$ as a function of the bath gas and the number of bath gas atoms or molecules attached. In concert with the experiments, Jasper will use trajectory simulations to compare with experimental results.

As the work on propane proceeds, including high-pressure MPIMS measurements, we will begin similar studies related to the development an accurate mechanism for the high-pressure combustion chemistry of butanols. First measurements of OH formation in high-pressure Cl-initiated oxidation of *n*-butanol have been carried out in the Taatjes lab. The butanol studies will include collaboration with the Princeton-led CEFRC, whose first target for mechanism development is *n*-butanol.

DOE Supported Publications, 2008-Present

1. **Theoretical Rate Coefficients for Allyl + HO_2 and Allyloxy Decomposition**, C. F. Goldsmith, S. J. Klippenstein, and W. H. Green, *Proc. Comb. Inst.*, submitted (2010).
2. **High Temperature Shock Tube and Theoretical Studies on the Decomposition of Propane: Evidence of Roaming Radical Mechanism**, R. Sivaramakrishnan, M.-C. Su, J. V. Michael, S. J. Klippenstein, and L. B. Harding, *J. Phys. Chem. A*, in preparation (2010).

Theoretical modeling of spin-forbidden channels in combustion reactions

Anna I. Krylov

Department of Chemistry, University of Southern California,
Los Angeles, CA 90089-0482

krylov@usc.edu

1 Scope of the project

The goal of our research is to develop predictive theoretical methods, which can provide crucial quantitative data (e.g., rate constants, branching ratios, heats of formation), identify new channels and refine reaction mechanisms. Specifically, we are developing tools for computational studies of spin-forbidden and non-adiabatic pathways of reactions relevant to combustion, and applying these tools to study electronic structure and reactions of open-shell and electronically excited species involved in these processes.

2 Summary of recent major accomplishments

During the past year, we conducted several computational studies of open-shell and electronically excited species. The common theme in these studies is interactions between states of different character and intersections between the corresponding potential energy surfaces (PESs). We also continued to develop computational methods for modeling electronic structure and spectroscopy of open-shell species. The DOE support is acknowledged in seven publications[1, 2, 3, 4, 5, 6, 7]. The previous year DOE-supported publications are [8, 9, 10]. Some of the recent results are highlighted below.

2.1 Diazirine

Motivated by the experiments conducted in Prof. Hanna Reisler group, we investigated the electronic structure of diazirine[2]. Our calculations of excitations energies and transition probabilities identified the initial electronic state in Reisler's experiments to be a valence 1^1A_2 ($\pi^* \leftarrow \sigma_{NN}$) state, which is reached via the intermediate 1^1B_2 ($\pi^* \leftarrow n$) state in a two-photon process.

2.2 Electronically excited and ionized states of 2-hydroxy-ethyl radical

In collaboration with Prof. Hanna Reisler’s group, we investigated electronically excited and ionized states of the $\text{CH}_2\text{CH}_2\text{OH}$ radical[7]. Our calculations revealed that vertical ionization from the ground-state conformers and saddle points leads to an unstable structure of the open-chain $\text{CH}_2\text{CH}_2\text{OH}^+$ cation (see Fig. 1). Consequently, adiabatic ionization energies (IEs) differ by more than 1 eV from vertical IE, and are therefore difficult to determine experimentally.

Fig.1

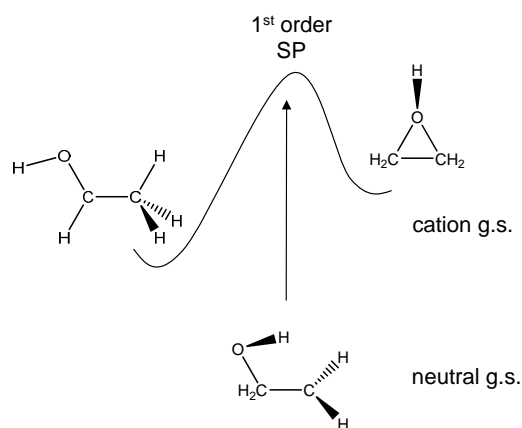


Figure 1: First ionization of $\text{CH}_2\text{CH}_2\text{OH}$. On the cation PES there is a first order saddle point in the Franck-Condon region which connects the CH_3CHOH^+ and $\text{CH}_2(\text{OH})\text{CH}_2^+$ isomers. The calculated vertical and adiabatic IEs are: $\text{VIE}=8.93$ eV, $\text{AIE}=6.21$ and 7.37 eV.

The ion isomerizes promptly either to the 1-hydroxyethyl ion, CH_3CHOH^+ , or to the cyclic oxirane ion, $\text{CH}_2(\text{OH})\text{CH}_2^+$, and the Rydberg states are expected to display a similar behavior (see Fig. 2). The isomerization pathway depends on the dOCC angle in the ground state. The lowest valence state is repulsive and its dissociation along the CC , CO and CH bonds, which leads to $\text{CH}_2 + \text{CH}_2\text{OH}$, $\text{CH}_2\text{CH}_2 + \text{OH}$, and $\text{H} + \text{CH}_2\text{CHOH}$ should be prompt. The branching ratio among these channels depends sensitively on the dihedral angles. Surface crossings among Rydberg and valence states and with the ground state are likely to affect dissociation as well. We concluded that the proximity of several low-lying excited electronic states, which can either dissociate directly or via isomerization and predissociation pathways, would give rise to prompt dissociation leading to several simultaneous dissociation channels.

2.3 Benzoxide diradical and its role in the benzene + O^3P reaction

In collaboration with several experimental and theoretical groups, we investigated electronic structure of benzoxide, an important combustion intermediate[5]. We characterized multiple closely lying electronic states of the initial benzene + oxygen adduct (see Fig. 3). Using our code for minimal minimum energy crossing points (MECP) within EOM-CC, we also located and characterized the singlet-triplet MECP. Our results helped to reproduce experimental branching ratios, yielding pressure-dependent rate expressions for the reaction channels,

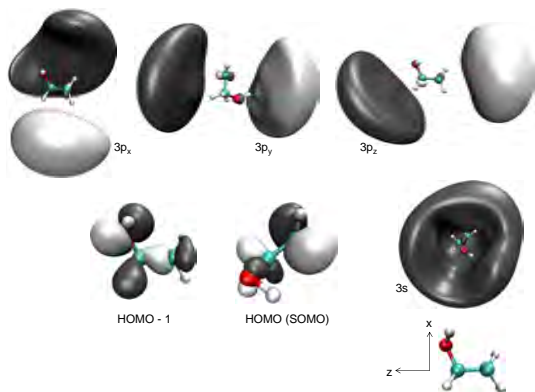
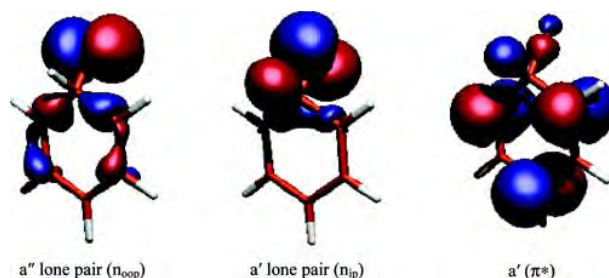


Figure 2: Relevant molecular orbitals involved in the lowest valence and Rydberg transitions. Rydberg states' PESs are similar to that of the cation, while the valence state is dissociative. The relative state ordering depends sensitively on the conformation.

including phenoxy + H, phenol, cyclopentadiene + CO, which are proposed for kinetic modeling of benzene oxidation[5].

Figure 3: Frontier MOs of the C_6H_6O adduct at the ${}^3A'$ -state geometry. In the open-shell diradical state, the a' π^* -like orbital is always singly occupied, whereas different populations of the a'' or a' lone pair orbitals give rise to A' and A'' electronic states, respectively. The lowest singlet states are of open-shell character. The the closed-shell singlet state, which gives rise to the phenol product, is about 1 eV above the triplet state vertically, however, the respective MECP is only 1.4 kcal/mol above the minimum.



2.4 Dyson orbitals and calculations of absolute and differential cross sections for photodetachment and photoionization

We developed a computational method for calculating total and differential cross sections for the photoionization and photdetachment experiments. As the first step, we benchmarked and validated our approach for negative ion photodetachment[4]. The energy dependence of the cross sections is reproduced well, however, the accuracy of absolute values varies. For F^- , C^- , NH_2^- , H^- , the calculated cross sections are within the error bars from the experimental values, whereas the errors for Li^- and OH^- are about 20%. The largest errors are observed for O^- and O_2^- for which the calculated cross sections differ from the experimental ones by factors of 3 and 2, respectively. Calculated anisotropy parameters for atomic anions exhibit too slow decrease, which suggests that the diffuseness of the computed Dyson orbitals is underestimated. Moreover, in the asymptotic region, the orbitals exhibit artifactual oscillations probably due to the limitations of Gaussian basis sets. The analysis of the trends in the experimental anisotropy parameters suggests that the interaction of the detached electron with the core, which is neglected in the present model, is important.

3 Current developments and future plans

Currently, we are pursuing modeling of dynamics of $\text{CH}_2\text{CH}_2\text{OH}$ using full-dimensional PES to quantify branching ratios of different dissociation/isomerization channels. We are benchmarking and validating our code for modeling absolute photoionization cross sections, and improving our description of the free electron to achieve better accuracy.

References

- [1] H. Reisler and A.I. Krylov, Interacting Rydberg and valence states in radicals and molecules: Experimental and theoretical studies, *Int. Rev. Phys. Chem.* **28**, 267 (2009).
- [2] I. Fedorov, L. Koziol, A.K. Mollner, A.I. Krylov, and H. Reisler, Multiphoton ionization and dissociation of diazirine: A theoretical and experimental study, *J. Phys. Chem. A* **113**, 7412 (2009).
- [3] L. Koziol, V. Mozhayskiy, B.J. Braams, J.M. Bowman, and A.I. Krylov, Ab initio calculation of the photoelectron spectra of the hydroxycarbene diradicals, *J. Phys. Chem. A* **113**, 7802 (2009).
- [4] C.M. Oana and A.I. Krylov, Cross sections and photoelectron angular distributions in photodetachment from negative ions using equation-of-motion coupled-cluster Dyson orbitals, *J. Chem. Phys.* **131**, 124114 (2009).
- [5] C.A. Taatjes, D.L. Osborn, T.M. Selby, G. Meloni, A.J. Trevitt, E. Epifanovsky, A.I. Krylov, B. Sirjean, E. Dames, and H. Wang, Products of the benzene + $\text{O}(^3\text{P})$ reaction, *J. Phys. Chem. A* **114**, 3355 (2010).
- [6] E. Kamarchik, O. Kostko, J.M. Bowman, M. Ahmed, and A.I. Krylov, Spectroscopic signatures of proton transfer dynamics in the water dimer cation, *J. Chem. Phys.* (2010), submitted.
- [7] B. Karpichev, L. Koziol, K. Diri, H. Reisler, and A.I. Krylov, Electronically excited and ionized states of the $\text{CH}_2\text{CH}_2\text{OH}$ radical: A theoretical study, *J. Chem. Phys.* **132**, 114308 (2010).
- [8] B. Karpichev, H. Reisler, A.I. Krylov, and K. Diri, Effect of hyperconjugation on ionization energies of hydroxyalkyl radicals, *J. Phys. Chem. A* **112**, 9965 (2008).
- [9] L. Koziol, Y. Wang, B.J. Braams, J.M. Bowman, and A.I. Krylov, The theoretical prediction of infrared spectra of trans- and cis- hydroxycarbene calculated using full dimensional ab initio potential energy and dipole moment surfaces, *J. Phys. Chem. A* **113**, 7802 (2008).
- [10] B.C. Shepler, E. Epifanovsky, P. Zhang, J.M. Bowman, A.I. Krylov, and K. Morokuma, Photodissociation dynamics of formaldehyde initiated at the T_1/S_0 minimum energy crossing configuration, *J. Phys. Chem. A* **112**, 13267 (2008).

SYNCHROTRON STUDIES OF COMBUSTION RADICAL REACTIONS AND AEROSOL CHEMISTRY

*Stephen R. Leone, Jared Smith, Kevin Wilson, Daphne Che, Chen-Lin Liu, Adam Trevitt,
Satchin Soorkia, Theodora Nah, and Musahid Ahmed*

*Departments of Chemistry and Physics and Lawrence Berkeley National Laboratory
University of California
Berkeley, California 94720
(510) 643-5467 srl@berkeley.edu*

Scope of the Project

Combustion is a complex process involving short-lived radical species, highly excited states, kinetics, transport processes, heterogeneous chemistry on aerosols such as organic liquid nanoparticles and soot, fluid dynamics, and energy transfer. Vacuum ultraviolet (VUV) light from the Chemical Dynamics Beamline of the Advanced Light Source (ALS) provides a powerful tool to selectively detect reaction products of carbon-based radical species (e.g. C₂H, CH, C₃H₃, C₅H₅ ...) with other hydrocarbons and oxygen by photoionization mass spectrometry. A multiplexed photoionization mass spectrometer apparatus at the ALS was jointly constructed with David Osborn and Craig Taatjes of the Sandia Combustion Research Facility. Products from key combustion reactions can now be detected and branching ratios estimated. In addition, an aerosol apparatus coupled to photoionization mass spectrometry is used to study aerosol heterogeneous chemistry. This endeavor explores aerosol particulate species chemistries, such as in fuel sprays, their production in combustion, and impact on the environment.

C₂H + 1-butyne

The gas phase reaction of ethynyl radical (C₂H) with 1-butyne (C₄H₆) is studied at room temperature (295 K) using a multiplexed photoionization mass spectrometer coupled to tunable VUV synchrotron radiation [Soorkia et al., JPC A, 2010]. Ethynyl radicals are formed by 193 nm laser photolysis of CF₃CCH. Two product channels are identified, i.e. C₅H₄ and C₆H₆ corresponding to the CH₃-loss and H-loss channels of the reaction, respectively. Photoionization efficiency curves are used to analyze the isomeric composition of both product channels. The C₅H₄ products are found to be exclusively linear isomers composed of ethynylallene and methyl diacetylene in a 4:1 ratio. In contrast, the C₆H₆ product channel includes two cyclic isomers, fulvene 18(±5)% and 3,4-dimethylenecyclobut-1-ene (DMCB) 32(±8)%, as well as three linear isomers, 2-ethynyl-1,3-butadiene 8(±5)%, 3,4-hexadiene-1-yne 28(±8)%, and 1,3-hexadiyne 14(±5)%. Within experimental uncertainties, we do not observe appreciable amounts of benzene and an upper limit of 10% is estimated for the yield of benzene. Diacetylene (C₄H₂) formation *via* the C₂H₅-loss channel is also thermodynamically possible but cannot be observed due to experimental limitations. These results provide insight into the formation of small cyclic molecules, especially C₆H₆ isomers, in the reaction of C₂H with unsaturated linear hydrocarbons, which might play an important role in the early stages of molecular weight growth processes leading to soot formation in combustion flames.

CH + pyrrole: formation of pyridine via a ring expansion reaction

The gas phase reaction of the ground state methylidyne radical CH (X²Π) with pyrrole (C₄H₅N) has been studied in a slow flow tube reactor using multiplexed photoionization mass spectrometry coupled to quasi-continuous tunable VUV synchrotron radiation at room temperature (295 K) and 90 °C (363 K) [Soorkia et al., PCCP, 2010]. Laser photolysis of bromoform (CHBr₃) at 248 nm is used to produce CH radicals that are free to react with pyrrole molecules in the gaseous mixture. A signal at m/z = 79 (C₅H₅N) is identified as the product of the reaction, and the result is consistent with CH addition to pyrrole followed by H-elimination. The photoionization efficiency curve unambiguously identifies m/z = 79 as pyridine. With deuterated methylidyne radicals (CD), the product mass peak is shifted by +1 mass unit,

consistent with the formation of C_5H_4DN and identified as deuterated pyridine (d-pyridine). Within detection limits, there is no evidence that the intermediate addition complex undergoes hydrogen scrambling. The results are consistent with a reaction mechanism that proceeds *via* the direct CH (CD) cycloaddition or insertion into the five-member pyrrole ring, giving rise to ring expansion, followed by H atom elimination from the nitrogen atom in the intermediate to form the resonance stabilized pyridine (d-pyridine) molecule. The N-H bond in pyrrole is weaker than any of the C-H bonds in pyrrole, providing a thermodynamic driving force for this selective outcome and the lack of randomization of the H atoms in the adduct. The possible generality of such ring expansion reactions in combustion will be important to characterize.

CH + propene

A key goal of this study is to examine whether the general trends learned from our earlier CH studies of CH reactions with molecules like acetylene and ethene [Goulay et al., JACS, 2009] can be extended to higher molecular weight systems, so that informed predictions can be made about even larger molecular species. The major product branching ratios of the CH + propene reaction are investigated at room temperature using the multiplexed photoionization mass spectrometer coupled with tunable VUV synchrotron radiation. Preliminary results show that the dominant product channel involves CH addition, followed by elimination of a H atom. Fitting the photoionization efficiency (PIE) curve on the C_4H_6 product channel reveals the presence of 3 isomers that, because their absolute photoionization cross sections are known, allows quantitative assignment of the branching fractions. The preliminary isomer contributions corresponding to the best fit are 1,3-butadiene (70%), 1,2-butadiene (22%) and 1-butyne (8%). We also investigated the CD + propene reaction to aid in unraveling the mechanism. The D:H elimination ratio is measured to be 1:4. Analysis is ongoing and made somewhat complex by the possibility of multiple addition complexes formed by either cycloaddition or insertion.

CH + benzene

The gas phase CH + benzene reaction has been investigated at room temperature. Benzene is purportedly central to soot formation in many combustion systems and the fate of this reaction impacts possible soot-forming pathways. The reaction is also of particular significance as the addition of CH to benzene forms an intermediate of the formula C_7H_7 that could implicate the benzyl radical or cycloheptatrienyl radical. The high exothermicities of CH + hydrocarbon reactions are interesting and informative high-energy probes of the relevant potential energy surfaces. Photoionization mass spectra of the species involved in the CH + benzene reaction reveals a dominant product on the C_7H_6 mass channel corresponding to CH addition followed by H elimination. The PIE curve of this mass channel has a signal onset and general morphology that is consistent with fulvenallene (c- $C_5H_4-CCH_2$). This product is a ring-contracted species that has recently been predicted to be the dominant benzyl radical thermal decomposition product [da Silva, et al., JPC A, 2010]. Further studies are currently underway to elucidate the mechanism of the CH + benzene reaction.

CN + benzene and toluene

The room-temperature product branching of CN reactions with benzene and toluene is also studied with vacuum ultraviolet photoionization at the Advanced Light Source [Trevitt et al., JPC A, 2010]. The only products observed are cyanobenzene and cyanotoluene. There is no evidence for direct abstraction pathways, and neither is benzyl radical $C_6H_5CH_2$ detected. The ortho, meta and para configurations for the reaction of CN with toluene were not resolvable in the vacuum ultraviolet photoionization because of their similar ionization energies. Corresponding kinetic rate coefficient results suggest that both reactions proceed without an energy barrier *via* addition complexes.

Aerosol Chemistry – reactions of squalane with Cl in the absence/presence of oxygen

An important process in complex combustion reactions is heterogeneous reactions between sprayed fuel droplets and reactive gas-phase radicals or molecules. Compared to the gas phase, there are potentially more coupled reactions of reactants, products, and intermediates occurring in the particle phase or gas-liquid phase. A simple atomic radical, Cl, is used to understand the reaction mechanism initiated *via* a heterogeneous H abstraction reaction by a gas phase radical at the surface of a sub-micron droplet of squalane. In the absence of O₂, chlorinated reaction products are formed and radical chain chemistry is observed; propagated by the R· + Cl₂ → RCl + Cl· reaction in the particle phase. Effective reactive uptake coefficients vary from 0.8 to 3.5, corresponding to radical chain propagation lengths of 1.4 and 6.4, respectively. The magnitude of the effective uptake coefficient is found to be approximately proportional to the [Cl₂] in the flow reactor. Molecular oxygen competes with molecular chlorine for reaction with R· and replaces the chain propagation mechanism by a terminating reaction through the formation of stable oxygenated products. Adding as much as 20% O₂ to the reaction effectively shuts off the chain cycling reaction, producing oxygenated products and decreasing the uptake coefficient to a diffusion-corrected value of 0.65±0.07. Additionally, the chemical evolution of the particle follows a sequential oxidation mechanism. Under these conditions the Cl initiated oxidation of the particle is nearly identical to that found for the OH + squalane reaction albeit ~2.2 times faster, due to the larger initial reactive uptake coefficient of Cl atoms compared to OH.

Aerosol Chemistry – reactivity of aerosols composed of unsaturated molecules

Oleic acid, linoleic acid, linolenic acid, and squalene, containing 1, 2, 3, and 6 C-C double bonds, respectively, are utilized to explore the reactivity of droplets composed of unsaturated molecules. These molecules are similar in structure to the long chain alkyl (methyl, ethyl, or propyl) esters found in biodiesel and are reasonable model systems to begin to examine the fundamental heterogeneous reactions between hydrocarbon droplets and gas phase radicals and molecules. A closed shell molecule, Cl₂, is found to react with these droplets despite the fact that analogous reactions in the gas phase occur very slowly or not at all at room temperature. The rates of these heterogeneous reactions are higher for the compounds containing more unsaturated reaction sites. For example, squalene (6 C-C double bonds) reacts with Cl₂ more rapidly than oleic acid (1 C-C double bond). From the chemical evolution of the particle phase, it is found that one Cl atom replaces one H atom for each reaction. Efforts are underway to construct a detailed heterogeneous reaction mechanism.

Cl radicals are also used to probe the heterogeneous reactivity of gas phase radicals with C-C double bonds in hydrocarbon droplets. These studies are designed to examine how hydrogen abstraction reactions compete with radical addition when C-C double bonds are present. Very large effective uptake coefficients are observed and depend upon [O₂] in the reactor as well as the number of unsaturated sites in the organic droplets. Effective uptake coefficients are 1.7 – 4.2, 14 – 47, and 50 – 130 for oleic acid, linolenic acid, and squalene, respectively, at [O₂] from 0 to 20%. The effective uptake coefficient of Cl with squalene droplets increases from 50 to 95 when the chlorine molecule concentration increases from 4 ppm to 12 ppm in the absence of O₂. Effective uptake coefficients much larger than 1 are clear indications of chain reaction chemistry, which has the net effect of making the reaction rate 100 times faster than the Cl atom collision frequency. Efforts are currently underway to develop a detailed molecular explanation for these heterogeneously initiated chain reactions.

Future plans

New studies will focus on additional gas phase radical-molecule reactions. In particular, we are examining the trends of insertion reactions compared to cycloaddition reactions of the CH radical. Products of the reaction of CH with cyclopentadiene (c-C₅H₆) and indene (C₉H₈) will be investigated to determine the influence of resonance-stabilized intermediates on the final product branching fractions of the reaction, in particular benzene and naphthalene, the smallest

polycyclic aromatic hydrocarbons, PAHs, which are believed to be molecular precursors of soot formation. Also, radical reaction/heterogeneous chemistry on carbonaceous soot particles has yet to be explored at the level of detail that is now possible by using aerosol generation and introduction instruments, flow tube reactors, and mass spectrometric detection tools. By preparing fresh soot particles in a flame and immediately introducing them into a flow tube system, we will study their reactivity and products with radicals, such as Cl atoms or C₂H radicals. The formation of larger PAH molecules that partition to the particle phase, produced by the reaction of hydrocarbon radicals with naphthalene and higher aromatic ring compounds derived from oil shales, will be investigated using the VUV photoionization aerosol mass spectrometer. Since PAH molecules have low ionization energies, they are readily identified by both their mass spectra and ionization energy. The oxidation of PAHs is a heterogeneous process that competes with the formation of soot. Oxidation reactions take place on the surfaces of soot particles and decrease the mass of PAHs and soot material through the formation of CO and CO₂. The main oxidation reactants are with OH radicals (under fuel-rich conditions) and O₂ (under fuel-lean conditions). Experiments will be carried out to determine the mechanisms by which these oxidants react with heterogeneous phase PAHs. These studies will shed light on how different types of combustion particulate emissions also evolve in the atmosphere.

Recent Publications Citing DOE Support (2008-2010)

S. Soorkia, A. J. Trevitt, T. M. Selby, D. L. Osborn, C. A. Taatjes, K. R. Wilson and S. R. Leone, "Reaction of the C₂H Radical with 1-Butyne (C₄H₆): Low-Temperature Kinetics and Isomer-Specific Product Detection," *J. Phys. Chem. A* (in press) (2010).

S. Soorkia, C. A. Taatjes, D. L. Osborn, T. M. Selby, A. J. Trevitt, K. R. Wilson and S. R. Leone, "Direct detection of pyridine formation by the reaction of CH (CD) with pyrrole: a ring expansion reaction," *Phys. Chem. Chem. Phys.* (submitted) (2010).

F. Goulay, A. J. Trevitt, G. Meloni, T. M. Selby, D. L. Osborn, C. A. Taatjes, L. Vereeken, and S. R. Leone, "Cyclic versus linear isomers produced by reaction of the methylidyne radical (CH) with small unsaturated hydrocarbons," *J. Am. Chem. Soc.* **131**, 993 (2009).

A. J. Trevitt, F. Goulay, C. A. Taatjes, D. L. Osborn, and S. R. Leone, "Reactions of the CN radical with benzene and toluene: product detection and low temperature kinetics," *J. Phys. Chem. A*, **114**, 1749 (2010).

J. D. Smith, J. H. Kroll, C. D. Cappa, D. L. Che, C. L. Liu, M. Ahmed, S. R. Leone, D. R. Worsnop, and K. R. Wilson, "The heterogeneous reaction of hydroxyl radicals with sub-micron squalane particles: a model system for understanding the oxidative aging of ambient aerosols," *Atmos. Chem. Phys.* **9**, 3209 (2009).

D.L. Che, J. D. Smith, S. R. Leone, M. Ahmed and K. R. Wilson, "Quantifying the Reactive Uptake of OH by Organic Aerosols in a Continuous Flow Stirred Tank Reactor" *Phys. Chem. Chem. Phys.* **11**, 7885 (2009).

A. J. Trevitt, F. Goulay, G. Meloni, D. L. Osborn, C. A. Taatjes, and S. R. Leone, "Isomer-specific product detection of CN radical reactions with ethene and propene by tunable VUV photoionization mass spectrometry," *Int. J. Mass. Spectrom.* **280**, 113 (2009).

T. M. Selby, G. Meloni, F. Goulay, S. R. Leone, C. A. Taatjes, A. Fahr, and D. L. Osborn, "Synchrotron photoionization mass spectrometry measurements of kinetics and product formation in the allyl radical (H₂CCHCH₂) self-reaction," *J. Phys. Chem. A* **112**, 9366 (2008).

D. L. Osborn, P. Zou, H. Johnsen, C. C. Hayden, C. A. Taatjes, V. D. Knyazev, S. W. North, D. S. Peterka, M. Ahmed, and S. R. Leone, "The multiplexed chemical kinetic photoionization mass spectrometer: a new approach to isomer-resolved chemical kinetics," *Rev. Sci. Instrum.* **79**, 104 (2008).

Intermolecular Interactions of Hydroxyl Radicals on Reactive Potential Energy Surfaces

Marsha I. Lester

Department of Chemistry, University of Pennsylvania
Philadelphia, PA 19103-6323
milester@sas.upenn.edu

I. Program Scope

Hydroxyl radicals are important in combustion and atmospheric environments, where they are often detected by laser-induced fluorescence (LIF) on the $A^2\Sigma^+ - X^2\Pi$ band system. However, collision partners known to quench electronically excited $OH A^2\Sigma^+$ radicals are ubiquitous in these environments. Thus, great effort has been made to quantify the rates and/or cross sections for collisional quenching, so that its effects on LIF signals may be taken into account to allow an accurate determination of OH concentrations.^{1,2} Despite extensive kinetic measurements, fundamental questions remain regarding the fate of the collisionally quenched molecules and the mechanism by which these nonadiabatic processes occur. The experimental work carried out under DOE funding in this laboratory is aimed at understanding the fundamental chemical dynamics governing quenching of $OH A^2\Sigma^+$ by molecular partners (M) of significance in combustion environments. In addition, we are examining the binary interaction of an open-shell $OH X^2\Pi$ radical with a water molecule as a prototype for interactions of radicals in aqueous environments.

II. Recent Progress

A. Quantum state distribution of the $OH X^2\Pi$ products from collisional quenching of $OH A^2\Sigma^+$ by molecular partners in combustion environments

Collisional quenching of electronically excited $OH A^2\Sigma^+$ can occur through two types of processes: non-reactive quenching that returns $OH A^2\Sigma^+$ population to its ground $X^2\Pi$ electronic state and reaction. The outcomes for collisional quenching of $OH A^2\Sigma^+$ by H_2/D_2 and N_2 partners have been studied extensively in this laboratory. For these systems, both reactive³⁻⁵ and non-reactive⁶⁻¹⁰ quenching processes have been investigated experimentally. The $OH A^2\Sigma^+$ by H_2/D_2 system is emerging as a benchmark system with new theoretical calculations of the potentials and dynamics as discussed below.

Recent work has expanded experimental studies on the outcomes of collisional quenching of $OH A^2\Sigma^+$ to include quenching by O_2 and CO_2 . These systems are more complex than those previously studied since they exhibit multiple low-lying electronic states and/or reactive channels that are depicted in Fig. 1. We have examined the $OH X^2\Pi$ product state distribution from quenching of $OH A^2\Sigma^+$ by O_2 and CO_2 as well as the branching fraction for $OH X^2\Pi$ production from non-reactive quenching.¹¹

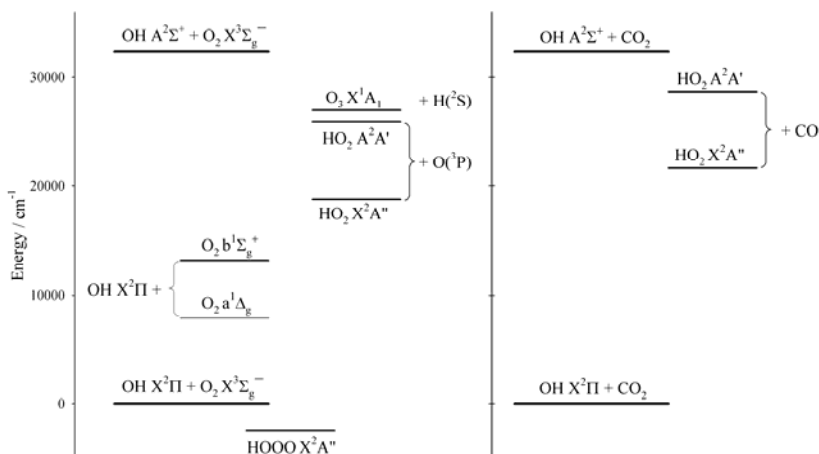


Fig. 1 Schematic energy level diagram illustrating possible non-reactive and reactive quenching channels for $OH A^2\Sigma^+$ with O_2 and CO_2 .

Comprehensive quantum state distributions have been measured for the $OH X^2\Pi$ products from quenching $OH A^2\Sigma^+$ ($v'=0, N'=0$) by O_2 and CO_2 . For both collision partners, OH products are formed

predominantly in $v''=0$ with less population in $v''=1$ and none detected in $v''=2$. No fine-structure effects are observed with either collision partner. With O_2 as the collision partner, the ground-state OH $X^2\Pi$ products are generated with a significant degree of rotational excitation, peaking at $N'' \sim 17$ with ~ 4800 cm^{-1} of rotational energy on average. Branching fraction measurements reveal that 40(1)% of the products are OH $X^2\Pi$ ($v''=0, 1$). With CO_2 as the collision partner, OH $X^2\Pi$ radicals are produced with a more moderate degree of rotational excitation, peaking at $N'' \sim 5$ with an average rotational energy of ~ 1800 cm^{-1} . In the case of quenching by CO_2 , 62(5)% of the products are identified as OH $X^2\Pi$ ($v''=0, 1$). For both systems, the balance may be found in higher OH $X^2\Pi$ vibrational levels $v'' \geq 2$ or more likely reactive quenching channels.

These results differ from previous observations made using H_2/D_2 and N_2 collision partners. In particular, quenching by O_2 and CO_2 show markedly different branching for production of OH $X^2\Pi$. For H_2 and D_2 , only 12(5)% and 15(8)% of the quenched products are OH $X^2\Pi$ with the balance being lost through reaction.⁸ For N_2 , non-reactive quenching collisions dominate, with >88 (3)% of the quenched population accounted for as OH $X^2\Pi$ and the balance thought most likely to be in yet higher undetected rotational states of $v''=0$ and 1.¹⁰

B. State-to-state vibrational energy transfer in OH $A^2\Sigma^+$ with N_2

For OH $A^2\Sigma^+ + N_2$, collisional quenching results in the nonradiative removal of population from the $A^2\Sigma^+$ state, principally through non-reactive transfer back to the ground $X^2\Pi$ state. In this system, collisions also induce transfer of population to other rovibrational levels within the excited OH $A^2\Sigma^+$ electronic state, namely vibrational energy transfer (VET), with comparable efficiency as quenching.

Vibrational energy transfer from $v'=0$ to $v'=1$ in the excited OH $A^2\Sigma^+$ electronic state has been investigated at low energies in the collisional region of a free-jet expansion.¹² High rotational levels of OH in its excited $A^2\Sigma^+$ ($v'=0$) electronic state, the starting point for the state-to-state VET studies presented here, are populated by a multi-step process illustrated in Fig. 2: A pump laser (blue arrow) initially prepares OH $A^2\Sigma^+$ ($v'=0, N'=0$), which is quenched by collision with N_2 , producing highly rotationally excited levels of OH in its ground $X^2\Pi$ ($v''=0$) electronic state,¹⁰ which is shown for reference in Fig. 2. OH $X^2\Pi$ ($v''=0$) population in high rotational levels is then excited with a second UV laser (red arrow) to prepare OH in specific rotational levels ($N'=14-22$) of the excited $A^2\Sigma^+$ ($v'=0$) state, which lie above the energetic threshold for OH $A^2\Sigma^+$ ($v'=1$).

Subsequent collisions with N_2 result in population of a distribution of OH $A^2\Sigma^+$ ($v'=1$) product rotational levels that is characterized through dispersed fluorescence spectra. The OH $A^2\Sigma^+$ ($v'=1$) products of VET are characterized through dispersed fluorescence spectra. Spectral simulations based on an assumed energy gap relationship are used to extract the OH $A^2\Sigma^+$ ($v'=1$) product rotational distributions for each initially prepared level. The majority of the OH $A^2\Sigma^+$ ($v'=1, N'$) products are observed in the most near-resonant level of $v'=1$ with population falling off rapidly in lower rotational levels. The near-resonant transfer involves a substantial change in rotational quantum number which increases as the initial rotational level of OH $A^2\Sigma^+$ ($v'=0$) is decreased. The efficiency of transfer from the initially prepared OH $A^2\Sigma^+$ ($v'=0, N'$) level to $v'=1$ is

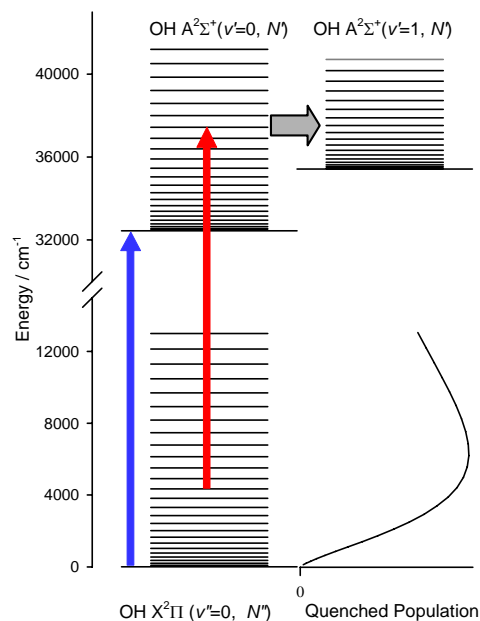


Fig. 2 Schematic energy level diagram depicting two step laser excitation scheme, quenched population distribution and vibrational energy transfer (VET) process within the OH $A^2\Sigma^+$ state.

assessed by comparing the intensity of emission from $v'=0$ and $v'=1$. This analysis reveals that the fractional transfer changes by an order of magnitude over the range of initial rotational levels of OH $A^2\Sigma^+$ ($v'=0$) investigated; a larger fraction is transferred to $v'=1$ for higher initial rotational levels. The fractional transfer correlates inversely with the magnitude of the change in angular momentum between initial and final states, which range from $\Delta N = 5-9$, suggesting that angular momentum constraints control the efficiency of VET at low collision energies.

C. Infrared spectrum and stability of the H₂O-HO complex: Experiment and theory

Hydroxyl radicals (OH) form strong hydrogen bonds with water. Such interactions are found in the gaseous environment of the atmosphere, the interface of liquid water and ice, and bulk regions of liquid water, snow, and ice. Hydroxyl radicals are also important products of electron-driven processes in water.¹³ The study of the binary H₂O-HO complex provides insight on the interactions of OH with a single water molecule and larger water networks found in the aforementioned systems. The experimental and theoretical study in this laboratory utilized experimental gas-phase vibrational spectroscopy in the OH radical stretching region and a two-dimensional vibrational approach to investigate the binary H₂O-HO complex,¹⁴ the latter in collaboration with Anne McCoy (OSU). We also benefited from collaboration with Joe Francisco (Purdue) on high-level ab initio calculations.

Binary H₂O-HO complexes are produced by association of photolytically generated OH radicals with H₂O from dilute nitric acid and identified by infrared action spectroscopy. The spectra display two distinct spectral bands: a dominant feature at 3490 cm⁻¹, assigned to the fundamental OH stretch of H₂O-HO, and a weaker feature at 3475 cm⁻¹, shifted by 78 and 93 cm⁻¹ to lower frequency of the OH stretch in an isolated OH molecule. The shift in frequency of the 3490 cm⁻¹ band is consistent with the harmonic shift calculated at the CCSD(T) level with very large basis sets and the shifts previously reported for the H₂O-HO complex in matrices. The rotational substructure in both bands is in accord with prior FTMW studies of H₂O-HO.¹⁵⁻¹⁷

In an effort to elucidate the assignment of the weaker band, we constructed a two-dimensional potential incorporating both ν_2 , the OH radical stretching mode, and ν_6 , the H₂O out-of-plane bending mode. Adiabatic potentials incorporating OH stretch with $\nu_2=0$ and 1 were generated as a function of the angle out-of-plane. This study demonstrates the coupling between these two modes, which leads to changes in the effective potential for the out-of-plane bending motion upon OH vibrational excitation, in particular the height of the barrier to planarity. Based on these calculations, we assign both bands as transitions within the nominally $^2A'$ electronic surface. The 3475 cm⁻¹ band is likely a hot band originating from a state with one quantum in the out-of-plane bend. The latter is calculated to be 13.7 cm⁻¹ lower in energy than the fundamental in the OH stretch with a comparable transition moment to the ν_2 fundamental transition.

Finally, using action spectroscopy to monitor the absorption of a photon by the H₂O-HO complex enables us to obtain an upper bound on the binding energy of the complex based on the OH product state distribution. Analysis of the distribution arising from exciting the complex at 3491.3 cm⁻¹ yields an experimental binding energy of $D_0 \leq 5.14$ kcal mol⁻¹. For comparison, the electronic binding energy D_e calculated at the CCSD(T) level of theory and the CBS limit is 5.6 kcal mol⁻¹. Interestingly, the H₂O-HO complex is predicted to have a larger electronic binding energy than those from the best calculations available to date for the water dimer! Future work is aimed at experimental and theoretical studies of partially and fully deuterated H₂O-HO complexes to ascertain their OH/D radical stretching frequencies, OH/D product state distributions, and binding energies.

III. Ongoing Work

High-level theoretical calculations of potentials and dynamical outcomes are being carried out for quenching in the benchmark OH $A^2\Sigma^+ + H_2$ system by several groups. Bowman and coworkers have very recently reported classical trajectory calculations of the post-quenching dynamics based on MRCI/aVTZ potentials, starting the trajectories at previously identified conical intersections.¹⁸ Product state distributions for the ground electronic state of OH and H-atom translational energy distributions for

abstraction and insertion mechanisms have been calculated and compare favorably with our experimental distributions. They find that the branching between reactive and non-reactive quenching agrees with experiment only when using diabatic sampling. Stimulated by this theoretical breakthrough, we are currently examining the reactive and non-reactive quenching outcomes for the OD $A^2\Sigma^+ + H_2$ system, so far having measured the OD $X^2\Pi$ product state distribution and branching fraction, while Bowman and coworkers are investigating the isotopic variants theoretically.

IV. References

- ¹ D. R. Crosley, *J. Phys. Chem.* **93**, 6273 (1989).
- ² M. I. Lester, R. A. Loomis, R. L. Schwartz, and S. P. Walch, *J. Phys. Chem. A* **101**, 9195 (1997).
- ³ D. T. Anderson, M. W. Todd, and M. I. Lester, *J. Chem. Phys.* **110**, 11117 (1999).
- ⁴ M. W. Todd, D. T. Anderson, and M. I. Lester, *J. Phys. Chem. A* **105**, 10031 (2001).
- ⁵ M. Ortiz-Suárez, M. F. Witinski, and H. F. Davis, *J. Chem. Phys.* **124**, 201106 (2006).
- ⁶ I. B. Pollack, Y. X. Lei, T. A. Stephenson, and M. I. Lester, *Chem. Phys. Lett.* **421**, 324 (2006).
- ⁷ P. A. Cleary, L. P. Dempsey, C. Murray, M. I. Lester, J. Kłos, and M. H. Alexander, *J. Chem. Phys.* **126**, 204316 (2007).
- ⁸ L. P. Dempsey, C. Murray, and M. I. Lester, *J. Chem. Phys.* **127**, 151101 (2007).
- ⁹ L. P. Dempsey, C. Murray, P. A. Cleary, and M. I. Lester, *Phys. Chem. Chem. Phys.* **10**, 1424 (2008).
- ¹⁰ L. P. Dempsey, T. D. Sechler, C. Murray, M. I. Lester, and S. Matsika, *J. Chem. Phys.* **130**, 104307 (2009).
- ¹¹ L. P. Dempsey, T. D. Sechler, C. Murray, and M. I. Lester, *J. Phys. Chem. A* **113**, 6851 (2009).
- ¹² T. D. Sechler, L. P. Dempsey, and M. I. Lester, *J. Phys. Chem. A* **113**, 8845 (2009).
- ¹³ B. C. Garrett, D. A. Dixon, D. M. Camaioni, D. M. Chipman, M. A. Johnson, et al., *Chem. Rev.* **105**, 355 (2005).
- ¹⁴ P. Soloveichik, B. A. O'Donnell, M. I. Lester, J. S. Francisco, and A. B. McCoy, *J. Phys. Chem. A* **114**, 1529 (2010).
- ¹⁵ Y. Ohshima, K. Sato, Y. Sumiyoshi, and Y. Endo, *J. Am. Chem. Soc.* **127**, 1108 (2005).
- ¹⁶ C. S. Brauer, G. Sedo, E. M. Grumstrup, K. R. Leopold, M. D. Marshall, and H. O. Leung, *Chem. Phys. Lett.* **401**, 420 (2005).
- ¹⁷ C. S. Brauer, G. Sedo, E. Dahlke, S. Wu, E. M. Grumstrup, K. R. Leopold, M. D. Marshall, H. O. Leung, and D. G. Truhlar, *J. Chem. Phys.* **129**, 104304 (2008).
- ¹⁸ E. Kamarchik, B. Fu, and J. M. Bowman, *J. Chem. Phys.* **132**, 091102 (2010).

V. Publications supported by this project 2008-2010

1. L. P. Dempsey, C. Murray, P. A. Cleary, and M. I. Lester, "Electronic quenching of OH $A^2\Sigma^+$ radicals in single collision events with H_2 and D_2 : A comprehensive quantum state distribution of the OH $X^2\Pi$ products", *Phys. Chem. Chem. Phys.* **10**, 1424-1432 (2008).
2. L. P. Dempsey, T. D. Sechler, C. Murray, M. I. Lester, and S. Matsika, "State-resolved distribution of OH $X^2\Pi$ products arising from electronic quenching of OH $A^2\Sigma^+$ by N_2 ", *J. Chem. Phys.* **130**, 104307 (2009).
3. L. P. Dempsey, T. D. Sechler, C. Murray and M. I. Lester, "Quantum state distribution of the OH $X^2\Pi$ products from collisional quenching of OH $A^2\Sigma^+$ by O_2 and CO_2 ", *J. Phys. Chem. A* **113**, 6851-6858 (2009).
4. T. D. Sechler, L. P. Dempsey, and M. I. Lester, "State-to-state vibrational energy transfer in OH $A^2\Sigma^+$ with N_2 ", *J. Phys. Chem. A* **113**, 8845-8851 (2009).
5. P. Soloveichik, B. A. O'Donnell, M. I. Lester, A. B. McCoy, and J. S. Francisco, "Infrared spectrum and stability of the H_2O -HO complex: Experiment and theory", *J. Phys. Chem. A* **114**, 1529-1538 (2010).

Theoretical Studies of Molecular Systems

William A. Lester, Jr.
Chemical Sciences Division,
Ernest Orlando Lawrence Berkeley National Laboratory and
Kenneth S. Pitzer Center for Theoretical Chemistry
Department of Chemistry, University of California, Berkeley
Berkeley, California 94720-1460
walester@lbl.gov

Program Scope

This research program is directed at extending fundamental knowledge of atoms and molecules. The approach combines the use of ab initio basis set methods and the quantum Monte Carlo (QMC) method to describe the electronic structure and energetics of systems of primarily combustion interest.

Recent Progress

Electronic structure and chemical activity of polyaromatic hydrocarbons for combustion processes and energy storage

The significance of electronic structure studies of graphene and related systems comes from the high relevance of the chemistry of polyaromatic hydrocarbons (PAHs) for the most challenging fundamental issues, such as the design of novel semiconducting materials, and applied areas, such as the thermodynamics of combustion and energy storage in batteries. With the increasing size of PAHs of interest, the application of very accurate quantum chemical methods becomes prohibitively expensive. This situation is more drastically pronounced in the studies of substrates that are presently too large to use single-molecule electronic structure methods, but too small to be treated as an infinite system. Therefore the development of simple models that capture the essential features of PAH chemistry and that are readily transferable to large systems is desirable.

a) Local aromaticity and relative stability of oxy radicals of linear and rectangular PAHs

Attention here is drawn mostly to the oxidation of PAH substrates and the relationship between local electronic structure of substrates and oxidation thermodynamics. The recent investigation of the local electronic structure of linear PAHs as models of zigzag graphene edges by this group showed that the relative stability of linear pentacene oxyradicals can be explained by fragmentation of the delocalized pi-electron system of the precursor pentacene molecule and formation of locally aromatic fragments. Linear PAHs provide less flexibility for rearrangement of pi-electron structure compared to realistic two-dimensional systems. In the latter case, both the influence of adjacent edges and interior regions need to be accounted for. Local aromaticity appears to be a robust

concept for assessment of local electronic structure and stability of PAHs. In addition, local aromaticity is closely related to structural properties of PAHs, including bond length in six-atom rings, and is, therefore, easily computable for systems of essentially any size.

In the present study, the relative stability of oxyl radicals of two-dimensional PAH substrates was investigated to establish the role of adjacent edges and interior regions and to identify the structural fragments responsible for the structural relaxation and stabilization upon oxidation.

b) Nature of diradical states of graphene at correlated levels of theory.

For larger PAHs, it is important to identify the nature of the ground state in view of the possibility of there being multi-configurational open-shell states with energies close to the ground state. The implications of spin-polarization for model systems also requires investigation. It is important here to clarify how interior and exterior (edge) regions, and exterior regions of different types (zigzag/armchair) of a finite-size graphene patch contribute to spin-polarization so that it is clear what kinds of effects are important in model studies.

A family of small graphene patches, i.e., rectangular PAHs, that display both zigzag and armchair edges was investigated to establish their ground state electronic structure. Broken symmetry density functional theory (DFT) and plane wave DFT were used to characterize the onset of diradical character via relative energies of open-shell and closed-shell singlet states. The perfect pairing (PP) active space approximation of coupled cluster theory was also used to characterize diradical character on the basis of promotion of electrons from occupied to unoccupied molecular orbitals. The role of zigzag and armchair edges in the formation of open-shell singlet states was clarified. In particular, it was found that elongation of the former results in increase of diradical character whereas elongation of the latter leads to decrease of diradical character. Analysis of orbitals from PP calculations suggests that diradical states are formally Möbius aromatic multiconfigurational systems.

c) Thermodynamics of soot oxidation: dissociation of OH bond in phenol at the QMC level.

The chemistry of phenol and the phenoxyl radical play fundamental roles in diverse scientific domains. For example, benzene is the smallest cyclic aromatic hydrocarbon used to model the small soot molecules that are produced by incomplete combustion processes and the phenoxyl radical is a representative product of the oxidation reactions that initiate thermal decomposition of soot. In biological contexts, conversion between the phenol and phenoxyl forms of tyrosine serves as a one-electron redox reaction that mediates the reduction of ribonucleotides and the metabolism of galactose. In light of the broad significance of phenol and the controversy over the value of the O–H bond dissociation energy (BDE) that fomented in the literature a few years ago, we have used the diffusion Monte Carlo (DMC) method to compute benchmark values for this BDE.

The homolytic O–H bond BDE of phenol was determined from DMC calculations using single determinant trial wave functions. The DMC method yields an O–H BDE of 87.0 ± 0.3 kcal/mol with restricted Hartree-Fock orbitals and 87.5 ± 0.3 kcal/mol with restricted B3LYP Kohn-Sham orbitals. These results are in good accord with the extrapolated B3P86 results of Costa Cabral and

Canuto (88.3 kcal/mol) and the recommended experimental value of Borges dos Santos and Martinho Simões (88.7 ± 0.5 kcal/mol).

This study shows that the O–H BDE of the phenol molecule can be accurately obtained using single determinant trial wave functions constructed from restricted HF and DFT orbitals. The results are encouraging for the application of the current methodology to larger aromatic molecules. Exploration of possible improvements from multi-determinant trial wave functions on DMC BDEs remains for future work. Further investigation is needed to understand why CCSD(T), which is typically very accurate, over estimates the O–H BDE of phenol.

Future Plans

We shall continue exploration of reactions on graphene edges in collaboration with Michael Frenklach's group. Following DFT studies of the reaction systems, QMC computations will be performed on the most critical reaction steps arising from the DFT analysis. For every reaction system, the Frenklach group will determine a complete set of rate coefficients.

DoE Supported Publications (2008-2010)

1. D. Domin, W. A. Lester, Jr., R. Whitesides, and M. Frenklach, "Isomer Energy Differences for the C₄H₃ and C₄H₅ Isomers Using Diffusion Monte Carlo," *J. Phys. Chem. A*, **112**, 2065 (2008).
2. M. T. Nguyen, M. H. Matus, W.A. Lester, Jr., and D. A. Dixon, "Heats of Formation of Triplet Ethylene, Ethylidene, and Acetylene," *J. Phys. Chem. A*, **112**, 2082 (2008).
3. R. Whitesides, D. Domin, R. Salomon-Ferrer, W.A. Lester, Jr., and M. Frenklach, "Graphene Layer Growth Chemistry: Five- and Six-Member Ring Flip Reaction," *J. Phys. Chem. A*, **112**, 2125 (2008).
4. W. A. Lester, Jr. and D. Domin, "Some Recent Developments of Quantum Monte Carlo to Molecular Systems," in *Nuclei and Mesoscopic Physics*, P. Danielewicz, P. Piecuch, and V. Zelevinsky, eds., AIP Conference Proceedings 995, (2008), p. 72.
5. D. Domin, B. Braida, and W. A. Lester, Jr., "The Breathing Orbital Valence Bond Method in Diffusion Monte Carlo: C-H Bond Dissociation of Acetylene," *J. Phys. Chem. A*, **112**, 8964 (2008).
6. R. Olivares-Amaya, R. Salomón-Ferrer, W. A. Lester Jr., and C. Amador-Bedolla, "Creation of a GUI for Zori, a Quantum Monte Carlo program, using Rappture," *Computing in Science and Engineering*, January/February 2009, Vol. 11, No.1, p. 41.
7. R. Whitesides, D. Domin, R. Salomon-Ferrer, W.A. Lester, Jr., and M. Frenklach, "Embedded-Ring Migration on Graphene Zigzag Edge," *Proc. Int. Symp. Combustion*, **32**, 577 (2009).
8. D. Y. Zubarev, N. Robertson, D. Domin, J. McClean, J. Wang, W.A. Lester, Jr., R. Whitesides, X. You, and M. Frenklach, "Local Electronic Structure and Stability of Pentacene Oxyradicals," *J. Phys. Chem. C* **114**, 5429 (2010).

Advanced Nonlinear Optical Methods for Quantitative Measurements in Flames

Robert P. Lucht

School of Mechanical Engineering, Purdue University

West Lafayette, IN 47907-2088

Lucht@purdue.edu

I. Program Scope

Nonlinear optical techniques such as laser-induced polarization spectroscopy (PS), resonant wave mixing (RWM), and electronic-resonance-enhanced (ERE) coherent anti-Stokes Raman scattering (CARS) are techniques that show great promise for sensitive measurements of transient gas-phase species, and diagnostic applications of these techniques are being pursued actively at laboratories throughout the world. We have continued our fundamental theoretical and experimental investigations of these techniques. We have also initiated both theoretical and experimental efforts to investigate the potential of femtosecond (fs) laser systems for sensitive and accurate measurements in gas-phase media. Our initial efforts have been focused on fs CARS, although the systems will be useful for a wide range of future diagnostic techniques involving two-photon transitions.

The objective of this research program is to develop and test strategies for quantitative concentration and temperature measurements using nonlinear optical techniques in flames and plasmas. We are investigating the physics of these processes by direct numerical integration (DNI) of the time-dependent density matrix equations for the resonant interaction. Significantly fewer restrictive assumptions are required using this DNI approach compared with the assumptions required to obtain analytical solutions. Inclusion of the Zeeman state structure of degenerate levels has enabled us to investigate the physics of PS and of polarization effects in DFWM and ERE CARS. We are concentrating on the accurate simulation of two-photon processes, including Raman transitions, where numerous intermediate electronic levels contribute to the two-photon transition strength. The DNI numerical methods can be extended to the calculation of the interaction of laser pulses as short as 50 fs simply by decreasing the integration time step (for pulses shorter than this the rotating wave approximation will no longer be valid and the density matrix equations will need to include terms that are negligible for longer pulses).

During the last year we continued our numerical simulations of high-resolution two-photon-induced laser-induced fluorescence (LIF) spectroscopy and ERE CARS spectroscopy of nitric oxide (NO). We have incorporated an effective intermediate electronic level in our calculations to account for the effects of the numerous intermediate electronic levels for the $A^2\Sigma^+ - X^2\Pi$ two-photon resonances. We also continued a detailed investigation of ERE CARS spectroscopy of nitric oxide, concentrating on a DNI analysis of saturation effects in the ERE CARS process, and we have further developed a DNI model for broadband Stokes, single-pulse ERE CARS measurements. During the last year we incorporated the effects of AC Stark shifting in both the two-photon absorption code and, with even more striking results, in the NO ERE CARS code. We have continued a detailed DNI analysis of the fs CARS process for gas-phase N_2 . We have demonstrated the acquisition of single-shot fs CARS signals from flames using a chirped pulse probe pulse following excitation of the Raman coherence using nearly Fourier-transform-limited pump and Stokes pulses. We have developed analytical techniques and numerical codes for the accurate determination of temperature from chirped-pulse probe fs CARS signals, and we continue to work on improving and optimizing these codes. We have also continued our development and application of injection-seeded optical parametric sources for high-resolution spectroscopy. In particular, we have demonstrated the use of an optical parametric oscillator (OPO) system with pulsed dye amplification (PDA) for the generation of pulsed, tunable, single-axial-mode laser radiation in the blue region of the spectrum. This system was used NO PLIF imaging.

II. Recent Progress

A. Electronic-Resonance-Enhanced CARS Spectroscopy of Nitric Oxide

We continue to investigate the physics and explore the diagnostic potential of ERE CARS for measurements of NO [P2, P5, P6, P8]. The primary motivation for the work is to determine whether ERE CARS can be used to measure NO in high-pressure environments, where LIF measurements are very difficult because of interfering LIF signals from species such as O₂, H₂O, and CO₂. ERE CARS is inherently more selective because of the requirement for both electronic and Raman resonance for signal generation. We have completed a detailed investigation of saturation effects in narrowband, scanning NO ERE CARS spectroscopy. The coupling of saturation effects for the Raman transition and the ultraviolet probe transition is quite complex and was investigated in detail. The inclusion of the AC Stark effect in the ERE CARS code was necessary to obtain good agreement between theory and experiment. In the ERE CARS measurements, the energy of the probe level is shifted due the near resonant coupling of single-photon transitions from the probe level to higher levels with the visible pump and Stokes laser radiation. This interaction is depicted schematically in Fig. 1 and has now been incorporated in the ERE CARS code, and we have obtained excellent agreement between experimental and calculated ERE CARS spectra. We have also continued our development of a DNI model for single-shot, broadband Stokes ERE CARS. The broadband Stokes laser is simulated using a multimode laser model with random phases for the modes and Gaussian-distributed mode amplitudes. The temporal dependence of the resulting ERE CARS signal is calculated using DNI methods, and the signal is then Fourier transformed to generate the ERE CARS spectrum for comparison with experiment. The theoretical spectra are in good qualitative agreement with experimental single-shot spectra. We have also incorporated the AC Stark effect in the broadband Stokes ERE CARS code. At this point the effect of the ac Stark effect on the detection limit for broadband Stokes ERE CARS is not clear. It may actually act to increase signals by sweeping neighboring probe transitions into resonance with the probe laser during the ERE CARS interaction.

B. Femtosecond CARS Calculations

Fs CARS offers several major potential advantages compared with nanosecond (ns) CARS; i.e., CARS as usually performed with nanosecond pump and Stokes lasers. These potential advantages include an elimination of collisional effects in the generation of the signal and the capability of performing real-time temperature and species measurements at data rates of 1 kHz or greater as compared to 10-50 Hz for ns CARS. During the past year single-laser-shot temperature measurements at a data rate of 1 kHz were performed in a gas cells, in near-adiabatic laminar flames, in a driven laminar flame, and in a turbulent Bunsen burner flame. room-pressure cell at temperatures of 300 K, 500K, 700K, and 900K.

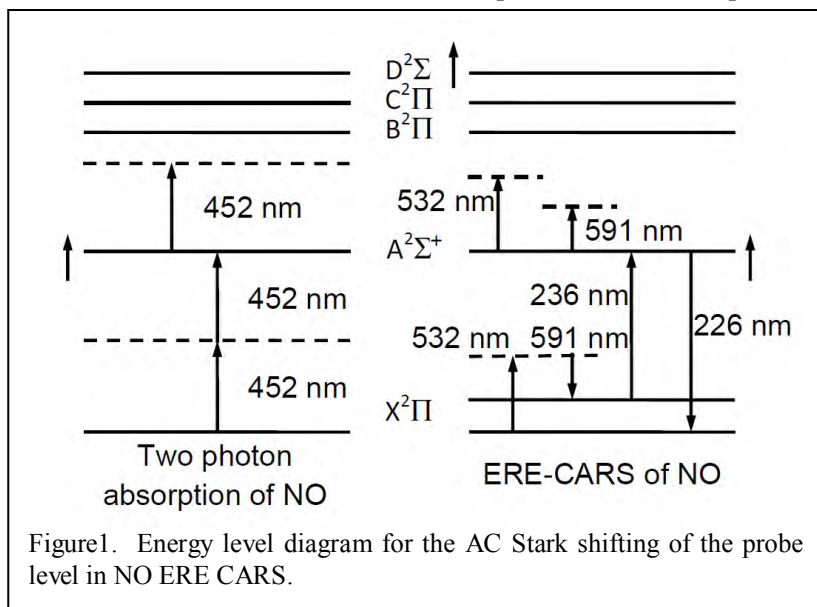
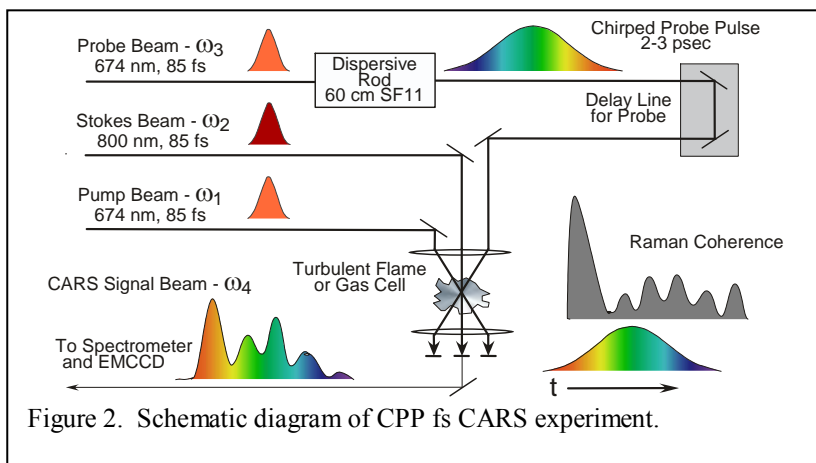


Figure1. Energy level diagram for the AC Stark shifting of the probe level in NO ERE CARS.

The measurements were performed using a laser system at Wright-Patterson Air Force base in collaboration with Drs. Sukesh Roy and James R. Gord; a schematic diagram of the experiment is shown in Fig. 2. The single-laser-shot measurements were performed by using a chirped probe pulse to map the time-dependent frequency-spread decay of the Raman coherence into the spectrum of the CARS signal pulse. Temperature was determined from the spectral shape of the chirped-probe-pulse (CPP) fs CARS signal for probe



equations for the fs CARS process were formulated and manipulated into a form suitable for solution by direct numerical integration (DNI). The temporal shapes of the pump, Stokes, and probe laser pulses are specified as an input to the DNI calculations. Based on these numerical results, a much faster fitting code

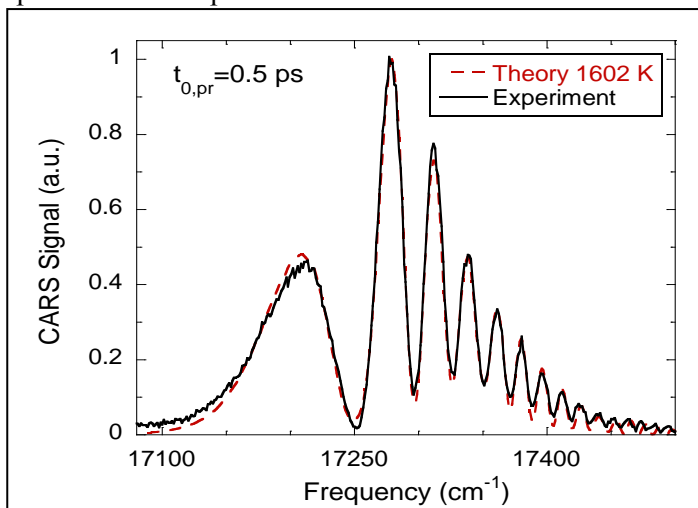


Figure 3. Comparison of experimental and theoretical spectra for CPP fs CARS.

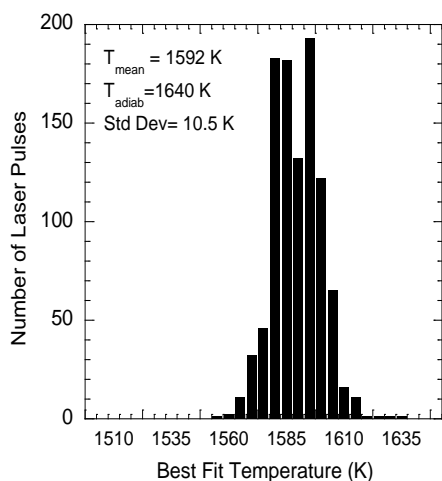


Figure 4. Histogram of single-shot temperatures determined near-adiabatic H₂/air flame using CPP fs CARS.

delays of approximately 2 ps with respect to the impulsive pump-Stokes excitation of the Raman coherence. Measured and calculated CPP fs CARS spectra from a flame with an equivalence ratio of 0.5 are shown in Fig. 3, and comparison of experiment and theory is excellent.

The physics of the CPP fs CARS process was previously analyzed using a time-dependent density matrix analysis. The time-dependent density matrix

was developed to generate synthetic CPP fs CARS spectra. The parameters in the fitting code were varied to obtain the best fit theoretical spectrum for a given experimental spectrum, and temperature was determined as one of the best-fit parameters. A histogram of 1000 single-laser-shot measurements, recorded in 1 second) for the $\Phi=0.5$ flame is shown in Fig. 4. The temperature histogram has standard deviation of less than 1%. Our results from the past year indicate that the precision of the single-pulse CPP fs CARS temperature measurements is approximately a factor of two better than for well-optimized single-pulse ns CARS measurements.

C. Modeling of Two-Photon Resonances and Six-Wave Mixing Processes

We are continuing our collaborative efforts with Dr. Thomas B. Settersten at Sandia's Combustion Research facility on six-wave mixing (6WM) spectroscopy and polarization spectroscopy of atomic hydrogen. The DNI computer code for the calculation of 6WM and PS signals from atomic hydrogen was significantly modified to incorporate all of the different possible photon mixing processes that can potentially contribute to both the 6WM and PS signals. The modeling of collisional processes in atomic hydrogen has also been modified to account for coherence transfer as well as

population transfer. However, the AC Stark effect has not yet been included in the model, and this is a very significant effect and explains much of the disagreement between our previous model results and the experimental data. The AC Stark shift of the upper level for the 243-nm two-photon transition will be incorporated in the numerical model during the next year.

III. Future Work

We plan to pursue further theoretical and experimental investigations of the ERE CARS process for species such as NO, OH, CH, and C₂H₂, especially at higher pressures where collisional narrowing may result in significant improvement in the detection limits. The DNI code for single-pulse, broadband Stokes ERE CARS has been developed and, now that the AC Stark effect has been incorporated, will be used to further explore the physics of the single-pulse ERE CARS process. Further theoretical investigations of the interaction of fs laser radiation with gas-phase resonances will be performed, and the computer code to extract temperature from single-shot, chirped-probe fs CARS signals will be optimized. Also, we will begin experimental fs CARS experiments in our laboratory after the delivery of a new ultrafast laser system to our laboratory later this year. This laser system operates at 5 or 10 kHz with pulse energies of >2.6 mJ and >1.05 mJ, respectively. This system is significantly more powerful and capable than the system at WPAFB that has been used for CPP fs CARS measurements to date. Our investigation of the physics of two-photon, two-color PS and 6WM for H-atom measurements will continue in collaboration with Tom Settersten at Sandia; incorporation of the AC Stark effect in the atomic hydrogen code is a high priority. We will continue to explore the physics of these processes using our DNI code. We plan to develop the capability for simultaneous operation of injection-seeded OPG/PDA and OPO/PDA systems. We will use the systems for two-color PS and 6WM measurements of atomic hydrogen and atomic oxygen.

IV. Publications and submitted journal articles supported by this project 2008-2010

1. S. V. Naik, J. Hwang, R. P. Lucht, and N. M. Laurendeau, "Measurement and Calculation of the Q-Branch Spectrum of Nitrogen Using Inverse Raman Spectroscopy and cw Raman-Induced Polarization Spectroscopy," *J. Raman Spectrosc.* **39**,68-78 (2008).
2. J. P. Kuehner, W. D. Kulatilaka, N. Chai, S. V. Naik, N. M. Laurendeau, R. P. Lucht, A. Patnaik, M. O. Scully, S. Roy, and J. R. Gord, "Perturbative Theory and Modeling of Electronic-Resonance-Enhanced Coherent Anti-Stokes Raman Scattering Spectroscopy of Nitric Oxide," *J. Chem. Phys.* **128**, Art. No. 174308 (2008).
3. A. H. Bhuiyan, D. R. Richardson, S. V. Naik, and R. P. Lucht, "Development of an Injection-Seeded Optical Parametric Generator/Pulsed Dye Amplifier System for High-Resolution Spectroscopy," *Appl. Phys. B* **94**, 559-567 (2009).
4. S. Roy, D. R. Richardson, P. J. Kinnius, R. P. Lucht, and J. R. Gord, "Effects of N₂-CO Polarization Beating on Femtosecond Coherent Anti-Stokes Raman Scattering (CARS) Spectroscopy of N₂," *Appl. Phys. Lett.* **94**, Article No. 144101 (2009).
5. A. K. Patnaik, S. Roy, R. P. Lucht, and J. R. Gord, "Collisional Effects on Molecular Dynamics in Electronic-Resonance-Enhanced CARS," *J. Mod. Opt.* **55**, 3263-3272 (2008).
6. A. K. Patnaik, S. Roy, R. P. Lucht, J. R. Gord and T. B. Settersten, "Effects of Collisions on Electronic-Resonance-Enhanced Coherent Anti-Stokes Raman Scattering of Nitric oxide," *J. Chem. Phys.* **130**, Article No. 214304 (2009).
7. S. Roy, D. R. Richardson, W. D. Kulatilaka, R. P. Lucht, and J. R. Gord, "Gas-Phase Thermometry at 1-kHz Using Femtosecond Coherent Anti-Stokes Raman Scattering (fs-CARS) Spectroscopy," *Opt. Lett.* **34**, 3857-3859(2009).
8. N. Chai, R. P. Lucht, W. D. Kulatilaka, S. Roy, and J. R. Gord, "Electronic-Resonance-Enhanced Coherent Anti-Stokes Raman Scattering Spectroscopy of Nitric Oxide: Nonperturbative Time-Dependent Modeling and Saturation Effect," *J. Chem. Phys.*, accepted for publication (2010).

Time-Resolved Infrared Absorption Studies of Radical Reactions

R. G. Macdonald
Chemistry Division
Argonne National Laboratory
Argonne, IL 60439
Email: rgmacdonald@anl.gov

Background

Information about the dynamics of radical-radical reactions is sparse. However, these processes are important in combustion being either chain propagating or terminating steps as well as potentially producing new molecular species. For almost all radical-radical reactions, multiple product channels are possible, and the determination of product channels will be a central focus of this experimental effort. In the current experiments, both transient species are produced by excimer laser photolysis of suitable photolytes, and if possible, two species are detected simultaneously using different continuous-wave laser sources operating in the red, near infrared and infrared spectral regions. This approach allows for the direct determination of the second-order rate constant under any concentration conditions if the appropriate absorption cross sections have been measured. The time dependence of individual ro-vibrational states of the reactants and/or products is followed by frequency- and time-resolved absorption spectroscopy. The simultaneous detection of multiple species ensures that species concentration profiles can be normalized to a common set of reaction conditions. In order to determine branching ratios and second-order rate constants, it is necessary to measure state-specific absorption coefficients and transition moments of radicals. These measurements play an important role in this experimental study.

Recent Results

The recently acquired continuous wave infrared OPO laser has been integrated into the experimental data acquisition procedures using Lab View and PXI data acquisition modules. In an absorption experiment, amplitude fluctuations of the probe beam are the largest source of noise in an experiment. In the present arrangement, laser amplitude fluctuations from the source laser are suppressed using software differential subtraction of I_0 and I temporal profiles from balanced detectors directly following each photolysis laser pulse. Previously, tuning the laser frequency to the peak of an absorption feature was facilitated using box-car signal averaging over the widest box car gate of 20 μ sec. This procedure has been replaced by displaying the moving average of a signal derived from recording separate I_0 and I profiles for 2 ms, calculating the integral of this differential signal and normalized to the ArF photolysis laser intensity. The peak position of a spectroscopic transition with an absorbance as low as 0.1% can be determined using this method.

$\text{NH}_2(\text{X}^2\text{B}_1) + \text{NH}_2(\text{X}^2\text{B}_1)$ Recombination. The NH_2 radical is an important intermediate in both the production of NO_x in combustion processes and the removal of NO_x from combustion exhaust gases. The removal processes are based on the addition of NH_3 , $(\text{HOCN})_3$ or $(\text{NH}_2)_2\text{CO}$ to the gas stream, resulting in the Thermal De NO_x , RAPRENO $_x$ and NO $_x$ OUT treatment processes, respectively. A key reaction in these processes is the

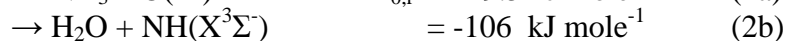
NH₂ + NO reaction. The NH₂ radical also plays a key role in the pyrolysis of NH₃ and other environments where nitrogen chemistry is important. However, in spite of its importance, the chemistry of the NH₂ radical, especially in reactions with other transient species, has not been widely studied.

In a continuation of the study of the NH₂ + OH, it became necessary to extend the number of species in the gas flow, as will be discussed in the next section. Thus, a study of the self-recombination of the NH₂ radical, reaction 1, in a variety of third bodies is being carried out to provide a larger data base to further the understanding of three body effects on this reaction. To date, work has been conducted on reaction 1 in He, CO₂ and H₂O. Future work will also involve SF₆ to see if these experiments can be extended over a sufficient pressure range to experimentally estimate the high pressure limit for NH₂ + NH₂. Klippenstein *et al.* (S. J. Klippenstein *et al.* *J. Phys. Chem. A* **113**, 10241 (2009)) have provide detailed theoretical and experimental guidance for many radical-radical and radical-molecule reactions of interest to this program. In particular, they have calculate the high pressure limit for reaction 1 using high level *ab initio* theoretical techniques to describe the NH₂ + NH₂ PES and variational transition state theory to calculate rate constants. At 293 K, only one product channel is energetically accessible:



In the present investigation, the NH₂ radical was created by the 193 nm photolysis of NH₃ dilute in CF₄ and the third body. Temporal concentration profiles of both NH₃ and NH₂ were recorded simultaneously using time- and frequency-resolved absorption spectroscopy. Unlike previous work, NH₃ was monitored on the ν₁ ⁹Q₃(3) fundamental transition, providing much larger signals to monitor the NH₃ temporal concentration profiles. The loss of NH₃ was directly related to the production of NH₂ in order to calculate the peak absorption cross section for the NH₂ transition used. Preliminary analysis provides the relative three body efficiency for NH₂ self-recombination: He < Ar < N₂ < CO₂ < H₂O, with H₂O about 10 times more efficient than He.

NH₂(X²B₁) + OH(X²Π). Experiments have continued on the NH₂ + OH reaction system in order to identify and measure the product branching ratios for this reaction. The OH radical possess electronic angular momentum so that the singlet and triplet spin manifolds now have A' and A'' electronic symmetry in planar geometry. There are several possible product channels:



As mentioned, Klippenstein *et al.* investigated reaction 2 both theoretically and experimentally at high temperatures. Theoretically, at 300 K channel 2b was predicted to have a rate constant of 1.6x10⁻¹¹ cm³ molecules⁻¹ s⁻¹. Preliminary experiments, reported last year were in reasonable agreement with this total rate constant but the branching into channel 2b was much smaller than the theoretical prediction. However, these experiments used high concentrations of N₂O to generate large concentrations of OH

from the reaction $O(^1D) + H_2O$; thus, potential secondary reactions, $O(^3P) + OH$ and NH_2 and $NO + NH$ and NH_2 could complicate the data interpretation. Initially, work was directed to a study of the $O(^3P) + NH_2$ reaction to verify the literature branching ratio. This is the only other reaction producing NH . The data was not interpretable using a simple straightforward mechanism. Unidentified secondary chemistry was contributing to the kinetics and is under further investigation. Although not efficient, the photodissociation of H_2O at 193 nm provides a clean source of OH radicals without the addition of any secondary chemistry. An example of the data collected using this OH source is shown in Figure 1b. The addition of small quantities of N_2O enhances the OH radical concentration but keeps secondary concentrations of $O(^3P)$ and $NO < 1 \times 10^{10}$ molecules cm^{-3} . An OH profile obtained under these conditions is shown in Figure 1d. Both NH_2 and OH or other infrared absorbing species were monitored simultaneously. The chemical model describing this system is more complicated than the sum of the individual self-reaction mechanisms because of the large number of cross-reactions between the two systems, and consists of over 80 reactions and 28 species. Under the conditions of these experiments no NH was detectable although the predicted model concentration peaked at 1×10^{11} (an absorbance of 0.5%) if the only product channel was 2b. The solid curves in panels b and d show the model predictions for the OH concentration profile using the recent rate constant measurement for the $OH + N_2H_4$ reaction, k_3 . (Vaghjiani Int. J. Chem. Kinet. **33**, 354 (2001)). Better fits to the OH profile are obtained if k_3 is reduced to $k_3 = 1.0 \times 10^{-11} \text{ cm}^3 \text{ molecule}^{-1} \text{ s}^{-1}$, as shown by the dashed lines in the figures. This adjustment reduces the scatter in the data for k_{2D} and shows a definite increase in k_{2D} with increasing pressure.

Publications 2008-present.

Determination of the rate constant for the $NH_2(X^2B_1) + NH_2(X^2B_1)$ reaction at low pressure and 293 K.

-Mi-Kyung Bahng and R. G. Macdonald
J. Phys. Chem. A **112**, 13432-13443 (2008).

Determination of the rate constants for the radical-radical reactions $NH_2(X^2B_1) + NH(^3\Sigma)$ and $NH_2(X^2B_1) + H(^2S)$ at 293 K.

-Mi-Kyung Bahng and R. G. Macdonald
J. Phys. Chem. A **113**, 2415-2423 (2009).

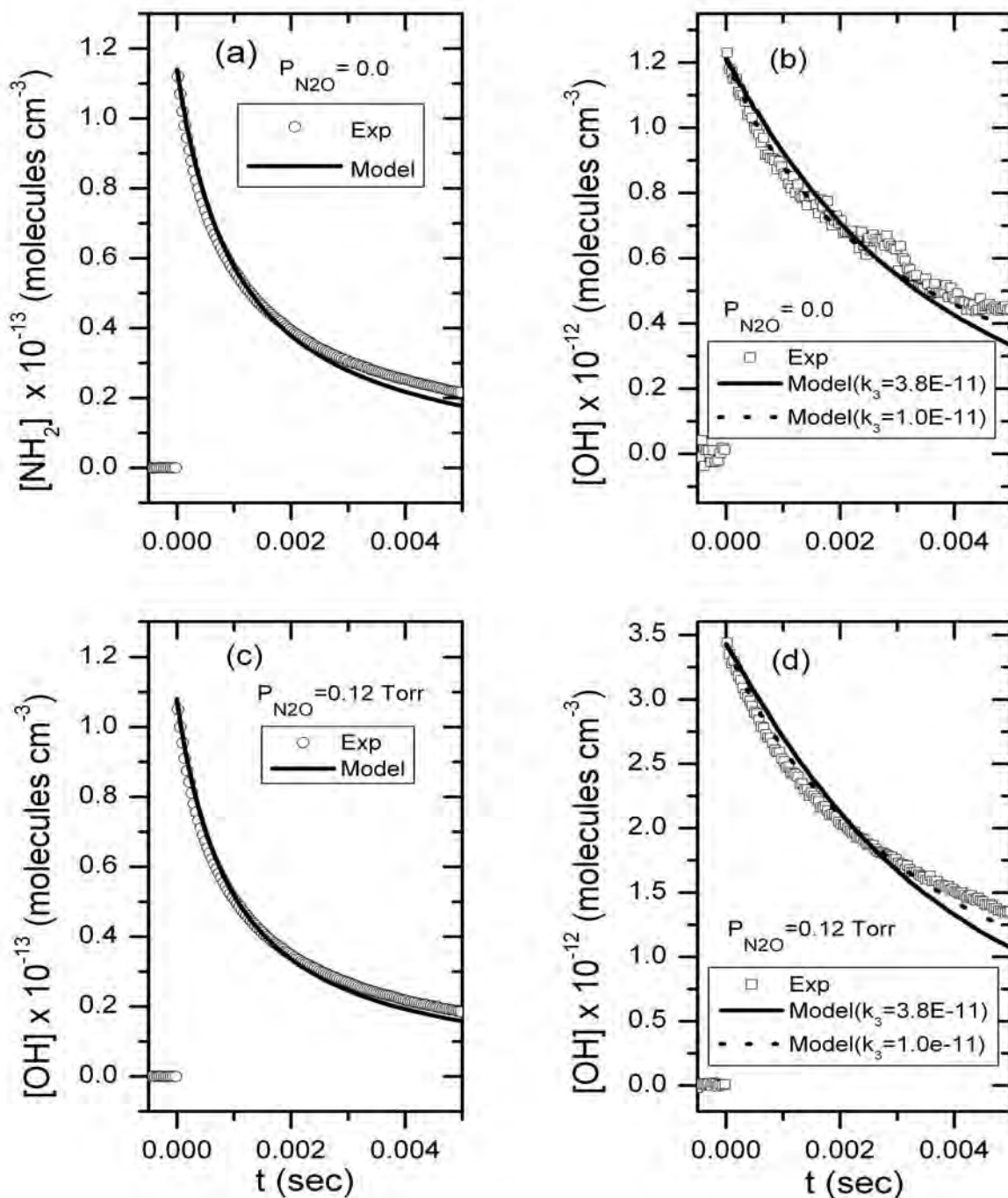


Fig. 1 Determination of k_1^{H2O} and k_{2C} under conditions which minimize $O(^3P)$ and NO formation. Panels a and b show NH_2 and OH temporal concentration profiles, respectively, where OH is produced only from H_2O photolysis. The model predictions are $k_1^{H2O} = 3.53 \times 10^{-11} \text{ cm}^3 \text{ molecules}^{-1} \text{ s}^{-1}$ and $k_{2C} = 1.53 \times 10^{-11} \text{ cm}^3 \text{ molecules}^{-1} \text{ s}^{-1}$ with $k_3 = 3.8 \times 10^{-11} \text{ cm}^3 \text{ molecules}^{-1} \text{ s}^{-1}$ (— solid curve). A much better fit gives $k_{2D} = 2.56 \times 10^{-11} \text{ cm}^3 \text{ molecules}^{-1} \text{ s}^{-1}$ if $k_3 = 1.0 \times 10^{-11} \text{ cm}^3 \text{ molecules}^{-1} \text{ s}^{-1}$ (- - - dashed curve). The conditions of the experiment: $P_{NH_3} = 3.86 \times 10^{-3}$ Torr, $P_{CF_4} = 0.392$ Torr, $P_{He} = 2.215$ Torr, and $P_{H_2O} = 4.52$ Torr. Panels c and d show the same except $P_{N_2O} = 0.12$ Torr has been added to increase the OH signal. The model predictions are $k_1^{H2O} = 4.08 \times 10^{-11} \text{ cm}^3 \text{ molecules}^{-1} \text{ s}^{-1}$, and $k_{2C} = 1.16 \times 10^{-11} \text{ cm}^3 \text{ molecules}^{-1} \text{ s}^{-1}$ with $k_3 = 3.8 \times 10^{-11} \text{ cm}^3 \text{ molecules}^{-1} \text{ s}^{-1}$ (— solid curve), and $k_{2D} = 2.02 \times 10^{-11} \text{ cm}^3 \text{ molecules}^{-1} \text{ s}^{-1}$ if $k_3 = 1.0 \times 10^{-11} \text{ cm}^3 \text{ molecules}^{-1} \text{ s}^{-1}$ (- - - dashed curve).

Theoretical studies of chemical reactions related to the formation and growth of polycyclic aromatic hydrocarbons and molecular properties of their key intermediates

Alexander M. Mebel

Department of Chemistry and Biochemistry, Florida International University
Miami, Florida 33199. E-mail: mebela@fiu.edu

Program Scope

We perform theoretical studies of the reactions of PAH formation and growth using ab initio molecular orbital and density functional calculations of potential energy surfaces (PES) and statistical (RRKM and TST) computations of absolute rate constants and relative product yields. In particular, we address the reactions of cyclopentadienyl radicals and cyclopentadiene involving the C₁₀H₁₁, C₁₀H₁₀, and C₁₀H₉ PES and producing naphthalene, azulene, fulvalene, and indene, and investigate the formation mechanisms of naphthalene and indene from smaller hydrocarbons, alternative to the HACA sequences. Our studies also include related chemical reactions under single-collision conditions, such as crossed molecular beam reactions of singlet and triplet C₂ with C₄H₆ isomers and C₆H₆ accessing previously unexplored regions of the C₆H₆ (benzene) and C₈H₆ (phenylacetylene) surfaces and the reactions of phenyl radical with C₃H₄, C₃H₆, and C₄H₆ occurring on the C₉H₉, C₉H₁₁, and C₁₀H₁₁ PES and directly linked to the indene, naphthalene, and azulene formation routes. The objective of these studies is to untangle elementary reaction mechanisms for these complex reactions and to predict their rate constants and product yields in a broad range of reaction conditions. In addition, we investigate molecular properties, potential energy surfaces, and dissociation mechanisms of hydrocarbon cations, which are relevant to the photoionization spectroscopy and mass spectrometry diagnostics of various products of elementary combustion reactions.

Recent Progress

Reactions of phenyl radical with C₄H₆ isomers. G3(MP2,CC)//B3LYP/6-311G** calculations were performed to investigate the potential energy surface and mechanism of the reaction of phenyl radical with 1,2-butadiene followed by kinetic RRKM-ME calculations of the reaction rate constants and product branching ratios at various temperatures and pressures. The results showed that the reaction can proceed by direct hydrogen abstraction producing benzene and C₄H₅ radicals or by addition of phenyl to different carbon atoms in CH₂CCHCH₃ followed by isomerizations of C₁₀H₁₁ adducts and their dissociation by H or CH₃ losses. The H abstraction channels were found to be kinetically preferable and to contribute 70-90% to the total product yield in the 300-3000 K temperature range, with the products including C₆H₆ + CH₂CHCCH₂ (~40%), C₆H₆ + CH₃CHCCH (5-31%), and C₆H₆ + CH₂CCCH₃ (24-20%). The phenyl addition channels were calculated to be responsible for 10-30% of the total product yield, with their contribution decreasing as the temperature increases. The products of the addition channels include collisionally stabilized C₁₀H₁₁ adducts, 1-phenyl-2-buten-2-yl, 1-methyl-3H-inden-2-yl, 3-phenyl-2-buten-2-yl, and 2-phenyl-2-buten-1-yl / 2-phenyl-1-buten-3-yl, which are favored under low temperature - high pressure conditions, as well as their dissociation products, indene + CH₃, 1-phenyl-propyne + CH₃, phenylallene + CH₃, and 2-phenyl-1,3-butadiene + H, preferred at higher temperatures. The maximal yield of indene, 7.5%, was found at 500 K and 7.6 Torr, however, at the temperatures relevant to combustion, its branching ratio does not exceed 1%.

Three-parameter modified Arrhenius expressions were generated for the total reaction rate constants and rate constants for the most important product channels, which can be utilized in future kinetic modeling of the formation mechanism of cyclopentafused polycyclic aromatic hydrocarbons.

The computed PES of the $C_6H_5 + 1,2$ -butadiene reaction and molecular and energetic parameters of its intermediates, transition states, and products were also used to interpret the results of crossed molecular beam experiments by Ralf Kaiser's group at the University of Hawaii within the DOE Combustion Research Program. Based on the combined experimental observations and theoretical data, the reaction, carried out under single collision at two collision energies of 109 ± 3 and 156 ± 5 kJmol^{-1} , was found to follow indirect scattering dynamics via an addition of the phenyl radical with its radical center to the sterically favorable C1 atom of the 1,2-butadiene reactant. Under the experimental conditions, the initial reaction intermediate decomposed via atomic hydrogen loss to form two $C_{10}H_{10}$ isomers, 1-phenyl-3-methylallene and 1-phenyl-butyne-2, via tight exit transition states. The failure to observe in crossed beams the CH_3 loss and direct H abstraction products predicted by the RRKM calculations may be explained by difficulties in experimental detection of C_6H_6/C_4H_5 fragments and possible deviations of the reaction system from the statistical behavior at the high collision energies used.

In a similar way, Kaiser's group studied the reactions of phenyl radical with 1-butyne and 2-butyne in a crossed molecular beams machine at collision energies of about 150 kJmol^{-1} . Combining the crossed beams data with our electronic structure calculations on the $C_6H_5 + HCCC_2H_5$ and $C_6H_5 + CH_3CCCH_3$ PESs, we found that both reactions involve indirect scattering dynamics and are initiated by additions of the phenyl radical with its radical center to the (sterically more accessible) acetylenic carbon atoms of the reactants. With respect to the formation of $C_{10}H_{10}$ isomers, the reaction intermediates fragmented through the ejection of hydrogen atoms yielding 1-phenyl-3-methylallene and 1-phenyl-1-butyne (both from 1-butyne) as well as 1-phenyl-1-methylallene (from 2-butyne); all decomposition pathways involved tight exit transition states. Meanwhile, we have studied theoretically all other possible pathways of the reactions of phenyl radical with 1- and 2-butyne. The initial adduct of the $C_6H_5 + 1$ -butyne reaction can lose not only a hydrogen atom but also the methyl group producing a C_9H_9 isomer phenylallene. The CH_3 loss channel is energetically preferable as compared to the H elimination pathways; according to our RRKM calculations, the branching ratios are 11.8 : 4.9 : 83.3 for the formation of 1-phenyl-1-butyne, 1-phenyl-3-methylallene, and phenylallene, respectively, at the collision energy of 150 kJ mol^{-1} . Phenyl radical can also add to the second acetylenic carbon in 1-butyne linked to the C_2H_5 moiety producing another initial intermediate, which in turn can decompose to phenylacetylene + C_2H_5 . Besides the addition channels, the reaction can also proceed by direct H abstractions by the phenyl radical from C_4H_6 producing benzene in conjunction with C_4H_5 isomers, CH_3CHCCH , CH_2CH_2CCH , or CH_3CH_2CC products. The initial intermediate formed in the $C_6H_5 + 2$ -butyne reaction can lose the CH_3 group attached to the C atom also linked to the phenyl moiety to form 1-phenyl-2-methylacetylene. RRKM calculations suggested that the CH_3 pathway dominates with a fraction above 99%. Also, one direct H abstraction channel is possible leading to $C_6H_6 + CH_2CCCH_3$. Statistical theories, such as TS and RRKM-ME, can be applied to compute temperature and pressure dependent reaction rate constants and relative product yields of the C_6H_5 reaction with 1- and 2-butyne at thermal conditions relevant to combustion and this will be a subject of our future theoretical work. The electronic structure calculations predicted a greater variety of products in the reactions of phenyl radical with 1- and 2-butyne than the $C_{10}H_{10}$ isomers detected in the crossed molecular beams

study. As for $C_6H_5 + 1,2\text{-butadiene}$, this deviation may be attributed to several factors, such as possible non-statistical behavior of the reactions at the high collision energy of 150 kJ mol^{-1} and experimental difficulties in detection of product pairs containing heavier fragments (CH_3 , C_2H_5 , C_4H_5).

Formation of the phenyl radical under single collision conditions in the reaction of C_2 with 1,3-butadiene. Reactions of C_2 with C_4H_6 isomers such as 1,3-butadiene represent a potential route to synthesize the first aromatic C_6 ring in hydrocarbon flames where concentrations of dicarbon transient species are significant. Ralf Kaiser's group conducted crossed molecular beams experiments of dicarbon molecules in their $X^1\Sigma_g^+$ electronic ground state and in the first electronically excited $a^3\Pi_u$ state with 1,3-butadiene and two partially deuterated counterparts (1,1,4,4-D4-1,3-butadiene and 2,3-D2-1,3-butadiene) at two collision energies of 12.7 and 33.7 kJ mol^{-1} . These scattering experiments were combined with our electronic structure and RRKM calculations on the singlet and triplet C_6H_6 surfaces and our joint experimental/theoretical investigation revealed that the aromatic phenyl radical is formed predominantly on the triplet surface via indirect scattering dynamics through a long-lived reaction intermediate. Initiated by a barrierless addition of triplet dicarbon to one of the terminal carbon atoms of 1,3-butadiene, the collision complex undergoes trans-cis isomerization followed by ring closure and hydrogen migration prior to hydrogen atom elimination, ultimately forming the phenyl radical. On the singlet surface, smaller contributions of phenyl radical could not be excluded; experiments with partially deuterated 1,3-butadiene indicated the formation of the thermodynamically less stable acyclic $H_2CCHCCCCH_2$ isomer. This study presented the very first experimental evidence, contemplated by theoretical studies, that under single collision conditions an aromatic hydrocarbon molecule can be formed in a bimolecular gas-phase reaction via reaction of two acyclic molecules involving cyclization processes at collision energies highly relevant to combustion flames. Based on the results of our RRKM calculations, on the triplet surface, phenyl is almost the exclusive reaction product with fractions of 98-99%, whereas on the singlet surface, the computed product distribution included 32-21% of phenyl + H, 34-35% of propargyl + propargyl, and 34-44% of various acyclic C_6H_5 isomers + H.

Ionization potential of C_4H_3 radicals. Ralf Kaiser and Musahid Ahmed investigated the ionization potentials of resonantly stabilized C_4H_3 radicals utilizing laser ablation of graphite in combination with seeding the ablated species in neat methylacetylene gas, which also played a role of a reagent. Photoionization efficiency (PIE) curves were recorded of photoionized isomers at the Advanced Light Source. To assist in the interpretation and assignment of these experimental measurements, our group conducted highly accurate CCSD(T)/CBS calculations of vertical and adiabatic ionization energies of various C_4H_3 isomers and Franck-Condon factors for their ionization processes. The fit of the experimental PIE curve using the computed ionization potentials and Franck-Condon factors suggested the formation of four C_4H_3 radicals: two acyclic structures i- C_4H_3 and E/Z-n- C_4H_3 and two cyclic isomers. This study provided a novel interpretation of previous data on C_4H_3 radicals in hydrocarbon flames.

Future Plans

Our immediate focus will be on RRKM-ME calculations of temperature and pressure dependent rate constants and product branching ratios for which our studies of PESs are now complete. This will include the $C_5H_5 + C_5H_5 \rightarrow C_{10}H_{10} \rightarrow C_{10}H_9 + H$ and $C_5H_5 + C_5H_6 \rightarrow C_{10}H_{11} \rightarrow C_9H_8 + CH_3 / C_{10}H_{10} + H$ reactions, unimolecular decomposition of 9-H-fulvalenyl radical, reactions of phenyl radical with 1- and 2-butyne, and $C_6H_5 + O_2$. Meanwhile,

we will continue theoretical calculations of PESs in our systematic survey of chemical reactions potentially leading to the formation of indene and/or naphthalene in combustion flames, including reactions of cyclopentadienyl radical with $2\text{C}_2\text{H}_2$ and C_4H_4 , phenyl radical with C_3H_6 , C_4H_2 , and C_4H_4 as well as oxidation of C_5H_5 , unimolecular decomposition of pyranyl, and C_{10}H_7 (naphthyl radical) + O_2 , with the eventual goal to predict their absolute rate constants and product branching ratios under combustion conditions.

DOE/BES sponsored publications (2008-2010)

1. Kislov V.V., Mebel A.M., “An ab initio G3-type / statistical theory study of the formation of indene in combustion flames. II. The pathways originated from reactions of cyclic C_5 species - cyclopentadiene and cyclopentadienyl radical”, *J. Phys. Chem. A*, 112, 700-716 (2008).
2. Gu X., Kaiser R.I., Mebel A.M., “Chemistry of energetically activated cumulenes – from allene (H_2CCCH_2) to hexapentaene ($\text{H}_2\text{CCCCCCH}_2$)”, *ChemPhysChem*, 9, 350-369 (2008).
3. Wang Q., Wu D., Jin M., Liu F., Hu F., Cheng X., Liu H., Hu Z., Ding D., Mineo H., Dyakov Y.A., Mebel A.M., Chao S.D., Lin S.H., “Experimental and theoretical investigation of ionization / dissociation of cyclopentanone molecule in a femtosecond laser field”, *J. Chem. Phys.*, 2008, 129, 204302 (15 pp.).
4. Mebel A.M., Bandrauk A.D., “Theoretical study of unimolecular decomposition of allene cations”, *J. Chem. Phys.*, 2008, 129, 224311 (12 pp.).
5. Gu X., Zhang F., Kaiser R.I., Kislov V.V., Mebel A.M., “Reaction dynamics of the phenyl radical with 1,2-butadiene”, *Chem. Phys. Lett.*, 2009, 474, 51-56.
6. Mebel A.M., Kislov V.V., “Can the $\text{C}_5\text{H}_5 + \text{C}_5\text{H}_5 \rightarrow \text{C}_{10}\text{H}_{10} \rightarrow \text{C}_{10}\text{H}_9 + \text{H} / \text{C}_{10}\text{H}_8 + \text{H}_2$ reaction produce naphthalene? An ab initio/RRKM study”, *J. Phys. Chem. A*, 2009, 113, 9825-9833.
7. Zhou W., Mebel A.M., Li X.-Y., “An ab initio/Rice-Ramsperger-Kassel-Marcus study of the reactions of propenols with OH. Mechanism and Kinetics”, *J. Phys. Chem. A*, 2009, 113, 10667-10677.
8. Kaiser R.I., Zhang F., Gu X., Kislov V.V., Mebel A.M., “Reaction dynamics of the phenyl radical (C_6H_5) with 1-butyne (HCCC_2H_5) and 2-butyne (CH_3CCCH_3)”, *Chem. Phys. Lett.*, 2009, 481, 46-53.
9. Kaiser R.I., Mebel A.M., Kostko O., Ahmed M., “On the Ionization Energies of C_4H_3 Isomers”, *Chem. Phys. Lett.*, 2010, 485, 281-285.
10. Zhang F., Jones B., Maksyutenko P., Kaiser R.I., Chin C., Kislov V.V., Mebel A.M., “Formation of the Phenyl Radical [$\text{C}_6\text{H}_5(\text{X}^2\text{A}_1)$] under Single Collision Conditions – A Crossed Molecular Beam and Ab Initio Study”, *J. Am. Chem. Soc.*, 2010, 132, 2672-2683.
11. Kislov V.V., Mebel A.M., “Ab Initio/RRKM-ME Study on the Mechanism and Kinetics of the Reaction of Phenyl Radical with 1,2-Butadiene”, *J. Phys. Chem. A*, submitted.
12. Kislov V.V., Xu Z.F., Lin M.C., Mebel A.M., “Variational calculations of thermal rate constants and relative product yields for the $\text{C}_6\text{H}_5 + \text{O}_2$ association reaction”, *Proc. Combust. Inst.*, submitted.

FLASH PHOTOLYSIS-SHOCK TUBE STUDIES

Joe V. Michael

Chemical Dynamics Group, Chemical Sciences & Engineering Division
Argonne National Laboratory, Argonne, IL 60439
E-mail: jmmichael@anl.gov

The scope of the program is to measure high-temperature thermal rate constants for use in high-temperature combustion with the reflected shock tube technique. We have adapted the OH multi-pass optical system¹⁻⁴ to detect CH₃ radicals at 214 nm and continued Atomic Resonance Absorption Spectrometry (ARAS) studies for detecting H- and/or D-atoms.⁵⁻⁷

During the past year, the reflected shock tube technique has been used to study the thermal decompositions of CH₃I and C₃H₈ using a Zn resonance lamp and a 12-pass optical system for detecting CH₃-radical absorption at 214 nm. H- and D- atoms were measured in two sets of studies, one aimed at characterizing contributions to the roaming mechanism under thermal conditions and the other used to study the thermal decompositions of single-ring aromatics.

CH₃ Multi-Pass Absorption

Similar to our prior OH-radical absorption studies using a multi-pass cell, the CH₃-radical electronic absorption band at ~205 to 220 nm⁸ was used in a white-cell configuration to detect CH₃. Specifically, absorption from a radio frequency driven continuous wave Zn lamp (Imaging and Sensing Technology, with a strong resonance line at 214 nm) was used in the present application. The White cell was constructed from two flat fused silica windows (3.81 cm) mounted on the tube across from one another that were coated so as to have near zero reflectance at 214 nm. The split and notched mirrors were externally mounted and with this white cell configuration, up to 24 multiple passes could be obtained, but the resulting signal was weak. We therefore used just 12 multiple passes for the kinetics studies on the thermal decomposition of CH₃I and C₃H₈.

The thermal decomposition of CH₃I, CH₃I + M → CH₃ + I + M, is a well characterized reaction, and, at high temperatures (>1200 K), the rate constant is expected to be at its low pressure limit (at P < 1 atm). A recent high temperature study by Yang et al.,⁹ using laser schlieren densitometry, reports rate constants in reasonable agreement with previous I-atom ARAS studies from our laboratory by Kumaran et al.¹⁰ and by Takahashi et al.¹¹ The present experiments that span a T-range, 1137-1440 K are in good agreement with the prior I-atom ARAS studies of Kumaran et al.¹⁰ and Takahashi et al.¹¹ thereby providing a cross-check on the CH₃ multi-pass detection system and verifying the absorption cross section used.

The 12-pass CH₃ detection system has also been used to probe the dissociation of propane, C₃H₈ → CH₃ + C₂H₅. Experiments were performed at three reflected shock densities ~ 2, 3, and 6 x 10¹⁸ molecules cm⁻³ over the T-range 1202-1543 K. The CH₃-absorption diagnostic allows dissociation experiments to be performed at lower-T and in combination with the data obtained using the H-ARAS technique an extensive set of measurements that span 1202-1819 K is obtained in the present work. The data are in good agreement with the higher temperature laser-schlieren studies of Al-Alami and Kiefer¹² and the more recent CH₃ Laser absorption studies of Oehlschlaeger et al.¹³

Roaming Radical Mechanisms in Thermal Systems

The dissociation of a molecule by simple bond cleavage generally leads to two radical fragments. However, as the radicals separate they can roam, sampling large volumes of orientation space. This roaming occurs at large radical-radical separations ($> 3 \text{ \AA}$). During this roaming, the radicals may sample orientations where there is a barrierless path leading to the abstraction of a radical from one radical to the other and thereby forming two stable molecules. Most commonly, this abstraction involves the transfer of an H atom from one radical to another.^{14,15} An example for this roaming process occurs in acetaldehyde, CH_3CHO .^{16,17} Acetaldehyde undergoes C-C bond fission giving CH_3 and HCO . However, with a roaming mechanism, the CH_3 can abstract the H atom in HCO thereby yielding two stable molecular products CH_4 and CO . In order to unambiguously determine the branching ratios leading to roaming products, we have performed thermal experiments on a series of molecules under high temperature conditions with the ANL flash photolysis shock tube. The high sensitivity H-atom ARAS detection technique used with the shock tube provides an excellent diagnostic for quantitative measurements of the roaming fraction. Figure 1 depicts the branching ratios measured for the roaming channel in CH_3CHO . Experiments have also been performed on propane, neo-pentane and iso-butane at high temperatures (1200 – 1800 K). The roaming mechanism contributes only 10% to the total dissociation flux in propane. However larger contributions have been observed in neo-pentane and iso-butane with the roaming channel contributing $\sim 22\text{-}25\%$.

Thermal Decompositions of Aromatics

The combustion chemistry of mono and di-alkyl substituted aromatics such as toluene and the xylenes are poorly understood because of a lack of consensus on the rate constants for the primary dissociation channels¹⁸ and mechanistic pathways for the primary radicals produced from these channels, i. e. the benzyl^{19,20} and xylyl radicals.²¹ Experiments using the H- and D-atom ARAS diagnostic with the completely protonated and partially deuterated species have offered some insights on the contributions of potential decomposition pathways suggested by theory.

The thermal decompositions of benzyl ($\text{C}_6\text{H}_5\text{CH}_2$) and benzyl, α,α -d₂ ($\text{C}_6\text{H}_5\text{CD}_2$) (using bromides as a source of benzyls) have been studied at high temperatures with the reflected shock tube technique using H- and D-atom ARAS. The experiments were performed at high-T (1437-1801 K) at nominal pressures $\approx 0.3\text{-}1.3 \text{ atm}$. The present experiments utilizing the ultra-sensitive H- and D-atom ARAS technique reveal that there are three unique channels that contribute to benzyl decomposition: H-atom removal from the ring, H/D-atom removal from the side-chain, and a non-atom producing process (postulated to be cyclopentadienyl + acetylene). The rate constants for the three channels can be represented by,

$$\begin{aligned}k_{\text{H,ring}} &= 1.14 \times 10^{12} \exp(-32180 \text{ K/T}) && (1475\text{-}1801 \text{ K}) \\k_{\text{H/D,side-chain}} &= 4.50 \times 10^{13} \exp(-40650 \text{ K/T}) && (1487\text{-}1789 \text{ K}) \\k_{\text{non-atom}} &= 1.55 \times 10^9 \exp(-23470 \text{ K/T}) && (1437\text{-}1627 \text{ K})\end{aligned}$$

The present study gives reliable determinations of rate constants for the three channels that, when coupled with the postulated mechanistic interpretations for these processes, should be useful in future theoretical and experimental characterizations of benzyl decomposition.

The thermal decomposition of toluene-d₅ (C₆D₅CH₃) has also been studied at high temperatures with the reflected shock tube technique using H- and D-atom ARAS. The experiments were performed at high-T (1469-1859 K) and nominal pressures ≈ 0.25-1.50 atm. The isotope effect is minimal, and since our prior benzyl decomposition study confirms that the major benzyl decay channel is ring H-atom removal, the present H-ARAS results therefore represent direct measurements of branching ratios and rate constants for toluene decomposition. The branching ratios to benzyl + H vary from ≈ 0.9 at lower-T (<1600 K) to ≈ 0.75 at higher-T (>1700 K). The excellent agreement between the present experiments and the theoretical predictions by Klippenstein et al. (Fig. 2) lead us to conclude that the thermal decomposition of toluene is now well-characterized.

We also have completed work on determining contributions to the roaming mechanism in dimethyl ether (DME) and obtaining rate constants for H + DME. We are planning thermal decomposition studies using H/D/Br-atom ARAS on the xylylbromides.

This work was supported by the U. S. Department of Energy, Office of Basic Energy Sciences, Division of Chemical Sciences, Geosciences, and Biosciences, under Contract No. DE-AC02-06CH11357.

References

1. Srinivasan, N. K.; Su, M.-C.; Sutherland, J. W.; Michael, J. V. *J. Phys. Chem. A* **2005**, *109*, 1857.
2. Su, M.-C.; Kumaran, S. S.; Lim, K. P.; Michael, J. V. *Rev. Sci. Inst.* **1995**, *66*, 4649.
3. Su, M.-C.; Kumaran, S. S.; Lim, K. P.; Michael, J. V.; Wagner, A. F.; Dixon, D. A.; Kiefer, J. H.; DiFelice, J. *J. Phys. Chem.* **1996**, *100*, 15827.
4. Su, M.-C.; Kumaran, S. S.; Lim, K. P.; Michael, J. V.; Wagner, A. F.; Harding, L. B.; Fang, D.-C. *J. Phys. Chem. A* **2002**, *106*, 8261.
5. S. L. Mielke, K. A. Peterson, D. W. Schwenke, B. C. Garrett, D. G. Truhlar, J. V. Michael, M.-C. Su, and J. W. Sutherland, *Phys. Rev. Lett.* **2003**, *91*, 063201.
6. J. V. Michael, M.-C. Su, and J. W. Sutherland, *J. Phys. Chem. A* **2004**, *108*, 432.
7. J. V. Michael, M.-C. Su, J. W. Sutherland, L. B. Harding, and A. F. Wagner, *Proc. Combust. Inst.* **2004**, *30*, 965.
8. D. F. Davidson, A. Y. Chang, M. D. Di Rosa, R. K. Hanson, *J. Quant. Spectrosc. Radiat. Transfer* **1993**, *49*, 559.
9. X. Yang, C. F. Goldsmith, R. S. Tranter, *J. Phys. Chem. A* **2009**, *113*, 8307.
10. S. S. Kumaran, M.-C. Su, and J. V. Michael, *Int. J. Chem. Kinet.* **1997**, *29*, 535.
11. K. Takahashi, A. Inoue, T. Inomata, *In Shock Waves Proceedings of the 20th International Symposium on Shock Waves*, Pasadena, USA, July 1995. Sturtevant, B., Shepard, J. E., Hornung, H. G., Eds.; World Scientific Publishing Co. Pte. Ltd.: Singapore, 1996; pp 959-964.
12. M. Z. Al-Alami and J. H. Kiefer, *J. Phys. Chem.* **1983**, *87*, 499.
13. M. A. Oehlschlaeger, D. F. Davidson and R. K. Hanson, *Proc. Comb. Inst.* **2005**, *30*, 1119.
14. D. Townsend, S. A. Lahankar, S. K. Lee, S. D. Chambreau, A. G. Suits, X. Zhang, J. Rheinecker, L. B. Harding, J. M. Bowman, *Science*, **2004**, *306*, 1158-1161.
15. P. L. Houston and S. H. Kable, *Proc. Nat. Acad. Sci.*, **2006**, *103*, 16079-16082.
16. R. Sivaramakrishnan, J. V. Michael and S. J. Klippenstein, *J. Phys. Chem. A* **2010**, *114*, 755.
17. L. B. Harding, Y. Georgievskii and S. J. Klippenstein, *J. Phys. Chem. A* **2010**, *114*, 765.
18. S. J. Klippenstein, L. B. Harding and Y. Georgievskii, *Proc. Combust. Inst.* **2007**, *31*, 221.
19. C. Cavallotti, M. Derudi and R. Rota, *Proc. Combust. Inst.* **2009**, *32*, 115.
20. G. DaSilva, J. A. Cole and J. W. Bozzelli, *J. Phys. Chem. A* **2009**, *113*, 6111.
21. G. DaSilva, E. E. Moore and J. W. Bozzelli, *J. Phys. Chem. A* **2009**, *113*, 10264.

PUBLICATIONS FROM DOE SPONSORED WORK FROM 2008-2010

- *Thermal Decomposition of CF₃ and the Reaction of CF₂ + OH → CF₂ + H*, N. K. Srinivasan, M.-C. Su, J. V. Michael, S. J. Klippenstein, and L. B. Harding, *J. Phys. Chem. A* **112**, 31 (2008).

- *High Temperature Rate Constants for OH + Alkanes*, R. Sivaramakrishnan, N. K. Srinivasan, M.-C. Su, and J. V. Michael, Proc. Combust. Inst. **32**, 107 (2009).
- *Shock Tube Measurements of High Temperature Rate Constants for OH with Cyclo-alkanes and Methyl-cycloalkanes*, R. Sivaramakrishnan and J. V. Michael, Combust. and Flame, **156**, 1126 (2009).
- *Rate Constants for OH with Selected Large Alkanes; Shock-Tube Measurements and An Improved Group Scheme*, R. Sivaramakrishnan and J. V. Michael, J. Phys. Chem. A **113**, 5047 (2009).
- *The Thermal Decomposition of NH₂OH and Subsequent Reactions: Ab initio Transition State Theory and Reflected Shock Tube Experiments*, S. J. Klippenstein, L. B. Harding, B. Ruscic, N. K. Srinivasan, R. Sivaramakrishnan, M.-C. Su, and J. V. Michael, J. Phys. Chem. A, **113**, 10241 (2009).
- *The Direct Observation of Roaming Radicals in the Thermal Decomposition of Acetaldehyde*, R. Sivaramakrishnan, J. V. Michael, and S. J. Klippenstein, J. Phys. Chem. A, **114**, 755 (2010).
- *H- and D-atom formation from the Pyrolysis of C₆H₅CH₂Br and C₆H₅CD₂Br: Implications for High-temperature Benzyl Decomposition*, R. Sivaramakrishnan, M.-C. Su, and J. V. Michael, In Review, Proc. Combust. Inst. (2010).
- *Pyrolysis of C₆D₅CH₃: Rate Constants and Branching Ratios in the High Temperature Thermal Decomposition of Toluene*, R. Sivaramakrishnan, and J. V. Michael, In Review, Proc. Combust. Inst. (2010).
- *Reflected Shock Tube and Theoretical Studies on the Thermal Decomposition of C₂H₅OH and OH + C₂H₅OH → Products*, R. Sivaramakrishnan, M.-C. Su, J. V. Michael, S. J. Klippenstein, and L. B. Harding, J. Phys. Chem. A, In Preparation (2010).
- *Shock Tube and Theoretical Studies on the Thermal Decomposition of Propane: Evidence for Roaming Radical Mechanisms in Alkanes*, R. Sivaramakrishnan, M.-C. Su, J. V. Michael, S. J. Klippenstein, L. B. Harding, J. Phys. Chem. A, In Preparation (2010).
- *Roaming Radical Mechanisms in the Thermal Decompositions of Alkanes: Isobutane and neo-pentane*, R. Sivaramakrishnan, J. V. Michael, S. J. Klippenstein, L. B. Harding, J. Phys. Chem. A, In Preparation (2010).

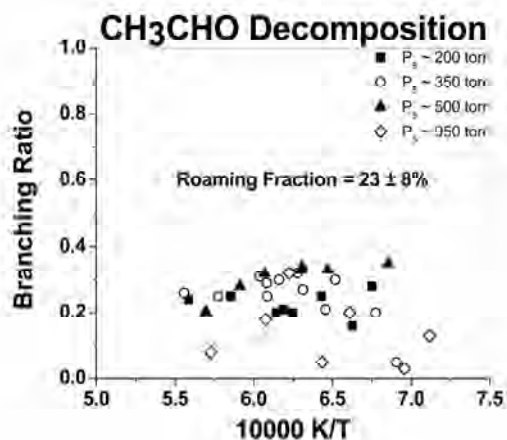


Fig. 1. Branching ratios for the roaming mechanism in CH₃CHO decomposition, CH₃CHO → CH₄ + CO.

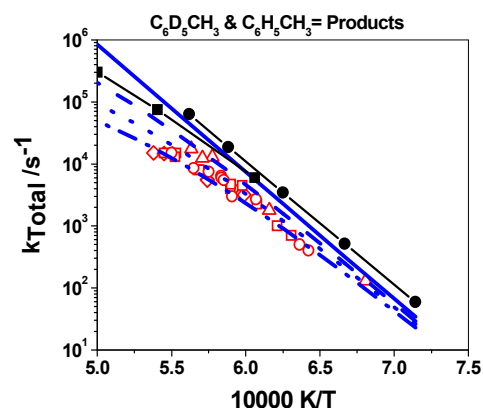


Fig. 2. Arrhenius plot for k_{Total} . Red open symbols – Data from present work (0.25 -1.5 atm). [---] – $P = 0.1$ atm; [***] – $P = 0.3$ atm; [—] – $P = 1.5$ atm; [—] – $P = \infty$; lines are predictions of Klippenstein et al., [●—●] – $P = 1.5$ atm, Oehlschlaeger et al., [■—■] – $P = 1.5$ atm, Eng. et al.

Particle Diagnostics Development

H. A. Michelsen

Sandia National Labs, MS 9055, P. O. Box 969, Livermore, CA 94551

hamiche@sandia.gov

I. Program Scope

Combustion processes often produce solid carbon particles, i.e., soot. These particles may be oxidized to form gas-phase species or released into the exhaust stream, where they can be coated with liquid coatings. These coatings can be comprised of any of a number of components, including unburned fuel, lube oil, sulfuric acid, water, and other combustion by-products.^{1,2} The research program described here focuses on the development of optical diagnostics for soot particles in combustion environments and combustion exhaust plumes. The goal of this work is *in situ* measurements of volume fraction, size, composition, and morphology of combustion-generated particles with fast time response and high sensitivity. Measurement techniques are targeted for studies of soot formation and evolution and must be versatile enough to probe particles throughout their entire life cycle. Techniques are being developed for detection and characterization of particles in combustion environments from incipient particles that are 2-20 nm in diameter and composed of condensed large organic species to mature soot particles composed of aggregates of carbonaceous primary particles resembling polycrystalline graphite. Diagnostics are also being developed for characterization of inhomogeneous exhaust particles.

II. Recent Progress

Our work has focused on developing a detailed understanding of the chemical and physical mechanisms that influence the applicability of laser-based techniques for soot detection under a wide range of conditions. In recent work, for instance, we have investigated the optical properties of soot in a flame. Using a combination of laser-induced incandescence (LII), extinction, and particle temperature measurements from spectrally- and temporally-resolved radiative emission, we have studied the wavelength and temperature dependence of the scattering and absorption cross sections of soot. We have used these results in a model that describes the energy- and mass-balance equations for laser-heated soot and compared the model predictions of time-resolved incandescence signals and particle temperatures to observed LII and temperature temporal profiles.

A. Soot optical properties

Quantitative information about soot scattering and absorption cross sections is critically important for developing optical measurement techniques for soot particles. The accuracy of these parameters determines the reliability of techniques, such as extinction, scattering, laser-induced incandescence, optical pyrometry, and photoacoustic methods. Because these techniques are often used under a variety of conditions, from high-temperature combustors to low-temperature atmospheric conditions with probe wavelengths ranging from X-rays to the infrared, accurate optical measurements also require a firm understanding of the wavelength and temperature dependence of scattering and absorption cross sections. Large uncertainties plague measured optical parameters, however, largely because such measurements and their interpretation are complicated by the non-spherical morphology of soot, the variability of its fine structure and composition as it ages, and the wide range of conditions under which measurement techniques have been implemented. In order to address some of the questions associated with soot optical parameters, we have coupled several techniques to investigate particle absorption and scattering properties.³ To gain information about the wavelength dependence of the emissivity of soot, we have used LII to measure the relative absorption cross section at 532 and 1064 nm of hot, uncoated soot produced in a laminar diffusion flame. Combining this information with measurements of the transmittance at 532 and 1064 nm provides information about the scattering cross section.

The absorption cross section for a particle in the Rayleigh regime (i.e., $\pi D|m| \ll \lambda$, where D is the particle size, m is the refractive index, and λ is the absorption wavelength) is generally expressed as

$$\sigma_{abs} = \frac{\pi^2 D^3 E(m)}{\lambda} . \quad (1)$$

Central to this expression is the dimensionless refractive-index function for absorption, which is given by

$$E(m) = -\text{Im}\left(\frac{m^2 - 1}{m^2 + 2}\right) = \frac{6nk}{(n^2 - k^2 + 2)^2 + 4n^2k^2} \quad (2)$$

for a complex index of refraction of $m=n-ki$. When the refractive index is wavelength independent, $E(m)$ is constant with respect to wavelength. Several studies have suggested, however, that the wavelength dependence of σ_{abs} deviates from the $1/\lambda$ -dependence given in Eq. (1), implying that $E(m)$ is wavelength dependent.⁴⁻⁸ Results of some of these studies are shown in Fig. 1 and demonstrate that uncertainty surrounds even the sign of the slope of the wavelength dependence of $E(m)$ for uncoated soot. These differences lead to uncertainties as large as 500 K for temperatures of soot inferred by optical pyrometry.⁹

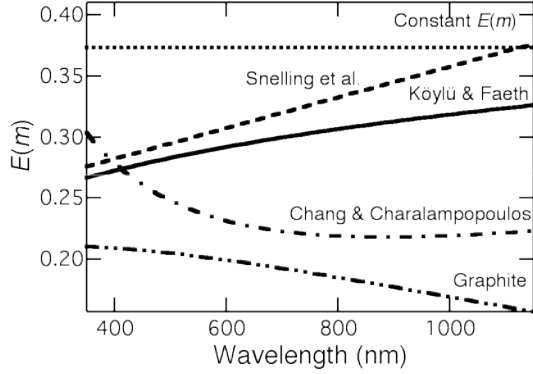


Figure 1. Wavelength dependence of the refractive-index function. The refractive-index function is calculated using Eq. (2) with a value of the index of refraction from Williams et al.,⁵ Chang and Charalampopoulos,⁶ or Michelsen⁴ for graphite. Values are also shown using equations based on the work of Köylü and Faeth⁷ and Snelling et al.⁸

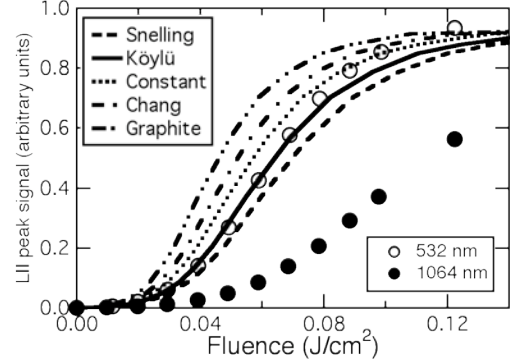


Figure 2. Fluence dependence of the peak LII signal. The peak of the LII temporal profile is shown as a function of fluence for laser wavelengths of 532 and 1064 nm (symbols). The lines represent values measured at 1064 nm plotted against an equivalent fluence given by Eq. (3) using the ratios for $E(m)$ derived from Fig. 1. Error bars are smaller than the size of the symbols.

Figure 2 shows the peaks of the LII temporal profiles from hot, uncoated soot at 532 and 1064 nm as a function of laser fluence. The lines on the figure show the 1064-nm data plotted against the 1064-nm laser fluence $F(1064)$ modified by the relative absorption cross section for the two wavelengths, i.e.,

$$F'(1064) = F(1064) \left(\frac{532}{1064} \right) \left[\frac{E(m)_{1064}}{E(m)_{532}} \right]. \quad (3)$$

The result should reproduce the 532-nm data at fluences below 0.08 J/cm². The only wavelength dependence that reproduces the data within experimental error is the relationship from Köylü and Faeth.⁷

Knowing the wavelength dependence of the absorption cross section, the transmittance measured at both wavelengths can provide information about the scattering cross section. The single-scattering albedo is defined as the ratio of the total scattering cross section to the sum of the scattering and absorption cross sections (i.e., the extinction cross section) at a specific wavelength λ_2 , i.e.,

$$\omega_{\lambda_2} = \frac{\sigma_{scat}^{agg}(\lambda_2)}{\sigma_{scat}^{agg}(\lambda_2) + \sigma_{abs}^{agg}(\lambda_2)}. \quad (4)$$

where σ_{scat}^{agg} is the total scattering cross section of a soot aggregate, and σ_{abs}^{agg} is the absorption cross section of the aggregate. The single-scattering albedo at λ_2 can be derived from the measurements of the transmittance at λ_2 (T_{λ_2}) relative to the transmittance at another wavelength λ_1 (T_{λ_1}) according to³

$$\omega_{\lambda_2} = \left[\frac{\ln(T_{\lambda_1})}{\ln(T_{\lambda_2})} - \frac{\lambda_2 E(m)_{\lambda_1}}{\lambda_1 E(m)_{\lambda_2}} \right] \left[\left(\frac{\lambda_2}{\lambda_1} \right)^4 \Gamma_{RDG} - \frac{\lambda_2 E(m)_{\lambda_1}}{\lambda_1 E(m)_{\lambda_2}} \right]^{-1}. \quad (5)$$

where Γ_{RDG} accounts for the Rayleigh-Debye-Gans correction to the Mie scattering cross section for a fractal aggregate of a given fractal dimension and radius of gyration.³ Assuming a constant concentration of particles C_{agg} across the sample path length l , the concentration-weighted aggregate absorption cross section at λ_2 can be expressed as

$$\sigma_{abs}^{agg} C_{agg} l = -\ln(T_{\lambda_2}) (1 - \omega_{\lambda_2}). \quad (6)$$

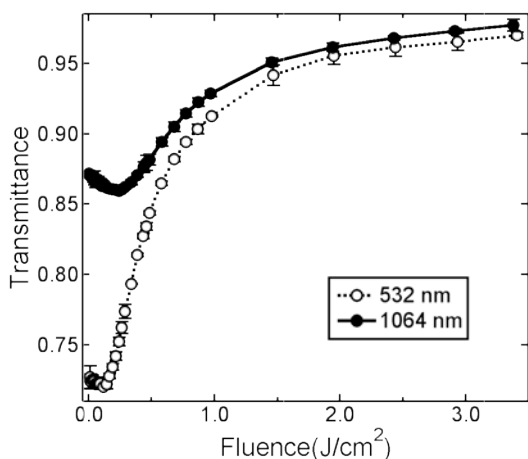


Figure 3. Fluence dependence of the flame transmittance. The symbols represent the measured values. The error bars represent 1σ standard deviation about the mean of 3-6 measured values.

Figure 3 shows the measured transmittance, and Fig. 4 shows the inferred concentration-weighted absorption cross section at 532 and 1064 nm as a function of fluence. These results suggest that the absorption cross section increases with increasing fluence. Using fluence-dependent temperature temporal profiles, we have estimated the increase in absorption cross section expected for an increase in particle size as the density decreases with increasing temperature. The values inferred from the data lie in between values predicted based on thermal expansion coefficients measured for polycrystalline graphite¹⁰ and perpendicular to the basal plane of single-crystal graphite¹¹ and are consistent with the swelling of the particle with increasing temperature. Figure 4 also shows results for a fit to the 532- and 1064-nm cross sections simultaneously using the thermal expansion coefficient as an adjustable parameter. The fits were performed for fluences $\leq 0.1 \text{ J/cm}^2$ at 532 nm and $\leq 0.2 \text{ J/cm}^2$ at 1064 nm and extrapolated to higher fluences in the figure.

III. Future Work

Current work builds on these results and extends them to combustion-generated particles with inorganic and organic coatings representative of particles found in exhaust plumes. In order to simulate exhaust-plume particulates, we have modified our flow-tube system to allow controlled deposition of a coating with low volatility on flame-generated soot. The thickness of the coating can be varied, and the particles collected for analysis by transmission electron microscopy (TEM) and near-edge X-ray absorption fine structure (NEXAFS) spectroscopy. Coatings investigated to date have been selected for diagnostic development for diesel exhaust and include sulfuric acid, heptamethylnonane, and oleic acid. These experiments are currently limited by our inability to determine the mass loading of particle coatings. Developing an understanding of the cause and magnitude of the effects of coatings will require characterization of the particle coatings. Coating the particles increases the mean aggregate size as measured by a scanning mobility particle sizer (SMPS), but measurements of mobility diameter provided by the SMPS do not provide a quantitative measure of the volatile coating fraction either by volume or by mass. In order to measure the volatile fraction, we will build a chamber that includes a temperature-controlled oscillating crystal microbalance for differential mass measurements on coated and evaporatively dried particles.

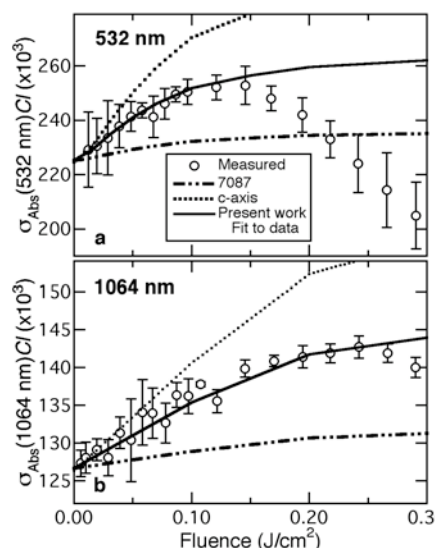


Figure 4. Fluence dependence of the absorption cross section. Concentration-weighted absorption cross sections are shown for (a) 532 nm and (b) 1064 nm. The symbols were derived using Eq. (6). The lines show predictions based on values of the thermal-expansion coefficient for polycrystalline graphite (7087)¹⁰ and for expansion along the c-axis of single-crystal graphite.¹¹ Results are also shown for a fit to the data using the thermal expansion coefficient as an adjustable parameter.

We have also recently started a project led by Prof. Angela Viola to develop a validated predictive multiscale model to describe the chemical composition of soot nanoparticles in premixed and diffusion flames. This project closely couples experimental investigations of soot precursors and incipient particle characteristics with the development of a predictive model for the chemical composition of soot nanoparticles. The co-investigators on the project are Profs. Angela Violi (University of Michigan) and Bernhard Schlegel (Wayne State University) for model development and Drs. Hope Michelsen (Sandia), Nils Hansen (Sandia), and Kevin Wilson (LBNL ALS) for experimental investigations.

Experimental and modeling studies will be carried out for several low- and atmospheric-pressure flames fueled by the hydrocarbons of interest. A new counter-flow burner and sampling probe will be designed and built for this project. Polycyclic aromatic hydrocarbons (PAHs) and small soot particles will be extracted from the counter-flow flames via a microprobe. The flames will vary from lean to rich conditions in order to cover a wide range of practical conditions. The composition of incipient particles will be measured using the aerosol mass spectrometer developed by Kevin Wilson and coworkers at the ALS. The corresponding particle size distributions will be measured using an SMPS. Angela Violi and coworkers will use the experimental results in the development and validation of a predictive multiscale soot model.

IV. References

1. Kittelson, D. B. *J. Aerosol Sci.* **1998**, *29*, 575.
2. Lighty, J. S.; Veranth, J. M.; Sarofim, A. F. *J. Air Waste Manage. Assoc.* **2000**, *50*, 1565.
3. Michelsen, H. A.; Schrader, P. E.; Goulay, F. *Carbon* **2010**, in press.
4. Michelsen, H. A. *J. Chem. Phys.* **2003**, *118*, 7012.
5. Williams, T. C.; Shaddix, C. R.; Jensen, K. A.; Suo-Anttila, J. M. *Int. J. Heat Mass Transfer* **2007**, *50*, 1616.
6. Chang, H.; Charalampopoulos, T. T. *Proc. R. Soc. London, A* **1990**, *430*, 577.
7. Snelling, D. R.; Liu, F.; Smallwood, G. J.; Gülder, Ö. L. *Combust. Flame* **2004**, *136*, 180.
8. Köylü, Ü. Ö.; Faeth, G. M. *J. Heat Transfer* **1996**, *118*, 415.
9. Goulay, F.; Schrader, P. E.; Michelsen, H. A. *Appl. Phys. B* **2009**, submitted.
10. Rasor, N. S.; McClelland, J. D. *J. Phys. Chem. Solids* **1960**, *15*, 17.
11. Tsang, D. K. L.; Marsden, B. J.; Fok, S. L.; Hall, G. *Carbon* **2005**, *43*, 2902.

V. Publications and submitted journal articles supported by this project 2008-2010

1. H. A. Michelsen, P. E. Schrader, and F. Goulay "Wavelength and temperature dependences of the absorption and scattering cross sections of soot", *Carbon*, in press (2010).
2. F. Goulay, P. E. Schrader, and H. A. Michelsen, "Effect of the wavelength dependence of the emissivity on inferred soot temperatures measured by spectrally resolved laser-induced incandescence", *Appl. Phys. B*, submitted (2009).
3. F. Goulay, L. Nemes, P. E. Schrader, and H. A. Michelsen, "Spontaneous emission from $C_2(d^3\Pi_g)$ and $C_3(A^1\Pi_u)$ during laser irradiation of soot particles", *Mol. Phys.*, in press (2010).
4. F. Goulay, P. E. Schrader, and H. A. Michelsen, "The effects of pulsed laser injection seeding and triggering on the temporal behavior and magnitude of laser-induced incandescence from soot", *Appl. Phys. B* **96(4)**, 613-621 (2009).
5. H. A. Michelsen, "Derivation of a temperature-dependent accommodation coefficient for use in modeling laser-induced incandescence of soot", *Appl. Phys. B* **94**, 103-117 (2009).
6. F. Goulay, P. E. Schrader, and H. A. Michelsen, "A dataset for validation of models of laser-induced incandescence from soot; Temporal profiles of LII signal and particle temperature", *Appl. Phys. B*, submitted (2009).
7. F. Goulay, P. E. Schrader, L. Nemes, M. A. Dansson, and H. A. Michelsen, "Photochemical interferences for laser-induced incandescence of flame-generated soot", *Proc. Comb. Inst.* **32**, 963-970 (2009).
8. H. A. Michelsen, M. A. Linne, B. F. Kock, M. Hofmann, B. Tribalet, and C. Schulz, "Modeling laser-induced incandescence of soot: Enthalpy changes during sublimation, conduction, and oxidation", *Appl. Phys. B* **93**, 645-656 (2008).

Chemical Kinetics and Combustion Modeling

James A. Miller

Combustion Research Facility, Sandia National Laboratories
MS 9055, Livermore, CA, 94551-0969
email: jamille@sandia.gov

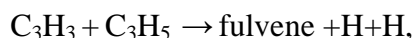
Program Scope

The goal of this project is to gain qualitative insight into how pollutants are formed in combustion systems and to develop quantitative mathematical models to predict their formation and destruction rates. The approach is an integrated one, combining theory, modeling, and collaboration with experimentalists to gain as clear a picture as possible of the processes in question. My efforts and those of my collaborators are focused on problems involved with the nitrogen chemistry of combustion systems and the formation of soot and PAH in flames, as well as on general problems in hydrocarbon combustion. Current emphasis is on determining phenomenological rate coefficients from the time-dependent, multiple-well master equation for reactions involved in the pre-cyclization and cyclization chemistry of flames burning aliphatic fuels.

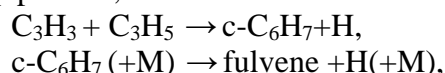
Recent Results

The Reaction between Propargyl and Allyl (with Yuri Georgievskii, Stephen Klippenstein, Larry Harding, Andy Simmonett, and Wesley Allen)

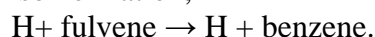
Our modeling indicates that, overall, the reaction between propargyl and allyl is the second most important cyclization step in rich flames of aliphatic fuels, after propargyl+propargyl. The reaction in our model is written as



which is short for a two-step process,



where c-C₆H₇ is a hydrofulvenyl radical. In rich flames fulvene is relatively easily converted to benzene by H-atom assisted isomerization,



The rate constant used in the model is an estimate based on the high pressure limit of the C₃H₅+C₃H₅ rate constant – there is no experimental or theoretical rate information available. In view of this situation it seemed desirable to analyze the reaction in some detail. In this analysis we employed high-level electronic-structure calculations to characterize the potential energy surface and various forms of transition-state theory (TST) to calculate microcanonical, J-resolved rate coefficients – conventional TST for isomerizations and the variable-reaction-coordinate form of variational TST for the “barrierless” association/dissociation processes. These rate coefficients were used in a time-dependent, multiple-well master equation to determine phenomenological rate coefficients, k(T,p), for various product channels – 8 wells and 6 sets of bimolecular products were included in the analysis. The bimolecular-product channels in the reaction all involve the recombination or production of two radicals (i.e., C₃H₃ + C₃H₅, C₂H₃ + i-C₄H₅, and H + C₆H₇, where there are numerous isomers of the latter). For such processes, with a couple of exceptions, the minimum-energy-path potentials in the recombination direction are barrierless, and both variational and anharmonic effects have a major

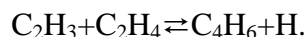
impact on the rate coefficients predicted by transition state theory (TST). Consequently, for these processes we implemented the direct variable-reaction-coordinate (VRC) transition-state theory approach (developed by Klippenstein and co-workers), which has been shown to provide an effective means for treating these complications. The calculations were performed as described previously for the $C_3H_3 + C_3H_5$ system and in close analogy with those described for the recombination of H atoms with resonance-stabilized radicals. An additional complication arose as a consequence of several of the intermediate structures being singlet biradicals. The rQCISD(T) calculations for these structures showed relatively large T1 diagnostics, indicating that the electronic wave functions have significant multi-reference character. Corrections for this effect ranged between 0 and 7 kcal/mole. The final analysis of the rate coefficients indicates that the formation of (cyclic) $c-C_6H_7$ and $c-C_6H_8$ species is suppressed by elevated pressure. Overall, the results suggest that the formation of these five-membered rings from the reaction is not as important as previously thought. A simplified description of the kinetics of the reaction was developed, and corresponding rate coefficients were calculated.

The Propargyl + OH Reaction (in collaboration with Stephen Klippenstein)

We have resumed our analysis of the C_3H_3+OH reaction. Because propargyl is resonance stabilized, it does not react readily with molecular oxygen. Consequently, in rich flames propargyl is oxidized primarily by reacting with hydroxyl. Because there is no information available, either experimental or theoretical, on the rate coefficient or product distribution of this reaction, we initiated a detailed theoretical investigation to provide this information for use in modeling. We believe that our electronic structure calculations of the relevant parts of the singlet PES are now finally complete. The deepest accessible wells on the PES correspond to CH_2CHCHO and CH_3CHCO structures. Both of these wells can be reached easily from the CH_2CCHOH adduct (formed by OH adding to the CH end of propargyl) by one or more hydrogen transfers. Additionally, there are several cyclic structures on the potential. The most important of these is cyclopropene-2-ol, which serves as an intermediate between the 2 initial adducts, completely analogous to the role played by cyclopropene in the allene-propyne isomerization. Fragmentation of the complexes into bimolecular products involves barrierless transition states as described above. We are currently in the process of calculating these rate coefficients, $k(E,J)$, using the same methods as for the $C_3H_3 + C_3H_5$ reaction. Even though the rate-coefficient calculations are not yet finished, it is clear that the most significant product channels at flame temperatures are $C_2H_3 + HCO$, $C_2H_4 + CO$, CH_3+HCCO , and triple propargylene + H_2O . The latter products are formed by direct abstraction on the triplet potential.

The Reaction between Vinyl and 1,3 Butadiene (in collaboration with Stephen Klippenstein)

The refinements to our kinetic model brought about by our theoretical analyses of the $C_3H_3+C_3H_3$ and $C_3H_3+C_3H_5$ reactions have generally resulted in better agreement between our model predictions and results from flame experiments. The exception is for flames fueled by ethylene. In these flames our predictions for benzene lie significantly lower than the experimental results. It is certainly possible that our prediction of the product distribution of the $C_3H_3+C_3H_3$ reaction is at fault. However, it seems more likely that there is a reaction leading to benzene that is not accurately accounted for in the modeling. After testing several plausible reactions, the only one that appears to be a realistic possibility is the reaction between vinyl and 1,3 butadiene. Note that 1,3 butadiene is likely to be more abundant in rich ethylene flames than in most others, because it is formed readily by a reaction between the fuel molecule and the “primary radical,”



We are now in the earliest stages of a detailed theoretical investigation of the reaction between C_2H_3 and 1,3 butadiene.

Future Directions

We shall continue our work on the chemical kinetics of rich flames of aliphatic fuels, particularly that concerned with the formation of the first aromatics containing one or two rings. In the next year we expect to complete our research on the reaction of OH with propargyl and perhaps that on the $C_2H_3+C_4H_6$ reaction. We shall continue to develop our chemical kinetic model, particularly in conjunction with the flame experiments at the Advanced Light Source. We expect in the next year to make progress in using the rate-controlled, constrained-equilibrium formalism to predict the concentrations of aromatic compounds with more than 2 rings. We shall also continue to maintain our interest in the nitrogen chemistry of combustion, particularly that concerned with NO_x control technologies such as reburning, Thermal De- NO_x , and RAPRENO $_x$.

Publications of James A. Miller 2008-2010

- J. A. Miller, S.J. Klippenstein, Y. Georgievskii, L. B. Harding, W. D. Allen, and A. C. Simmonett, "Reactions between Resonance Stabilized Radicals: Propargyl + Allyl," *J. Phys. Chem. A*, in press (2010)
- J. A. Miller, S.J. Klippenstein, S. H. Robertson, M. J. Pilling, and N. J. B. Green, "Detailed Balance in Multiple-Well Chemical Reactions," "Perspective" for *Phys. Chem. Chem. Phys.* **11**, 1128-1137 (2009)
- J. Zádor, A. W. Jasper, and J. A. Miller, "The Reaction between Propene and Hydroxyl," *Phys. Chem. Chem. Phys.* **11**, 11040-11053 (2009)
- A. W. Jasper and J. A. Miller, "Collisional Energy Transfer in Unimolecular Reactions: Direct Classical Trajectories for $CH_4 \rightleftharpoons CH_3 + H$ in Helium," *J. Phys. Chem. A* **113**, 5612-5619 (2009)
- J. A. Miller, J. P. Senosiain, S. J. Klippenstein, and Y. Georgievskii, "Reactions Over Multiple, Interconnected Potential Wells: Unimolecular and Bimolecular Reactions on a C_3H_5 Potential", *J. Phys. Chem. A* **112**, 9429-9438 (2008)
- S. R. Sellevåg, Y. Georgievskii, and J. A. Miller, "Kinetics of the Gas-Phase Recombination Reaction of Hydroxyl Radicals to form Hydrogen Peroxide," *J. Phys. Chem. A* **113**, 4457-4467 (2009)
- N. Hansen, J. A. Miller, P. R. Westmoreland, T. Kasper, K. Kohse-Höinghaus, J. Wang, and T. A. Cool, "Isomer-Specific Combustion Chemistry in Allene and Propyne Flames," *Combustion and Flame* **156**, 2153-2164 (2009)
- R. X. Fernandes, J. Zádor, L. E. Jusinski, J. A. Miller, and C. A. Taatjes, "Formally Direct Pathways and Low-Temperature Chain Branching in Hydrocarbon Autoignition: The Cyclohexyl + O_2 Reaction at High Pressure," *Phys. Chem. Chem. Phys.* **11**, 1320-1327(2009)
- L. B. Harding, S. J. Klippenstein, and J. A. Miller, "The Kinetics of $CH+N_2$ Revisited with Multi-Reference Methods," *J. Phys. Chem. A* **112**, 522-532 (2008)

- N. Hansen, J. A. Miller, T. Kasper, K. Kohse-Höinghaus, P. R. Westmoreland, J. Wang, and T. A. Cool, "Benzene Formation in Premixed Fuel-Rich 1,3 Butadiene Flames," *Proc. Combust. Inst.* **32**, 623-630 (2009)
- S. R. Sellevåg, Y. Georgievskii, and J. A. Miller, "The Temperature and Pressure Dependence of the Reactions $\text{H} + \text{O}_2(+\text{M}) \rightleftharpoons \text{HO}_2(+\text{M})$ and $\text{H} + \text{OH}(+\text{M}) \rightleftharpoons \text{H}_2\text{O}(+\text{M})$," *J. Phys. Chem. A* **112**, 5085-5095 (2008)
- J. Zádor, R. X. Fernandes, Y. Georgievskii, G. Meloni, C. A. Taatjes, and J. A. Miller, "The Reaction of Hydroxyethyl Radicals with O_2 : A Theoretical Analysis and Experimental Product Study," *Proc. Combust. Inst.* **32**, 271-277 (2009)

Detection and Characterization of Free Radicals Relevant to Combustion Processes

Terry A. Miller

Laser Spectroscopy Facility, Department of Chemistry

The Ohio State University, Columbus OH 43210, email: tamiller@chemistry.ohio-state.edu

1 Program Scope

Combustion processes have been studied for many years, but the chemistry is very complex and yet to be fully understood. Modern computer codes for its modeling typically employ hundreds of reaction steps with a comparable number of chemical intermediates. The predictions of such models are obviously limited by the dynamical and mechanistic data that is input. Spectroscopic identifications and diagnostics for the chemical intermediates in the reaction mechanisms constitute an important experimental benchmark for the models, as well as providing molecular parameters that are “gold standards” against which quantum chemistry computations of molecular properties may be judged. Our recent work has emphasized the spectroscopy of reactive organic peroxy radicals that are known to be key intermediates in combustion reactions.

2 Recent Progress

Our earlier cavity ringdown spectroscopic (CRDS) studies mainly involved the $\tilde{A} - \tilde{X}$ absorptions of simple alkyl peroxy radicals. Recently we have extended these studies towards unsaturated and hydroxy-substituted peroxies. Unsaturated hydrocarbon radicals are significant as precursors to polycyclic aromatic hydrocarbons and soot; understanding reaction mechanisms which contribute to their removal, such as peroxy formation, is fundamentally important in combustion chemistry. We have obtained the CRDS spectra of peroxy radicals derived from the resonance-stabilized allyl and propargyl radicals, two species expected to be important agents in soot formation. We have acquired the $\tilde{A} - \tilde{X}$ absorption spectra of the β -hydroxyethyl peroxy radical (β -HEP) which is an important intermediate in oxidation of ethanol and represents a model system for the OH-initiated oxidation of olefins of atmospheric importance, such as ethylene, isoprene, and terpenes. We have also recently targeted the vinoxy radical, an intermediate in the combustion of ethylene and acetylene. It possesses an electronic transition which is similar in frequency and strength to the $\tilde{A} - \tilde{X}$ systems of organic peroxies, and is therefore accessible in our experimental apparatus.

Another recent focus has been on the accurate measurement of the absorption cross-section of the $\tilde{A} - \tilde{X}$ electronic transition of organic peroxy radicals. Monitoring the concentration of these species in complex chemical environments requires the selectivity of the $\tilde{A} - \tilde{X}$ transition and knowledge of its absorption cross-section. We have developed an experimental method for cross-section determination which utilizes only absorption measurements. We describe the capability of this method and compare our first results for ethyl peroxy with cross-section values obtained with other experimental techniques.

2.1 Unsaturated peroxy radicals

Allyl peroxy The origin band region of the $\tilde{A} - \tilde{X}$ spectrum of allyl peroxy is shown in Fig. 1, along with rotational simulations for the 0_0^0 transitions of the five stable conformers. These are distinguished by dihedral angles $\angle\text{OCC}$ and $\angle\text{OCCC}$; the first angle is labeled T_1/G_1 (values of $180^\circ/\pm 60^\circ$, respectively), while the second is labeled C_2/G_2 ($0^\circ/\pm 120^\circ$, respectively). The three conformers having $-\text{G}_2$ arrangements are predicted to be the major contributors to the experimental spectrum (Table 1). In Fig. 1 the G_1G_2 conformer origin is identified as the source of the strong band at 7605 cm^{-1} with some vibrational sequence band structure also partially resolved. Band origins of the remaining conformers are predicted to be contained in the other strong feature at $\approx 7400\text{ cm}^{-1}$ with most of its intensity being attributable to the T_1G_2 and $\text{G}'_1\text{G}_2$ conformers. Although absent from Fig. 1, we have also measured the spectrum in the O-O stretching region, which appears as a replica of the origin region shifted $\sim 920\text{ cm}^{-1}$ to the blue and with $\sim 50\%$ the intensity.

Propargyl peroxy In Fig. 2 the propargyl peroxy radical spectrum is depicted along with rotational simulations. Since propargyl radical has two major resonance forms, O_2 can add at either of two sites to

yield acetylenic or allenic peroxy radical isomers. Electronic structure calculations predict that each isomer has two conformers related by the OOCC torsion (Table 1). The acetylenic isomer possesses conformers with dihedral angles $\angle\text{OOCC} = 180^\circ$ (ace-T) and $\pm 60^\circ$ (ace-G) in both \tilde{X} and \tilde{A} states; the conformers of the allenic isomer have $\angle\text{OOCC} = 0^\circ$ (all-C) and 180° (all-T) in the \tilde{X} state, and all-C/all-G (the latter with $\angle\text{OOCC} \sim \pm 128^\circ$) in the \tilde{A} state. In Fig. 2 the 0_0^0 band of the ace-T species can be identified at 7637 cm^{-1} by its rotational profile. We tentatively assign the ace-G band origin to the feature at ca. 7380 cm^{-1} . The broad experimental feature centered at $\sim 7500\text{ cm}^{-1}$ falls in reasonable agreement with the expected energy of the most intense transition for the all-T species; that is, the transition to the top of the \tilde{A} state torsional barrier at $\angle\text{OOCC} = 180^\circ$ separating the two all-G minima. The 0_0^0 band of the all-C species is predicted to be outside of our scan range and to have lower intensity (Table 1).

Table 1: Calculated \tilde{X} and \tilde{A} state energies (cm^{-1}), origin frequencies (T_{00}), oscillator strengths (f), and relative intensities (I) for conformers of allyl, propargyl, and β -hydroxyethyl peroxy radicals. Energies are ZPE-corrected and Boltzmann weights are given in parentheses. Relative intensities are given as products of Boltzmann weights and oscillator strengths. Relative energies and oscillator strengths are computed at the G2 and UCIS/6-31G(d) levels of theory, respectively.

Propargyl peroxy						Allyl peroxy					
Conformer	\tilde{X}	\tilde{A}	T_{00}	$10^5 f$	I	Conformer	\tilde{X}	\tilde{A}	T_{00}	$10^5 f$	I
ace-T (1.00)	0	7636	7636	1.9	1.9	G ₁ G ₂ (2.00)	0	7604	7604	3.4	6.8
ace-G (1.19)	107	7480	7373	0.7	0.8	G' ₁ G ₂ (1.65)	40	7375	7335	2.1	3.4
all-T (0.56)	120	7696 ^a	7576 ^b	4.2	2.4	T ₁ G ₂ (1.27)	94	7468	7374	2.5	3.1
all-C (0.09)	494	7356	6862	3.6	0.3	G ₁ C ₂ (0.77)	197	7508	7311	0.8	0.6
β -HEP ^c						T ₁ C ₂ (0.22)	315	7581	7266	2.1	0.5
G ₁ G ₂ G ₃ (1.00)	0	7356	7356	7.1	7.1	^a Top of OOCC torsion barrier in \tilde{A} state					
G' ₁ G ₂ G ₃ (0.76)	57	7326	7269	1.8	1.4	^b Transition to top of OOCC barrier in \tilde{A} state					
T ₁ G ₂ G' ₃ (0.24)	292	7474	7181	2.5	0.6	^c Four most stable conformers					
G ₁ G ₂ T ₃ (0.11)	451	8111	7660	2.2	0.2						

2.2 The vinoxy \tilde{A} - \tilde{X} absorption

Vinoxy, the smallest alkenyloxy radical, possesses a weak ($f \sim 10^{-4}$) $\tilde{A}^2A' - \tilde{X}^2A''$ electronic transition at $\approx 8000\text{ cm}^{-1}$ which has been observed previously by absorption and by photoelectron SEVI experiments. The latter studies have yielded \tilde{A} state vibrational frequencies whose precision is improved by the present study. Additionally, Fig. 3 reveals several strong bands in the CRDS trace that are neither predicted by the Franck-Condon simulations nor observed by the photoelectron SEVI experiments. We have performed electronic structure calculations that demonstrate that the “additional” bands in the CRDS trace are Herzberg-Teller-allowed bands which correspond to single quantum excitations in asymmetric (a'') \tilde{A} state normal modes.

2.3 β -hydroxyethyl peroxy radical

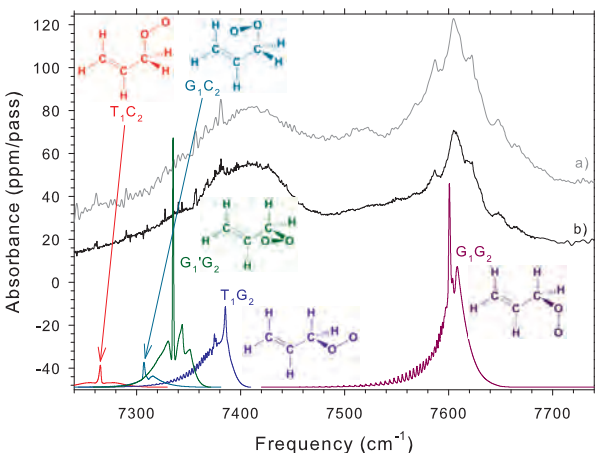


Figure 1: CRDS spectra of allyl peroxy, obtained from a) 193 nm and b) 248 nm photolysis of allyl bromide, with rotational simulations. Relative intensities and band positions for the simulations are taken from Table 1.

The CRDS $\tilde{A} - \tilde{X}$ electronic spectrum of β -HEP is shown in Figure 4. Quantum chemical calculations predict that β -HEP has 13 distinct conformers; the four most stable are listed in Table 1, where conformer labels T/G refer to values of $180^\circ/\pm 60^\circ$ for the $\angle\text{OOCC}(1)$, $\angle\text{OCCO}(2)$ and $\angle\text{CCOH}(3)$ dihedral angles, respectively. The most stable conformer, G₁G₂G₃, possesses a six-membered cyclic geometry where the OH group is weakly hydrogen-bonded to the peroxy moiety. This conformer also exhibits a larger $\tilde{A} - \tilde{X}$ oscillator strength than other β -HEP conformers. As indicated by the tentative assignments in Fig. 4, most of the observed vibrational features can be rationalized in terms of the G₁G₂G₃ conformer, while two weaker bands, an origin and O-O stretch, can be ascribed to the G'₁G₂G₃ conformer.

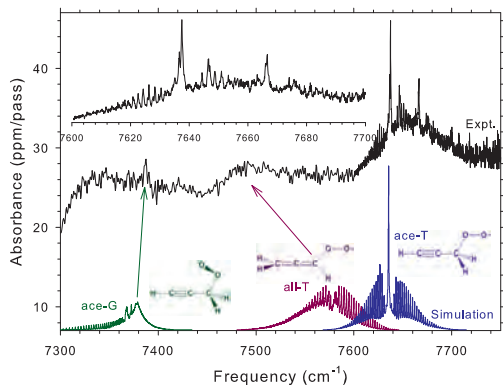


Figure 2: CRDS spectrum of propargyl peroxy, obtained from 193 nm photolysis of a propargyl chloride/ O_2 mixture, with rotational simulations. Relative intensities and band positions for the simulations are taken from Table 1. The 7600-7700 cm^{-1} region in the experimental trace is expanded (upper left) to better display the observed rotational structure.

2.4 Absorption cross-sections

To measure the absolute absorption cross-section of the $\tilde{A} - \tilde{X}$ transition of organic peroxy radicals, we have built a dual cavity ring down spectrometer (DCRDS), shown schematically in Fig. 5, which simultaneously measures along optically equivalent paths the absorption at two different wavelengths. “Arm A” measures the peak absorption of the $\tilde{A} - \tilde{X}$ transition of peroxy radicals, whereas “Arm B” measures the absorption of a non-transient product of the peroxy radical synthesis generated stoichiometrically with the radical.

We have measured the peak cross-section, σ_P^{EP} , of ethyl peroxy, $C_2H_5O_2$, for the origin transition of the G conformer. The radicals are produced using hydrogen abstraction from an organic precursor, RH, by chlorine atoms, resulting in the formation of an equal number of ethyl peroxy (EP) radicals and HCl molecules,



The cross-section σ_P^{EP} of $C_2H_5O_2$ can be expressed as

$$\sigma_P^{EP} = \left[\left(\frac{\Delta I}{I} \right)_G^{EP} / \left(\frac{\Delta I}{I} \right)_{\eta\eta'}^{HCl} \right] \frac{S_{\eta\eta'}}{\pi\gamma_{\eta\eta'}} \quad (4)$$

where $(\Delta I/I)$ are peak absorptions of, respectively, the $C_2H_5O_2$ G conformer’s $\tilde{A} - \tilde{X}$ origin band at 7596 cm^{-1} and an HCl transition between rovibronic levels η and η' , $\gamma_{\eta\eta'}$ is HWHM of the collisionally broadened HCl line, and $S_{\eta\eta'}$ is its integrated absorption line strength precisely available from the HITRAN database.

To accurately measure peak absorption using CRDS, it is important that the laser linewidth be substantially smaller than the molecular absorption linewidth. For this reason, we used an optical parametric oscillator (OPO) operating single mode (HWHM ≈ 300 MHz) to measure “reporter” HCl absorption lines (HWHM ≈ 640 -1100 MHz under the conditions of the experiments), whereas the stimulated Raman shifted output of a dye laser (HWHM ≈ 1200 MHz) was used to measure the broader absorption of ethyl peroxy. As Fig. 6 shows, the dye laser is scanned over the absorption of $C_2H_5O_2$, while the OPO scans repeatedly over a narrow (0.5 cm^{-1}) region centered at an HCl line. Since the absorption signals of HCl are fairly strong, several relatively weak lines, P(1), P(5) and P(6), of the vibrational overtone of the lesser abundant $H^{37}Cl$ isotopologue were used to avoid saturation effects and associated systematic errors. Several HCl transitions gave consistent results and the measured value of σ_P^{EP} is $5.51(32) \times 10^{-21} \text{ cm}^2$.

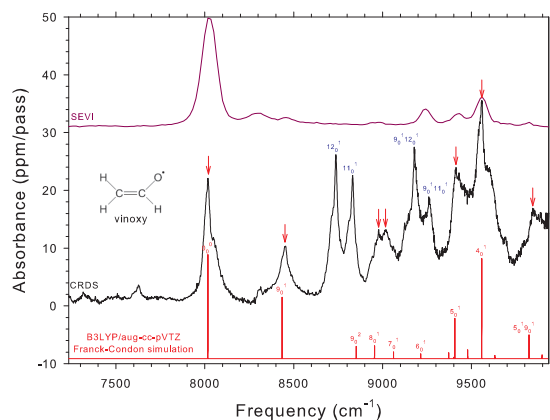


Figure 3: Ambient temperature CRDS $\tilde{A} - \tilde{X}$ spectrum of vinyloxy radical, with Franck-Condon simulation showing contribution of allowed bands to the spectrum (indicated by arrows above the experimental trace), and SEVI spectrum (courtesy of D. Neumark) of the $\tilde{A} - \tilde{X}$ vinoxide transition. CRDS features labeled in blue correspond to Herzberg-Teller transitions and are absent in the SEVI spectrum.

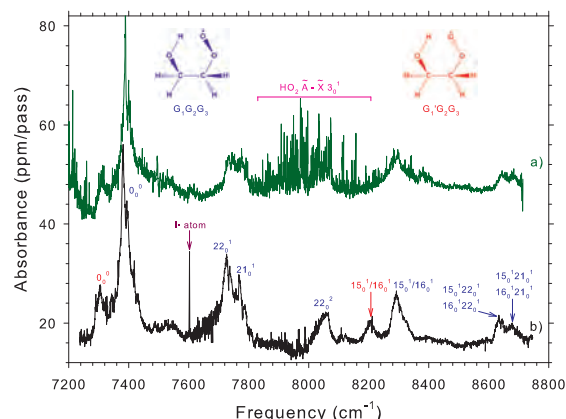


Figure 4: CRDS spectra of β -HEP radical obtained from a) OH addition to ethylene and b) photolysis of 2-iodoethanol, in both cases followed by O_2 reaction. Vibrational assignments are color coded to the indicated conformers. The O-O stretch is shared between ν_{15} and ν_{16} , while ν_{22} and ν_{21} correspond to OCCO torsion and COO bend vibrations, respectively.

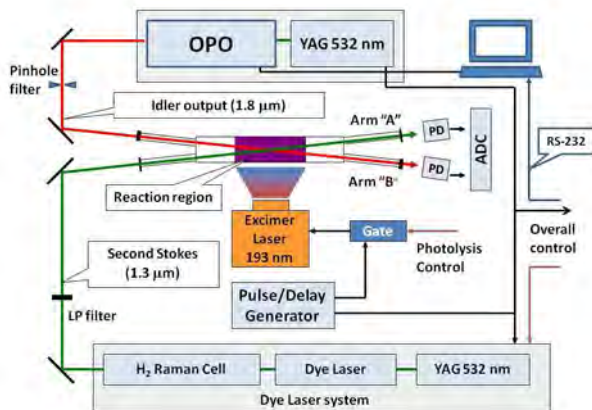


Figure 5: Block diagram of DCRDS apparatus. The radiation sources indicated are chosen to monitor simultaneously transitions in $C_2H_5O_2$ and HCl.

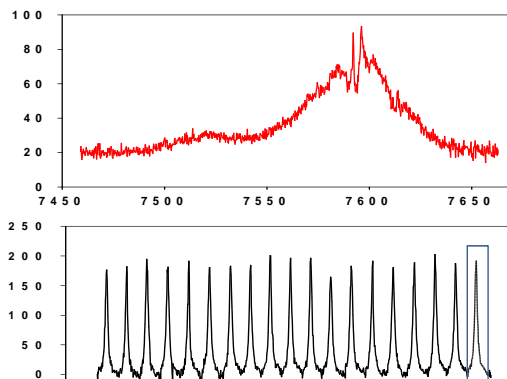


Figure 6: The $\tilde{A} - \tilde{X}$ origin band of G $C_2H_5O_2$ (top panel) and P(1) line of the vibrational overtone of $H^{37}Cl$ at 5643.1 cm^{-1} , taken repeatedly (bottom panel).

We compare this result with two alternative methods of measurement. In one series of experiments, we monitored the temporal decay of the $C_2H_5O_2$ absorption due to self-reaction of radicals which determines a value of k_{obs}/σ_P^{EP} . Using the literature value of k_{obs} yields a value of σ_G^{EP} of $5.37(42) \times 10^{-21} \text{ cm}^2$. An independent experiment by Atkinson and Spillman using this approach obtained $3.0(15) \times 10^{-21} \text{ cm}^2$. Another determination of σ_P^{EP} can be obtained by measuring the peak absorption of ethyl peroxy with simultaneous measurement of the absorption of the photolysis beam by the chlorine atom precursor $(COCl)_2$, assuming a Cl quantum yield of 2. The resulting value of σ_P^{EP} is $6.15(51) \times 10^{-21} \text{ cm}^2$. Comparing the measurements of σ_P^{EP} shows that the values obtained by different methods are consistent; however, results obtained with the DCRDS technique are the most precise. Additionally, these measurements of σ_P^{EP} are independent of the accuracy of the kinetic rate constants or photolysis cross-sections.

3 Future Directions

We plan to extend the work in unsaturated organic peroxy radicals to the CRDS spectra of other intermediates. These include vinyl and ethynyl peroxy, the smallest unsaturated peroxy radicals. To complement our previous observation of phenyl peroxy, we will pursue other cyclic unsaturated systems beginning with cyclopentadienyl peroxy. It is our goal to observe and analyze the CRDS spectra of larger members of the β -hydroxy peroxy series to include those species formed in the OH-initiated oxidation of propene, butene isomers, isoprene, and 1,3-butadiene.

We plan to extend the measurements of the absolute absorption cross-sections to other peroxy radicals, such as propyl, cyclopentyl, and cyclohexyl peroxy radicals with the DCRDS apparatus. Additionally, using data from high resolution studies of these species, we can obtain values of the $\tilde{A} - \tilde{X}$ electronic transition dipole moment of these radicals. Such results allow us to both derive absolute absorption cross-sections for a variety of experimental conditions and provide a benchmark for quantum chemistry calculations.

Publications Supported by DOE (2008-2010)

- [1] "Observation of the $\tilde{A} - \tilde{X}$ Electronic Transition of the Isomers and Conformers of Pentyl Peroxy Radical Using Cavity Ringdown Spectroscopy," E. N. Sharp, P. Rupper, and T. A. Miller, *J. Phys. Chem. A* **112**, 1445 (2008).
- [2] "The Structure and Spectra of Organic Peroxy Radicals," E. N. Sharp, P. Rupper, and T. A. Miller, *Phys. Chem. Chem. Phys.* **10**, 3955 (2008). [Invited Perspective Article]
- [3] "Observation of the $\tilde{A} - \tilde{X}$ Electronic Transitions of Cyclopentyl and Cyclohexyl Peroxy Radicals Via Cavity Ringdown Spectroscopy," P. S. Thomas, R. Chhantyal-Pun and T. A. Miller, *J. Phys. Chem. A* **114**, 218 (2010).
- [4] "The $\tilde{A} - \tilde{X}$ Absorption of Vinyloxy Radical Revisited: Normal and Herzberg-Teller Bands Observed Via Cavity Ringdown Spectroscopy," P. S. Thomas, R. Chhantyal-Pun, N. D. Kline and T. A. Miller, *J. Chem. Phys.* **132**, 114302 (2010).
- [5] "Cavity Ringdown Spectroscopy of the NIR $\tilde{A} - \tilde{X}$ Electronic Transition of Allyl Peroxy Radical ($H_2C=CH-CH_2OO\cdot$)," P. S. Thomas and T. A. Miller, *Chem. Phys. Lett.* (accepted).

Reaction Dynamics in Polyatomic Molecular Systems

William H. Miller

Department of Chemistry, University of California, and
Chemical Sciences Division, Lawrence Berkeley National Laboratory
Berkeley, California 94720-1460
millerwh@berkeley.edu

Program Scope or Definition

The goal of this program is the development of theoretical methods and models for describing the dynamics of chemical reactions, with specific interest for application to polyatomic molecular systems of special interest and relevance. There is interest in developing the most rigorous possible theoretical approaches and also in more approximate treatments that are more readily applicable to complex systems.

Recent Progress

Research efforts are being focused on the problem of how to add quantum mechanical effects to the classical molecular dynamics (MD) simulations that are now so ubiquitously applied to all types of dynamical processes in complex molecular systems, e.g., chemical reactions in clusters, nano-structures, molecules on or in solids, bio-molecular systems, etc. Semiclassical (SC) theory — since it is based on the classical trajectories of the molecular system — is a natural way to approach the problem, and one knows from much work¹ in the early 1970's that SC theory describes *all* quantum effects in molecular dynamics at least qualitatively, and typically quite quantitatively; the primary challenge is thus to develop methods for implementing it for large molecular systems. In this regard, the 'initial value representation'² (IVR) of SC theory has emerged as the most useful starting point since it replaces the non-linear boundary value problem of earlier SC approaches by a Monte Carlo average over the initial conditions of classical trajectories, a procedure more amenable to systems with many degrees of freedom.³

Particularly interesting is that electronically non-adiabatic processes can be treated within the general SC-IVR framework by using the approach of Meyer and Miller⁴ (MM) for replacing a finite set of electronic states of a molecular system (i.e., the various potential energy surfaces and their couplings) by a set of harmonic oscillators (one for each electronic state). Classical trajectory calculations — which are used as 'input' for the SC-IVR approach — can then be carried out treating the nuclear and electronic degrees of freedom in an equivalent dynamical framework (i.e., by classical mechanics), thereby describing non-adiabatic dynamics in a more unified manner. Stock and Thoss⁵ (ST) showed much later that the MM model is actually not an approximate 'model', but rather an exact 'representation' of the nuclear-electronic system; i.e., were this MMST nuclear-electronic Hamiltonian taken as a Hamiltonian *operator* and used in the Schrödinger equation, the exact (quantum) nuclear-electronic dynamics would be obtained. Thus the only approximation is that of the SC-IVR itself, and this realization has greatly revitalized interest in this approach to electronically non-adiabatic dynamics.

One recent application⁶ of the MMST approach to non-adiabatic dynamics has been to treat a model for coherence in electronic energy transfer in the Fenna-Mathews-Olson pigment protein complex that is involved in the light-harvesting step of photosynthesis. (This is motivated by experiments⁷ in Fleming’s lab observing direct evidence of such coherent energy transfer.) Fig. 1 shows the time-dependent electronic population of site 1, for various values of the ‘reorganization energy’ assumed for the model. Results of the SC-IVR treatment are in excellent agreement with those of a reduced density matrix approach used by Ishizaki and Fleming,⁸ while the simpler treatment given by traditional Redfield theory is not accurate in this case. The attractiveness of MMST/SC-IVR approach is that it can be applied to any model for which classical MD simulations are possible, all the way up to a full ‘all atom’ MD simulation of the protein system, treating the electronic and nuclear dynamics on an equivalent basis.

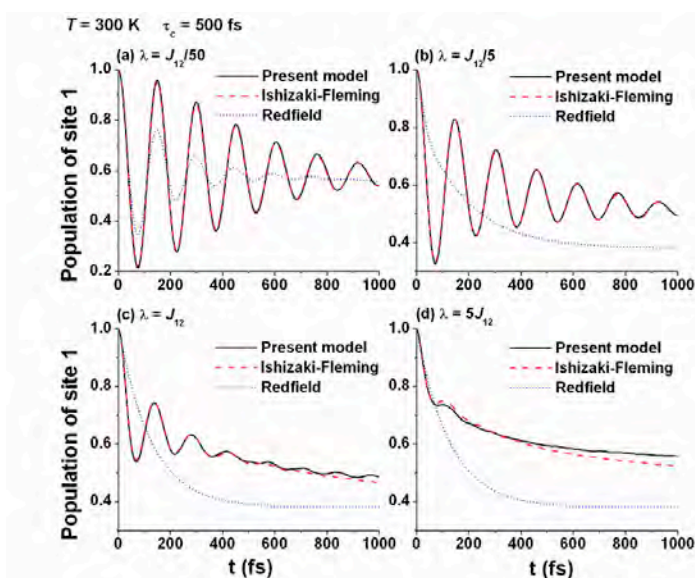


Figure 1. Electronic population dynamics of site 1. The results are calculated by the present semiclassical model for various reorganization energies, in comparison with those by using Ishizaki and Fleming’s hierarchy equation approach and Redfield theory taken from Ref 8.

A particularly interesting feature of the MMST Hamiltonian is that the classical trajectories generated from it are ‘Ehrenfest’ trajectories; i.e., the force experienced by the nuclei at any time is the Ehrenfest (i.e., average) force. Yet when these trajectories are used as input to SC theory, the nuclear motion emerges

from a non-adiabatic region moving (correctly) on one potential energy surface (PES) or another, and not on an average PES as in the traditional Ehrenfest model. This is due to coherence that is contained within the SC description, as is readily evident since the ‘linearized’ approximation to the SC-IVR (which does many things well, but which does not contain true quantum coherence effects) does not produce this correct behavior.

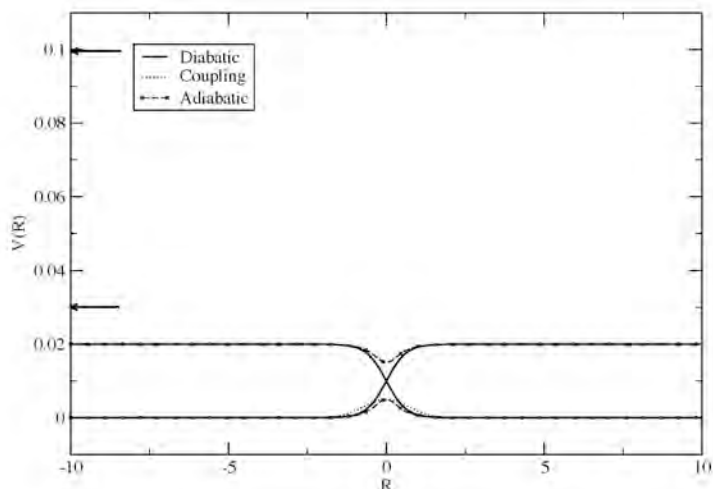
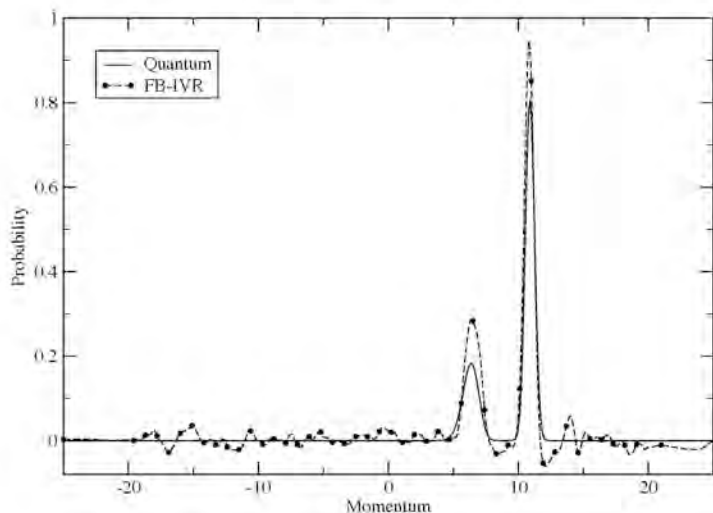


Figure 2. Potential curves for the symmetric version of the electronically non-adiabatic scattering problem discussed in ref. 10. Both diabatic and adiabatic potentials are shown. The two arrows on the vertical (energy) axes indicate the two collision energies for which calculations were carried out.

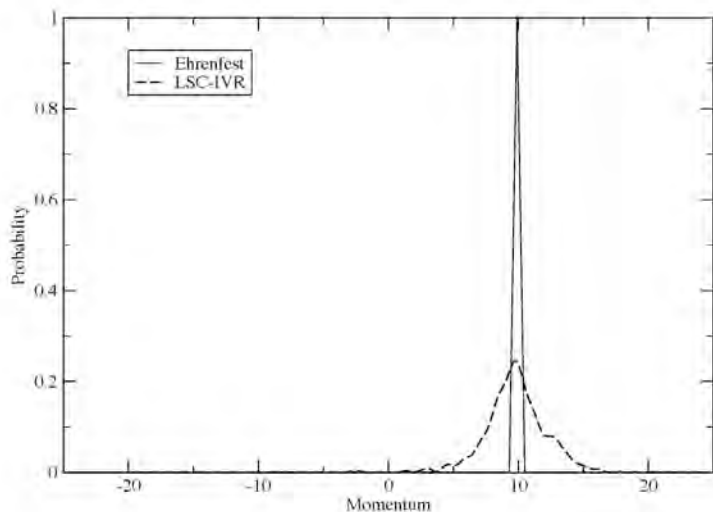
Figures 2 and 3 show a representative calculation^{9,10} that

illustrates the behavior described in the above paragraph. Fig. 2 shows two electronic potential ‘surfaces’ (actually ‘curves’ for this system of only one nuclear degree of freedom, translation). The initial state corresponds to translation motion coming from the left ($R \ll 0$) with a well-defined (positive) nuclear momentum, with the total energy indicated by the arrow on the abscissa. Fig. 3 shows the distribution of final ($t \rightarrow \infty$) nuclear momenta. The (exact) quantum result shows two peaks, corresponding to whether the nuclei emerge on one PES or the other, as does the FB-IVR (a version of the SC-IVR that is able to describe coherence).



The traditional Ehrenfest model, however, and the ‘linearized’ approximation (LSC-IVR) to the SC-IVR, are not able to describe this correctly.

Figure 3. Probability distribution of the final ($t \rightarrow \infty$) translational momentum for the potentials shown in Fig 2. See ref. 10 for more details.



Future Plans

The ‘linearized’ approximation to the general SC-IVR is now readily applicable to essentially any molecular system for which classical MD calculations are feasible, and it describes some quantum effects quite well. To describe true quantum coherence effects, however, requires a more accurate version of the SC-IVR. The ‘forward-backward’ IVR is the simplest step up the ‘ladder of rigor’ that is able to do so, but it is considerably more awkward to apply than the ‘linearized’ version. Effort is therefore focused on developing a way to

implement SC-IVR methodology that is both more accurate than the ‘linearized’ approximation and more convenient than the FB-IVR approach. There are such approaches in development.

References

1. For reviews, see W. H. Miller, *Adv. Chem. Phys.* **25**, 69 (1974); **30**, 77 (1975).
2. W. H. Miller, *J. Chem. Phys.* **53**, 1949 (1970).
3. For reviews, see (a) W. H. Miller, *J. Phys. Chem. A* **105**, 2942-2955 (2001); (b) W. H. Miller, *Proceedings of the National Academy of Sciences*, **102**, 6660-6664 (2005); (c) W. H. Miller, *J. Chem. Phys.* **125**, 132305.1-8 (2006).
4. H. D. Meyer and W. H. Miller, *J. Chem. Phys.* **70**, 3214-3223 (1979).
5. G. Stock and M. Thoss, *Phys. Rev. Lett.* **78**, 578 (1997).
6. G. Tao and W. H. Miller, *J. Phys. Chem. Lett.* **1**, 891-894 (2010).
7. G. S. Engel, T. R. Calhoun, E. L. Read, T. K. Ahn, T. Mancal, Y. C. Cheng, R. E. Blankenship, and G. R. Fleming, *Nature* **446**, 782-786 (2007).
8. A. Ishizaki and G. R. Fleming, *J. Chem. Phys.* **130**, 234110.1-8 (2009).
9. N. Ananth, C. Venkataraman and W. H. Miller, *J. Chem. Phys.* **127**, 084114.1-9 (2007).
10. W. H. Miller, *J. Phys. Chem.* **113**, 1405-1415 (2009).

2008 - 2010 (to date) DOE Publications

1. W. H. Miller, "The initial value representation of semiclassical theory: A practical way for adding quantum effects to classical molecular dynamics simulations of complex molecular systems," in *Physical Biology – From Atoms to Medicine*, ed. A. Zewail, Imperial College Press, London, UK, pp. 505-525 (2008).
2. J. Liu and W. H. Miller, "Test of the consistency of various linearized semiclassical initial value time correlation functions in application to inelastic neutron scattering from liquid *para*-hydrogen," *J. Chem. Phys.* **128**, 144511.1-15 (2008).
3. J. Liu and W. H. Miller, "Linearized semiclassical initial value time correlation functions with maximum entropy analytic continuation," *J. Chem. Phys.* **129**, 124111.1-17 (2008).
4. W. H. Miller, "Electronically non-adiabatic dynamics via semiclassical initial value methods," *J. Phys. Chem.* **113**, 1405-1415 (2009). LBNL-1582E.
5. G. Tao and W. H. Miller, "Semiclassical description of vibrational quantum coherence in a 3d I₂Ar_n (n≤6) cluster: A forward-backward initial value implementation," *J. Chem. Phys.* **130**, 184108.1-7 (2009).
6. J. Liu and W. H. Miller, A simple model for the treatment of imaginary frequencies in chemical reaction rates and molecular liquids, *J. Chem. Phys.* **131**, 074113.1-19 (2009).
7. J. Liu, W. H. Miller, F. Paesani, W. Zhang and D. A. Case, Quantum dynamical effects in liquid water: A semiclassical study on the diffusion and the infrared absorption spectrum, *J. Chem. Phys.* **131**, 164509.1-12 (2009).
8. G. Tao and W. H. Miller, Gaussian approximation for the structure function in semiclassical forward-backward initial value representations of time correlation functions, *J. Chem. Phys.* **131**, 224107.1-8 (2009).
9. G. Tao and W. H. Miller, Semiclassical description of electronic excitation population transfer in a model photosynthetic system, *J. Phys. Chem. Lett.* **1**, 891-894 (2010).

Dynamics of Activated Molecules

Amy S. Mullin

Department of Chemistry and Biochemistry, University of Maryland

College Park, MD 20742

mullin@umd.edu

I. Program Scope

The focus of my research program is to investigate the collisional energy transfer of molecules with large amounts of internal energy. Collisional energy transfer is ubiquitous in gas-phase chemistry and can have important effects on overall reaction rates and branching ratios. However there are substantial challenges to making detailed experimental measurements of molecular energy transfer at energies that are relevant to chemistry under combustion conditions. High energy molecules contain extremely large densities of states, are of transient nature and have poorly understood interactions with other molecules. Currently, there are no first-principle theories of collisional energy transfer and the lack of fundamental knowledge often results in cursory and insufficient treatments in reactive models. A goal of my research is to gain new insights into the microscopic details of relatively large complex molecules at high energy as they undergo quenching collisions.

We use state-resolved transient IR absorption to characterize the energy transfer pathways that are responsible for the collisional cooling of high energy molecules. To overcome the inherent difficulties in developing a molecular level understanding of collisions involving high energy molecules, we use high-resolution IR probing to measure population changes in small collision partners that undergo collisions with high energy molecules. Using this technique, we have performed in-depth spectroscopic studies that provide a greater understanding of high energy molecules and their collisional energy transfer.

II. Recent Progress

A. Probing dynamics of weak (but significant!) collisions

Until recently, high-resolution probing of collisional energy transfer of high energy molecules has been limited to measuring large ΔE collisions that scatter bath molecules into previously unpopulated states. We have recently developed a new approach to measure the outcome of small ΔE collisions for states of the bath gas that are thermally populated prior to collisions with high energy molecules. This development represents an important breakthrough because it allows us to investigate for the first time the dynamics that are associated with so-called “weak” collisions. The terms “weak” and “strong” are qualitative descriptors that refer to collisions leading to small- ΔE and large- ΔE energy transfer, based historically on Hinshelwood’s strong collision assumption.

To investigate the outcome of weak collisions we use transient IR absorption to measure the simultaneous appearance and depletion of population in low energy rotational states of bath molecules that are involved in the collisional quenching of high energy molecules. This approach allows the measurement of state-resolved dynamics and rates for the full distribution of molecules that result from collisions. Our measurements so far have focused on the nascent products generated from single collisions, but could be applied to mapping out how energy distributions in the bath molecule evolve under higher pressure conditions.

Collisions that induce small exchanges of energy make up the vast majority of energy transfer events but they are difficult to distinguish from the ambient background population in low- J states at 300 K. Parallel energy transfer processes that excite bath vibrational states (V-to-V energy transfer) interfere with high-resolution absorption measurements by moving population into upper states of the IR probe transitions. If this is the case, it is impossible to sort out how state-specific energy flow pathways contribute to the overall absorption signals. We overcome this problem by judiciously choosing probe transitions that have negligible cross sections for V-to-V energy transfer. For CO_2 probing, we use $00^0_0 \rightarrow 10^0_1$ transitions near $\lambda=2.7 \mu\text{m}$. The 10^0_1 state of CO_2 is of sufficiently high energy that it is not

excited in single collisions with high energy molecules. For HOD, DCl and HCl probing, direct collisional excitation of the bath stretching modes are not observed and single quantum probe transitions are used to measure weak collisions.

During this funding cycle, we have used our approach for measuring weak CO₂ collisions to investigate the balance between strong and weak collisions for a series of related highly excited molecules each containing different densities and types of internal energy. We measured the full CO₂ product distributions following collisions with pyrazine, 2-methylpyridine (picoline) and 2,6-dimethylpyridine (lutidine), each initially excited to $E_{\text{vib}} \sim 38500 \text{ cm}^{-1}$ with 266 nm light. The internal energy of highly excited pyrazine corresponds to the average vibrational energy at $T_{\text{vib}} = 4000 \text{ K}$. At the same photon excitation energy, the energies of excited picoline and lutidine correspond to cooler molecules, with $T_{\text{vib}} = 2300 \text{ K}$ and 1990 K , respectively, since these donors contain low frequency methyl rotors.



We investigated the outcome of weak collisions for these donors by measuring transient Doppler-broadened IR line profiles for individual rotational states of CO₂ immediately following single collisions with the highly excited molecules. The simultaneous appearance and depletion of population in low rotational states is extracted from transient line profile data by fitting to double Gaussian profiles.

The rotational energy distributions for CO₂ $J=2-80$ are shown in Figure 1 following single collisions with the highly excited donor molecules. For CO₂ collisions with these donors, we see evidence for biexponential rotational energy distributions. We interpret this observation as arising from two subpopulations of scattered molecules. The strongest collisions for each donor involve large increases in rotational energy of CO₂, but the extent of these large ΔJ -changing collisions is donor-dependent. Of these

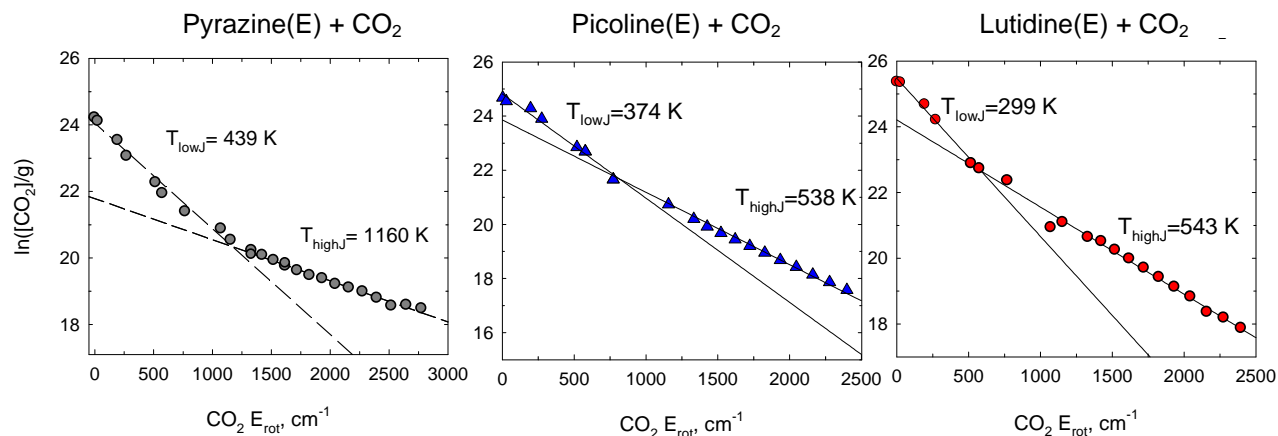


Figure 1. Nascent rotational distributions of scattered CO₂ molecules in $J=2-80$ from three different highly excited donor molecules. Evidence of bimodal distributions is present for each of the highly excited donors, but the extent of large ΔJ -collisions drops dramatically for methylated donor molecules.

donors, pyrazine has the highest energy content per mode and exhibits the “strongest” of strong collisions for this group of donor. It is likely that pyrazine’s higher energy content is in part responsible for the large ΔJ tail observed in the distribution of scattered CO₂ molecules. In other studies, we found that when the internal energy of pyrazine is dropped by 14% to $E=32000 \text{ cm}^{-1}$, the propensity of large ΔJ collisions also drops. It is likely that replacing C-H stretching modes in the excited donors with methyl rotors also reduces the number of impulsive collisions that lead to large changes in bath rotation. We observe translational energy distributions of the product states that are consistent with this picture.

It is worth noting that a separate high energy subpopulation is not observed for all collision partners. When the energy-accepting bath molecule is H₂O, HOD or DCl, single rotational distributions are observed. It is likely that linear, rigid molecules such as CO₂ with its relatively long lever arm are excellent candidates for large ΔJ -changing and Δv -changing collisions.

The CO₂ rotational distribution for each donor is fit to a biexponential function to characterize the subsets of quenching collisions. The lower energy distribution in each case has a temperature near the initial 300 K distribution. We associate the low energy distributions with elastic and weakly inelastic collisions. The high energy distributions are associated with strongly inelastic collisions leading to large changes in angular momentum and velocity. The ratio of weak to strong collisions is 3:1 for pyrazine, and 1:1 for picoline and lutidine. However, the strong component for the methylated donors is much less pronounced than for pyrazine.

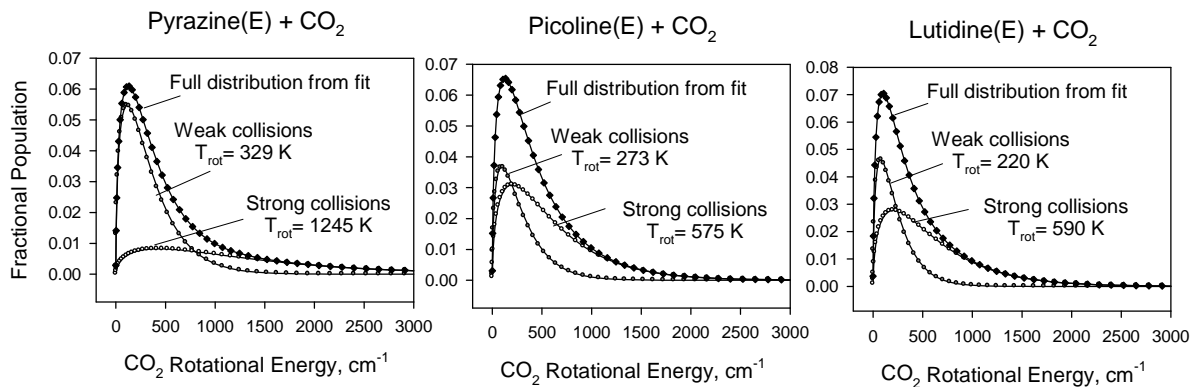


Figure 2. Results of fitting each rotational distribution for donor(E) + CO₂ collisions to a biexponential distribution. The sum of weak and strong collisions yields the total distribution of CO₂ states that result from V-RT collisions.

Absolute rate constants for appearance and depletion measurements provide a lower limit to the actual collision rates for highly excited molecules with CO₂. The measured rates include essentially all CO₂ molecules that undergo collisions and end up in the 00⁰ vibrational state. The observed rate for pyrazine(E):CO₂ is very close to the Lennard-Jones collision rate. However, for the methylated donors that we have studied, the observed collision rates are bigger than the Lennard-Jones rate by a factor of 1.6 for picoline(E) and a factor of 2 for lutidine(E). At this point, we do not know if the observed enhancements in CO₂ collisions are due to internal energy content or to the vibrational structure of the excited donor molecules. Nor do we yet know how the internal energy content of the methylated donors affects their quenching. We do know that the collision rates for pyrazine(E) with CO₂ show almost no dependence on the initial energy E.

B. Energy gain profiles of scattered HCl ($v=0, J$)

We have also made progress in the past year on studies of inelastic collisions of highly excited molecules with HCl. For studies on HCl scattering, we perform transient IR measurements using P-branch transitions of the $v=0 \rightarrow 1$ vibrational fundamental at $\lambda=3.3$ μm . This project entailed a number of development steps that are now complete. We have modified an existing transient absorption spectrometer for HCl detection, developed the means for spectral characterization and reconfigured our data collection protocols to adapt them for HCl studies. To date we have collected transient absorption signals for a number of HCl states with $J=0-8$. Transient signals for HCl following collisions with pyrazine(E) are shown in Figure 3. This initial data shows that the $J=0$ state is dominated by population depletion at the center frequency of the probe transition, while the $J=7$ state shows overall appearance. We are now poised to collect transient line profiles from which we will extract the transient populations and Doppler profiles for appearance and depletion. We would like to collect data for higher J states, but spectral contamination of our diode lasers makes them unsuitable for probing the higher J states.

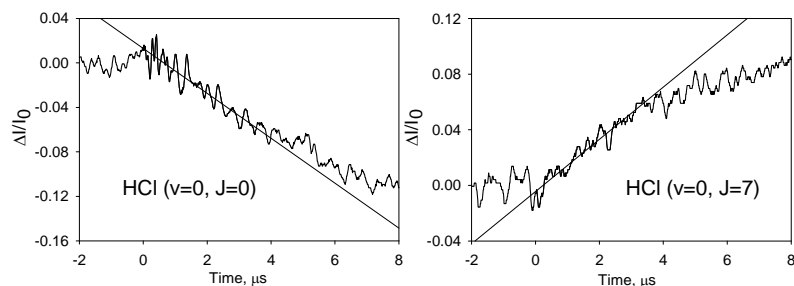


Figure 3. Transient absorption signals for scattered HCl molecules resulting from collisions of pyrazine(E) with HCl, where $E=38000\text{ cm}^{-1}$. The $J=0$ states show population loss at the center probe frequency, while $J=7$ shows overall appearance.

III. Future Work

We plan to continue our studies on the energy transfer dynamics of highly excited molecules in collisions with HCl. These studies are designed to test how the rotational energy structure of the energy-accepting bath molecule affects the energy exchange dynamics in collisions of highly excited molecules. We have already reported the full energy profiles for collisions of pyrazine(E) with DCl and the current studies on HCl will provide important benchmarks for developing models that account for energy partitioning in molecular collisions. We also plan new studies that will address how internal energy content in high energy molecules affects their collision rates. We have seen that collision rates of water and HOD with high energy molecules are as large as 3 times larger than Lennard-Jones collision rates. In the case of water collisions, it is likely that strong hydrogen bonding is a major factor for the enhanced collision rates. For CO_2 collisions, it is not clear whether the donor energy content enhances the collision rate or whether the Lennard-Jones model is in error by a factor of two. We plan to investigate this issue by measuring full energy transfer distributions for additional donor molecules with a wide range of internal energies.

IV. Publications supported by this project 2007-2010

1. D. K. Havey, Q. Liu, Z. Li, M. S. Elioff, M. Fang, J. Neudel and A. S. Mullin, "Direct determination of collision rates beyond the Lennard-Jones model through state-resolved measurements of strong and weak collisions," *J. Phys. Chem. A* **111**, 2458-2460 (2007).
2. Q. Liu, J. Du, D. K. Havey, Z. Li, E. M. Miller and A. S. Mullin, "Strong collisions of highly vibrationally excited alkylated pyridines ($E_{\text{vib}}\sim 38800\text{ cm}^{-1}$) with CO_2 " *J. Phys. Chem. A* **111**, 4073-4080 (2007).
3. D. K. Havey, Q. Liu, Z. Li, M. S. Elioff, and A. S. Mullin, "Collisions of highly vibrationally excited pyrazine with HOD: State-resolved probing of strong and weak collisions," *J. Phys. Chem. A* **111**, 13321-13329 (2007).
4. L. Yuan, J. Du and A. S. Mullin, "State resolved strong collisions of vibrationally excited azulene ($E_{\text{vib}}=20,100$ and $38,500\text{ cm}^{-1}$) with CO_2 ," *J. Chem. Phys.* **129**, 014303/1-11 (2008).
5. J. Du, L. Yuan, S. Hsieh, F. Lin and A. S. Mullin, "Energy transfer dynamics of weak and strong collisions between vibrationally excited pyrazine ($E_{\text{vib}}=37900\text{ cm}^{-1}$) + DCl," *J. Phys. Chem. A* **112**, 9396-9404 (2008).
6. D. K. Havey, Q. Liu and A. S. Mullin, "Energy transfer dynamics in the presence of preferential hydrogen bonding: Collisions of highly vibrationally excited pyridine- h_5 , -d_5 , and -f_5 with water," *J. Phys. Chem. A* **112**, 9509-9515 (2008).
7. Q. Liu, D. K. Havey, Z. Li and A. S. Mullin, "Effects of alkylation on deviations from Lennard-Jones collision rates for highly excited aromatic molecules: Collisions of methylated pyridines with HOD" *J. Phys. Chem. A* **113**, 4387-4396 (2009).
8. D. K. Havey, J. Du and A. S. Mullin, Full state-resolved energy gain profiles of CO_2 ($J=2-80$) from collisions with highly vibrationally excited molecules. I. Relaxation of pyrazine ($E=37900\text{ cm}^{-1}$)" *J. Phys. Chem. A* **114**, 1569-80 (2010).

Reacting Flow Modeling with Detailed Chemical Kinetics

Habib N. Najm

Sandia National Laboratories
P.O. Box 969, MS 9051, Livermore, CA 94551
hnnajm@sandia.gov

I. Program Scope

The goal of this research program is to improve our fundamental understanding of reacting flow, thereby advancing the state of the art in predictive modeling of combustion. The work involves: (1) Using computations to investigate the structure and dynamics of flames using detailed chemical kinetics; (2) Developing techniques for analysis of multidimensional reacting flow; (3) Developing numerical methods for the efficient solution of reacting flow systems of equations with detailed kinetics and transport; (4) Developing massively parallel codes for computing large scale reacting flow with detailed kinetics; and (5) Developing numerical methods for uncertainty quantification in reacting flow computations, including methods for the construction of uncertain chemical models from experimental data.

II. Recent Progress

A. Reacting Flow Computations, Analysis, and Model Reduction

We have concluded our study of methane-air edge flame structure using computational singular perturbation (CSP) analysis. We analyzed the global flame structure, outlining the spatial distribution of the dimensionality of the fast subspace, as well as the breakdown into frozen, exhausted, active, and dormant modes.

The modal distribution highlighted the global structure of the flame, as composed of a premixed front and a trailing non-premixed region. Analysis of individual modes revealed more detailed dynamical structure. We identified two explosive modes in the premixed front, consistent with earlier findings in 1D premixed flames. No explosive modes were found elsewhere in the flame. We also presented a detailed analysis of the structure of the fastest exhausted mode, which is consequential to requisite time integration strategies. We identified the dominant processes defining this mode, and highlighted their spatial distribution. Analyzing all modes, we outlined the spatial distribution of CSP radicals in the flame. We also identified reactions dominating relevant local equilibria in different layers in the edge flame. Further, we examined the progression of flame structure from premixed layers, through the transitional zone immediately behind the premixed branches, towards the downstream limiting non-premixed flame structure, identifying locally significant reactive processes. We also examined time scales of chemical and transport processes inside the flame highlighting their relative amplitudes in different regions.

Further, we presented a range of results highlighting important chemical/transport processes relevant to the slow/fast time evolution of specific species in the flame. In this context, we compared the results available from CSP slow/fast importance index analysis with those based on reaction flux analysis. One clear advantage of the importance indices is their utility for examining both transport and chemical processes, as well as highlighting reactions not involving the particular species at hand. Both of these capabilities are not available from straightforward reaction flux analysis. Of course, sensitivity analysis has been used to examine the importance of both transport processes and reactions not involving the target species in flames. However, local sensitivity analysis, in this post-processing context, does not discriminate between fast and slow subspaces, and therefore cannot address specific questions pertaining to a relevant time scale of interest. The CSP importance indices do provide that sharper focus on each subspace. Moreover, with this sharper focus we found a clear distinction between the findings for major and CSP-radical species. We illustrated how, for major species, slow importance index results highlight largely the same set of reactive processes as reaction flux analysis, albeit not necessarily with the same ordering. On the other hand, for highly-unstable CSP-radical species, the slow importance index results largely highlight reactive processes involving *other* species, namely those that are important in the algebraic constraints defining this radical species. In contrast, the fast importance index for these radicals, capturing the importance of processes in the fast subspace, again predicts largely the same set of important reactions as the reaction flux analysis. Clearly, while the fast reactions dominating the high consumption rates of unstable radicals are important in the fast subspace, captured by the fast importance index and the reaction flux analysis for these radicals,

these reactions are *not* important to the slow time evolution of these radicals over flame time scales of interest, as revealed by the CSP slow importance index. The strength of the dynamical analysis provided by CSP is precisely the decomposition of the dynamics into fast and slow subspaces, and the targeted and discriminating analysis of the chemical structure of the flame in each subspace.

We have also concluded development and demonstration of our two-dimensional (2D) high-order adaptive mesh refinement (AMR) low Mach number reacting flow solver. Achieving requisite 4^{th} -order spatial convergence in 2D required careful redesign of the momentum projection solver to guarantee solvability of the elliptic equation for the pressure while at the same time retaining 4^{th} -order accuracy. This involved transformation of the discrete fluxes from the native finite-difference construction to a finite-volume discretization, and back. This was done with requisite high-order interpolation operations. With this construction in place, we demonstrated 4^{th} -order spatial convergence, along with 2^{nd} -order temporal convergence, in a transient 2D reacting flow configuration. The robustness of the AMR discretizations was demonstrated employing targeted test problems with scalar structures transported along diagonal directions in and out of refined mesh regions. We also demonstrated the overall solver in a canonical reacting flow context involving the interaction of a premixed methane-air flame with a counter-rotating vortex-pair, using a C_1 methane-air kinetic mechanism. We have also continued our transition of the AMR code from the *Grace* mesh library to *Chombo*. We have demonstrated the operation of the full 2D reacting flow solver with *Chombo* using our custom-designed interfaces. Verification testing in comparison to *Grace* is in progress employing a number of test cases.

We have continued development of the CSP-tabulation adaptive chemical reduction algorithms, and have demonstrated their operation in both H_2 -air and CH_4 -air ignition computations. Performance gains over time-integration of the original stiff chemical source term were achieved with the methane-air case, but not in the Hydrogen case. This is as expected, as the dimensionality, complexity, and stiffness of the methane-chemistry is significantly above that of H_2 , such that the savings from CSP-tabulation become more significant. We have conducted detailed parametric studies exploring the effect of time step size, table-distance threshold, number of ignition conditions used to tabulate the table, and number of states used from each ignition computation, on the CPU performance and accuracy of the results. These studies outline the evident trade-offs in table construction and use, and will be relevant in appropriate table design for efficient and accurate computations with a given chemical model.

B. Uncertainty Quantification in Reacting Flow

In previous work, we had explored the impact of correlations among uncertain parameters on the structure of the uncertain solution, in the context of exothermal ignition of a methane-air mixture. For perfectly correlated parameters, we observed a strong dependence of the structure of the probability density function, and the maximum standard deviation of temperature ($\sigma_{T,\max}$), on the particular slope (χ) of the dependence relationship between the uncertain Arrhenius rate parameters ($\ln A, \ln E$). Specifically, we observed a range of $[0, 400]$ K in $\sigma_{T,\max}$ depending on the value of χ . Moreover, in the case of independent parameters, we find that $\sigma_{T,\max}$ reaches nearly ~ 600 K. These observations indicate strongly the need for learning the structure of the uncertain input space in order to have meaningful and accurate uncertainty quantification (UQ) in chemical systems. On the other hand, the only available means of discovering this structure is typically through experimental data. However, raw data on the Arrhenius parameters for each reaction-rate in a given chemical mechanism is simply not available. Therefore, we have been working on means of capturing the inherent parametric correlations as constrained by the physical model itself, nominal parameter values and error bars, along with the range of validity of the model. The idea is that such sufficient statistics do constrain the correlations that would be discovered based on any given data set that leads to parameters satisfying these statistics. Based on these concepts, we have arrived at a data-free inference (DFI) procedure for discovering the joint distribution of uncertain parameters in the absence of data. We have so far demonstrated the efficacy of this procedure in simple model fitting scenarios.

We have also begun work addressing the context of model reduction under uncertainty. This work is based on extending CSP analysis and model reduction methods to uncertain chemical systems. We have been able to identify the distribution of eigenvalues of the uncertain system, outlining relationships between the uncertain and nominal dynamical landscapes. Work is in progress on analyzing the uncertain eigenvectors, and therefore uncertain invariant manifolds that are pre-requisite objects for model reduction strategies.

III. Future Plans

A. Reacting Flow Computations, Analysis, and Model Reduction

We will continue our development of advanced massively parallel reacting flow algorithms and codes. Our key algorithmic development presently in progress is an axisymmetric construction. We are taking an incremental approach, starting with a second-order implementation, given its immediate utility, before progressing towards a 4th-order construction. This work is currently underway. It will pave the way for our handling of axisymmetric laminar jet flows, and enable comparisons with published experimental measurements, as well as ongoing CRF-experiments, involving axisymmetric jet flames.

We also plan to further explore the performance of our existing MPI/OpenMP low Mach number rectangular-coordinates code as far as parallel efficiency. We need to identify the dominant bottlenecks for strong scalability. Of course, communication loads at processor boundaries are bound to become dominant as the number of processors is increased, and processor-regions are shrunk, given the fixed problem size in the strong scalability exercise. We know that chemistry is our key computational bottleneck on moderate numbers of processors. We need to observe how this changes for large numbers of processors. We need to also evaluate the quality of the load balancer performance at $o(10^4)$ cores. We will study the performance of the code employing timing-measures with both strong and weak scalability studies, to identify dominant causes for the decay in parallel efficiency and what can be done to eliminate them.

We will continue our analysis of iso-octane/air ignition using CSP. We will examine this system under a range of conditions, analyzing the dynamical structure of the ignition process, and its dependence on the mixture conditions. We will compare the iso-octane ignition results with n-heptane ignition, and ultimately with the ignition picture in simple fuels. We will also take this analysis towards 1D premixed flames. It is of particular interest to study the structure of the preheat region in these flames using CSP, in comparison with the structure of igniting systems during the slow preheat phase when low temperature chemistry is active. We will conduct this study over a range of reactants mixture conditions, and for a range of fuels. Complex fuels, with two-stage ignition behavior, are of particular interest.

We will also continue our studies of edge flames, focusing on their detailed structure for complex fuels. We are currently working on the analysis of n-heptane/air edge flames, employing both detailed (560-sp, 2538-rn) and simplified (139-sp, and 66-sp) chemical models. We are working on interpretation of the information available from CSP analysis of this flame. We will examine the edge flame structure using the detailed model over a range of variation of the composition of the two streams, varying the amount of premixing in the fuel-stream, or N₂-dilution in the air-stream. We plan to extend this study towards more complex fuels, in particular iso-octane. The complexity of the iso-octane model, with 857-sp, will likely raise new computational challenges in this 2D flow. However, with our massively-parallel code, and the NERSC hardware, we should have sufficient resources to compute this system. Further, our hitherto edge-flame studies, whether with methane or n-heptane, have focused exclusively on mixing layers with uniform-velocity inflow. We will extend these to inflows that involve a shear layer between two streams with different velocity.

We are also interested in following up our edge flame studies with detailed studies of lifted unsteady jet flames, with a focus on the internal chemical structure and dynamical landscape of these flames. The above edge flame studies will provide valuable information about the structure of the base of the lifted jet, while full jet studies will examine the structure of downstream regions, and the dependence of this structure on flow dynamics. Forcing of jet inflow with tailored disturbances will allow analysis of these processes for specific length/time scales of vortical flow structures.

B. Uncertainty Quantification in Reacting Flow

We will continue our work on methods development for reduction of chemical models under uncertainty. We will pursue an understanding of the eigenstructure of uncertain ODE systems, and of underlying low dimensional manifolds. Uncertainties will generally affect both the manifold structure and the slow and fast dynamical subspaces. Properly accounting for these uncertainties will allow development of suitable model reduction strategies that are robust under uncertainty.

We also plan to examine/improve the performance, accuracy, and utility of our DFI algorithm in simple model scenarios, before proceeding to single-step chemical models with Arrhenius rate kinetics. Taking this algorithm to realistic reaction kinetics, one would have to address the hierarchical nature of the problem. Submodels, be

they thermodynamic or kinetic, would have to be built one at a time, depending on the relevant experiment used to determine the parameters in each. Once assembled they can be coupled together hierarchically, employing Bayesian methods, and marginalizing over nuisance parameters, to arrive at a properly specified uncertain input space for the final model.

Significant challenges exist in the development of efficient Polynomial Chaos (PC) UQ methods. One specific challenge is the formulation of optimal PC bases. Existing methods present non-trivial numerical challenges in this regard. Moreover, while the PDFs of uncertain inputs could be known *a priori*, those of the computational model outputs are not. Thus the PC basis has to be adapted in space and time to retain an optimal representation of general nonlinear model fields/outputs. We intend to work in this direction, in order to evaluate the utility of existing methods and advance the state of the art accordingly. We have begun work in this context, exploring the construction of specialized functions that are orthogonal with respect to a given measure.

Moreover, the forward UQ problem brings in challenges related to high-dimensionality, non-linearity, and long-term dynamics. In particular, the long-term dynamics challenge is primarily about the growth-rate of phase-variances in time for systems with nonlinear oscillatory dynamics. One available solution involves (a) focusing on non-intrusive/sampling-based forward UQ methods, and (b) choosing smooth observables. Given this, we will focus our development on non-intrusive PC methods. We will focus on (a) the use of sparse-quadrature methods for efficient computation of high-dimensional integrals, and (b) methods for stochastic domain decomposition to ensure accurate representation of uncertain fields in non-linear systems, particularly those with bifurcations/discontinuities. In the latter context, the support of the input space is decomposed into multiple elements, each of which becomes an independent UQ problem, with its own local PC representation of uncertain fields. One key reason for using these constructions is to deal with bifurcations, which are manifested as discontinuities in the dependence of uncertain variables on the inputs. We plan to work on the development of a flexible domain-decomposition functionality for the general representation of random variables within our UQ toolkit. In particular, this capability will be developed to be easily usable in a non-intrusive sparse-quadrature context.

IV. BES-Supported Published/In-Press Publications [2008-2010]

- [1] Najm, H.N., Valorani, M., Goussis, D.A., and Prager, J., Analysis of Methane-Air Edge Flame Structure, *Combustion Theory and Modelling* in press.
- [2] Najm, H.N., Uncertainty Quantification in Fluid Flow, in *Turbulent Combustion Modeling: Advances, New Trends and Perspectives* (T. Echehki and N. Mastorakos, Eds.), Springer-Verlag, Berlin, in press.
- [3] Ray, J., Armstrong, R., Safta, C., Debusschere, B.J., Allan, B.A., and Najm, H.N., Computational frameworks for advanced combustion simulations, in *Turbulent Combustion Modeling: Advances, New Trends and Perspectives* (T. Echehki and N. Mastorakos, Eds.), Springer-Verlag, Berlin, in press.
- [4] Najm, H.N., Debusschere, B.J., Marzouk, Y.M., Widmer, S., and Le Maître, O.P., Uncertainty Quantification in Chemical Systems, *Int. J. Num. Meth. Eng.*, 80:789–814 (2009).
- [5] Marzouk, Y. M., and Najm, H. N., Dimensionality reduction and polynomial chaos acceleration of Bayesian inference in inverse problems, *Journal of Computational Physics*, 228(6):1862–1902 (2009).
- [6] Valorani, M., and Paolucci, S., The *G-Scheme*: A framework for multi-scale adaptive model reduction, *Journal of Computational Physics*, 228:4665–4701 (2009).
- [7] Najm, H.N., Uncertainty Quantification and Polynomial Chaos Techniques in Computational Fluid Dynamics, *Annual Review of Fluid Mechanics*, 41(1):35–52 (2009).
- [8] Prager, J., Najm, H., Valorani, M., and Goussis, D., Skeletal Mechanism Generation with CSP and Validation for Premixed n-Heptane Flames, *Proc. Comb. Inst.*, 32(1):509–517 (2008).
- [9] Najm, H.N., Ponganis, D., and Prager, J., Analysis of NO Structure in a Methane-Air Edge Flame, *Proc. Comb. Inst.*, 32(1):1117–1124 (2008).
- [10] Najm, H.N., Ray, J., Safta, C., Marzouk, Y., Valorani, M., and Goussis, D.A., High-order AMR computations of reacting flow with adaptive reduction of chemical stiffness, *Journal of Physics: Conference Series*, 125:012032 (2008).
- [11] Valorani, M., Creta, F., Li Brizzi, A., Najm, H.N., and Goussis, D.A., Surrogate Fuel Analysis and Reduction using Computational Singular Perturbation, *AIAA-2008-1009* (2008) AIAA 46th AIAA Aerospace Sciences Meeting and Exhibit, Reno, NV.

Spectroscopy, Kinetics and Dynamics of Combustion Radicals

David J. Nesbitt

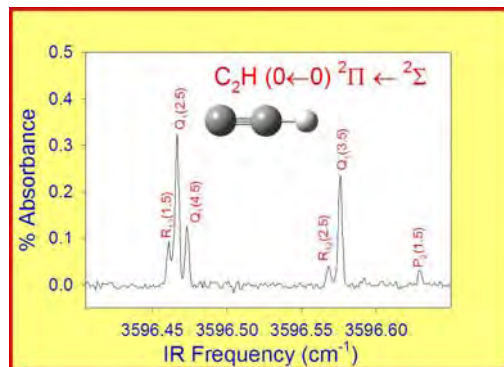
*JILA, University of Colorado and National Institute of Standards and Technology, and
Department of Chemistry and Biochemistry, University of Colorado, Boulder, Colorado*

Spectroscopy, kinetics and dynamics of jet cooled hydrocarbon transients relevant to the DOE combustion mission have been explored, exploiting i) high resolution IR lasers, ii) slit discharge sources for formation of jet cooled radicals, and iii) high sensitivity detection with direct laser absorption methods and near the quantum shot noise limit. What makes this combination powerful is that such transients can be made under high concentrations and pressures characteristic of actual combustion conditions, and yet with the resulting species rapidly cooled ($T \approx 10\text{-}20\text{K}$) in the slit supersonic expansion. Combined with the power of IR laser absorption methods, this provides novel access to spectral detection and study of many critical combustion species. Selected highlights from work over the last year are summarized below.

I. Acetylenic Radical (C_nH) Species

Due to elimination of hydrogen from aliphatic radical species under typical flame conditions, unsaturated radicals play a critical role in combustion even for saturated hydrocarbon aliphatic feedstock. Particularly important is the formation the ethyne radical, C_2H , which is thought to be a strategic intermediate in sequential formation of large aromatic species.^{1,2} The high resolution IR spectroscopy of C_2H in the acetylenic stretch region has been studied under room temperature conditions by Curl and coworkers, using UV excimer laser to photolytically generate C_2H radical and magnetic rotation spectroscopy to Zeeman shift mJ levels of the open shell species and thereby isolate absorption contributions while scanning over single rovibrational/ rovibronic lines.^{1,2} Complicating matters is the fact that there is an electronic band due to the presence of a low lying electronic A state in 3300 cm^{-1} region, which is relatively weak by electronic transition standards but in fact relatively strong compared to normal vibrational lifetimes and intensity standards.

Given the critical importance of this radical species, we have undertaken a spectroscopic reinvestigation of C_2H radical under sub-Doppler conditions of the slit jet apparatus. The data, taken under discharge conditions of trace acetylene (0.04% C_2H_2) in a 70%/30% mix of Ne/He, reveal an intense sequence of 5 absorption bands beginning at 3300 cm^{-1} and continuing up into the 4100 cm^{-1} region. There is significant new data content in these studies for the following reasons. First is that the much colder temperatures (15 K) in the slit jet have compressed the spectra down into the lowest end-over-end tumbling N states, therefore sampling lines not observed under room temperature conditions with high S/N. This in fact proves to be critical, as these low J ($= N \pm 0.5$) lines give substantial oscillator strength to additional "satellite" spectral structure arising from spin orbit state changing transitions (e.g. $R_{12}(1.5)$ and $R_{12}(2.5)$) which are not observable at high N. Secondly, the slit supersonic jet offers further sub-Doppler resolution of the radical transitions ($< 50\text{ MHz}$). In combination

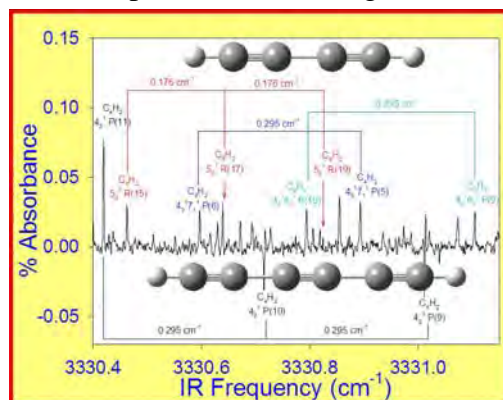


with the enhanced intensity in low J satellite transitions, the present work reveals fine structure transitions due to spin-rotation splittings in the lower S state, and which are indeed in excellent agreement with the predictions from microwave studies of Thaddeus and coworkers. Of special importance, however, is that the present study under direct absorption and higher resolution has permitted an independent spectral analysis of C_2H under much lower jet temperatures. This much colder and higher resolution analysis unambiguously reveals a systematic misassignment in the previous spectroscopic efforts, specifically regarding parity ordering and labeling of the upper vibronic manifolds. This reanalysis also permits a first and much closer look at the presence of perturbations in low N states of C_2H , the high N states of which are thought to be significantly complicated due to mixing with other vibronic levels.

II. IR Spectroscopy of Longer Chain Acetylenic (C_nH_m) Species

As a reward for our efforts with C_2H , this has permitted us to detect and analyze the first high resolution, jet cooled spectrum of *diacetylene* (C_4H_2), formed from sequential reaction of C_2H radicals with acetylene in the discharge. For example, the accompanying figure shows a small region of the full diacetylene spectrum, in particular revealing

excitation of the asymmetric CH stretch as fundamental and what is thought to be hot band combination transitions with ν_6 or ν_7 bending modes.³ The full spectral analysis of this is currently underway, but there are already suggestions of spectral surprises under these low temperatures and high resolution conditions. For example, the much higher collision density in the slit jet expansion is known to cool low frequency vibrations extremely effectively; thus it is actually quite surprising to see any appreciable bending

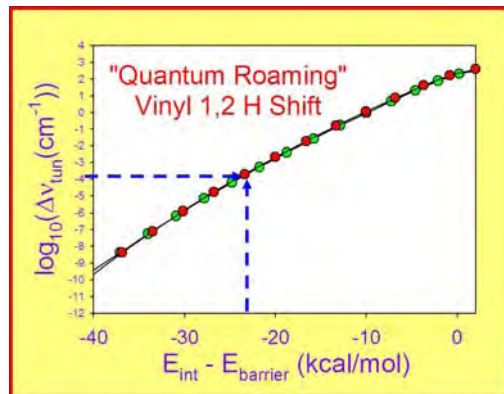


excitation in the present spectra, and may suggest some interesting pathways for C_2H addition chemistry in the slit jet. By way of further example, the chemistry of C_2H to form diacetylene is sufficiently fast to even to form *triacetylene* (C_6H_2) in the jet, a sample region of which is shown in the accompanying figure, and which also permits us to obtain a first jet cooled high resolution spectrum of this hydrocarbon species.⁴ Indeed, the fact that reactions to form diacetylene and triacetylene can and do occur so rapidly in the slit jet discharge expansion region provides strong support for the rich chemistry of linear chain growth with C_2H radical, as well as offers novel opportunities for study of such kinetics as a function of downstream distance.

III. “Quantum Roaming” Dynamics in Vinyl Radical Tunneling

Unimolecular H atom migration in energized closed shell molecules and radicals is of critical interest to a complete understanding of the combustion process. In recent years, there has been considerable interest in novel “roaming” dynamics observed initially by Suits and coworkers and predicted by Bowman and coworkers.^{5,6} As a result, there have been substantial experimental and theoretical interest in determining whether such roaming phenomena are general, and furthermore if they might represent an important channel for unimolecular rearrangement in combustion. One manifestation of

this phenomenon would be unimolecular 1,2, hydride shift from one radical center to another. A classic example of this would be the 1,2, H-atom shift in vinyl radical, which is known from early work by Harding^{7,8} to have an in-plane C_{2v} barrier on the order of 17500 cm^{-1} , with an out-of-plane barrier found by Bowman and Harding to be of comparable magnitude. Interestingly, this barrier is close in energy to the CH bond dissociation strength, due to stabilization of the resulting CC triple bond in acetylene. Thus one might expect 1,2 H-atom shift rates to compete effectively with rates for dissociation.

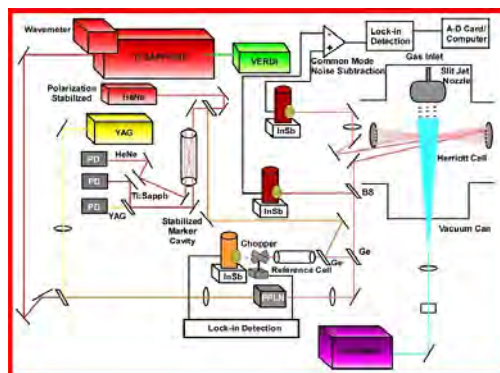


An intriguing alternative picture for roaming at energies substantially below the barrier is via *quantum mechanical tunneling*. For example, high-resolution infrared spectroscopy of vinyl radical by Dong *et al.* in a slit jet discharge expansion revealed that bands out of the lowest (0^+) and first excited (0^-) tunneling states exhibited anomalous 4:4 nuclear spin statistics for $K_a = \text{even}:\text{odd}$ states.^{9,10} One explanation was large amplitude "roaming" of all three H-atoms in vinyl radical on the μsec time scale of the expansion. It was furthermore speculated that this exchange would only be feasible for highly internally excited vibrational states, based on the *ab initio* barrier heights for this process. We have explored this "roaming" mechanism by means of approximate 1-D large amplitude tunneling potentials, followed by semi-classical and full quantum calculations of the associated tunneling splittings. In conjunction with the time scale of the expansion, these splittings provide a rigorously quantitative metric for assessing the amount of internal vibrational energy required to facilitate proton/nuclear spin exchange. Specifically, we use the Harding internal reaction coordinate potential for in-plane tunneling in conjunction with an exact treatment based on Hougen, Bunker and Johns for the large amplitude dependence of the reduced mass.^{11,12} This analysis permits us to report tunneling splittings associated with large amplitude 1,2 H-atom migration between the two global minima in the vinyl radical. These calculations have been pursued also in collaboration with Bowman and coworkers, based on a recent full-dimensional *ab initio* potential energy surface (PES) but based on a completely different but equivalent Hamiltonian formulation of the large amplitude dynamics.¹³ The tunneling splittings have been calculated over a large range of internal energies, with results from the two sets of calculations in excellent agreement as a function of energy below the global 1,2 hydride shift barrier. The major results of this work are: i) tunneling splittings for a 1,2 hydride shift in vinyl are quite small ($< 10^{-6}\text{ cm}^{-1}$) for vibrational states near the bottom of the well, but ii) grow *exponentially* with internal vibrational excitation, and iii) predict unimolecular tunneling dynamics on the sub- μsec time scale for energies with $E_{\text{int}} > 21\text{ kcal/mol}$ in the tunneling coordinate. As these energies are still more than 2-fold *below* the CH bond dissociation limit, these results indicate that "quantum roaming" pathways may indeed be relevant for unimolecular isomerization dynamics in energized combustion radicals.

IV. Apparatus Modification

We have incorporated a single mode tunable Ti:sapphire laser with a fixed frequency Nd:YAG cw single laser for difference frequency generation access to the near

IR region. The Ti:sapphire laser has been engineered for automated computer controlled scanning and spectral calibration throughout its tuning range, with transmission through a pair of high resolution Fabry-Perot cavities (at 250 MHz and 1 GHz free spectral ranges, respectively) for determining the absolute frequency. Each of the two cavities is optically locked via servo loop control onto a single mode HeNe laser, which in turn is stabilized to < 1 MHz absolute frequency accuracy by polarization stabilization methods already well established in our group. This generates two reference cavities with a long term comparable stability (< 1 MHz) and precision in the optical cavity length at the few Angstrom length scale. The larger FSR cavity then is used in conjunction with the built in wavemeter (which systematically provides an accuracy of < 200 MHz over the complete tuning curve) to establish the absolute number count in the Fabry-Perot interferometer for any fringe peak. The smaller FSR cavity then provides a convenient and stable interpolation scheme for laser scanning between these larger FSR fringes, thereby easily offering an absolute stability of < 5 -10 MHz over the full tuning range. This accuracy in the absolute IR frequency also relies on a comparable stability in the Nd:YAG laser frequency, which is therefore simultaneously locked via a combination of piezoelectric and thermoelectric servo loop cavity onto the smaller Fabry-Perot cavity. IR light generation between Ti:sapphire and Nd:YAG is accomplished in a set of periodically poled Lithium Niobate crystals (PPLN), which provides > 50 μ W of tunable, narrowband (< 1 MHz) IR light from the CH/OH stretch region (3600 - 3800 cm^{-1}) down to the LiNbO₃ cutoff (< 2450 cm^{-1}). Finally, absolute frequency calibration for the spectrometer is provided by reference gas cells of HOD, ethane, etc, and other well known absorbing species through these spectral regions.



References

- 1 W. B. Yan, C. B. Dane, D. Zeitz, J. L. Hall, and R. F. Curl, *J. Mol. Spectrosc.* **123** (2), 486 (1987).
- 2 R. F. Curl, P. G. Carrick, and A. J. Merer, *J. Chem. Phys.* **82** (8), 3479 (1985).
- 3 G. Guelachvili, A. M. Craig, and D. A. Ramsay, *J. Mol. Spectrosc.* **105** (1), 156 (1984).
- 4 K. Matsumura, K. Kawaguchi, D. McNaughton, and D. N. Bruget, *J. Mol. Spectrosc.* **158** (2), 489 (1993).
- 5 S. A. Lahankar, S. D. Chambreau, D. Townsend, F. Suits, J. Farnum, X. B. Zhang, J. M. Bowman, and A. G. Suits, **125** (4) (2006).
- 6 D. Townsend, S. A. Lahankar, S. K. Lee, S. D. Chambreau, A. G. Suits, X. Zhang, J. Rheinecker, L. B. Harding, and J. M. Bowman, **306** (5699), 1158 (2004).
- 7 L. B. Harding, *J. Am. Chem. Soc.* **103** (25), 7469 (1981).
- 8 L. B. Harding, private communication (2009).
- 9 F. Dong, M. Roberts, and D. J. Nesbitt, *J. Chem. Phys.* **128** (4) (2008).
- 10 F. Dong, M. Roberts, and D. J. Nesbitt, *J. Chem. Phys.* **128**, 044305 (2008).
- 11 J. T. Hougen, P. R. Bunker, and J. W. C. Johns, *J. Mol. Spectrosc.* **34** (1), 136 (1970).
- 12 D. J. Rush and K. B. Wiberg, *J. Phys. Chem. A* **101** (17), 3143 (1997).
- 13 A. R. Sharma, B. J. Braams, S. Carter, B. C. Shepler, and J. M. Bowman, *J. Chem. Phys.* **130** (17) (2009).

Radical Photochemistry and Photophysics

Daniel M. Neumark
Chemical Sciences Division
Lawrence Berkeley National Laboratory
Berkeley, CA 94720

Our research program is focused on fundamental aspects of radical photochemistry and photophysics, with particular emphasis on radicals that play an important role in the combustion of hydrocarbons. Radicals are generated from neutral or anionic precursors and photodissociated in the ultraviolet. We then determine which fragmentation channels occur and measure the photofragment translational energy and angular distributions for each channel. These measurements address the following central issues. First, they yield the primary photochemistry for a particular radical as a function of excitation energy. While many photodissociation experiments provide extremely sensitive probes of particular products (i.e. Rydberg tagging to detect H atoms), our experiments incorporate more universal detection schemes that are sensitive to all or most photofragmentation channels. Secondly, measurements of the product translational energy distributions provide considerable insight into the dissociation mechanism following photoexcitation and how this mechanism might vary with excitation energy. For example, very different translational energy distributions are expected if dissociation occurs on an excited state surface as opposed to internal conversion (IC) to the ground state followed by statistical decay. The relative importance of these two limiting mechanisms is a sensitive probe of the conical intersections that govern the dynamics of electronically excited polyatomic molecules. Moreover, results for radicals that decay from the ground state can be directly compared to experiments in which the thermal decomposition rates and products of radicals are determined, since in both cases internal energy tends to be randomized prior to dissociation. Finally, photodissociation experiments can provide direct measures of bond dissociation energies in free radicals, information that is critical in developing kinetic mechanisms for complex combustion processes in which radicals serve as key intermediates.

The radical photodissociation experiments are carried out on two instruments with complementary capabilities: a fast beam photofragment translational spectroscopy apparatus, and a molecular beam photodissociation instrument. In the fast beam experiment, radicals are generated by laser photodetachment of a fast (8–10 keV) beam of mass-selected negative ions. The radicals are then photodissociated by a second laser, and the photofragments are collected with high efficiency. We can measure the total dissociation signal as a function of excitation wavelength, thereby mapping out the photofragment yield spectrum of the radical. In addition, at fixed wavelengths, photofragment coincidence imaging yields the position and arrival times for all photofragments from each photodissociation event, from which the photofragment translational energy and angular distribution are obtained for each mass channel. In the molecular beam experiments, radicals are generated by either photolysis or pyrolysis of a stable

precursor and then photodissociated at either 248 or 193 nm. Photofragments are detected and analyzed using a rotating mass spectrometer with electron impact ionization. The choice of experiment for a particular radical depends on whether it can be generated more easily by photodetachment or by photolysis/pyrolysis. Also, compared to the fast beam experiment, the molecular beam instrument is more suitable for radicals that dissociate via loss of H atoms.

Recent experimental efforts have focused on the ultraviolet photodissociation of the phenyl and tert-butyl radicals and the three-body decay dynamics of ozone. The phenyl radical, $c\text{-C}_6\text{H}_5$, plays a central part in the combustion chemistry of aromatic hydrocarbons, compounds used in industry as additives to fuels. During combustion the phenyl radical can undergo oxidation to form phenyl peroxy and phenoxy radicals, it can polymerize to form polycyclic aromatic hydrocarbons, or it can decompose. A better understanding of the phenyl radical has been a priority in many laboratories since the rate-limiting step in this process is formation of the first aromatic ring. The phenyl radical is an intermediate in the thermal decomposition of benzene, so its bimolecular reactivity and unimolecular decay kinetics are of considerable interest in formulating a complete mechanism for this process.

We have used molecular beam photofragment translational spectroscopy (PTS) to study the photodissociation dynamics of the phenyl radical at 193 and 248 nm. The phenyl radical was generated by flash pyrolysis of nitrosobenzene. Time of flight data collected for the C_6H_4 , C_4H_3 , and C_2H_2 photofragments showed the presence of two decomposition channels, as indicated in the accompanying

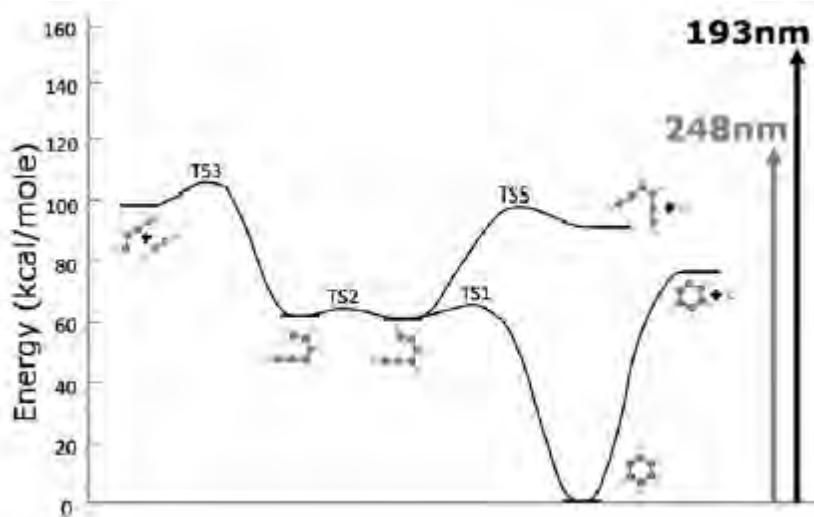


figure. The only C_6H_5 decomposition channel observed at 248 nm corresponded to C—H bond fission from the cyclic radical producing *ortho*-benzyne. The translational energy distribution peaked at 0 kcal/mol, consistent with no exit barrier for the H loss process. At 193 nm however, we observed significant decyclization of the C_6H_5 radical and subsequent fragmentation to $n\text{-C}_4\text{H}_3$ and C_2H_2 . These two momentum matched photofragments were described by a translational energy distribution that peaked around 9 kcal/mol, indicative of a process that proceeds through a tighter transition state. This is a higher energy channel than H + *ortho*-benzyne, and we are in the process of quantifying the branching ratio for the two channels in order to gain a better understanding of the unimolecular decay of phenyl.

PTS studies on the photodissociation dynamics of the *tert*-butyl radical at 248nm were also performed in our lab. *Tert*-butyl radicals were produced from the flash pyrolysis of azo-*t*-butane molecules entrained in a helium beam. Time of flight spectra taken at different laboratory angles for the C₄H₈, C₃H₆ and CH₃ photofragments showed the presence of a previously observed hydrogen atom loss channel as well as a methyl loss channel. The P(E_T) for the H loss channel is consistent with previous work and peaks well away from zero, indicating a dissociation channel with a significant exit barrier. Decomposition of the *tert*-butyl radical by CH₃ loss, however, was not previously observed and can proceed either by direct dissociation to form dimethylcarbene or by isomerization to the *iso*-butyl radical and subsequent fragmentation to propene. The P(E_T) for this channel peaks at 13 kcal/mol and does not extend past 30 kcal/mol. These energetics are consistent with the formation of dimethylcarbene as opposed to propene. Although isomerization of the *tert*-butyl radical to *iso*-butyl and subsequent dissociation to propene appears to be a favorable dissociation route it is not believed to take place due to a substantial isomerization barrier. The branching ratio for these two different decomposition pathways was found to be close to unity, imparting equal importance to the methyl loss channel and hydrogen atom loss channel alike.

We have investigated the photodissociation dynamics of ozone on our fast radical beam instrument, with particular focus on the competition between two-body and three-body decay at the two wavelengths. In our experiments, we generate the ozonide anion O₃⁻ and make a fast beam of O₃ by detaching above the ozone electron affinity, 2.103 eV. The ozone is then dissociated at either 193 nm or 157 nm. With our coincidence imaging detector, we can measure the branching between two- and three-body dissociation of ozone and map out the photofragment momenta for both channels. For the two-body channel, we can identify the O and O₂ electronic states by the translational energy release. For three-body decay, only the production of 3 O(³P) atoms is accessible at 157 nm. For this channel, measurement of the photofragment momenta leads to the construction of a “Dalitz plot”, from which one can extract information on the ozone geometry at the instant of the three-body breakup and thereby determine whether the three-body decay is concerted or sequential. Results so far have shown that three-body decay is considerably more important at 157 nm than at 193 nm; further analysis of this channel is in progress.

Publications:

D. M. Neumark, “Probing Chemical Dynamics with Negative Ions,” J. Chem. Phys. 125, 132303 (2006).

N. E. Sveum, S. J. Goncher, and D. M. Neumark, “Determination of Absolute Photoionization Cross Sections of the Phenyl Radical,” Phys. Chem. Chem. Phys. 8,

592 (2006).

D. S. Peterka, J. H. Kim, C. C. Wang, L. Poisson, and D. M. Neumark. "Photoionization Dynamics in Pure Helium Droplets," *J. Phys. Chem. A* 111, 7449 (2007).

D. Szpunar, A. E. Faulhaber, K. E. Kautzman, P. E. Crider, and D. M. Neumark, "D Atom Loss in the Photodissociation of the DNCN Radical: Implications for Prompt NO Formation," *J. Chem. Phys.* 126, 114311 (2007).

K. E. Kautzman, P. E. Crider, D. E. Szpunar, and D. M. Neumark, "Dissociative Photodetachment Studies of $I_2^- \cdot Ar$: Coincident Imaging of Two and Three-body Product Channels," *J. Phys. Chem. A.* 111, 12795 (2007).

C. C. Wang, O. Kornilov, O. Gessner, J. H. Kim, D. Peterka, and D. M. Neumark. "Photoelectron Imaging of Helium Droplets Doped with Xe and Kr Atoms," *J. Phys. Chem A.* 112, 9356 (2008).

S. J. Goncher, D. T. Moore, N. E. Sveum, and D. M. Neumark, "Photofragment Translational Spectroscopy of Propargyl Radicals at 248nm," *J. Chem Phys.* 128, 114303 (2008).

P. E. Crider, L. Castiglioni, K. K. Kautzman, and D. M. Neumark, "Photodissociation of the Propargyl and Propynyl (C_3D_3) Radicals at 248 nm and 193 nm," *J. Chem Phys.* 130, 044310 (2009).

Determination of Accurate Energetic Database for Combustion Chemistry by High-Resolution Photoionization and Photoelectron Methods

C. Y. Ng

Department of Chemistry, University of California, Davis, California 95616

E-mail Address: cyng@chem.ucdavis.edu

I. Program Scope:

The main goal of this research program is to obtain accurate thermochemical data, such as ionization energies (IEs), 0 K dissociative photoionization thresholds or appearance energies (AEs), 0 K bond dissociation energies (D_0 's), and 0 K heats of formation (ΔH_{f0}° 's) for small and medium sizes molecular species and their ions of relevance to combustion chemistry. Accurate thermochemical data determined by high-resolution photoionization and photoelectron studies for selected polyatomic neutrals and their ions are also useful for benchmarking the next generation of *ab initio* quantum computational procedures.

II. Recent Progress:

While standard quantum computation packages can be used routinely to provide reliable energetic information with chemical accuracy, such as IEs and D_0 of molecules of main group elements, a different scenario exists for the theoretical treatment of transition metal-containing molecules. Even for simple transition metal-containing diatomic molecules, such as FeC, the IE predictions of 7.1 eV for FeC calculated at the state-of-the-art multi-reference *ab initio* quantum C-MRCI+Q level are found to deviate from the experimental $IE(\text{FeC}) = 7.5932$ eV by ≈ 0.5 eV. We have recently successfully employed the CCSDTQ(Full)/CBS approach for energetic calculations of transition metal carbides and their cations [K.-C. Lau, et al., *J. Phys. Chem. A*, **113**, 14321 (2009)]. As shown in the example below, this approach seems very promising to give reliable energetic predictions with chemical accuracy.

The $IE(\text{FeC})$, $D_0(\text{Fe-C})$, $D_0(\text{Fe}^+-\text{C})$, $\Delta H_{f0}^\circ(\text{FeC})$ and $\Delta H_{f0}^\circ(\text{FeC}^+)$ values based on the CCSDTQ(Full)/CBS approach, which involves the approximation to the complete basis set (CBS) limit at the coupled cluster level up to full quadruple excitations. The zero-point vibrational energy (ZPVE) correction, the core-valence electronic corrections (up to CCSDT level), spin-orbit couplings and relativistic effects (up to CCSDTQ level) are included in the calculations. The present calculations provide the correct symmetry predictions for the ground states of FeC and FeC^+ to be $^3\Delta$ and $^2\Delta$, respectively. As shown in Table 1, the CCSDTQ(Full)/CBS $IE(\text{FeC}) = 7.565$ eV is found to compare favorably with the experimental IE value of 7.59318 ± 0.00006 eV, suggesting that the single-reference based coupled cluster theory is capable of providing reliable IE prediction for FeC, despite of its multi-reference character. The CCSDTQ(Full)/CBS $D_0(\text{Fe}^+-\text{C})$ and $D_0(\text{Fe-C})$ give the prediction of $D_0(\text{Fe}^+-\text{C}) - D_0(\text{Fe-C}) = 0.334$ eV, which is consistent with the experimental determination of 0.3094 ± 0.0001 eV. The D_0 calculations also support the experimental $D_0(\text{Fe}^+-\text{C}) = 4.1 \pm 0.3$ eV and $D_0(\text{Fe-C}) = 3.8 \pm 0.3$ eV determined by the previous ion photodissociation study. The present calculations also provide the $\Delta H_{f0}^\circ(\Delta H_{f298}^\circ)$ predictions for FeC/ FeC^+ . The analysis of the correction terms in these calculations (see Table 1) shows that the core-valence and valence-valence electronic correlations beyond CCSD(T) wavefunction and the relativistic effects make significant contributions to the calculated thermochemical properties of FeC/ FeC^+ . For the experimental D_0 and ΔH_{f0}° values of FeC/ FeC^+ , which are not known to high precision, we recommend the CCSDTQ(Full)/CBS predictions [$D_0(\text{Fe-C}) = 3.778$ eV, $D_0(\text{Fe}^+-\text{C}) = 4.112$ eV, $\Delta H_{f0}^\circ(\text{FeC}) = 760.8$ kJ/mol and $\Delta H_{f0}^\circ(\text{FeC}^+) = 1490.6$ kJ/mol] based on the ZPVE corrections using the experimental vibrational frequencies of FeC and FeC^+ .

Table 1. Individual energy contributions to the CCSDTQ(Full)/CBS predictions for the IE(FeC), IE(Fe), $D_0(\text{Fe}-\text{C})$ and $D_0(\text{Fe}^+-\text{C})$ predictions.

		IE(FeC) (eV)	IE(Fe) (eV)	$D_0(\text{Fe}-\text{C})$ (eV)	$D_0(\text{Fe}^+-\text{C})$ (eV)
$\Delta E_{\text{extrapolated CBS}}^{\text{a)}$	wCTQ5	7.425	7.799	3.770	4.144
	wCQ5	7.426	7.802	3.799	4.176
	Average	7.426	7.801	3.785	4.160
$\Delta E_{\text{CV}}^{\text{b)}$	(T) \rightarrow T	0.008	-0.005	-0.006	-0.019
$\Delta E_{\text{ZPVE}}^{\text{c)}$		0.005	---	-0.073	-0.078
		0.004 ^{d)}		-0.053 ^{d)}	-0.057 ^{d)}
$\Delta E_{\text{SO}}^{\text{e)}$		-0.039	-0.001	-0.049	-0.012
$\Delta E_{\text{SR}}^{\text{f)}$	CCSD(T)	0.147	0.093	-0.088	-0.142
	(T) \rightarrow T	0.002	0.000	0.001	-0.001
	T \rightarrow Q	-0.005	0.001	0.000	0.005
	subtotal	0.144	0.094	-0.087	-0.138
$\Delta E_{\text{HOC}}^{\text{h)}$	(T) \rightarrow T	-0.013	0.008	-0.162	-0.142
	T \rightarrow Q	0.034	0.003	0.350	0.320
	subtotal	0.021	0.011	0.188	0.178
CCSDTQ(Full)/CBS IE or $D_0^{\text{h)}$		7.565	7.899	3.758	4.092
		7.564 ^{d)}		3.778 ^{d)}	4.112 ^{d)}
Experimental ⁱ⁾		7.59318 \pm 0.00006	7.9024 \pm 0.0001	3.8 \pm 0.3	4.1 \pm 0.3
		7.74 \pm 0.09		3.4 \pm 0.2	3.7 \pm 0.2

- a) Extrapolated from the core and valence correlation energies with the cc-pwCV[T-5]Z and cc-pwCV[Q,5]Z basis sets, respectively.
- b) Core-valence electronic correlation obtained as the energy difference between CCSD(T) and CCSDT levels using the cc-pwCVTZ basis set.
- c) Based on the harmonic vibrational frequencies at the CCSD(T)/aug-cc-pV5Z level.
- d) Values obtained using the experimental vibrational frequencies of FeC/FeC⁺ for ZPVE corrections.
- e) Spin-orbit coupling obtained at the MRCI level with the uncontracted cc-pVTZ basis set.
- f) Scalar relativistic effect calculated at the CCSD(T)/aug-cc-pV5Z-DK, CCSDT/aug-cc-pVQZ-DK and CCSDTQ/cc-pVTZ-DK levels.
- g) Higher-order effect calculated at the CCSDT/aug-cc-pVQZ and CCSDTQ/cc-pVTZ levels.
- h) IE or $D_0 = \Delta E_{\text{extrapolated CBS}} + \Delta E_{\text{CV}} + \Delta E_{\text{ZPVE}} + \Delta E_{\text{SO}} + \Delta E_{\text{SR}} + \Delta E_{\text{HOC}}$.
- i) Y.-C. Chang, C.-S. Lam, B. Reed, K.-C. Lau, H. T. Liou, and C. Y. Ng, *J. Phys. Chem. A*, **113**, 4242 (2009); and references therein.

III. Ongoing experiments and Future Plans:

We have recently implemented the VUV threshold photoelectron imaging (VUV-TPE-EI) technique, and found that this method provides an energy resolution close to the pulsed field ionization-photoelectron (PFI-PE) measurement. Figures 1(a), 1(b), and 1(c) depict the VUV photoionization energies: (a) 9.114eV, (b) 9.185eV, (c) 9.377eV. The photoelectron spectra obtained from the e-images observed under different VUV photoionization energies (marked by the red arrows) are shown in Fig. 2.

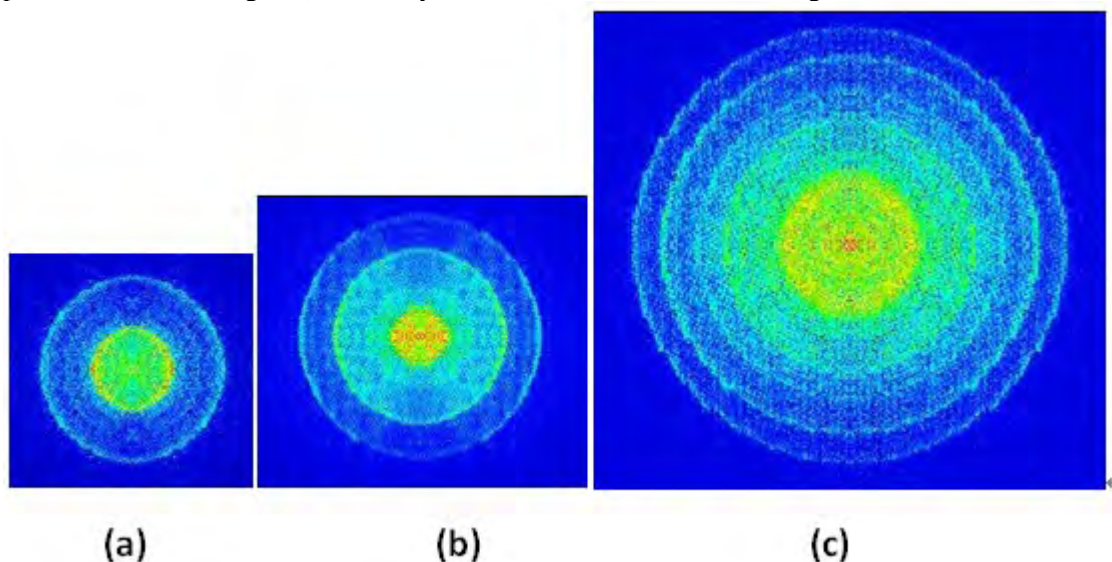


Figure 1. Raw images with VUV photoionization energies: (a) 9.114eV, (b) 9.185eV, (c) 9.377eV

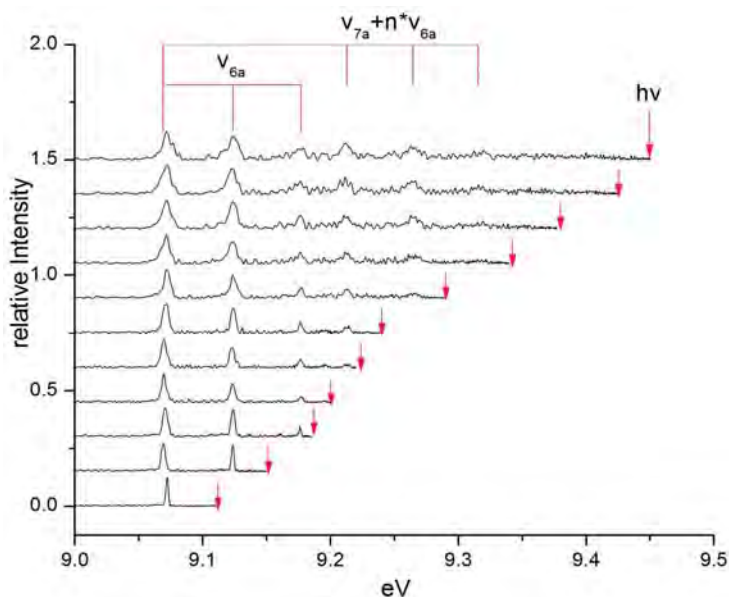


Figure 2. Photoelectron spectrum converted from the e-images observed under different VUV photoionization energies. The red arrows marked the energies of the VUV photon energies in eV used in the measurement.

The comparison of VUV near threshold e-imaging spectra obtained at different VUV photoionization energies (see Fig. 2) clearly shows that the photoelectron energy resolution increase (or the photoelectron peak becomes narrower) as the VUV photoionization energy used is closer to the ionization energy of the vibrational band of interest. Since the VUV-TPE-EI method is significantly more efficient than the VUV-PFI-PE technique, the VUV-TPE-EI method is ideal for high-resolution photoelectron measurements of radicals. By changing the VUV laser energy, excited photoelectron bands for radicals can be measured with high sensitivity.

We are making progress in PIE, PFI-PE, and VUV-TPE-EI measurements of small radicals, such as propargyl (C_3H_3), allyl (C_3H_5), and phenyl C_6H_5 radicals, using the VUV laser photoion/photoelectron imaging apparatus. In collaboration with Xu Zhang (Jet propulsion Laboratory, NASA), Barney Eillison (Univ. of Colorado, Boulder), Ralf Kaiser (Univ. of Hawaii, Manoa) and Branko Ruscic (Argonne National Laboratory), progress is also made in the study of the IR spectroscopy and photoionization-photoelectron spectroscopy measurements of hydrocarbon radicals of

relevance to combustion chemistry using the single-photon and two-color IR-VUV PI, and IR-VUV-PFI-PE methods, which have recently developed in our laboratory.

IV. Publications of DOE sponsored research (2008-present)

1. J. Zhou, B. Jones, X. Yang, W. M. Jackson, and C. Y. Ng, "A vacuum ultraviolet laser photoionization and pulsed field ionization study of nascent $S(^3P_{2,1,0}; ^1D_2)$ formed in the 193.3 nm photodissociation of CS_2 ", *J. Chem. Phys.* **128**, 014305 (2008). Selected for the February 2008 issue of Virtual Journal of Ultrafast Science.
1. X. Yang, J. Zhou, B. Jones, C. Y. Ng, and W. M. Jackson, "Single-photon vacuum ultraviolet excitation spectroscopy of autoionizing Rydberg states of atomic sulfur", *J. Chem. Phys.* **128**, 084303 (2008).
2. X. Xing, M.-K. Bahng, B. Reed, C. S. Lam, K.-C. Lau, and C. Y. Ng, "Rovibrationally selected and resolved pulsed field ionization photoelectron study of propyne: Ionization energy and spin-orbit interaction in the propyne cation", *J. Chem. Phys.* **128**, 094311 (2008).
3. X. Xing, B. Reed, M.-K. Bahng, S. J. Baek, P. Wang, and C. Y. Ng, "Infrared-vacuum ultraviolet pulsed field ionization-photoelectron study of CH_3I^+ using a high-resolution infrared laser", *J. Chem. Phys.* **128**, 104306 (2008).
4. J. Wang, Y. Li, T. Zhang, Z. Tian, B. Yang, K. Zhang, F. Qi, A. Zhu, Z. Cui, and C. Y. Ng, "Interstellar Enols Are Formed in Plasma Discharge of Alcohols", *Astrophys. J.* **676**, 416-419 (2008).
5. X. Xing, B. Reed, M.-K. Bahng, and C. Y. Ng, "Infrared-vacuum ultraviolet pulsed field ionization-photoelectron study of $C_2H_4^+$ using a high-resolution infrared laser", *J. Phys. Chem. A* **112**, 2572-2578 (2008).
6. M. Oku, Y. Hou, X. Xing, B. Reed, H. Xu, C. Y. Ng, K. Nishizawa, K. Ohshimo, and T. Suzuki, "3s Rydberg and cationic states of pyrazine studied by photoelectron spectroscopy", *J. Phys. Chem. A* **112**, 2293-2310 (2008).
7. X. Xing, P. Wang, H.-K. Woo, M.-K. Bahng, S.-J. Baek, and C. Y. Ng, "Rotationally resolved infrared-vacuum ultraviolet pulsed field ionization-photoelectron depletion method for infrared spectroscopic studies of neutral molecules", *Chem. Phys. Lett.* **455**, 321 (2008).
8. X. Xing, B. Reed, M.-K. Bahng, P. Wang, H.-K. Woo, S.-J. Baek, C. S. Lam, and C. Y. Ng, "High-resolution infrared-vacuum ultraviolet photoion and pulsed field ionization-photoelectron methods for spectroscopic studies of neutrals and cations", *Chinese J. Chem. Phys.* **21**, 193 (2008).
9. C. Chang, Q.-Z. Yin, and C. Y. Ng, "Testing of self-shielding model for early solar nebula with laboratory experiment", *Geochimica et Cosmochimica Acta* **72**, A148, Suppl. 1 (2008).
10. Xi Xing, Peng Wang, Beth Reed, S. J. Baek, and C. Y. Ng, "Infrared-vacuum ultraviolet pulsed field ionization-photoelectron study of CH_3Br^+ ", *J. Phys. Chem. A*, **112**, 9277 (2008).
11. Y. Hou, H.-K. Woo, P. Wang, X. Xing, C. Y. Ng, and K.-C. Lau, "Vacuum ultraviolet pulsed field ionization-photoelectron and infrared-photoinduced Rydberg ionization study of 1,3-butadiene", *J. Chem. Phys.* **129**, 114305 (2008).
12. B. Jones, J. Zhou, L. Yang, and C. Y. Ng, "High-resolution Rydberg tagging time-of-flight measurements of atomic photofragments by single-photon vacuum ultraviolet Laser Excitation", *Rev. Sci. Instrum.* **79**, 123106 (2008).
13. C. Y. Ng, "Spectroscopy and Dynamics of Neutrals and Ions by high-resolution infrared-vacuum ultraviolet photoionization and photoelectron methods", in "Frontiers of Molecular Spectroscopy", edited by Jaan Laane (Elsevier Science and Technology, 2009) Chap. 19, page 659-691.
14. B. Reed, C.-S. Lam, Y.-C. Chang, X. Xing, and C. Y. Ng, "A high-resolution photoionization study of ^{56}Fe using vacuum ultraviolet laser", *Astrophys. J.*, **693**, 940 (2009).
15. Y.-C. Chang, C.-S. Lam, B. Reed, K.-C. Lau, H. T. Liou, and C. Y. Ng, "Rovibrationally selected and resolved two-color laser photoionization and photoelectron study of the iron carbide cation", *J. Phys. Chem. A* (invited), **113**, 4242 (2009).
16. Kai-Chung Lau, Yih-Chung Chang, Chow-Sheng Lam, and C. Y. Ng, "High-level *ab initio* predictions of the ionization energy, bond dissociation energies and heats of formations for Iron carbide (FeC) and its cation (FeC⁺)", *J. Phys. Chem. A* (invited), **113**, 14321 (2009).

Large Eddy Simulation of Turbulence-Chemistry Interactions in Reacting Multiphase Flows

Joseph C. Oefelein

Combustion Research Facility, Sandia National Laboratories
Livermore, CA 94551-9051 (oefelei@sandia.gov)

Program Scope

Application of the Large Eddy Simulation (LES) technique within the Diagnostics and Reacting Flows program at the CRF was initiated with two primary objectives. The first is to establish a set of high-fidelity computational benchmarks that identically match the geometry (i.e., experimental test section and burner) and operating conditions of selected experimental target flames. The second is to establish a scientific foundation for advanced model development. The goal is to provide a direct one-to-one correspondence between measured and modeled results at conditions unattainable using the Direct Numerical Simulation (DNS) technique by performing a series of detailed simulations that progressively incorporate the fully coupled dynamic behavior of reacting flows with detailed chemistry and realistic levels of turbulence. Our focal point is the series of flames that have been studied as part of the Experimental Reacting Flow Research program in collaboration with Rob Barlow and Jonathan Frank (see related abstracts). This represents a direct extension of joint activities being pursued as part of the International Workshop on Measurement and Computation of Turbulent Nonpremixed Flames organized by Barlow *et al.* (www.ca.sandia.gov/TNF).

Recent Progress

Our primary goals over this review period were to: 1) continue to develop our theoretical-numerical capabilities in LES through application of advanced SGS models, 2) maximize the benefits of high performance computing through close coordination with key DOE Office of Science computational facilities, and 3) continue to establish key links between our basic and applied science programs. All of the cases considered involve direct coupling with key target experiments and the common objective of establishing a one-to-one correspondence with these experiments while adhering to the strictest accuracy requirements for LES. These requirements include use of clean numerics with non-dissipative spatial stencils and no artificial dissipation terms, high-quality grids, and science-based SGS models that take full advantage of the LES formalism and are designed specifically for high-resolution applications.

Over the past several years we have been successful in linking our LES activities under the BES program to various applied programs, both within the DOE and elsewhere. Figure 1 shows an example of the synergy established with the CRF Advanced Engine Combustion program. This program is funded by the DOE Office of Vehicle Technologies (OVT), with emphasis placed on development of high-pressure, low-temperature combustion concepts for design of internal combustion engines. A subset of turbulent flames being studied as part of the BES program are shown on the left. A subset of experiments associated with the Advanced Engine Combustion program are shown on the right. Objectives and milestones for both projects are aimed at establishing high-fidelity computational benchmarks that identically match the geometry and operating conditions of key target experiments using a single unified theoretical-numerical framework. The projects are complementary in that BES funded research provides the basic science foundation for advanced

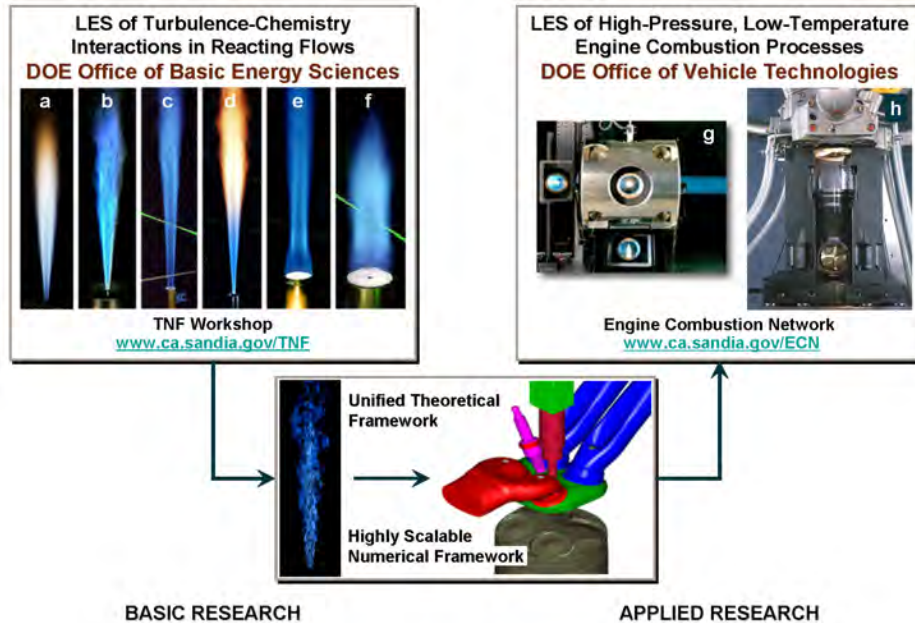


Figure 1: Advanced capabilities in LES provide a programmatic link between basic and applied sciences. A subset of turbulent flames associated with the BES Experimental Reacting Flow Research program are shown on the left (a,b: Simple jet flames, c,d: Piloted jet flames, e: Bluff-body; f: Bluff-body with swirl). A subset of experiments associated with the CRF Advanced Engine Combustion program are shown on the right (g: Constant-volume Diesel combustion facility, h: Typical single-cylinder optically accessible internal combustion engine).

model development and OVT funded research provides the applied component for advanced engine development. This combination of projects directly addresses targeted research areas identified as part of a BES sponsored workshop entitled *Basic Research Needs for Clean and Efficient Combustion of 21st Century Transportation Fuels*. Note that the approach applies in a broad sense to any propulsion and power device.

Our efforts to combine state-of-the-art LES, experiments, and High Performance Computing (HPC) over the past several years has catalyzed significant growth and collaborative opportunities. Much of this growth has been facilitated by establishing the Computational Combustion and Chemistry Laboratory. The dedicated local-capacity clusters provide a significant production level computing capability for routine calculations, and also serve as staging platforms for more efficient use of large-scale computing facilities such as the Lawrence Berkeley National Laboratory, National Energy Research Scientific Computing Center (www.nersc.gov); and the Oak Ridge National Laboratory, National Center for Computational Science (www.nccs.gov). Using these platforms in concert with grants such as the Innovative and Novel Computational Impact on Theory and Experiment (www.sc.doe.gov/ascr/INCITE) has enabled access to the full hierarchy of computing resources needed for state-of-the-art combustion simulations. From 2008 to present, the LES effort has been among the new projects awarded under the INCITE program. The LES component involves a combination of studies related to the experiments shown in Fig. 1.

Using the hierarchy of HPC resources described above to its full potential requires the development of specialized massively-parallel flow solvers that can be easily ported to a variety of platforms and scale efficiently on $\mathcal{O}(10^5)$ processing cores (and beyond). From this perspective, the approach described above has been enabled through a unique theoretical-numerical framework developed over the last eighteen years called "RAPTOR." Unlike conventional LES solvers, RAPTOR is a massively-parallel DNS solver that has been designed specifically for application of LES to turbulent, chemically reacting, multiphase flows in complex geometries. In the most general case it solves the fully coupled conservation equations of mass, momentum, total-energy, and species for a chemically reacting system. It also accounts for real gas/liquid phenomena, detailed thermodynamics, and transport processes for both multicomponent and mixture aver-

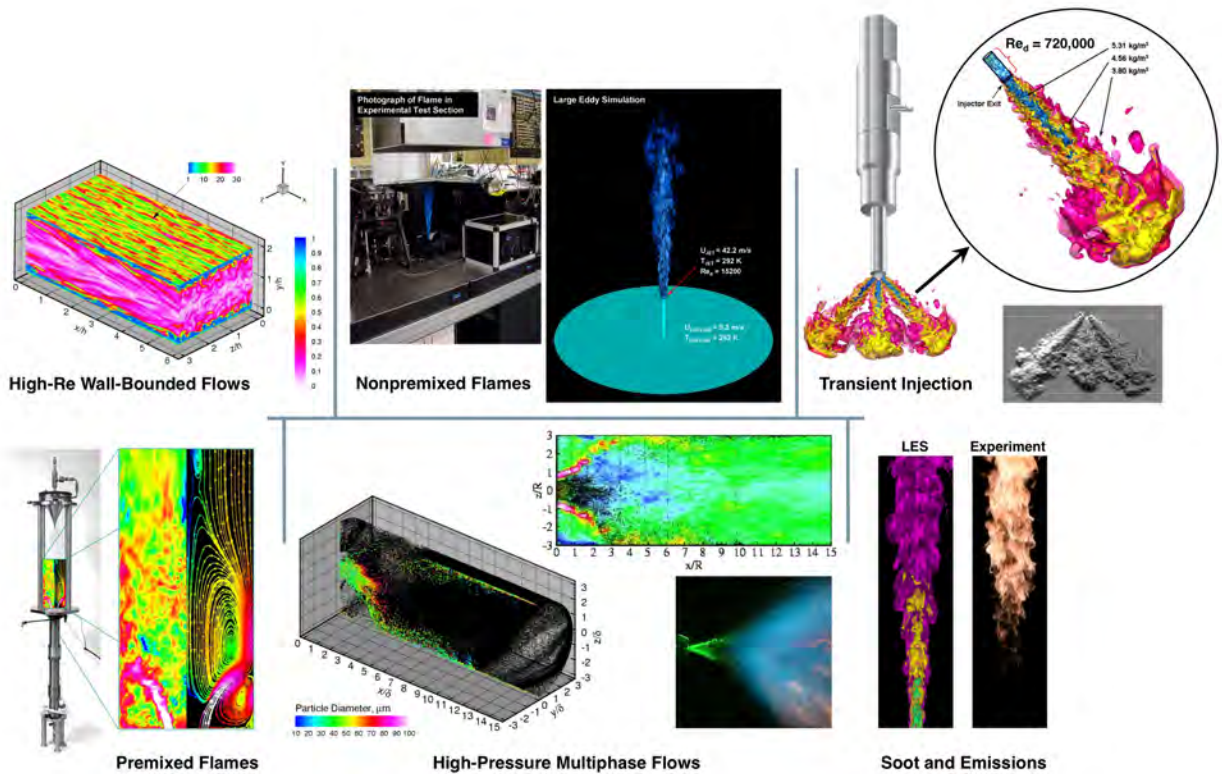


Figure 2: “RAPTOR” has now been validated for a wide range of turbulent reacting multiphase flows.

aged systems. The code framework has been optimized to provide excellent parallel scalability attributes using a distributed multiblock domain decomposition with a generalized connectivity scheme. Distributed-memory message-passing is performed using MPI and the Single-Program–Multiple-Data (SPMD) model. It accommodates complex geometric features and time varying meshes with generalized hexahedral cells while maintaining the high accuracy attributes of structured spatial stencils. The numerical framework has been ported to all major platforms and provides highly efficient coarse- and fine-grain (i.e., weak and strong) scalability attributes. Over the current review period, we have continued to perform a combination of validation and performance studies to anchor the accuracy and computational efficiency of the code. A suite of sample results associated with our research over this period are shown in Fig. 2.

In 2009, RAPTOR was selected as one of the application codes to be evaluated under the DOE Office of Advanced Scientific Computing Research (ASCR) annual “Joule Metric on Computational Effectiveness.” A key element of this program was to evaluate the existing baseline performance of the code and demonstrate that it could scale linearly on DOE “capability-class” computers. To achieve this goal, a series of weak scaling studies were performed to demonstrate the combined computational effectiveness of the ORNL NCCS Cray-XT platform (Jaguar) and RAPTOR. The first step toward measuring the performance was defining a realistic model problem that was representative of actual production simulations. For this study we chose the turbulent nonpremixed $\text{CH}_4/\text{H}_2/\text{N}_2$ jet flame known as the “DLR-A” configuration. A photograph of this flame is shown in Fig. 1b, and also in Fig. 2 at center with a corresponding LES solution. Using this configuration, we successfully demonstrated that the code scaled linearly well beyond 100,000 processor cores for extremely fine-grain problems. Collaborative activities such as this have now anchored RAPTOR as a capability-class flow solver and set the stage for future improvements that coincide with the evolution of HPC hardware. Details related to this activity can be found in a recent report by Kothe *et al.*

Future Plans

Using the framework described above, we continue to investigate two new modeling approaches. The first employs a stochastic reconstruction methodology that treats detailed chemistry directly within the LES formalism. This model is “science-based” in that it facilitates direct treatment of turbulence-chemistry interactions and multiple-scalar mixing in a manner consistent with the application of DNS. The second employs a tabulated combustion closure based on the Linear Eddy Model. With this it is clear that quality assessment techniques and uncertainty quantification for LES must be further to make meaningful progress in model development. Addressing these issues will be a priority in future studies.

BES Sponsored Publications (2007–Present)

1. A. M. Kempf, B. J. Geurts, and J. C. Oefelein. Error analysis of large eddy simulation of the turbulent non-premixed sydney bluff-body flame. *Combustion and Flame*, 2010. Submitted.
2. R. C. Knaus, C. Pantano, and J. C. Oefelein. Statistical analysis and modeling of scalar dissipation and its relation to the filtered mixture fraction. *Physics of Fluids*, 2010. Submitted.
3. J. H. Frank, S. A. Kaiser, and J. C. Oefelein. Analysis of scalar mixing dynamics in LES using high-resolution imaging of laser rayleigh scattering in turbulent non-reacting jets and non-premixed jet flames. *Proceedings of the Combustion Institute*, 33, 2010. Submitted.
4. D. Kothe, K. Roche, R. Kendall, M. Adams, S. Ahern, C.-S. Chang, H. Childs, E. D’Azevedo, K. Evans, T. Evans, J. Hack, S. Klasky, S.-H. Ku, J. Oefelein, D. Pugmire, J. Rosinski, R. Sankaran, and P. Worley. FY 2009 Annual report of joule software metric SC GG 3.1/2.5.2, improve computational science capabilities. Technical Report ORNL/TM-2009/322, Oak Ridge National Laboratory, December 2009.
5. J. C. Oefelein and R. Sankaran. Large eddy simulation of turbulence-chemistry interactions in reacting flows: Experiences on the ORNL NCCS Cray-XT platforms (Jaguar). *Proceedings of the 21st International Conference on Parallel Computational Fluid Dynamics*, May 18-22 2009. Moffett Field, California.
6. J. C. Oefelein, J. H. Chen, and R. Sankaran. High-fidelity simulations for clean and efficient combustion of alternative fuels. *Journal of Physics*, 180:1–5, 2009. DOI 10.1088/1742-6596/180/1/012033.
7. L. Lu, P. M. Najt, T.-W. Kuo, V. Sankaran, and J. C. Oefelein. A fully integrated linear eddy model and chemistry agglomeration model with detailed chemical kinetics for studying the effect of stratification on HCCI combustion. *Proceedings of the 6th Joint Meeting of the US Sections of the Combustion Institute, Paper 13C2*, May 17-20 2009. Ann Arbor, Michigan.
8. J. H. Frank, S. A. Kaiser, and J. C. Oefelein. Coupling imaging measurements and LES of dissipation structures in turbulent nonreacting jets and nonpremixed jet flames. *Proceedings of the 6th Joint Meeting of the US Sections of the Combustion Institute, Paper 32D1*, May 17-20 2009. Ann Arbor, Michigan.
9. J. H. Frank, S. A. Kaiser, and J. C. Oefelein. Coupling imaging diagnostics and large eddy simulation in turbulent nonreacting jets and nonpremixed jet flames. *Proceedings of the 4th European Combustion Meeting*, April 14-17 2009. Vienna, Austria.
10. V. Sankaran, T. G. Drozda, and J. C. Oefelein. A tabulated closure for turbulent nonpremixed combustion based on the linear eddy model. *Proceedings of the Combustion Institute*, 32:1571–1578, 2009.
11. T. G. Drozda, G.-H. Wang, V. Sankaran, J. R. Mayo, J. C. Oefelein, and R. S. Barlow. Scalar filtered mass density functions in non-premixed turbulent jet flames. *Combustion and Flame*, 155:54–69, 2008.
12. J. H. Chen, C. S. Yoo, R. Sankaran, and J. C. Oefelein. High-fidelity simulations for clean and efficient combustion of alternative fuels. *Journal of Physics*, 125:1–6, 2008. DOI 10.1088/1742-6596/125/1/012028.

KINETICS AND DYNAMICS OF COMBUSTION CHEMISTRY

David L. Osborn

Combustion Research Facility, Mail Stop 9055

Sandia National Laboratories

Livermore, CA 94551-0969

Telephone: (925) 294-4622

Email: dlosbor@sandia.gov

PROGRAM SCOPE

The goal of this program is to elucidate mechanisms of elementary combustion reactions through the use of multiplexed optical spectroscopy and mass spectrometry. We employ time-resolved Fourier transform spectroscopy (TR-FTS) to probe multiple reactants and products with broad spectral coverage ($> 1000 \text{ cm}^{-1}$), moderate spectral resolution (0.1 cm^{-1}), and a wide range of temporal resolution (ns – ms). The inherently multiplexed nature of TR-FTS makes it possible to simultaneously measure product branching ratios, internal energy distributions, energy transfer, and spectroscopy of radical intermediates. Together with total rate coefficients, this additional information provides further constraints upon and insights into the potential energy surfaces that control chemical reactivity. Because of its broadband nature, the TR-FTS technique provides a global view of chemical reactions and energy transfer processes that would be difficult to achieve with narrow-band, laser-based detection techniques.

More work has recently been focused on a complementary approach, time-resolved multiplexed photoionization mass spectrometry (MPI MS), which is used to sensitively and selectively probe unimolecular and bimolecular reactions. This work is in collaboration with Craig Taaftjes and many scientists from other institutions in the US and abroad. The Sandia-designed MPIMS instrument utilizes tunable vacuum ultraviolet light from the Advanced Light Source synchrotron at Lawrence Berkeley National Laboratory for sensitive, isomer-specific ionization of reactant and product molecules in chemical reactions.

RECENT PROGRESS

Isomer-resolved mass spectrometry

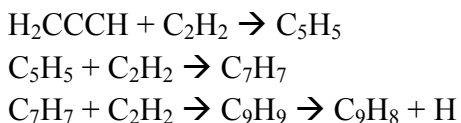
The multiplexed chemical kinetics photoionization mass spectrometer operates both at Sandia National Laboratories (using a discharge lamp to create VUV radiation), and at the Chemical Dynamics Beamline of the Advanced Light Source (ALS) synchrotron of LBNL. The chemical reactor is based on the Gutman design,¹ which allows the study of photodissociation and bimolecular reactions at pressures of 1 – 10 Torr and temperatures of 300 – 1000 K.

While the study of chemical kinetics using PI MS is well-established, this apparatus has two unique features that make it especially powerful for chemical kinetics. First, the widely tunable, intense VUV radiation from the ALS enables isomer-specific ionization of product species. As an example, we have studied the isomer-resolved products of the CN radical with benzene and toluene, measuring the branching ratios of the product isomers.

The second unique feature is the high repetition rate mass spectrometer that allows us to take snapshots of the complete chemical composition in our reactor as a function of time. Towards this end, a significant upgrade to the multiplexed photoionization mass spectrometer became operational in the past year. Leveraging designs from the analytical chemistry community, we have replaced the small magnetic sector mass spectrometer in the original design with an orthogonal acceleration time-of-flight mass spectrometer (OA-TOF), suitable for continuous ionization sources. Although the OA-TOF approach does not have 100% duty cycle, the duty cycle is as high as possible for a time-of-flight system, operating at a repetition rate of 50 kHz. In return, mass resolution of $m/\Delta m \sim 2000$ has been achieved using a simple linear (i.e., not reflectron) approach. This mass resolution has already been used to separate HCCO^+ from C_3H_5^+ (both nominally mass 41) and will be increasingly valuable in separating other O \leftrightarrow CH₄ substitutions in larger hydrocarbons (e.g., acetone vs. butane, ketene vs. propene) in the chemistry of hydrocarbon oxidation. The increase in mass resolution by more than a factor of 10 has been accompanied with greater reliability and increased sensitivity (due to the lack of beam-defining slits in OA-TOF).

The C₃H₃ + C₂H₂ reaction sequence

One original goal motivating construction of the MPIMS apparatus was the desire to follow reaction sequences relevant to combustion chemistry. The reaction of propargyl radical with acetylene,



previously investigated by Knyazev and Slagle,² is an interesting example of such sequences that may be relevant in molecular weight growth chemistry leading to soot. Their work has shown that the initial product (C₅H₅) can react with excess acetylene to form C₇H₇. This process continues to form C₉H₈ and perhaps larger species. However, no isomeric information was obtained in these studies. Knowing which isomers are produced and in what amounts are critical constraints in testing reaction mechanisms. In addition to studying this reaction starting with propargyl radicals, we can also start the reaction at intermediate points by photolytic production of known isomers of C₅H₅ and C₇H₇, which then react with acetylene.

We have acquired MPIMS spectra of this reaction at 800, 900, and 1000K at a total density of $\sim 1.5 \times 10^{17}$ molecules cm⁻³. In the first reaction step, the results show the presence of two isomers of C₅H₅ (cyclopentadienyl radical and the ethynyl allyl radical), with the latter becoming less important with increasing temperature. Because the experiment records the complete time profile of each species simultaneously, and as a function of ionizing photon energy, we can compare the time constant of a product's rise with that of the reactant's decay. A

match of these profiles kinetically links the production of C_5H_5 (for example) to the decay of H_2CCCH . Kinetic links such as this can be performed at each stage of this reaction sequence.

For the larger radicals, we see production of three isomers of C_7H_7 as a function of temperature and starting point of the reaction (i.e., starting with propargyl vs. cyclopentadienyl). A main contributor is the benzyl radical; the other isomers are yet to be conclusively identified. The C_9H_9 radical is apparently unstable at the temperatures investigated, and appears to produce only indene (C_9H_8) upon loss of a hydrogen atom.

The $C_3H_3 + C_6H_5 \rightarrow C_9H_8$ reaction

The most important reaction in the formation of the first aromatic ring in combustion appears to be the propargyl (C_3H_3) self reaction. Propargyl radicals are resonance stabilized, leading to slow reactivity with closed-shell species, and can therefore attain concentrations much higher than most free radicals. By analogy, it seems probable that the next steps in soot formation, beyond the first aromatic ring, might involve reactions of propargyl with radicals that already contain a benzene ring, such as phenyl (C_6H_5).

In collaboration with Talitha Selby (University of Wisconsin), Ahren Jasper, and Stephen Klippenstein, we have nearly completed a combined experimental and theoretical study on the isomer distributions of the C_9H_8 product from this reaction from 1 – 10 Torr and from 300 – 1000 K. At low temperature (300 K), the experiment shows that the only C_9H_8 products formed are the expected initial adducts of the barrierless association of propargyl with phenyl, namely, phenyl allene and 3-phenyl propyne. As temperature increases to 600 K, a clear signature of an additional isomer is present, which is most easily explained by including 1-phenyl propyne in the fits to the data. At the highest temperature investigated, 1000K, we observe strong evidence for isomerization forming indene, a resonance-stabilized compound consisting of a 6-member ring fused to a 5-member ring. This structural motif leads to polycyclic aromatic hydrocarbons that are non-planar.

To aid in interpretation of these results, we have investigated several isomerization pathways using high level electronic structure calculations. We have calculated the rates of barrierless addition of the two reactants using variable reaction coordinate variational transition state theory (VRC-TST). In addition, multiple well master equation calculations are used to predict the final branching ratios among the different isomers observed in the experiment.

Future Directions

Using TR-FTS, we will continue to investigate photodissociation reactions that show evidence for roaming dynamics. Following on the recent work of Suits and coworkers³ on acetone photodissociation, we plan to study production of C_2H_6 in this system.

A new modification of the MPIMS apparatus is the creation of a low temperature flow tube accessing the temperature range 230 – 300 K. This improvement will allow us to access a much broader range of reciprocal temperature space, providing more stringent tests of global mechanisms in combustion reactions.

BES-sponsored publications, 2008 – present

- 1) "Reactions of the CN radical with benzene and toluene: product detection and low temperature kinetics," A. J. Trevitt, F. Goulay, C. A. Taatjes, D. L. Osborn, and S. R. Leone, *J. Phys. Chem. A* **114**, 1749 (2010).
- 2) "Reaction of the C₂H radical with 1-butyne (C₄H₆): Low temperature kinetics and isomer-specific product detection," S. Soorkia, A. J. Trevitt, T. M. Selby, D. L. Osborn, C. A. Taatjes, K. R. Wilson, and S. R. Leone, *J. Phys. Chem. A* **114**, 3340 (2010).
- 3) "Products of the benzene + O(³P) reaction," C. A. Taatjes, D. L. Osborn, T. M. Selby, G. Meloni, A. J. Trevitt, E. Epifanovsky, A. Krylov, B. Sirjean, E. Dames, and H. Wang, *J. Phys. Chem. A* **114**, 3355 (2010).
- 4) "Direct detection of pyridine formation by the reaction of CH (CD) with pyrrole: a ring expansion reaction," S. Soorkia, C. A. Taatjes, D. L. Osborn, T. M. Selby, A. J. Trevitt, K. R. Wilson, and S. R. Leone, *Phys. Chem. Chem. Phys.* (accepted, 2010).
- 5) "Isomer-selective study of the OH initiated oxidation of isoprene in the presence of O₂ and NO: I. The minor inner OH-addition channel" E. E. Greenwald, B. Ghosh, K. C. Anderson, K. S. Dooley, P. Zou, T. M. Selby, D. L. Osborn, G. Meloni, C. A. Taatjes, F. Goulay, and S. W. North, *J. Phys. Chem. A* **114**, 904 (2009).
- 6) "Cyclic versus linear isomers produced by reaction of the methylidyne radical (CH) with small unsaturated hydrocarbons" F. Goulay, A. J. Trevitt, G. Meloni, T. M. Selby, D. L. Osborn, C. A. Taatjes, L. Vereecken, and S. R. Leone, *Journal of the American Chemical Society* **131**, 993 (2009).
- 7) "Temperature-Dependent Kinetics of the Vinyl Radical (C₂H₃) Self-Reaction," H. Ismail, P. Abel, W. Green, A. Fahr, L. Jusinski, A. Knepp, J. Zádor, G. Meloni, T. M. Selby, D. L. Osborn, C. A. Taatjes, *Journal of Physical Chemistry A* **113**, 1278 (2009).
- 8) "Isomer-specific product detection of CN radical reactions with ethene and propene by tunable VUV photoionization mass spectrometry," A. J. Trevitt, F. Goulay, G. Meloni, D. L. Osborn, C. A. Taatjes, and S. R. Leone, *International Journal of Mass Spectrometry* **208**, 113 (2009).
- 9) "Enol Formation and Ring-Opening in OH-Initiated Oxidation of Cycloalkenes," G. Meloni, T. M. Selby, and D. L. Osborn, and C. A. Taatjes, *Journal of Physical Chemistry A* **112**, 13444 (2008).
- 10) "The multiplexed chemical kinetic photoionization mass spectrometer: a new approach to isomer-resolved chemical kinetics," D. L. Osborn, P. Zou, H. Johnsen, C. C. Hayden, C. A. Taatjes, V. D. Knyazev, S. W. North, D. S. Peterka, M. Ahmed, and S. R. Leone, *Review of Scientific Instruments* **79**, 104103 (2008).
- 11) "Synchrotron photoionization mass spectrometry measurements of kinetics and product formation in the allyl radical (H₂CCHCH₂) self-reaction," T. M. Selby, G. Meloni, F. Goulay, S. R. Leone, A. Fahr, C. A. Taatjes, and D. L. Osborn, *Journal of Physical Chemistry A* **112**, 9366 (2008).
- 12) "Absolute photoionization cross-section of the methyl radical," C. A. Taatjes, D. L. Osborn, T. M. Selby, G. Meloni, H. Fan, and S. T. Pratt, *Journal of Physical Chemistry A* **112**, 9336 (2008).
- 13) "Roaming is the dominant mechanism for molecular products in acetaldehyde photodissociation" B.R. Heazlewood, M.J.T. Jordan, S.H. Kable, T.M. Selby, D.L. Osborn, B. C. Shepler, B.J. Braams, and J.M. Bowman, *Proceedings of the National Academy of Sciences* **105**, 12719 (2008).
- 14) "Direct Observation of the Gas-Phase Criegee Intermediate (CH₂OO)" C. A. Taatjes, G. Meloni, T. M. Selby, A. J. Trevitt, D. L. Osborn, C. J. Percival, and D. E. Shallcross, *Journal of the American Chemical Society* **130**, 11883 (2008).
- 15) "Ultraviolet photodissociation of vinyl iodide: understanding the halogen dependence of photodissociation mechanisms in vinyl halides" P. Zou, K. E. Strecker, J. Ramirez-Serrano, L. E. Jusinski, C. A. Taatjes, D. L. Osborn, *Physical Chemistry Chemical Physics* **10**, 713 (2008).
- 16) "Imaging combustion chemistry via multiplexed synchrotron-photoionization mass spectrometry" C. A. Taatjes, N. Hansen, D. L. Osborn, K. Koehse-Hoinghaus, T. A. Cool, P. R. Westmoreland, *Physical Chemistry Chemical Physics* **10**, 20 (2008).
- 17) "Exploring multiple reaction paths to a single product channel" D. L. Osborn, *Advances in Chemical Physics* **138**, 213 (2008).

References

- ¹ I. R. Slagle and D. Gutman, *J. Am. Chem. Soc.* **107**, 5342 (1985).
- ² V. D. Knyazev and I. R. Slagle, *J. Phys. Chem. A* **106**, 5613 (2002).
- ³ V. Goncharov, N. Herath, and A. G. Suits, *J. Phys. Chem. A* **112**, 9423 (2008).

Theoretical Studies of the Combustion Reactions of Asphaltene Model Compounds

Carol A. Parish

Department of Chemistry, University of Richmond
Richmond, VA 23173
cparish@richmond.edu

I. Program Scope

We seek to utilize theoretical methods to understand the gas phase structures and energies of the combustion and pyrolysis reactions of the molecular constituents of asphaltenes contained in oil sand and oil shale. Asphaltenes represent an untapped source of hydrocarbon fuels in North America; however, information about the molecular nature of these deposits has only recently become available.¹ Theoretical and experimental evidence suggests that asphaltenes are composed of molecules that contain 4-10 fused ring cores, with alkyl chain arms extending from the core. Sulfur and nitrogen may also be present.² Very little is known about the reaction pathways of these heteroaromatic species.

II. Summary of Recent Accomplishments related to the project

A. Singlet Excited States of *p*-benzyne

Understanding the potential energy surfaces of species important in asphaltene combustion mandates an accurate and efficient characterization of radical intermediates. Towards this end, we have recently completed a collaboration with Hans Lischka of the University of Vienna, to characterize the 4 lowest states (1^1A_g , $3B_{3u}$, $1B_{3u}$ and 2^1A_g ; D_{2h} oriented in the *yz* plane) and associated vertical excitations of *p*-benzyne using MCSCF state-averaging and MR-AQCC methods.¹⁴ There have been numerous studies¹⁵⁻²⁴ of the *p*-benzyne open shell singlet ground state (1^1A_g); however, to our knowledge there have been very few reports of the characterization of the other three states ($3B_{3u}$, $1B_{3u}$ and $2^{nd} 1^1A_g$). Slipchenko and Krylov have characterized the ground and lowest triplet state and reported that there is a high density of states in the range from 4 to 7 eV due to extensive orbital degeneracy.²⁵ Our results were obtained in large part by undergraduate student Evan Wang (UR '09) using state-averaged MCSCF, CISD, CISD+Q with *a posteriori* Davidson-type corrections (for size extensivity) and MR-AQCC. A variety of basis sets were employed and initial calculations included only the diradical orbitals in the (2,2) active space; however, results indicated that this reference space was not large enough. Therefore, we expanded the active space to (8,8) by adding the bonding and anti-bonding π orbitals. Even within this larger space, the second 1^1A_g singlet state was difficult to converge, likely due to interactions between this state and a low lying Rydberg state. Our results indicate that there is a very high density of electronic states in this diradical system – there are more than seventeen states within 7 eV of the ground state including two 3s Rydberg states. All excitations, except 2^1A_g , are from the π system to the $\sigma\sigma^*$ system. Of the thirty-two states characterized, fifteen were multi-configurational, including the ground 1^1A_g state, which provides further evidence for the necessity of a multireference approach for the *p*-benzyne diradical.

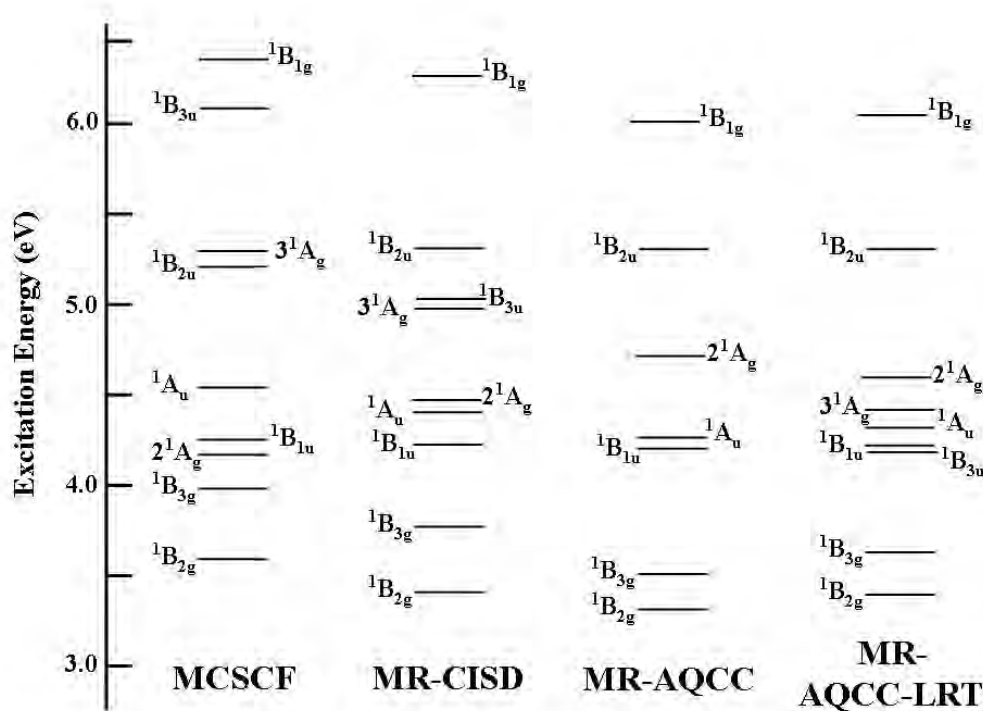


Figure 3. A comparison of valence states for *p*-benzyne calculated using 10-SA and MCSCF, MR-CISD, MR-AQCC and MR-AQCC-LRT. Results are not shown for MRCISD+Q as they are within 0.03 eV agreement of the AQCC results.

III. Future Work

Initially, the reactions of methyl thiophene will be utilized as a model for larger asphaltene heteroaromatic constituents. Work is currently underway to characterize the singlet and triplet combustion surfaces of methyl thiophene reaction with triplet oxygen; in particular we are investigating a hydrogen abstraction and ring opening pathway. We are also pursuing a complete characterization of the singlet and triplet surfaces of the electrocyclic reaction of (*Z*)-hexa-1,3,5-triene leading to *p*-benzyne.

IV. References

1. Mullins, O. C.; Sheu, E. Y.; Hammami, A.; Marshall, A. G. *Asphaltenes, Heavy Oils and Petroleomics*; Springer: New York, 2007.
2. Ruiz-Morales, Y.; Wu, X.; Mullins, O. C. *Energy and Fuels* **2007**, *21*, 944-952.

V. Recent publications and journal articles (undergraduate co-authors underlined).

1. "Conformational Analysis of a Model for the trans-fused FGH Ether Rings in Brevetoxin A," Evan B. Wang and Carol A. Parish, *Journal of Organic Chemistry*, **2010** *75*, 1582-1588.
2. "Triphenylamine-Based Receptors for Selective Recognition of Dicarboxylates," Kumaresh Ghosh, Indrajit Saha, Goutam Masanta, Evan B. Wang and Carol A. Parish, *Tetrahedron Letters*, **2010** *51*, 343-347.

3. Conformational Analysis of Trimeric Maleimide Substituted 1,5,9-triazacyclododecane HIV Fusion Scaffolds,” Sarah Remmert, Heather Hollis and Carol Parish, *Bioorganic and Medicinal Chemistry*, **2009** *17*, 1251-1258.
4. “Energetic Analysis of Chair and Boat Conformations of Maleimide Substituted Cyclohexane Derivatives,” Sarah Remmert and Carol Parish, *Journal of Computational Chemistry*, **2009** *30*, 992-998.
5. “An Extended Multireference Study of the Electronic States of para-benzyne,” Evan Wang, Carol Parish and Hans Lischka, *Journal of Chemical Physics*, **2008** *129*, 44306:1-44306:8.
6. “Synthesis, Spectroscopy and Theoretical Calculations for a Series of Push-Pull [14]-pyridoannulenes,” Matthew M. Lauer, James W. Leslie, Ashley Mynar, Shelly A. Stamper, Anthony D. Martinez, Adrian J. Bray, Senai Negassi, Kevin McDonald, Eric Ferraris, Aaron Muzny, Shawn McAvoy, Keith Walters, Keith C. Russell, Evan Wang, Betsy Nuez and Carol Parish, *Journal of Organic Chemistry*, **2008**, *73*, 474-484.

The Dynamics of Large-Amplitude Motion in Energized Molecules

David S. Perry, Principal Investigator
Department of Chemistry, The University of Akron
Akron OH 44325-3601
DPerry@Uakron.edu

I. Program Scope

Most theories of reaction rely, either explicitly or implicitly, on a separation of the large-amplitude degrees of freedom from the other nuclear motions. For example, transition state theory (including its unimolecular variant RRKM theory) identifies a reaction coordinate and assumes thermal equilibrium among the other degrees of freedom. The transition state is a dividing hypersurface between reactants and products located at some point along the reaction coordinate so as to minimize recrossing. At high energies, particularly just below the threshold for a new fragmentation channel, there may be “roaming” trajectories, which may favor particular product channels and which clearly involve more than one large-amplitude degree of freedom. An alternative to transition state theory is the adiabatic channel model in which the excitation in one of more of the orthogonal degrees of freedom is assumed to be conserved as the system moves along the reaction coordinate. At the other end of the spectrum from statistical theories, close-coupled quantum scattering calculations are limited by practical considerations to a few degrees of freedom. Thus in systems larger than 3 or 4 atoms, one must define the active degrees of freedom and separate them in some way from the other degrees of freedom.

In this research, we test the limits of the adiabatic separation of different nuclear degrees of freedom, in particular, the separation of the large amplitude nuclear degrees of freedom (LADF) from the small amplitude vibrations (SAV). We will call this *vibrational adiabaticity* to distinguish it from *electronic adiabaticity*, that is, from the Born-Oppenheimer approximation. Nonadiabatic coupling terms scale as $(m/M)^{1/4}$ where m is the reduced mass for the fast degree of freedom and M is that for the slow degree of freedom. In the Born-Oppenheimer approximation, $m \ll M$, but in the vibrational case, often $m \approx M$. Therefore, the vibrational adiabatic approximation is on much more tenuous ground. The limits of its usefulness and the consequences of its failure are examined in this project.

While scattering systems are of primary interest in reactive chemistry, the collision complexes are relatively short lived and can rarely be probed directly. For this reason, we choose bound molecules, including methanol, nitromethane and methylamine, as our laboratory for studying adiabatic separations and consequent nonadiabatic effects. Bound systems are by definition long-lived, which means that we are able to use high-resolution spectroscopy to probe the interactions with a high level of precision and detail. In addition to cavity ringdown experiments and calculations at the University of Akron, experimental work on this project involves a collaboration with Brooks Pate's group at the University of Virginia (CD-FTMW-IR). A new collaboration with Michel Herman of the Université Libre de Bruxelles on the rotationally dependent dynamics of acetylene was initiated during the past year.

II. Recent Progress

A. Torsion-Vibration Dynamics and the Adiabatic Approximation

The work on methanol and nitromethane under this project, when taken together with work by other authors on these molecules (i, ii) and on hydrogen peroxide (iii), points to a number of conclusions that may have some generality [3]:

- The coupling of the torsion to the stretching vibrations of adjacent hydrogens is strong, typically 40 to 80 cm^{-1} per quantum of XH stretch. The peak-to-peak values reach 270, 500, 265, 460 cm^{-1} by $\nu_{\text{XH}}=6$ in the methanol OH, CH, nitromethane CH, and hydrogen peroxide OH manifolds

respectively. The magnitude of the torsion-vibration coupling is generally similar in these systems even though the ground state torsional potentials are very different.

- The form of the leading torsion-vibration coupling term is determined by the symmetry of the rotor at the opposite end of the torsional bond from the excited stretching vibration, with the lower symmetry contributions being larger ($\cos\alpha$ terms $>$ $\cos2\alpha$ or $\cos3\alpha$ terms).
- The adiabatic treatment of torsional motion as occurring in an effective potential determined by the high frequency vibrations is a useful tool for analyzing torsion-vibration spectra, and appears to offer a general means of predicting the occurrence of inverted torsional tunneling but it does not account for the pattern of CH stretch-torsion levels in CH_3OH at high torsional excitation.
- In the high CH overtone region of CH_3OH and CH_3NO_2 ($\nu_{\text{CH}} \geq 4$), there is a transition from adiabatic to diabatic behavior [1, 3], a consequence of the transition from normal mode CH vibrations to local modes as the CH stretch excitation is increased.
- In CH_3OH , we found that neither the adiabatic nor the diabatic approximation is quantitatively accurate relative to fully coupled calculations, even within its respective domain of applicability [1, 3]. The torsion-vibration coupling results in “nonadiabatic” IVR coupling matrix elements, which results in energy exchange between the torsion and the CH vibrations. The scaling properties of the IVR coupling, which derive from the nature of the 1-dimensional torsional motion, indicate a role for direct high-order coupling.

B. Two-Dimensional Large-Amplitude Motion

The two-dimensional torsion-inversion potential energy surfaces of methylamine, protonated methanol, and ethyl radical have been investigated with partially optimized *ab initio* calculations [4]. All three molecules belong to the G_{12} molecular symmetry group and each has six equivalent minima. CH_3NH_2 has a high barrier to inversion ($\sim 1950 \text{ cm}^{-1}$), whereas in CH_3OH_2^+ the barrier is lower ($\sim 875 \text{ cm}^{-1}$). In CH_3CH_2^- , there is no barrier to inversion. The torsional barriers in these systems are about 704, 400, and 21 cm^{-1} respectively. The computed torsion-inversion surfaces were fit to a function of the form (Fig. 1),

$$V(\alpha, \tau) = \sum_{n=0}^4 \sum_{m=0}^{12} V_{m,3n} \tau^m \cos(3n\alpha),$$

where α , is the torsional angle, τ is the inversion angle, and $m+n = \text{even}$. Even though the three surfaces are quite different (Fig. 1(a)), we find that the torsion-inversion coupling is similar in strength (Fig. 1(b)). The dominant torsion-inversion coupling term in all three cases has the form, $V_{1,3}\tau \cos3\alpha$, with $V_{1,3}$ in the range 280 to 450 cm^{-1} .

The synthesis these results with those of section A. above indicates that the coupling terms, whether torsion-vibration or torsion-inversion, have typical values that vary by less than a factor of two in a range of systems where the barriers to torsion or inversion vary by orders of magnitude.

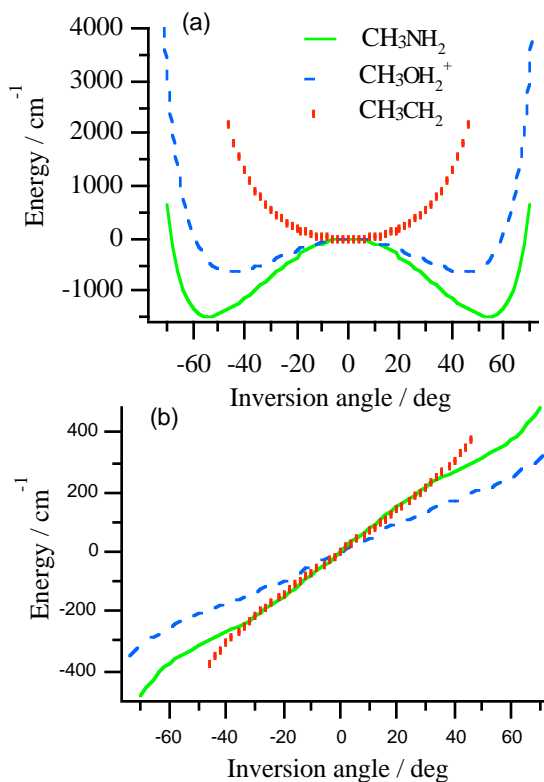


Fig. 1. *Ab initio* results at the CCSD(T)/6-311++G(3df,2p)//MP2/6-311++G(3df,2p) level on three CH_3XH_2 molecules. (a) The torsionally invariant part ($V_{m,0}$ terms) of the fitted potentials. (b) The $\cos3\alpha$ part of the torsion-inversion coupling ($V_{m,3}$ terms).

C. Spectroscopy and Torsion-Vibration Coupling in the CH Stretch Region of Methanol

The three CH stretch fundamentals of methanol have been resolved at high resolution and assigned in detail and those results have contributed to the analysis in section A above; nonetheless, there is a great deal of additional spectral complexity in this region. To understand the responsible interactions, a new experimental technique for rotationally selected infrared spectra has been applied to obtain assignments for dozens of additional vibrational bands in the range 2700 – 3000 cm^{-1} for the E species of both CH_3OH and CH_3OD [2, 5].

The technique, developed at the University of Virginia, is coherence-detected Fourier transform microwave – infrared spectroscopy (CD-FTMW-IR). Population transfer induced by a pulsed IR laser is detected by FTMW spectroscopy using a sequence of two microwave pulses. The first pulse converts the thermal population difference to a coherence using an approximate “ $\pi/2$ ” pulse. Then, an IR laser pulse interacts with the polarized sample. Finally, a second microwave pulse with a 180° phase shift is applied to perform a “ $-\pi/2$ ” excitation. The sequence of two microwave pulses produces a null signal in the absence of the IR pulse and hence a flat baseline upon which the state-detected infrared transitions are observed.

In the ν_3 symmetric CH stretch region (2750 - 2890 cm^{-1}) of CH_3OH , a total of 12 interacting vibrations are observed [2]. By contrast, this region of CH_3OD is almost unperturbed. The pattern of the combined spectra can be explained by the following coupling pathway:

- ν_3 CH stretch \Rightarrow HCH bend + COH bend (tier 1)
- \Rightarrow HCH bend + methyl rock + torsion (tier 2)
- \Rightarrow combination states with additional quanta of torsion (tier 3 and higher)

The data allow insightful comparisons with time-domain solution-phase spectra.

The higher frequency region of CH_3OD (2890 - 3020 cm^{-1}) contains the asymmetric CH stretches (ν_2 and ν_9) and 15 additional bands that have been rotationally assigned. The number of observed vibrational bands indicates that the CH stretch bright states couple first to the binary CH bend combinations, and then to higher order combinations of the normal modes, including torsional excitation. This region of CH_3OH is even more complicated and that analysis is underway.

The OD stretch fundamental of CH_3OD (2710 - 2736 cm^{-1}) has been resolved and assigned.

D. Rotational Dependence of the Intramolecular Dynamics in Acetylene

In a linear molecule like acetylene, there is no torsional motion in the unexcited molecule, but in vibrationally excited states where non-linear geometries are accessed, the vibrational angular momenta take on a key role in the dynamics. In acetylene, the couplings involving the vibrations, vibrational angular momenta, and overall rotation are understood in detail up to 8600 cm^{-1} from the analysis of high-resolution spectra (iv). We have explored the calculated time-dependent dynamics of polyads in this region [6]. The dynamics of single rotational levels show the recurrences characteristic of the sparse coupling limit, but thermal distributions of rotational levels yield apparent irreversible decays that result from the dephasing of the inhomogeneous distribution of rotational levels. The form of the decays in a given polyad depends critically on the definition of the bright state. This work elucidates significant issues that must be considered when comparing time-resolved and frequency-resolved spectra.

III. Future Work

The development of the continuous-wave cavity ringdown (CW-CRDS) and CD-FTMW-IR techniques will continue, targeting experiments on the CH manifolds in methylamine and methanol. A new wavelength scanning mechanism is being developed for the CW OPO laser system. The parts have been ordered for the extension of the CD-FTMW-IR technique to the 48 GHz range to allow improved sensitivity and access to the methanol A species. CD-FTMW-IR experiments on methylamine are

planned. The calculations on the CH₃XH₂ systems will be extended to include the coupling of the two large amplitude motions to CH stretch vibrations. The time-dependent dynamics of acetylene will be extended to higher energy where there are new kinds of large-amplitude vibrational modes, such as the local bender and the counter rotator.

IV. References

- i. B. Fehrensen, D. Luckhaus, M. Quack, M. Willeke, and T. R. Rizzo, *J. Chem. Phys.* **119**, 5534 (2003).
- ii. D. Cavagnat, L. Lespade, *J. Chem. Phys.* 106 (1997) 7946-7957.
- iii. H. R. Dübal, F. F. Crim, *J. Chem. Phys.* 83 (1985) 3863-72; B. Kuhn, T. R. Rizzo, D. Luckhaus, M. Quack, M. A. Suhm, *J. Chem. Phys.* 111 (1999) 2565-2587.
- iv. B. Amyay, S. Robert, M. Herman, A. Fayt, B. Raghavendra, A. Moudens, J. Thiévin, B. Rowe, and R. Georges, *J. Chem. Phys.* **131**, 114301 (2009).

VI. Publications from this Project, 2008-2010

1. David S. Perry, Torsion-vibration coupling in methanol: Diabatic behavior in the CH overtone region, *J. Phys. Chem. A* **112**, 215-223 (2008). <http://dx.doi.org/10.1021/jp077269q>.
2. Sylvestre Twagirayezu, David S. Perry, Justin L. Neill, Matt T. Muckle, Brooks H. Pate, Vibrational coupling pathways in the ν_3 CH stretch fundamental region of methanol as revealed by coherence-detected FTMW-IR spectroscopy, *Bull. Am. Phys. Soc.* **54**(1), V37.00007 (2009). http://absimage.aps.org/image/MWS_MAR09-2008-001026.pdf
3. David S. Perry, The Adiabatic Approximation as a Diagnostic Tool for Torsion-Vibration Dynamics, *J. Mol. Spectrosc.* **257**(1), 1-10, 2009 (feature article), <http://dx.doi.org/10.1016/j.jms.2009.05.002>.
4. Ram S Bhatta, Amy Gao, David S Perry, A comparative ab initio study of torsion-inversion coupling in CH₃NH₂, CH₃OH₂⁺ and CH₃CH₂, *J. Mol. Struct.: THEOCHEM*, **941**, 22-29, 2009, <http://dx.doi.org/10.1016/j.theochem.2009.10.033>.
5. Sylvestre Twagirayezu, David S. Perry, Justin L. Neill, Matt T. Muckle, Brooks H. Pate, Coherence-converted population transfer FTMW-IR double resonance spectroscopy of CH₃OD in the asymmetric CH-Stretch Region, *Bull. Am. Phys. Soc.* **55**(2), P27.00003 (2010), http://absimage.aps.org/image/MWS_MAR10-2009-006226.pdf.
6. David Perry, Anthony Miller, B. Amyay, A. Fayt and M. Herman, Vibration-rotation alchemy in acetylene (¹²C₂H₂), X ¹Σ_g⁺ at low vibrational excitation: From high resolution spectroscopy to fast intramolecular dynamics, *Mol. Phys.*, 2010, in press.

New Single- and Multi-Reference Coupled-Cluster Methods for High Accuracy Calculations of Ground and Excited States

Piotr Piecuch

Department of Chemistry, Michigan State University
East Lansing, MI 48824
piecuch@chemistry.msu.edu

I. Program Scope

This research program focuses on the development and applications of new generations of *ab initio* electronic structure methods and computer codes, exploiting coupled-cluster (CC) wave function ansatz, which can provide an accurate description of chemical reaction pathways, radicals, biradicals, potential energy surfaces (PESs), properties other than energy, and electronic excitations in molecules. The goal is to design and apply affordable computational methods that enable precise modeling of molecular processes and properties relevant to combustion, catalysis, and photochemistry. Among the most promising methods developed in this program are (i) the renormalized CC and equation-of-motion CC (EOMCC) approaches, and the low-order scaling, local correlation extensions of the conventional and renormalized CC methods to larger systems involving hundreds of correlated electrons, (ii) the active-space CC and EOMCC methods, and (iii) the genuine multi-reference CC (MRCC) theories. The renormalized CC methods and their open-shell, local correlation, and excited-state extensions extend the standard single-reference theories to multi-reference situations created by radicals, biradicals, bond breaking, and two-electron excitations with an ease of a black-box calculation that can be performed by non-experts. The active-space CC and EOMCC approaches, and their open-shell generalizations via the electron attached (EA) and ionized (IP) theories as well as the genuine MRCC methods have the flexibility that enables accurate *ab initio* calculations for all kinds of closed- and open-shell electronic states with manageable computer costs. All methods pursued in this program can utilize modern multi-node computer architectures and are well suited for pursuing novel coding strategies, such as the automated computer implementation. They address two main challenges of electronic structure theory, which are (i) the development of practical and systematically improvable computational schemes that can provide a balanced and accurate description of closed- and open-shell systems, and the rapidly changing electron correlation effects along reaction coordinates, and (ii) the development of algorithms that can reduce prohibitive costs of traditional high-accuracy *ab initio* calculations by attacking the scaling laws that define the dependence of computer costs on the system size. Methods developed in this program are shared with the community by incorporating them in the GAMESS package.

II. Recent Progress (2008-2010)

We have extended the left-eigenstate, completely renormalized (CR) CC method with singles, doubles, and non-iterative triples [CR-CC(2,3)] to excited states of open-shell systems [17]. The resulting CR-EOMCC(2,3) approach corrects the EOMCCSD energies for triples using the non-iterative N^7 steps similar to those used in CCSD(T) and CR-CC(2,3). The CR-EOMCC(2,3) code, using the computationally efficient expressions from [17], and the modified variant of CR-EOMCC(2,3) that enforces size intensivity of excitation energies have been added to GAMESS. These new codes, along with the EA- and IP-EOMCC options mentioned below, will become part of the official GAMESS release within the next month or so. The open-shell CR-EOMCC(2,3) approach utilizing the ROHF reference provides great improvements in the EOMCCSD results for doublet and quartet states of radicals and other open-shell species, particularly for the excited states dominated by two-electron processes, where errors in the excitation energies obtained with EOMCCSD often exceed 1 eV, as shown for CH, CNC, C₂N, N₃, and NCO [15,17]. We have provided the alternative derivation of the biorthogonal method of moments of CC equations, on which CR-CC(2,3) and CR-EOMCC(2,3) are based [6]. This has enabled us to explain why CR-CC(2,3) is more accurate than the earlier CR-CCSD(T) approach and its CCSD(2)_T analog, which are, in turn, more robust than CCSD(T) in situations involving bond breaking and biradicals. We have illustrated the advantages of CR-CC(2,3) over other non-iterative triples CC methods by examining singlet-triplet gaps of magnetic systems [6]. We have developed the initial CR-CC(2,4) and CR-

EOMCC(2,4) codes that correct the CR-CC(2,3)/CR-EOMCC(2,3) energies for quadruples [10] and completed work on the non-iterative CC/EOMCC methods using multi-reference MP2 wave functions [8]. We have also developed the simplified CR-CC(2,4) model, termed CR-CC(2,3)+Q, which reduces the non-iterative N^9 steps associated with quadruples corrections to the less expensive N^7 steps [1,5,14].

We have developed the local correlation CCSD, CCSD(T), and CR-CC(2,3) approaches [12,19-22]. The resulting CIM-CCSD, CIM-CCSD(T), and CIM-CR-CC(2,3) methods use orthonormal localized orbitals and enable high accuracy calculations for systems with hundreds of correlated electrons and thousands of basis functions. Our CIM-CC codes [12,19-22] are characterized by the linear scaling of the CPU time with the system size when single-level CIM-CC is used, coarse-grain parallelism, and non-iterative character of local triples corrections to CCSD. They enable one to mix different theory levels (e.g., canonical CCSD with local triples corrections [12,19-21]). By comparing the canonical and CIM-CC results for alkanes and water clusters of varying size, we have demonstrated that CIM-CCSD, CIM-CCSD(T), and CIM-CR-CC(2,3) recover the corresponding CC correlation energies to within 0.1 % or so, while offering savings in the computer effort by orders of magnitude. By examining bond breaking in alkanes and low-energy structures of the $(\text{H}_2\text{O})_n$ clusters, we have shown that the CIM-CC methods accurately reproduce the relative energetics of the canonical CC calculations. We have applied CIM-CR-CC(2,3), combined with the embedded cluster QM/MM method called SIMOMM, to the etching and diffusion of atomic oxygen on the Si(100) surface, obtaining accurate information about the activation barriers and energetics characterizing these processes [23]. Thanks to CIM-CC, we could perform the CR-CC(2,3) calculations for clusters as large as $\text{Si}_{15}\text{H}_{16}\text{O}$ [23]. We have also worked toward improvements in the CIM-CC methodology that are particularly relevant for large weakly bound molecular clusters, where the relative energies between different structures on the PES are on the order of a few kcal/mol and where one has to use basis sets with diffuse functions, obtaining excellent results [21]. We have proposed multi-level CIM-CC methods that combine the high-level CC approaches, such as CR-CC(2,3), which are used to treat the reactive parts of a large molecular system, with the lower-order schemes, such as MP2, to handle the chemically inactive regions, without splitting the system into *ad hoc* fragments and saturating dangling bonds [22]. The results of multi-level CIM-CC/MP2 calculations for bond breaking in large alkanes and the reaction between the bis(2,4,4-trimethylpentyl)dithiophosphinic acid and water (important for nuclear waste management) are outstanding [22]. If the reactive region treated by CC has a fixed size and the system is grown by adding MP2 regions, the size dependence of the costs of multi-level CIM-CC/MP2 computations is virtually none.

We have continued applying the CR-CC methods to important chemical problems [1-5,7,10,11,14]. Calculations for the diverse set of reaction barrier heights included in the DBH24 database of Truhlar et al. have shown that CR-CC(2,3) provides high accuracy results for thermochemical kinetics [2] that can compete with those obtained with CCSD(T), while eliminating failures of CCSD(T) in bond breaking regions [1,5,11,14]. We have shown that CR-CC(2,3) offers an excellent description of the bond breaking reactions of several open-shell species consisting of C, H, Si, and Cl, relevant to the gas-phase chemistry of the silicon carbide chemical vapor deposition [11]. In particular, the non-singlet PESs characterizing bond breaking in open-shell species obtained with the ROHF-based CR-CC(2,3) have substantially smaller non-parallelity errors than those obtained with the frequently used UHF-based CCSD(T), while reducing the reaction energy errors obtained with multi-reference MP2, in spite of the single-reference ‘black-box’ nature of CR-CC(2,3) [11]. We have also proposed an efficient computational strategy to estimate the CR-CC(2,3)/cc-pVTZ PESs, in which the most expensive steps are defined by the MP2/cc-pVTZ and CR-CC(2,3)/cc-pVDZ calculations [11]. We have demonstrated that the CR-CC(2,3)+Q approach, in which one corrects the CR-CC(2,3) energy in a relatively inexpensive fashion for the quadruples effects, describes the PESs of H_2O and H_2S , all the way up to the dissociation of H_2O into $2\text{H}+\text{O}$ and H_2S into $2\text{H}+\text{S}$ [including the $\text{Y}(2p^4\ ^1\text{D})+\text{H}_2(\text{X}^1\Sigma_g^+) \rightarrow \text{YH}(\text{X}^2\Pi)+\text{H}(1s\ ^2\text{S})$, $\text{Y}=\text{O},\text{S}$, processes, of significance in combustion and atmospheric chemistry], in the accurate and computationally efficient manner, comparable to the best multi-reference configuration interaction (MRCI) data [1,5]. The CR-CC(2,3)+Q method has been used to make the new best estimates of the stationary point energetics for the cycloadditions of ozone to ethyne and ethane [14].

We have examined the low-lying states of CNC, C₂N, N₃, and NCO [15,17], and the singlet-triplet gaps in the challenging BN and C₂ molecules [10]. In the former case, we have shown that CR-CC(2,3) and CR-EOMCC(2,3) provide an excellent description of the low-lying states that are poorly described by EOMCCSD [15,17]. In the latter case, the black-box CR-CC(2,4) approach has provided excellent values of the tiny singlet-triplet gaps in BN and C₂ that agree with the expert, reduced MRCC (RMRCC) calculations with multi-reference singles and doubles, and non-iterative triples, and with experiment. We have also continued our work on the copper-dioxygen systems, of significance in catalysis and activation of oxygen by metalloenzymes [3]. By comparing the CR-CC(2,3), CASPT2, and density-functional theory (DFT) results, we have explained why the relative energies and singlet-triplet gaps of the various CuO₂ motifs are sensitive to the nature of the supporting ligands, and how and why these characteristics depend upon the geometric arrangement of ligands relative to the O₂ binding site [3].

We have developed the extrapolation procedure which predicts the smooth molecular PES corresponding to a larger basis set or to the CBS limit from a series of inexpensive calculations using smaller basis sets by scaling the electron correlation energies [4,7]. By examining the isomerization pathways of bicyclobutane to butadiene, we have shown that the CR-CC(2,3)/cc-pVQZ PESs obtained by the extrapolation from the smaller basis set calculations are virtually identical to the true CR-CC(2,3)/cc-pVQZ PESs [4,7]. The same applies to the CR-CC and MRCI calculations for other PESs. Our extrapolation procedure predicts the CBS limits of the calculated PESs from the results of smaller basis set calculations at a tiny fraction of the effort required by point-wise CBS extrapolations [4,7].

We have continued our earlier work on extending the active-space CC and EOMCC theories to ground and excited states of radicals and other valence systems by combining them with the EA/IP EOMCC methodology [15,17]. We have demonstrated a superb performance, in terms of accuracy and computational efficiency, of the active-space EA-EOMCCSD(3p2h) and IP-EOMCCSD(3h2p) approaches in calculations of the excitation energies in CH, CNC, C₂N, N₃, and NCO, where the low-lying excited states have a significant multi-reference character, causing problems to EOMCCSD, EA-EOMCCSD(2p1h), and IP-EOMCCSD(2h1p) [15,17]. We have shown that the active-space EA/IP EOMCC schemes, which use small subsets of higher-than-2p1h and 2h1p excitations, reproduce the results of their parent methods, where all such excitations are included, while requiring computational effort similar to CCSD. The EA-EOMCCSD(2p1h), IP-EOMCCSD(2h1p), and full and active-space EA-EOMCCSD(3p2h) codes have been incorporated in GAMESS. Their official release is expected to occur within a month or so. Work is under way to add the full and active-space IP-EOMCCSD(3h2p) options to GAMESS. We have applied the method of moments of CC equations to the generalized MRCC formalism representing the continuous transition between the state-specific Brillouin-Wigner-type and state-universal Rayleigh-Schrödinger-type MRCC theories, and derived the novel formula for the non-iterative corrections to the corresponding MRCC energies that recover the exact energies in the general model space case [16]. As in the past, we have applied CC methods to nuclei [9,13,18].

III. Immediate Future Plans (2010/2011)

- Development of the multi-level local correlation CIM-CC methods mixing CR-CC(2,3) or CCSD(T) with CCSD and MP2. Work toward open-shell extensions of CIM-CC and multi-level CIM-CC.
- Development of the PES extrapolation procedure based on the concept of correlation energy scaling that uses lower-order methods to calculate correlation energy scaling factors for high-level calculations.
- Development of the active-space doubly electron attached (DEA) and doubly ionized (DIP) EOMCC methods. Completing the migration of full and active-space IP-EOMCCSD(3h2p) codes to GAMESS.
- New studies of radical and biradical reactions, and molecular electronic (including radical) spectra.

IV. Publications and submitted journal articles supported by this project (2008-2010)

1. P. Piecuch, M. Włoch, and A.J.C. Varandas, "Application of Renormalized Coupled-Cluster Methods to Potential Function of Water," *Theor. Chem. Acc.* **120**, 59-78 (2008).
2. J. Zheng, J.R. Gour, J.J. Lutz, M. Włoch, P. Piecuch, and D.G. Truhlar, "A Comparative Assessment of the Perturbative and Renormalized Coupled Cluster Theories with a Non-iterative Treatment of Triple Excitations for Thermochemical Kinetics, Including a Study of Basis Set and Core Correlation Effects," *J. Chem. Phys.* **128**, 044108-1 - 044108-7 (2008).

3. C.J. Cramer, J.R. Gour, A. Kinal, M. Włoch, P. Piecuch, A.R.M. Shahi, and L. Gagliardi, "Stereochemical Effects on Molecular Geometries and State-Energy Splittings of Ligated Monocopper Dioxygen Complexes," *J. Phys. Chem. A* **112**, 3754-3767 (2008).
4. J.J. Lutz and P. Piecuch, "Extrapolating Potential Energy Surfaces by Scaling Electron Correlation: Isomerization of Bicyclobutane to Butadiene," *J. Chem. Phys.* **128**, 154116-1 – 154116-12 (2008).
5. Y.Z. Song, A. Kinal, P.J.S.B. Caridade, A.J.C. Varandas, and P. Piecuch, "A Comparison of Single-Reference Coupled-Cluster and Multi-Reference Configuration Interaction Methods for Representative Cuts of the H₂S(¹A₁) Potential Energy Surface," *J. Mol. Struct.: THEOCHEM* **859**, 22-29 (2008).
6. P. Piecuch, J.R. Gour, and M. Włoch, "Biorthogonal Method of Moments of Coupled-Cluster Equations: Alternative Derivation, Further Considerations, and Application to a Model Magnetic System," *Int. J. Quantum Chem.* **108**, 2128-2149 (2008).
7. J.J. Lutz and P. Piecuch, "Extrapolating Potential Energy Surfaces by Scaling Electron Correlation: Isomerization of Bicyclobutane to Butadiene," in: *Nuclei and Mesoscopic Physics*, AIP Conference Proceedings, Vol. 995, edited by P. Danielewicz, P. Piecuch, and V. Zelevinsky (AIP, Melville, NY, 2008), pp. 62-71.
8. M.D. Lodriguito and P. Piecuch, "Method of Moments of Coupled Cluster Equations Employing Multi-Reference Perturbation Theory Wavefunctions: General Formalism, Diagrammatic Formulation, Implementation, and Benchmark Studies," in: *Progress in Theoretical Chemistry and Physics*, Vol. 18, edited by S. Wilson, P. Grout, J. Maruani, G. Delgado-Barrio, and P. Piecuch (Springer, Dordrecht, 2008), pp. 67-174.
9. J.R. Gour, M. Horoi, P. Piecuch, and B.A. Brown, "Coupled-Cluster and Configuration-Interaction Calculations for Odd-A Heavy Nuclei," *Phys. Rev. Lett.* **101**, 052501-1 - 052501-4 (2008).
10. X. Li, J.R. Gour, J. Paldus, and P. Piecuch, "On the Significance of Quadruply Excited Clusters in Coupled-Cluster Calculations for the Low-Lying States of BN and C₂," *Chem. Phys. Lett.* **461**, 321-326 (2008).
11. Y. Ge, M.S. Gordon, P. Piecuch, M. Włoch, and J.R. Gour, "Breaking Bonds of Open-Shell Species with the Restricted Open-Shell Size Extensive Left Eigenstate Completely Renormalized Coupled-Cluster Method," *J. Phys. Chem. A* **112**, 11873-11884 (2008).
12. W. Li, P. Piecuch, and J.R. Gour, "Local Correlation Calculations Using Standard and Renormalized Coupled-Cluster Methods," in: *Theory and Applications of Computational Chemistry - 2008*, AIP Conference Proceedings, Vol. 1102, edited by D.-Q. Wei and X.-J. Wang (AIP, Melville, NY, 2009), pp. 68-113.
13. R. Roth, J.R. Gour, and P. Piecuch, "Ab Initio Coupled-Cluster and Configuration Interaction Calculations for ¹⁶O Using V_{UCOM}," *Phys. Rev. C* **79**, 054325-1 - 054325-19 (2009).
14. Y. Zhao, O. Tishchenko, J.R. Gour, W. Li, J.J. Lutz, P. Piecuch, and D.G. Truhlar, "Thermochemical Kinetics for Multireference Systems: Addition Reactions of Ozone," *J. Phys. Chem. A* **113**, 5786-5799 (2009).
15. M. Ehara, J.R. Gour, and P. Piecuch, "Low-Lying Valence Excited States of CNC, C₂N, N₃, and NCO Studied Using the Electron-Attached and Ionized Symmetry-Adapted-Cluster Configuration-Interaction and Equation-of-Motion Coupled-Cluster Methodologies," *Mol. Phys.* **107**, 871-880 (2009).
16. J. Pittner and P. Piecuch, "Method of Moments for the Continuous Transition Between the Brillouin-Wigner-Type and Rayleigh-Schrödinger-Type Multireference Coupled Cluster Theories," *Mol. Phys.* **107**, 1209-1221 (2009).
17. P. Piecuch, J.R. Gour, and M. Włoch, "Left-Eigenstate Completely Renormalized Equation-of-Motion Coupled-Cluster Methods: Review of Key Concepts, Extension to Excited States of Open-Shell Systems, and Comparison with Electron-Attached and Ionized Approaches," *Int. J. Quantum Chem.* **109**, 3268-3304 (2009).
18. R. Roth, J.R. Gour, and P. Piecuch, "Center-of-Mass Problem in Truncated Configuration Interaction and Coupled-Cluster Calculations," *Phys. Lett. B* **679**, 334-339 (2009).
19. W. Li, J.R. Gour, P. Piecuch, and S. Li, "Local Correlation Calculations Using Standard and Renormalized Coupled-Cluster Approaches," *J. Chem. Phys.* **131**, 114109-1 - 114109-30 (2009).
20. W. Li, P. Piecuch, and J.R. Gour, "Linear Scaling Local Correlation Extensions of the Standard and Renormalized Coupled-Cluster Methods," in: *Progress in Theoretical Chemistry and Physics*, Vol. 19, edited by P. Piecuch, J. Maruani, G. Delgado-Barrio, and S. Wilson (Springer, Dordrecht, 2009), pp. 131-195.
21. W. Li and P. Piecuch, "Improved Design of Orbital Domains within the Cluster-in-Molecule Local Correlation Framework: Single-Environment Cluster-in-Molecule Ansatz and its Application to Local Coupled-Cluster Approach with Singles and Doubles," *J. Phys. Chem. A*, in press (2010).
22. W. Li and P. Piecuch, "Multi-level Extension of the Cluster-in-Molecule Local Correlation Methodology: Merging Coupled-Cluster and Møller-Plesset Perturbation Theories," *J. Phys. Chem. Lett.*, submitted (2010).
23. P. Arora, W. Li, P. Piecuch, J.W. Evans, M. Albao, and M.S. Gordon, "Diffusion of Atomic Oxygen on the Si(100) Surface," *J. Phys. Chem. C*, submitted (2010).

Chemical Kinetic Modeling of Combustion Chemistry

William J. Pitz and Charles K. Westbrook

Lawrence Livermore National Laboratory

Livermore, CA 94551

pitz1@llnl.gov

I. Program Scope

Our research project focuses on developing detailed chemical kinetic reaction mechanisms for the combustion of a wide variety of hydrocarbon and alternative fuels. These reaction mechanisms are designed to be applicable over extended ranges of operating conditions, including temperature, pressure, and fuel/oxidizer ratio, making them so-called “comprehensive” reaction mechanisms. They can then be systematically reduced in size and complexity as needed for specific types of modeling applications. We also use these detailed kinetic mechanisms to carry out modeling studies of practical combustion systems.

II. Recent Progress

Detailed chemical kinetic models are needed to accurately reproduce the behavior of transportation fuels like gasoline and diesel fuel. These chemical kinetic models typically describe the behavior of a limited number of fuel components to represent the hundreds of components in real fuels. During the last year, we have improved the accuracy our fuel component models over the large pressure and temperature range needed to model combustion in practical devices. We also have improved our ability to represent mixtures of the large hydrocarbons present in transportation fuels.

A. Fuel components and surrogates for gasoline and diesel fuels

We improved the ability of our detailed chemical kinetic mechanisms to model straight-chain pentenes and hexenes. These are important fuel components that can be used to represent alkenes in gasoline fuels. The improved detailed chemical kinetics models can better simulate the ignition behavior at low temperatures in a rapid compression machine (RCM) and at high temperature in a shock tube. In Fig. 1, the predictions of the model for ignition delay times of the three isomers of hexene are compared to the RCM experimental data of Vanhove et al.¹ and the newly acquired high-pressure shock tube data from Curran’s group in Galway². The detailed chemical kinetic models simulate the measured ignition behavior of the hexenes very well. At low temperature, 1- and 2-hexene exhibit shorter ignition delay times than 3-hexene due to the formation of hex-1-en-3-yl radicals that can undergo O₂ addition and start the pathway leading to ketohydroperoxides. On the other hand at high temperature, 3-hexene exhibits smaller ignition delay times due to its decomposition to ethyl and but-1-en-3-yl radicals, both of which react by eliminating H radicals that speed reactivity.

We have been performing collaborative research with the combustion chemistry research teams at Nancy, France and Milano, Italy to improve the ability to model toluene and its related intermediate compounds in many fundamental laboratory devices such as low pressure flames, shock tubes, and flow reactors. With the Nancy team, we modeled the low pressure flames of Li et al.³ for toluene, obtaining good agreement over a wide carbon range of intermediate species including two-ring aromatic hydrocarbons, methylnaphthalene and phenanthrene. With the Milano team, we validated the chemical kinetic mechanisms from our two groups for the ignition and oxidation of cyclopentadiene, benzene and toluene over a wide range of conditions in shock tubes and flow reactors. This range includes temperatures from 1100 to 1800 K, pressures from 1 to 50 atm, and equivalence ratios of 0.5 to 2, conditions that are relevant to combustion in internal combustion engines.

N-hexadecane (n-cetane) and 2,2,4,4,6,8,8-heptamethylnonane (iso-cetane) are used as primary reference fuels to rate ignition properties of diesel fuel through the Cetane number. We have combined our recently developed chemical kinetic models for these compounds to create a primary reference fuel model for diesel fuels. This development has improved our ability to model fuel mixtures relevant to diesel. Figure 2 shows that as the primary reference fuel mixture is changed from a Cetane number of 15 (pure iso-cetane) to a Cetane number of 100 (pure n-cetane), the CO increases at low temperatures and the

H₂O₂ increases at both low and intermediate temperatures. This increased H₂O₂ production for high Cetane number fuels leads to the formation of OH radicals and increased reactivity.

B. Components and mixtures biodiesel fuels

We have developed chemical kinetic models for C5 esters and validated the mechanisms by comparison to the low pressure flame data from Yang, Cool and Hansen⁴. Good agreement between the model predictions and experiments demonstrated that three main factors were needed to properly account for methyl ester chemistry in the model. The first factor was unimolecular decomposition of the fuel, especially by rapid molecular elimination reactions through 6-membered ring transition states, when possible. Second, H-atom abstraction reactions followed by β -scission of the resulting radicals leads to nearly all of the observed intermediate species detected experimentally in each flame. Finally, the rates of these H-atom abstraction reactions are effectively the same from each distinct type of terminal alkyl radical group (i.e., methoxy, ethoxy, methyl, ethyl, propyl).

Soy- or rapeseed-based biodiesel mainly consists of 5 different large methyl esters. During the past year, we have developed detailed chemical models for two of these methyl esters: methyl stearate and methyl oleate. This development brings us closer to being able to simulate all the actual components in these important types of biodiesel. Figure 3 shows the ignition behavior of these two methyl esters compared to n-heptane⁵, n-decane⁶, and n-hexadecane⁷. The predicted ignition delay times for methyl stearate are shorter than methyl oleate which has the same structure except for the presence of a carbon-carbon double bond in the C18 carbon chain. Methyl stearate ignites quite similarly to the large n-alkanes, while methyl oleate ignites more slowly due to the presence of the double bond.

III. Summary

Improved detailed chemical kinetic mechanisms for components and mixtures of importance for transportation fuels have been developed. These components are of interest for gasoline, diesel and biodiesel fuels. Also, we have obtained improved understanding of the chemistry of C5 methyl esters which will help in improving the chemical kinetic description of large methyl esters important for biodiesels.

IV. Future Work

We plan on developing chemical kinetic mechanisms of additional saturated and unsaturated alkyl esters, and comparing simulations with molecular beam sampling measurements taken in low pressure flames and with ignition delay times measured in rapid compression machines.

This work was performed under the auspices of the U.S. Department of Energy by Lawrence Livermore National Laboratory under Contract DE-AC52-07NA27344.

V. References

1. G. Vanhove; M. Ribaucour; R. Minetti, *Proceed. of the Combust. Inst.* **2005**, 30, 1065-1072.
2. M. Mehl; W. J. Pitz; C. K. Westbrook; K. Yasunaga; H. J. Curran in: Proceedings of the Combustion Institute, Beijing, China, 2010, submitted.
3. Y. Y. Li; L. D. Zhang; Z. Y. Tian; T. Yuan; J. Wang; B. Yang; F. Qi, *Energy&Fuels* **2009**, 23, 1473-1485.
4. B. Yang; T. A. Cool; C. K. Westbrook; N. Hansen in: The 33rd International Symposium on Combustion, Beijing, China, submitted.
5. H. K. Ciezki; G. Adomeit, *Combustion and Flame* **1993**, 93, 421-433.
6. U. Pfahl; K. Fieweger; G. Adomeit, *Proc. Combust. Inst.* **1996**, 26, 781-789.
7. C. K. Westbrook; W. J. Pitz; O. Herbinet; H. J. Curran; E. J. Silke, *Combust. Flame* **2009**, 156, (1), 181-199.

VI. Publications and submitted journal articles supported by this project 2009-2010

1. Kohse-Hoinghaus, K., P. Osswald, T. A. Cool, T. Kasper, N. Hansen, F. Qi, C. K. Westbrook and P. R. Westmoreland (2010). "Biofuel combustion chemistry: from ethanol to biodiesel." *Angewandte Chemie*, in press.
2. Yang, B., Cool, T. A., Westbrook, C.K., and Hansen, N., "A Detailed Chemical Kinetic Reaction Mechanism for Oxidation of Four Small Alkyl Esters in Laminar Premixed Flames," The 33rd International Symposium on Combustion, Beijing, China, 2010, submitted.
3. Veloo, P. S., Y. L. Wang, F. N. Egolfopoulos and C. K. Westbrook (2010). "A comparative experimental and computational study of methanol, ethanol, and n-butanol flames." *Combustion and Flame*, submitted.
4. S. M. Sarathy, M. J. Thomson, W. J. Pitz and T. Lu, "An Experimental and Kinetic Modeling Study of Methyl Decanoate Combustion," The 33rd International Symposium on Combustion, Beijing, China, 2010, submitted.
5. Z. Tian, W. J. Pitz, R. Fournet, P.-A. Glaude and F. Battin-Leclerc, "A detailed kinetic modeling study of toluene oxidation in a premixed laminar flame," The 33rd International Symposium on Combustion, Beijing, China, 2010, submitted.
6. M. Mehl, W. J. Pitz, C. K. Westbrook, K. Yasunaga and H. J. Curran, "Autoignition behavior of unsaturated hydrocarbons in the low and high temperature regions," The 33rd International Symposium on Combustion, Beijing, China, 2010, submitted.
7. M. Mehl, W. J. Pitz, C. K. Westbrook and H. J. Curran, "Kinetic Modeling of Gasoline Surrogate Components and Mixtures under Engine Conditions," The 33rd International Symposium on Combustion, Beijing, China, 2010, submitted.
8. C. Naik, C. K. Westbrook, O. Herbinet, W. J. Pitz and M. Mehl, "Detailed Chemical Kinetic Reaction Mechanism for Biodiesel Components Methyl Stearate and Methyl Oleate," The 33rd International Symposium on Combustion, Beijing, China, 2010, submitted.
9. C. K. Westbrook, W. J. Pitz, M. Mehl and H. J. Curran, "Detailed Chemical Kinetic Reaction Mechanisms for Primary Reference Fuels for Diesel Cetane Number and Spark-Ignition Octane Number," The 33rd International Symposium on Combustion, Beijing, China, 2010, submitted.
10. W. J. Pitz and C. J. Mueller, "Recent Progress in the Development of Diesel Surrogate Fuels," *Progress in Energy and Combustion Science* (2010), submitted.
11. Herbinet, O., W.J. Pitz, and C.K. Westbrook, "Detailed chemical kinetic mechanism for the oxidation of biodiesel fuels blend surrogate". *Combustion and Flame*, 157 (2010) 893-908.
12. Westbrook, C. K., Pitz, W. J., Westmoreland, P. R., Dryer, F. L., Chaos, M., Osswald, P., Kohse-Hoinghaus, K., Cool, T. A., Wang, J., Yang, B., Hansen, N. and Kasper, T., "A Detailed Chemical Kinetic Reaction Mechanism for Oxidation of Four Small Alkyl Esters in Laminar Premixed Flames," *Proceedings of the Combustion Institute*, 32 (2009) 221-228.
13. M. A. Oehlschlaeger, J. Steinberg, C. K. Westbrook and W. J. Pitz, "The Autoignition of iso-Cetane: Shock Tube Experiments and Kinetic Modeling," *Combustion and Flame*, 156 (11) (2009) 2165-2172.
14. Westbrook, C. K., Pitz, W. J., Herbinet, O., Curran, H. J. and Silke, E. J., "A Detailed Chemical Kinetic Reaction Mechanism for n-Alkane Hydrocarbons from n-Octane to n-Hexadecane," *Combustion and Flame* 156 (1) (2009) 181-199.
15. Seshadri, K., Lu, T., Herbinet, O., Humer, S., Niemann, U., Pitz, W. J. and Law, C. K., "Ignition of Methyl Decanoate in Laminar Nonpremixed Flows," *Proceedings of the Combustion Institute* 32 (2009) 1067-1074.
16. Sakai, Y., Miyoshi, A., Koshi, M. and Pitz, W. J., "A Kinetic Modeling Study on the Oxidation of Primary Reference Fuel-Toluene Mixtures Including Cross Reactions between Aromatics and Aliphatics," *Proceedings of the Combustion Institute*, 32 (2009) 411-418. Awarded best paper of the year by the Japanese Section of the Combustion Institute.

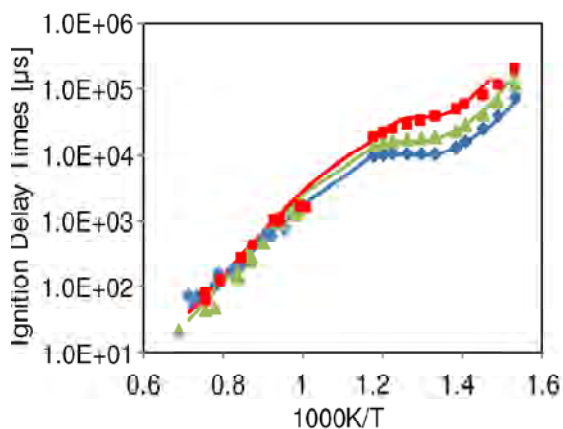


Figure 1. Ignition delay times of 1-hexene (diamonds), 2-hexene (triangles) and 3-hexene (squares) in a shock tube² (on the left) and in a rapid compression machine¹ (on the right). The symbols are the experiments and the curves are the model simulations.

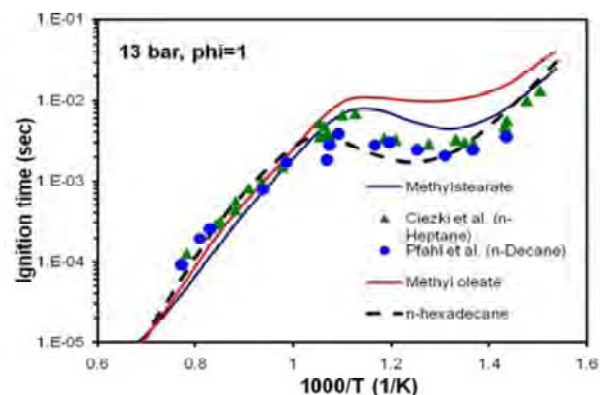


Figure 3. Autoignition of stoichiometric methyl stearate/air and methyl oleate/air at 13.5 atm. Also shown are experimental results at the same conditions for n-heptane/air⁵, n-decane/air⁶ and computed results for n-hexadecane⁷.

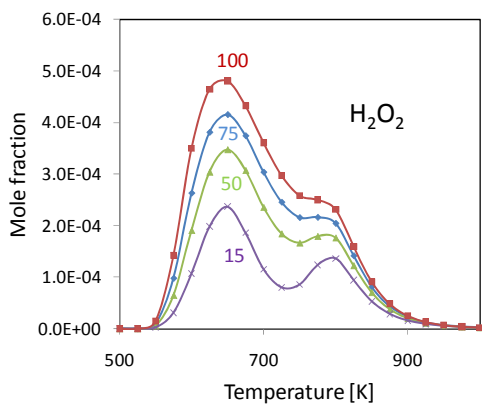
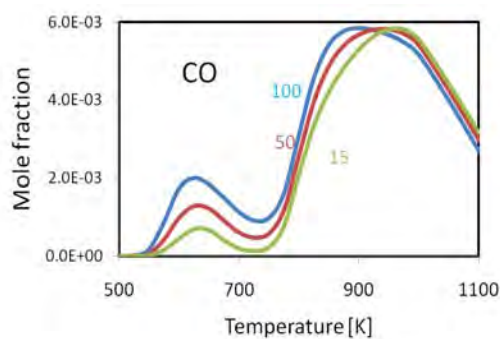


Figure 2. Computed fuel and intermediate species concentrations for selected diesel primary reference fuel mixtures under stirred reactor conditions of 10 atm pressure, 1 sec residence time and stoichiometric mixtures. Cetane number (CN) of each fuel mixture indicated on each frame. CN=15 is defined as pure n-hexadecane. CN=100 is defined as pure 2,2,4,4,6,8,8-heptamethyl nonane.

INVESTIGATION OF NON-PREMIXED TURBULENT COMBUSTION

Grant: DE-FG02-90ER14128

Stephen B. Pope
Sibley School of Mechanical & Aerospace Engineering
Cornell University
Ithaca, NY 14853
s.b.pope@cornell.edu

1 Scope of the Research Program

The focus of the current work is on the development of computational approaches which allow our detailed knowledge of the chemical kinetics of combustion to be applied to the modeling and simulation of combustion devices. In the past year, the work has been focused in two general areas. The first area is the evaluation and implementation of different algorithms for the treatment of molecular diffusion and mixing in large-eddy simulations (LES) using the probability density function (PDF) approach for turbulence chemistry interactions. The second area of research is the combination of dimension-reduction schemes and tabulation strategies for the computationally-efficient implementation of combustion chemistry in LES/PDF and other modeling approaches.

2 Recent Progress

The principal research results from this program are described in the publications listed in Section 4. The first subsection describes the progress made in developing efficient numerical implementations for the treatment of molecular diffusion and mixing. The next subsection details the progress made in the computationally-efficient implementation of combustion chemistry.

2.1 Treatment of molecular diffusion and mixing in LES-PDF methods

In probability density function (PDF) methods for turbulent reactive flows, reaction is treated exactly without modeling approximations while modeling the effects of molecular diffusion and mixing are crucial [1]. Various mixing models have been developed and studied extensively in previous studies [2, 3, 4]. In this study, the Interaction by Exchange with the Mean (IEM) mixing model is used and the effects of molecular diffusion are incorporated as a mean drift term in the mixing model [5]. This is done in the context of large-eddy simulation (LES). Three algorithms developed for the treatment of molecular diffusion and mixing in LES-PDF methods have been implemented and their properties and performance characteristics studied.

The current implementation of the algorithms has the following favorable properties: (i) the three schemes satisfy detailed conservation, (ii) they ensure boundedness of species mass fractions, (iii) they achieve second-order accuracy in both space and time, (iv) they are based on an implicit scheme and hence are unconditionally stable, (v) their computational cost scales linearly with the grid size, (vi) they account for the effects of molecular diffusion without giving rise to spurious production of variance, and (vii) they have the capability to incorporate the effects due to differential diffusion without violating conservation principles. The implementation also ensures that the axis

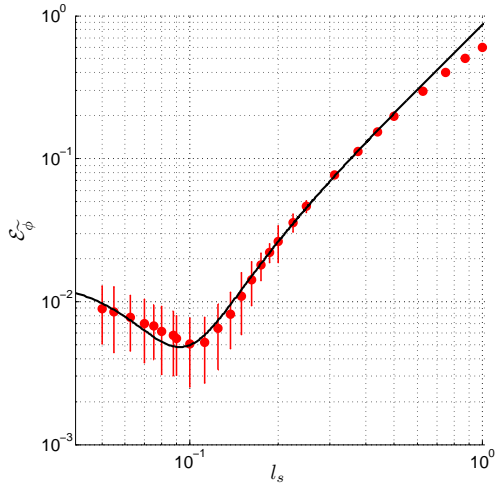


Figure 1: Plot of the global error in the scalar mean, $\mathcal{E}_{\tilde{\phi}}$ against smoothing lengthscale, l_s non-dimensionalized by the period of the scalar mean field: solid line represents the modeled error; symbols represent the estimate of the error obtained from PDF calculations

in cylindrical geometry is treated correctly. In addition, an implicit smoothing scheme has been developed for use in combination with the implementation of the mixing algorithm. Our studies show that an appropriate amount of smoothing can improve accuracy significantly, by reducing the variance in the estimated statistics, for no substantial increase in the computational cost.

The three algorithms developed as part of this study have been evaluated in the context of LES-PDF methods using the method of manufactured solutions in a three dimensional constant-density flow in a Cartesian coordinate system. Results obtained from this study indicate that all of the above mentioned properties are satisfied. Figure 1 plots the estimated global error [6] in the scalar mean, $\mathcal{E}_{\tilde{\phi}}$ for a range of smoothing lengthscales, l_s from the calculation performed on a 20^3 grid with a nominal number of one particle per grid cell (*i.e.* $N_{pc} = 1$ and hence, the total number of particles $N_{tot} = 20^3 N_{pc}$). The solid line corresponds to a model of the form, $\mathcal{E}_{\tilde{\phi}} = \alpha l_s^2 + \beta [1 / (N_{tot} l_s^3 + \gamma N_{pc})]$, that is fit to the data obtained from the PDF calculations. The model parameters α, β and γ are chosen to minimize the least-squares error. One can infer from this figure that an appropriate choice of the smoothing lengthscale can result in as much as 50% reduction in the estimated error. A publication describing these advances will be written in the near future.

2.2 Efficient Implementation of the Combustion Chemistry

Modern chemical mechanisms for real fuels typically involve hundreds of species and thousands of reactions. Computational calculations of reactive flows involving real fuels with detailed chemistry are prohibitive even on a distributed computing platform. Thus, dimension reduction is essential to the use of detailed chemical kinetics in reactive flow simulations.

Here we report recent progress made in developing a combined dimension-reduction and tabulation methodology for the efficient implementation of combustion chemistry. We are working on integrating the “rate-controlled constrained equilibrium” (RCCE) [7] and the “invariant constrained-equilibrium edge manifold with pre-image curve method” (ICE-PIC) [8] dimension reduction methods with the “*in situ* adaptive tabulation” (ISAT) [9] algorithm. In this combined methodology, the reactive flow calculations are performed using a small number (say, around 10) of represented species, and the combined reduction-storage methodology determines and tabulates (*in situ*) the reduced space in terms of the represented species based on the detailed mechanism. An automated greedy algorithm [10] has been devised to select good represented species for the accurate representation of chemistry using the RCCE and ICE-PIC dimension reduction methods.

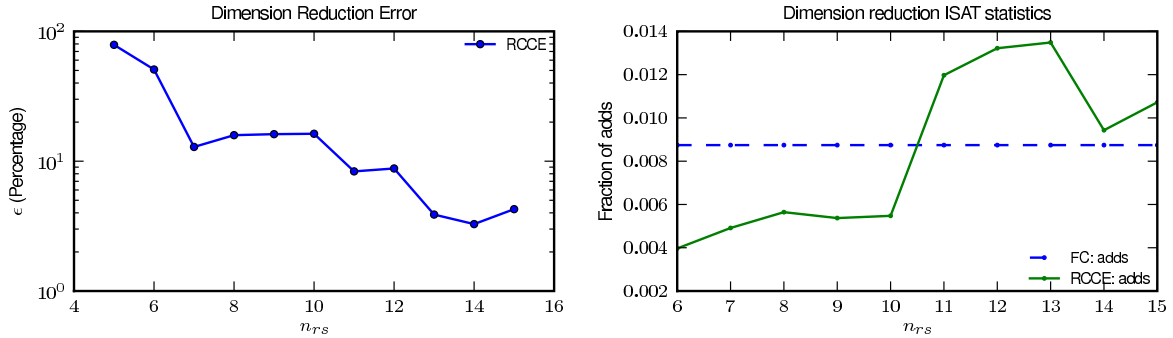


Figure 2: PaSR test for ethylene/air combustion: plotted are the dimension reduction error using RCCE (left) and ISAT adds (right) against the number of represented species, n_{rs} .

2.2.1 Partially-Stirred Reactor (PaSR)

The combined methodology has been extensively tested using the partially-stirred reactor (PaSR) for the ethylene/air premixed combustion with the chemistry described by the USC Mech II detailed mechanism (optimized in 2009) involving 111 species and 784 reactions.

The PaSR has two inflowing streams: one premixed stream of ethylene/air mixture at 600 K and a pilot stream of equilibrium products of the stoichiometric ethylene/air mixture. Other important parameters involved are: number of particles, $N_P = 100$; residence time, $\tau_{res} = \times 10^{-4}$ s; mixing time, $\tau_{mix} = 10^{-5}$ s and pairing time, $\tau_{pair} = 10^{-5}$ s. The PaSR is run for $N_T = 350$ time steps, resulting in more than 10^6 queries to ISAT. An ISAT error tolerance of $\epsilon_{tol} = 10^{-5}$ is used.

2.2.2 Dimension Reduction Error

To compute the dimension reduction error, PaSR calculations are performed with and without dimension reduction, and the compositions obtained with the two approaches are compared to estimate errors incurred by the dimension reduction. The dimension reduction error, ϵ , is defined as

$$\epsilon = \frac{[\mathbf{z}_{DR}^r - \mathbf{z}_{FC}^r]_{rms}}{[\mathbf{z}_{FC}^r]_{rms}}, \quad (1)$$

where \mathbf{z} denotes the specific moles of the species; DR and FC denote the predictions with dimension reduction and full chemistry (no reduction) respectively, and the superscript r denotes the represented species. The error is computed over all the particles for all time steps as follows:

$$[\mathbf{z}]_{rms} = \sqrt{\frac{1}{N_P N_T} \sum_{n=1}^{N_P} \sum_{t=1}^{N_T} |\mathbf{z}^{(n)}(t)|_{rms}^2}. \quad (2)$$

The dimension reduction error and ISAT ‘‘adds’’ (direct evaluations) for the ethylene premixed combustion are shown in Fig.2. We see that even for a large ethylene mechanism involving 111 species, using just 13 to 15 represented species with RCCE results in less than 5% error with good ISAT performance.

2.3 Conclusions

The numerical implementations developed for the treatment of molecular diffusion and mixing satisfy conservation and boundedness constraints while ensuring second order accuracy in space and time. Moreover, when mixing is implemented with smoothed statistics, an appropriate choice

of the smoothing lengthscale can lead to a significant improvement in accuracy for little or no increase in the computational cost.

The combined dimension-reduction and tabulation methodology has proved successful for the efficient and accurate representation of combustion chemistry.

3 Future Plans

The focus of current and future work is on the development of a computationally-efficient implementation of “local” turbulent mixing models, and combustion chemistry. A combined LES/PDF/ISAT with dimension reduction code is being developed for simulating turbulent reactive flows.

4 Publications from DOE Research 2008-2010

1. Z. Ren and S.B. Pope (2008) “Sensitivity calculations in PDF modelling of turbulent flames,” Proceedings of the Combustion Institute, **32**, 1629–1637.
2. S. Viswanathan and S.B. Pope (2008) “Turbulent dispersion behind line sources in grid turbulence,” Physics of Fluids, **20**, 101514.
3. H. Wang and S.B. Pope (2008) “Lagrangian investigation of local extinction, re-ignition and auto-ignition in turbulent flames,” Combustion Theory and Modelling, **12**, 857-882.
4. Z. Ren and S.B. Pope (2009) “Sensitivity calculations in PDF modelling of turbulent flames,” Proceedings of the Combustion Institute, **32**, 1629–1637.
5. V. Hiremath, Z. Ren and S.B. Pope (2010) “A Greedy Algorithm for Species Selection in Dimension Reduction of Combustion Chemistry” Combustion Theory and Modelling, (submitted).

References

- [1] S.B. Pope, Prog. Energy Combust. Sc. 11 (1985) 119-192.
- [2] S. Subramaniam and S.B. Pope, Combust. Flame 117 (1999) 732-754.
- [3] Z. Ren and S.B. Pope, Combust. Flame 136 (2004) 208-216.
- [4] R. Cao, H. Wang and S.B. Pope, Proc. Comb. Inst. 31 (2007) 1543-1550.
- [5] R. McDermott and S.B. Pope, J. Comp. Phys. 226(1) (2007) 947-993.
- [6] H. Wang, P. P. Popov, and S. B. Pope 229 J. Comp. Phys. (2010) 1852-1878.
- [7] J.C. Keck, Prog. Energy Combust. Sci. 16 (1990) 125-154.
- [8] Z. Ren, S.B. Pope, A. Vladimirov, J.M. Guckenheimer, J. Chem. Phys. 124 (2006) 114111.
- [9] L. Lu, S.B. Pope, J. Comput. Phys. 228 (2009) 361-386.
- [10] V. Hiremath, Z. Ren and S.B. Pope (2010), Combustion Theory and Modelling, (submitted)

OPTICAL PROBES OF ATOMIC AND MOLECULAR DECAY PROCESSES

S.T. Pratt
Building 200, B-125
Argonne National Laboratory
9700 South Cass Avenue
Argonne, Illinois 60439
E-mail: spratt@anl.gov

PROJECT SCOPE

Molecular photoionization and photodissociation dynamics can provide considerable insight into how energy and angular momentum flow among the electronic, vibrational, and rotational degrees of freedom in isolated, highly energized molecules. This project involves the study of these dynamics in small polyatomic molecules, with an emphasis on understanding the mechanisms of intramolecular energy flow and determining how these mechanisms influence decay rates and product branching ratios. It is also aimed at understanding how internal energy can influence photoionization cross sections and dissociative ionization processes. The experimental approach combines double-resonance laser techniques, which are used to prepare selected highly excited species, with mass spectrometry, ion-imaging, and high-resolution photoelectron spectroscopy, which are used to characterize the decay of the selected species.

RECENT PROGRESS

We have continued to focus on using a combination of ion imaging, vuv single-photon ionization, and resonant multiphoton ionization to probe the photodissociation dynamics of small polyatomic molecules, and to characterize the photoionization dynamics of combustion-relevant radicals. Most recently, we have been studying the photodissociation of acetaldehyde into $\text{CH}_3 + \text{HCO}$, and using vacuum ultraviolet (vuv) photoionization to determine the absolute photoionization cross section of HCO. In particular, by photodissociating at 266 nm and ionizing both the CH_3 and the HCO with vuv light, we would compare the ion images and translational energy distributions from the two products. Although the 266 nm photons have sufficient energy to allow secondary dissociation of the HCO, the translational energy distributions from the CH_3^+ and HCO^+ images are essentially identical, indicating that very little secondary dissociation occurs at this wavelength. Thus, with some additional considerations, the ratio of the ion signals for the two ions could be used with the absolute photoionization cross section of CH_3 to determine the absolute photoionization cross section of HCO. The data analysis is still underway, but the HCO cross section is very small--even less than that of CH_3 . Interestingly, this observation is consistent with the very small threshold photoionization cross section of the isoelectronic species NO, and can be rationalized by considering the atomic d-like character of the HOMO in the two molecules.

New experiments were performed using velocity-map ion imaging to study the predissociation and dissociative ionization of the rare-gas dimers Xe_2 and KrXe , as well as the photodissociation of the corresponding ions. In this work, two-photon excitation was used to prepare low-lying Rydberg states of these van der Waals molecules. Some of these states predissociated into a ground-state atom and an excited-state atom, and the latter was ionized by the absorption of an additional photon. Ion imaging provides the translational energy of the fragments, and thus

allows the assignment of the predissociation products. Identification of the fragments by using photoelectron spectroscopy had been performed previously, but the resolution of the imaging technique is somewhat better, allowing more definitive assignments. This approach should be general, and could be used as an alternative to photoelectron spectroscopy in a variety of different systems. Some of the molecular Rydberg states were photoionized to produce bound states of the molecular ion, which were subsequently photodissociated by the absorption of additional photons. This observation allowed us to identify the specific dissociation mechanism for both molecular ions. Interestingly, photodissociation only produced a single set of products: $\text{Xe } ^1\text{S}_0 + \text{Xe}^+ ^2\text{P}_{1/2}$ for Xe_2^+ and $\text{Xe } ^1\text{S}_0 + \text{Kr}^+ ^2\text{P}_{1/2}$ for KrXe^+ .

I spent one month working with the group of Valerie Blanchet at the CNRS in Toulouse, France, where we performed experimental studies on the time-resolved femtosecond photoelectron imaging spectroscopy of CH_3I and its fragments CH_3 and I . Femtosecond laser pulses near 200 nm were used to excite the origin band of the B state of CH_3I , which corresponds to the lowest Rydberg state and predissociates on a ps timescale. The excited molecules were photoionized at several probe wavelengths and as a function of time delay, and the photoelectron energy and angular distributions provided insight into the character of the B state and the photoionization dynamics. The CH_3 fragments were also selectively detected as a function of vibrational level, and the time dependence of these signals were also determined. Essentially all of the I atoms produced by the predissociation are in the spin-orbit excited $^2\text{P}_{1/2}$ level. One manuscript based on this work has already been submitted and a second is in preparation.

In collaboration with Christian Jungen, I have continued to work on theoretical models of vibrational autoionization and, in particular, dissociative recombination. We are currently working on a manuscript exploring the ramifications of our simple model for electron capture by ions into vibrationally and rotationally excited Rydberg states. This capture process is the first step in indirect dissociative recombination processes, and in many instances it is also the rate limiting step. We have examined low-energy dissociative recombination data and have identified general features of these cross sections. In particular, the cross sections for many small polyatomic ions such as H_3O^+ , NH_4^+ , CH_3^+ , and CH_5^+ show significant drops at the threshold for excitation of the fundamental of one of the vibrational levels of the ion, and this vibration is typically Renner-Teller or Jahn-Teller active. This observation is consistent with our earlier work on Renner-Teller and Jahn-Teller induced vibrational autoionization, and may ultimately lead to a more general understanding of the dissociative recombination electrons and polyatomic ions. We are also exploring electron capture into rotationally excited Rydberg states, which provides a potentially important alternative to vibrational capture at very low electron energies.

Finally, last fall I participated in two weeks of beamtime at the Linac Coherent Light Source (LCLS) at SLAC. The LCLS is the world's first hard x-ray free-electron laser, and this was the first beamtime for external users. In the first set of user experiments at this facility, I worked with Linda Young's group from Argonne on the multiple ionization of atomic Ne, which showed that high charge states are produced by sequential absorption of multiple x-ray photons. Most of this ionization occurs through a series of inner shell ionization processes to remove 1s electrons and Auger decay processes that replenish them. However, in some instances, the intensity is sufficiently high that both 1s electrons are removed by the sequential absorption of two photons before Auger decay can occur. If the FEL pulse is shorter than (or approximately the same

duration as) the Auger lifetime, inner-shell absorption terminates after the absorption of two photons. In the second week of beamtime, I worked with Nora Berrah's group (University of Western Michigan) on experiments on molecular systems, including N_2 , CO, H_2S , and SF_6 . These experiments show similar effects as the Ne experiments, but with the added complexity of molecular fragmentation. Interestingly, the possibility of making two core holes, for example, one on each atom in N_2 , also exists, and the decay dynamics of such states are of considerable interest. I am currently helping with the analysis of the results on molecular nitrogen, and helping prepare several manuscripts for publication. I have learned a significant amount about the capabilities of this new facility and I am developing ideas for future experiments that probe chemical dynamics more directly.

FUTURE PLANS

We plan on continuing our studies of the photodissociation and photoionization of combustion-relevant radicals by using ion-imaging techniques, vacuum-ultraviolet single-photon ionization, and resonant multiphoton ionization techniques. In particular, we will finish the analysis of the data on acetaldehyde and the absolute photoionization cross section of HCO. We may extend this work to longer photodissociation wavelengths, and place a greater emphasis on recording the vuv photoionization spectrum of HCO as a function of wavelength. We have performed imaging experiments on formic acid and deuterated formic acid as a means of producing a number of interesting combustion radicals including OH, HCO, HOCO, and HCOO, and hope to pursue these studies. Unfortunately, to date it has been difficult to obtain unambiguous results on the most interesting species, HOCO and HCOO. By using selectively deuterated precursors, we hope to be able to study HOCO and HCOO species separately, to study their photoionization dynamics, and ultimately to determine their photoionization cross sections. Testing of a new apparatus for photoelectron imaging has begun, and we hope it will be fully operational in early in the coming year. This apparatus affords easy access to the region close to the pulsed molecular beam valve, allowing both photodissociation in the expansion and discharge or pyrolysis sources to produce cold radicals.

I will continue to collaborate with Christian Jungen on theoretical models of vibrational autoionization and dissociative recombination in polyatomic molecules. In particular, we will work to develop the connection between our simple model for dissociative recombination and the large-scale theoretical calculations of Greene and Kokoouline. We will continue to work on understanding the discrepancies between high-level theoretical calculations and the experimental dissociative recombination data, in particular, the surprising lack of resonant structure in the experimental cross sections. Finally, we will explore the possible importance of dissociative recombination for the generation of radicals in the first steps of spark ignition.

I will finish the analysis and publication of data from my work with Valerie Blanchet's group, as well as the analysis and publication of data from the initial experiments at the LCLS. I will continue to participate in experiments at the LCLS, which are scheduled for August of this year. These experiments are moving towards larger polyatomic molecules and are increasingly concerned with controlling the excitation process to localize core holes in particular locations within the molecule.

This work was supported by the U.S. Department of Energy, Office of Science, Office of Basic Energy Sciences, Division of Chemical Sciences, Geosciences, and Biological Sciences under contract No. DE-AC02-06CH11357.

DOE-SPONSORED PUBLICATIONS SINCE 2008

1. E. R. Peterson, C. Buth, D. A. Arms, R. W. Dunford, E. P. Kanter, B. Krässig, E. C. Landahl, S. T. Pratt, R. Santra, S. H. Southworth, and L. Young
X-RAY ABSORPTION BY LASER-ALIGNED MOLECULES
Appl. Phys. Lett. **92**, 094106 (2008).
2. C. A. Taatjes, D. L. Osborn, T. Selby, G. Meloni, H. Fan, and S. T. Pratt
ABSOLUTE PHOTOIONIZATION CROSS SECTION OF THE METHYL RADICAL
Phys. Chem. A **112**, 9336-9343 (2008).
3. I. Thomann, R. Lock, V. Sharma, E. Gagnon, S. T. Pratt, H. C. Kapteyn, M. M. Murnane, and W. Li
DIRECT MEASUREMENT OF THE ANGULAR DEPENDENCE OF THE SINGLE-PHOTON IONIZATION OF ALIGNED N₂ AND CO₂
J. Phys. Chem. A **112**, 9382-9386 (2008).
4. Ch. Jungen and S. T. Pratt
RENNER-TELLER INTERACTIONS IN THE VIBRATIONAL AUTOIONIZATION OF POLYATOMIC MOLECULES
J. Chem. Phys. **129**, 164310 (2008).
5. Ch. Jungen and S. T. Pratt
RENNER-TELLER INTERACTIONS IN THE DISSOCIATIVE RECOMBINATION OF HCO⁺
J. Chem. Phys. **129**, 164311 (2008).
6. Ch. Jungen and S. T. Pratt
JAHN-TELLER INTERACTIONS IN THE DISSOCIATIVE RECOMBINATION OF H₃⁺
Phys. Rev. Lett. **102**, 023201 (2009).
7. S. T. Pratt
HIGH-RESOLUTION VALENCE-SHELL PHOTOIONIZATION
in *Handbook of High-Resolution Spectroscopies*, edited by M. Quack and F. Merkt (Wiley, New York, XXXX). (in press).
8. V. A. Shubert, M. Rednic, and S. T. Pratt
PHOTODISSOCIATION OF I-C₃H₇I WITHIN THE A BAND AND ANISOTROPY-BASED DECOMPOSITION OF THE TRANSLATIONAL ENERGY DISTRIBUTIONS
J. Chem. Phys. **130**, 134306 (2009).
9. V. A. Shubert, M. Rednic, and S. T. Pratt
PHOTODISSOCIATION OF 2-IODOETHANOL WITHIN THE A BAND
J. Phys. Chem. A **113**, 9057-9064 (2009).
10. V. A. Shubert, M. Rednic, and S. T. Pratt
PREDISSOCIATION AND DISSOCIATIVE IONIZATION OF RYDBERG STATES OF Xe₂ AND THE PHOTODISSOCIATION OF Xe₂⁺
J. Chem. Phys. (in press).

Photoinitiated Reactions of Radicals and Diradicals in Molecular Beams

Hanna Reisler

Department of Chemistry, University of Southern California

Los Angeles, CA 90089-0482

reisler@usc.edu

Program Scope

Open shell species such as radicals and diradicals are central to reactive processes in combustion and environmental chemistry. Our program is concerned with photoinitiated reactions of hydroxyalkyl radicals and carbenes. The goal is to investigate the detailed dynamics of dissociation of free radicals and diradicals for which multiple pathways including molecular rearrangements compete, and compare them with high level calculations. Studies include unimolecular reactions on the ground state as well as photodissociation dynamics on excited Rydberg and valence states that involve multiple potential energy surfaces. The photodissociation of triplet methylene, the prototypical carbene, exhibits conical intersections and the experiments will be compared with high-level electronic structure calculations. The detailed measurements on simple systems will serve as benchmarks for homologous series.

Recent Progress

I. Theoretical studies of the electronic spectroscopy and ionization of $\text{CH}_2\text{CH}_2\text{OH}$

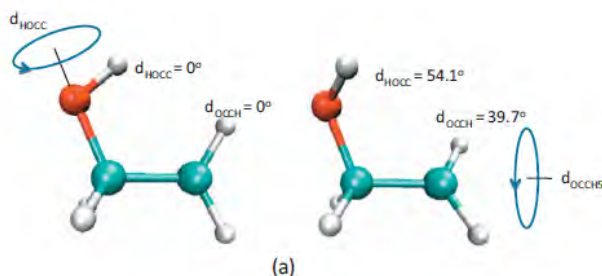
Of the two structural isomers of the hydroxyethyl radical, 1-hydroxyethyl (CH_3CHOH) has its radical center placed on the carbon adjacent to the oxygen, and thus its electronic structure is similar to CH_2OH . On the other hand, the 2-hydroxyethyl radical, $\text{CH}_2\text{CH}_2\text{OH}$, in which the unpaired electron is located on the outermost carbon, should exhibit a different electronic structure and excited states. The $\text{CH}_2\text{CH}_2\text{OH}$ radical is interesting from both theoretical and experimental perspectives. Whereas the neutral species has a typical open chain configuration, the cation has no minima in this configuration. Instead, the Franck-Condon region has a saddle point which leads to the only two minima on the cation's surface: a non-classical cyclic bridged structure, $\text{CH}_2(\text{OH})\text{CH}_2^+$, which can be described as protonated oxirane, and CH_3CHOH^+ , which is obtained by shifting a hydrogen atom from the central to the terminal carbon atom. Likewise, excitation to Rydberg states may lead to both dissociation and isomerization. In addition, the radical has several conformers on the ground state, and excitation from each conformer may lead to a different outcome.

In collaboration with the Krylov theory group, two stable conformers on the ground potential energy surface of $\text{CH}_2\text{CH}_2\text{OH}$ were identified. In addition, the low-lying excited electronic states (valence and Rydberg) have been investigated theoretically in the range 5-7 eV by using coupled-cluster and equation-of-motion coupled-cluster methods. Both dissociation and isomerization pathways were characterized. A dense manifold of electronic states was found, consisting of close-lying valence and Rydberg states and leading to rich and complex dissociation and isomerization dynamics following excitation from the stable conformers and saddle points on the ground state.

Two stable conformers and six saddle points have been found on the ground electronic potential energy surface at energies below $\sim 900 \text{ cm}^{-1}$. Vertical excitation energies and oscillator strengths for the lowest-lying excited valence state and the 3s, 3p_x, 3p_y and 3p_z Rydberg states have been calculated and it is predicted that the absorption spectrum at $\sim 270\text{-}200 \text{ nm}$ would be featureless. The stable conformers and saddle points differ primarily in their two dihedral coordinates, labeled d_{HOCC} (OH torsion around CO), and d_{OCCCH} (CH_2 torsion around CC).

Vertical ionization from the ground-state conformers and saddle points leads to an unstable structure of the open-chain $\text{CH}_2\text{CH}_2\text{OH}^+$ cation. The ion isomerizes promptly either to CH_3CHOH^+ or to the cyclic oxirane ion, $\text{CH}_2(\text{OH})\text{CH}_2^+$, with isomerization pathway depending primarily on the $d_{\text{OCC}}^{\text{H}}$ angle in the ground state. The Rydberg states are expected to display a similar behavior.

Fig. 1: Conformers and dihedral angles in ground state $\text{CH}_2\text{CH}_2\text{OH}$.

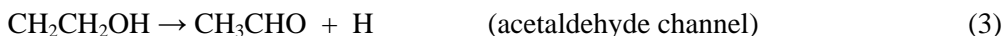
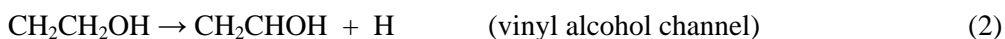
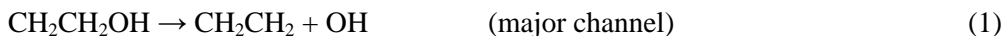


The lowest valence state is repulsive and its dissociation along the CC, CO and CH bonds is prompt, leading to $\text{CH}_2 + \text{CH}_2\text{OH}$, $\text{CH}_2\text{CH}_2 + \text{OH}$, and $\text{H} + \text{CH}_2\text{CHOH}$ product channels. The branching ratio among these channels depends sensitively on the dihedral angles. Surface crossings among Rydberg and valence states and with the ground state are likely to affect dissociation. It is concluded that the proximity of several low-lying excited electronic states, which can either dissociate directly or via isomerization and predissociation pathways, would give rise to rapid dissociation leading to several simultaneous dissociation channels.

II. Predissociation of rovibrationally excited $\text{CD}_2\text{CD}_2\text{OH}$: D-atom fragments

Acetaldehyde and vinyl alcohol products have been implicated in the decomposition of $\text{C}_2\text{H}_5\text{O}$ structural isomers. Of particular interest is the vinyl alcohol (ethenol) product, CH_2CHOH . Vinyl alcohol tautomerizes readily to the more thermodynamically stable acetaldehyde isomer. Its recent discovery in significant concentrations in flames, as well as its identification as a dissociation product in electronically excited 1-hydroxyethyl radicals, has underscored the importance of this species. The presence of the acetaldehyde tautomer in combustion reactions is well established.

Predissociation to the lowest channel, $\text{OH} + \text{C}_2\text{H}_4$, is dominant in the dissociation of the $\text{CH}_2\text{CH}_2\text{OH}$ radical. Theoretical assessments suggest, however, that at high excitation energies other pathways, such as dissociation to vinyl alcohol and acetaldehyde, can also play a role.^{1,2} To date no report has been published on dissociation pathways of $\text{CH}_2\text{CH}_2\text{OH}$ or $\text{CD}_2\text{CD}_2\text{OH}$ leading to H(D) fragments. The three relevant dissociation channels are:

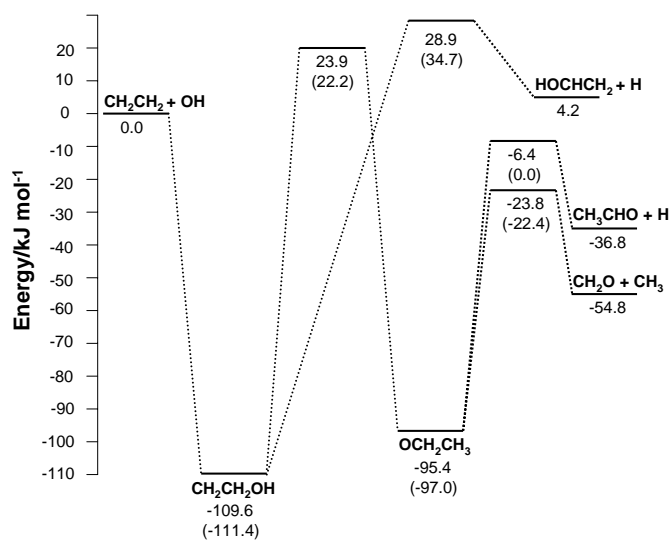
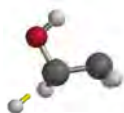


Relatively little experimental work has been published on the $\text{CH}_2\text{CH}_2\text{OH}$ radical, because a clean source of cold radicals is yet unavailable. However, upon dissociation of haloethanols rovibrationally excited $\text{CH}_2\text{CH}_2\text{OH}$ radicals are produced by secondary dissociation, some of which having sufficient internal energy to dissociate.³⁻⁷ Previous work characterized the fraction of radicals that dissociate and concluded that some of the radicals are born with high rotational excitation and do not dissociate within the observation time due to centrifugal barriers even when their internal energies exceed the dissociation barrier to channel (1). OH radicals produced via channel (1) have been characterized experimentally, but the production of D atoms via channels (2) and (3) has not been investigated.

In collaboration with S.J. Klippenstein, we investigated the appearance of D photofragments following 202–215 nm photolysis of BrCD₂CD₂OH and conclude that they are generated by predissociation of internally excited CD₂CD₂OH. The partially deuterated product was used in order to distinguish between O- and C-bound hydrogens, and improve the signal-to-noise ratio in the experiment. D atoms were detected by 1+1' REMPI, and their TOF distributions were determined. Bromoethanol was chosen as the precursor because around 202 nm the product CD₂CD₂OH radicals should contain enough internal energy to predissociate via reactions (1)–(3).^{1,2} D-atom maximum velocities and kinetic energies confirmed that it was generated by reactions (2) and (3). The relative importance of the vinyl alcohol and acetaldehyde channels in generating D-photofragments was assessed on the basis of experimental findings and theoretical calculations.

The theoretical calculations predict the energy dependence of the branching between channels (1)–(3) in CD₂CD₂OH dissociation via RRKM calculations based on the model of ref. 1. The relevant channels and barriers are shown in Fig. 2.

Fig. 2. Energies and barrier heights for CH₂CH₂OH and CD₂CD₂OH (values in parentheses) relevant to the vinyl alcohol dissociation channel. Calculations by Klippenstein and co-workers.



The underlying microcanonical RRKM analysis of ref. 1 could be compared directly to the present observations. However, the partial deuteration may have some effect on the predicted rate constants and branching ratios. Thus, to properly compare with the present experiments, we have evaluated the rovibrational properties of the stationary points for the relevant partially deuterated species at the B3LYP/6-311++G(d,p) level, and the energies and reaction barriers for these species are included in parentheses in Fig. 2. These rovibrational properties were then incorporated in a revised RRKM analysis for the partially deuterated species. Calculations of microcanonical dissociation rates and branching ratios were carried out for the range of available excess energies in the experiment (up to 5000–8000 cm⁻¹ above the OH + C₂D₄ threshold). The major results are:

(i) The reaction channels terminating in D products are minor -- only a few percent of all products. Nevertheless, there is no problem in detecting these channels via the sensitive 1+1' REMPI scheme.

(ii) The acetaldehyde product correlated with H(D) co-fragments could not be discerned experimentally from vinyl alcohol in our study because dissociation to both species proceeds via C–D bond cleavage. Calculations show that it should be a minor channel relative to vinyl alcohol and that isomerization to the ethoxy radical that precedes dissociation to acetaldehyde is inefficient. Additionally, the dissociation of ethoxy to acetaldehyde competes with the channel that yields H₂CO + CH₃, which has a

lower barrier (Fig. 1), and the latter should comprise the major dissociation channel of the ethoxy radical, in agreement with previous work.^{1,2}

(iii) The calculations for CD₂CD₂OH in rotational states J of 4, 20, 52, and 100 show that the branching to reaction (2) relative to reaction (1) decreases with increasing J as the rotational barriers become more significant. Thus, the contribution of the D channel is largest for those “hot” 2-hydroxyethyl radicals that are born with modest rotational excitation. These are also the radicals that dissociate the fastest and whose products are likely to be observed in our detection region.

References

1. Senosiain, J. P.; Klippenstein, S. J.; Miller, J. A. *J. Phys. Chem. A* 2006, *110*, 6960.
2. Xu, Z. F.; Xu, K.; Lin, M. C. *ChemPhysChem* 2009, *10*, 972.
3. Chandler, D. W.; Thoman, J. W.; Hess, W. P. *Inst. Phys. Conf. Ser.* 1991, 355.
4. Sapers, S. P.; Hess, W. P. *J. Chem. Phys.* 1992, *97*, 3126.
5. Shubert, V. A.; Rednic, M.; Pratt, S. T. *J. Phys. Chem. A* 2009, *113*, 9057.
6. Hintsä, E. J.; Zhao, X. S.; Lee, Y. T. *J. Chem. Phys.* 1990, *92*, 2280.
7. Ratliff, B. J. W., CC; Tang, X.N.; Landau, M.; Butler, L. J.; Szpunar, D.E. *J. Phys. Chem. A* (in press, 2010).

Future Work

Our next goals are to study the vibrational predissociation of CH₂OH and the photodissociation of the triplet methylene radical. The latter is being produced efficiently by pyrolysis of diazirine. We will also continue the work with our theory collaborators in order to fully characterize the potential energy surface of CH₂CH₂OH on the ground electronic state at energies above the isomerization and dissociation barriers.

Publications, 2008-2010

1. Karpichev, B., Reisler, H., Krylov, A. I., and Diri, K. "Effect of hyperconjugation on ionization energies of hydroxyalkyl radicals," *J. Phys. Chem. A* 112 (2008): 9965-9969.
2. Karpichev, B., Edwards, L. W., Wei, J., and Reisler, H. "Electronic spectroscopy and photodissociation dynamics of the 1-hydroxyethyl radical CH₃CHOH," *J. Phys. Chem. A* 112 (2008): 412-418.
3. Fedorov, I., Koziol, L., Mollner A. K., Krylov, A. I., and Reisler H, "Multiphoton ionization and dissociation of diazirine: A theoretical and experimental study" *J. Phys. Chem. A* 113 (2009): 7412-7421.
4. Reisler, H and Krylov, A.I. "Interacting Rydberg and valence states in radicals and molecules: Experimental and theoretical studies", *Int. Rev. Phys. Chem.* 28 (2009): 267-308.
5. B. Karpichev, L. Koziol, K. Diri, H. Reisler and A. I. Krylov, "Electronically excited and ionized states of the CH₂CH₂OH radical: A theoretical study", *J. Chem. Phys.*, 132 (2010), 114308.
6. L.W. Edwards, M. Ryazanov, H. Reisler and S. J. Klippenstein, "D-atom products in predissociation of CD₂CD₂OH from the 202-215 nm photodissociation of 2-bromoethanol", *J. Phys. Chem. A* (in press, 2010).

Active Thermochemical Tables – Progress Report

Branko Ruscic

Chemical Sciences and Engineering Division, Argonne National Laboratory,
9700 South Cass Avenue, Argonne, IL 60439
ruscic@anl.gov

Program Scope

The *spiritus movens* of this program is the need to provide the scientific community with accurate and reliable thermochemical, spectroscopic, and structural information on chemical species that are relevant in combustion, or play prominent roles in the associated post-combustion environmental chemistry, thus contributing to the comprehension of the underlying chemical reactions and/or providing reliable benchmark values for development and testing of state-of-the-art theoretical approaches. In particular, thermochemistry is one of the essential underpinning scientific blocks that is enabling DOE to successfully interpret, analyze, model, and optimize energy-producing chemical reactions and thus fulfill its mission, and is, as such, a long-term component of the DOE BES research program. The current focus of this program is on bringing substantial innovations to the field of thermochemistry through the development of new tools and methodologies, and utilizing these new approaches to systematically advance the quality and quantity of available thermochemical data relevant to energy-producing processes. In order to accomplish the stated goals, this program has undertaken the development of a novel approach that is centered on the idea of analyzing and optimally utilizing the knowledge content of thermochemically relevant measurements. The aim of these developments is not only to produce *the best currently possible* thermochemical parameters for the targeted chemical species, but also to allow *efficient updates with new knowledge*, properly propagating its consequences through all affected chemical species, as well as to provide *critical tests of new experimental or theoretical data*, and, if possible, to develop *pointers to future determinations that will most efficiently improve the thermochemical knowledge base*. The effort of this program is synergistically coordinated with related experimental and theoretical efforts within the Argonne Chemical Dynamics Group to provide a broad perspective of this area of science.

Recent Progress

Development of Active Thermochemical Tables and the Core (Argonne) Thermochemical Network

Active Thermochemical Tables (ATcT) are a new paradigm of how to develop accurate, reliable, and internally consistent thermochemical values for stable, reactive, and transient chemical species by utilizing to the fullest all available experimental measurements as well as state-of-the-art theoretical data. Availability of reliable thermochemical values, accompanied by properly quantified uncertainties, is central to chemistry and chemical engineering. High-quality dependable values are critical in such areas as experimental and computational chemical kinetics and dynamics, development of credible chemical reaction mechanisms, and formulation of realistic models for complex chemical environments such as flames, internal combustion engines, or the atmosphere. Equally importantly, the availability of accurate and reliable thermochemical benchmarks has been historically the strongest *spiritus movens* for the advancement of sophisticated electronic structure theories.

The power of ATcT is rooted in the underlying Thermochemical Network (TN) approach.^{1,2,3} Traditional sequential thermochemistry (A begets B, which begets C, etc.) utilizes the available information in an inherently incomplete manner, is prone to cumulative errors, and results in tabulations that are encumbered by a hidden maze of progenitor-progeny relationships and thus cannot be updated with new knowledge without introducing serious inconsistencies. As opposed to this, ATcT operate on the underlying Thermochemical Network (TN), which explicitly contains the available thermochemically-

relevant determinations and thus allows statistical scrutiny and manipulation of the intricate manifold of relationships characterizing thermochemistry. The end result of this scrutiny is the extraction of the best possible thermochemical values for all chemical species described by the TN, based on optimal use of all the available knowledge, hence making conventional tabulations of thermochemical values obsolete.

The cardinal TN from which ATcT derives new thermochemical insights is the Core (Argonne) Thermochemical Network, C(A)TN. The overarching goal is to create a TN that describes in the best possible manner the thermochemistry of all radicals and stable species relevant to combustion. C(A)TN currently encompasses no less than 920 chemical species of C/H/O/N/Hal composition, intertwined by more than 13,000 thermochemically-relevant determinations. C(A)TN is under continuous development, which entails periodic expansions toward new species as well as sustained improvements in the thermochemical definitions of existing chemical species. The latter, which is largely driven by ATcT scrutinies of the constructed TN, has been the primary focus of our effort during the past year. The TN improvement and expansion processes involve, among others, critical analyses of all available experimental and theoretical determinations from the literature and from our laboratory, further extended by targeting new critical measurements. The experimental information is routinely complemented by additional high-quality electronic structure computations, using standardized composite methods that in the past have shown a reasonably good track record of thermochemical fidelity, such as G3, G3B3, G3X, CBS-Q, CBS-QB3, and CBS-APNO, as well as – when warranted and possible – thermochemical quantities computed using cutting edge methods, which presently start approaching for small chemical species accuracies of ~ 1 kJ/mol or even better (such as higher members of the W_n series, the HEAT protocol, and Focal Point approaches). As opposed to a *localized* TN (which we use only during initial testing of new TN sections), C(A)TN is an *ab ovo* TN, i.e. it does not contain any species that are constrained to an externally selected or imposed value of enthalpy of formation (other than the definitions of the reference state for each element). The fact that C(A)TN is devoid of non-transparent external dependences allows ATcT to coerce the knowledge contained in the TN toward full self-consistency.

The C(A)TN is now large enough to allow us to concentrate on groups of key chemical species that are spanned by reasonably complete dependency manifolds and capable of producing thermochemistry that has converged toward a stable value, and to undertake the effort of bringing the thermochemistry of such species to a ‘release-quality’ level. The first group of such species are those having an H/O composition, and our continued effort on finalizing their thermochemistry has, *inter alia*, resulted in highly accurate values for two quantities: the proton affinities (as well as the related gas-phase basicities) of H_2 and O_2 (see Ref. 4). Both of these quantities are important as firm pegs that place substantial sections of the general proton affinity scale (which relies on a myriad relative proton affinity measurements) on an absolute scale. In addition, knowledge of these two quantities with very high accuracy turns out to be of paramount importance in interstellar astrochemistry, where it directly relates to the thermochemistry of the nearly thermoneutral proton exchange between H_2 and O_2 , and thus defines the chemical equilibrium between the very abundant protonated hydrogen, H_3^+ , and (otherwise not readily detectable) protonated oxygen, HO_2^+ . The latter ATcT-derived equilibrium was a topic of a recent extensive collaborative effort (with Ben McCall, U. Illinois Urbana-Champaign), which explored how much of the ‘missing’ interstellar O_2 may be in fact ‘hidden’ in a protonated form that eludes detection by usual radioastronomical methods. We are currently in the process of preparing a manuscript with the latest ATcT values for the principal O/H species and their positive and negative ions.

The effort of finalizing the values for a number of key species (O/H species, simple C/H/O species, N/H species, NO_x species) has also resulted in stabilizing the thermochemistry for the C and N atoms. The correct values for the enthalpies of formation of atoms are of intense interest to theoretical chemists, where a large number of electronic structure computations resort to the atomization energy scheme as a vehicle to producing enthalpies of formation. Given the wide interest in these quantities, we are giving here the current interim ATcT values for several first-row atoms (see Table 1). While the initial efforts of improving on the values for C and N have benefited from collaborations with out theoretical colleagues

(J. Stanton, UT Austin; A. G. Csaszar, Eotvos U.; J. M. L. Martin, Weizmann), the current values rely heavily on two^{5,6} ATcT-driven photoionization experimental studies (in collaboration with C.-Y. Ng, UC Davis) and on the fact that the dependency manifold for these two atoms has now reached a ‘critical mass’. It is noteworthy that, similar to what happened previously¹ with O, the current ATcT values for the enthalpies of formation of C and N are essentially an order of magnitude more accurate than those originally recommended by CODATA and listed in all conventional thermochemical tabulations.

We are also in the finishing stages of providing accurate ATcT thermochemistry for phenyl radical and its positive and negative ions.⁷ This effort was conducted in collaboration with Tom Baer (UNC) and the researchers at the Swiss Light Source, and not only clarifies the so far rather uncertain thermochemistry of phenyl (where historic values of the enthalpies of formation differ by several times the declared uncertainties) and its ionization energy (the knowledge of which affects attempts to monitor combustion processes via photoionization mass spectrometric sampling), but it also provides accurate and validated thermochemistry of benzene itself and a number of monohalosubstituted benzenes. (The latter are important in numerous kinetic studies, where they are often used as convenient reactants.)

Pleasingly, the ATcT results have also found an instrumental role in developing and benchmarking the latest state-of-the-art sub-kJ/mol electronic structure methods, since ATcT is currently the only approach providing thermochemical data that consistently possesses sufficient accuracy and reliability for this task. Thus, the development of the higher members of the *Wn* electronic structure methods (Jan Martin, Weizmann Institute) and the development of the HEAT approaches (John Stanton, UT Austin) relied almost entirely on ATcT results. The vogue continues, and in collaboration with Wim Klopper (U. Karlsruhe), the current ATcT results are used to test electronic structure approaches that focus on incorporating promising explicitly-correlated coupled-cluster methods, such as CC-R12 and CC-F12. This testing and development process has, *inter alia*, resulted in producing a new ATcT thermochemical benchmark set containing 73 well-defined total atomization energies.⁸

Table 1. Current ATcT thermochemical values for atoms^a

Quantity	0 K	298.15 K	uncert.	units	comment
$\Delta_f H^\circ(\text{C})$	711.39	716.87	± 0.06	kJ/mol	<i>b</i>
$\Delta_f H^\circ(\text{H})$	216.034	217.998	± 0.000	kJ/mol	<i>c</i>
$\Delta_f H^\circ(\text{O})$	246.844	249.229	± 0.002	kJ/mol	<i>c</i>
$\Delta_f H^\circ(\text{N})$	470.57	472.43	± 0.03	kJ/mol	<i>b</i>
$\Delta_f H^\circ(\text{F})$	77.26	79.37	± 0.06	kJ/mol	<i>d</i>
$\Delta_f H^\circ(\text{Cl})$	119.621	121.302	± 0.002	kJ/mol	<i>c</i>
$\Delta_f H^\circ(\text{Br})$	117.92	111.85	± 0.06	kJ/mol	<i>b</i>
$\Delta_f H^\circ(\text{I})$	107.157	106.757	± 0.002	kJ/mol	<i>b</i>

^a All values are interim values based on C(A)TN ver. 1.098; uncertainties are 95% confidence limits, as customary in thermochemistry; see Ref. 7 for an updated set of interim values

^b supersedes earlier interim values disseminated by private communication(s)

^c essentially unchanged from previously published ATcT value, see Ref. 1

^d improved from previously published ATcT value, see Ref. 1

Future Plans

Future plans of this program pivot around further developments and expansive use of Active Thermochemical Tables, providing accurate thermochemistry, and driving targeted theoretical and laboratory experimental investigation of radicals and transient species that are intimately related to combustion processes. The most pressing task for the forthcoming period is to continue the effort toward finalizing and disseminating the ATcT results. A necessary prerequisite is to coerce the related thermochemistry to converge to a stable, “release quality” value, and we intend to continue expanding the number of species that belong to this category. Another prerequisite is the continuation of the current

effort on designing and producing an entirely computer-generated ATcT web site that will be populated by “release quality” results automatically by a suitable post-processing step in ATcT. Besides full automation with archival capability, a desideratum is the automatic inclusion of sufficient background information to document an extensive pedigree tree for every recommended value.

This work is supported by the U.S. Department of Energy, Office of Basic Energy Sciences, Division of Chemical Sciences, Geosciences, and Biosciences, under Contract No. DE-AC02-06CH11357.

References

- ¹ B. Ruscic, R. E. Pinzon, M. L. Morton, G. von Laszewski, S. Bittner, S. G. Nijssure, K. A. Amin, M. Minkoff, and A. F. Wagner, *J. Phys. Chem. A* **108**, 9979 (2004)
- ² B. Ruscic, R. E. Pinzon, G. von Laszewski, D. Kodeboyina, A. Burcat, D. Leahy, D. Montoya, and A. F. Wagner, *J. Phys. Conf. Ser.* **16**, 561 (2005)
- ³ B. Ruscic, “Active Thermochemical Tables”, in *2005 Yearbook of the McGraw-Hill Encyclopedia of Science and Technology*, pp. 3–7, McGraw-Hill, New York (2004)
- ⁴ S. L. Widicus Weaver, D. E. Woon, B. Ruscic, and B. J. McCall, *Astrophys. J.* **697**, 601 (2009)
- ⁵ X. Tang, Y. Hou, C. Y. Ng, and B. Ruscic, *J. Chem. Phys.* **123**, 074330 (2005)
- ⁶ C.-Y. Ng and B. Ruscic, *unpublished data.*
- ⁷ W. R. Stevens, B. Ruscic, and T. Baer, *to be published*
- ⁸ W. Klopper, B. Ruscic, D. P. Tew, F. A. Bischoff, and S. Wolfsegger, *Chem. Phys.* **356**, 14 (2009)

Publications resulting from DOE sponsored research (2007 - present)

- *Unimolecular Thermal Fragmentation of ortho-Benzyne*, X. Zhang, A. T. Maccarone, M. R. Nimlos, S. Kato, V. M. Bierbaum, B. K. Carpenter, G. B. Ellison, B. Ruscic, A. C. Simmonett, W. D. Allen, and H. F. Schaefer III, *J. Chem. Phys.* **126**, 044312/1-20 (2007).
- *Benchmark Atomization Energy of Ethane: Importance of Accurate Zero-point Vibrational Energies and Diagonal Born-Oppenheimer Corrections for a ‘Simple’ Organic Molecule*, A. Karton, B. Ruscic, and J. M. L. Martin, *J. Mol. Struct. (Theochem)* **811**, 345-353 (2007).
- *Kinetics of the Reaction of Methyl Radical with Hydroxyl Radical and Methanol Decomposition*, A. W. Jasper, S. J. Klippenstein, L. B. Harding, and B. Ruscic, *J. Phys. Chem. A* **111**, 3932-3950 (2007).
- *Portal-based Knowledge Environment for Collaborative Science*, K. Schuchardt, C. Pancerella, L. A. Rahn, B. Didier, D. Kodeboyina, D. Leahy, J. D. Myers, O. O. Oluwole, W. Pitz, B. Ruscic, J. Song, G. von Laszewski, and C. Yang, *Concurrency Computat.: Pract. Exper.* **19**, 1703-1716 (2007).
- *HEAT: High Accuracy Extrapolated ab initio Thermochemistry. III. Additional Improvements and Overview*, M. E. Harding, J. Vazquez, B. Ruscic, A. K. Wilson, J. Gauss, and J. F. Stanton, *J. Chem. Phys.* **128**, 114111/1-15 (2008).
- *Accurate ab initio Computation of Thermochemical Data for C₃H_x (x = 0,...,4) Species*, J. Aguilera-Iparraguirre, A. D. Boese, W. Klopper, and B. Ruscic, *Chem. Phys.* **346**, 56-68 (2008).
- *Atomization Energies from Coupled-Cluster Calculations Augmented with Explicitly-Correlated Perturbation Theory*, W. Klopper, B. Ruscic, D. P. Tew, F. A. Bischoff, and S. Wolfsegger, *Chem. Phys.* **356**, 14-24 (2009).
- *Is HO₂⁺ a Detectable Interstellar Molecule?*, S. L. Widicus Weaver, D. E. Woon, B. Ruscic, and B. J. McCall, *Astrophys. J.* **697**, 601-609 (2009).
- *Thermal Decomposition of NH₂OH and Subsequent Reactions: Ab Initio Transition State Theory and Reflected Shock Tube Experiments*, S. J. Klippenstein, L. B. Harding, B. Ruscic, R. Sivaramakrishnan, N. K. Srinivasan, M.-C. Su, and J. V. Michael, *J. Phys. Chem A* **113**, 10241-10259 (2009).

Gas-Phase Molecular Dynamics: High Resolution Spectroscopy and Collision Dynamics of Transient Species

Trevor J. Sears

Department of Chemistry, Brookhaven National Laboratory
Upton, NY 11973-5000

sears@bnl.gov

Program Scope

This research is carried out as part of the Gas-Phase Molecular Dynamics program in the Chemistry Department at Brookhaven National Laboratory. High-resolution spectroscopy, augmented by theoretical and computational methods, is used to investigate the structure and collision dynamics of chemical intermediates in the elementary gas-phase reactions involved in combustion chemistry. Applications and methods development are equally important experimental components of this work.

I. Recent Progress

A. Sub-Doppler spectroscopy of radicals

The development of frequency comb-based spectrometers (see below) opens up the potential for exceptional improvements in both the accuracy and precision of optical spectroscopy. We have been developing experimental tools for sub-Doppler measurements needed to take full advantage of these spectrometers. Initial measurements, reported last year, were made on the cyanogen radical where we have recorded multiple rotational lines in the (1,0) band of the $A\ ^2\Pi_i - X\ ^2\Sigma^+$ system at sub-Doppler resolution. The CN radical was produced by 193 nm photodissociation of NCCN and detected using a Ti:sapphire ring laser operating near $10,900\text{ cm}^{-1}$. The sample was exposed to a weak, frequency-modulated probe beam and a strong, counterpropagating bleach laser beam. Lorentzian saturation dip line widths (HWHM) of 4-6 MHz are typical and result from a combination of pressure dependent broadening, laser frequency instability during the measurement, and a geometrical factor resulting from the pump-probe beam crossing angle. Recently, we have made Stark effect measurements to determine the very small, electric dipole moment of the excited A state of CN. Static fields of less than 1kV/cm are sufficient to mix the closely-spaced Λ -doublets in the A state, leading to shifts in the resonance lines and the appearance of new resonances. Figure 1 shows an example of the A -state hyperfine level shifts caused by the fields used in the experiments for the $J=5/2$ rotational level. The zero field energies of the $F=3/2(-)$ and $F=5/2(+)$ are separated by less than 3 MHz, while the $5/2(-)$ and $7/2(+)$ levels are separated by about 13 MHz. Avoided crossings between these nearly degenerate pairs occur as the field is increased, leading to spectral line shifts and the appearance of new resonances. These avoided crossings make spectroscopic transitions terminating in $J=5/2$ particularly sensitive to Stark effects and we determined an A -state dipole moment of 0.06 ± 0.02 Debye.

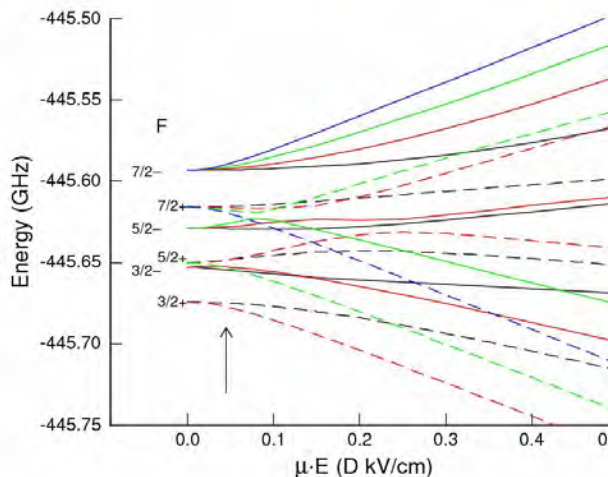


Figure 1. Calculated Stark splitting of the hyperfine and parity components of CN ($A\ ^2\Pi_{3/2}$, $v=1$, $J=5/2$). The zero-field hyperfine levels are labeled by F and parity, dashed and solid lines depict correlation to zero-field levels of + and - parities while the colors label states of the same M . The vertical arrow labels a region near the observed pattern at a laboratory field of 800 V/cm.

Using similar techniques, sub-Doppler spectra of transitions in the $\tilde{b}\ ^1B_1 \leftarrow \tilde{a}\ ^1A_1$ band of CH_2 have also been observed. Most of the rovibronic levels involved in this transition do not show resolved

hyperfine structure even at the sub-Doppler resolution of our experiments. This is expected because the *para* nuclear spin states are non-degenerate, and the *ortho* states have hyperfine splitting dominated by

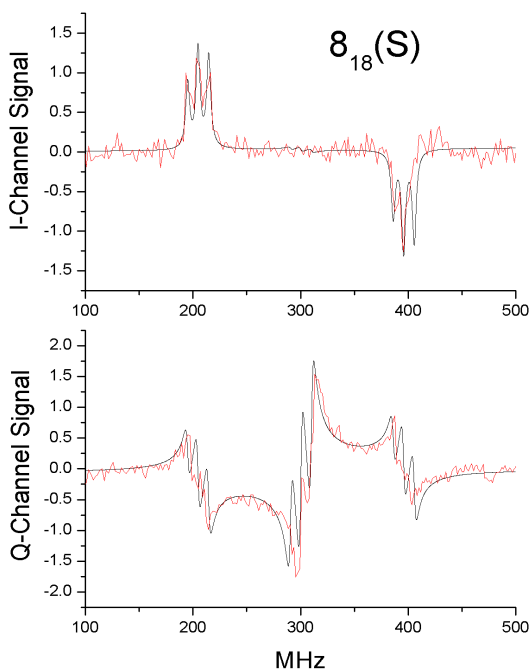


Figure 2. Sub-Doppler measurement of the hyperfine splitting in the 8_{18} \tilde{a}^1A_1 rotational level. This level is perturbed by the nearby 9_{37} level of the excited (020) vibrational level of \tilde{X}^3B_1 . The upper and lower traces are the absorption and dispersion measurements, respectively with the data in red and fitted lineshape function in black. In the absorption trace, the spectrum is recorded twice, as each sideband interacts with the bleach laser beam going in the opposite direction. In the dispersion phase, both carrier and sidebands produce a signal. For $J = 8$ of the 9_{37} level in the ground triplet state, the hyperfine splittings are approximately 50-60 MHz. We measure splittings of approximately 7-10 MHz for the ‘singlet’ level above, and ~25 MHz for its triplet partner.

or the simple 2-state picture is not adequate.

B. New spectroscopy of singlet CH_2

As reported last year, transitions in the $\tilde{b} - \tilde{a}$ origin band of CH_2 near 1200 nm were detected for the first time, using OODR spectroscopy. In collaboration with Professor Bor-Chen Chang from National Central University, Taiwan, the origin band transitions were observed and unambiguously assigned using pulsed infrared light from a scanning OPO laser system to induce transient depletion in absorptions from known lower state rotational levels monitored using lines in the 780 – 800 nm region with a diode laser. To extend and complete the measurements, a Faculty and Student Team group from Bloomsburg University helped to record the entire region between approximately 8150 and 8410 cm^{-1} last summer. This region includes the expected positions of both the $K_a = 0-1$ and $K_a = 1-0$ sub-bands and many additional rotational assignments were made. Unexpectedly, the spectra also contained many additional absorption lines. Hot band absorption lines can be eliminated on the basis of the known spectroscopy, and in this wavelength region, the only other possible origin for such absorptions is to vibrational overtone and combination levels of the lower \tilde{a}^1A_1 state. Previous theoretical and computational work suggested their intensities should be lower than are observed and some additional work is required to

the very weak nuclear spin-rotation coupling, of the order of kHz, well below our current resolution. However, a few \tilde{a}^1A_1 levels are known to be perturbed by nearby vibrationally excited triplet state levels of the same symmetry, via spin-orbit coupling. These perturbed levels act as gateway states and are crucial to the observed very efficient collision-induced intersystem crossing in CH_2 . The triplet contamination of the singlet electronic wavefunction leads to a non-zero electron spin-nuclear spin hyperfine interaction characterized by Fermi-contact and spin-magnetic dipolar coupling terms. In pure triplet state levels, these interactions result in hyperfine splittings of the order of 10’s of MHz. Measurement of any observed hyperfine splittings in perturbed singlet state levels provides a direct estimate of the amount of triplet state mixing and provide a means of validating CI-ISC models.

Figure 2 illustrates sub-Doppler spectra of transitions involving one of these perturbed rotational levels: 8_{18} in the \tilde{a}^1A_1 zero point level. The spectrum indeed shows a resolved hyperfine splitting of about 7-10 MHz. Its perturbing triplet partner (not shown) exhibits splittings of approximately 25 MHz. A simple two-state mixing model would imply the sum of the observed splittings should match the pure triplet level value, which (from published results for the \tilde{X}^3B_1 ground state) would be 50-60 MHz. This suggests either the hyperfine interaction decreases with bending vibrational excitation in triplet CH_2 ,

investigate this observation, which may imply the singlet stretching potential is more anharmonic than previously thought.

C. Double resonance and sub-Doppler studies of radical collision dynamics

Rotational energy transfer within the \tilde{a} state of CH_2 and between rotational levels of CN has been studied by saturation recovery and saturation transfer double resonance kinetic spectroscopy. In addition, new sub-Doppler probes of the collisional loss of transient holes burned into specific velocity groups of the radical sample are being investigated in both radicals. These measurements give a new and insightful view of the various contributions to pressure-broadening in spectroscopic measurements. The results are discussed in G. Hall's abstract from our group.

D. Spectroscopy with comb-stabilized extended cavity diode lasers

Our recent demonstration of sub-Doppler resolution spectra of transient species has illustrated the limitations associated with the use of wavelength standards for spectral calibration. While it is often possible to measure fine and hyperfine spacings in spectra to within a few MHz using stabilized etalon markers, absolute measurements, or precise relative line position measurements when the features are separated by an interval corresponding to larger than a radio frequency, are difficult. Such measurements are limited by wavelength standards such as the iodine spectrum or wavelength measurement precision to (at the best) a 10^{-8} fractional uncertainty. In the case of the CN and CH_2 measurements, we were hampered by our inability to prevent long-term (i.e., longer than a few seconds) drifts of up to 10 MHz in the laser frequency during a measurement. Our ability to precisely measure line shapes is compromised by the same factors. Recently, we have successfully locked an extended cavity diode laser to a single component of a near-infrared Er-fiber laser-based comb operating at 250 MHz. The diode laser has been used to record absorption spectra of $(\nu_1 + \nu_3)$ combination band lines in acetylene near $1.5\mu\text{m}$, that were previously adopted as a secondary frequency standard. Figure 3 shows an example of the recent measurements.

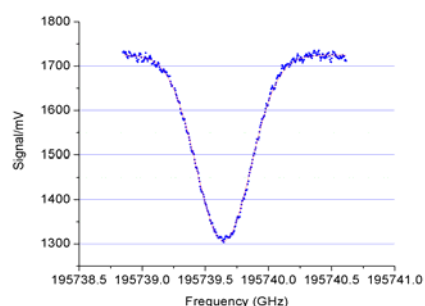


Figure 3. Doppler-limited rotational line in the $\nu_1+\nu_3$ combination band of acetylene recorded at a pressure of 2 mT using a comb-stabilized extended-cavity diode laser in a cavity-enhanced absorption experiment.

E. Low energy photoelectron spectroscopy of aromatic species

In collaboration with Prof. Philip Johnson (Stony Brook University) we have recently completed a new study of phenylacetylene, comparing a more thorough vibronic calculation to the jet-cooled REMPI $S_1 \leftarrow S_0$ spectrum. To provide more information for vibrational assignments, velocity map imaging photoelectron spectra were also recorded for the resonant ionization process through the vibrational features of the spectrum. In addition to being a good candidate for a test of computational methods, phenylacetylene was chosen in order to gather more information about the character of its S_1 state. It has recently been discovered there is an anomalous photochemical transformation that occurs in this molecule when excited to S_1 . Although strong fluorescence is seen, about 20% of excitations immediately result in the formation of a species with a low ionization potential and a lifetime exceeding 100 μs . The relative production of the short- and long-lifetime products varies with the S_1 vibronic level excited, however the identity of the long-lived photoproduct has not yet been determined.

II. Future Work

A. Precision spectroscopy and dynamics

Time resolved measurements of the collisional loss of saturation in both CH_2 and CN radicals as a function of pressure and collision partner are continuing. These measurements will provide new insights

into the function describing the intermolecular potential and the various contributions leading to pressure broadening and dephasing in gaseous systems. More details are given elsewhere in G. Hall's abstract. For the spectroscopic focus of our work, the implementation of frequency comb measurements of the laser frequencies so that both Doppler-limited lineshapes and sub-Doppler line positions in our spectra can be measured precisely is a major theme. Currently, our measurement precision is limited by a combination of laser source instability over the time required to acquire data and the limitations of our high resolution wavemeters. Locking the laser to a component of a stabilized frequency comb will eliminate both these issues and spectroscopic line positions in the visible and near-IR region will be able to be measured to 3×10^{-10} fractional accuracy. This will have an immediate effect on the quality of our sub-Doppler measurements, but also open the path to extremely precise line shape measurements to compare to theory.

Frequency-based optical measurements will have a broad impact on future analytical measurements. In particular a major focus of ourselves and other research groups is to take advantage of the potential for parallel measurements by making use of many, rather than just one, comb components. While the power in any single comb component is not sufficient to saturate transitions, there is ample for linear absorption measurements. The combination of a Fourier Transform spectrometer with a comb source offers one way to make such measurements and has already been demonstrated at near-IR wavelengths. Alternatively, a two-comb method can achieve identical results with the advantage that the mechanical moving reflector of a FT instrument can be eliminated. The field is at a very exciting point, and we are actively investigating the various alternatives.

Continued ultra-high resolution spectroscopy efforts using comb-stabilized single frequency lasers will target increased sensitivity through the use of cavity-enhanced techniques. We have already demonstrated measurements in which a resonant cavity mode is locked to a diode laser that is itself locked to the comb. This technique is needed for sub-Doppler measurements using relatively low-power extended cavity diode lasers. In the near future, we will combine this with a transient molecule measurement. In the longer term, we also plan to make high resolution measurements of the A-X origin band of PbF, in collaboration with Prof Neil Shafer-Ray (University of Oklahoma). This DOE EPSCoR funded project is directed toward investigating parity violation effects in small molecules containing a heavy atom.

Publications supported by this project since 2008

- State mixing and predissociation in the $\tilde{c} - \tilde{a}$ band system of singlet methylene studied by optical-optical double resonance, Z. Wang, Y. Kim, G. E. Hall and T. J. Sears, *J. Phys. Chem. A*, **112**, 9248-9254 (2008)
- The fate of excited states in jet-cooled aromatic molecules: Bifurcating pathways and very long-lived species from the S₁ excitation of phenylacetylene and benzonitrile, J. Hofstein, H. Xu, T. J. Sears, and P. M. Johnson, *J. Phys. Chem. A*, **112**, 1195-1201 (2008).
- Sub-Doppler laser absorption spectroscopy of the $A^2\Pi_i - X^2\Sigma^+$ (1,0) band of CN. Measurement of the ¹⁴N hyperfine parameters in $A^2\Pi_i$ CN. M. L. Hause, G. E. Hall, and T. J. Sears, *J. Mol. Spectr.* **253** 122-128 (2008).
Corrigendum: *J. Mol. Spectr.* **260** 138 (2010).
- The Zeeman effect on lines in the (1,0) band of the $F^4\Delta - X^4\Delta$ transition of the FeH radical. J. J. Harrison, J. M. Brown, J. Chen. T. Steimle and T. J. Sears. *Astrophys. J.* **679**, 854-861 (2008).
- Sub-Doppler Stark spectroscopy in the $A - X$ (1,0) band of CN. M. L. Hause, G. E. Hall, and T. J. Sears, *J. Phys. Chem. A*, **113** 13342-13346 (2009).
- The halocarbenes: model systems for understanding the spectroscopy and dynamics of carbenes. S. H. Kable, S. A. Reid and T. J. Sears, *Int. Revs. Phys. Chem.* **28** 435-480 (2009).
- Pseudo-continuous resonance-enhanced multiphoton ionization: application to the determination of the hyperfine constants of ²⁰⁸Pb¹⁹F. P. Sivakumar, C. P. McRaven, P. M. Rupasinghe, T. Zh. Yang, N. E. Shafer-Ray, G. E. Hall and T. J. Sears, *Mol. Phys.* (2010). (in press, DOI: 10.1080/00268970903567304).

Picosecond Nonlinear Optical Diagnostics

Thomas B. Settersten and Roger L. Farrow
Combustion Research Facility, Sandia National Laboratories
P.O. Box 969, MS 9055
Livermore, CA 94551-0969
tbsette@sandia.gov

Program Scope

This program focuses on the development of innovative laser-based techniques for measuring temperature and concentrations of important combustion species as well as the investigation of fundamental physical and chemical processes that directly affect quantitative application of these techniques. Our development efforts focus on laser-induced fluorescence (LIF) and crossed-laser-beam techniques, which can be used in cases where LIF is not feasible. A critical aspect of our research includes the study of fundamental spectroscopy, energy transfer, and photochemical processes. This aspect of the research is essential to the development of accurate models and *quantitative* application of techniques to the complex environments encountered in combustion systems. Many of these investigations use custom-built tunable picosecond (ps) lasers, which enable efficient nonlinear excitation, provide high temporal resolution for pump/probe studies of collisional processes, and are amenable to detailed physical models of laser-molecule interactions.

Recent Progress

Multiplexed time-resolved picosecond CARS. Frequency-domain coherent anti-Stokes Raman spectroscopy (CARS) using nanosecond-duration laser pulses is a well developed technique for concentration and temperature measurement in flames. By using broadband excitation of rovibrational Raman coherences and probing with a narrowband probe, an entire vibrational CARS (VCARS) spectrum can be recorded on a single shot. A similar “multiplexed” measurement of the pure-rotational (RCARS) spectrum is possible through Raman excitation via a single broadband laser. Unfortunately collisional line-mixing, nonresonant CARS contributions, and resonant interferences can restrict the utility of CARS, particularly at high pressures. We are addressing these issues through joint theoretical-experimental development of a new variant of RCARS using ps lasers. We use ps-duration laser pulses and a time-delayed probe to significantly simplify complex RCARS spectra by (1) effectively eliminating contributions from rotational Raman coherences excited in large molecules by exploiting large differences in species-dependent coherence dephasing rates and (2) imposing a time-ordering of photon interactions in the four-wave-mixing process that eliminates interference from non-resonant four-wave mixing and from smeared VCARS.^{1,2} Because gas-phase applications of RCARS almost exclusively use nanosecond-duration laser pulses and because coherence lifetimes for practical conditions are considerably shorter than these laser pulses, such time-dependent discrimination against these Raman-resonant contributions has not been demonstrated previously. Although this approach eliminates complex coherent interferences in practical measurement environments, it is still sensitive to collisions that occur during the probe delay. To develop robust and accurate analysis tools requires detailed understanding of collisional effects in combustion-relevant conditions. The signal decay rates in these time-domain measurements are a direct measure of dephasing rates and can be used to extract J -dependent linewidths that are equivalent to those obtained in high-resolution experiments. Figure 1b displays the results for N_2 , where the J -dependent (S-branch) Raman linewidth was calculated from the measured decay rates (Fig. 1a). As can be seen in Fig. 1b, the values compare exceptionally well with Q-branch

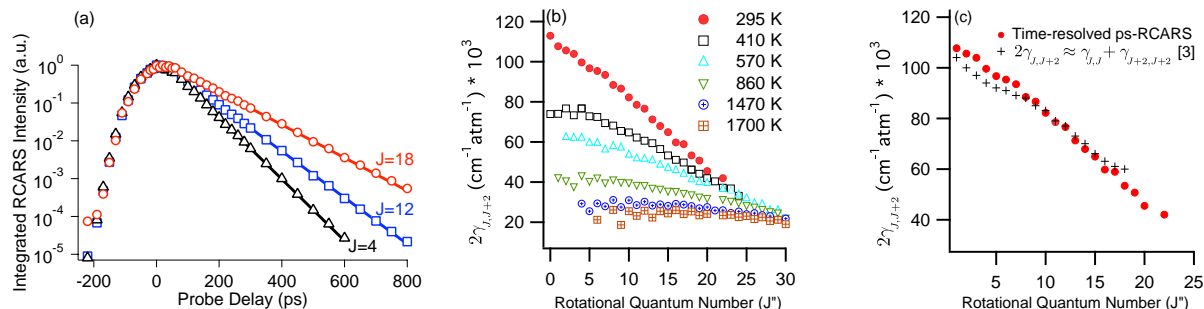


Figure 1: (a) J -dependent time-resolved DBB-RCARS decays for N₂ at 295 K. (b) Compilation of N₂ S-branch Raman linewidths calculated from measured J -dependent decay rates. (c) Comparison of the room- T N₂ S-branch linewidths reported in panel (b) and those estimated from Q-branch linewidths reported in [3].

linewidths based on high-resolution inverse Raman spectroscopy (IRS) measurements.³In Fig. 1b, the linewidths approximated from the frequency-domain Q-branch measurements are smaller at low J because the anisotropic dephasing, which is typically ignored for RCARS calculations, is not negligible. Our approach not only more accurately measures S-branch collisional dephasing, but also has significantly higher data rates than high-resolution measurements. The rapid, direct, and accurate measurement of broadening coefficients from time-domain data is a key capability that we plan to exploit in the development of collision models for nonlinear spectroscopy of combustion-relevant molecules and collision partners. Such broadening rates can also be used to test molecular potential energy surfaces important in elastic and inelastic collisions.

RCARS flame measurements. We have successfully used time-delayed ps-RCARS to produce interference-free N₂ and O₂ spectra in a range of fuel-rich and sooting flames.⁴ Spectra have been evaluated for temperature and relative O₂/N₂ concentration ratios using frequency-domain analysis, and corrections for collisional bias were empirically approximated from cell measurements.

Development of 1-D ps-RCARS imaging. Because only modest pulse energies are necessary when exciting Raman coherences with ps pulses, it is feasible to implement a CARS imaging configuration that enables single-shot measurements of temperature and concentrations along a line. In this case, the pump, Stokes, and probe laser beams are formed into sheets that intersect along a line. The signal from the 1-D probe volume is relay-imaged onto the spectrometer slit, dispersed, and the spatially resolved CARS spectra detected with a 2-D CCD array. Initial imaging experiments employed time-delayed probing to eliminate fuel interference in a rich ($\Phi=2.8$) propane jet flame, enabling 1-D imaging along a 9-mm line through the flame. Spectra were fitted to produce a 1-D map of temperature and relative O₂/N₂ concentration. See Fig. 2.

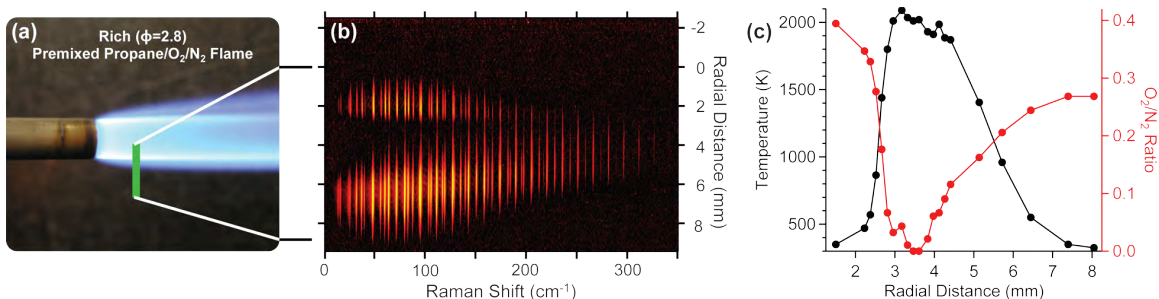


Figure 2: 1-D RCARS imaging through a rich propane jet flame. (a) Photograph of flame with imaged area indicated by the green line. (b) Spatially and spectrally resolved RCARS spectra using delayed probing to eliminate interference. (c) Temperature and relative O₂/N₂ concentration from fitted spectra.

Future Plans

Model development and validation for time-resolved CARS. We are well into the development of a versatile simulation and fitting code for time-resolved CARS, capable of treating both coherent and incoherent (stochastic) laser pulses. To analyze data provided by our current experimental capabilities, the ps-RCARS code will allow simulation and fitting of either dispersed or non-dispersed signal pulse energies as a function of time delay. Pulses are described in terms of duration and coherence length, permitting greater than transform-limited bandwidths as required by the use of an incoherent broadband dye laser in experiments. The code will allow analysis of temperature and relative concentrations from least-squares fits of spectra, and molecular parameters such as coherence decay rates, relative transition amplitudes, and transition splittings from fits of spectral peaks versus delay. Development and validation of the analysis code will rely on ps-RCARS measurements of well characterized gas mixtures in heated cells and premixed flames. A significant advantage of these experiments is that we extract J -dependent coherence decay rates from observations of the spectrally integrated signal decay and the decay of spectrally resolved rotational peaks. The latter provides excellent measurements of individual decays, but we expect the total decay waveform to be an exceptionally sensitive test of the relative decays, rotation constants, and transition strengths because of beats between time-varying rotational amplitudes.

High-pressure line mixing. As we develop nonlinear diagnostics for high-pressure applications, it is essential to further develop collision models relevant to line broadening and line mixing. To this end, we propose a multiplexed coherence transfer diagnostic, which will enable rapid and direct measurement of state-to-state rates for an entire rotational manifold. This approach relies on the unique capability provided by our independently tunable, transform-limited, picosecond lasers to excite individual rotational coherences on a time scale that is short compared to dephasing times. A third delayed laser pulse will simultaneously probe the directly excited coherence as well as all collisionally coupled coherences. The exceptional dynamic range already demonstrated in our lab is critical to the success of this effort. Because the signals from all Raman coherences are simultaneously recorded in a single spectrum, their relative calibration is automatic. Time-dependent spectra will map both total relaxation rates and state-to-state rates for the entire manifold. These experiments measure coherence transfer rather than population transfer, and through comparison with measurements of the latter we will gain new information on decay of alignment by collisions.

Ignition Experiments using ps H-atom LIF. Based on the success of our ps two-photon LIF imaging of H, we plan to continue collaboration with J. H. Frank to apply this technique to study preferential diffusion in edge flames during extinction and re-ignition in pulsed counterflows. Studies of H-atom preferential diffusion in flames with different Lewis numbers are also envisioned.

Energy transfer studies for quantitative CO imaging. We are collaborating with Volker Sick (Univ. Michigan) to characterize collisional energy transfer processes in the CO $A^2\Pi$ electronic state using ps time-resolved two-photon LIF. This work contributes to the development of a new fluorescence detection technique for spatially-resolved, quantitative measurements of CO at the high pressures and elevated temperature relevant to combustion regimes that will be employed in next-generation devices.

Energy transfer studies for quantitative Kr imaging. We are developing a predictive model for collisional quenching of Kr $5p^2[3/2]_2$ in collaboration with Jonathan Frank. This work will contribute to development of a new mixture-fraction diagnostic technique using Kr two-photon LIF. Because the natural radiative lifetime of this excited state is only 27 ns and collisions at even modest pressures (< 10 Torr) of strongly quenching species reduce the effective fluorescence

lifetime to a few ns, excitation by standard dye lasers (10-ns pulses) is not sufficient for accurate time-resolved studies, and excitation with picosecond (ps) laser pulses is necessitated.

References

- [1] T. Seeger, J. Kiefer, A. Leipertz, B. D. Patterson, C. J. Kliewer, T. B. Settersten, *Opt. Lett.* **34**, 3755 (2009).
- [2] T. Seeger, J. Kiefer, Y. Gao, B. D. Patterson, C. J. Kliewer, T. B. Settersten, "Suppression of Raman-resonant interferences in rotational CARS using time-delayed picosecond probe pulses," *Opt. Lett.* submitted (2010).
- [3] L. A. Rahn, P. R. E., *J. Opt. Soc. Am. B* **3**, 1164 (1986).
- [4] C. J. Kliewer, T. Seeger, Y. Gao, J. Kiefer, B. D. Patterson, T. B. Settersten, "Picosecond time-resolved pure-rotational coherent anti-Stokes Raman spectroscopy in sooting flames," *Proc. Comb. Instit.* **33**, submitted (2010).

BES-Supported Publications (2008-present)

1. W. D. Kulatilaka, B. D. Patterson, J. H. Frank, and T. B. Settersten, "Comparison of nanosecond and picosecond excitation for interference-free two-photon laser-induced fluorescence detection of atomic hydrogen in flames," *Appl. Opt.* **47**, 4672–4683 (2008).
2. X. Chen, T. B. Settersten, P. P. Radi, and A. P. Kouzov, "Two-color resonant four-wave mixing spectroscopy: New perspectives for direct studies of collisional state-to-state transfer," *Spectral Line Shapes* **15**, 128–130 (2008).
3. T. B. Settersten, B. D. Patterson, and W. H. Humphries, IV, "Radiative lifetimes of NO $A^2\Sigma^+(v' = 0, 1, 2)$ and the electronic transition moment of the $A^2\Sigma^+ - X^2\Pi$ system," *J. Chem. Phys.* **131**, 104309 (2009).
4. T. B. Settersten, B. D. Patterson, and C. D. Carter, "Collisional quenching of NO $A^2\Sigma^+(v' = 0)$ between 125 and 294 K," *J. Chem. Phys.* **130**, 204302 (2009).
5. A. K. Patnaik, S. Roy, J. R. Gord, R. P. Lucht, and T. B. Settersten, "Effects of collisions on electronic-resonance-enhanced coherent anti-Stokes Raman scattering of nitric oxide," *J. Chem. Phys.* **130**, 214304 (2009).
6. V. Ebert, T. B. Settersten, and D. K. Killinger, "Laser applications to chemical, security, and environmental analysis: introduction to the feature issue," *Appl. Opt.* **48**, A1 (2009).
7. W. D. Kulatilaka, J. H. Frank, B. D. Patterson, and T. B. Settersten, "Analysis of 205-nm photolytic production of atomic hydrogen in methane flames," *Appl. Phys. B* **97**, 227 (2009).
8. X. Chen, T. B. Settersten, and A. P. Kouzov, "State- and time-resolved rotational relaxation signatures in two-color resonant four-wave mixing spectra," *J. Raman Spectrosc.* **40**, 847 (2009).
9. R. W. Schefer, W. D. Kulatilaka, B. D. Patterson, and T. B. Settersten, "Visible emission of hydrogen flames," *Combust. Flame* **156**, 1234 (2009).
10. W. D. Kulatilaka, J. H. Frank, and T. B. Settersten, "Interference-free two-photon LIF imaging of atomic hydrogen in flames using picosecond excitation," *Proc. Comb. Instit.* **32**, 955 (2009).
11. T. Seeger, J. Kiefer, A. Leipertz, B. D. Patterson, C. J. Kliewer, and T. B. Settersten, "Picosecond time-resolved pure-rotational coherent anti-Stokes Raman spectroscopy for N₂ thermometry," *Opt. Lett.* **34**, 3755 (2009).
12. J. M. Headrick, T. A. Reichardt, T. B. Settersten, R. P. Bambha, and D. A. V. Kliner, "Application of laser photofragmentation-resonance enhanced multi-photon ionization to ion mobility spectrometry," *Appl. Opt.*, in press (2010).
13. T. Seeger, J. Kiefer, Y. Gao, B. D. Patterson, C. J. Kliewer, and T. B. Settersten, "Suppression of Raman-resonant interferences in rotational CARS using time-delayed picosecond probe pulses," *Opt. Lett.*, submitted (2010).
14. C. J. Kliewer, T. Seeger, Y. Gao, J. Kiefer, B. D. Patterson, and T. B. Settersten, "Picosecond time-resolved pure-rotational coherent anti-Stokes Raman spectroscopy in sooting flames," *Proc. Comb. Instit.*, submitted (2010).

Theoretical Studies of Potential Energy Surfaces and Computational Methods

Ron Shepard

Chemical Sciences and Engineering Division,
Argonne National Laboratory, Argonne, IL 60439
[email: shepard@tcg.anl.gov]

Program Scope: This project involves the development, implementation, and application of theoretical methods for the calculation and characterization of potential energy surfaces (PES) involving molecular species that occur in hydrocarbon combustion. These potential energy surfaces require an accurate and balanced treatment of reactants, intermediates, and products. This difficult challenge is met with general multiconfiguration self-consistent field (MCSCF) and multireference single- and double-excitation configuration interaction (MR-SDCI) methods. In contrast to the more common single-reference electronic structure methods, this approach is capable of describing accurately molecular systems that are highly distorted away from their equilibrium geometries, including reactant, fragment, and transition-state geometries, and of describing regions of the potential surface that are associated with electronic wave functions of widely varying nature. The MCSCF reference wave functions are designed to be sufficiently flexible to describe qualitatively the changes in the electronic structure over the broad range of molecular geometries of interest. The necessary mixing of ionic, covalent, and Rydberg contributions, along with the appropriate treatment of the different electron-spin components (e.g. closed shell, high-spin open-shell, low-spin open shell, radical, diradical, etc.) of the wave functions are treated correctly at this level. Further treatment of electron correlation effects is included using large-scale multireference CI wave functions, particularly including the single and double excitations relative to the MCSCF reference space. This leads to the most flexible and accurate large-scale MR-SDCI wave functions that have been used to date in global PES studies.

Recent Progress: ELECTRONIC STRUCTURE CODE MAINTENANCE, DEVELOPMENT, AND APPLICATIONS: A major component of this project is the development and maintenance of the COLUMBUS Program System. The COLUMBUS Program System computes MCSCF and MR-SDCI wave functions, MR-ACPF (averaged coupled-pair functional) energies, MR-AQCC (averaged quadratic coupled cluster) energies, spin-orbit CI energies, analytic energy gradients, and nonadiabatic coupling. Geometry optimizations to equilibrium and saddle-point structures can be done automatically for both ground and excited electronic states. The COLUMBUS Program System is maintained and developed collaboratively with several researchers including Isaiah Shavitt (University of Illinois), Russell M. Pitzer (Ohio State University), Thomas Mueller (Central Institute for Applied Mathematics, Juelich, Germany), and Hans Lischka (University of Vienna, Austria). The nonadiabatic coupling and geometry optimizations for conical intersections is done in collaboration with David R. Yarkony (Johns Hopkins University). The distributed development effort and software coordination uses an svn repository of source code. The parallel sections of the code are based on the single-program multiple-data (SPMD) programming model with explicit

This work was performed under the auspices of the Office of Basic Energy Sciences, Division of Chemical Sciences, Geosciences, and Biosciences, U.S. Department of Energy, under contract number DE-AC02-06CH11357.

message passing using the portable MPI library, and the portable Global Array Library (distributed from PNNL) is used for data distribution. The next major release of the COLUMBUS codes will begin to incorporate the newer language features of F90/F95. This will facilitate future development and maintenance effort.

GRAPHICALLY CONTRACTED FUNCTION METHOD: We have recently developed a novel expansion basis for electronic wave functions [*J. Phys. Chem. A* **109**, 11629 (2005)]. In this approach, the wave function is written as a linear combination of *graphically contracted functions* (GCFs), and each GCF in turn is formally equivalent to a linear combination of configuration state functions (CSFs) that comprise an underlying linear expansion space of dimension N_{csf} . The CSF coefficients that define the GCFs are nonlinear functions of a smaller number of variables $N_{\phi} \ll N_{\text{csf}}$. GCF expansions with 10 to 20 basis functions can approach the full-CI PES to within chemical accuracy (1 kcal/mole or better) [*Int. J. Quantum Chem.* **107**, 3203 (2007)]. The method is formulated in terms of spin-eigenfunctions using the Graphical Unitary Group Approach (GUGA) of Shavitt, and consequently it does not suffer from spin contamination or spin instability.

Our new method is characterized by several important features. First, open-shell spin-eigenfunctions are included in the wave function expansions. This allows our new method to be used for the reactions that are important to combustion chemistry (i.e. involving radicals and other open-shell electronic states) without introducing spin contamination. Second, we place no intrinsic restrictions on the orbital occupations, so our GCFs are not restricted to only geminals or to other preselected molecular fragments, and there are no artificial excitation-level or occupation restrictions with respect to a reference function or reference space. Third, we use linear combinations of N_{GCF} basis functions rather than a single expansion term. This allows our method to be used for both ground and excited electronic states, the increased wave function flexibility leads to more accurate wave functions, and it will allow the computation of transition moments, nonadiabatic coupling, and other properties that at present can only be computed reliably with MCSCF and MRCI approaches.

Efficient procedures to compute hamiltonian matrix elements and reduced one- and two-particle density matrices for this nonlinear expansion have been developed [*J. Phys. Chem. A* **110**, 8880 (2006)]. The effort required to construct an individual hamiltonian matrix element between two GCFs $H_{PQ} = \langle P | \hat{H} | Q \rangle$ scales as $\mathcal{O}(\omega n^4)$ for a wave function expanded in n molecular orbitals. The prefactor ω depends on the complexity of the underlying Shavitt Graph and scales between N^0 and N^2 for N electrons. The corresponding metric matrix element $S_{PQ} = \langle P | Q \rangle$ requires effort that scales as $\mathcal{O}(\omega n)$, the one-particle transition density \mathbf{D}^{MN} requires $\mathcal{O}(\omega n^2)$ effort, the two-particle density \mathbf{d}^{MN} requires $\mathcal{O}(\omega n^4)$ effort. There is no component of the effort or storage for matrix element computation or wave function optimization that scales as N_{csf} . This feature allows very large wave functions to be employed, much larger than would be possible with any of the traditional electronic structure methods. Timings with our initial implementation of this method are very promising. A hamiltonian matrix element involving GCFs corresponding to an underlying linear expansion space with dimension $N_{\text{csf}} \approx 5.5 \cdot 10^{24}$ requires only 10 to 15 seconds on a typical laptop or desktop computer. The computation of this same matrix element would require over a million times the age of the universe

using traditional full-CI technology. H_{PQ} timings for expansions as large as $N_{csf} \approx 4.0 \cdot 10^{56}$ were shown in last year's abstract.

An efficient algorithm has been developed and implemented to compute spin-density matrices from wave functions expanded in a basis of GCFs. The spin-density matrix allows expectation values to be computed for spin-dependent operators that depend on the M quantum number of the \hat{S}_z operator. Through the Wigner-Eckart theorem, the spin-density matrix also allows entire spin-blocks of matrix elements to be computed, $\langle \psi, S, M | \hat{A} | \psi, S, M \rangle$ for $M, M' = -S, -S+1, \dots, S$. Because the GUGA is a "spin-free" formulation of the electronic wave function, the computation of the $S=M$ component of the spin-density matrix elements is first cast in terms of the one-particle and two-particle charge-density matrix elements (which are independent of M).

$$D_{qp}^{(1,0;S)} = \frac{(2 - \frac{1}{2}N)}{(S+1)} D_{qp}^{(0)} - \frac{1}{(S+1)} \sum_k d_{qkpk}$$

If computed in this form, all n^2 elements of the matrix $\mathbf{D}^{(1,0;S)}$ would require $\mathcal{O}(N_{\text{GCF}}^2 \omega n^3)$ total effort where N_{GCF} is the dimension of the GCF basis. A more efficient recursive algorithm was developed that allows the spin-density matrix to be computed with only $\mathcal{O}(N_{\text{GCF}}^2 \omega n^2)$ total effort. Because the "spin-free" GCF formulation eliminates the need to expand the wave function in a spin-dependent Slater determinant basis, it is possible to treat wave functions with large numbers of electrons and orbitals. Timings have been presented for wave functions that correspond to determinantal expansions over 10^{200} in length. Fig. 1 shows timings for triplet wave functions for fixed N and increasing n (such as might be appropriate for computing complete basis set (CBS) limits for some arbitrary spin-dependent property). These timings verify the above predicted scaling of the algorithm. The implementation is applicable to arbitrary spin states and to both ground and excited electronic states.

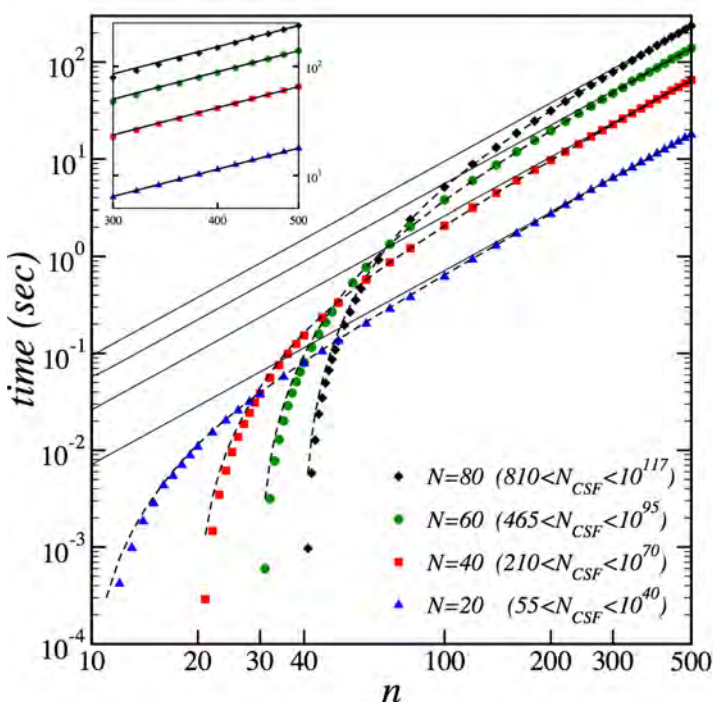


Fig. 1 Timings for the transition spin-density matrix computation for a set of triplet wave functions based on full-CI Shavitt graphs. Four sets of curves are given, each of which corresponds to a fixed number of electrons ($N=20, 40, 60,$ and 80) and with up to 500 orbitals. For each set of curves, the measured values are shown, the $f(n)=an^2$ fit from the measured large n values is shown with a solid line, and the timing estimates using ω_p based on the actual number of nodes at each orbital level are indicated by the dashed lines.

Future Plans: GCF METHOD: Our applications have so far used single-headed Shavitt graphs appropriate for describing individual molecular states with a given number of electrons, with a particular spin state, and that belong to a particular irrep. We will generalize this in several respects. First, we will introduce state averaging over individual irreps and state averaging over multiple irreps. This will allow the nonlinear arc factor parameters to be optimized for several electronic states simultaneously rather than for individual electronic states. For the multiple irrep case, this will allow the computation of several molecular states with essentially no additional effort over single-irrep calculations. Next, we will employ multiheaded Shavitt graphs in the state-averaging procedure. This will allow the computation of hamiltonian matrix elements corresponding to states with different numbers of electrons, different spin values, and different irreps simultaneously with only a relatively small increase in effort over the current single-state approach.

We have recently developed a new algorithm to compute the gradients of the energy with respect to the nonlinear arc factor parameters. These gradients are used during the wave function optimization. Our previous algorithm required $\mathcal{O}(\omega^5)$ effort; the new algorithm requires $\mathcal{O}(\omega^4)$ effort and is comparable to that of the energy evaluation itself. This is an extension of our *deferred propagation* algorithm for the contributions of the Shavitt loop upper and lower walks described in last year's abstract. An initial implementation of this algorithm has been developed, and during the next year a robust implementation will be distributed through the COLUMBUS svn repository.

Publications:

- “The Accuracy of Molecular Bond Lengths Computed by Multireference Electronic Structure Methods”, R. Shepard, G. S. Kedziora, H Lischka, I. Shavitt, T. Müller, P. G. Szalay, M. Kállay, M. Seth, *Chem. Phys.* **349**, 37-57 (2008).
- “Advanced Software for The Calculation of Thermochemistry, Kinetics, and Dynamics,” R. Shepard, *J. Physics: Conference Series* **125**, 012016 (2008).
- “Computation of Determinant Expansion Coefficients Within the Graphically Contracted Function Method”, G. Gidofalvi and R. Shepard, *J. Comp. Chem.* **30**, 2414 (2009).
- “The Evaluation of Spin-Density Matrices Within the Graphically Contracted Function Method”, G. Gidofalvi and R. Shepard, *Int. J. Quantum Chem.* **109**, 3552 (2009).
- “Evaluation of the Spin-Orbit Interaction Within the Graphically Contracted Function Method”, S. R. Brozell and R. Shepard, *J. Phys. Chem. A* **113**, 12741 (2009).
- “Computational and Methodological Elements for Nonadiabatic Trajectory Dynamics Simulations of Molecules,” M. Barbatti, R. Shepard, and H. Lischka, in “Conical Intersections: Theory, Computation and Experiment”, W. Domcke, D.R. Yarkony and H. Köppel, Eds., *Advanced Series in Physical Chemistry*, **17** (World Scientific, Singapore, *in press*).

COMPUTATIONAL AND EXPERIMENTAL STUDY OF LAMINAR FLAMES

M. D. Smooke and M. B. Long
Department of Mechanical Engineering
Yale University
New Haven, CT 06520
mitchell.smooke@yale.edu

Program Scope

Our research has centered on an investigation of the effects of complex chemistry and detailed transport on the structure and extinction of hydrocarbon flames in coflowing axisymmetric configurations. We have pursued both computational and experimental aspects of the research in parallel. The computational work has focused on the application of accurate and efficient numerical methods for the solution of the boundary value problems describing the various reacting systems. Detailed experimental measurements were performed on axisymmetric coflow flames using two-dimensional imaging techniques. Spontaneous Raman scattering and laser-induced fluorescence were used to measure the temperature, and major and minor species profiles. Laser-induced incandescence (LII) has been used to measure soot volume fractions and particle sizes. A new approach to optical pyrometry has been developed to measure temperatures where the other techniques fail due to the presence of soot. Our goal has been to obtain a more fundamental understanding of the important fluid dynamic and chemical interactions in these flames so that this information can be used effectively in combustion modeling.

Recent Progress

Time-Varying Flames:

Fully coupled implicit algorithms are used extensively in flame calculations for steady-state problems due to their good stability properties with large time steps (see [1] and references therein). Generally, the governing partial differential equations are discretized in space and time with low order (≤ 2) difference schemes, and the resulting system of nonlinear algebraic equations is solved by Newton's method. Within each Newton iteration, the linearized problem involving the Jacobian matrix is solved with a preconditioned iterative solver, typically some kind of Krylov method [1,2]. Pseudo-time continuation facilitates a very rapid approach to the steady state. In this way, excellent agreement has been achieved with experimental profiles of major and minor species concentrations, as well as with other variables such as temperature [1]. The extension of the low order implicit solver to model time-dependent chemically reacting flows is hindered by the presence of large artificial diffusion, in particular from the first-order upwind discretizations of the convective terms in the governing equations. As in the steady-state problem, this can be reduced through grid refinement. In a time-evolving flow, however, node clustering must be adjusted dynamically to follow the movement of flow structures such as vortices. Otherwise, during some stages of the computations, important flow nonuniformities may penetrate regions of the domain having insufficient grid resolution and experience a significant amount of artificial diffusion, thus spuriously altering the flow dynamics. As an alternative approach, high order discretization schemes with negligible numerical diffusion can be used for flame computations.

We are applying high order compact spatial discretizations in a fully implicit framework that avoid these problems, and offer many advantages over other current approaches to solving reacting flow problems. Compact schemes are well suited to the simulation of time-dependent

flows with complicated structures due to their excellent resolution characteristics [3,4]. Their integration into an efficient Newton-based flame code is an extremely challenging problem requiring research in modern iterative linear algebra solvers and preconditioning, novel storage/retrieval methodologies, fast Jacobian matrix algorithms, and domain decomposition methods. The necessity of implementing all these numerical techniques on message-passing parallel architectures only compounds the difficulty. However, an operation count/cost estimate indicates that the use of compact spatial discretizations with implicit time stepping may be able to reduce overall computation times by upwards of two orders of magnitude compared to other numerical methods commonly employed in detailed-chemistry combustion simulations [5].

More recently, we completed the first implicit, fully coupled, two-dimensional forced (20 Hz) axisymmetric coflow diffusion flame computation with compact methods employing Arrhenius chemistry. The steady velocity field of the fuel jet was modulated with a sinusoidal velocity perturbation. Although only a simple chemical mechanism was used, the results of these computations (Fig. 1) for forcing amplitudes up to 90% illustrate the superior ability of the compact method compared to the low order method in its ability to resolve the flame structure without significant dissipation. We plan to continue to use laser diagnostic techniques such as Raman and Rayleigh scattering to measure temperature and major species profiles from forced time-varying flames using this burner.

Measurements of Soot Particle Sizes:

In support of our soot modeling efforts we have undertaken experiments to measure the size distribution of soot particles. Typically, particle size distributions are determined with LII using point measurements by evaluating the temporal decay of the signal as the heated soot cools back down to flame temperatures [6]. For the purpose of this study, two-dimensional measurements of particle sizes are the most practical for comparison with the computational results. For two-dimensional particle sizing, short exposure images are taken at a series of time delays [7,8]. Care must be taken when choosing which delays to use and the best method of combining the images so as to provide size data with the least degree of uncertainty.

LII was generated using a pulsed, Nd:YAG laser operating at 1064 nm. Modeling of the LII process assumes that all particles in the measurement volume are heated to the same temperature, requiring a top-hat laser profile. Therefore, the beam shaping lenses and apertures were carefully designed using relay imaging of the apertures to maximize the depth of field of the imaged beam sheet and to provide as uniform a beam profile as possible across the measurement volume (~2 cm tall and 300 μm wide). The LII signal was detected at a wavelength of 455 nm using a fast-gate (~5 ns) ICCD camera at discrete gate times (0, 50, then 100 - 1000 ns in steps of 100ns) relative to the temporal peak of the LII signal. The results were analyzed to determine the optimal

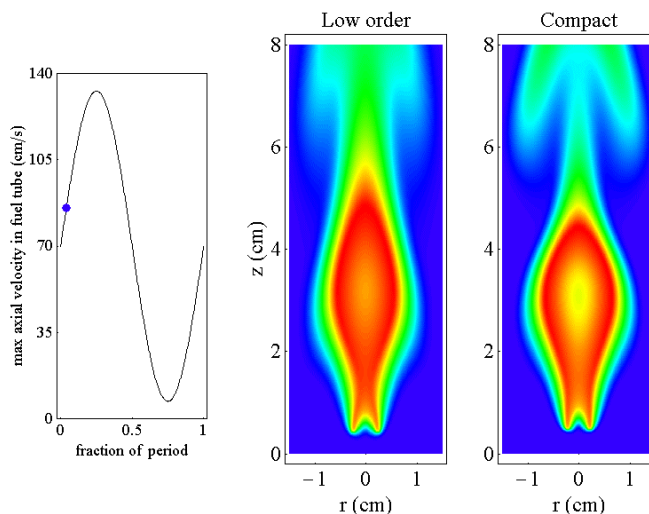


Fig. 1 A comparison of the temperature profiles in a forced (20 Hz), coflow, axisymmetric diffusion flame with Arrhenius chemistry and a 90% velocity perturbation. The image on the left is the velocity point indicated on the sinusoid. The comparisons are made for both a low order and a high order compact computation after the solutions have evolved through 10 cycles (500 ms).

combination of images taken at different gate delays that gave the least uncertainty in particle size and size distribution. This was done following the approach of Daun *et al.* [9] and is discussed in detail in Ref. [10]. Briefly, a library of simulated LII signals for a range of log-normal size distributions was generated to correspond to discrete gate times following LII excitation. A series of minimization functions was formed which represent the difference between measured and simulated signal ratios. Combining several minimization criteria provided the least ambiguity in the particle-size/log-normal-distribution-width space that is of interest.

As a test of the measurement technique, initial measurements were made in the well-characterized Santoro burner [11], and the results were compared to the values in the literature. A particle diameter of 35.1 nm was measured on the flame centerline with a geometric width of 1.17 (3.2 nm). This compares well with results from other studies, which were summarized in Ref. [6] as: 29.3 nm, 1.18 geometric width; 35 ± 3 nm; 31 nm; 33.3 ± 3.2 nm; and 32 nm. With the successful comparison of results from the Santoro burner, the experiments were repeated in the same standard flames that have been measured and modeled computationally. Fig. 2 shows a comparison of computed and measured particle sizes in an 80% C₂H₄ flame. Computational particle sizes were determined by calculating the geometric mean diameter from the 20 computed size sections, assuming a log-normal distribution. The comparison is encouraging, as the trends in the computation are captured well both qualitatively and quantitatively. Compared with the experiments, the computations predict both larger particles overall and less variation in size on the centerline, relative to the wings.

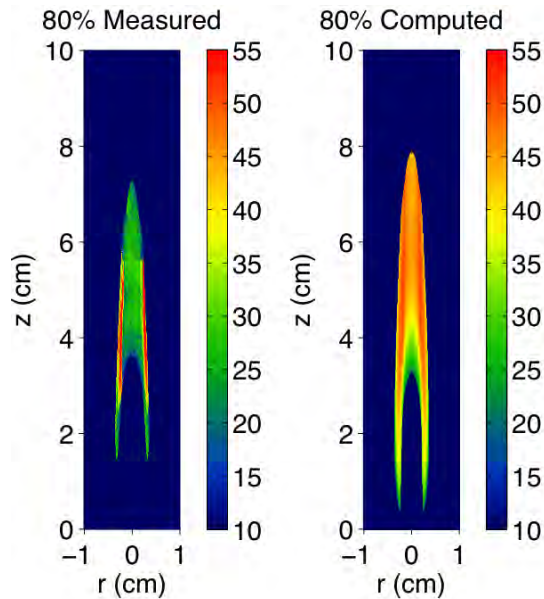


Fig. 2 Experimental and computational particle sizes for an 80% C₂H₄ flame.

Future Plans

During the next year we will continue our study of time-varying flames with the goal of fully implementing higher-order compact-based methods. We plan to study both sooting and nonsooting hydrocarbon flames. Experimentally we will continue our work on improving the accuracy of our soot particle size measurement, as well as applying other diagnostic techniques that can provide information on soot aggregation. Finally, using the same techniques that we have developed for the steady sooting flames, we will perform phase-averaged measurements to characterize the soot in the time-varying flames.

References

1. M.D. Smooke and B.A.V. Bennett, "Computational Fluid Dynamics in Industrial Combustion," in Numerical Modeling of Multidimensional Laminar Flames, C.E. Baukal, V.Y. Gershtein and X. Li, eds., CRC Press, Boca Raton, FL, pp. 209–245, 2001.
2. A. Ern, Ph.D. Thesis, Yale University, 1994.
3. S.K. Lele, "Compact Finite Difference Schemes with Spectral-Like Resolution," J. Comput. Phys., 103, 16–42, 1992.

4. R.V. Wilson, A.O. Demuren, and M. Carpenter, "Higher-Order Compact Schemes for Numerical Simulation of Incompressible Flows, Part II: Applications," *Numer. Heat Transfer, Part B*, 39, 231–255, 2001.
5. M. Noskov, Ph.D. Thesis, Yale University, 2004.
6. C. Schulz, B.F. Kock, M. Hofmann, H. Michelsen, S. Will, B. Bougie, R. Suntz and G. Smallwood, "Laser-Induced Incandescence: Recent Trends and Current Questions," *Applied Physics B-Lasers and Optics*, **83**, 333-354, (2006).
7. S. Will, S. Schraml and A. Leipertz, *Optics Letters*, "2-Dimensional Soot-Particle Sizing by Time-Resolved Laser-Induced Incandescence," **20**, 2342-2344, (1995).
8. S. Will, S. Schraml, K. Bader and A. Leipertz, "Performance Characteristics of Soot Primary Particle Size Measurements by Time-Resolved Laser-Induced Incandescence," *Applied Optics*, **37**, 5647-5658, (1998).
9. K.J. Daun, B.J. Stagg, F. Liu, G. Smallwood, and D.R. Snelling, D.R., *Applied Physics B-Lasers and Optics*, **87**: p. 363-372 (2007).
10. B. C. Connelly, Ph.D. Thesis, Yale University, 2009.
11. R.J. Santoro, H.G. Semerjian and R.A. Dobbins, *Combustion and Flame*, "Soot Particle Measurements in Diffusion Flames," **51**, 203, (1983).

DOE Sponsored Publications since 2008

1. B. A. V. Bennett, M. D. Smooke, R. J. Osborne and R. W. Pitz, "Computational and Experimental Study of Oxy-Fuel Diffusion Flames," *Comb. Theory and Modelling*, **12**, (2008).
2. B. C. Connelly, B. A. V. Bennett, M. D. Smooke, M. B. Long, "A Paradigm Shift in the Interaction of Experiments and Computations in Combustion Research," *Proceedings of the Combustion Institute*, **32**, (2009).
3. B. C. Connelly, M. B. Long, M. D. Smooke, R. J. Hall and M. B. Colket, "Computational and Experimental Investigation of the Interaction of Soot and NO_x in Coflow Diffusion Flames," *Proceedings of the Combustion Institute*, **32**, (2009).
4. S. B. Dworkin, M. D. Smooke and V. Giovangigli, "The Impact of Detailed Multicomponent Transport and Thermal Diffusion Effects on Soot Formation in Ethylene/Air Flames," *Proceedings of the Combustion Institute*, **32**, (2009).
5. J. H. Miller, B. McAndrew, M. P. Puccio, S. B. Dworkin, A. M. Schaffer, B. C. Connelly, M. B. Long and M. D. Smooke, "Measurements and Calculations of Formaldehyde Concentrations in a Methane/N₂/Air, Non-Premixed Flames," *Proceedings of the Combustion Institute*, **32**, (2009).
6. B. A. V. Bennett, C. S. McEnally, L. D. Pfefferle, M. D. Smooke and M. B. Colket, "Computational and Experimental Study of the Effects of Adding Dimethyl Ether and Ethanol to Nonpremixed Ethylene/Air Flames," *Comb. and Flame*, **156**, (2009).
7. H. Bufferand, L. Tosatto, B. La Mantia, M. D. Smooke and A. Gomez, "The Structure of Methane Counterflow Diffusion Flames Perturbed by Trace Amounts of Either JP-8 or a Six-Component Surrogate," accepted for publication *Comb. and Flame*, **156**, (2009).
8. S. B. Dworkin, J. A. Cooke, B. A. V. Bennett, B. C. Connelly, M. B. Long, M. D. Smooke, R. J. Hall and M. B. Colket, "Distributed-Memory Parallel Computation of a Forced, Time-Dependent, Sooting, Ethylene/Air Coflow Diffusion Flame," *Comb. Theory and Modelling*, **13**, (2009).
9. P. B. Kuhn, B. Ma, B. C. Connelly, M. D. Smooke, and M. B. Long, "Soot and Thin-filament Pyrometry Using a Color Digital Camera," accepted to the *Proceedings of the Combustion Institute*, 2010.
10. M. Sanchez-Sanz, B. A. V. Bennett, M. D. Smooke and A. Linan, "Influence of Strouhal Number on Pulsating Methane/Air Coflow Jet Diffusion Flames," accepted for publication *Comb. Theory and Modelling*, (2010).

Quantum Chemistry of Radicals and Reactive Intermediates

John F. Stanton
Institute for Theoretical Chemistry
University of Texas
Austin, TX 78712

Scope of Research

My research group works in the area of theoretical chemical physics, especially on the properties and chemistry of organic radicals and other reactive intermediates. This research follows a number of paths, including first-principles calculations of bond energies and other thermochemical information (as well as development of methodology for such calculations), methods for the simulation and analysis of molecular spectroscopy, especially relevant to those experiments that can be used to glean thermochemical information, and the development of *ab initio* methods needed for the accurate treatment of transient organic molecules.

Summary of recent accomplishments

Progress has been made in the development methods based on the equation-of-motion coupled-cluster (EOM-CC) model, originally proposed by Monkhorst more than thirty years ago¹. In particular, we have put together an efficient implementation of the so-called EOMIP-CCSDT model², in which the very accurate CCSDT treatment of electron correlation is used in both the reference state and final state parametrizations. This represents a significant improvement in our current computational capabilities; calculations at this level of theory were previously based on a computational convenience that “wasted” significant amounts of computer time³. In an EOMIP-CCSDT calculation, there are two stages: in the first, the CCSDT wavefunction for the reference state (usually a closed-shell species) is calculated and the wavefunction parameters are used to affect a similarity transformation of the electronic Hamiltonian. The second stage of the calculation involves the (iterative) diagonalization of this Hamiltonian. Due to the parametrization of this method, in which the final state has one fewer electron than the initial state, the costs of these two steps scale differently; the first goes - roughly - with the eighth power of the basis set size, while the second goes with N^7 . Due to the costly nature of the reference state CCSDT calculation, we have investigated the use of triples amplitudes given by the so-called (T) approximation⁴ in the transformation of the Hamiltonian. Initial results are excellent, and suggest that this - now approximate - EOMIP-CCSDT model might offer a powerful treatment of radicals with a computational scaling cost (N^7) that is the same as CCSD(T). In addition, we have also made an implementation of EOMDIP-CCSDT, a method in which two, rather than one, electrons are “removed” from the reference state. This latter method, which offers great promise of the treatment of biradicals and which offers many of the same virtues as the spin-flip methods of Krylov⁵ for such problems, has an N^8 reference state calculation followed by an N^6 diagonalization. The same (T)-based approximation mentioned above in the context of EOMIP-CCSDT can be used for EOMDIP-CCSDT, but other (and more severe) problems associated with the latter method are rooted in the choice of the reference state orbitals. We have explored several possibilities for the latter, and have found the best results are obtained when using restricted orbitals for the triplet state, in conjunction with the QRHF approach of Rittby and Bartlett⁶. Finally, in collaboration with Anna Krylov’s group, we have developed and studied a method for EOMIP calculations that is “better” than CCSD, while retaining the same (N^6) asymptotic cost⁷.

In the area of theoretical thermochemistry, we have a few projects to report. First, we have worked with the group of Tomas Baer in a TPEPICO study of acetic and formic acids. An important part of this work was the finding of an unexpected barrier in the loss of hydrogen atom from the cation of formic acid. This barrier is along a dissociation pathway leading to a closed-shell cation and a hydrogen atom, a fundamentally different type of bond-breaking process than the homolytic cleavage of covalent bonds, with which standard single-reference coupled-cluster methods have pronounced difficulties. Hence, straightforward CCSD(T) calculations are possible (and useful), and the results obtained are in good agreement with a one-dimensional Eckart tunneling model fit to the experimental data.

¹H.J. Monkhorst *Int. J. Quantum Chem.* 11, 421 (1978).

²M. Musial, S.A. Kucharski and R.J. Bartlett *J. Chem. Phys.* 118, 1128 (2003).

³J.F. Stanton and J. Gauss *J. Chem. Phys.* 111, 8785 (1999).

⁴K. Raghavachari, G.W. Trucks, J.A. Pople and M. Head-Gordon *Chem. Phys. Lett.* 157, 479 (1989).

⁵A.I. Krylov *Acc. Chem. Res.* 39, 83 (2006).

⁶M. Rittby and R.J. Bartlett *J. Phys. Chem* 92, 3033 (1988).

⁷P.U. Manohar, J.F. Stanton and A.I. Krylov *J. Chem. Phys.* 131, 114112 (2009).

Second, we are nearing completion of a project in which the HEAT family of thermochemical methods are applied to three prototype stable radicals: vinyl, allyl and vinoxy. These calculations should give enthalpies of formation within *ca.* 1 kJ mol⁻¹; in addition to being useful as is, they can also provide useful information for Ruscic's Active Thermochemical Tables (ATcT) project⁸. In addition, members of my group are working on a project in which the HEAT methods are applied to calculate ionization potentials of several compounds. The results are striking - errors are typically on the order of 50 cm⁻¹ or less - and it is believed that this area of application could prove useful to members of the combustion community that are using photoionization mass spectroscopy as an analytical method. Finally, the excellent work done in parallelization of our CFOUR program package (which is freely available to the scientific community⁹) by my current postdoc Michael Harding has permitted us to extend the HEAT method - originally applicable only to very small molecules - significantly. While the radicals mentioned above are all beyond the range of possible applications a few years ago, we have recently succeeded in calculating the enthalpy of formation of benzene with the HEAT approach.

Future Research Directions

Given our successful application of HEAT to benzene, the scope of the method is now beginning to approach the C₆H₆ isomers that are involved in the Miller-Klippenstein¹⁰ model of benzene formation that I have wanted to target for some time. Due to the lower symmetries encountered, the calculations will be more difficult and costly, but they are no longer in the realm of fantasy. Work will also begin soon on a benchmark study of HEAT as applied to the calculation of barriers for certain classes of reaction (those which do not involve significant multireference character in the activated complex), mostly conformation isomerizations and processes involving the homolytic cleavage of single bonds. Also related to transition states is a collaboration that we have begun very recently with John Barker (Michigan) on the development and application of a method based on Miller's non-separable semi-classical transition state theory¹¹ which should be applicable to relatively large reactive systems, due to a recent advance in Barker's laboratory¹². The model requires accurate calculations of anharmonicities along the reaction pathway, which will be my contribution to the project.

In addition, we are planning to work with W.D. Allen (Georgia) on the calculations (via HEAT) of small (up to five carbon atoms) hydrocarbons that are the key species in his recently-proposed scheme for hydrocarbon thermochemistry¹³. These molecules will serve as building blocks that will allow the thermochemistry of *all* hydrocarbon molecules to be calculated with simple and affordable computational methods *via* appropriately-chosen reaction schemes.

We continue to collaborate with the Field group at MIT on the study of acetylene and related systems. Currently, we are working towards the development of a diabatic model that should provide a great deal of qualitative insight into the nature of the first excited state of acetylene, and are also applying the same formalism (the approach of Köppel, Domcke and Cederbaum¹⁴) to the C₂H radical. Frequently, the diabatic approach offers a helpful alternative perspective to situations that are extremely complicated (*i.e.* conical intersections) in the adiabatic representation¹⁵. This has been a major part of my research program in recent years, and the acetylene and C₂H work is an area of effort at the present time.

Finally, and motivated by discussions with others in the combustion group, we plan to begin working on the calculation of photoionization efficiency (PIE) curves in the coming year. In the simplest approximation - where the ion does not fragment after absorbing the photon, all absorption of photons leads directly to ionization, and the photoionization cross-section is constant - the PIE is the "integral" of the photoelectron spectrum. In the last several years, my group and I have done a great deal of work in the parametrization of model Hamiltonians and their subsequent application to the simulation of various kinds of electronic spectra, especially in cases where vibronic coupling plays an important role. Thus, we are ready to embark on the zeroth-order part of the project, but we are also planning to address the more complex issues associated with autoionizing resonances and energy-dependent cross-sections. The EOM-CC methods that are a major part of our program seem especially well-suited to the calculation of the former, which are high-lying electronic states of the neutral above the ionization limit, due to their immunity with regard to variational collapse. My able postdoc Takatoshi Ichino has done some work in the calculation of photodetachment cross sections, and has begun to think about the more complicated issue of photoionization, where one must address the coulomb interaction between the outgoing electron and the ion.

⁸B. Ruscic, R.E. Pinzon, M.L. Morton, G.v. Laszewski, S.J. Bittner, S.G. Nijssure, K.A. Amin, M. Minkoff and A.F. Wagner *J. Phys. Chem. A* 108, 9979 (2004).

⁹See www.cfour.de.

¹⁰J.A. Miller and S.J. Klippenstein *J. Phys. Chem. A* 107, 7783 (2003).

¹¹W.H. Miller *J. Phys. Chem. A* 102, 793 (1998).

¹²T.L. Nguyen and J.R. Barker *J. Phys. Chem. A* 114, 3718 (2010).

¹³S.E. Wheeler, K.N. Houk, P.v.R. Schleyer and W.D. Allen *J. Amer. Chem. Soc.* 131, 2547 (2009).

¹⁴H. Köppel, W. Domcke and L.S. Cederbaum *Adv. Chem. Phys.* 57, 59 (1984).

¹⁵See, for example, J.F. Stanton *J. Chem. Phys.* 126, 134309 (1997).

References supported by DE-FG02-07ER15884 (2008-)

- [1] Barney Ellison, Evan Jochnowitz, Xu Zhang, Mark Nimlos, Bradley Flowers, and John Stanton. Infrared Spectrum of the Propargyl Peroxyl Radical. *J. Phys. Chem. A* 114, 1498 (2010).
- [2] Etienne Garand, Kerstin Klein, John F. Stanton, Jia Zhou, Tara I. Yacovitch, and Daniel M. Neumark. Vibronic Structure of the Formyloxyl Radical (HCO_2) via Slow Photoelectron Velocity-Map Imaging Spectroscopy and Model Hamiltonian Calculations. *J. Phys. Chem. A* 114, 1374 (2010).
- [3] Juergen Gauss Juana Vazquez, Michael E. Harding and John F. Stanton. High-Accuracy Extrapolated ab Initio Thermochemistry of the Propargyl Radical and the Singlet C_3H_2 Carbenes. *J. Phys. Chem. A* 113, 12447 (2009).
- [4] Mychel E. Varner, Michael E. Harding, Juana Vazquez, Juergen Gauss, and John F. Stanton. Dissociation Energy of the HOOO Radical. *J. Phys. Chem. A* 113, 11238 (2009).
- [5] Takatoshi Ichino, Juergen Gauss, and John F. Stanton. Quasidiabatic states described by coupled-cluster theory. *J. Chem. Phys.* 130, 174105 (2009).
- [6] Michael E. Harding, Juana Vazquez, Branko Ruscic, Angela K. Wilson, Juergen Gauss, and John F. Stanton. High-accuracy extrapolated ab initio thermochemistry. III. Additional improvements and overview. *J. Chem. Phys.* 128, 114111 (2008).
- [7] John F. Stanton. On the vibronic level structure in the NO_3 radical: II. Adiabatic calculation of the infrared spectrum. *Mol. Phys.* 107, 1059 (2009).
- [8] Sandra L. Hobson, Edward F. Valeev, Attila G. Csaszar, and John F. Stanton. Is the adiabatic approximation sufficient to account for the post-Born-Oppenheimer effects on molecular electric dipole moments? *Mol. Phys.* 107, 8 (2009).
- [9] John F. Stanton and Mitchio Okumura. On the vibronic level structure in the NO_3 radical Part III. Observation of intensity borrowing via ground state mixing. *Phys. Chem. Chem. Phys.* 11, 4742 (2009).
- [10] Devin A. Matthews and John F. Stanton. Quantitative analysis of Fermi resonances by harmonic derivatives of perturbation theory corrections. *Mol. Phys.* 107, 213 (2009).
- [11] Dominique S. Kumkli, Simon Lobsiger, Hans-Martin Frey, Samuel Leutwyler, and John F. Stanton. Accurate determination of the structure of cyclooctatetraene by femtosecond rotational coherence spectroscopy and ab initio calculations. *J. Phys. Chem. A* 112, 9134 (2008).
- [12] John F. Stanton, Bradley A. Flowers, Devin A. Matthews, Asa F. Ware, and G. Barney Ellison. Gas-phase infrared spectrum of methyl nitrate. *J. Mol. Spect.* 251, 384 (2008). SEP-OCT 2008.
- [13] Takatoshi Ichino, Scott W. Wren, Kristen M. Vogelhuber, Adam J. Gianola, W. Carl Lineberger, and John F. Stanton. The vibronic level structure of the cyclopentadienyl radical. *J. Chem. Phys.* 128, 084310 (2008).
- [14] Holger Schneider, Kristen M. Vogelhuber, Florian Schinle, John F. Stanton, and J. Mathias Weber. Vibrational spectroscopy of nitroalkane chains using electron autodetachment and Ar predissociation. *J. Phys. Chem. A* 112, 7498 (2008).
- [15] Mychel E. Varner, Michael E. Harding, Juergen Gauss, and John F. Stanton. On the geometry of the HO_3 radical. *Chem. Phys.* 346, 53 (2008).
- [16] Henrik G. Kjaergaard, Anna L. Garden, Galina M. Chaban, R. Benny Gerber, Devin A. Matthews, and John F. Stanton. Calculation of vibrational transition frequencies and intensities in water dimer: Comparison of different vibrational approaches. *J. Phys. Chem. A* 112, 4324 (2008).

Universal and State-Resolved Imaging Studies of Chemical Dynamics

Arthur G. Suits
Department of Chemistry, Wayne State University
5101 Cass Ave
Detroit, MI 48202
asuits@chem.wayne.edu

Program Scope

The focus of this program is on combining universal ion imaging probes providing global insight, with high-resolution state-resolved probes providing quantum mechanical detail, to develop a molecular-level understanding of chemical phenomena. Particular emphasis is placed upon elementary reactions important in understanding and predicting combustion chemistry. This research is conducted using state-of-the-art molecular beam machines, photodissociation, reactive scattering, and vacuum ultraviolet lasers in conjunction with ion imaging techniques. An ongoing parallel effort is made to develop new tools and experimental methods with which to achieve these goals.

Recent Progress

Systematic studies of polyatomic reaction dynamics

We have developed an intense Cl atom source and combined this with loosely focused 157nm single photon ionization of the radical reaction product in crossed beam DC slice imaging studies. The result is that we can now obtain very intense scattering signals with minimal background interference. Although it took us some time to develop the full set of tools needed to undertake these studies and analyze these results, we can now complete a crossed-beam reaction at a single energy in a matter of hours, *including data analysis*. This opens the door to very detailed and systematic studies such as were never possible before. We can study reaction dynamics across a series of isomers, such as the pentanes described below, or for a single system as a function of carbon chain length, functional group, etc.

The reaction of chlorine atoms with hydrocarbons (RH) has been an important touchstone in exploring the dynamics in polyatomic systems, and there are a number of reasons for this. In general these are fast reactions, affording good signal-to-noise in challenging scattering studies. Moreover, the reaction energetics lie in an intermediate regime, i.e., some are endoergic, others thermoneutral or exoergic, and with either a modest barrier or no barrier to reaction. In addition, there are different abstraction sites and the possibility to investigate the associated reactivity. Finally, the H abstraction process leads to the diatomic product HCl, which can be detected with quantum state specificity and good sensitivity using resonance-enhanced multiphoton ionization (REMPI). In the past we reported an initial investigation of these reactions using state-resolved imaging of HCl from the Cl+ethane reaction.

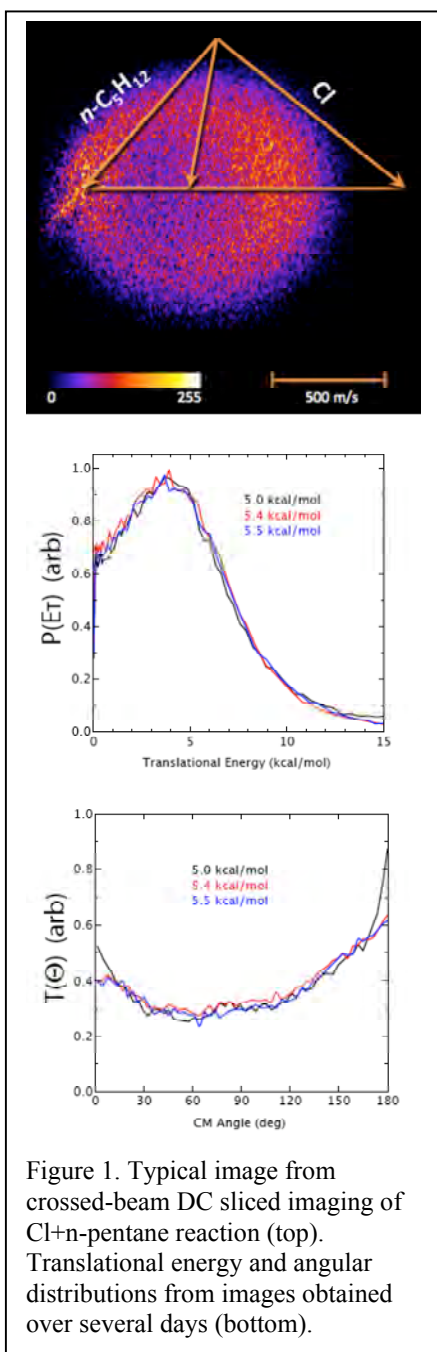


Figure 1. Typical image from crossed-beam DC sliced imaging of Cl+n-pentane reaction (top). Translational energy and angular distributions from images obtained over several days (bottom).

There are a number of key questions we can hope to address with such detailed and systematic dynamical studies: Are there different dynamics for primary, secondary and tertiary H abstraction? What is the fraction of energy appearing in translation, vibration or rotation of the two products, and what factors govern this disposition of energy? How do these issues change with collision energy or temperature? What effect do structural or stereochemical influences have on the dynamics? These questions have been examined with varying degrees of success in the many studies reported over the years for these systems, but inconsistencies persist and many open questions remain. Our slice imaging experiments promise some new insights into these fundamental questions.

Our first series of molecules in this investigation is n-pentane, isopentane and neopentane, ranging from a linear molecule with equal numbers of primary and secondary H sites to a quasi-spherical molecule with only primary H atoms. A typical DC sliced image for n-pentane is shown in Fig. 1. We have essentially eliminated the background interference from photochemistry of the parent hydrocarbon the plagued us before, so that now we can recover the full scattering distribution directly. Fig. 1 also includes the translational energy and angular distributions derived from three separate data sets over many days, showing excellent reproducibility.

One way to explore the rich information contained in these images is to examine the translational energy distributions for different scattering regions, and do this for each target isomer and varied collision energies. The distributions tend to preserve the collision energy into product recoil, as expected for collinear Heavy-Light-Heavy systems,

and it suggests plotting all of the translational energy distributions on a reduced scale as shown in Fig. 2. The plots are extraordinary in the similarity of the trends shown regardless of target isomer. For the high collision energy result averaged over recoil direction, more than 70% of the products possess a translational energy equal to or less than the collision energy. At low collision energy, this fraction is smaller, i.e., a greater fraction of the energy appears in translation. This trend is perhaps not surprising, as the exoergicity is a larger fraction of the collision energy, and some of it finds its way into product recoil. The most probable translational energy release is similar in all cases, about 80% of E_c , independent of target isomer and collision energy.

Further insight can be obtained by examining these same trends for different scattering regions, also shown in Fig. 2. The forward scattered (0° - 60°) distributions show sharp peaking at $0.8 E_c$. It is sharpest for neopentane and isopentane, somewhat broader for n-pentane. The forward scattered distributions all show much less variation with collision energy compared to the sideways (60° - 120°) or backscattered (120° - 180°) contributions. The backscattered distributions show a strong dependence on collision energy, for n-pentane and isopentane we see a change from about $1.02 E_c$ at low collision energy to $0.68 E_c$ at high collision energy. This observation shows rather clearly that low impact parameter collisions are required to couple the exoergicity into recoil.

Roaming dynamics

We continue our study of roaming dynamics that began with state-correlated studies of formaldehyde photodissociation in collaboration with the Bowman group. Our proposal for a Workshop on this topic has found broad support, with fifty participants expected at Argonne in a few weeks.

We have recently published a study of roaming in decomposition of formaldehyde-d2 at energies above the radical dissociation threshold, again in collaboration with the Bowman group. The experimental results are quite reminiscent of those for H_2CO , clearly confirming roaming dynamics in this system as well. Detailed analysis of the branching shows surprisingly little change in the roaming fraction compared to H_2CO .

We have extended our state-resolved study of acetone photodissociation dynamics to 193nm where we access the S_2 excited state. The dynamics are remarkably similar to those we reported at 230nm, showing a slow component in the low j_{CO} product that we ascribed to roaming. The branching into this channel is quite similar, confirming earlier suggestions that internal conversion to S_1 is the first step, and the additional excess energy has little impact on the dynamics.

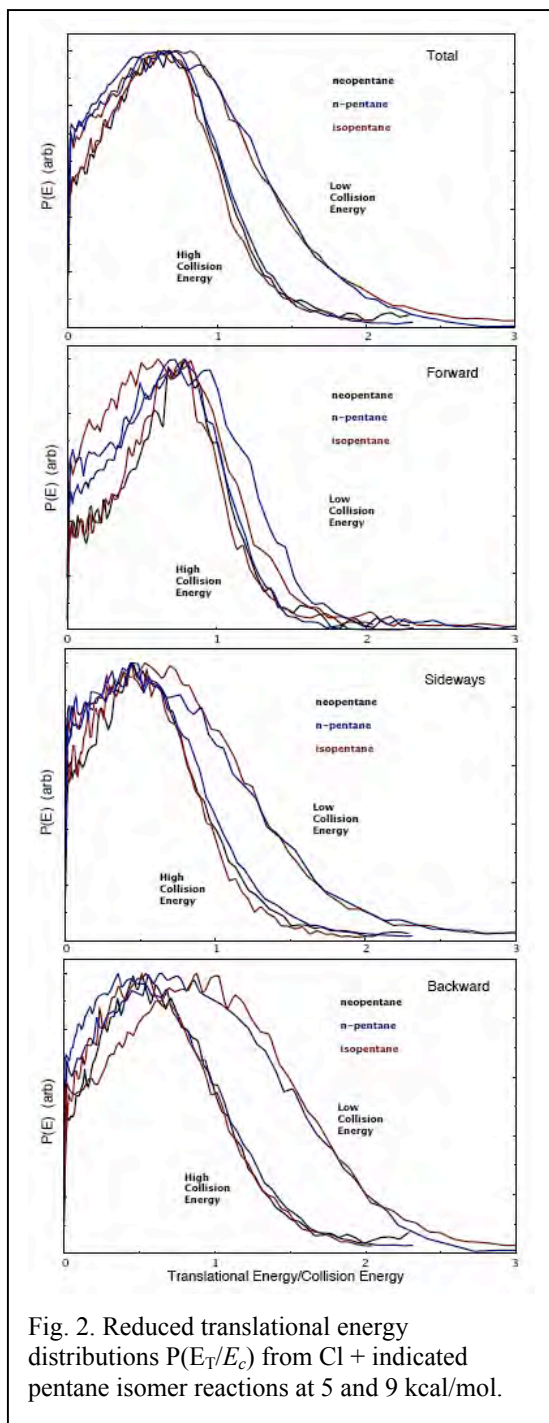


Fig. 2. Reduced translational energy distributions $P(E_T/E_c)$ from Cl + indicated pentane isomer reactions at 5 and 9 kcal/mol.

Selected Future Plans

Roaming atom reaction dynamics. We will perform DC slice imaging a range of systems to investigate the generality of the roaming mechanism. One promising system is NO₃ radical which we are pursuing in collaboration with the North group at Texas A&M. This is known to dissociate to yield NO+O₂ and an energy just below the O atom loss threshold, but the dynamics responsible are not clear, and roaming is a plausible explanation. By applying state-resolved imaging of the NO product, and comparing this to O(³P) + NO₂ reactive scattering results, we expect the state-correlated product distributions will clearly reveal the underlying dynamics. In a sense, this is an example of a *roaming-mediated isomerization* to the nitrite, and one future aspect of our roaming investigations will be to investigate this aspect of roaming dynamics.

State-resolved and universal crossed-beam DC slice imaging. We have plans to continue exploring a range of systems using our crossed-beam sliced imaging approach. We will finish an extended series of studies of Cl atom reactions, looking at unsaturated hydrocarbons as a function of unsaturation site and chain length; at saturated hydrocarbons as a function of chain length, and at alcohols as a function of isomer and chain length. Much of this data is already in-hand. We will complement these studies in some cases with state-selected detection of the HCl product.

With our enhanced sensitivity, we now expect our CH reaction studies to bear fruit, and we will explore systems and pathways complementary to those under investigation in the Kaiser lab.

DOE Publications 2008-present

S.A. Lahankar, V. Goncharov, F. Suits, J.D. Farnum, J.M. Bowman and A. G. Suits.

“Further aspects of the roaming mechanism in formaldehyde dissociation,” *Chem. Phys.* **347**, 288 (2008).

C. Huang, A. D. Estillore and A. G. Suits, “State-selected imaging of HCCO radical photodissociation dynamics,” *J. Chem. Phys.* **128** 134301 (2008).

A. G. Suits, “Roaming atoms and radicals: A new mechanism in molecular dissociation,” *Acc. Chem. Res.* **41**, 873 (2008).

V. Goncharov, N. Herath and A. G. Suits, “Roaming dynamics in acetone dissociation,” *J. Phys. Chem. A* 10.2021/jp802534r (2008).

C. Huang, A. Estillore, W. Li, and A. G. Suits, “Dynamics of CN + alkane reactions by crossed-beam dc slice imaging,” **129**, 074301 (2008).

V. Goncharov, N. Herath, A. Arregui, L. Banares, A. G. Suits, “Masked velocity map imaging: A one-laser-beam Doppler-free spectroscopic technique,” *J. Phys. Chem A*, (2009) DOI: 10.1021/jp809711n.

A. Estillore, L. Visger and A. G. Suits, “Crossed-beam DC slice imaging of chlorine atom reactions with pentane isomers,” *J. Chem. Phys.* (accepted).

Elementary Reaction Kinetics of Combustion Species

Craig A. Taatjes

Combustion Research Facility, Mail Stop 9055, Sandia National Laboratories,
Livermore, CA 94551-0969

cataatj@sandia.gov www.ca.sandia.gov/CRF/staff/taatjes.html

SCOPE OF THE PROGRAM

This program aims to develop new methods for studying chemical kinetics and to apply these methods to the investigation of fundamental chemistry relevant to combustion science. One central goal is to perform accurate measurements of the rates at which important free radicals react with each other and with stable molecules. Another goal is to characterize complex reactions that occur via multiple potential wells by investigating the formation of products. Increasingly, these investigations are moving towards simultaneous time-resolved detection of multiple species in well-characterized photolytically-initiated reaction systems where multiple consecutive and competing reactions may occur. Understanding the reactions in as much detail as possible under accessible experimental conditions increases the confidence with which models can treat the inevitable extrapolation to the conditions of real-world devices. Another area of research is the investigation and application of new detection methods for precise and accurate kinetics measurements. Absorption-based techniques and mass-spectrometric methods have been emphasized, because many radicals critical to combustion are not amenable to fluorescence detection.

An important part of our strategy, especially for complex reaction systems, is using experimental data to test and refine detailed calculations (working in close cooperation with Stephen Klippenstein at Argonne and Jim Miller and Judit Zádor at Sandia), where the theory offers insight into the interpretation of experimental results and guides new measurements that will probe key aspects of potential energy surfaces. This methodology has been applied in our investigations of the reactions of alkyl radicals with O₂, where the combination of rigorous theory and validation by detailed experiments has made great strides toward a general quantitative model for alkyl oxidation.

PROGRESS REPORT

We continue to apply frequency-modulation and direct absorption spectroscopy to measurements of product formation in reactions of alkyl radicals with O₂ and kinetics of unsaturated hydrocarbon radicals. In addition, the multiplexed photoionization mass spectrometric reactor at the Advanced Light Source (ALS), a close collaboration with David Osborn, has become a major part of our investigations of low-temperature hydrocarbon oxidation chemistry. Some highlights of the recent work are described briefly below.

Product branching in the O(³P) + benzene reaction. The gas-phase reaction of benzene with O(³P) is of considerable interest for modeling of aromatic oxidation, and also because there exist fundamental questions concerning the prominence of intersystem

crossing in the reaction. While its overall rate constant had been studied extensively, there remained significant uncertainties in the product distribution. The reaction proceeds mainly through the addition of the O atom to benzene, forming an initial triplet diradical adduct, which can either dissociate directly, forming phenoxy radical and H atom, or undergo intersystem crossing onto a singlet surface, followed by a multiplicity of internal isomerizations, leading to several possible reaction products. We examined the product branching ratios of the reaction between benzene and O(³P) over the temperature range of 300 to 1000 K and pressure range of 1 to 10 Torr, using the multiplexed chemical kinetics photoionization mass spectrometer at the ALS. Phenol and phenoxy radical were detected and quantified. Cyclopentadiene and cyclopentadienyl radical were directly identified as products of this reaction for the first time. In collaboration with Hai Wang and Anna Krylov (USC), *ab initio* calculations and master equation/RRKM modeling were used to reproduce the experimental branching ratios, yielding recommended pressure-dependent rate expressions for the reaction channels to phenoxy + H, phenol, and cyclopentadiene + CO.

OH formation in ethyl + O₂ and propyl + O₂ reactions. The formation of OH was previously measured by LIF in the Cl-initiated oxidation of alkanes, a method that required extensive modeling to calibrate the OH yield. The predictions of the master equation (ME) models were in only qualitative agreement with the experimental data, but the uncertainties in the experimental analysis prevented reliable validation of the stationary-point energies. We reinvestigated both systems using long-path direct-absorption probing of OH, which yields the absolute concentration of OH. The experimental data were modeled using rate coefficients derived from ME calculations of the alkyl + O₂ systems.¹⁻³ The propyl + O₂ results are in essentially complete agreement with the model after a 0.25 kcal mol⁻¹ reduction in the barriers for isomerization of both *i*- and *n*-propylperoxy to their corresponding 2-hydroperoxypropyl radicals. Because of the smaller OH yield, the OH concentration in the ethyl + O₂ system is sensitive to ethyl + HO₂ → OH + ethoxy. Taking the rate coefficient for that reaction from the Jasper et al.⁴ calculation of the analogous methyl + HO₂ reaction gives quantitative agreement between experiment and the ME model, employing the transition state energies from earlier work.¹ The improved experiments now validate the transition state for isomerization to 2-hydroperoxyalkyl radicals in both systems.

HO₂ and OH formation in ethanol oxidation. The Cl-initiated oxidation of ethanol proceeds via the reactions of 1-hydroxyethyl and 2-hydroxyethyl radicals with O₂. We investigated these reactions earlier by a combination of *ab initio* theory, master equation calculations, and photoionization mass spectrometry experiments. The yield of CH₂O, from the reaction of 2-hydroxyethyl radicals with O₂, was substantially greater than predicted by the quantum chemistry / master equation model.⁵ We have recently investigated the formation of OH and HO₂ in Cl-initiated oxidation of ethanol. The OH formation, particularly at high pressure, contains a substantial component from the reactions of hydroxyalkyl radicals with HO₂ product, and from decomposition of the 2-hydroxyethyl radical above about 700 K. The HO₂ is slightly but systematically overpredicted by the model, suggesting that the HO₂ + ethanol channel in the 2-hydroxyethyl + O₂ reaction may be too prominent in the calculations, at the expense of branching to the 2 CH₂O + OH channel.

OH + propene reaction. In collaboration with the Olzmann group in Karlsruhe we have measured the kinetics of the OH reaction with propene and propene-d6 from room temperature to 900 K and over a range of pressures. The results are modeled using the calculated values of Zádor, Jasper and Miller,⁶ which reproduce the experiments from both laboratories over the entire temperature range, from the addition-dominated low temperature regime through the multiexponential decays in the transition region through to the high temperature where abstraction dominates. This gives an explicit validation for the predicted rate coefficients over a wide temperature and pressure range.

FUTURE DIRECTIONS

Characterization of R + O₂ reactions will continue, both in the laser absorption work and in the ALS kinetics machine, with increasing emphasis on oxidation of alternative fuel molecules. Butanol isomers and isomeric 5-carbon branched alcohols will be early targets; the butanol work will complement experiments carried out as part of the Argonne-Sandia consortium on high-pressure combustion chemistry (abstract elsewhere in this volume). Low-pressure experiments often probe a larger or different range of stationary points on the potential surface than do high-pressure measurements and serve as an additional constraint in the high-pressure mechanism. Oxidation of selectively deuterated alkanes will be carried out to distinguish among different internal abstraction pathways in R + O₂ reactions. Characterization of OH and Cl-initiated oxidation of alkenes and aromatics will extend the previous work on alkyl + O₂ systems to reactions relevant for low-temperature oxidation of unsaturated fuels.

The most important unexplored area for autoignition chemistry is the chain branching initiated by the “second O₂ addition,” that is, the reaction of molecular oxygen with the hydroperoxyalkyl radicals QOOH. It has been a consistent goal of this program over at least the past ten years to obtain experimental information about these QOOH species and their reactions. That quest will continue, including efforts to directly form QOOH radicals and detect them by synchrotron photoionization. The more stable peroxy isomers most often do not have stable cations but many cations in the QOOH configuration are calculated to be bound.

References

- (1) DeSain, J. D.; Klippenstein, S. J.; Miller, J. A.; Taatjes, C. A. *J. Phys. Chem. A* **2003**, *107*, 4415
- (2) DeSain, J. D.; Klippenstein, S. J.; Miller, J. A.; Taatjes, C. A. *J. Phys. Chem. A* **2004**, *108*, 7127
- (3) DeSain, J. D.; Taatjes, C. A.; Miller, J. A.; Klippenstein, S. J.; Hahn, D. K. *Faraday Discuss.* **2001**, *119*, 101
- (4) Jasper, A. W.; Klippenstein, S. J.; Harding, L. B. *Proc. Combust. Inst.* **2009**, *32*, 279.
- (5) Zádor, J.; Fernandes, R. X.; Georgievskii, Y.; Meloni, G.; Taatjes, C. A.; Miller, J. A. *Proc. Combust. Inst.* **2009**, *32*, 271
- (6) Zádor, J.; Jasper, A. W.; Miller, J. A. *Phys. Chem. Chem. Phys.* **2009**, *11*, 11040.

Publications acknowledging BES support, 2008 –

1. Craig A. Taatjes, “Recent developments in the coupling of theory and experiment to study the elementary chemistry of autoignition,” *J. Combust. Soc. Japan* **50**, 29–38 (2008).
2. Peng Zou, Kevin E. Strecker, Jaime Ramirez-Serrano, Leonard E. Jusinski, Craig A. Taatjes, and David L. Osborn, “Ultraviolet photodissociation of vinyl iodide: understanding the halogen dependence of

- photodissociation mechanisms in vinyl halides,” *Phys. Chem. Chem. Phys.* **10**, 713–728 DOI: 10.1039/b712117b (2008).
3. Craig A. Taatjes, Nils Hansen, David L. Osborn, Katharina Kohse-Höinghaus, Terrill A. Cool, Phillip R. Westmoreland, “ ‘Imaging’ Combustion Chemistry with Multiplexed Synchrotron-Photoionization Mass Spectrometry,” *Phys. Chem. Chem. Phys.* **10**, 20–34 (2008).
 4. Craig A. Taatjes, Giovanni Meloni, Talitha M. Selby, Adam J. Trevitt, David L. Osborn, Carl J. Percival, and Dudley E. Shallcross, “Direct Observation of the Gas-Phase Criegee Intermediate (CH₂OO),” *J. Am. Chem. Soc.* **130**, 11883–11885 (2008).
 5. Craig A. Taatjes, Giovanni Meloni, Talitha M. Selby, David L. Osborn, Haiyan Fan, and Stephen T. Pratt, “Absolute Photoionization Cross Section of Methyl Radical” *J. Phys. Chem. A* **112**, 9336–9343 (2008).
 6. Talitha M. Selby, Giovanni Meloni, Fabien Goulay, Stephen R. Leone, Askar Fahr, Craig Taatjes, and David L. Osborn, “Synchrotron Photoionization Mass Spectrometry Measurements of Kinetics and Product Formation in the Allyl Radical (H₂CCHCH₂) Self-Reaction,” *J. Phys. Chem. A* **112**, 9366–9373 (2008).
 7. David L. Osborn, Peng Zou, Howard Johnsen, Carl C. Hayden, Craig A. Taatjes, Vadim D. Knjazev, Simon W. North, Darcy S. Peterka, Musahid Ahmed, and Stephen R. Leone, “The Multiplexed Chemical Kinetic Photoionization Mass Spectrometer: A New Approach for Isomer-Resolved Chemical Kinetics,” *Rev. Sci. Instrum.* **79**, 104103 (2008).
 8. Giovanni Meloni, Talitha M. Selby, David L. Osborn, and Craig A. Taatjes, “Enol Formation and Ring Opening in OH-Initiated Oxidation of Cycloalkenes,” *J. Phys. Chem. A* **112**, 13444–13451 (2008).
 9. Judit Zádor, Ravi X. Fernandes, Yuri Georgievskii, Giovanni Meloni, Craig A. Taatjes, and James A. Miller, “The reaction of hydroxyethyl radicals with O₂: a theoretical analysis and experimental product study,” *Proc. Combust. Inst.* **32**, 271–277 (2009).
 10. Adam J. Trevitt, Fabien Goulay, Giovanni Meloni, David L. Osborn, Craig A. Taatjes and Stephen R. Leone, “Isomer specific product detection of CN radical reactions with ethylene and propene by tunable VUV photoionization mass spectrometry,” *Int. J. Mass Spectrom.* **280**, 113–118 (2009).
 11. Fabien Goulay, Adam J. Trevitt, Giovanni Meloni, Talitha M. Selby, David L. Osborn, Craig A. Taatjes, Luc Vereecken and Stephen R. Leone, “Cyclic Versus Linear Isomers Produced by Reaction of the Methylidyne (CH) Radical with Small Unsaturated Hydrocarbons,” *J. Am. Chem. Soc.* **131**, 993–1005 (2009).
 12. Huzeifa Ismail, Paul R. Abel, William H. Green, Askar Fahr, Leonard E. Jusinski, Adam M. Knepp, Judit Zádor, Giovanni Meloni, Talitha M. Selby, David L. Osborn, and Craig A. Taatjes, “Temperature-Dependent Kinetics of the Vinyl Radical (C₂H₃) Self Reaction,” *J. Phys. Chem. A* **113**, 1278–1286 (2009).
 13. T. Kasper, P. Oßwald, U. Struckmeier, K. Kohse-Höinghaus, C. A. Taatjes, J. Wang, T. A. Cool, M. E. Law, A. Morel, and P. R. Westmoreland, “The combustion chemistry of propanol isomers investigated by electron ionization and VUV-photoionization molecular-beam mass spectrometry,” *Combust. Flame* **156**, 1181–1201 (2009).
 14. Erin E. Greenwald, Buddhadeb Ghosh, Katie C. Anderson, Kristin S. Dooley, Peng Zou, Talitha Selby, David L. Osborn, Giovanni Meloni, Craig A. Taatjes, Fabien Goulay, and Simon W. North, “Isomer-Selective Study of the OH Initiated Oxidation of Isoprene in the presence of O₂ and NO: I. The Minor Inner OH-Addition Channel,” *J. Phys. Chem. A* **114**, 904–912 (2009).
 15. Adam J. Trevitt, Fabien Goulay, Craig A. Taatjes, David L. Osborn and Stephen R. Leone, “Reactions of the CN Radical with Benzene and Toluene: Product Detection and Low Temperature Kinetics,” *J. Phys. Chem. A* **114**, 1749–1755 (2010).
 16. Satchin Soorkia, Adam J. Trevitt, Talitha M. Selby, David L. Osborn, Craig A. Taatjes, Kevin R. Wilson and Stephen R. Leone, “Reaction of the C₂H radical with 1-butene (C₄H₆): Low temperature kinetics and isomer-specific product detection,” *J. Phys. Chem. A* **114**, 3340–3354 (Benoît Soep festschrift) (2010).
 17. Craig A. Taatjes, David L. Osborn, Talitha M. Selby, Giovanni Meloni, Adam J. Trevitt, Evgeny Epifanovsky, Anna Krylov, Baptiste Sirjean, Enoch Dames, Hai Wang, “Products of the Benzene + O (³P) Reaction,” *J. Phys. Chem. A* **114**, 3355–3370 (Benoît Soep festschrift) (2010).
 18. Satchin Soorkia, Craig A. Taatjes, David L. Osborn, Talitha M. Selby, Adam J. Trevitt, Kevin R. Wilson and Stephen R. Leone, “Direct detection of pyridine formation by the reaction of CH (CD) with pyrrole: a ring expansion reaction,” accepted to *Phys. Chem. Chem. Phys.*
 19. Judit Zádor, Craig A. Taatjes, Ravi X. Fernandes, “Kinetics of Elementary Reactions in Low-Temperature Autoignition Chemistry,” accepted to *Prog. Energy Combust. Sci.*

Elementary Reactions of PAH Formation

Robert S. Tranter

Chemical Sciences and Engineering Division, Argonne National Laboratory

Argonne, IL-60439

tranter@anl.gov

I. Program Scope

This program is focused on the experimental determination of kinetic and mechanistic parameters of elementary reactions, in particular those involved in the formation and destruction of the building blocks for aromatic species. Recently, the program has also encompassed the study of cyclic species that are representative of oxygenated intermediates in combustion mechanisms. In addition, thermal sources of radicals are investigated and characterized for use in more complex reaction systems where secondary chemistry can be significant. The approach involves a diaphragmless shock tube (DFST) equipped with laser schlieren (LS) and a time-of-flight mass spectrometer (TOF-MS) and the development of a low pressure, fast flow, reactor equipped with a quadrupole MS. The combination of these techniques permit a wide range of reaction temperatures and pressures to be accessed.

II. Recent Progress

A. Dissociation of 1,4-dioxane and ethylene vinyl glycol ether

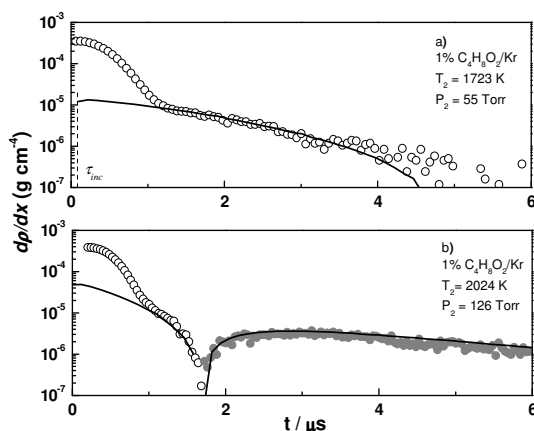


Figure 1 Semi-log density gradient plots derived from laser schlieren experiments of 1,4-dioxane pyrolysis. Open symbols represent positive values while closed symbols represent negative values. The solid black lines are the results of model simulations. Note the small incubation delay introduced into the modeling of (a)

part of the density gradient, $d\rho/dx$, profile obtained from the LS experiments, thereby hindering determination of $(d\rho/dx)_0$, the density gradient at $t=0 \mu\text{s}$, from which the rate of dissociation of 1,4-dioxane is obtained. Example semi-log plots of the LS density gradient profiles are shown in Fig. 1. The lower temperature, pressure and concentration experiments are less sensitive to the secondary chemistry and permit accurate determinations of the rate of dissociation of 1,4-dioxane to be made which can be extended to the higher temperature, pressure and concentration experiments facilitating development of the reaction mechanism. The reaction products are identified from the TOF-MS results and used to further guide mechanism development. In these experiments the mass spectra indicate the formation of CH_3 and OH radicals with the hydroxyl radical being inferred from the presence of peaks representing CH_4 and

Preliminary results of shock tube TOF-MS and LS experiments on the cyclic ether 1,4-dioxane, in collaboration with J.H. Kiefer, were previously reported. The range of the LS experiments has been greatly extended during the last year and now covers reaction pressures of 55 ± 2 Torr and 120 ± 2 Torr, reagent concentrations of 1, 2 and 4% and a temperature range of 1550-2100 K. Such a wide range is necessary because of the complex dissociation of 1,4-dioxane arising from competing initial dissociation channels and the formation of high concentrations of H , OH and CH_3 radicals early on that subsequently consume the parent molecule. At the higher pressures and concentrations these secondary reactions significantly affect the early

H₂O, respectively. A significant peak corresponding to H₂ is also observed which indicates that H-atoms are also formed in significant amounts.

In a collaborative effort A. W. Jasper, has explored the potential energy surface for the dissociation of 1,4-dioxane and the immediate products, details of the theoretical work and an illustration of the PES can be found in his abstract. The theoretical studies revealed that four dissociation channels

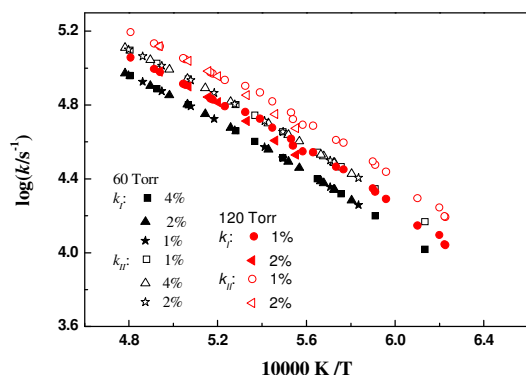


Figure 2. The first order rate coefficients for 1,4-dioxane dissociation to CH₂CH₂OH + CH₂CHO (I) and CH₃CH₂O + CH₂CHO (II) derived from the simulation of laser schlieren experiments of 1%, 2% and 4% 1,4-dioxane dilute in Krypton

are potentially accessible. Two channels correspond to C-O fission with H transfer to the terminal C or O atom. These channels have similar barrier heights that are significantly lower than those for reaction by C-C fission or a concerted breaking of three bonds, c.f. pyrolysis of 1,3,5-trioxane.ⁱ The C-O fission channels produce the intermediates ethylene glycol vinyl ether (EGVE) and ethoxyacetaldehyde (EOA), reactions I and II respectively. The dissociation products of I and II ultimately yield the reaction products observed in TOF-MS experiments and also result in the early formation of CH₃ and OH radicals and eventually H-atoms. The barrier to reaction by C-C is too high for this to be a major route for 1,4-dioxane dissociation and reaction by the concerted breaking of three bonds has a barrier ~20 kcal/mol higher than the C-O fission channels. Furthermore, the

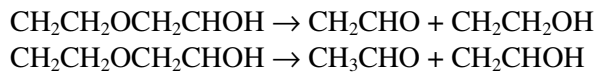
concerted mechanism yields stable products that, at the experimental conditions, will not initiate a rapid chain reaction or yield CH₃ and OH radicals.



Based on the theoretical results and TOF-MS studies a model for the dissociation of 1,4-dioxane has been constructed that incorporates the production of EGVE and EOA as the sole routes for dissociation of 1,4-dioxane. The subsequent dissociation of these molecules and their products generates a chain mechanism that initially produces OH radicals by the dissociation of ethenol, CH₂CH₂OH, and methyl radicals from dissociation of CH₃CH₂O. H-atoms are subsequently formed by a number of paths of which dissociation of HCO is one of the most important. In many of the experiments H and OH attack on 1,4-dioxane play an important role and estimates of the rates of these reactions have been made by Jasper and incorporated in the mechanism.

From the CH₄ and H₂O peaks in the TOF-MS results the branching ratio for k_I/k_{II} can be crudely estimated as 0.5 which is consistent with what might be expected from the theoretical work. This estimate has subsequently been refined in the modeling work to $k_I/k_{II}=0.44$. Rate coefficients obtained from the LS experiments for reactions (I) and (II), assuming rapid dissociation of EGVE and EOA, are shown in Fig. 2.

In the mechanism for 1,4-dioxane pyrolysis, it is assumed that EGVE and EOA decompose rapidly and only to radical products. Whereas, theoretical studies by Jasper indicate that EGVE can dissociate via C-O fission giving either radical products, reaction (III), or molecular products (IV) and the branching between these channels will affect the observed density gradients in part due to the very different heats of reaction to which LS is sensitive. Jasper also predicts reactions that are analogous to (III) and (IV) for the dissociation of EOA.



$$\Delta H_{r,298} = 66.3 \text{ kcal/mol (III)}$$

$$\Delta H_{r,298} = -0.9 \text{ kcal/mol (IV)}$$

Consequently, EGVE pyrolysis has also been studied by TOF-MS and LS in the DFST to examine the branching between reactions (III) and (IV) and to determine rate coefficients for the two channels. The EGVE LS studies were conducted over 1250-1800 K and reaction pressures of 30 and 60 Torr. Similar to the 1,4-dioxane studies, low pressures and temperatures are necessary to suppress the secondary chemistry sufficiently to allow accurate determination of $(d\rho/dx)_0$.

The results of the EGVE LS experiments are shown in Fig.3. Clearly, reaction (III) is favored at all temperatures and k_{IV}/k_{III} decreases from ~ 0.3 at 1250 K to ~ 0.1 at 1800 K. Thus, in the temperature range of the 1,4-dioxane study EGVE dissociation is facile and occurs almost exclusively by reaction (III).

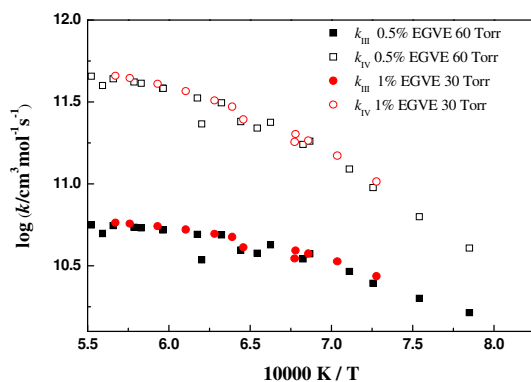


Figure 3 Second order dissociation rate of EGVE to $\text{CH}_2\text{CH}_2\text{OH} + \text{CH}_2\text{CHO}$ (III) and $\text{CH}_2\text{CHOH} + \text{CH}_3\text{CHO}$ (IV)

It has not yet been possible to conduct a LS study of EOA as it polymerizes readily and is not commercially available. However, it may be possible to create a stable, dilute mixture of EOA by immediately blending freshly synthesized EOA with krypton..

B. Ethyl Iodide

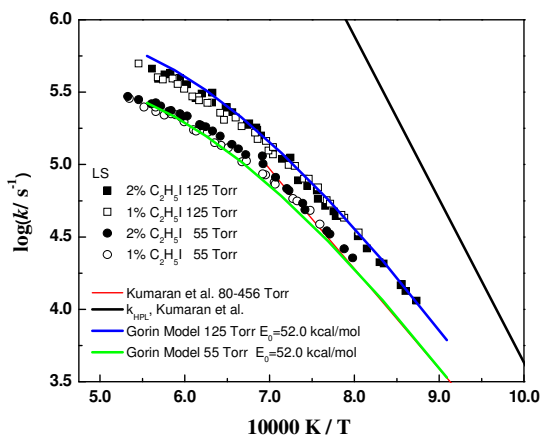


Figure 4: Comparison of first order rate coefficients for $\text{C}_2\text{H}_5\text{I} \rightarrow \text{C}_2\text{H}_5 + \text{I}$ from the LS experiments, the I-ARAS results of Kumaran et al.ⁱⁱ and the results of a Gorin model calculation using the parameters from Kumaran et al.

at high temperatures and are perhaps better considered in second order form. Rate coefficients were also obtained for the dissociation of C_2H_5 to $\text{C}_2\text{H}_4 + \text{H}$ that are in excellent agreement with theoretical predictions by Miller and Klippenstein.ⁱⁱⁱ

The dissociation of ethyl iodide has been studied by LS over the temperature range 1150-1870 K and at pressures of 54 ± 2 Torr and 123 ± 3 Torr as part of a project to characterize radical sources for use in DFST/LS and TOF-MS experiments. Ethyl iodide readily eliminates an I-atom which is followed by fast dissociation of the C_2H_5 product to ethylene and H-atoms, providing a clean, high temperature source of H-atoms. The kinetics of ethyl iodide dissociation has previously been studied by Kumaran et al.ⁱⁱ using I-ARAS and in addition to decomposition by C-I fission they determined that about 13% of $\text{C}_2\text{H}_5\text{I}$ dissociates by elimination of HI. A reaction model has been developed to simulate the LS experiments that incorporates both channels for $\text{C}_2\text{H}_5\text{I}$ dissociation with the branching ratio taken from Kumaran et al., a sub-mechanism for CH_3 reactions which was developed in previous studies of diacetyl and CH_3I dissociation, and additional reactions for H-atom attack on a variety of species. The rate coefficients for the C-I dissociation channel are compared in Fig. 4 with the results of RRKM calculations using the Gorin model of Kumaran et al.ⁱⁱ The LS data show considerable falloff from k_∞

C. Self-reaction of phenyl radicals and the dissociation of phenyl iodide

In collaboration with J. H. Kiefer, S. J. Klippenstein and L. B. Harding an experimental and theoretical study of the self reaction of phenyl radicals has been conducted. The experimental work used both TOF-MS and LS DFST experiments with phenyl iodide dissociation serving as a source of phenyl radicals. Both the LS and TOF-MS results indicate that self-reaction of phenyl radicals do not only form biphenyl as indicated in the literature but that a significant fraction undergo disproportionation to give benzene and *o/m/p*-benzynes which is in agreement with the theoretical predictions. A reaction model for C₆H₅I dissociation and phenyl self-reaction has been developed that incorporates the results of master equation calculations from the theoretical work and good agreement between experiment and theory is obtained although the experiments favor a rate for the disproportionation reactions that is a factor of two lower than the theoretical predictions. However, this lower rate is just within the estimated error bars of the calculations. Of particular importance, the study indicates that the disproportionation reactions will generate *o*-benzyne at much lower temperatures than would be predicted from pyrolysis of phenyl radicals with implications for soot and PAH modeling

III. Future Work

DFST studies of the reactions of phenyl radicals with a number of species e.g. C₂H₂ and CH₃ are planned that will utilize phenyl iodide as the C₆H₅ source., The studies on halogenated benzenes are being extended to include bromo- and chloro-benzene to examine their potential as sources of benzyne radicals with a view to studying the self-reaction of *o*-benzyne and possibly addition reactions of *o*-benzyne. It is also intended to study the dissociation of 1,5-hexadiene to characterize it as a potential source of allyl radicals in the DFST and to study their dissociation kinetics. A modified DFST has been designed and is being tested with finally improvements to be made in the coming year. The new design should increase the range of shock strengths available. The nozzle/skimmer interface between the shock tube and TOF-MS has been redesigned and the new interface will be installed during the year along with a new mass spectrometer which should improve the resolution in the mass spectra and the temporal resolution of the DFST/TOF-MS experiments.

IV. References

- i. Irdam E. A., Kiefer J. H., *Chem. Phys. Lett.*, **1990** 166, 491; Vasudevan V., Davidson D. F., Hanson R. K., Bowman C. T., Golden D. M., *Proc. Combust. Inst.*, **2007**, 31, 175.
- ii. Kumaran S. S., Su M. C., Lin K. P., Michael J. V., *Proc. Combust. Symp.* **1996**, 26, 605.
- iii. Miller J. A., Klippenstein S. J., *Phys. Chem. Chem. Phys.*, **2004**, 6 1192.

V. Publications and submitted journal articles supported by this project 2008-2010

1. Tranter R. S., Klippenstein S. K., Harding L. B., Giri B. R., Yang X., Kiefer J. H., "An experimental and theoretical investigation of the self-reaction of phenyl radicals" Submitted *J. Phys. Chem. A*, March **2010**.
2. Yang X., Jasper A.W., Kiefer J. H., Tranter R. S., "The Dissociation of Diacetyl: A Shock Tube and Theoretical Study" *J. Phys. Chem. A*, **2009**, 29, 8318.
3. Yang X., Goldsmith C. F. and Tranter R. S., "Decomposition and Vibrational Relaxation in CH₃I and Self-Reaction of CH₃ Radicals" *J. Phys. Chem. A*, **2009**, 113, 8307.
4. Hessler J. P., Tranter R. S., De Lurgio P. M., Jennings G., Seifert S., Guoeb L. and McNaney J., "A high-speed one-dimensional detector for time-resolved small-angle x-ray scattering: commissioning results" Submitted *J. Synchrotron Rad.* Nov **2009**
5. Giri B. R., Klippenstein S. J., Kiefer J. H. and Tranter R. S., "An Experimental and Theoretical High Temperature Kinetic Study of the Thermal Unimolecular Dissociation of Fluoroethane", *Phys. Chem. Chem. Phys.*, **2008**, 10, 6266.
6. Tranter R. S. and Giri B. R., "A Diaphragmless Shock Tube for High Temperature Kinetic Studies", *Rev. Sci. Instrum.*, **2008**, 79, 094103.

Variational Transition State Theory

Donald G. Truhlar

Department of Chemistry, University of Minnesota
207 Pleasant Street SE, Minneapolis, Minnesota 55455
truhlar@umn.edu

Program scope

This project involves the development of variational transition state theory (VTST) with optimized multidimensional tunneling (OMT) contributions and its application to gas-phase reactions. For overbarrier processes, we are employing both methods suitable for tight transition states, employing isoinertial minimum energy paths and curvilinear generalized normal mode coordinates (Garrett, Truhlar 1979; Isaacson, Truhlar 1982; Jackels, Gu, Truhlar 1995; Fast, Truhlar 1998), and methods suitable for loose transition states, employing multifaceted dividing surfaces and Monte Carlo integration over transition modes (Georgievskii, Klippenstein 2003). For optimized multidimensional tunneling, we employ small curvature tunneling (Skodje, Truhlar, Garrett 1981; Liu, Lynch, Truong, Lu, Truhlar, Garrett 1993), large curvature tunneling (Garrett, Truhlar, Wagner, Dunning 1983; Fernandez and Truhlar 2001), and least-action tunneling (Garrett, Truhlar, 1983; Meana-Pañeda, Truhlar, Fernandez 2010).

The further development of VTST/OMT as a useful tool for combustion kinetics involves advancing the ability of electronic structure calculations (both wave function and density functional theory) of the required potential energy surface, which we now take as an implicit surface defined by a level of electronic structure theory (direct dynamics: Baldrige, Gordon, Steckler, Truhlar, 1989; González-Lafont, Truong, Truhlar 1991). We are developing new methods to interface reaction-path and reaction-swath dynamics calculations with electronic structure theory, for example, multiconfiguration Shepard interpolation (Kim, Corchado, Villà, Xing, Truhlar 2000; Tishchenko, Truhlar, 2010). We are developing and implementing practical techniques and software for applying these theoretical methods to various classes of reactions and making applications to specific reactions, with special emphasis on combustion reactions and reactions that provide good test cases for methods needed to study combustion reactions.

Recent progress

We have incorporated the variable-reaction-coordinate multifaceted-dividing-surface algorithm for treating dividing surfaces appropriate for barrierless association reactions into a new parallel version of the freely available POLYRATE program.

We are also developing improved electronic structure methods and using them for rate constant calculations. One class of new methods involves wave function theory, especially generally defined electronic wave function methods with empirical elements, such as BMC-CCSD; another class of methods is based on new density functionals. These methods are then used in direct dynamics calculations or with efficient interpolation schemes. Direct dynamics denotes that, instead of using a pre-defined potential energy function, all required energies and forces for each geometry that is important for evaluating dynamical properties are obtained directly from electronic structure calculations. We have now developed new functionals, especially the M06-2X functional (Minnesota 2006 functional with double nonlocal exchange), that are quite accurate for these properties, and we have also developed multi-coefficient correlation methods for using wave function theory for these properties. Density functional theory is very attractive as an electronic structure method for direct dynamics because of its relatively low cost and the availability of analytic gradients and Hessians. Density functional theory is applicable to large, complex systems

because of favorable cost scaling. Using the new POLYRATE program, we showed that the difficulty in efficiently generating accurate potential surfaces for radical-radical interaction energies is alleviated by the new M06 suite of density functionals, which often provide a better compromise of efficiency, convenience, and accuracy for calculating radical association rate constants.

The diverse barrier height database DBH24 was updated by using W4 and W3.2 data to replace previous W1 values. We used the new database to assess 348 model chemistries, each consisting of a combination of a wave function theory level or a density functional approximation with a one-electron basis set. A test of the M06-2X and M08-SO functionals on DBH24 with the cc-pVTZ+ basis set yielded a mean unsigned error of only 0.9 kcal/mol, better than the accuracy of CCSD(T) with the same basis set. A key advantage of M06-2X as compared to other density functionals is the improved accuracy for attractive noncovalent interactions. This is important for barrierless reactions and for reactions with low, early saddle points (like OH + H₂S), where it is necessary to have a consistent treatment of the energy along the reactant approach coordinate.

The calculation of chemical reaction barrier heights often requires multireference methods, but well-defined and validated multireference methods for barrier height calculations have not been available. Now we have developed three model chemistries based on multireference methods, and we demonstrated their use and validated them for calculating barrier heights of chemical reactions by applying them to a new database of diverse-reaction barrier heights.

In order to generate reactive potential energy surfaces with minimal computational effort, we have introduced an algorithm called multiconfiguration Shepard interpolation (MCSI). In earlier work we called this multiconfiguration molecular mechanics (MCMM) to emphasize that the cost is as low as for molecular mechanics, but now we changed the name to emphasize that it is an interpolation method that can be used to fit potential energy surfaces to arbitrary accuracy. MCSI describes polyatomic potential energy surfaces by interacting molecular mechanics configurations (each of which is the analog of a valence bond configuration) and can thus be viewed as an extension of standard MM to chemical reactions or as an extension of semiempirical valence bond theory to be systematically improvable. MCMM fitting is accomplished by combining molecular mechanics potentials for the reactant and product wells with electronic structure data (energy, gradient, and Hessian) at the saddle point and a small number of non-stationary points. We have now identified the key elements required both to make MCMM more accurate and to make it more efficient, and these have been incorporated in a new non-Hermitian version of the algorithm, with very stable analytic gradients.

At the suggestion of Wing Tsang, the rate constants of three intramolecular hydrogen-transfer isomerization reactions, namely, 1-4 isomerization of the 1-pentyl radical and 1-4 and 1-5 isomerizations of the 1-hexyl radical, were calculated using variational transition state theory with multidimensional tunneling, in particular by using canonical variational theory (CVT, which is the version of variational transition state theory in which the transition state dividing surface is optimized for a canonical ensemble) with small-curvature tunneling (SCT) for the transmission coefficient. The required potential energy surfaces were obtained implicitly by direct dynamics employing interpolated variational transition state theory with mapping (IVTST-M) and variational transition state theory with interpolated single-point energies (VTST-ISPE). Single-level direct dynamics calculations were performed for all of the reactions by IVTST-M using M06-2X/MG3S or M08-HX/cc-pVTZ+ potential energy surfaces or both. The stationary points of 1-4 isomerization of 1-pentyl and the stationary points for the forward reactions of 1-4 and 1-5 isomerizations of 1-hexyl were also optimized by BMC-CCSD, and for all three reactions we also performed dual-level direct dynamics calculations using VTST-ISPE

in which MCG3-MPW single-point energies served as the higher level. The calculated MCG3-MPW//M06-2X/MG3S rate constants agree well with experimental values for 1-4 isomerization of the 1-pentyl radical at high temperature, and this validates the accuracy of this theoretical method for 1-4 isomerization. The MCG3-MPW//M06-2X/MG3S method was therefore used to make a reliable prediction for the rate constants of 1-4 isomerization of the 1-hexyl radical for which a direct experimental measurement is not available. The calculated CVT/SCT/M08-HX/cc-pVTZ+ rate constants agree well with experimental values for 1-5 isomerization of the 1-hexyl radical, and they show that the tunneling effect for these reactions was underestimated in previous work.

Software distribution

We have developed several software packages for applying variational transition state theory with optimized multidimensional tunneling coefficients to chemical reactions and for carrying out MCCM calculations and direct dynamics. The URL of our software distribution site is comp.chem.umn.edu/Truhlar. The license requests that we fulfilled for rate constant programs during the period Jan. 1, 2008–Mar. 31, 2010 for software packages developed wholly or partially under DOE support is as follows:

	<i>Total</i>	<i>academic</i>	<i>government/DoD</i>	<i>industry/nonprofit</i>
POLYRATE	189	171	13	5
GAUSSRATE	103	95	1	7
GAMESSPLUSRATE	17	15	1	1
NWCHEMRATE	6	4	2	0
5 others	14	14	0	0

In addition we distributed 10 license packages for MCMM calculations.

Future plans

We have several objectives for the next few years: (1) treat the stabilization of intermediate complexes by energy transfer collisions; (2) integrate the above methods with tight transition state methods to treat multiwell reactions and reactions with inner and outer dynamical bottlenecks; (3) further improve our multi-coefficient correlation methods for potential energy surfaces; (4) further develop the multi-configuration molecular mechanics approach as an efficient tool for the semiautomatic fitting of complex-system potential energy surfaces and apply it to calculate reaction rates for complex systems; (5) develop more reliable methods for including anharmonicity at variational transition states, especially for torsions and mode-mode coupling; (6) continue our calculations of reaction rates of peroxides and enols; (8) enhance our user-friendly computer program packages to allow more researchers to carry out calculations conveniently by the new methods.

Publications supported in whole or in part by this grant, 2008-present

Journal articles

1. "The M06 Suite of Density Functionals for Main Group Thermochemistry, Thermochemical Kinetics, Noncovalent Interactions, Excited States, and Transition Elements: Two New Functionals and Systematic Testing of Four M06 Functionals and Twelve Other Functionals," Y. Zhao and D. G. Truhlar, *Theoretical Chemistry Accounts*, Y. Zhao and D. G. Truhlar, *Theoretical Chemistry Accounts* **120**, 215-241 (2008) Erratum: **119**, 525 (2008).
2. "A Comparative Assessment of the Perturbative and Renormalized Coupled Cluster Theories with a Non-iterative Treatment of Triple Excitations for Thermochemical Kinetics, Including a Study of Basis Set and Core Correlation Effects," J. Zheng, J. R. Gour, J. J. Lutz, M. Włoch, P. Piecuch, and D. G. Truhlar, *Journal of Chemical Physics* **128**, 44108/1-7 (2008).

3. "How Well Can New-Generation Density Functionals Describe the Energetics of Bond Dissociation Reactions Producing Radicals?" Y. Zhao and D. G. Truhlar, *Journal of Physical Chemistry A* **112**, 1095-1099 (2008).
4. "VBSM: A Solvation Model Based on Valence Bond Theory," P. Su, W. Wu, C. J. Cramer, C. P. Kelly, and D. G. Truhlar, *Journal of Physical Chemistry A* **112**, 12761-12768 (2008).
5. "Assessment of New Meta and Hybrid Meta Density Functionals for Predicting the Geometry and Binding Energy of a Challenging System: the Dimer of H₂S and Benzene," H. R. Leverentz and D. G. Truhlar, *Journal of Physical Chemistry A* **112**, 6009-6016 (2008).
6. "Multireference Model Chemistries for Thermochemical Kinetics," O. Tishchenko, J. Zheng, and D. G. Truhlar, *Journal of Chemical Theory and Computation* **4**, 1208-1219 (2008).
7. "Effects of ¹⁸O Isotopic Substitution on the Rotational Spectra and Potential Splitting in the OH–H₂O Complex: Improved Measurements for ¹⁶OH–¹⁶OH₂ and ¹⁸OH–¹⁸OH₂, New Measurements for the Mixed Isotopic Forms, and Ab Initio Calculations of the 2A' – 2A" Energy Separation," C. S. Brauer, G. Sedo, E. Dahlke, S. Wu, E. Grumstrup, K. R. Leopold, M. D. Marshall, H. O. Leunge, and D. G. Truhlar, *Journal of Chemical Physics* **129**, 104304/1-11 (2008).
8. "Density Functional Study of Methyl Radical Association Reaction Kinetics," J. Zheng, S. Zhang, and D. G. Truhlar, *Journal of Physical Chemistry A* **112**, 11509-11513 (2008).
9. "The DBH24/08 Database and Its Use to Assess Electronic Structure Model Chemistries for Chemical Reaction Barrier Heights," J. Zheng, Y. Zhao, and D. G. Truhlar, *Journal of Chemical Theory and Computation* **5**, 808-821 (2009).
10. "Efficient Diffuse Basis Sets: cc-pVxZ+ and cc-pV(x+d)Z+," E. Papajak, H. R. Leverentz, J. Zheng, and D. G. Truhlar, *Journal of Chemical Theory and Computation* **6**, 597-601 (2010). Errata and addendum: **5**, 3330 (2009).
11. "Thermochemical Kinetics for Multireference Systems: Addition Reactions of Ozone," Y. Zhao, O. Tishchenko, J. R. Gour, W. Li, J. J. Lutz, P. Piecuch, and D. G. Truhlar, *Journal of Physical Chemistry A* **113**, 5786–5799 (2009).
12. "Non-Hermitian Multiconfiguration Molecular Mechanics," O. Tishchenko and D. G. Truhlar, *Journal of Chemical Theory and Computation* **5**, 1454-1461 (2009).
13. "The Muonic He Atom and a Preliminary Study of the ⁴Heμ + H₂ Reaction," D. J. Arseneau, D. G. Fleming, O. Sukhorukov, J. H. Brewer, B. C. Garrett, and D. G. Truhlar, *Physica B: Condensed Matter* **404**, 946-949 (2009). (Proceedings of the Eleventh International Conference on Muon Spin Rotation, Relaxation and Resonance).
14. "Direct Dynamics Study of Hydrogen-Transfer Isomerization of 1-Pentyl and 1-Hexyl Radicals," J. Zheng and D. G. Truhlar, *Journal of Physical Chemistry A* **113**, 11919-11925 (2009).
15. "Steric Effects and Solvent Effects on S_N2 Reactions," Y. Kim, C. J. Cramer, and D. G. Truhlar, *Journal of Physical Chemistry A* **113**, 9109-9114 (2009).
16. "Homogeneous Nucleation with Magic Numbers: Aluminum," S. L. Girshick, P. Agarwal, and D. G. Truhlar, *Journal of Chemical Physics* **131**, 134305/1-11 (2009).
17. "Phase Space Prediction of Product Branching Ratios: Canonical Competitive Nonstatistical Model," J. Zheng, E. Papajak, and D. G. Truhlar, *Journal of the American Chemical Society* **131**, 15754-15760 (2009).
18. "Least-Action Tunneling Transmission Coefficient for Polyatomic Reactions," R. Meana-Pañeda, D. G. Truhlar, and A. Fernández-Ramos, *Journal of Chemical Theory and Computation* **6**, 6-17 (2010).
19. "Efficient Diffuse Basis Sets for Density Functional Theory," E. Papajak and D. G. Truhlar, *Journal of Chemical Theory and Computation*, *Journal of Chemical Theory and Computation* **6**, 597-601 (2010).
20. "Kinetics of Hydrogen-Transfer Isomerizations of Butoxyl Radicals," J. Zheng and D. G. Truhlar, *Physical Chemistry Chemical Physics*, submitted Dec. 29, 2009.

Chemical Kinetic Data Base for Combustion Modeling

Wing Tsang
National Institute of Standards and Technology
Gaithersburg, MD 20899
Wing.tsang@nist.gov

Program Scope and Definition

The increasing use of simulations as a tool in combustion technology has focused interest in the use of fundamental or transferable inputs into these programs. This is a reflection of the great advances in Computational Fluid Dynamics that can combine fluid dynamics and realistic chemistry [1]. The thrust of this program is to aid in the development of the fundamental chemical kinetics information base that are necessary ingredients into such programs. The unique aspect is the emphasis on real fuels. It is obvious that a kinetic database based on real fuels will be able to simulate their behavior in real combustion devices. This means the creation of a new tool for innovation and optimization. It will bring combustion technology to the stage of other cutting edge areas where the design process is intimately linked with simulations.

Real fuels are complex mixtures of many organic compounds. They belong to a very limited set of classes of compounds. There is agreement among those who work in the fuel area that a limited palette of compounds can effectively represent the combustion behavior of real fuel mixtures. This has become an increasing focus of research in combustion technology [2]. In terms of chemical kinetics database development the emphasis remains that of fundamental and transferable reaction rate constants and expressions. This work is focused on increasing coverage to include the newer and larger structures when real fuels are involved. A particular challenge is the size of the molecules. The need is for fuels containing as many as 16 carbon atoms (hexadecane in diesel). It is necessary to determine correlations for the various types of reactions that are possible. At the experimental level the work is similar to that carried out to determine Structural Activity Relations. For these relatively simple systems, transition state theory serves as a guide and the added features arising from chemical activation, fall-off effects and tunneling can be used to further refine the results. An important feature of fundamental or transferable kinetic data is their use in mixtures. It is simple to consider new formulations and compounds by the use of different mixture fractions or through addition of new species into the database.

Recent Progress

Background: The present work has focused on pyrolytic decomposition. The rationale for this emphasis is the lack of attention on this aspect of combustion in current databases. They have focused on oxidative degradation since the emphasis is on matching ignition behavior. The processes involved in pyrolysis are of key importance for the treatment of Soot/PAH formation [3], since the products of such reactions are their precursors. A pyrolysis database complements and extends the range of current fuel mechanisms. From an experimental point of view it is difficult to study oxidation at high temperatures without a thorough understanding of the competing pyrolytic processes.

Linear Radicals	Ranched Radicals	Cyclic Radicals	1-olefinyl radicals
1-butyl *	4-methylpentyl-1*	Cyclopentyl *	4-pentenyl-1*
1-pentyl *	5-methylhexyl-1*	Cyclohexyl*	5-hexenyl-1*
1-hexyl *		Cyclohexylmethyl*	6-heptenyl-1*
1-heptyl * [4]		2-cyclohexylethyl-1*	
1-octyl * [5]			
1-nonyl *			

Table 1: Fuel radicals that have been studied divided into various classes

The quantitative details of the kinetics of radical forming processes from fuel molecules are well established. The present work on mechanism and rate constants of fuel radical degradation is a natural follow up to the earlier studies. In practically all cases fuel radicals are generated from an appropriate organic iodide. Advantage is taken of the weak C-I bond and the appropriate radicals are released into the high temperature shock tube environment. The experimental aspect of this work is supported by the AFOSR. The analysis of this data and associated information is the focus of the present work. The results are unimolecular rate expressions for beta bond scission and isomerization. The latter is a particular challenge due to the necessity of considering tunneling. This has not been considered earlier and is a major scientific accomplishment of this work and has now been confirmed by ab initio calculations.

Table 1 contains a listing of the radicals that have been studied experimentally. The work under this project involves the analysis of the data in terms of the rate constants for the various decomposition and isomerization channels. The results include not only the high pressure rate expressions but also the dependence of the rate constants on pressure obtained through the solution of the master equation. It is clear that the amount of work required to analyze each set of data increases dramatically as the radical becomes larger and, through substitution, loses symmetry.

In terms of the compounds in a particular fuel mixture, the radicals are derived from linear, branched (as from Fischer-Tropsch fuels), cyclic and olefinyl fuels. The only important class of compounds not treated are the branched aromatic fuels. The data on the linear fuels and properties of the reaction of aromatic compounds in the literature is sufficient to make predictions regarding the radicals derived from such compounds. This will be demonstrated subsequently.

Specific Radicals: We have recently completed an analysis of the experimental results (in terms of the olefin branching ratio derived from the decomposition of 5-methyl-hexyl-1 radical. Figure 1 is illustrative of the many products that are formed and the high quality of the experimental data. The experimental conditions are set so that only unimolecular decomposition and isomerizations occur. The general mechanism is summarized in Figure 2. The high pressure rate expressions are given in Table 2. Due to space problems we have not included the values of the rate constants at various pressures. The

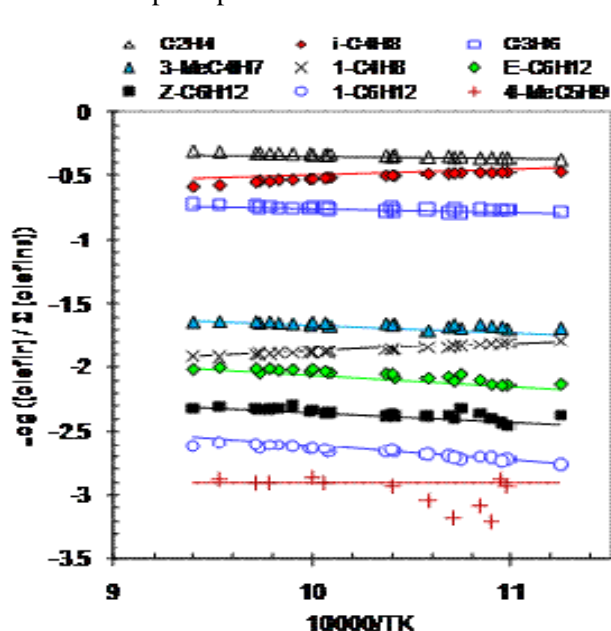


Figure 1: Olefinic branching ratios from 5-methyl hexyl-1 breakdown

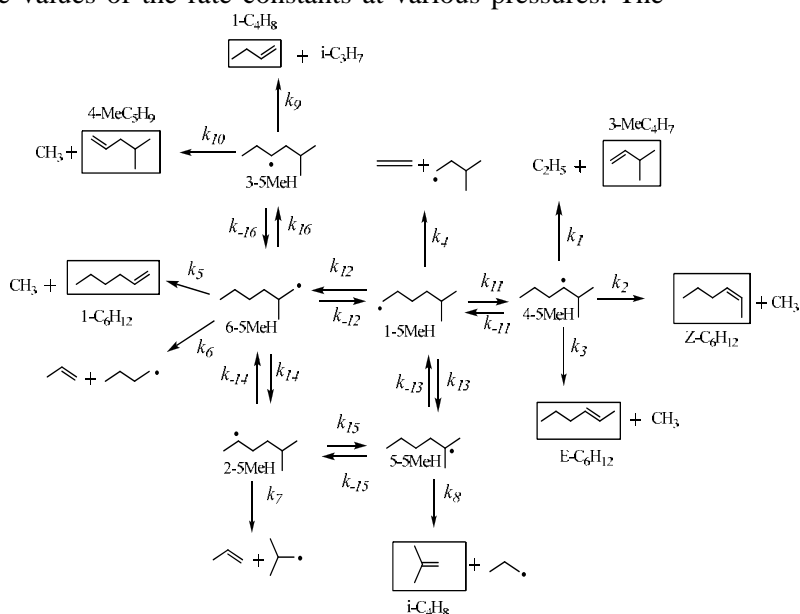


Figure 2: Mechanism for 5-methylhexyl-1 breakdown

	Reaction	Log A	<i>n</i>	E/R	Log (<i>k/s</i> ⁻¹) 1000 K
<i>k</i> ₁	4-5MeH → C ₂ H ₅ + 3-MeC ₄ H ₇	13.57	0.033	14591	7.25
<i>k</i> ₂	4-5MeH → CH ₃ + <i>E</i> -C ₆ H ₁₂	13.52	0.11	15371	6.90
<i>k</i> ₃	4-5MeH → CH ₃ + <i>Z</i> -C ₆ H ₁₂	12.97	0.14	14866	6.59
<i>k</i> ₄	1-5MeH → C ₂ H ₄ + 3-MeC ₄ H ₈	14.06	-0.55	15670	6.96
<i>k</i> ₅	6-5MeH → CH ₃ + 1-C ₆ H ₁₂	13.52	-0.59	15396	6.52
<i>k</i> ₆	6-5MeH → C ₃ H ₆ + <i>n</i> -C ₄ H ₉	14.18	-0.56	15782	7.03
<i>k</i> ₇	2-5MeH → C ₃ H ₆ + <i>i</i> -C ₄ H ₉	13.20	0.07	13651	7.31
<i>k</i> ₈	5-5MeH → <i>i</i> -C ₄ H ₈ + <i>n</i> -C ₃ H ₇	13.00	0.31	13392	7.34
<i>k</i> ₉	3-5MeH → <i>i</i> -C ₃ H ₇ + 1-C ₄ H ₈	13.24	0.16	12563	7.87
<i>k</i> ₁₀	3-5MeH → 4-MeC ₅ H ₉ + CH ₃	13.05	0.16	14326	6.91
<i>k</i> ₁₁	1-5MeH → 4-5MeH	9.19	2.13	7937	6.86
<i>k</i> ₋₁₁	4-5MeH → 1-5MeH	8.64	2.84	8985	6.23
<i>k</i> ₁₂	1-5MeH → 6-5MeH	8.79	2.36	6969	7.01
<i>k</i> ₋₁₂	6-5MeH → 1-5MeH	8.54	2.31	7020	6.71
<i>k</i> ₁₃	1-5MeH → 5-5MeH	8.67	1.71	4041	7.81
<i>k</i> ₋₁₃	5-5MeH → 1-5MeH	8.17	2.62	6044	6.92
<i>k</i> ₁₄	6-5MeH → 2-5MeH	8.69	1.69	4748	7.52
<i>k</i> ₋₁₄	2-5MeH → 6-5MeH	8.65	2.28	6005	7.24
<i>k</i> ₁₅	2-5MeH → 5-5MeH	8.91	2.70	8081	6.82
<i>k</i> ₋₁₅	5-5MeH → 2-5MeH	8.70	3.07	8776	6.51
<i>k</i> ₁₆	6-5MeH → 3-5MeH	9.28	2.01	8103	6.82
<i>k</i> ₋₁₆	3-5MeH → 6-5MeH	8.99	2.79	9403	6.38
<i>k</i> ₁₇	5-5MeH → 2-CH ₃ -hex-1-ene + H	13.17 ^a	0.71 ^a	17787 ^a	5.82 ^a
<i>k</i> ₁₈	5-5MeH → 2-CH ₃ -hex-2-ene + H	12.76 ^a	0.69 ^a	17287 ^a	5.61 ^a

Table 2. High pressure limiting rate expressions, $k/s^{-1} = A (T/298)^n \exp(-E/T)$, from 500-1900 K, derived for reactions in the thermal decomposition of 5-methylhexyl-1 radical

noteworthy feature of these results are the large number of olefins and reactions for this radical. The rate expressions for all these channels are not really needed in any model for 5-methylhexyl-1 radical. Decomposition. However they give insights into related processes. This is the reason that rate expressions can be given for all the processes enumerated in Figure 2. Nine products are detected. Rate expressions are given for 18 reactions. This arises from the use of rate expressions derived from earlier studies on related molecules. One of the most interesting observations from this analysis is the relationship between structure and reactivity. For high temperature applications the olefin branching ratio can be directly used.

With these results and literature information it is possible to predict the breakdown patterns of related fuels. Table 3 contains predictions on the rate expressions for the breakdown of the phenylbutyl radical. The stability of the aromatic ring simplifies the estimation procedures. Branched aromatics are important as a soot precursor. The results will permit direct simulations of the sooting propensities of such compounds. The remaining class of fuel compounds are the branched cyclic radicals. The problems in the analysis of data on such such compounds are the constraint arising from the linkage of radical and olefinic sites and the effects from tunneling in transferring the H-atom into and out of the ring.

Future Work

As indicated earlier we plan to conclude our work on the thermal stability of alkyl radicals by analyzing the experimental data on the various cyclohexyl and branched cyclohexyl radicals.. This will be followed

Reactions	Rate Expressions		
	Log A	N	E/R
Beta bond scissions			
$C_6H_5CH^*CH_2CH_2CH_3 = C_6H_5CH=CH_2 + CH_2CH_3$	13.54	.178	16234
$C_6H_5CH_2CH^*CH_2CH_3 = C_6H_5CH_2CH=CH_2 + CH_3$	13.27	.039	15221
$C_6H_5CH_2CH_2CH^*CH_3 = C_6H_5CH_2^* + CH_2=CHCH_3$	13.35	.128	11980
$C_6H_5CH_2CH_2CH_2CH_2^* = C_6H_5CH_2CH_2 + CH_2=CH_2$	13.06	.146	13445
$C_6H_5CH(CH_2^*)CH_2CH_3 = C_6H_5CH=CH_2 + CH_2CH_3$	13.36	.13	13491
$C_6H_5CH(CH_3)CH_2CH_2^* = C_6H_5CH^*CH_3 + CH_2=CH_2$	13.37	.138	11732
$C_6H_5CH^*CH_3 = C_6H_5CH=CH_2 + H$	13.23	.405	23191
$C_6H_5CH_2CH_2^* = C_6H_5CH=CH_2 + H$	13.33	.22	17950
$C_6H_5CH_2CH_2^* = C_6H_5 + CH_2=CH_2$	13.70	.18	20969
Isomerizations			
$C_6H_5CH_2CH^*CH_2CH_3 = C_6H_5CH(CH_2^*)CH_2CH_3$ (neophyl rearrangement)	13.36	.130	7955
$C_6H_5CH_2CH_2CH_2CH_2^* = C_6H_5CH^*CH_2CH_2CH_3$ (1,4-Hydrogen shift)	11.46	1.64	9233
$C_6H_5CH(CH_2^*)CH_2CH_3 = C_6H_5CH(CH_3)CH_2CH_2^*$ (1,4-Hydrogen shift)	11.79	1.60	11684

Table 3: High pressure rate expressions for the decomposition of phenylbutyl radicals [6].

by the analysis of the chemically activated decomposition of alkyl radicals. Particular attention will be paid to the existing results on radical isomerization and their compatibility with the rate expressions derived from the shock tube experiments. This will set the stage for work on the oxidative degradation of organic radicals where sufficient oxygen will be added to the system so as to swamp the pyrolytic process. These are chemical activation reactions but have rarely been treated in this fashion and hence represents a serious deficiency in existing databases.

Publications 2008-2009

1. McGovern WS, Awan IA, Tsang W Isomerization and Decomposition Reactions in the Pyrolysis of Branched Hydrocarbons; 4-methyl-pentyl, J. Phys. Chem.,A 112 6908-6917, 2008
- 2 Tsang, W., Awan, I., McGovern, S., Manion, J. A., "Soot Precursors from Real Fuels: The Unimolecular Reactions of Fuel Radicals" in "Combustion Generated Fine Carbon Particles" (H. Bockhorn, A. D'Anna, A. Sarofim, H. Wang, ed) KIT Scientific Publishing, 2009, pg.55-74
3. Tsang, W., McGovern, S., Manion, J. A., "Multichannel Decomposition and Isomerization of Octyl Radicals" Proc Comb. Institute 32, 131-138, 2009
4. Tsang, W., "Pathways and Rate Constants for the Breakdown of n-Butylbenzene" (submitted)

References

1. Kee, R. J., Coltrin, M. E. and Glarborg, P., "Chemically Reacting Flow" Theory and Practice, Wiley, Interscience, New York, 2003
2. Colket M., Edward, C. T., Williams, S., Cernansky, N. P., Miller, D. L., Egolfopoulos, F., Lindstedt, P., Seshadri, K., Dryer F. L., Law, C. K., Friend, D., Lenhart, D. B., Pitts, H., Sarofim, A., Smooke, M., Tsang, W., "Development of an Experimental Database and Kinetic Models for Surrogate Fuels", 45th AIAA Aerospace Sciences Meeting and Exhibit, Reno, Nevada, January 9, 2007
3. Richter H, and Howard J.B., Prog. Energ. Combust.: 4 565, 2000
- 4 Tsang, W., Awan, I., McGovern, S., Manion, J. A., "Soot Precursors from Real Fuels: The Unimolecular Reactions of Fuel Radicals" in "Combustion Generated Fine Carbon Particles" (H. Bockhorn, A. D'Anna, A. Sarofim, H. Wang, ed) KIT Scientific Publishing, 2009, pg.55-74
5. Tsang, W., McGovern, S., Manion, J. A., "Multichannel Decomposition and Isomerization of Octyl Radicals" Proc Comb. Institute 32, 131-138, 2009
6. Tsang, W., "Pathways and Rate Constants for the Breakdown of n-Butylbenzene" (submitted)

SISGR: Developing a predictive model for the chemical composition of soot nanoparticles: Integrating Model and Experiment

Principal Investigator Angela Violi
Department of Mechanical Engineering, University of Michigan
Ann Arbor, MI 48109-2125
avioli@umich.edu

I. Program Scope

In order to provide the scientific foundation to enable technology breakthroughs in transportation fuel, it is important to develop a combustion modeling capability to optimize the operation and design of evolving fuels in advanced engines for transportation applications. The goal of this proposal is to develop a validated predictive multiscale model to describe the chemical composition of soot nanoparticles in premixed and diffusion flames.

Multiscale computational studies in conjunction with state-of-the-art experiments are the distinguishing characteristics of this unique interdisciplinary effort. The modeling effort is conducted at the University of Michigan by Prof. A. Violi. The experimental work will entail a series of studies using different techniques to analyze gas-phase soot precursor chemistry and soot particle production in premixed and diffusion flames. The experimental team includes Dr. N. Hansen and H. Michelsen at Sandia National Labs' Combustion Research Facility, and Dr. K. Wilson at Lawrence Berkeley National Lab's Advanced Light Source.

Recent studies show that the chemical and physical properties of nanoparticles affect the coagulation behavior in soot formation, and an experimentally validated, predictive model for the chemical composition of soot nanoparticles will not only enhance our understanding of soot formation since but will also allow the prediction of particle size distributions under combustion conditions. These results will provide a novel description of soot formation based on physical and chemical properties of the particles for use in the next generation of soot models and an enhanced capability for facilitating the design of alternative fuels and the engines they will power.

II. Recent Progress

A. Rotationally resolved infrared spectroscopy of the hydroxymethyl radical (CH₂OH)

The formation of soot begins with the nucleation of nanoparticles, a process difficult to model due to the complexity of the constituent particles. Fullerenes have characteristics resembling the particles found in soot, but their simpler structure makes simulations more tractable. We propose that the nucleation of fullerenes may serve as a window to the formation of soot. Using Molecular Dynamics simulations, we analyze the nucleation rates of homomolecular systems of C₆₀, C₈₀, C₁₈₀, and C₂₄₀ fullerenes as function of temperature and molecular mass. For temperatures lower than 1000K, the four systems show similar characteristics, with significant nucleation rates, due to the low energy that favors binding. At higher temperatures, the high kinetic energy limits the binding probability between fullerenes and molecular clusters are only detected in systems composed of C₁₈₀ and C₂₄₀. The analysis shows that particles with molecular masses between those of C₈₀ and C₁₈₀ could be critical for the transition from monomers to clusters. The computational findings are then related to experimental data of combustion-generated particles present in the literature to assess the feasibility of a physical nucleation pathway in the transition from bi-dimensional structures to three-dimensional particles in high temperature regimes. The results obtained using Molecular Dynamics simulations highlight the importance of a physical nucleation pathway to describe the formation of molecular clusters when the particle concentration exceeds a critical value. These results represent the first step toward a more complete description of nanoparticle formation and soot nucleation in high temperature regimes.

Homo-molecular systems of C₆₀, C₈₀, C₁₈₀, and C₂₄₀ were simulated using the canonical NVT ensemble with cubical periodic boundary conditions. The familiar form of a short-range 6-12 Lennard-

Jones (LJ) potential was employed to model the non-bonded interactions between atoms. The total conformational energy between two fullerene molecules was defined as:

$$(1) \quad V = \sum_{ij} -\frac{A}{r_{ij}^6} + \frac{B}{r_{ij}^{12}}$$

where A and B are the attractive and repulsive constants and r_{ij} is the distance between two interacting atoms. The values of A and B were taken from the discrete carbon-carbon potential for C60 - C60 developed by Girifalco et al.^{16,17} ($A = 15.2 \text{ eV} \times \text{\AA}^6$, and $B = 34.8 \times 10^3 \text{ eV} \times \text{\AA}^{12}$), who determined the energy of sublimation and the lattice parameters of a face-centered cubic fullerene cluster using first-, second-, and third-neighbor interactions. This potential has been used by other research groups to compute molecular properties of C60 and compared with experimental data for the heat of sublimation and lattice constant.^{i,ii,iii} The LJ potential cut off was set at 30 Å, and the molecules were considered to be rigid. The elimination of intramolecular potential is related to the continuum model proposed by Girifalco¹⁶, which simplifies the system by averaging the potential over the surfaces of the molecules. This model has been used to study the growth of fullerene clusters, interaction of C60 with a graphite surface and thermal expansion of C60.¹⁹ The discrete atom-atom model was used in this study to facilitate the scale up of the potential to bigger fullerene molecules. The temperature was controlled using the Nosé-Hoover thermostat. Keeping the temperature constant is very important and an inefficient thermalization may have a strong influence on the results. A recent work by Wedekind et al.^{iv} investigated the influence of carrier gases and thermostats on nucleation processes described with MD. The authors analyzed the efficiency of velocity rescaling, Nosé-Hoover, and a carrier gas (mimicking the experimental condition), and reported that the choice of the thermostating method does not have a significant influence on the nucleation rate, obtaining deviations of less than a factor of 1.7.

The trajectories were integrated using the Velocity Verlet method, using a time step of 0.05 ps. All calculations were performed using the DL_POLY_2.18 software package.^v

The systems studied contained 343 molecules for the C60 and C80 systems ($35 \times 35 \times 35 \text{ nm box}$) and 125 molecules for the C180 and C240 cases ($25 \times 25 \times 25 \text{ nm box}$).

Figure 1 reports the percentages of fullerenes present in the system as monomers and the number of fullerenes per cluster for C60 and C240 molecules as function of time at different temperatures. At 500 K, the systems show a significant number of “sticky” collisions and the percentage of monomers decreases by 80% over a time interval of 1000 ps reaching an average of 3.5 - 4 fullerenes per cluster. The nucleation rate at 500 K, identified by the disappearance of monomers in the system, is the highest among the conditions investigated.

However, for the system composed of C240, the growth of nuclei at 500 K reaches a plateau between 600 and 700 ps. This result can be explained using the Maxwell-Boltzmann molecular speed distributions of two homogeneous systems at different temperatures, as their conceptual plots are drawn in Figure 2 (a). At Tlow (e.g. 500 K in our simulations), molecules with relatively high translational energies participate to the formation of nuclei since they are able to reach each other within a relative short time, and their energy levels favor binding (Figure 2 (b)). Since this process can be faster than the energy transfer, molecules with low translational kinetic energies require longer time to reach the adjacent species and remain in the system as monomers. In this situation, shown as Tlow in Figure 2 (c), the system looks “frozen” due to the low speed of the molecules and nuclei. At higher temperatures, this effect is negligible since the binding probability is relatively low due to the high kinetic energies of the molecules.

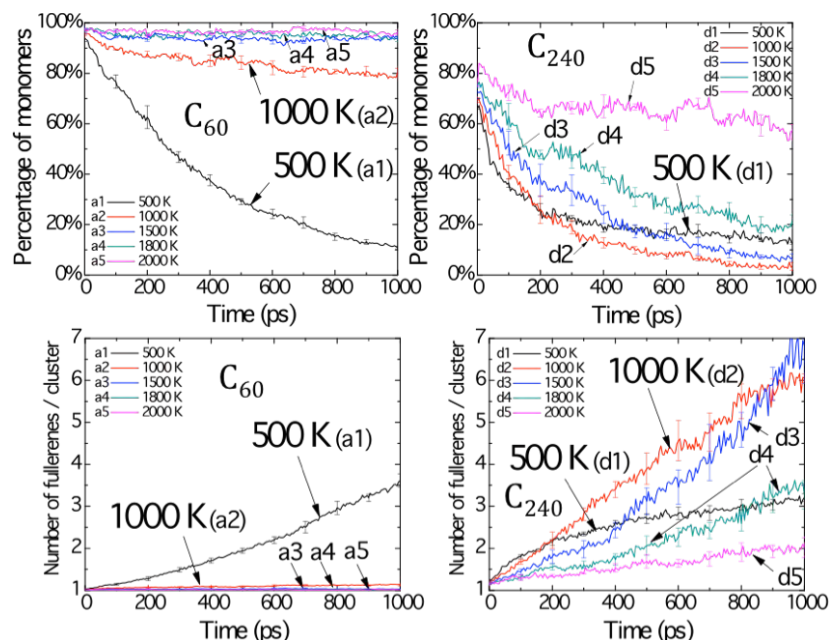


Figure 1. Percentages of C₆₀ and C₂₄₀ fullerene molecules in the state of monomers (top panels) and mean cluster size as function of time at various temperatures.

At 1000 K, the four systems (C₆₀, C₈₀, C₁₈₀ and C₂₄₀) show different behaviors. The average size of C₆₀ and C₈₀ clusters does not exceed 1.35 fullerenes (Curves a2 and b2 in Figure 2) and the percentages of monomers in the systems are ~ 80% for C₆₀ and ~ 60% for C₈₀ at the end of 1 ns simulation. C₆₀ and C₈₀ nuclei are constantly formed but they dissociate because of thermal fluctuations and the majority of the clusters exist as dimers. Differently, in these conditions, C₁₈₀ and C₂₄₀ systems still show nucleation events. At 2000 K, only the biggest molecules - C₂₄₀ - present some nucleation events.

III. Future Work

The goal of this study is to relate the results obtained using MD simulations to the nucleation process occurring in flame environments, characterized by the presence of gaseous species along with nanoparticles. We will therefore study different configurations and relate the gas-phase species distributions and temperature to nucleation rates.

Experimental work is in progress for simple fuels. Measurements will provide spatial distributions of polycyclic aromatic hydrocarbons and other gas-phase species and size and composition of incipient soot nanoparticles for comparison with model results.

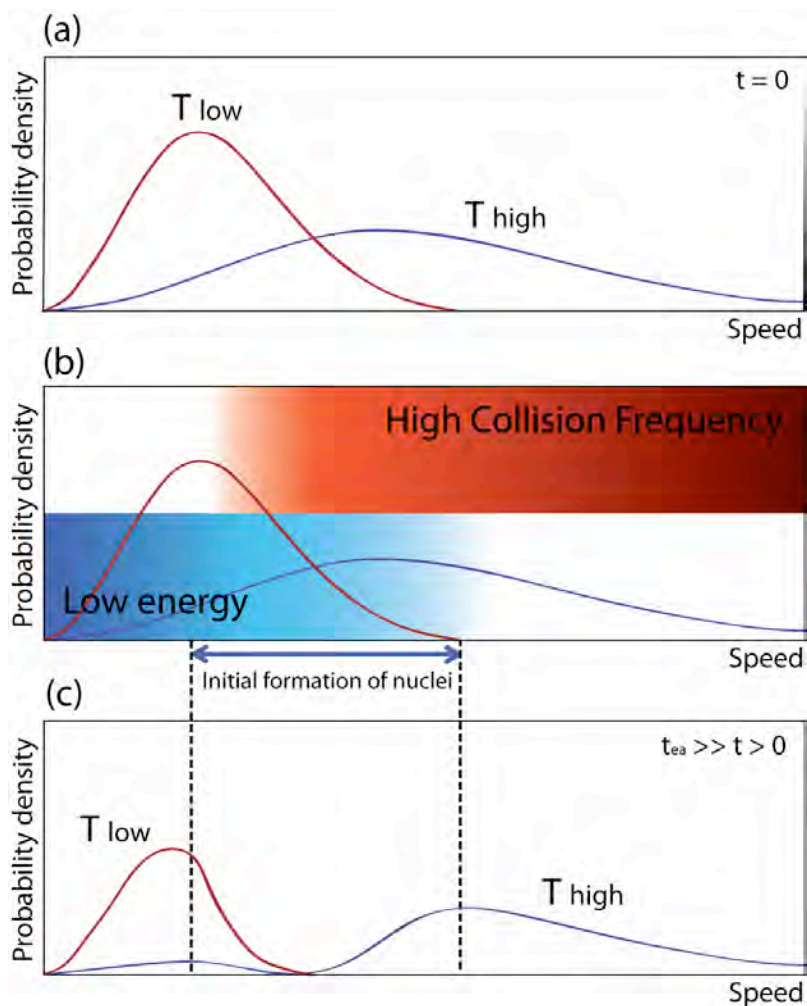


Figure 2. Speed probability density functions of molecules at two temperatures using the Maxwell-Boltzmann distributions.

IV. References

- i. Girifalco, L.A.; *J. Phys. Chem.* **1992**, 96, 858.
- ii. Girifalco, L.A.; Hodak, M.; and Lee, R.S. *Phys. Rev.* **2000**, 62, 13104.
- iii. Yannoni C.S.; Johnson, R. D.; Meijer, G.; Bethune, D.S.; Salem, J.R. *J. Phys. Chem.* **1991**, 95, 9.
- iv. Wedekind, J.; Reguera, D.; Strey, R. *J. Chem. Phys.* **2007**, 127, 064501.
- v. Smith, W.; Forester, T. R. *J. Mol. Graph.* **1996**, 14, 36.

V. Publications and submitted journal articles supported by this project 2006-2008

1. S.H. Chung, A. Violi “Nucleation of Fullerenes as a Model for Examining the Formation of Soot” *J. Chemical Physics*, 2010, in press.

Ultrafast Structural Dynamics in Combustion Relevant Model Systems

Peter M. Weber
Department of Chemistry
Brown University, Providence, Rhode Island 02912
Peter_Weber@brown.edu

I. Program Scope

Rydberg electrons are uniquely capable sensors of the geometric structure of molecular ion cores: As the Rydberg electron passes the ion core it experiences a phase shift that depends on the geometrical arrangement of all atoms and charges in the molecule. The phase shift, in turn, determines the binding energy of the Rydberg electron. Thus, the measurement of the Rydberg electron binding energy provides a measure of the molecular structure. In our experiments, the Rydberg electron binding energies are observed by photoionization-photoelectron spectroscopy. Because the experiment is done with ultrafast time resolution, we can characterize molecular structures through photoelectron spectroscopy of Rydberg states.

The spectroscopy of the structure-sensitive Rydberg electron binding energies has several intriguing characteristics. Because the entire Franck-Condon envelope is enclosed in a narrow band originating from the electronic transition, the spectra are insensitive toward internal energy. The method can therefore be used to explore molecules at high temperatures, or very high internal energies such as encountered when they undergo a chemical reaction. Importantly, because the number of Rydberg states is determined by the radial and angular momentum quantum numbers of hydrogenic systems, the complexity of the spectra does not scale with the size of the molecule. As a result, the method can be applied to fairly large molecules. Because the Rydberg electron's orbit is large, it covers the entire molecule. Therefore, the shape specificity covers the global molecular structure. In our experiments we have found that it is possible to distinguish isomeric and conformeric forms even of large molecules. Finally, it is straightforward to extend the method to the time-domain, thereby providing us with a uniquely capable tool for ultrafast structural dynamics experiments.

To implement Rydberg ionization spectroscopy we use a pump-probe multi-photon ionization/photoelectron scheme in which a first laser pulse excites the molecule to a Rydberg state, and a probe pulse ionizes the molecule. Photoelectrons are detected and their kinetic energies are analyzed using a time-of-flight detector. The photoelectron spectrum directly provides the binding energy of the electron, and thereby reveals the molecule's time-dependent structural fingerprint. The time resolution of the measurement is given by the duration of the laser pulses, which in our experiment is on the order of 100 fs. The spectral resolution is limited by the bandwidth of the laser and, for fast electrons, the resolution of the photoelectron spectrometer. To measure structural dynamics in Rydberg-excited states we time-delay the ionization photon from the pump photon. To measure the dynamics in ground or excited valence states we induce the dynamics using a near UV laser pulse, and use a multi-photon ionization scheme via the

Rydberg state as a probe process. Helpful in this context is that there are often many Rydberg states on the way to ionization, so that the likelihood of observing the fingerprint spectra for a given molecule is quite large.

II. Recent Progress

Electronic curve crossing dynamics in cyclic polyenes

Electronic curve crossing reactions through conical intersections are at work in the opening and closing of hydrocarbon rings containing double bonds. These mechanisms are also in play in the formation of soot during combustion processes. We have continued our studies of the electronic conversion dynamics in cyclopentadienes and cyclohexadienes. Once excited to the optically active 1^1B_2 surface, these molecules quickly convert to the 2^1A_1 state. From there, a conical intersection leads down to the molecular ground state, leaving the molecule in either an open or a closed form.

We have succeeded in following this path from the initial excitation to the final product state. Ionization with one, two, or three photon provides views of the molecules in the 1^1B_2 , the 2^1A_1 , and the 1^1A_1 ground state.

As previously reported, we find that the cyclopentadiene systems cross the electronic states such that the ground state molecular structure is completely recovered (figure 1, 2009 report). Consequently, the binding energies of the Rydberg states that we observe during the curve crossing process do not change with time. In contrast, in the cyclohexadiene systems, we observed that the crossing through the conical intersections leads to a depletion of the original structure, and the creation of a new structure, i.e. the 1,3,5 hexatrienes.

The sensitivity of the Rydberg spectra coupled with their narrow line shapes even when large amounts of internal energy are present allows us to follow the time-dependent molecular structures. In CHD, we have now been able to observe the structural signature of the ring opening while it happens. When the molecule is ionized out of the ultrashort lived, transient 2^1A_1 state, we observe the Rydberg states that are passed during the ionization transition with the two probe photons. The binding energies of those Rydberg orbits change with delay time, see figure 1: all

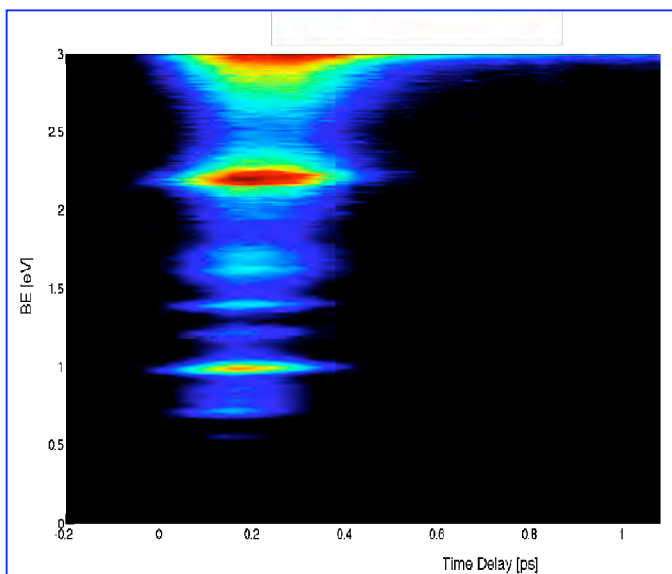


Figure 1: The Rydberg fingerprints of 1,3 cyclohexadiene during the electronic curve crossing. Note that all the Rydberg peaks change their binding energies on an ultrafast time scale, reflecting the structural dynamics.

the sharp peaks are slanting upward with increasing delay time. This constitutes the first truly structural dynamics observation of the ring opening process while it happens!

The analysis of the binding energy spectra uses peak fits of the Rydberg lines. A preliminary analysis shows that the rates of change of the Rydberg electron binding energies depend on the Rydberg orbit. This is understandable as different Rydberg states probe the molecular structures in different ways. Ongoing experimental work seeks to improve the time resolution of the experiment, while the analysis focuses on the deconvolution of the time dependent peak position information.

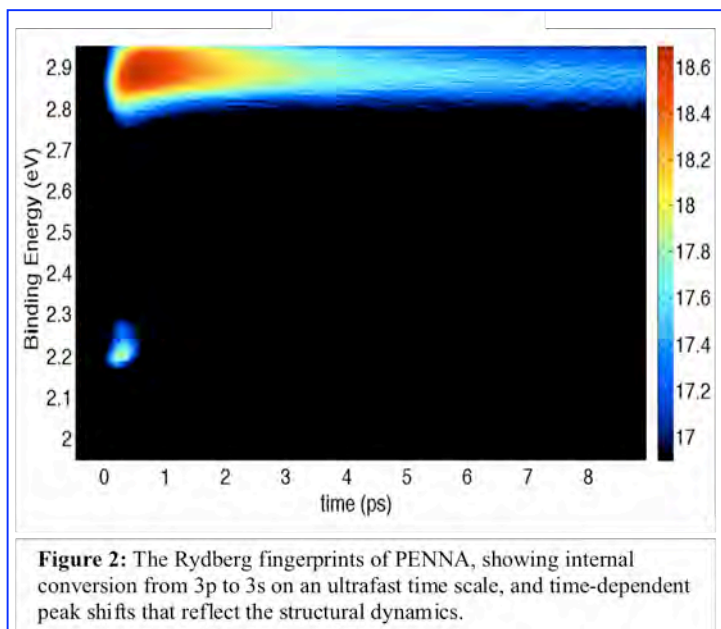
Ultrafast Dynamics of flexible model systems: formation of a cation- π bond

Like all chemical reactions, conformeric transitions depend strongly on the potential energy landscape and the temperature at which the system is observed. We seek to explore conformational transformations in model systems under varying experimental conditions. Our measurements can serve as important benchmarks that can be compared to computational results.

From the conformer distributions at the beginning and the end of a reaction one can infer the relative depths of the minima in the potential landscape.

In phenyl ethyl N,N dimethyl amine (PENNA) we observe a rapid internal conversion from 3p (BE=2.2 eV) to 3s (BE = 2.9 eV) (figure 2). The initial conformer distribution in 3p reflects the structures present in the neutral ground state molecules. Rapid planarization of the

molecule is evident by the peak shift on a very fast, femtosecond time scale. On a slower, picosecond time scale, we note that the position of the 3s band, observed at around 2.9 eV, is shifting with time. Upon excitation to the Rydberg state, PENNA has two structurally active components: the positive charge at the amine ion core, and the aromatic electrons at the phenyl ring. The interaction between those two moieties drives a structural rearrangement that leads to the formation of a cation- π bond. It is this structural motion, which competes with a curve crossing to a dissociative state as seen from the rapid and biexponential intensity profile, which leads to the Rydberg electron binding energy shift.



III. Future Plans

The Rydberg fingerprint method continues to be very rewarding for the study of molecular dynamics on ultrafast time scales. We will continue our work along several lines. First, we will continue to explore dynamics in model systems. This includes the derivatives of the cyclic polyenes, where our efforts are directed to further observe and analyze the time-dependent Rydberg energy shifts. Current experimental work is directed toward improving the time resolution, so that the peak shifts can be observed with greater clarity. Work also continues in the mapping of conformeric dynamics in model systems with internal degrees of freedom. Of particular interest to combustion and soot formation are molecules with flexible hydrocarbon chains.

We will also continue our collaborations with theorists to calculate the Rydberg electron binding energies using model systems. The goal of that work is to better understand how attributes of the molecular structure determine the binding energy.

Finally, we will seek to construct a new spectrometer that will permit the coincident observation of mass spectra and Rydberg spectra. This instrument will be uniquely useful in many applications, in particular the analysis of flames.

IV. Publications resulting from DOE sponsored research (2008 - 2010)

1. "Ultrafast Curve Crossing Dynamics through Conical Intersections in Methylated Cyclopentadienes," Fedor Rudakov and Peter M. Weber, in print, JPC-A.
2. "Electron Diffraction with Bound Electrons: the Structure Sensitivity of Rydberg Fingerprint Spectroscopy" Xiao Liang, Michael G. Levy, Sanghamitra Deb, Joseph D. Geiser, Richard M. Stratt, and Peter M. Weber, in print, JMS.
3. "Ground State Recovery and Molecular Structure upon Ultrafast Transition through Conical Intersections in Cyclic Dienes," Fedor Rudakov and Peter M. Weber, *Chemical Physics Letters* 470, pp 187-190, (2009).
4. "Excited-state ions in femtosecond time-resolved mass spectrometry: An investigation of highly excited chloroamines", R. Y. Brogaard, N. Rusteika and T. I. Sølling, F. M. Rudakov and P. M. Weber, *J. Phys. Chem. A*, 2009, 113 (1), pp 40–43.
5. "Electronic Spectroscopy and Ultrafast Energy Relaxation Pathways in the lowest Rydberg States of Trimethylamine," Job D. Cardoza, Fedor M. Rudakov and Peter M. Weber; *J. Phys. Chem. A*, 2008, 112 (43), pp 10736–10743.
6. "Identification of isomeric flame components by Rydberg ionization spectroscopy," J. D. Cardoza, F. M. Rudakov, N. Hansen, P. M. Weber, *Journal of Electron Spectroscopy and Related Phenomena*, 65, 15–20 (2008).

Probing Flame Chemistry with MBMS, Theory, and Modeling

Phillip R. Westmoreland

Department of Chemical and Biomolecular Engineering, North Carolina State University

Raleigh, NC 27695-7905

phil.westmoreland@ncsu.edu

I. Program Scope

The objective of this research is obtaining kinetics of fuel combustion and molecular-weight growth in flames. Our approach combines molecular-beam mass spectrometry (MBMS) experiments on low-pressure flat flames; ab initio thermochemistry and transition-state structures; rate constants predicted by transition-state and chemical activation theories; whole-flame modeling using sets of elementary reactions; and hypothesis, inference, and testing of reaction mechanisms.

MBMS is a particularly powerful technique because it can be used to measure a wide range of species quantitatively, including radicals, with minimal flame perturbation. By using two complementary instruments, we obtain remarkably complete sets of flame data that are useful for direct insights, testing of mechanistic models, and selected measurement of rate constants. Our electron-ionization quadrupole MS (presently being moved to North Carolina State University from UMass Amherst) provides species profiles with high signal sensitivity and mass resolution. At the Advanced Light Source (ALS) at LBNL, we obtain species profiles with more precise isomer resolution and identification using time-of-flight MS with VUV photoionization. Professor Westmoreland is part of the team of DOE-BES contractors - Terry Cool (team leader), Andy McIlroy, Craig Taatjes, and Nils Hansen - that has developed this system. Additional collaborators in making measurements include the group of Katharina Kohse-Höinghaus of Universität Bielefeld, while DOE-BES contractors Jim Miller, Stephen Klippenstein, Charlie Westbrook, and Fred Dryer have collaborated in modeling thermochemistry, kinetics, and flame structure.

II. Recent Progress

A. Data from the MBMS systems

Flames of a wide range of hydrocarbon and biomass-related fuels have been mapped by our team of researchers at the Advanced Light Source at Lawrence Berkeley National Laboratory in the past year:

- Ethyne (acetylene) at $\phi=1.0$ and 2.41;
- C_6H_{12} isomers at $\phi=1.7$: Cyclohexane, 1-hexene, methylcyclopentane, 3,3-dimethylbutene; also 1-hexene at $\phi=0.70$, 1.0, and 2.0;
- Methylcyclohexane $\phi=2.0$ (complementing previous $\phi=1.75$ data);
- n-Heptane at $\phi=1.7$;
- Iso-octane at $\phi=1.7$;
- Toluene+ CH_4 and toluene+ C_2H_2 mixtures at $\phi=1.5$;
- Biofuel model compounds with N: Ethylamine at $\phi=1.3$; dimethyl amine at $\phi=1.0$ and 1.3;
- Esters at $\phi=1.2$ as biofuel model compounds: ethyl formate, methyl propenoate (and at 1.56), ethyl propenoate (and at 1.56), ethyl propanoate (and at 1.56), methyl butanoate (and at 1.56), methyl isobutanoate (and at 1.56), methyl acetate, vinyl acetate (and 1.56), ethyl acetate, methyl crotonate, methyl methacrylate (1.56 only);
- Tetrahydropyran, the monoether analogue to cyclohexane, at $\phi=1.0$ and 1.75.

B. Modeling of cyclohexane flames reveals pathways and cycloalkane generalizations.

The influences of stoichiometry on cyclohexane combustion and benzene-formation pathways were analyzed using detailed data from low-pressure, premixed, flat flames at stoichiometric and fuel-rich conditions ($\phi=1.0$, cyclohexane/ O_2 /32.5% Ar, 30 Torr, 35.0 cm/s burner velocity at 298 K; $\phi=2.0$, cyclohexane/ O_2 /30% Ar, 30 Torr, 50.0 cm/s). We obtained 70 and 40 stable and radical species in the stoichiometric and fuel-rich flames, respectively. For modeling, we used a newly revised reaction set.

Numerous improvements were added, most notably the new 1-hexene decomposition kinetics of Kiefer *et al.* (*J. Phys. Chem. A* **2009**) and additional treatments of falloff.

Fuel destruction was dominated by H-abstractions to make cyclohexyl, followed by beta-scissions to hex-5-enyl and some cyclohexyl with subsequent H-abstractions, beta-scissions, and oxidation of the small alkenes.

The simulation showed that in $\phi=1.0$ flame, cyclohexane was solely destroyed via H-abstractions to generate cyclohexyl, and initial aromatic species were formed by sequential dehydrogenation, as previously proposed by Law *et al.* (2007). The majority of cyclohexyl destruction was to linear 5-hexenyl, which can further isomerize to 2-hexenyl; both 5-hexenyl and 2-hexenyl decomposed to form smaller C_2 and C_4 alkyls. A small fraction of cyclohexyl consumption was through H-by-H stepwise dehydrogenation, leading toward cyclohexene, cyclohexenyl, cyclohexadiene, cyclohexadienyl, and finally benzene. Nevertheless, this route provided the main benzene formation pathway (more than 72%), and the contribution from small-radical additions and combinations was small.

At the fuel-rich condition, H-abstraction still dominated cyclohexane consumption, although isomerization into 1-hexene appears to contribute about 10%. The dominant effect of richer stoichiometry was lower OH and O-atom, leading to higher abundance of small alkyls. Benzene formation through stepwise cyclohexane dehydrogenation still contributed, but small-alkyl routes increased to become dominant. Benzene formation was predicted to be dominated by C_4+C_2 associations (46%, mostly from $i/n-C_4H_5+C_2H_2$ directly and through fulvene), H_2 elimination from 1,3-cyclohexadiene and beta-scission from cyclohexadienyl (20% and 10%, respectively, with both precursors from stepwise dehydrogenation), and from C_3H_3 via $C_3H_3+C_3H_3$ directly and $C_3H_3+C_3H_3$ and C_3H_3 +allyl via fulvene (9% total).

Comparison of cyclohexane combustion pathways to those of acyclic alkanes reveals insights that extend to cycloalkanes in general. First, H-abstraction from cycloalkanes should dominate fuel destruction, as with acyclic alkanes. However, from cycloalkyls, beta-scission ring-breaking or H-elimination both lead to forming allylic positions in the fuel-destruction intermediates, unlike acyclic alkanes. Two potential consequences are (1) steering intermediates toward even-carbon-number products vs. odd-carbon-number intermediates and (2) stepwise dehydrogenation to an aromatic ring

C. Modeling of 1-hexene flames shows fuel destruction by thermal decomposition.

Modeling a fuel-rich ($\phi=2.0$) 1-hexene flame measured by the ALS team shows that decomposition is its dominant fuel-destruction pathway, an uncommon route for hydrocarbon fuels. This fuel is dominantly destroyed by decomposition to allyl and *n*-propyl, again based on the new Kiefer *et al.* kinetics (2009). In flames, fuels are generally destroyed by low-activation-energy radical attack: H abstraction for saturated molecules, and for unsaturated species like alkenes, alkynes, and aromatics, some combination of H abstraction and chemically activated radical additions like $O+C_2H_2 \rightarrow H+HCCO$. Another, earlier exception to this generalization we have seen is 1,3-butadiene [Paper 7], where concerted decomposition to $H_2CC+C_2H_4$ proceeded at a rate nearly as fast as the dominating H-abstraction mechanism at $\phi=2.4$, although it was less comparable at $\phi=1.8$.

Two aspects account for this unusual behavior in 1-hexene. First, its central, allylic C-C bond is much weaker than other C-C sigma bonds, causing the high-pressure-limit rate constant for decomposition to be higher at a given temperature. Second, 1-hexene has more rovibrational degrees of freedom than smaller molecules, reducing falloff in its decomposition rate constant. Thus, this rate constant is closer to the high-pressure rate constant than is the case for smaller molecules, and so it can compete favorably with abstraction kinetics, which is pressure-independent.

As with most of our flames, we are also interested in formation routes to the first aromatic ring of benzene or phenyl. Chemically activated combination of propargyl with allyl was dominant, based on the new rate constants computed by Miller *et al.* (*J. Phys. Chem. A* **2010**, doi:10.1021/jp910604b). This reaction formed fulvene, and the main route to benzene (64%) was H +fulvene \rightarrow benzene+H, a chemically activated addition/isomerization/decomposition. Chemically activated combination of propargyl with itself was included using the recent rate constant of Georgievskii, Miller, and Klippenstein (*Phys. Chem. Chem. Phys.* **2007**, doi:10.1039/b703261g) but was predicted to contribute only 15%. The

prominence of $C_3H_5+C_3H_3$ is due to allyl formation directly from the fuel and to rapid formation of C_3H_3 from allyl via C_3H_4 intermediates.

D. PrIME-based data handling and model analysis promises to aid model analysis.

With DOE contractor Michael Frenklach, we are working to use PrIME to archive the ALS flame team's unique set of raw and processed data. PrIME (primekinetics.org) is presently a virtual archive of detailed scientific data for experiments, thermochemistry, and reaction mechanisms of flame chemistry.

We have initially begun by inserting processed data: Analyzed mole-fraction profiles, temperature profiles, and metadata about the apparatus and experimental condition. We are also collaborating to create an "Instrument Model" of the system that can take the raw, unprocessed data (signal counts at a given burner position, ionizing photon energy, and m/z) and process it with photoionization cross-section and other calibration data, isotopic corrections (because of natural abundances of ^{13}C and 2H such as in benzene contribution to mass 80), mass-discrimination factor, photon-energy interferences and calibrations, experimental settings, and so on. This approach allows easier incorporation of new information such as newly measured PI cross-sections, as well as improved uncertainty quantification (UQ) of the data.

A future intent of our collaboration is to create a new cloud-based analysis of uncertainty quantification, the "Data Collaboration" method, that will allow both fast, more accurate UQ of the elementary-reaction-based model and dramatically improved testing against the data. Data Collaboration is a framework designed to make inferences from heterogeneous experimental observations in the context of a common underlying model. For example, consider data on methane combustion from a diverse range of experiments and analytical methods, as in the work that developed the chemical reaction set GRIMech 3.0 [Smith et al., 2000]. UQ of the experimental data and of the model parameters can be combined to assess model agreement with the data. Combining a large number of experiments, it should be possible to infer values and precision of the model parameters.

III. Future Work

We will conduct complementary experiments at NC State and at the ALS on mixed flames of acetylene, benzene, toluene, and their mixtures along with modeling at UMass Amherst. The dual purposes are to establish fuel-conversion kinetics and the formation and destruction chemistry of polycyclic aromatic hydrocarbons, using these fuels to focus on indene and naphthalene. Upcoming experiments will also study oxidation chemistry of JP-10, a liquid, single-compound, multi-cyclic $C_{10}H_{16}$ fuel chemically specified as exo-tetrahydrodicyclopentadiene or more formally as exo-tricyclo[5.2.1.0^{2,6}]decane. This fully hydrogenated dicyclopentadiene is of scientific interest because of its multi-ring alkane structure, providing a demanding test of our hypotheses about flame kinetics of cycloalkanes.

The ALS system has great power to resolve and identify isomers, while the NCSU system has a valuable role because it has higher signal sensitivity, especially for radicals, can be run at more fuel-rich conditions, and is more suitable for the thermocouple measurements. Our group will also seek to coordinate flame data-handling and modeling for the research team, and we will participate in the team objectives of improving the mass and signal sensitivity of the ALS apparatus and of studying flame kinetics for other hydrocarbons, biofuel analogues, and amines.

IV. Publications and submitted journal articles supported by this project 2008-2010

1. "Imaging' Combustion Chemistry via Multiplexed Synchrotron-Photoionization Mass Spectrometry." *Phys. Chem. Chem. Phys.* **10**, 20-34 (2008); [dx.doi.org/10.1039/b713460f](https://doi.org/10.1039/b713460f)
2. N. Hansen, S.J. Klippenstein, P.R. Westmoreland, T. Kasper, K. Kohse-Höinghaus, J. Wang, T.A. Cool, "A Combined ab initio and Photoionization Mass Spectrometric Study of Polyynes in Fuel-Rich Flames," *Phy. Chem. Chem. Phys.* **10**, 366-374 (2008); [dx.doi.org/10.1039/b711578d](https://doi.org/10.1039/b711578d)
3. J. Wang, U. Struckmeier, B. Yang, T. A. Cool, P. Osswald, K. Kohse-Höinghaus, T. Kasper, N. Hansen, P. R. Westmoreland, "Isomer-specific influences on the composition of reaction

- intermediates in dimethyl ether/propene and ethanol/propene flames,” *J. Phys. Chem. A* **112**(39), 9255-9265 (2008); dx.doi.org/10.1021/jp8011188
4. N. Hansen, T. A. Cool, K. Kohse-Höinghaus, P. R. Westmoreland, “Recent Contributions of Flame-Sampling Molecular-Beam Mass Spectrometry to a Fundamental Understanding of Combustion Chemistry,” *Prog. Energy Comb. Sci.* **35**(2) (2009) 168-191; dx.doi.org/10.1016/j.pecs.2008.10.001
 5. C. K. Westbrook, W. J. Pitz, P. R. Westmoreland, F. L. Dryer, M. Chaos, Patrick Oßwald, K. Kohse-Höinghaus, T. A. Cool, J. Wang, B. Yang, N. Hansen, T. Kasper, “A Detailed Chemical Kinetic Reaction Mechanism for Oxidation of Four Small Alkyl Esters in Laminar Premixed Flames,” *Proc. Combust. Inst.* **32** (2009) 221-228.
 6. A. Lucassen, Patrick Oßwald, U. Struckmeier, K. Kohse-Höinghaus, T. Kasper, N. Hansen, T. A. Cool, P. R. Westmoreland, “Species identification in a laminar premixed low-pressure flame of morpholine as a model substance for oxygenated nitrogen-containing fuels,” *Proc. Combust. Inst.* **32** (2009) 1268-1276.
 7. N. Hansen, J. A. Miller, T. Kasper, K. Kohse-Höinghaus, P. R. Westmoreland, J. Wang, T. A. Cool, “Benzene Formation in Premixed Fuel-Rich 1,3-Butadiene Flames,” *Proc. Combust. Inst.* **32** (2009) 623-630.
 8. J. Wang, M. Chaos, B. Yang, T. A. Cool, F. L. Dryer, T. Kasper, N. Hansen, K. Kohse-Höinghaus, P. Oßwald, P. R. Westmoreland, “Composition of reaction intermediates for stoichiometric and fuel-rich dimethyl ether flames: Flame-sampling mass spectrometry and modeling studies,” *Phys. Chem. Chem. Phys.* **11** (2009) 1328-1339; dx.doi.org/10.1039/b815988b
 9. T. Kasper, P. Oßwald, U. Struckmeier, K. Kohse-Höinghaus, C.A. Taatjes, J. Wang, T.A. Cool, M.E. Law, A. Morel, P.R. Westmoreland, “The combustion chemistry of the propanol isomers investigated by electron ionization and VUV-photoionization molecular-beam mass spectrometry,” *Combustion and Flame* **156**:6 (2009) 1181-1201; doi:10.1016/j.combustflame.2009.01.023
 10. N. Hansen, J. A. Miller, P. R. Westmoreland, T. Kasper, K. Kohse-Höinghaus, J. Wang, T. A. Cool, “Isomer-Specific Combustion Chemistry in Allene and Propyne Flames,” *Combustion and Flame* **156** (2009) 2153-2164; doi:10.1016/j.combustflame.2009.07.014
 11. K. Kohse-Höinghaus, P. Oßwald, T. A. Cool, T. Kasper, N. Hansen, F. Qi, C. K. Westbrook, P. R. Westmoreland, “Aspects of biofuel combustion chemistry,” *Angewandte Chemie* (in press).
 12. N. Hansen, T. Kasper, B. Yang, T. A. Cool, W. Li, P. R. Westmoreland, P. Oßwald, K. Kohse-Höinghaus, “Fuel-Structure Dependence of Benzene Formation Processes in Premixed Flames Fueled by C₆H₁₂ Isomers,” *Proc. Combustion Institute*, **33** (accepted).
 13. N. Hansen, W. Li, M. E. Law, T. Kasper, P. R. Westmoreland, B. Yang, T. A. Cool, A. Lucassen, “The Importance of Fuel Dissociation and Propargyl + Allyl Association for the Formation of Benzene in a Fuel-Rich 1-Hexene Flame” (submitted).
 14. W. Li, M. E. Law, P. R. Westmoreland, T. Kasper, N. Hansen, J. Wang, T. A. Cool, K. Kohse-Höinghaus “Competing Paths for Aromatic Species Formation in Cyclohexane Premixed Flat Flames” (submitted).

SISGR: The effects of oxygenated fuel compound structure on combustion and pollutant reaction chemistry

Margaret S. Wooldridge

Departments of Mechanical and Aerospace Engineering, University of Michigan

Ann Arbor, MI 48109-2121

mswool@umich.edu

I. Program Scope

The increased use of biofuels presents an exciting opportunity to improve combustion performance while simultaneously reducing greenhouse gases and pollutant emissions. Realization of this potential, however, requires a more complete understanding of the fundamental reaction chemistry at conditions relevant to advanced combustion systems, i.e. moderate temperatures and elevated pressures. This research program focuses on understanding the elementary combustion chemistry of ester compounds (relevant to biofuels) through comprehensive experimental and modeling efforts. The effects of varying carbon content and chemical structure of representative esters are examined through ignition studies. Ignition delay time measurements are used to quantify the effects of the esters on the fuel reaction rates. Gas-speciation analysis is used to interrogate the effects of the esters on fuel decomposition and oxidation pathways and on sentinel species for particulate production (e.g. propene). Additionally, fundamental studies of strong and weak ignition phenomena are used to develop improved methods to quantitatively validate reaction kinetics at moderate temperatures and high pressures. The outcomes of this work provide quantitative assessment of the reaction pathways important in ester compounds as a function of the critical properties of the ester compounds at moderate pressures (5-20 atm) and temperatures (800-1300 K) directly relevant to modern combustion systems.

The chemical physics of oxygenated fuels is an area which, until recently, has seen little scrutiny from the fundamental combustion science community. The chemistry of OHCs presents an exciting area to apply our learning from HCs and adapt our methods to develop a similar level of predictive capabilities for elementary reaction theory and combustion reaction mechanisms. Many of our experimental, computational and analytical HC tools can be applied with relative ease; whereas others will require adaptation to accommodate the complexities introduced by the presence of the fuel-bound oxygen. The efforts to advance the elementary reaction theory for OHCs will require significant experimental validation of model predictions, with an emphasis on methods that have high sensitivity to the basic effects of molecular structure. Additionally, we have learned from HC combustion chemistry, that we improve our predictive capabilities by expanding our consideration to the broadest possible parametric space in terms of theoretical and experimental parameters.

Recent studies address deficiencies in the literature on quantitative understanding of the reaction chemistry of esters and other oxygenated hydrocarbons (e.g. methylbutanoate [1,2,3,4], dimethyl ether [5], dimethyl carbonate [6], butyl alcohols [7], isomers of $C_5H_{10}O_2$ esters [8], methyl acetate [9], ethyl formate [9], and other alkyl ethers [10] to name a few). However, there are still few data on high molecular weight compounds and which isolate the effects of structure on reaction chemistry. Our program objectives are to provide a quantitative understanding of the reactivity of key oxygenate compounds particularly in comparison to their hydrocarbon counterparts.

II. Recent Progress

The technical approach to meet the project objectives focuses on the reaction kinetics of ignition of reference compounds. Ignition kinetics are relevant to understanding radical pool formation and fuel decomposition and oxidation pathways. Specifically, we use the University of Michigan rapid compression facility (UofM RCF) to create the temperature and pressure conditions of interest for experimental ignition studies. We partner with Dr. Charlie Westbrook for our modeling studies. Details on the dimensions, components and performance characterization of the UofM RCF can be found in Donovan et al. [11]. Results of previous ignition studies using the UofM RCF including the experimental

approach used in this work can be found in Walton et al. [12] and He et al. [13], and results of previous gas sampling studies can be found in He et al. [14].

A. Speciation studies of methyl butanoate

We recently completed speciation studies of the intermediates formed during methyl butanoate ignition [a]. The gas sampling experiments were conducted at $P = 10.2$ atm and $T = 985$ K, mixtures of $\chi_{mb} = 0.96\%$, $\chi_{O_2} = 20.79\%$, $\chi_{N_2} = 52.89\%$, and $\chi_{Ar} = 25.25\%$, mole fraction, percent basis; corresponding to $\phi = 0.30$ and an inert gas to O_2 molar ratio of 3.76. Gas chromatography was used to identify and quantify stable intermediate species formed during ignition. Figure 1 below presents some results of species measured by rapid gas sampling from the test section of the RCF during ignition. The time axis is normalized to the ignition delay time, τ_{ign} . The model predictions for the time histories during methyl butanoate ignition are in excellent agreement for several species. Model analyses indicates OH/HO₂/H₂O₂ kinetics do dominate the methyl butanoate ignition behavior. Discrepancies observed for propene indicate the H-atom abstraction rate for the methyl butanoate 3 site may be slightly too low at the conditions studied.

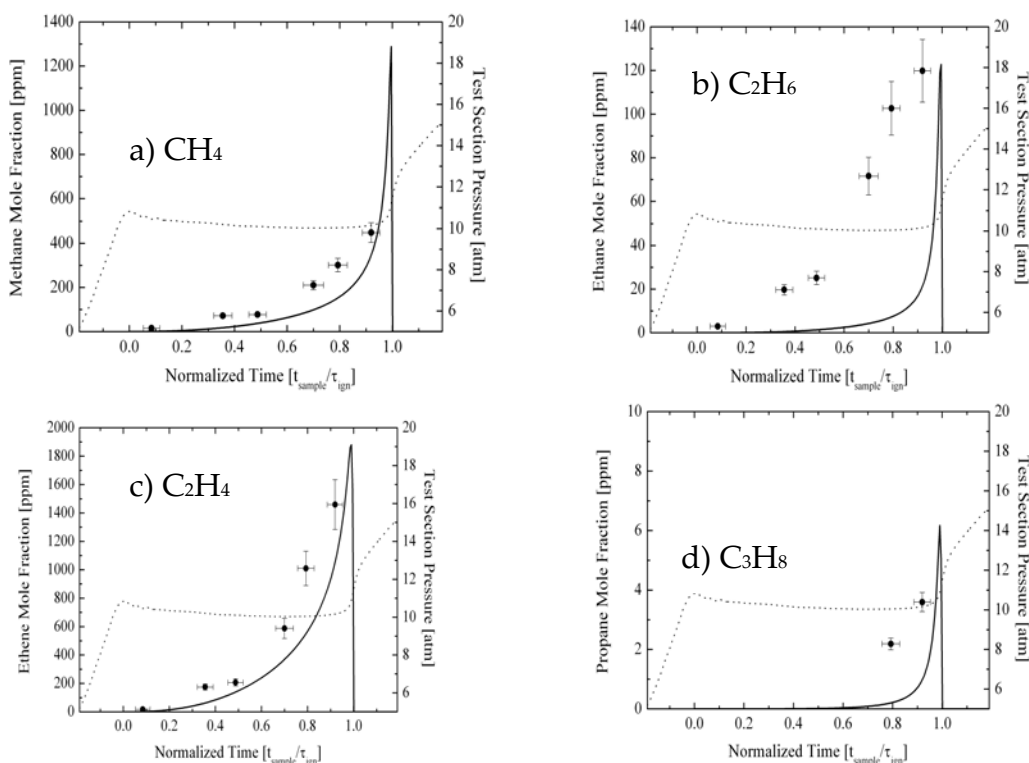


Figure 1. Comparison of measured (solid symbols) and predicted (solid lines) species time histories for methyl butanoate/air ignition studies. A typical pressure time history during ignition is provided for reference (dotted line). The experimental conditions are provided in the text.

B. Ignition studies of high molecular weight compounds

Experimental studies of long chain esters and hydrocarbons require modification of our experimental approach to create fuel/air mixtures of low vapor pressure compounds. We have adapted the UofM RCF for these studies by heating the driven section, test section and mixing manifold. For our initial studies, we investigated n-dodecane ignition. N-dodecane was selected for characterizing the modified experimental approach because it is an important reference alkane with strong negative temperature coefficient behavior at the conditions where we are interested. Our experiments target pressures from 3-10 atm and temperatures from approximately 700-840 K. These data are the only

experimental results of their kind at these conditions, and represent new contributions that complement the few experimental results currently available in the literature [15,16]. Results from a typical n-dodecane ignition experiment are presented in Fig. 2. Reaction during compression is expected to occur for n-dodecane at these conditions. Current work includes modeling of the compression and ignition processes including detailed reaction kinetics.

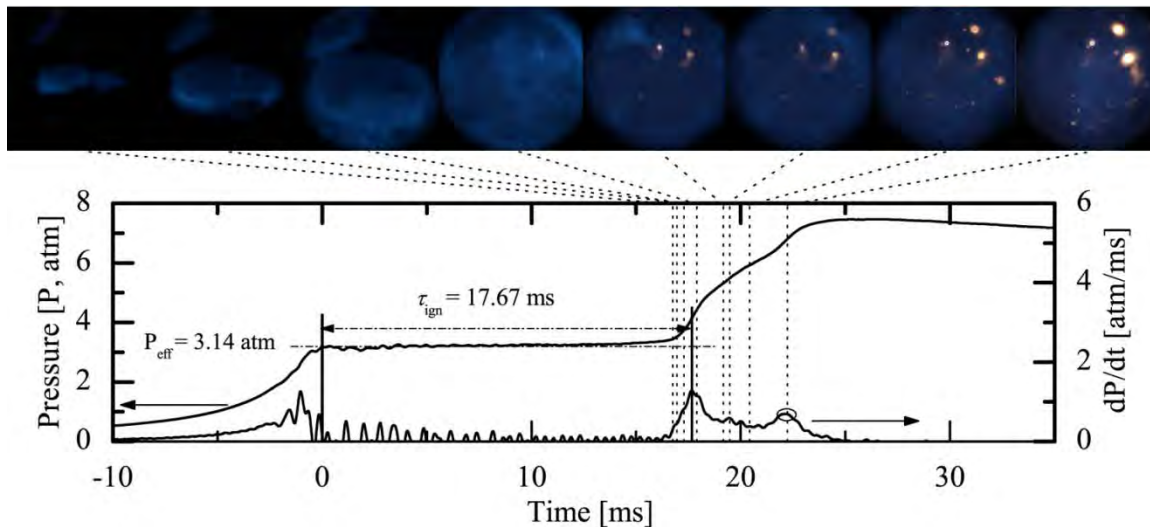


Figure 2: Results for n-dodecane ignition for conditions of $P_{eff} = 3.14$ atm, $T_{eff} = 745$ K, $\phi = 0.98$, Inert/O₂ = 3.77 and $\tau_{ign} = 17.76$ ms. The lower panel shows the pressure (P) in the test section and the rate of pressure rise (dP/dt). The end of compression corresponds to a time of $t = 0$ ms. The upper panel shows still images (end view) acquired at 26,000 fps of the chemiluminescence in the test section corresponding to various times during ignition (color adjusted for clarity).

III. Future Work

Our future work includes ignition and speciation studies of longer chain esters, as well as speciation studies of the intermediates formed during ignition of n-dodecane. We will also leverage our support to study blends of key hydrocarbon and oxygenate compounds.

IV. References

1. Westbrook, C. K., Pitz, W. J., Curran, H. J., (2006) "Chemical Kinetic Modeling Study of the Effects of Oxygenated Hydrocarbons on Soot Emissions from Diesel Engines," *J. Phys. Chem. A* **110** 6912.
2. Fisher, E. M., Pitz, W. J., Curran, H. J., Westbrook, C. K., (2000) "Detailed Chemical Kinetic Mechanisms for Combustion of Oxygenated Fuels," *Proc. Combust. Inst.* **28** 1579.
3. Walton, S. M., Wooldridge, M. S., and Westbrook, C. K., (2009) "An Experimental Investigation of Structural Effects on the Auto-Ignition Properties of Two C5 Esters" *Proc. Combust. Inst.*, **32** 255.
4. Milovanovic, N., Chen, R., Dowden, R., Turner, J., (2004) "An Investigation of Using Various Diesel-Type Fuels in Homogeneous Charge Compression Ignition Engines and Their Effects on Operational and Controlling Issues," *Int. J. Eng. Res.* **5**, 297.
5. Zheng, X.L., Lu, T.F., Law, C.K., Westbrook, C.K., Curran, H.J., Berces, T., Dryer, F.L., (2005) "Experimental and Computational Study of Nonpremixed Ignition of Dimethyl Ether in Counterflow," *Proc. Combust. Inst.* **30** 1101.
6. Glaude, P.A., Pitz, W.J., Thomson, M.J., Pitz, R., (2005) "Chemical Kinetic Modeling of Dimethyl Carbonate in an Opposed-Flow Diffusion Flame," *Proc. Combust. Inst.* **30** 1111.

7. McEnally, C.S., Pfefferle, L.D., Taatjes, C., Tsang, W., Hippler, H., (2005) "Fuel Decomposition and Hydrocarbon Growth Processes for Oxygenated Hydrocarbons: Butyl Alcohols," *Proc. Combust. Inst.* **30** 1363.
8. Schwartz, W.R., McEnally, C.S., Pfefferle, L. D., (2006) Decomposition and Hydrocarbon Growth Processes for Esters in Non-Premixed Flames," *J. Phys. Chem. A* **110** 6643.
9. Osswald, P., Struckmeier, U., Kasper, T., Kohse-Höinghaus, K., Wang, J., Cool, T. A., Hansen, N., Westmoreland, P. R., (2007) "Isomer-Specific Fuel Destruction Pathways in Rich Flames of Methyl Acetate and Ethyl Formate and Consequences for the Combustion Chemistry of Esters," *J. Phys. Chem. A*.
10. McEnally, C.S., Pfefferle, L.D. (2004) "Experimental Study of Fuel Decomposition and Hydrocarbon Growth Processes for Practical Fuel Components in Nonpremixed Flames: MTBE and Related Alkyl Ethers," *Int. J. Chem. Kin.* **36** 345.
11. Donovan, M. T., He, X., Zigler, B.T., Palmer, T.R., Wooldridge, M.S., Atreya, A. (2004) "Demonstration of a Free-Piston Rapid Compression Facility for the Study of High Temperature Combustion Phenomena" *Combust. Flame*, **137** 351.
12. Walton, S. M., Wooldridge, M. S., and Westbrook, C. K., (2009) "An Experimental Investigation of Structural Effects on the Auto-Ignition Properties of Two C5 Esters" *Proc. Combust. Inst.*, **32** 255.
13. He, X., Donovan, M.T., Zigler, B.T., Palmer, T.R., Walton, S. M., Wooldridge, M.S., Atreya, A., (2005) "An Experimental and Modeling Study of Iso-octane Ignition Delay Times under Homogeneous Charge Compression Ignition Conditions," *Combust. Flame* **142** 266.
14. He, X., Walton, S.M., Zigler, B.T., Wooldridge, M.S., Atreya, A., (2007) "An Experimental Investigation of the Intermediates of Iso-octane During Ignition," *Int. J. Chem. Kinet.* **39** 498.
15. Vasu, S.S., Davidson, D.F., Hong, Z., Vasudevan, V., Hanson, R.K., (2009) "N-Dodecane Oxidation at High-Pressures: Measurements of Ignition Delay Times and OH Concentration Time-Histories," *Proc. Combust. Inst.* **32** 173.
16. Shen, H.-P. S., Steinberg, J., Vanderover, J., Oehlschlaeger, M.A. (2009) "A Shock Tube Study of the Ignition of n-Heptane, n-Decane, n-Dodecane, and n-Tetradecane at Elevated Pressures," *Energy and Fuels*, **23**, 2482.

V. Publications and submitted journal articles supported by this project 2008-2010

- a. Walton, S. M., Karwat, D. M., Teini, P. D., Gorny, A., and Wooldridge, M. S., "Speciation Studies of Methyl Butanoate Ignition," in preparation, 2010.

THEORETICAL STUDIES OF THE REACTIONS AND SPECTROSCOPY OF RADICAL SPECIES RELEVANT TO COMBUSTION REACTIONS AND DIAGNOSTICS

DAVID R. YARKONY

DEPARTMENT OF CHEMISTRY, JOHNS HOPKINS UNIVERSITY, BALTIMORE, MD 21218

yarkony@jhu.edu

We continue our work on anion photoelectron spectra that describe states of a neutral that are strongly coupled by conical intersections. As part of a study of alkoxide photoelectron spectra, we have finished simulations of the photoelectron spectrum (PES) of ethoxide. A simulation of the related hydroxymethoxide anion has begun. We are also studying nonadiabatic photodissociation of the 1-hydroxyethyl radical, which builds on our previous work on hydroxymethyl radical.

As part of other funded research, we are developing new computational tools which will significantly impact our DoE funded research effort. A new, general, approach to describing strongly coupled adiabatic potential energy surfaces and their interstate interactions, based on quantifiably quasi-diabatic coupled state diabatic Hamiltonians, has been reported.¹ This tool will enable us to study the dynamics of nonadiabatic photodissociation. A theory of nonadiabatic electron scattering that takes full account of electron exchange and nonorthogonality effects has been developed. This will enable us to determine the partial photodissociation cross sections needed for a completely first principles simulation of a PES. A brief overview of these methods and their implications for our DoE funded research is provided.

I. Photoelectron Spectra of States Strongly Coupled by Conical Intersections

A. Ethoxide

We have completed our computational determinations and analyses of the photoelectron spectra of the alkoxides, isopropoxide (previously reported),² and ethoxide³ which yield the spectra of isopropoxy and ethoxy, respectively. This work complements experimental work in the groups of Lineberger,⁴ Neumark,⁵ and Terry Miller⁶. The unique computational tools we developed that have enabled us to simulate these nonadiabatic spectra have been described previously.⁷⁻⁹ The ethoxy radical, and other alkoxy radicals, play key roles in the chemistry of the troposphere¹⁰ and in the combustion of fossil fuels.¹¹ The PES of ethoxide has been measured by Lineberger's group⁴ and Neumark's group⁵ has reported a slow electron velocity-map imaging (SEVI) measurement. As a substitutional isomer of methoxy with a single H replaced by a methyl group, ethoxy is expected to have two low-lying states, an ²A" and an ²A' state, corresponding to the ²E state of methoxy, that are strongly coupled by conical intersections. In Fig. 1 below we compare our nonadiabatic simulation of

the ethoxide PES with the measured result of Lineberger.⁴

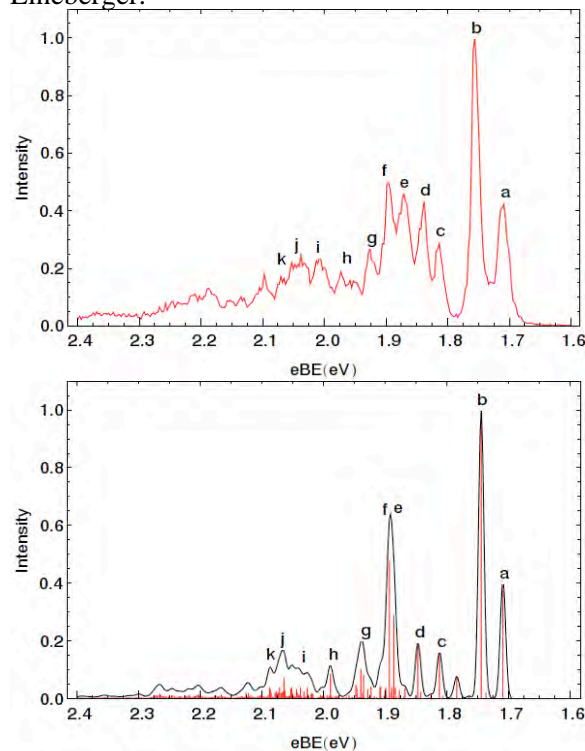


Figure 1: Photoelectron spectrum of ethoxide- h_5 (Ref. ³) lower plate compared with the experimental spectrum from Lineberger's group⁴ in upper plate. The computed spectrum is convoluted with a $10 \text{ meV} = 80.7 \text{ cm}^{-1}$ gaussian to simulate the instrumental resolution.

Good agreement between the measured and calculated spectra is seen with the exception of lines e and f which are too close in the simulation. These are challenging calculations, as evidenced by the fact that although the measured spectra are almost a decade old,⁴ our simulations were the first nonadiabatic simulations reported for ethoxy and isopropoxy. Simulations that ignore the effects of conical intersections are not able to reproduce this spectrum.⁴

One of the more interesting results to emerge from this study concerns the near threshold results of Neumark's, high resolution SEVI spectrum of ethoxide.⁵ The results of his study are summarized in Fig. 2. The thick black lines are the SEVI levels reported by Neumark. The lines labeled a and b agree with lines labeled a and b by Lineberger and well described in our ground state anion simulation (the red, solid line, peaks in Fig. 2).

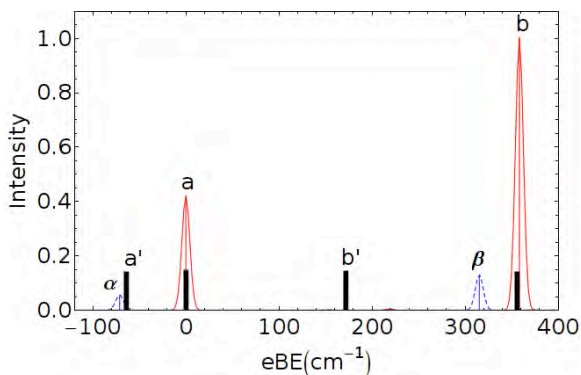


Fig. 2 Low energy portion of \mathbf{H}^d based PES showing sequences built on zero (red peaks, solid lines) and one (blue peaks, dashed lines) quantum in mode $\omega_7(a'')$. 10 cm^{-1} gaussian convolution used. Solid bars denote, from left to right, the peaks denoted a' , a , b' , b from SEVI spectrum of Neumark.⁵

The assignment of the line a' observed by Neumark at $\sim 63 \text{ cm}^{-1}$ to the red of a was perplexing. The separation of the lowest two lines in the isopropoxy spectrum is $\sim 66 \text{ cm}^{-1}$.¹⁶ Are these two results related? In isopropoxy, we assigned this splitting to the $\tilde{X}^2A - A^2A$ transition with the separation due principally to the spin-orbit interaction.² This, we explained, could not be the case in ethoxy.³ Instead, a' , was attributed to the peak labeled α in Fig. 2. This peak was obtained from a nonadiabatic simulation of the ethoxide spectrum, not with the anion in its ground vibrational state, but with one quantum of the lowest a'' mode, $\omega_7(a'')$, excited. The line in the SEVI spectrum labeled b' is unexplained at this time.

The combined studies of isopropoxide and ethoxide enabled us to provide a clear picture of the role and impact of conical intersections on the alkoxy radicals.⁵

II. Work in Progress

A. Photoelectron Spectrum of Hydroxy methoxide.

Hydroxymethoxy can be viewed as a derivative of methoxy with a hydrogen replaced by an OH group. Hence one would expect conical intersections to play a role in the electronic structure of the low-lying states of this molecule. Indeed a recent, very high quality theoretical study of the low-lying electronic \tilde{A} states of hydroxymethoxy found the excited \tilde{A} state only 3142 cm^{-1} above the ground state minimum.¹² We will determine the locus of what we expect to be a relatively low-lying seam of conical intersections and determine its impact on the PES of hydroxymethoxide. The referenced theoretical study did not address the issue of this seam and the PES has yet to be measured experimentally.

B. Photodissociation of the 1-hydroxyethyl radical.

The 1-hydroxyethyl radical, CH_3CHOH , is relevant to the combustion of ethanol and the photochemistry of ethoxy.¹³ Recently Reisler and coworkers¹³ have studied the (nonadiabatic) photodissociation of 1-hydroxyethyl to $\text{CH}_3\text{CHO} + \text{H}$ (onset at $19,600 \text{ cm}^{-1}$)¹³ or $\text{CH}_2\text{CHOH} + \text{H}$ (onset at $31,250 \text{ cm}^{-1}$)¹³. Much of Reisler's analysis¹³ of the nonadiabatic aspects of this photodissociation was based on our earlier studies of the role of conical intersections in the photodissociation of hydroxymethyl, H_2COH .¹⁴ We are currently extending that analysis to consider the role of conical intersections in the photodissociation of 1-hydroxyethyl. To date conical intersections of the $1,2^2A$ states in two regions of nuclear coordinate space have been located. The minimum energy $1,2^2A$ accidental conical intersection has been located and has a considerably extended O-H distance, $R(\text{O-H}) = 1.275 \text{ \AA}$, compared to the ground 1^2A state equilibrium distance, $R^{\text{eq}}(\text{O-H}) = 0.963 \text{ \AA}$. Preliminary calculations place this intersection at $\sim 21,000 \text{ cm}^{-1}$ relative to the ground state minimum. This conical intersection is relevant to the CH_3CHO channel. As a result of this conical intersection there is no local minimum on the 2^2A state potential energy surface. This is consistent with, the observed onset of photodissociation at $19,600 \text{ cm}^{-1}$, the absence of a REMPI signal in this region¹³ and our previous calculations on CH_2OH .¹⁴ The mechanism for the production of CH_2CHOH is currently under investigation.

C. Coupled Potential Energy Surfaces for Nonadiabatic Reactions from Quasi-diabatic Hamiltonians

As a result of other funded research, we have developed a procedure for describing coupled adiabatic potential energy surfaces and their interstate interactions using a quasi-diabatic Hamiltonian, \mathbf{H}^d ,¹ of the form, for $1 \leq \alpha, \beta \leq N^{\text{state}}$

$$H_{\alpha,\beta}^d(\mathbf{Q}) = E_{\alpha}(\mathbf{Q}^0)\delta_{\alpha,\beta} + \sum_{k=1}^{N^{\text{rc}}} V_k^{(1),\alpha,\beta} Q_k + \quad (1)$$

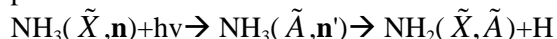
$$\frac{1}{2} \sum_{k,l=1}^{N^{\text{rc}}} V_{k,l}^{(2),\alpha,\beta} Q_k Q_l + \frac{1}{3} \sum_{k,l,m=1}^{N^{\text{rc}}} V_{k,l,m}^{(3),\alpha,\beta} Q_k Q_l Q_m + \dots$$

where the overcomplete nuclear coordinates Q_i are exponentially decreasing functions internuclear distances, and dot-cross product functions, and the $\mathbf{V}^{(i)}$ are determined from the pseudo constrained normal equations:

$$\begin{pmatrix} \mathbf{W}^{lsq\dagger} \mathbf{W}^{lsq} + \mathbf{t} & -\mathbf{W}^{\text{node}\dagger} \\ \mathbf{W}^{\text{node}} & \mathbf{0} \end{pmatrix} \begin{pmatrix} \mathbf{V} \\ \boldsymbol{\lambda} \end{pmatrix} = \begin{pmatrix} \mathbf{W}^{lsq\dagger} \mathbf{M}^{lsq} \\ \mathbf{M}^{\text{node}} \end{pmatrix} \quad (2)$$

where the λ_i are Lagrange multipliers. The right hand side involves, *ab initio* determined energies, energy gradients and derivative couplings. Here we introduced the idea of nodes, points in nuclear coordinate space at which the \mathbf{H}^d derived energies, energy gradients and derivative couplings are required to agree exactly with the *ab initio* results. The inclusion of nodes increased considerably the general accuracy of the fit. Further since we include derivative couplings in the fitting procedure our \mathbf{H}^d are quantifiably quasi diabatic. Illustrative of the potential of this approach, is the excellent reproduction of the derivative coupling for the $1,2^1A$ states of NH_3 in the range 10^{-2} to 10^3 justifying the attribute quasi-diabatic.¹ See Fig. 3.

We are currently extending our preliminary work on the $1,2^1A$ states of NH_3 to produce an \mathbf{H}^d with full permutational symmetry, suitable for simulating Fleming Crim's studies of ammonia photodissociation¹⁵⁻¹⁷



where \mathbf{n} and \mathbf{n}' denote the vibrational quantum numbers. Crim's studies revealed a pronounced dependence of the final state of NH_2 produced on \mathbf{n} , with the observed differences attributed to near conical intersection dynamics. These observations have yet to be fully explained by existing studies,^{18,19} based on an alternative method of describing and fitting²⁰ the $1,2^1A$ states of NH_3 .

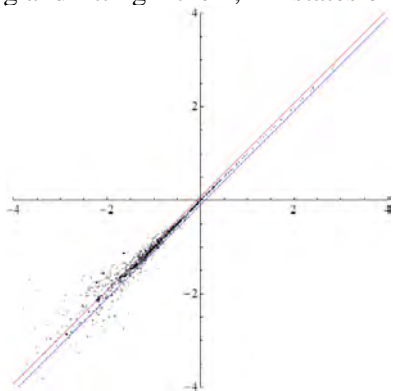
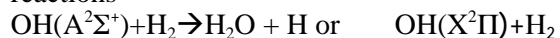


Figure 3: Comparison of *ab initio* and \mathbf{H}^d determined derivative couplings from NH_3 , $1,2^1A$. x-axis *ab initio* value and y-axis \mathbf{H}^d determined value, of a nonzero component of the derivative coupling. For points on the diagonal agreement is exact. Solid lines enclose 20% error.

We are also in the process of constructing an \mathbf{H}^d to describe the reactive and nonreactive quenching reactions



studied experimentally in the groups of Marsha Lester,^{21,22} and Floyd Davis²³ and analyzed theoretically by Bowman's group in a treatment that focused on post quenching dynamics.²⁴ We have considerable experience with this system,²⁵

having described several regions of accidental conical intersections, including those used in the study by Bowman's group. In this system the exploitation of permutational symmetry using the complete nuclear permutation inversion group is complicated by the fact that at our chosen D_{3h} origin of the coordinate system a degenerate E state exists. The algorithmic extensions necessary to deal with this situation are currently being developed as part of our DoE grant.

D. Transition Moments for Photoelectron Spectra

When simulating a PES where the molecule from which the electron has been detached has non degenerate electronic states strongly coupled by conical intersections, a first principles simulation of the spectrum requires the transition moments to the individual diabatic electronic states. The determination of these transition moments is a complex problem in electron scattering and is routinely ignored in current simulations. In our work, see also Ref. ²⁶, we have estimated the transition moments (assumed geometry independent) by comparing the simulated and measured photoelectron spectra. This procedure breaks down for SEVI experiments where the measured intensities may also reflect the Wigner threshold law.

We are developing, as part of other funded research, a formalism, using the sudden approximation,²⁷ to determine these transition moments. In this case the wave function for the target plus outgoing electron is expanded as:

$$\Psi^{(N^{el}+1)} = \sum_{\alpha=1}^{N^{state}} A^{(N^{el}+1)} \Psi_{\alpha}^d(\mathbf{r}; \mathbf{W}) \zeta_{\alpha}^k(\mathbf{W}) \phi_k^c(\mathbf{r}^{N^{el}+1})$$

where ϕ_k^c , which is to be determined, is the orbital that describes the outgoing electron, $\zeta_{\alpha}^k(\mathbf{W})$ is a vibrational function, Ψ_{α}^d is an N^{el} electron diabatic electronic state, $A^{(N^{el}+1)}$ is the $N^{el}+1$ electron antisymmetrizer and

$$\Psi_k^{(N^{el})} = \sum_{\alpha=1}^{N^{state}} A^{(N^{el})} \Psi_{\alpha}^d(\mathbf{r}; \mathbf{W}) \zeta_{\alpha}^k(\mathbf{W})$$

is the, known, k^{th} solution to the N^{el} electron total vibronic Schrödinger equation. In this approximation the scattering orbital, which depends on the vibronic state of the target, is *not* orthogonal to the target electrons, but is geometry independent (although the constructed transition moment is not). The target is unperturbed by the scattering electron, while the scattering electron is affected by the target. Our approach takes full account of the antisymmetrizer, which is not always the case. Initially, the complex rotation method of Han and Reinhardt^{28,29} will be used to determine the solution to the multichannel quantum scattering problem.

Once the algorithm is operational it will be used to determine the transition moments for electron photodetachment for molecules of interest to DoE, including 1-propynide³⁰ and ethoxide. In our previous analyses of those systems, the transition moments were estimated by comparing calculated and measured spectra. As pointed out in those works the estimates of the transition moments contained therein, will provide valuable benchmarks for these first principles calculations.

Literature Cited

¹ X. Zhu and D. R. Yarkony, *J. Chem. Phys.* 132, 104101 (2010).
² J. J. Dillon and D. R. Yarkony, *J. Chem. Phys.* 130, 154312 (11 pages) (2009).
³ J. J. Dillon and D. R. Yarkony, *J. Chem. Phys.* 131, 134303 (12 pages) (2009).
⁴ T. M. Ramond, G. E. Davico, R. L. Schwartz, and W. C. Lineberger, *J. Chem. Phys.* 112, 1158 (2000).
⁵ D. M. Neumark, *J. Phys. Chem. A* 112, 13287 (2008).
⁶ J. Jin, I. Sioutis, G. Tarczay, S. Gopalakrishnan, A. Bezanat, and T. A. Miller, *J. Chem. Phys.* 121, 11780 (2004).
⁷ M. S. Schuurman, D. E. Weinberg, and D. R. Yarkony, *J. Chem. Phys.* 127, 104309(12 pages) (2007).
⁸ B. N. Papas, M. S. Schuurman, and D. R. Yarkony, *J. Chem. Phys.* 129, 124104(10 pages) (2008).
⁹ M. S. Schuurman, R. A. Young, and D. R. Yarkony, *Chem. Phys.* 347, 57 (2008).
¹⁰ M. E. Jenkin and G. D. Hayman, *Atmos. Environ.* 33, 1275 (1999).
¹¹ R. Atkinson, *Int. J. Chem. Kinet.* 29, 99 (1997).
¹² W. Eisfeld and J. Francisco, *J. Chem. Phys.* 131, 134313 (2009).

¹³ B. Karpichev, L. Edwards, J. Wei, and H. Reisler, *J. Phys. Chem. A* 112, 412 (2008).
¹⁴ B. C. Hoffman and D. R. Yarkony, *J. Chem. Phys.* 116, 8300 (2002).
¹⁵ A. Bach, J. M. Hutchison, R. J. Holiday, and F. F. Crim, *J. Chem. Phys.* 116, 4955 (2002).
¹⁶ A. Bach, J. M. Hutchison, R. J. Holiday, and F. F. Crim, *J. Chem. Phys.* 118, 7144 (2003).
¹⁷ M. L. Hause, Y. H. Yoon, and F. F. Crim, *J. Chem. Phys.* 125, 174309 (2006).
¹⁸ D. Bonhommeau and D. G. Truhlar, *J. Chem. Phys.* 129, 014302 (2008).
¹⁹ D. Bonhommeau, R. Valero, D. G. Truhlar, and A. W. Jasper, *J. Chem. Phys.* 130, 234303 (17 pages) (2009).
²⁰ S. Nangia and D. G. Truhlar, *J. Chem. Phys.* 124, 124309 (2006).
²¹ P. A. Cleary, L. P. Dempsey, C. Murray, M. I. Lester, J. Kos, and M. H. Alexander, *J. Chem. Phys.* 126, 204316 (2007).
²² L. P. Dempsey, C. Murray, and M. I. Lester, *J. Chem. Phys.* 127, 151101 (2007).
²³ M. Ortiz-Suárez, M. F. Witinski, and H. F. Davis, *J. Chem. Phys.* 124, 201106 (2006).
²⁴ E. Kamarchik, B. Fu, and J. M. Bowman, *J. Chem. Phys.* 132, 091102 (2010).
²⁵ B. C. Hoffman and D. R. Yarkony, *J. Chem. Phys.* 113, 10091 (2000).
²⁶ T. Ichino, A. J. Gianola, W. C. Lineberger, and J. F. Stanton, *J. Chem. Phys.* 125, 084312 (2006).
²⁷ A. B. Trofimov, H. Köppel, and J. Schirmer, *J. Chem. Phys.* 109, 1025 (1998).
²⁸ W. P. Reinhardt and S. Han, *Int. J. of Quantum Chem.* 57, 327 (1995).
²⁹ S. Han and W. P. Reinhardt, *J. Phys. B* 28, 3347 (1995).
³⁰ B. N. Papas, M. S. Schuurman, and D. R. Yarkony, *J. Chem. Phys.* 130, 064306 (12 pages) (2009).

PUBLICATIONS SUPPORTED BY DE-FG02-91ER14189: 2008 – present

1. *The Photoelectron Spectrum of 1-propynide. Nonadiabatic Effects*

Brian N. Papas, Michael S. Schuurman and David R. Yarkony, *J. Chem. Phys.* **130**, 064306 (12 pages) (2009).

2. *The simulated spectrum of isopropoxide. Nonadiabatic effects due to conical intersections and the spin-orbit interaction*

Joseph J. Dillon and David R. Yarkony, *J. Chem. Phys.* 130 154312 (11 pages) (2009)

3. *The Photoelectron Spectrum of the Ethoxide Anion: Conical Intersections, the Spin-Orbit Interaction and Sequence Bands*

Joseph J. Dillon and David R. Yarkony, *J. Chem. Phys.* 131, 134303 (12 pages) (2009)

GAS-PHASE MOLECULAR DYNAMICS: THEORETICAL STUDIES IN SPECTROSCOPY AND CHEMICAL DYNAMICS

Hua-Gen Yu (hgy@bnl.gov) and James T. Muckerman (muckerma@bnl.gov)
Chemistry Department, Brookhaven National Laboratory, Upton, NY 11973-5000

Program Scope

The goal of this program is the development and application of computational methods for studying chemical reaction dynamics and molecular spectroscopy in the gas phase. We are interested in developing rigorous quantum dynamics algorithms for small polyatomic systems and in implementing approximate approaches for complex ones. Particular focus is on the dynamics and kinetics of chemical reactions and on the rovibrational spectra of species involved in combustion processes. This research also explores the potential energy surfaces of these systems of interest using state-of-the-art quantum chemistry methods.

Recent Progress

Kinetics and dynamics study of the reaction of HOCO radical with CH₃ and ClO radicals

A combined *ab initio* direct dynamics and RRKM (Rice-Ramsperger-Kassel-Marcus) study has been carried out for the reaction of HOCO radicals with CH₃ radicals. It is examined using the coupled cluster method (CCSD(T)) to locate and optimize the critical points on the ground-state potential energy surface as shown in Fig.1. The results show that the CH₃ + HOCO reaction can produce both the H₂O + CH₂CO and the CH₄ + CO₂ products through acetic acid (M₁) and enediol (M₂) intermediates. Direct *ab initio* dynamics calculations determine the thermal rate coefficients to be $k(T/K) = 3.24 \times 10^{-11} T^{0.1024}$ in $\text{cm}^3 \text{molec}^{-1} \text{s}^{-1}$ at $T \leq 1000$ K for the overall reaction. The product branching ratio of (H₂O + CH₂CO) to (CH₄ + CO₂) is predicted to be $R_{\text{H}_2\text{O}/\text{CH}_4}(T/K) = 1.52 + (1.95 \times 10^{-4})T$ using the RRKM approach. Both the thermal rate coefficients and the product branching ratios weakly depend on temperature. In addition, the kinetics of the ClO + HOCO reaction has been studied using the variational RRKM theory based on a CCSD(T) potential energy surface. This is a fast reaction leading to a diversity of products *via* an addition or direct hydrogen abstraction reaction mechanism. At room temperature, the thermal rate coefficient is obtained as $4.26 \times 10^{-12} \text{ cm}^3 \text{molec}^{-1} \text{s}^{-1}$ with the product branching fractions of Cl (0.518), HOCl (0.469), HCl (0.01), and HClO (0.003) at zero pressure. Furthermore, a simple RRKM/master equation simulation indicates that the stabilization of the HOC(O)Cl intermediates is noticeable at moderate

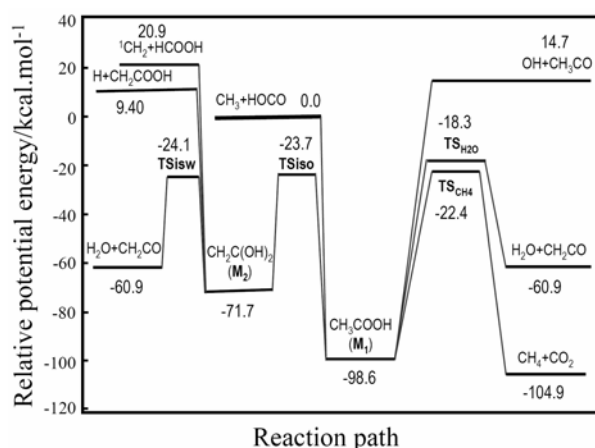


Figure 1. CCSD(T)/aug-cc-pVQZ energy diagram for the reaction pathway of the CH₃ + HOCO reaction.

pressures as its thermal rate constant reaches about $6.0 \times 10^{-13} \text{ cm}^3 \text{ molec}^{-1} \text{ s}^{-1}$. This work was done in collaboration with J. Francisco (Purdue).

Dynamics study of molecular ion-molecule reaction

The direct molecular dynamics method was employed to study the reaction of CO with H_3^+ and H_2D^+ using a scaling all correlation second-order Møller–Plesset perturbation theory (SAC-MP2) method with the cc-pVTZ basis set. Results show that total thermal rate coefficients for both the CO + H_3^+ and the CO + H_2D^+ reactions have a weakly positive temperature dependence. At room temperature, the rate coefficients are predicted to be $(1.42 \pm 0.03) \times 10^{-9} \text{ cm}^3 \text{ molec}^{-1} \text{ s}^{-1}$ with a product branching ratio of $[\text{HOC}^+]/[\text{HCO}^+] = 0.36 \pm 0.01$ for the CO + H_3^+ reaction, and $(1.26 \pm 0.03) \times 10^{-9} \text{ cm}^3 \text{ molec}^{-1} \text{ s}^{-1}$ with the product branching ratios: 0.37 ± 0.01 ($([\text{HOC}^+] + [\text{DOC}^+])/([\text{HCO}^+] + [\text{DOC}^+])$), 0.54 ± 0.02 ($[\text{DCO}^+]/[\text{HCO}^+]$), and 0.49 ± 0.02 ($[\text{DOC}^+]/[\text{HOC}^+]$) for CO + H_2D^+ . The product branching ratios have a noticeable temperature dependence as well as a pronounced isotopic effect for the H/DOC⁺ product channel.

Spherical electron cloud hopping molecular dynamics simulation on dissociative recombination (DR) of protonated water

The SECH MD method has been applied to study the DR of H_3O^+ at zero collision energy. The simulations give several product channels: 0.660 for (OH + 2H), 0.230 for (H_2O + H), 0.108 for (OH + H_2), and 0.002 for (O + H + H_2), which are in excellent agreement with the heavy-ion storage ring experimental results. It was noticed that the first excited state of H_3O plays a prominent role in DR of H_3O^+ . The OH + H_2 channel proceeds on this excited state and associated non-adiabatic transitions. Similar dynamics events were also observed by Lester and co-workers in their dynamics measurement of the OH ($A^2\Sigma$) + H_2 collisions. In addition, two different pathways leading to hydrogen atoms are identified in the H_3O^+ DR processes, by analysis of the trajectories, and the bimodal distribution of released kinetic energies of hydrogen atoms.

A general program for calculating vibrational spectra of five-atom systems

Besides the electronic structure and molecular dynamics calculations, our research is also focuses on quantum dynamics studies of molecular spectroscopy. In this project, we aim to develop computational algorithms to accurately calculate the rovibrational spectra of polyatomic molecules, and to assist experimentalists to interpret their observed spectra. By using the two layer Lanczos iterative diagonalization algorithm developed by us previously, we have programmed an exact variational algorithm for calculating vibrational energy levels of pentatomic molecules using a rigorous quantum dynamics method. The algorithm has exploited a common compact Hamiltonian expressed in a set of four orthogonal polyspherical vectors. Since the orthogonal coordinates are a set of scattering coordinates, the large amplitude motions of vibrations and molecular dissociation events are well described. It is possible to study highly excited vibrational states and resonances (metastable vibrational states) of molecules. With the intermediate use of atomic Cartesian coordinates, any functional form can be used for expressing the potential energy surface of the system of interest. In addition, the vibrational states are efficiently solved using a two-layer Lanczos algorithm in a mixed grid/basis representation. A non-direct product basis is used in the angular variables, which avoids the singularity of the Hamiltonian at $\sin\theta = 0$. The two-layer Lanczos algorithm solves the whole eigenvalue problem in two consecutive diagonalizations in a five dimensional

manner, and only requires the actions of Hamiltonian on a vector, without explicitly storing the Hamiltonian matrix. Thus, a very large basis set is allowed in calculations, which makes this work feasible. In particular, the algorithm is problem-independent so that it is universal and applicable to most penta-atomic molecules with small and/or large amplitude vibrations. A general code (PetroVib) has been programmed. The program has been successfully applied for calculating the vibrational states of three types of penta-atomic molecules, e.g., semi-rigid CH₄, floppy H₃O₂⁻, and the van der Waals complex He₃Cl₂, for numerical demonstrations.

Future Plans

Kinetics and dynamics study of combustion-related reactions

We will continue to study some important combustion reactions using the direct *ab initio* molecular dynamics program. Our study of a series of reactions involving the HOCO radical will conclude with the disproportionation of the HOCO radical. Here we will address the energies, geometries, and vibrational frequencies of the stationary points on the singlet ground-state surface, and the reaction mechanism. If one HOCO radical abstracts the hydrogen atom from the other, the products would be HC(O)OH and CO₂. If the two HOCO radicals form an intermediate oxalic acid (HOC(O)C(O)OH) complex, the products could be H₂O, CO and CO₂, or two CO₂ and H₂. The dynamics will be carried out using a dual level *ab initio* method. The aim of this research is to determine the mechanism and product branching ratio as well as rate coefficients.

A new direction in the study of combustion-related radical reactions using the direct *ab initio* molecular dynamics program will focus on the kinetics and dynamics of cyclic, N- and O-containing fuel molecules. The concentration of cyclic compounds in diesels and other future transportation fuels, produced largely from non-traditional sources such as oil shales and sand oils, are much higher than those in current fuels. There are only limited kinetics data on cyclic fuel molecules, yet they are required to design future internal combustion engines using such fuels. A new unique step in the chemistry is the ring-opening processes resulting in, for example cyclopentoxy (cyc-C₅H₉O) radicals discussed by us before. Such radicals may well contribute to enhanced formation of soot without a ring-opening reaction. In this work, we will start this project with the reactions of morpholine (1-oxa-4-aza-cyclohexane, i.e. cyclic -OCH₂CH₂NHCH₂CH₂-) and its derivatives with small radicals such as O₂, HO₂ and OH. Westmoreland et al. have recently demonstrated that morpholine is an ideal compound for modeling those hydrocarbon, oxygenated and N-containing fuels. Here, we will address the energies, geometries, and vibrational frequencies of the stationary points on the ground-state surfaces, and the reaction mechanism. The dynamics will be carried out using the DualOrthGT program, together with variational RRKM theory.

Vibronic spectrum calculations of CH₂ and its interactions with He

In our GPMD group, Sears and Hall have observed rich and complicated rovibronic levels of CH₂ near the C + H₂ and CH + H dissociation limits. They provide a challenge for multiple surface dynamics theory, with relevance to the reactive system as well as CH₂ spectroscopy. We have calculated five low-lying electronic potential energy surfaces of CH₂ using a multireference CI (MRCI) method. The adiabatic surfaces will be transformed into a set of diabatic ones using the quasi-adiabatic approximation of

Koppel et al. Full-dimensional quantum dynamics will then be performed on the five coupled surfaces. The principal interest is in the energy levels and non-adiabatic coupling effects, for detailed comparison with experimental observations. In addition, we also plan to calculate the singlet and triplet potential energy surfaces of the He-CH₂ (X/A) interaction system using the CCSD(T)/aug-cc-pVQZ level of theory. The surfaces will be used for investigating the dynamics of singlet and triplet states of CH₂ in collaboration with Tscherbul at Harvard, and rotationally inelastic scattering calculations in collaboration with Dagdigian and Alexander at Johns Hopkins and Maryland.

Non-adiabatic molecular dynamics studies of polyatomic molecular reactions

Electronically excited species such as ¹CH₂ also play an important role in combustion chemistry. However, the studies of their reactivity are rather limited, partially due to the non-adiabatic dynamics effects because those reactions often occur on multiple potential energy surfaces. In this research, we will extend the surface hopping direct *ab initio* molecular dynamics algorithm, developed for the SECH MD studies, to simulate the bimolecular reactions and the photo-dissociation chemistry. The first application would be the photodissociation dynamics of acetone at 193-230 nm. This system has been investigated by Suits et al. using an universal ion imaging technique. The photon excited acetone produces two major types of products: CH₃CO + CH₃ and CO + 2CH₃. The latter products result from poorly understood dissociation mechanisms. Here we will attempt to explore the dissociation pathways of acetone on its three low-lying electronic states.

Publications since 2008

- H.-G. Yu, G. Poggi, J.S. Francisco and J. T. Muckerman, *Energetics and molecular dynamics of the reaction of HOCO with HO₂ radicals*, J. Chem. Phys. **129**, 214307 (2008).
- H.-G. Yu, J.S. Francisco and J. T. Muckerman, *Ab initio and direct dynamics study of the reaction of Cl atoms with HOCO*, J. Chem. Phys. **129**, 064301 (2008).
- H.-G. Yu and J.S. Francisco, *Energetics and kinetics of the reaction of HOCO with hydrogen atoms*, J. Chem. Phys. **128**, 244315 (2008).
- H.-G. Yu, *A spherical electron cloud hopping model for studying product branching ratios of dissociative recombination*, J. Chem. Phys. **128**, 194106 (2008).
- B.J. Braams and H.-G. Yu, *Potential energy surface and quantum dynamics study of rovibrational states of HO₃(X²A'')*, Phys. Chem. Chem. Phys. **10**, 3150 (2008).
- W.-Q. Han, H.-G. Yu, C. Zhi, J. Wang, Z. Liu, T. Sekiguchi and Y. Bando, *Isotope effect on band gap and radiative transitions properties of boron nitride nanotubes*, Nano Lett. **10**, 491 (2008).
- H.-G. Yu and J.S. Francisco, *A theoretical study of the reaction of CH₃ with HOCO radicals*, J. Phys. Chem. A, **113**, 3844 (2009).
- H.-G. Yu and J.S. Francisco, *Ab initio and RRKM study of the reaction of ClO with HOCO radicals*, J. Phys. Chem. A, **113**, 12932 (2009).
- H.-G. Yu, *Product branching ratios of the reaction of CO with H₃⁺ and H₂D⁺*, Astrophys. J. Lett., **706**, L52 (2009).
- H.-G. Yu, *Spherical electron cloud hopping molecular dynamics simulation on dissociative recombination of protonated water*, J. Phys. Chem. A, **113**, 6555 (2009).
- H.-G. Yu, *A general rigorous quantum dynamics algorithm to calculate vibrational energy levels of pentaatomic molecules*, J. Mol. Spectrosc. **256**, 287 (2009).

Isomer-specific Spectroscopy and Isomerization in Aromatic Fuels

Timothy S. Zwier

Department of Chemistry, Purdue University, West Lafayette, IN 47907-2084
zwier@purdue.edu

Program Definition and Scope

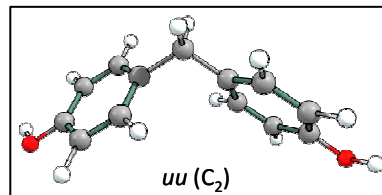
Gasoline and diesel fuels are complicated mixtures containing about 30% aromatics, including alkylbenzene, alkenylbenzene, and alkynylbenzenes of various chain lengths. The combustion of these molecules is influenced by their structural and conformational make-up, and by the rates of isomerization between them. Alternative energy sources, such as biofuels, will bring to the combustion process a wider array of chemical functionality, further challenging combustion models, especially at the large molecule end of the model where experimental data is less complete. In this size regime, conformational and structural isomers are pervasive. The objective of this research program is to develop and utilize laser-based methods to characterize the spectroscopy and isomerization dynamics of conformational and structural isomers of aromatic derivatives that play a role in soot formation, or that may be components of alternative energy fuels. As a first step in all these studies, UV-UV hole-burning and resonant ion-dip infrared (RIDIR) spectroscopy are being used to determine the number and identity of the isomers present, based on their ultraviolet and infrared spectral signatures. These structural studies then serve as a foundation for studies of the dynamics of conformational isomerization using stimulated emission pumping-population transfer (SEP-PT) spectroscopy, a method developed by our group to directly measure the energy thresholds separating individual A→B reactant-product isomer pairs, thereby mapping out key stationary points on the multi-dimensional potential energy surface for isomerization.

Recent Progress

Over the past year, we have expanded our studies of the spectroscopy and the conformational isomerization dynamics of a series of flexible bichromophores. We have also initiated work that takes our program in a new direction, involving isomer-specific spectroscopy and isomerization of lignin monomers and oligomers of importance in the breakdown and/or combustion of biofuels.

A. Conformational isomerization and internal mixing in bis-(4-hydroxyphenyl)methane

In previous work, we studied the jet-cooled spectroscopy and isomerization of diphenylmethane (DPM)^{1,4} and bis-(2-hydroxyphenyl)methane (b2HPM)^{5,6}, both symmetric flexible bichromophores containing two and four flexible coordinates, respectively. In both cases, the two chromophores were structurally equivalent, with identical excited state energies prior to excitonic coupling. The spectroscopy and isomerization of both these molecules were fascinating, particularly in that they revealed the presence of two close-lying, “intermingled” excitonic states, whose relative energy and degree of electronic localization/delocalization depend sensitively on the relative orientation of the two phenyl rings relative to one another. During the past year, we have studied another closely analogous molecule, bis-(4-hydroxyphenyl)methane (b4HPM). Three publications are currently in preparation describing this work. b4HPM places the two OH groups in *para* positions on the ring, at a distance too great to interact either with each other or with the other phenyl ring. Nevertheless, the asymmetry of the



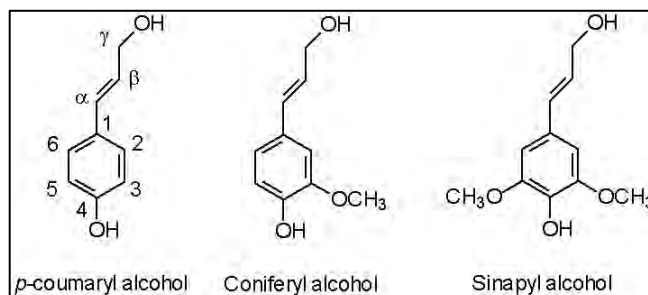
OH groups leads to formation of three conformational isomers, with ‘uu’, ‘ud’, and ‘dd’ designations indicating whether the OH groups point ‘up’ towards or ‘down’ away from the methylene group.

We have studied the single conformation UV spectroscopy of the two observed conformers of b4HPM, recording high resolution UV spectra of the S_0 - S_1 and S_0 - S_2 origins (in collaboration with David Plusquellic at NIST) and characterizing the state-to-state internal mixing, much as we did in DPM and b2HPM. In addition, the spectroscopically distinct conformers present in b4HPM provide an extraordinary opportunity to measure the barriers to isomerization involving phenyl ring torsion using SEP-PT spectroscopy. The observed energy thresholds for isomerization are startlingly low for conformer interconversion, with values of less than 50 cm^{-1} for all observed thresholds. This is a factor of ten lower than any other barriers we have measured by our methods. In order to understand these results, we have calculated the ground state 2D torsional surface, which shows a nearly flat trough in the surface along the antisymmetric torsional coordinate. Motion along this coordinate keeps the two rings nearly orthogonal to one another. Thus, the two phenyl rings undergo nearly free internal rotation, yet undergo a highly correlated motion in which the two rings maintain an orthogonality that minimizes the inter-ring interactions.

Furthermore, the combination of high resolution UV spectra and single vibronic level dispersed fluorescence spectra were used to study state-specific internal mixing in b4HPM. In particular, emission from the S_2 origin of both isomers proves that this level in fact has mixed excited state character, with components of the emission ascribable to the S_2 origin and the set of S_1 vibronic levels to which it is coupled. Unlike DPM, in which the levels involved in S_1/S_2 internal mixing violated the $\Delta v = \pm 1$ selection rules for vibronic coupling, in b4HPM, the low-frequency vibrations contain low-lying b-symmetry bending mode close in energy to the excitonic splitting ($\omega = 125\text{ cm}^{-1}$).

B. Single-conformation spectroscopy of lignin monomers

We are also in the midst of studies of the single-conformation spectroscopy of each of the three monomers that make up lignin, the second most abundant biopolymer on earth. Lignin is the principle biopolymer that makes up plant cell walls. Plant biologists interested in maximizing the efficiency of conversion of biomass into liquid fuels are focusing attention on lignin, because it is not easily converted into ethanol. Lignin adds structural integrity to plant cell walls by virtue of its interwoven, rigid framework (structure shown on the next page). This aromatic biopolymer is produced in the plant by the action of oxidative enzymes on the three lignin monomers p-coumaryl alcohol, coniferyl alcohol, and sinapyl alcohol, whose structures are shown to the right. There is an obvious and pressing need for a deeper understanding of the biological mechanisms for controlling the composition and structure of lignin in plants.



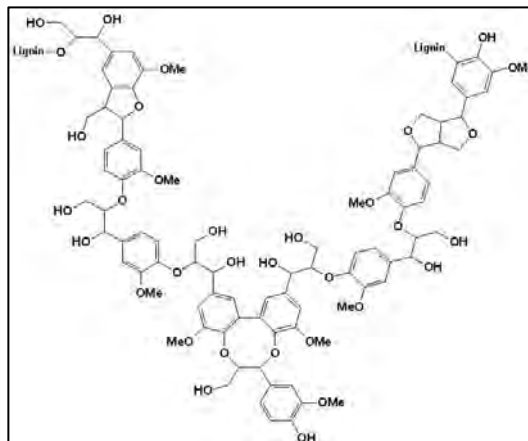
The recent U.S. Department of Energy Biomass to Biofuels Workshop highlighted the range of scientific problems that must be addressed in order to understand and control biomass synthesis and maximize its conversion to biofuels. Furthermore, pyrolysis or combustion of wood necessarily involves the breakdown of lignin, via a cascade of reactions that produce small oligomers, monomers, and smaller aromatic-containing intermediates.

The lignin monomers themselves are a natural starting point for our studies, forming a series of substituted aromatics (see above) with multiple small flexible side chains whose conformation-

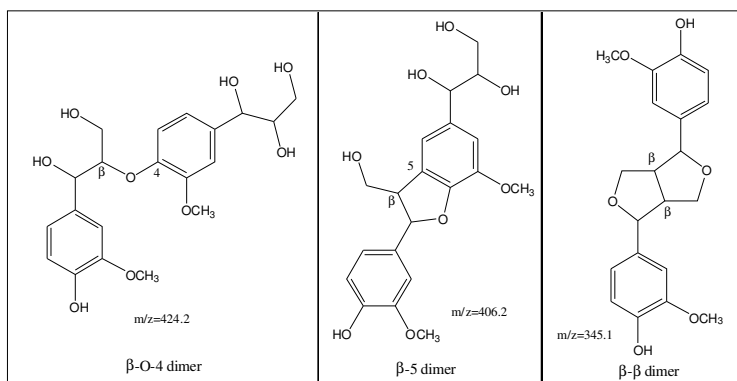
specific spectroscopy can be characterized and distinguished, and whose conformational isomerization can be studied in significant detail by our methods. To that end, we have recorded LIF, R2PI, UV hole-burning, and fluorescence-dip infrared spectra of the three molecules, determining the presence and spectral signatures of two conformational isomers of each, differing in the relative orientations of the C=C and OH groups.

Future work

Lignin oligomers (shown schematically above) are composed of these fundamental building blocks, linked together in one of several ways to produce structures whose rigidity varies with the nature and type of linkage and the degree of branching present. These, too, can be subjects of our study, with the goal of learning about the inherent conformational preferences, unique linkage-dependent spectroscopic signatures, conformational interconversion, and interchromophore electronic coupling. To that end, we have initiated a collaboration with P.V. Ramachandran's group here at Purdue, which has led



to their synthesis of the three prototypical lignin dimers shown to the right. During the coming year, we hope to explore the spectroscopy of these dimers. Sample handling will be an issue, since further polymerization at the temperatures needed to bring the molecules into the gas phase must be minimized. We are exploring laser desorption schemes for doing so.



We will also be exploring the isomer-specific spectroscopy of resonance-stabilized radicals, concentrating initially on the dispersed fluorescence and resonant ion-dip infrared spectra of the 1- and 2-hydronaphthyl radicals and 1,2,3-trihydronaphthyl radical.

Publications acknowledging DOE support, 2008-present

1. Nathan R. Pillsbury, Jaime A. Stearns, Alope Das, Talitha M. Selby, David F. Plusquellic, and Timothy S. Zwier, "State-specific studies of Internal Mixing in a Prototypical Flexible Bichromophore: Diphenylmethane", *J. Chem. Phys.* **129** 114301 (2008). 12 pages.
2. Nathan R. Pillsbury and Timothy S. Zwier, "Conformation-specific spectroscopy and excited state photophysics of 5-phenyl-1-pentene", *J. Phys. Chem. A* **113**, 118-125 (2009).
3. Nathan R. Pillsbury and Timothy S. Zwier, "Conformational isomerization of 5-phenyl-1-pentene probed by SEP-population transfer spectroscopy", *J. Phys. Chem. A* **113**, 126-134 (2009).
4. Jaime A. Stearns, Nathan R. Pillsbury, Christian W. Müller, Kevin O. Douglass, Timothy S. Zwier, and David F. Plusquellic, "Rotationally resolved studies of S_0 and the exciton coupled S_1/S_2 origin regions of diphenylmethane and its d_{12} isotopologue", *J. Chem. Phys.* **129**, 224305 (2009).
5. Nathan R. Pillsbury, Christian W. Muller, and Timothy S. Zwier, "Conformational Effects on Excitonic Interactions in a Prototypical H-bonded Bichromophore: Bis(2-hydroxyphenyl) methane", *J. Phys. Chem. A* **113**, 5000-5012 (2009).
6. Nathan R. Pillsbury and Timothy S. Zwier, "The Conformational Isomerization and Collisional Cooling Dynamics of Bis-(2-hydroxyphenyl)methane", *J. Phys. Chem. A* **113**, 5013-5021 (2009).

Participant List

31st Annual Combustion Research Meeting Participation List

Last Name	First Name	Organization	Email
Alexander	Millard	University of Maryland	mha@umd.edu
Allen	Wesley	University of Georgia	wdallen@uga.edu
Babikov	Dmitri	Marquette University	dmitri.babikov@mu.edu
Baer	Tomas	University of North Carolina	baer@unc.edu
Barlow	Robert	Sandia National Laboratories	barlow@sandia.gov
Bellan	Josette	Jet Propulsion Laboratory, California Institute of Technology	josette.bellan@jpl.nasa.gov
Bowman	Joel	Emory University	jmbowma@emory.edu
Brown	Nancy	Lawrence Berkeley National Lab	NJBrown@lbl.gov
Casassa	Michael	Office of Basic Energy Sciences, U.S. Department of Energy	michael.casassa@science.doe.gov
Chandler	David	Sandia National Laboratories	chand@sandia.gov
Chen	Jacqueline	Sandia National Labs	jhchen@sandia.gov
Continetti	Robert	University of California, San Diego	rcontinetti@ucsd.edu
Cool	Terrill	Cornell University	TAC13@CORNELL.EDU
Crim	Fleming	University of Wisconsin-Madison	fcrim@chem.wisc.edu
Davis	Floyd	Cornell University	hfd1@cornell.edu
Davis	Michael	Argonne National Laboratory	davis@tcg.anl.gov
Dibble	Theodore	SUNY-ESF	tsdibble@syr.edu
Ervin	Kent M.	University of Nevada, Reno	ervin@unr.edu
Fiechtner	Greg	Office of Basic Energy Sciences, U.S. Department of Energy	Gregory.Fiechtner@science.doe.gov
Field	Robert	MIT	rwfield@mit.edu
Flynn	George	Columbia University	gwf1@columbia.edu
Frank	Jonathan	Sandia National Laboratories	jhfrank@sandia.gov
Frenklach	Michael	Lawrence Berkeley Nat'l Lab/ U.C. Berkeley	myf@me.berkeley.edu

Green	William	MIT/Dept. of Chemical Engineering	balkwill@mit.edu
Guo	Hua	University of New Mexico	hguo@unm.edu
Hall	Gregory	Brookhaven National Lab	gehall@bnl.gov
Hansen	Nils	Sandia National Laboratories	nhansen@sandia.gov
Hanson	Ronald	Stanford University	rkhanson@stanford.edu
Harding	Lawrence	Argonne National Laboratory	harding@anl.gov
Head-Gordon	Martin	Lawrence Berkeley Nat'l Lab/ U.C. Berkeley	m_headgordon@berkeley.edu
Hershberger	John	North Dakota State University	john.hershberger@ndsu.edu
Hirata	So	University of Florida	hirata@qtp.ufl.edu
Hoffmann	Mark	University of North Dakota	mhoffmann@chem.und.edu
Jasper	Ahren	Sandia National Laboratories	ajasper@sandia.gov
Kaiser	Ralf	University of Hawaii	ralfk@hawaii.edu
Kellman	Michael	University of Oregon	kellman@uoregon.edu
Kerstein	Alan	Sandia National Laboratories	arkerst@sandia.gov
Khokhlov	Alexei	The University of Chicago	ajk@oddjob.uchicago.edu
Klippenstein	Stephen	Argonne National Laboratory	sjk@anl.gov
Krylov	Anna	University of Southern California	krylov@usc.edu
Lansdon	Connie	Oak Ridge Associated Universities	Connie.Lansdon@orise.ornl.gov
Leone	Stephen	Lawrence Berkeley Nat'l Lab/ U.C. Berkeley	srl@berkeley.edu
Lester	Marsha	University of Pennsylvania	milester@sas.upenn.edu
Lester, Jr.	William	Lawrence Berkeley Nat'l Lab/ U.C. Berkeley	walester@lbl.gov
Long	Marshall	Yale University	marshall.long@yale.edu
Longman	Douglas	Argonne National Laboratory	dlongman@anl.gov
Lucht	Robert	Purdue University	Lucht@purdue.edu
Macdonald	Robert	Argonne National Laboratory	rgmacdonald@anl.gov
McIlroy	Andrew	Sandia National Laboratories	amcrlr@sandia.gov
Mebel	Alexander	Florida International University	mebela@fiu.edu
Michael	Joe	Argonne National Laboratory	jmichael@anl.gov

Michelsen	Hope	Sandia National Laboratories	hamiche@sandia.gov
Miller	James A.	Sandia National Laboratories	jamilie@sandia.gov
Miller	Terry	Ohio State University	tamiller@chemistry.ohio-state.edu
Miller	William H.	Lawrence Berkeley Nat'l Lab/ U.C. Berkeley	millerwh@berkeley.edu
Mittal	Gaurav	University of Akron	gaurav@uakron.edu
Mullin	Amy	University of Maryland	mullin@umd.edu
Nesbitt	David	JILA, NIST, Department of Chemistry and Biochemistry	djn@jila.colorado.edu
Neumark	Daniel	Lawrence Berkeley Nat'l Lab/ U.C. Berkeley	dneumark@berkeley.edu
Ng	Cheuk-Yiu	University of California, Davis	cyng@chem.ucdavis.edu
Nizkorodov	Sergey	University of California, Irvine	nizkorod@uci.edu
Oefelein	Joseph	Sandia National Laboratories	oefelei@sandia.gov
Osborn	David	Sandia National Laboratories	dlosbor@sandia.gov
Parish	Carol	University of Richmond	cparish@richmond.edu
Pederson	Mark	Office of Basic Energy Sciences, U.S. Department of Energy	Mark.Pederson@science.doe.gov
Perry	David	The University of Akron	dperry@uakron.edu
Piecuch	Piotr	Michigan State University	piecuch@chemistry.msu.edu
Pitz	William	Lawrence Livermore National Laboratory	pitz1@llnl.gov
Pope	Stephen	Cornell University	s.b.pope@cornell.edu
Pratt	Stephen	Argonne National Laboratory	stpratt@anl.gov
Reisler	Hanna	University of Southern California	reisler@usc.edu
Rohlfing	Eric	Office of Basic Energy Sciences, U.S. Department of Energy	eric.rohlfing@science.doe.gov
Rouson	Damian	Sandia National Laboratories	rouson@sandia.gov
Ruscic	Branko	Argonne National Laboratory	ruscic@anl.gov
Sanov	Andrei	University of Arizona	sanov@u.arizona.edu
Schaefer	Henry	University of Georgia	sch@uga.edu
Sears	Trevor	Brookhaven National Laboratory	sears@bnl.gov
Settersten	Thomas	Sandia National Laboratories	tbsette@sandia.gov
Shepard	Ron	Argonne National Laboratory	shepard@tcg.anl.gov

Sheps	Leonid	Sandia National Laboratories	sheps@jila.colorado.edu
Sisk	Wade	Office of Basic Energy Sciences, U.S. Department of Energy	wade.sisk@science.doe.gov
Sivaramakrishnan	Raghu	Argonne National Laboratory	raghu@anl.gov
Smooke	Mitchell	Yale University	mitchell.smooke@yale.edu
Stanton	John	University of Texas at Austin	jfstanton@mail.utexas.edu
Stolow	Albert	National Research Council Canada	albert.stolow@nrc.ca
Streiffer	Stephen	Argonne National Laboratory	streiffer@anl.gov
Suits	Arthur	Wayne State University	asuits@chem.wayne.edu
Tranter	Robert	Argonne National Laboratory	tranter@anl.gov
Truhlar	Donald	University of Minnesota	truhlar@umn.edu
Tsang	Wing	NIST/DOE	wing.tsang@nist.gov
Vander Wal	Randy	Penn State University	ruv12@psu.edu
Violi	Angela	University of Michigan	avioli@umich.edu
Virgo	Wilton	Wellesley College	wvirgo@wellesley.edu
Wagner	Albert	Argonne National Laboratory	wagner@anl.gov
Weber	Peter	Brown University	Peter_Weber@brown.edu
Westmoreland	Phillip	NC State University	phil.westmoreland@ncsu.edu
Wittig	Curt	University of Southern California	wittig@usc.edu
Wooldridge	Margaret	University of Michigan	mswool@umich.edu
Yarkony	David	Johns Hopkins University	yarkony@jhu.edu
Yu	Hua-Gen	Brookhaven National Laboratory	hgy@bnl.gov
Zádor	Judit	Sandia National Laboratories	jzador@sandia.gov
Zheng	Xiaolin	Stanford University	xlzheng@stanford.edu
Zwier	Timothy	Purdue University	zwier@purdue.edu